

Design and Synthesis of Core-modified Porphyrin Sensitizers for Dye-Sensitized Solar Cells

A Thesis Submitted to the
National Taiwan Normal University

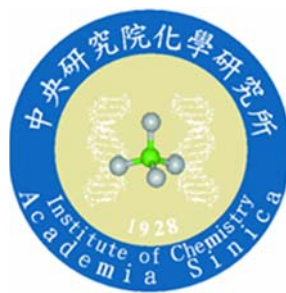
For the Degree of
DOCTOR OF PHILOSOPHY
(In Chemistry)

By
Sandeep Babruwahan Mane
(898420121)

Adviser
Dr. Chen-Hsiung Hung



Department of Chemistry,
National Taiwan Normal University



Institute of Chemistry,
Academia Sinica, Taipei, Taiwan



CERTIFICATE

This is to certify that the work incorporated in the thesis entitled “Design and Synthesis of Core-modified Porphyrin Sensitizers for Dye-sensitized Solar Cells” submitted by Sandeep Babruwahan Mane was carried out by him under my supervision at the Institute of Chemistry, Academia Sinica, Taipei, Taiwan.

*Dr. Chen-Hsiung Hung
Institute of Chemistry, Academia Sinica
128, Academia Rd, Sec. 2, Nankang,
Taipei 11529, Taiwan (ROC)
E-mail: chhung@gate.sinica.edu.tw
TEL: +886-2-27898570 FAX: +886-2-27831237*

CANDIDATE'S DECLARATION

I hereby declare that the work presented in the dissertation entitled "Design and Synthesis of Core-modified Porphyrin Sensitizers for Dye-sensitized Solar Cells" submitted for Ph.D. degree to National Taiwan Normal University, Taipei, Taiwan. The work has been carried out by myself at the Institute of Chemistry, Academia Sinica, Taipei, Taiwan (ROC), under the supervision of Dr. Chen-Hsiung Hung. The work is original and any of the part of this work was not submitted by me for another degree or diploma to this or any other university. In keeping with the general practice, due acknowledgements have been made, wherever the work described based on the findings of other investigators. Any inadvertent omissions that might have occurred, due to oversight or error in judgment are regretted.

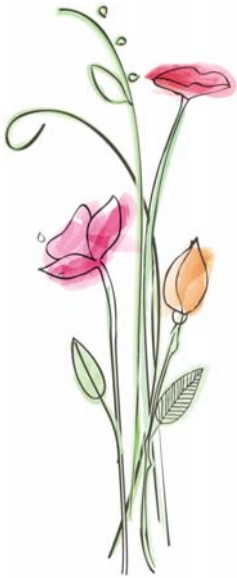
Date: June 2014

*Department of Chemistry,
National Taiwan Normal University,
Taipei 11677, TAIWAN (ROC)*

Sandeep Babruwahan Mane

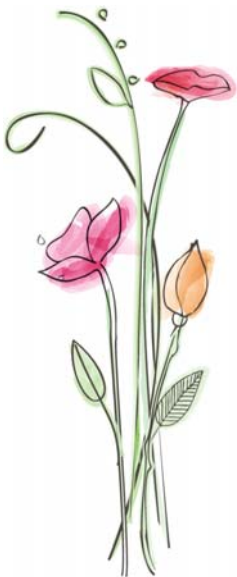


Dedicated to,



My Teachers.....

Teachers don't impact for a year or two, but for a lifetime.



My Family.....

In every conceivable manner, the family is link to our past and bridge to our future.

Acknowledgements

This thesis has been conducted in the Institute of Chemistry, Academia Sinica under the direction of Prof. Chen-Hsiung Hung. I wish to express my sincere gratitude to Prof. Hung for giving me the opportunity to get into research in his group. During the stay in this lab I enjoyed the freedom and support provided by my supervisor. Much helpful advice and the moral support from Prof. Hung has helped me to complete of the dissertation work within time.

My gratitude also goes to Prof. Jiann-T'suen Lin, Prof. Ching-Fa Yao, Prof. Way-Zen Lee and Prof. Eric Diau, who agreed to read my thesis and to participate as a referee in my final oral defense. I also wish to thank our collaborator Dr. Diau for his help for the photovoltaic measurements.

Completion of this thesis would not have been possible without the wonderful skills and valuable advices of Dr. Liyang Luo and Gao-Fong Chang. I would also like to thank my past and present colleagues, Dr. Anilkumar Pal, Dr. Amitava Dutta, Dr. Wei-min ching, Dr. Malgorzata Gajewska, Sam Chien, Chuan-Hung Chuang, Chien-Chen Yeh, Li-Ting Fong, Belete Bedemo, Shailaja Pingale, Jay-ar dela Cruz, Gong-Fong Lin, Chen-Yi Yu, Hsin-Han Tsai, Shan-Tung Liu, Yun-Ru Huang, Jia-Shan Li, Yi-Chieh Lo, Chih-Fu Cheng, Min-Hung Tsai, John, Quan-bo Chen, Amy, Denis, Luffy and Kai-tin for maintaining a congenial, fun filled atmosphere in the lab. Dr. Ram, my dear friend and colleague, indeed we had a great collaboration. I also want to express my sincere thanks to Dr. Ashutosh Singh, Dr. Pratap Patil, Surendhar Reddy and Dr. Rajeswara Rao for the untiring discussions about my work, great support in my depressed times and enduring well wishes.

My deep gratitude also goes to my teachers Dr. Sunil Joshi, Dr. R. P. Pawar, Dr. W. N. Jadhav, Dr. Ratnalikar, Mr. Santpure, Mr. Khupse, Mrs. Chavan and Mr. Selukar, without your guidance and encouragement I could never achieve what I have today.

At each step of my life, I had blessed with good friends who have healthy contribution in developing me as a better person. Life in Taiwan would never been as great without my friends here who helped me to relieve my hassles through small but merry events and concentrate back to my work. Friends from Parbhani and Pune, with whom I enjoyed some of the precious moments of my life, taught me to stay unite and focused in difficult times. I want to take this chance to be grateful to all my friends for always being there for me.

Finally, I would like to thank my parents for providing me with the unconditional love and support needed in order to continually push myself to succeed. Without you're love and

support, I wouldn't be here today! Dear bhauji, tai, pradip and sonali, your continuous encouragement and backing always kept me inspired and in the hunt for greater goals in my life. I preserve my gratitude to my late father-in-law for his blessings, mammy (mother-in-law), Suraj and Dhiraj for their emotive support and encouragement. Dear deepika, words cannot express how thankful I am for your unwavering care and love. I couldn't have made it through the past year of ups and downs without you! I love you with all my heart. Last but not the least, with a warm heart, I would like to thank my nephews and nieces Nikita, Asmita, Atharva and Rajdeep for keeping me cheerful throughout the PhD.



TABLE OF CONTENTS

<u>Content</u>	<u>Page</u>
Abbreviations	
List of publications	
Abstract	
Ch 1. Introduction	
1.1 Motivation	1
1.2 Natural photosynthesis	3
1.3 Basics of photovoltaics	5
1.4 Dye-sensitized solar cell	8
1.5 Sensitizers	13
1.5.1 Ruthenium sensitizers	13
1.5.2 Organic Dyes	15
1.5.3 Porphyrinoid sensitizers	16
1.5.3.1 Chlorins and Bacteriochlorins	17
1.5.3.2 Porphyrins	18
1.5.3.3 Corroles	33
1.5.3.4 Phthalocyanines and Subphthalocyanines	33
1.5.3.5 Core-modified Porphyrins	35
1.6 Scope of thesis	36
1.7 References	37

Section I: Core-modified porphyrins

Ch 2. Effects of core-modification on porphyrin sensitizers to the efficiency of dye-sensitized solar cells

2.1 Introduction	46
2.2 Results and Discussion	48
2.2.1 Syntheses	48
2.2.2 Optical Spectroscopy	49
2.2.3 Cyclic Voltammetry	52
2.2.4 DFT and TD-DFT calculations	53
2.2.5 Dye loading experiments	55
2.2.6 Photovoltaic measurements	56
2.2.7 TCSPC measurements	57

2.3 Conclusions	59
2.4 Experimental Section	60
2.5 References	67

Ch 3. Synthesis of carboxylate functionalized A₃B and A₂B₂ thiaporphyrins and their application in DSSCs

3.1 Introduction	69
3.2 Results and Discussion	70
3.2.1 Syntheses	70
3.2.2 Optical Spectroscopy	72
3.2.3 Electrochemical Spectroscopy	74
3.2.4 DFT and TD-DFT calculations	76
3.2.5 ATR-FTIR measurements	77
3.2.6 Dye loading experiments	79
3.2.7 Photovoltaic measurements	80
3.2.8 Electrochemical Impedance Spectroscopy	82
3.3 Conclusions	83
3.4 Experimental Section	84
3.5 References	93

Section II: Core-modified expanded porphyrins

Ch 4. Novel expanded porphyrin sensitized solar cell using boryl oxasmaragdyrins as the sensitizers

4.1 Introduction	94
4.2 Results and Discussion	96
4.2.1 Syntheses	96
4.2.2 Optical Spectroscopy	97
4.2.3 CV Studies	100
4.2.4 DFT and TD-DFT calculations	102
4.2.5 Dye loading experiments	104
4.2.6 Photovoltaic measurements	105
4.2.7 Transient photoelectric and Charge-Extraction Measurements	106
4.2.8 Femtosecond transient absorption studies	108
4.3 Conclusions	109
4.4 Experimental section	111

4.5 References	119
----------------	-----

Ch 5. Molecular engineering of boryl oxasmaragdyrin sensitizers through peripheral substituents: Effect of number and position of donor-acceptor groups

5.1 Introduction	121
5.2 Results and Discussion	122
5.2.1 Syntheses	122
5.2.2 Optical Spectroscopy	125
5.2.3 Electrochemical Spectroscopy	128
5.2.4 DFT and TD-DFT calculations	130
5.2.5 Dye loading measurements	133
5.2.6 Photovoltaic measurements	134
5.3 Conclusions	137
5.4 Experimental Section	138

Ch 6. Novel carboxylate functionalized N₂S₃ Sapphyrins: Synthesis, Photophysical and Photovoltaic properties

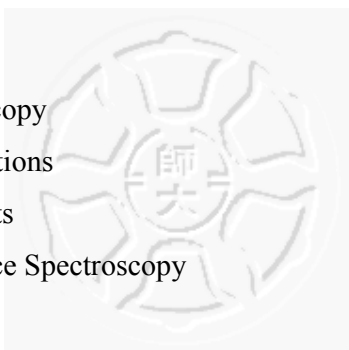
6.1 Introduction	158
6.2 Results and Discussion	160
6.2.1 Syntheses	160
6.2.2 Optical properties	162
6.2.3 Electrochemical properties	163
6.2.4 DFT calculations	164
6.2.5 Photovoltaic measurements	166
6.2.6 Electrochemical Impedance Spectroscopy	167
6.3 Conclusions	168
6.4 Experimental Section	169
6.5 References	175

Section III: Miscellaneous dyes

Ch 7. Co-sensitization of free-base and zinc porphyrins: An effective strategy to improve the photon to current conversion efficiency of DSSCs

7.1 Introduction	177
7.2 Results and Discussion	179

7.2.1 Syntheses	179
7.2.2 Optical Spectroscopy	180
7.2.3 Electrochemical Spectroscopy	182
7.2.4 DFT and TD-DFT calculations	184
7.2.5 Dye loading measurements	187
7.2.6 Photovoltaic measurements	187
7.3 Conclusions	190
7.4 Experimental Section	191
7.5 References	196
Ch 8. Novel D-π-A type organic dyes with oxadiazole ring as electron transporter for DSSC application	
8.1 Introduction	198
8.2 Results and Discussion	199
8.2.1 Syntheses	199
8.2.2 Optical Spectroscopy	200
8.2.3 Electrochemical Spectroscopy	201
8.2.4 DFT and TD-DFT calculations	202
8.2.5 Photovoltaic measurements	204
8.2.6 Electrochemical Impedance Spectroscopy	205
8.3 Conclusions	206
8.4 Experimental Section	207
8.5 References	211
Ch 9. Concluding Remarks	213
Appendix 1 Publications	216



Abbreviations

DSSCs	Dye-sensitized solar cells
DFT	Density functional theory
TD-DFT	Time-dependent density functional theory
HOMO	Highest occupied molecular orbital
LUMO	Lowest unoccupied molecular orbital
MLCT	Metal to ligand charge transfer
LHE	light harvesting efficiency
IPCE	Incident photon to current efficiency
WE	Working electrode
CE	Counter electrode
CV	Cyclic voltammetry
ATR-FTIR	Attenuated total reflectance-Fourier transform infrared
NMR	Nuclear magnetic resonance
HRMS-FAB	High resolution mass spectra-fast atom bombardment
HRMS-ESI	High resolution mass spectra-electrospray ionization
MALDI	Matrix Assisted Laser Desorption Ionization
ε	Extinction coefficient
η	Solar-to-electric power conversion efficiency
J_{sc}	Short-circuit current
V_{oc}	Open-circuit voltage
FF	Fill Factor
EIS	Electrochemical impedance spectroscopy
TCSPC	Time-correlated single photon counting
ν (C=O)	C=O stretching
$\nu_{sym}(\text{COO}^-)$	C-O symmetric stretching
$\nu_{asym}(\text{COO}^-)$	C-O asymmetric stretching
Hz	Hertz
ml	Milliliter
mg	Milligram
μm	Micrometer
μl	Microliter
ppm	Parts per million

eq.	Equivalents
mp	Melting point
bp	Boiling point
CDCA	Chenodeoxycholic acid
TBP	4- <i>tert</i> -Butyl pyridine
BMI	1-butyl-3-methylimidazolium iodide
I ₂	Diiodide
LiI	Lithium iodide
DMPII	1,2-Dimethyl-3-propylimidazolium iodide
GuSCN	Guanidinium thiocyanate
TFA	Trifluoroacetic acid
BF ₃ •OEt ₂	Boron trifluoride etherate
<i>n</i> -BuLi	<i>n</i> -Butyl lithium
TMEDA	Tetramethylethylenediamine
DDQ	2,3-Dichloro-5,6-dicyano-1,4-benzoquinone
TPA	Triphenylamine
NBS	N-Bromosuccinamide
KOH	Potassium hydroxide
THF	Tetrahydrofuran
CH ₃ CN	Acetonitrile
EtOH	Ethanol
MeOH	Methanol
CH ₂ Cl ₂	Dichloromethane
DMF	N,N-Dimethylformamide
DMSO	Dimethylsulfoxide
Pd ₂ (dba) ₃	Tris(dibenzylideneacetone)dipalladium(0)
AsPh ₃	Triphenyl Arsine
SI	Supporting information

List of publications

The work carried out during my doctoral studies has led so far to three first author and one co-author publications, whereas four manuscripts are under preparation (see Appendix 1).

First author

1. Synthesis of carboxylate functionalized A₃B and A₂B₂ thiaporphyrins and their application in dye-sensitized solar cells, **Sandeep B. Mane** and Chen-Hsiung Hung, *New Journal of Chemistry* (2014), DOI:10.1039/C4NJ00373J.
2. Effects of core-modification on porphyrin sensitizers to the efficiencies of dye-sensitized solar cells, **Sandeep B. Mane**, Liyang Luo, Gao-Fong Chang, Eric Wei-Guang Diao and Chen-Hsiung Hung, *J. Chin. Chem. Soc.* (2014), 61, 545-555.
3. Novel expanded porphyrin sensitized solar cells using boryl oxasmaragdyrin as the sensitizer, **Sandeep B. Mane**, Jyun-Yu Hu, Yu-Cheng Chang, Liyang Luo, Eric Wei-Guang Diao and Chen-Hsiung Hung, *Chem. Comm.* (2013), 49, 6882-6884.
4. Molecular engineering of boryl oxasmaragdyrins through peripheral substituents, **Sandeep B. Mane** and Chen-Hsiung Hung, *manuscript under preparation*.
5. Synthesis and photovoltaic properties of carboxylate functionalized A₃B and A₂B₂ type N₂S₃ sapphyrins, **Sandeep B. Mane** and Chen-Hsiung Hung, *manuscript under preparation*.
6. Co-sensitization of free-base and zinc porphyrins: an effective approach to improve the photon-to-current conversion efficiency in DSSCs, **Sandeep B. Mane**, Liyang Luo and Chen-Hsiung Hung, *manuscript under preparation*.

Co-author

7. Toward carboxylate group functionalized A₄, A₂B₂, A₃B oxaporphyrins and zinc complex of oxaporphyrins, Ram Ambre, Chien-Yi Yu, **Sandeep B. Mane**, Ching-Fa Yao, and Chen-Hsiung Hung, *Tetrahedron* (2011), 67; 4680-4688.
8. Anchoring Effects of Number and Position of *meta*-Carboxyphenyl and *para*-Carboxyphenyl Groups of Zinc Porphyrins in Dye-Sensitized Solar Cells: Structure-Performance Relationship, Ram Ambre, Sandeep B. Mane, Gao-Fong Chang and Chen-Hsiung Hung, *manuscript under preparation*.

Abstract in English

This thesis reported the design and synthesis of novel core-modified and expanded porphyrin sensitizers for dye-sensitized solar cells. The development of these sensitizers starts off with novel thiaporphyrin and oxaporphyrin, which consists of ethynylphenyl group as a conjugated linker and carboxylic acid as anchoring group. Comparative photovoltaic studies of these heteroporphyrins with regular N4 porphyrins show that core-modification results in decreased performance, with moderate efficiency for thiaporphyrin and minute efficiency for oxaporphyrin. Following parts of this thesis regard the development strategy through core-modification. The periphery of thiaporphyrin was modified to obtain five more derivatives with A₃B and A₂B₂ substitution pattern. The photophysical and electrochemical studies revealed that the π -extension through the ethynylphenyl group not only made the macrocycle planar but also increased their absorption bathochromically. Furthermore, substitution of the electron withdrawing cyano group produced higher polarizability required for the effective charge transfer from the porphyrin ring to the anchoring cyanoacrylic group. All these factors contributed to achieve the highest overall power conversion efficiency of 1.69% for N3S-ECN compared to other thiaporphyrin dyes.

We also devote effort to uncover the potential of applying expanded porphyrins to DSSC studies. Boron chelated oxasmaragdyrins, a class of aromatic core-modified expanded porphyrin with a 22 π -electron conjugation were synthesized. These dyes provided desired redox potentials, high absorption coefficients, high stability, and higher power conversion efficiencies. More importantly, broad absorption spreading over the entire visible region and its lower energy Q bands covering part of the NIR region. The factor above made this class of compound an optimistic candidate for being one of the future selections of porphyrin-sensitized solar cells. The molecular engineering of these oxasmaragdyrins through peripheral substitution with various donors and acceptors was also discussed. To our surprise, utilizing of triphenylamine unit as a donor and ethynylphenyl group as a linker did not improve the overall performance for these dyes. Finally, novel mono or dual carboxylate functionalized N₂S₃ sapphyrins were prepared and applied as sensitizers in DSSCs for the first time. From the electrochemical studies it was observed that, the potential difference between the LUMO level of the dyes and conduction band of TiO₂ was not sufficient for effective electron injection, which ultimately resulted in minute power conversion efficiencies for this class of dyes.

In an effort to enhance the overall performance of porphyrin dyes, we also evaluated the co-sensitization effect. We combined two discretely moderate dyes, a free-base porphyrin and its zinc derivative, with complementary absorption spectra to construct a mixed porphyrin DSSC. From photo-action spectra, it is evident that the incident photon collection for the mixed dyes is higher than both the individual dyes due to the broader absorption. For the Mix-1, consisting of N4CA (2.71%) and N4ZnCA (3.09%), we observed conversion efficiency of 3.28% which higher than both the individual dyes, while for Mix-2, comprising for N4CN (1.94%) and N4ZnCN (3.52%), overall photon-to-current conversion efficiency of 4.18% was observed. We also evaluated the effectiveness of oxadiazole group as electron transporter. We attached an electron donor, oxadiazole ring and phenyl or thiophenophenyl group as linkers and carboxylic or cyanoacrylic group as anchor in D- π -A fashion to prepare three novel OD dyes. Although, the optical and electrochemical properties and DFT calculations confirmed good absorption features and effective charge separation, only moderate efficiency of 2.72% was observed for OD3 dye.

So far, the work from this thesis has led to achieve the highest efficiency for thiaporphyrins and also unleashed a new class of porphyrinoids, the expanded porphyrins as highly efficient sensitizers for DSSCs.

Keywords: Dye-sensitized solar cells, core-modified porphyrins, expanded porphyrins, organic dyes.

Abstract in Chinese

環修飾之紫質的設計與合成以應用於太陽能光敏染

此篇論文報導了新的環修飾紫質以及大環紫質的設計與合成，以及其在太陽能光敏染料之應用。此些染料的發展由單硫取代紫質以及單氧取代紫質開始，並且其上有一ethynylphenyl基團為共振鏈以及以羧基為掛載基團。比較這些異原子取代紫質與傳統的四氮紫質，結果顯示異原子的取代降低了這些染料的光電伏打效率，其中單氧取代的紫質表現更低於單硫取代的紫質。接著我們對單硫取代紫質進行了環修飾得到了擁有A3B以及A2B2之不同取代型式的五種衍生物。經由光物理和電化學的研究顯示以ethynylphenyl基團延伸共振的鏈長不僅增加了環的平面性，同時也增加了光譜的紅位移。而在取代基上加上擁有拉電子能力的cyano基團亦可增加分子的極性而讓分子有較佳的電荷轉移效果。結合上訴修飾，單硫取代紫質的光電轉換效率可由沒有cyano基團的0.2 % 提升到有cyano基團的1.69 %。

我們亦致力於研究大環紫質於太陽能光敏染料的應用。我們合成出了有硼配位的oxasmaragdyrins，其是擁有22個 π 電子共振的芳香大環紫質。這些染料擁有合適的還原電位，高消光係數，良好的穩定性，以及高光電轉換效率。更重要的，其在可見光區段的吸光範圍廣泛，且其較低能量的Q band吸收位於在紅外光區段。基於上述條件，oxasmaragdyrins適合用來發展為太陽能光敏染料。我們亦於了oxasmaragdyrins環上掛載了不同的推拉電子基，並進行研究與討論。令人意外的，掛載上tripheylamine為推電子基以及ethynylphenyl為共振鏈的染料其光電轉換效能相較於未修飾的染料並未增加。

最後，我們合成了分別擁有一個和兩個羧基的新的二氮三硫 sapphyrins化合物並且將其應用於太陽能光敏染料。由電化學研究看來，其最低未佔軌域與二氧化鈦之傳導能帶間的差距太相近，使其不夠能讓激發的電子做有效的電子注入至二氧化鈦，故此染料的光電轉換效率不佳。

至目前為止，此論文完成了單硫取代紫質最高的光電轉換效率，並且開發出了一系列新的大環紫質為高效率的太陽能光敏染料。

關鍵字：太陽能光敏染料，環修飾紫質，大環紫質，硼配位的oxasmaragdyrins

1. Introduction

“Energy is the ‘oxygen’ of the economy and the life-blood of growth”

-Peter Voser, Energy Community Leader, 2011, World Economic Forum.

1.1 Motivation

In the old civilizations, energy was called as the source of all ‘life’, however for modern civilizations renewable energy will be the source of a better life. As of today, the world population exceeded 7 billion with a growth rate of 1.1% by 2011. With the increasing population, global energy consumption also grew by 2.5% in 2011. Fossil fuels still dominate energy consumption with 78% share of the market (Figure 1-1). Due to the tumultuous events of the ‘Arab Spring’ the balance between the oil production and sales disrupts resulting in record high oil prices of all-time.^[1] The reserves of fossil fuels are limited and one day they will be depleted. A large dependency on fossil fuels is not only causing geopolitical tensions but also damaging our environment severely (Figure 1-2). These environmental and economic concerns have encouraged researchers to find alternative renewable sources of energy that could replace fossil fuels.

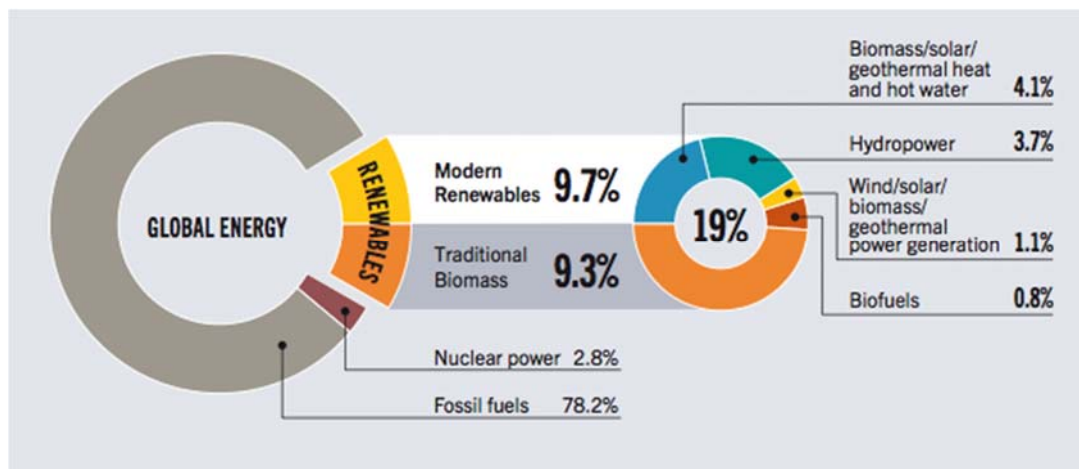


Figure 1-1. Renewable Energy Share of Global Energy Consumption, 2011.^[2]

Solar energy is the most abundant, clean and safe energy source that could also be harnessed in remote areas. Energy is consumed at a rate of about 15 Terawatts (TW) by global civilization, whereas total solar radiation on earth’s surface is around 1.22×10^5 TW_s.^[3-4] Energy from renewable sources like biomass, geothermal, hydropower, solar and wind currently accounts for about 19% of total energy. In terms of energy generation, the renewable energy comprises more than 25%. In last five years many renewable technologies

grew at rapid rates. Wind energy clearly outperforms photovoltaics (PV) in terms of installed capacity. However solar PV is the fastest growing power generation technology, with operating capacity increasing at an average of 58% annually.^[2] The PV sector shows extraordinary boom owing to a combination of growing demands, decreasing prices (\$ 1.26 per watt compared to \$ 3 per watt in 2005), huge government subsidies and the development of less expensive thin film technologies.

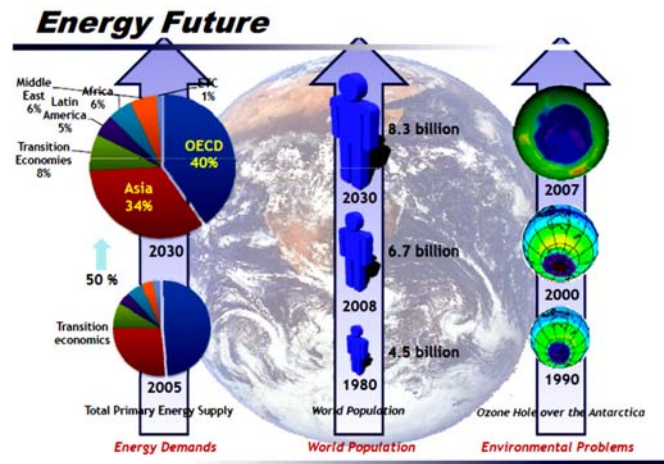


Figure 1-2. Energy future predictions. (Image courtesy: Y. S. Kang, Hanyang uni. Seoul)

Back in my country India, increasing economic development has resulted in growing electricity consumption by the commercial as well as residential sectors. The country is largely dependent on fossil fuel imports to meet its energy requirements, which is estimated to exceed 53% of its total energy consumption by 2030. Out of 100, about 70% of the country's energy generation capacity is from fossil fuels, with coal accounting for a large share (40%) of its total energy consumption. India being a tropical country receives adequate solar radiation for 300 days, amounting to 3000 hours of sunshine equivalent to over 5,000 trillion kWh. Therefore solar energy can play a pivotal role in the energy sector to fulfill our future energy demands and reduce the fossil fuel imports. Solar cell is the most suitable answer to this energy problem as the solar radiations are free and available all the year. Silicon solar cell is an outstanding performer of solar energy research with lab scale efficiency of 44% and for commercially available module efficiency of approximately 20%. Extensive research is underway all over the world to find efficient, low cost solar cells which can provide electrical energy affordable to all people. Continuous energy supply at economical price is necessary to get a better life. The dye-sensitized solar cell (DSSC), a technology invented by Ecole Polytechnique Federale de Lussane in 1991, fulfills these

requirements and most probably will be a major contributor to the future commercial photovoltaic scenario. This thesis aims to support the development of the DSSCs by synthesizing efficient, cost effective and stable core modified porphyrin sensitizers.

We are bathed in sunshine, and we can profit from it immensely. Thomas Edison told his friends Henry Ford and Harvey Firestone, back in 1931, *“I’d put my money on the sun and solar energy. What a source of power! I hope we don’t have to wait until oil and coal run out before we tackle that.”*

1.2 Natural Photosynthesis

The average rate of energy captured by photosynthesis globally is immense, approximately 130 TWs per year, which is ten times larger than the power consumption of human civilization (approximately 12 TW).^[3-4] Photosynthesis is the process in which light energy is converted in to chemical energy and stored in the form of chemical bonds of sugar. This process occurs in plants, algae and cyanobacteria. Photosynthesis uses carbon dioxide and water to produce sugars releasing oxygen as by product. Although all cells in the green parts of a plant have chloroplasts (Figure 1-3), most of the energy is captured in the leaves.

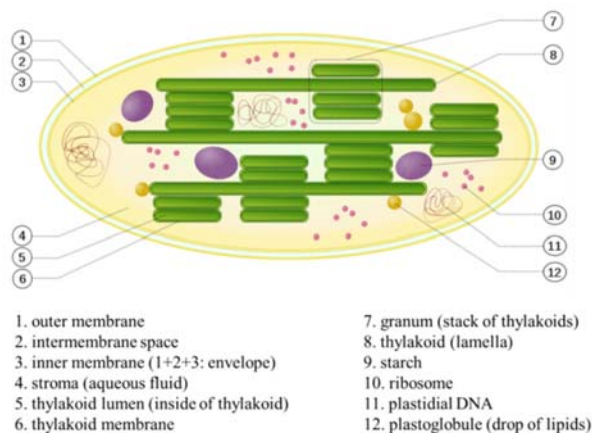


Figure 1-3. Schematic diagram of Chloroplast. (source:- <http://en.wikipedia.org>)

The cells in the interior tissues of a leaf, called the mesophyll, can contain between 450,000 and 800,000 chloroplasts per square millimeter of leaf. The surface of the leaf is uniformly coated with a water-resistant waxy cuticle that protects the leaf from excessive evaporation of water and decreases the absorption of ultraviolet or blue light to reduce heating. The transparent epidermis layer allows light to pass through to the palisade mesophyll cells where most of the photosynthesis takes place. There are two parts of photosynthesis:

The light reaction occurs in the thylakoid membrane (Figure 1-4) and converts light energy to chemical energy. One molecule of the pigment chlorophyll (PSII) absorbs one photon and loses one electron. This electron is passed to a modified form of chlorophyll called pheophytin, which passes the electron to a quinone molecule, allowing the start of a flow of electrons through an electron transport chain that leads to the ultimate reduction of NADP to NADPH. In addition, this creates a proton gradient across the chloroplast membrane; its dissipation is used by ATP synthase for the concomitant synthesis of ATP. The chlorophyll molecule regains the lost electron from a water molecule through a process called photolysis, which releases a dioxygen molecule. The overall equation for the light-dependent reactions under the conditions of non-cyclic electron flow in green plants is as given below.^[5]

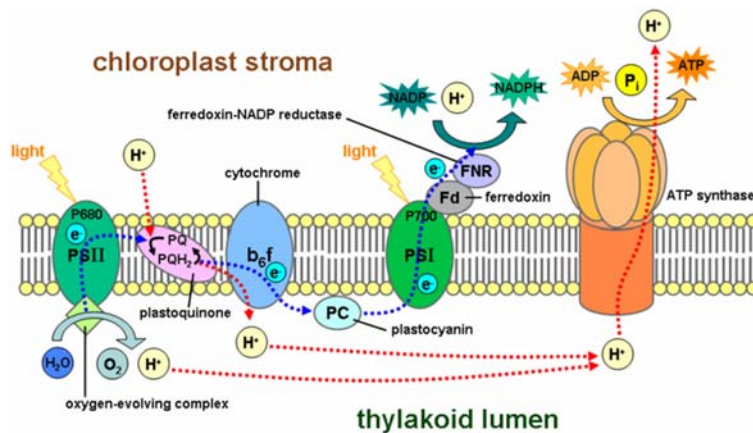


Figure 1-4. Schematic diagram of Thylakoid membrane. (source:- <http://en.wikipedia.org>)

The dark reaction takes place in the stroma within the chloroplast (Figure 1-5), and converts carbon dioxide to sugar. This reaction doesn't need light in order to occur, but it does need the products of the light reaction (ATP and NADPH). The dark reaction involves a cycle called the *Calvin cycle* in which CO_2 and energy from ATP are used to form sugar. The overall equation for the dark reaction is,



The fixation or reduction of carbon dioxide is a process in which carbon dioxide combines with a five-carbon sugar, ribulose-1,5-bisphosphate (RuBP), to yield two molecules of a three-carbon compound, glycerate-3-phosphate (GP), also known as 3-phosphoglycerate (PGA). GP, in the presence of ATP and NADPH from the light reaction, is reduced to glyceraldehyde-3-phosphate (G3P), sometimes referred to as 3-phosphoglyceraldehyde. Five out of six molecules of the G3P produced are used to regenerate RuBP so the process can continue.

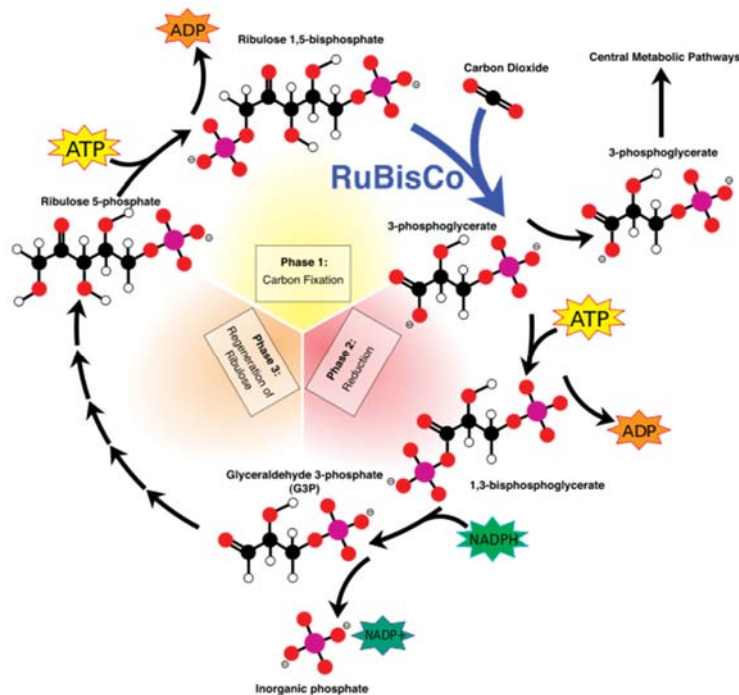


Figure 1-5. Schematic diagram of Stroma. (source:- <http://en.wikipedia.org>)

The remaining one molecule of the G3P condenses to form hexose phosphates, which ultimately yield sucrose, starch and cellulose. Plants usually convert light into chemical energy with a photosynthetic efficiency of 3–6%.^[6] Actual plant's photosynthetic efficiency varies with the frequency of light being converted, light intensity, temperature and proportion of carbon dioxide in the atmosphere, and can vary from 0.1% to 8%.^[7] Comparatively, solar panels convert light into electric energy at an efficiency of approximately 6–20% for mass-produced panels, and above 40% in laboratory devices. As seen from the above discussion, solar energy is effectively collected by chromophores based on porphyrins (chlorophylls, P680 and P700).

1.3 Basics of photovoltaic energy conversion

PV is a method of generating electrical power by converting solar radiations into current using semiconductors that exhibit the photovoltaic effect. The photovoltaic effect refers to photons of light exciting electrons into a higher state of energy acting as a charge carrier for an electric current. This effect was first observed by Edmond Becquerel in 1839, when he was experimenting with illuminated metal electrodes in an electrolyte.^[8] However, the photovoltaic effect was explained in 1905 with the pioneering theoretical work of Albert Einstein on the photoelectric effect for which he received the Noble prize.^[9]

1.3.1 The Solar Spectrum

Solar irradiation can be well estimated by a black body at a temperature of 5800 K emitting according to Plank's distribution.^[10] The solar radiation is attenuated by absorption, reflection, and scattering. Sunlight is absorbed in the visible and UV region by molecular nitrogen, oxygen, ozone, nitrous oxide, and methane in the mid-infrared region by water vapor and in the infrared region by carbon dioxide. The spectrum is strongly confined between the far infrared and near ultraviolet by the time it reaches the earth's surface. The air mass coefficient is used to characterize the solar spectrum after the solar radiation travels through the atmosphere and hence it is commonly used to characterize the performance of solar cells under standardized conditions.

The Air Mass (AM) is the ratio of the path length (y) of the sun light passing through the atmosphere when the sun is at a given angle θ to the zenith, to the path length (x) when sun is at its zenith (Figure 1-6). This relation is approximated as below,

$$AM = \frac{y}{x} \approx \frac{1}{\cos \theta} \quad (\text{eq. 3})$$

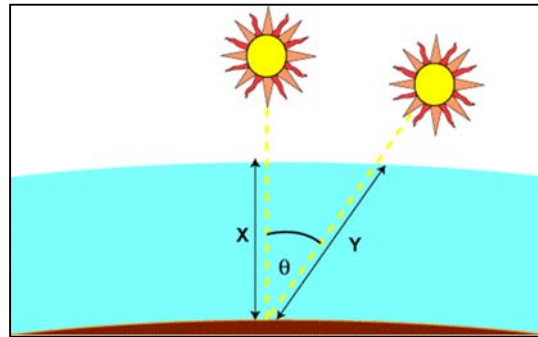


Figure 1-6. Cartoon drawing illustrating AM.

The solar irradiance outside the earth's surface (AM 0), at sea level (AM 1) and the standard reference spectrum are compared in (Figure 1-7). The spectrum outside the atmosphere, the 5,800 K black body, is denoted as AM 0, meaning 'zero atmospheres'. Solar cells for space power applications are generally characterized using AM 0. The spectrum after travelling through the atmosphere to sea level with the sun directly overhead is referred to as AM 1, meaning 'one atmosphere'. AM 1 ($\theta = 0^\circ$) to AM1.1 ($\theta = 25^\circ$) range is used to estimate performance of solar cells in equatorial and tropical regions. The standard reference spectrum in PV is denoted by AM 1.5 G, which corresponds to the total global (hemispherical) irradiance under specified atmospheric conditions at an incident angle of 48° .

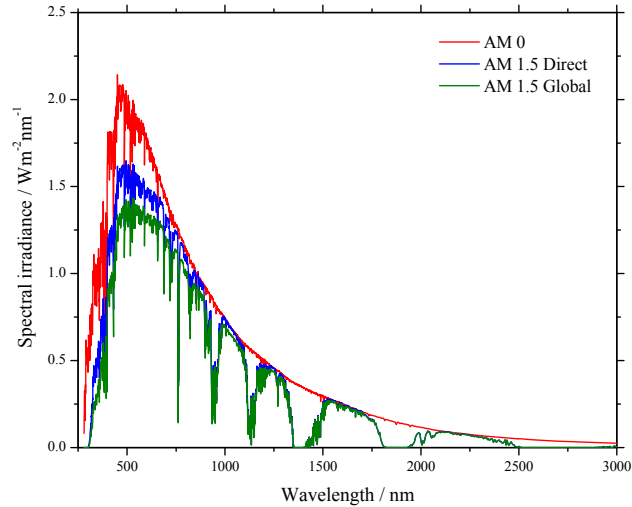


Figure 1-7. Solar irradiation spectra above atmosphere and at surface.

1.3.2 Photovoltaic Market overview

Renewable energy continued to grow strongly as investments increase, prices falls, and policies spread. In the span of last five years, total global installed capacity of many renewable energy technologies grew at very fast rates. Solar PV capacity in operation at the end of 2011 (70 GW) was about ten times the global total (7 GW) just five years earlier (Figure 1-8). It grew the fastest of all with operating capacity increasing at an average of 58% annually. It was followed by concentrating solar thermal power (CSP), which increased almost 37% and wind power increased 26%. In spite of this admirable progress, renewable energy only shares 17% shares of global energy consumption. Biomass, solar and geothermal collectively share a tiny amount of 3.3% among the all renewable resources. By the end of 2011, 30 GW of operating capacity of solar PV was added, increasing the total global capacity by 74% to almost 70 GW, sufficient to generate 85 TW/year.^[11]

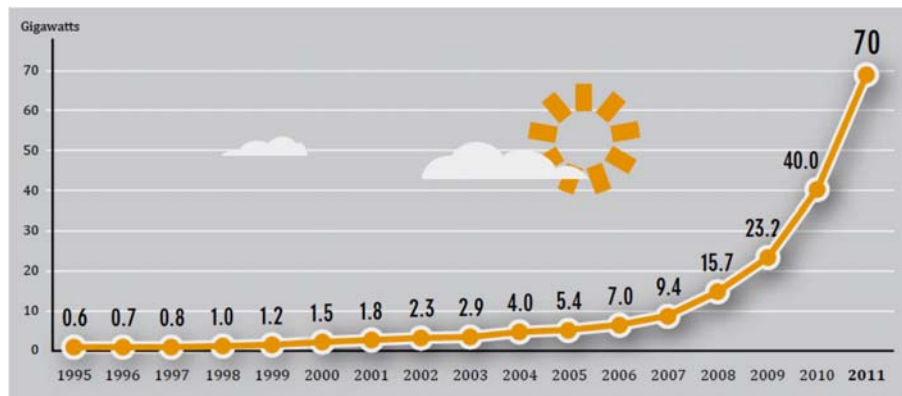


Figure 1-8. Solar PV Total World Capacity.^[2]

Solar PV is now the third most important renewable energy source following hydro and wind power, in terms of globally installed capacity. The number of countries having more than 1 GW capacity to their grids increases from three to six. So far the best efficiency solar cell is a multi-junction concentrator solar cell with the overall efficiency 44% (Figure 1-9). The highest efficiency of 35.8% was obtained by Sharp Corporation using a triple-junction technology in 2009^[12] and Boeing Spectrolab have achieved 40.7% using a triple layer design. Crystalline silicon based modules are facing great competition by thin-film solar cells, CdTe, amorphous Si, and microcrystalline Si, which are expected to account for 31% of the global installed power capacity by 2013. San Jose based company Sunpower produces cells with energy conversion ratio of 19.5%, which is well above the market average of 12-18%.^[13] Solar cell efficiency varies from 6% for amorphous silicon-based solar cells to 44% with multiple-junction concentrated photovoltaics. But for the commercially available photovoltaic modules, the efficiencies are around 14-22%. The cost of PV has already reached well below nuclear power in 2011 and is set to fall further. The average solar cell prices as monitored by Solarbuzz group fell from \$3.50/watt to \$2.43/watt over the course of 2011 and the prices below \$2.00/watt are looking inevitable. For large-scale installations, prices reached below \$1.00/watt. The declining prices of PV are directly proportional to the installation capacities.

Emerging technologies, such as DSSCs and organic solar cells are expected to grow rapidly in next few years. Although they have lower module efficiencies, their cost per watt is estimated to be three to four times lower than the conventional c-Si based systems. Currently these emerging technologies are being developed industrially in pilot plants and are very close to commercialization.

1.4 Dye-sensitized solar cell

DSSCs made from crystalline TiO₂ electrodes is one of the most promising candidates in recent quest for cheap, clean and green alternative to fossil fuels. In recent years a lot of research is focused on the development of highly efficient and stable dyes. It was revealed in the late 1960s that upon illumination, organic dyes can generate electricity at oxide electrodes in electrochemical cells.^[14] Current best PV research-cell efficiencies are displayed in Figure 1-9. To understand and simulate the primary processes in photosynthesis, the phenomenon was studied with chlorophyll extracted from spinach (bio-mimetic approach).^[15] In 1972, these experiments lead to demonstrate electric power generation from solar cell via the dye sensitization principle.^[16]

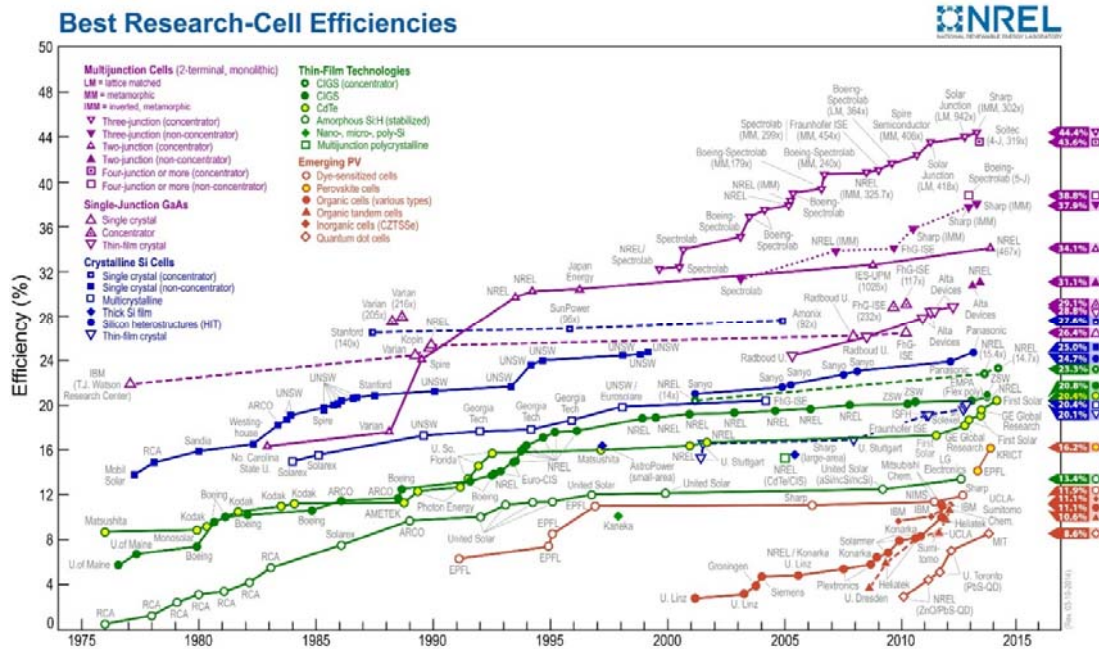


Figure 1-9. Current best photovoltaic research-cell efficiencies.^[17]

However, The instability of the DSSC was recognized as a main challenge.^[18] Nanocrystalline semiconductor films have been used in the direct conversion of solar energy into chemical or electrical energy.^[19-20] The conventional PVs having crystalline or amorphous silicon, have exceptional solar energy to electricity conversion efficiency of approximately 20%.^[21] However, the fabrication of these PVs is expensive. CuInSe and CdTe thin film PV cells reach efficiencies of around 15%.^[22] The scarcity of indium, selenium and tellurium can be a drawback for large scale production of these cells; also the high toxicity of cadmium has to be taken into account.

In 1991, Michael Grätzel and Brian O'Regan ignited the solar cell research area with a spark of 7% overall power conversion efficiency using a ruthenium sensitizer and porous TiO₂ layer as semiconducting material.^[23] Recently DSSCs achieved certified conversion efficiencies of around 11.9% for laboratory-scale devices based on ruthenium sensitizers^[24] and 12.7% for porphyrin-based devices^[25] and 8.5% with small submodules.^[26] The facile assembly, large choice of colors, transparency and mechanical flexibility are some features for extensive attraction towards the DSSCs.

1.4.1 Device structure

A schematic diagram of a typical DSSC device is shown in Figure 1-10. Dye-sensitized solar cells separate the two functions provided by silicon in a traditional cell design. Silicon not

only acts as the source of photoelectrons, but also it provides the electric field to separate the charges and create a current. In DSSCs, the semiconductor is used solely for charge transport, the photoelectrons are provided from a separate photosensitive dye. Charge separation occurs at the surfaces between the dye, semiconductor and electrolyte.

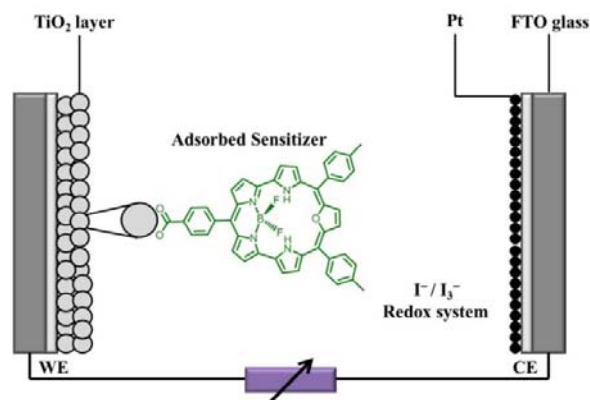


Figure 1-10. Schematic representation of Dye-Sensitized Solar Cell.

The nanocrystalline semiconductor is normally TiO₂ with typical sizes of 20-30 nm, film thickness of ~10 μm with a porosity of ~60%, although other wide band gap oxides like ZnO and SnO can be used.^[27] A monolayer of the sensitizer is attached to the surface of the semiconductor. A redox mediator, commonly iodide/tri-iodide redox couple in organic solvent is used as electrolyte. The electrode with the mesoporous film (the photoanode) is sandwiched together with a second conducting glass substrate. The second electrode is coated with catalytically active platinum for efficient reduction of oxidized redox species.

1.4.2 Electron Injection, Transport and Recombination

Efficient photon to current conversion occurs in DSSCs because of a judiciously well-adjusted interplay of different kinetic processes as illustrated in Figure 1-11. In the dark, the fermi level of electrons in the TiO₂ semiconductor is in equilibrium with the redox energy level of the electrolyte. When a photon is absorbed by the sensitizer (*S*), it is excited to the higher energy level (eq. 4). The excited state molecule (*S*^{*}) injects an electron into the conduction band (*E_c*) of the semiconductor in a femto to picosecond timescale (eq. 5) before the dye can relax back to its ground state (eq. 8). The oxidized sensitizer (*S*⁺) is regenerated by iodide in the electrolyte within a few microseconds (eq. 6), which generally occurs more rapidly than reduction by photoinjected electrons in the TiO₂ (eq. 9). The tri-iodide formed upon the dye regeneration is reduced at the platinized counter electrode (eq. 7). The additional charge in the TiO₂ under illumination defines a quasi-Fermi level *E_{Fn}*. Electrons in

the TiO_2 are affected by two competing processes: Recombination with tri-iodide in the electrolyte (eq. 10) and diffusion through the mesoporous TiO_2 to the front electrode. The effective time constants for these processes strongly depend on the trapping and detrapping events.

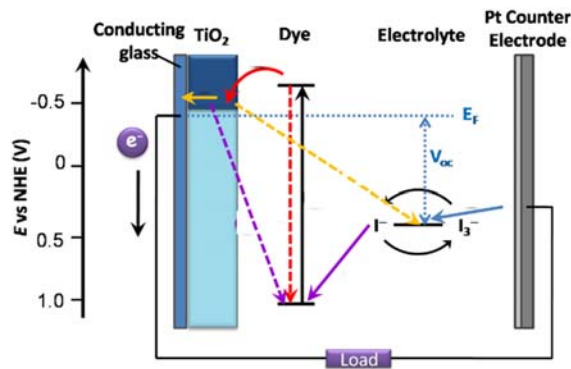


Figure 1-11. Schematic representation of the electron flow in DSSC.

Recombination occurs in the millisecond to second range, and diffusion ideally occurs on a timescale one to two orders of magnitude smaller such that a large fraction of electrons is extracted at the front electrode. The differences in the electrochemical potentials (or Fermi energies) of the electrons at the opposite electrodes, *i.e.* E_{Fn} and E_{redox} , defines the photovoltage generated by the cell. The quasi-fermi level E_{Fn} of electrons in the TiO_2 depends on the charge generation rate in the TiO_2 , the transport rate, and the recombination rate.

1.4.3 Incident Photon to Current Efficiency (IPCE)

The solar cell performance is measured with several parameters like incident photon to current efficiency (IPCE), short circuit current (J_{sc}), open circuit voltage (V_{oc}), fill factor (FF) and the overall efficiency of the photovoltaic cell (η). IPCE measures how efficiently

the incident photons are converted to electrons. The wavelength dependent IPCE can be expressed as the product of the light harvesting efficiency (LHE), quantum yield of charge injection (Φ_{inj}), charge collection efficiency (η_{coll}) at the back contact and quantum yield of regeneration (Φ_{reg}) (eq. 11).

$$\text{IPCE} = \text{LHE} \cdot \Phi_{inj} \cdot \eta_{coll} \cdot \Phi_{reg} \quad (\text{eq. 11})$$

Where, Φ and η are dependent on kinetic parameter, LHE depends on the active surface area of the semiconductor and on the light absorption of the sensitizers.^[28] In practice the IPCE measurements are carried out with monochromatic light and calculated according to eq. 12,

$$\text{IPCE (\%)} = \frac{1240 \cdot J_{ph}}{\lambda \cdot \Phi} \cdot 100 \quad (\text{eq. 12})$$

Where J_{ph} is the short-circuit photocurrent density for monochromatic irradiation and λ and Φ are the wavelength and the intensity, respectively.

1.4.4 Overall Efficiency of the Photovoltaic Cell (η)

The solar energy to electricity conversion efficiency is given by eq. 13,

$$\eta = \frac{J_{sc} \cdot V_{oc} \cdot FF}{\Phi} \quad (\text{eq. 13})$$

Where J_{sc} is the short circuit current, V_{oc} the open circuit voltage, FF the cell fill factor, and Φ the intensity of the incident light. The fill factor is defined by the ratio of the current and the voltage at the maximum power point to the short circuit current and the open circuit voltage. The fill factor measures the squareness of the I-V curve (Figure 1-12). DSSCs are advantageous over conventional $p-n$ junction solar cells by features like, less sensitivity to impurities, easy fabrication, operation over a wide range of temperatures, different angles of the incident light, and lower production costs. The applications of these cells are more flexible since they can be made of different substrates such as glass, plastics, ceramics, fabric and metal.^[27]

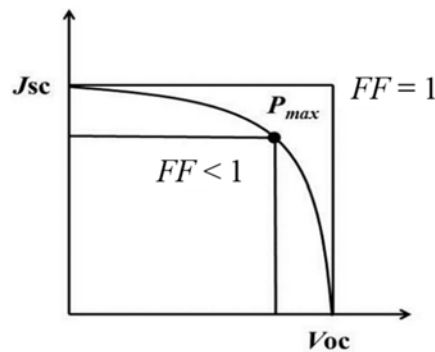


Figure 1-12. I-V curve.

1.5 Sensitizers

Design and synthesis of highly efficient sensitizers for DSSC is the most attractive and challenging field. Thousands of ruthenium,^[29] porphyrinoids,^[30-31] and organic dyes^[32-33] have been synthesized and utilized in DSSCs. To be a best candidate, the photosensitizer should fulfill some important characteristics:

1. The absorption spectrum of the sensitizer should cover the whole UV-visible region and even the part of the near-infrared (NIR) region in order to absorb as many photons as possible.
2. Lowest unoccupied molecular orbital (LUMO) of the sensitizer should be more negative than the conduction band (CB) of the semiconductor and highest occupied molecular orbital (HOMO) should be more positive than the redox potential of the electrolyte so as to trigger the efficient electron transfer.
3. The molar extinction coefficient (ϵ) of the dye must be as high as possible to enable efficient light harvesting with thinner TiO₂ film.
4. In order to minimize charge recombination between the injected electrons and the resulting oxidized dye, the positive charge resulting after electron injection should be localized at the donor part, so that it will be away from the TiO₂ surface.
5. The dye should not aggregate on TiO₂ film.
6. The synthesis should be easy and straightforward with minimum steps so that bulk production will be easy in future.
7. The dye should be enough stable and bind strongly on TiO₂.

Based on above requirements many sensitizers of ruthenium complexes, porphyrinoids and organic dyes have been designed, synthesized, and applied successfully in DSSC. Some of the best performers from ruthenium and organic sensitizers are discussed below. As this thesis deals with the synthesis of core-modified porphyrin dyes, porphyrinoids are discussed comprehensively.

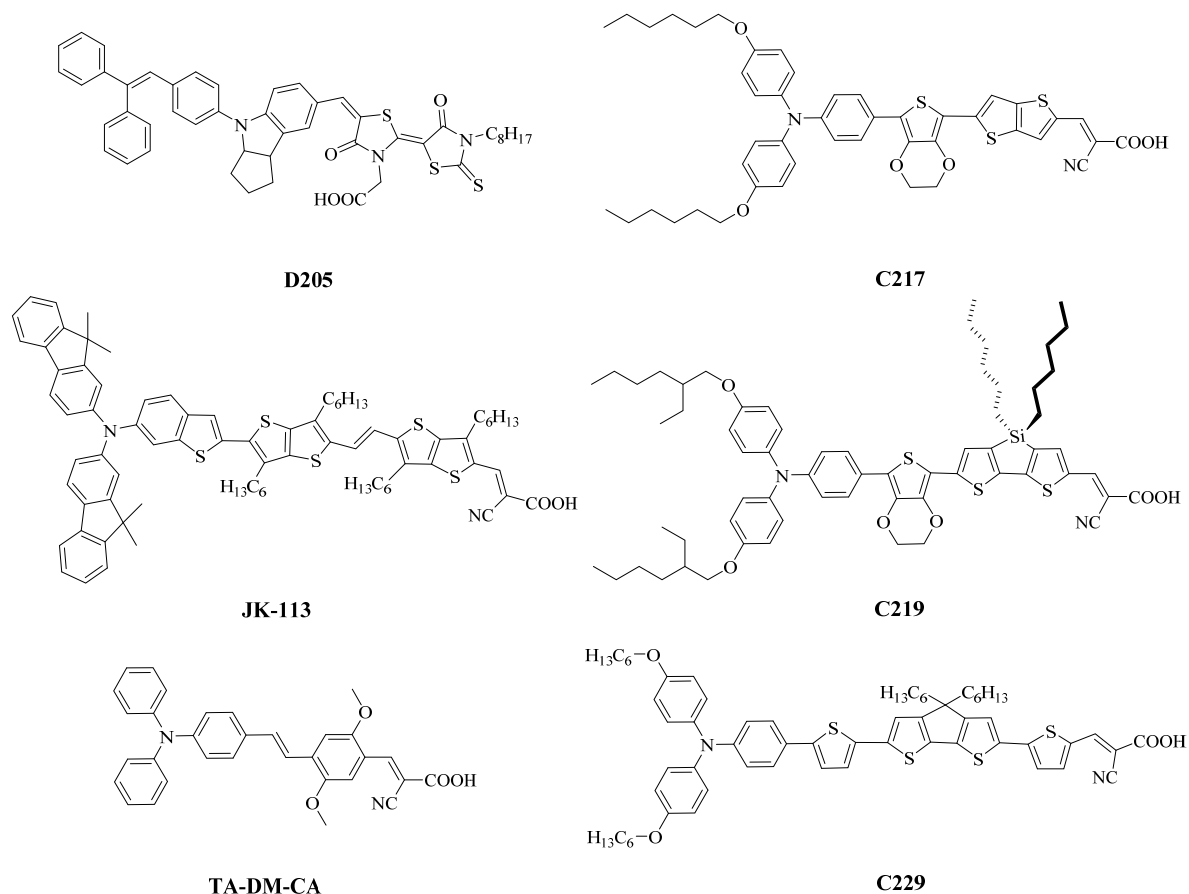
1.5.1 Ruthenium Sensitizers

The Ru complexes have shown the best photovoltaic properties due to their broad absorption spectrum, suitable excited and ground state energy levels, relatively long excited state life time and good electrochemical stability. Many Ru complexes used in DSSCs have achieved solar cell efficiency about 11%. The use of the Ru complexes with carboxylated bipyridine ligands for the TiO₂ sensitization was first reported long back in 1979.^[34] In 1985, a tris(2,2'-

Because of its high extinction coefficients, the TiO₂ film thickness can be reduced, which favors the charge collection efficiency.^[43-44] Recently, a new record efficiency of 11.4% is achieved by black dye using novel co-adsorbent **Y1** (Scheme 1-1). This co-adsorbent effectively reduces the competitive light absorption by I⁻/I₃⁻, avoids dye aggregation and decreases the charge recombination. This result is certified by AIST, Japan. Though these are the best performers in the DSSCs, their progress would be hindered due to the limited resources, sensitivity towards purity and high cost of ruthenium metal purification, demanding further search for new sensitizers.

1.5.2 Organic Sensitizers

Organic dyes are considered as dark horse in the solar cell field due to their easy synthesis, very high molar extinction coefficients compared to the Ru dyes, and lower cost of preparation.^[32-33] Their facile optimization can allow extension of the absorption wavelengths and tuning the HOMO-LUMO energy levels. Even though hundreds of organic dyes have been synthesized and applied in the DSSCs till date, only few of them gave efficiencies comparable to Ru dyes (Scheme 1-2).



Scheme 1-2. Organic Sensitizers.

Some important classes of the organic dye family are carbazoles,^[45-47] coumarins,^[48-51] fluorines,^[52-55] hemicyanines,^[56-58] heteroanthracenes,^[59-63] indolines,^[64-66] merocyanine,^[67] perylenes,^[68-69] quinaxolines,^[70-71] squarines^[72-77] and triphenylamines.^[78-81] Some of the best solar cell performers having photon to current conversion efficiencies more than 9% are depicted in Scheme 1-2.^[82-84] Dye **C219** (Scheme 1-2) is the first and only organic sensitizer to achieve 10% PCE. The performance of organic dyes remain subordinate compared to Ru complexes and porphyrinoid sensitizers due to their low light harvesting capacity, as the absorption spectra is limited up to 600 nm only and lower stability. Owing to the recent higher efficiency, easy structural modification and high molar extinction coefficients organic dyes can still be a popular candidate for commercial solar cell modules.

1.5.3 Porphyrinoid Sensitizers

Nature has utilized chlorophylls in plants as antennae to harvest light for the conversion of solar energy in the photosynthetic processes. In the photosynthetic cores of bacteria and plants, solar energy is collected at chromophores based on porphyrin,^[85] the captured radiant energy is converted efficiently to chemical energy. Inspired by the natural photosynthesis, scientists utilized artificial chlorophylls, “the porphyrins” as efficient centers to harvest light for solar cells sensitized with a porphyrin. This efficient energy transfer in naturally occurring photosynthetic reaction centers motivated a lot of researchers to design and synthesize numerous porphyrins for DSSC applications.^[30-31, 86-90] Porphyrins are heterocyclic macrocycles composed of four modified pyrrole subunits inter connected at their α -carbon atoms via methane bridges as shown in Figure 1-13. Porphyrin macrocycles are highly conjugated systems and as a consequence, they typically have very intense absorption bands in the visible region; the name "porphyrin" comes from a Greek word for *purple*.

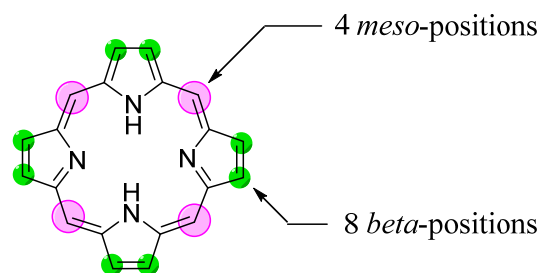


Figure 1-13. General structure of porphyrin.

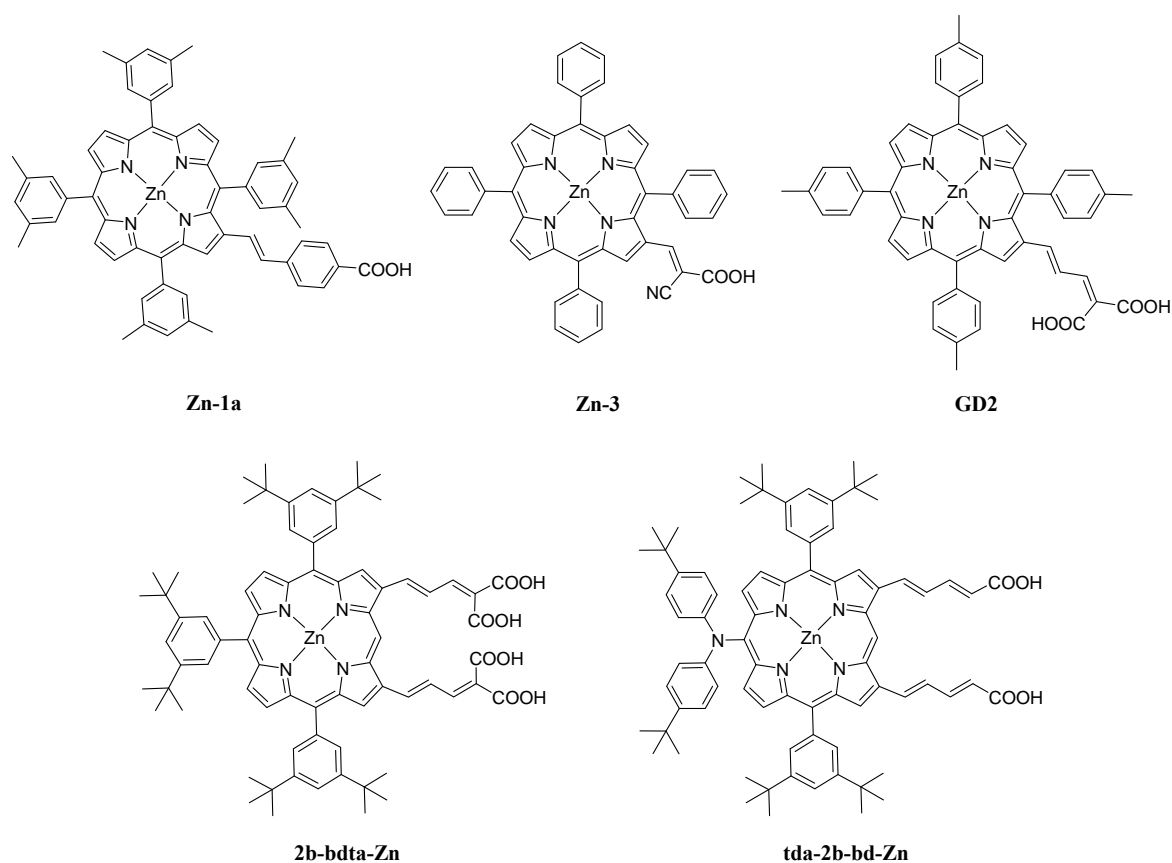
Due to their aromatic structure porphyrins have a similar chemical behavior as simple aromatics. The inherent advantages of porphyrin-based dyes are their rigid molecular

structures with large absorption coefficients in the visible region. Also, their various reaction sites, i.e., four *meso* and eight β -positions, are available for functionalization through which fine tuning of the optical, physical, electrochemical and photovoltaic properties of porphyrins thus becomes feasible. In principle, the free *meso*-carbon atoms are more reactive than the β -carbon atoms. Though regular N4 porphyrins are the most efficient and massively studied porphyrin analog, other porphyrinoids such as chlorins, bacteriochlorins, phthalocyanines and subphthalocyanines, corroles and thiaporphyrins have been efficiently used as sensitizers for DSSCs. In this section we reviewed various porphyrinoid sensitizers for DSSCs.

1.5.3.1 Chlorins and Bacteriochlorins

The use of chlorins in a DSSC was first reported in 1993 by Kay and Grätzel.^[91] In that report a variety of metallo and free-base carboxychlorins were prepared from natural chlorophylls via metallation and/or saponification. The best DSSC reported was with a copper chlorophyll derivative, **Cu-2- α -Oxymesoisochlorin *e*** as sensitizer (Scheme 1-3), which gave an efficiency value of 2.6%.^[91-92] Since this first report, chlorins have been studied in DSSCs using both free-base^[93] and zinc metalated^[94] forms. Ikegami *et al.* reported in 2008, the best performance of a DSSC using **Chlorin-e6** (Scheme 1-3), $\eta = 4.35\%$ was observed after optimizing the co-adsorbent to avoid molecular aggregate formation between dye molecules.^[95] The research by Wang *et al.* has had a profound impact on advances in chlorin and bacteriochlorin DSSCs,^[96-104] starting in 2006 with work on chlorin **PPB a** in which an $\eta = 4.2\%$ was achieved using β -carotene as a co-adsorbent (Scheme 1-3).^[97] Later **PPB a** was tested without the presence of the co-adsorbent and compared to other chlorins, bacteriochlorins, and porphyrins; in these tests an η of 3.8% was achieved and **PPB a** was the best sensitizer tested.^[100] Dyes **Chlorin 1-4** (Scheme 1-3) have carboxylic acid groups linked to the chlorin macrocycle *via* an ethylene moiety and gave η values in the range of 6.5%-8.0% in DSSC tests, comparable to **N719** which gave $\eta = 9.3\%$ under the same experimental conditions.^[104] An improved η value of 7% has been reported for **Chlorin 2** compared to **Chlorin 1** ($\eta = 6.5\%$).^[102, 104] **Chlorin 3** gave an $\eta = 8.0\%$ which is the best η value to date for a chlorin sensitizer.^[104] Work on bacteriochlorin sensitizers by Wang *et al.* has yielded the most efficient bacteriochlorin DSSC to date. The dye **BChlorin-1** (Scheme 1-3) uses dialkyl substitution at its second reduced pyrrole ring to increase the stability of the bacteriochlorin skeleton and avoid oxidation to the corresponding chlorin (a general problem with bacteriochlorins). The η value of **BChlorin-1** sensitized DSSC was found to be 6.2% and was improved to 6.6% when chenodeoxycholic acid was used as a coadsorbent.^[101]

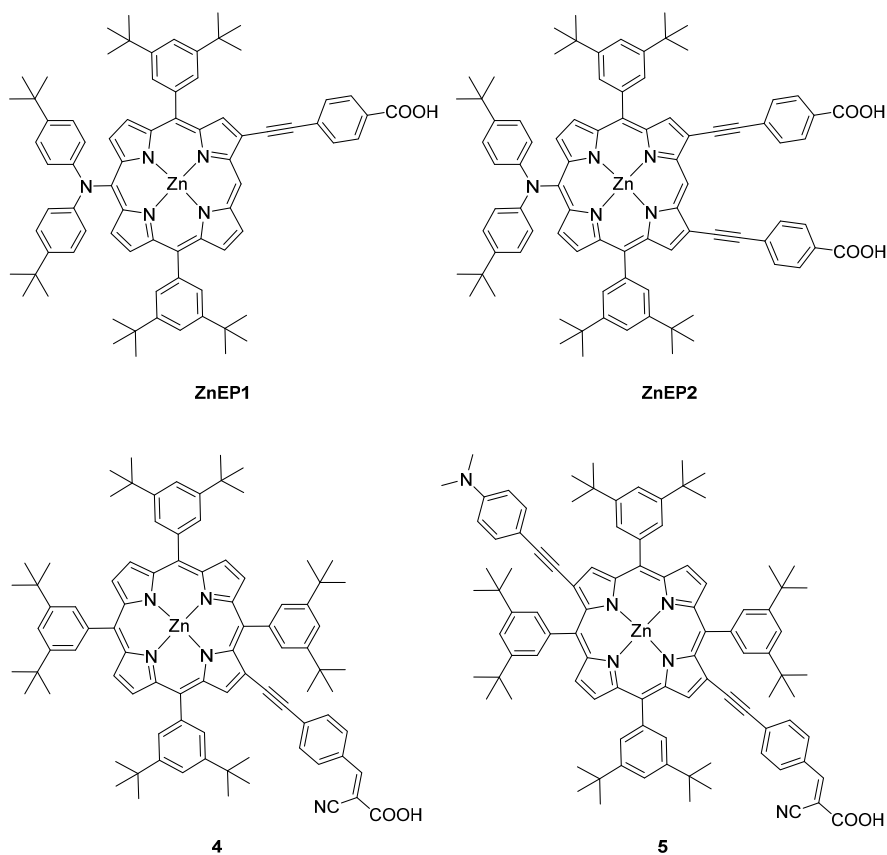
due to the splitting of the four frontier molecular orbitals. The first example of β -substituted porphyrins was reported by Officer, Grätzel and co-workers in 2004. They reported a series of β -substituted zinc porphyrins, among them **Zn-1a** (Scheme 1-4) attained promising efficiency of 4.8%.^[105] Further they investigated different derivatives, out of which **Zn-3** (Scheme 1-4) achieved $\eta = 5.6\%$ in the presence of co-adsorbent chenodeoxycholic acid (CDCA).^[110]



Scheme 1-4. Molecular structures of β -substituted porphyrins.

Later in 2007, the same group reported another series of porphyrin sensitizers with the best performer **GD2** (Scheme 1-4) obtaining impressive efficiency of $\eta = 7.1\%$ with liquid electrolytes.^[111] Kim and co-workers applied this strategy of attaching the π -conjugated linker at β -position of the porphyrin ring to design doubly anchored porphyrin sensitizers. They revealed that zinc porphyrin **2b-bdta-Zn** (Scheme 1-4) with double malonic acid linkers effectively enhance the electron injection and retarded charge recombination.^[112] The similar group in 2011, reported β -functionalized push-pull zinc porphyrins with diarylamino donor, **tda-2b-bd-Zn** (Scheme 1-4) presenting the best performance of $\eta = 7.5\%$ which is comparable with **N3** dye ($\eta = 7.7\%$) under the similar conditions.^[113] In 2013, the same group

also reported β -Ethynylbenzoic acid substituted push-pull porphyrins, **ZnEP1** and **ZnEP2** (Scheme 1-5). Surprisingly **ZnEP1** with single anchoring arm ($\eta = 5.9\%$) performed better than **ZnEP2** with $\eta = 4.0\%$. The overall conversion efficiency of **ZnEP1** was comparable with **YD1** ($\eta = 6.2\%$).^[114]

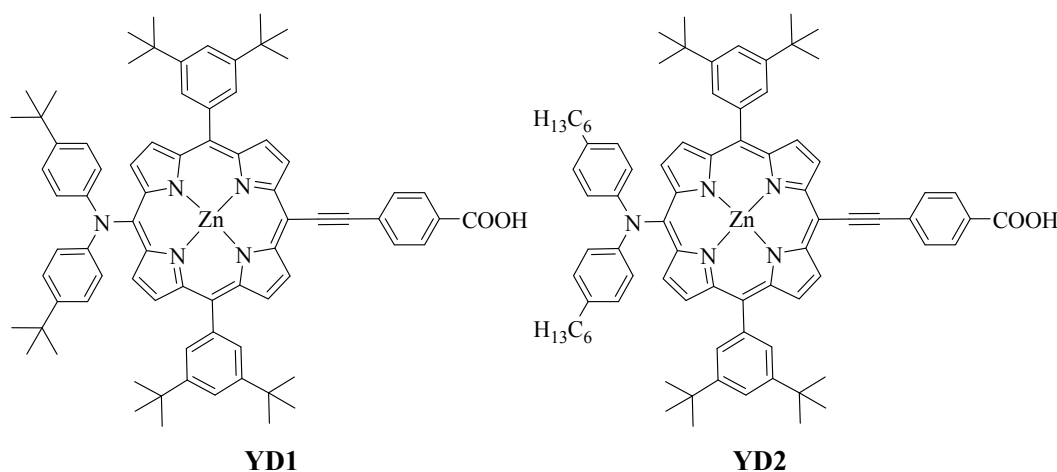


Scheme 1-5. Molecular structures of β -substituted porphyrins.

In a report, Pizzotti and co-workers synthesized five β -substituted porphyrins with ethynylphenyl linker and different anchoring acid groups and compared their DSSC performance with *meso*-substituted porphyrin derivatives.^[115] They have shown that, zinc porphyrin **4** (Scheme 1-5) attained $\eta = 4.6\%$, while the push-pull zinc porphyrin **5** (Scheme 1-5), achieved overall conversion efficiency of 4.7%. They also stated that the efficiency of **5** is better than the *meso* derivative ($\eta = 4.2\%$). Although some of the above mentioned dyes show that β -substituted porphyrins performed better than *meso*-substituted porphyrins, their progress is limited to the overall conversion efficiency of 7.5%. Also it is noteworthy that the π -conjugation at the β -substituted porphyrins has a narrow effect to extend the absorption spectra to greater wavelengths. These results encourage researchers to change the design of extending the π -conjugation through functionalization the porphyrins at *meso*-position.

b) Attachment through *meso*-position

The concept of the *meso* ethynyl substituted porphyrins was first reported by Anderson^[116] and Therian.^[117] The first *meso*-substituted free base porphyrin for DSSC application was reported in 2000 by Cherain and Wasmer^[118] with $\eta = 3.5\%$. After a long gap, in 2007 Galoppini *et al.* reported tetrachelated zinc porphyrins with *meta*-substituted linker on four *meso* positions to suppress dye aggregation. To solve the porphyrin aggregation, 3,5-di-*tert*-butylphenyl group were introduced at the *meso*-positions of the porphyrin ring. Following this concept, Yeh and co-workers designed and synthesized a library of *meso*- and β -substituted porphyrins with carboxyl anchoring group. Their study revealed that dyes with *meso*-substituents are better in terms of efficiency than their β -substituent counterparts. They designed dye **YD1** (Scheme 1-6), a push-pull porphyrin with a D- π -A skeleton, having diphenylamine as donor group, porphyrin chromophore as a π spacer and 4-ethynylbenzoic acid as acceptor group, to achieve 6.0% efficiency under AM 1.5 G illumination.^[119] It is noteworthy that it is comparable with **N3** dye ($\eta = 6.1\%$) under the similar conditions. The superlative performance of **YD1** reflects its remarkable short-circuit photocurrent density (J_{sc}) which arises from the large IPCEs broadly extending beyond 700 nm. The electron donor in **YD1** plays a role not only spectrally to extend the absorption to a greater wavelength but also spatially pushing the excited electrons towards TiO₂ for an improved separation of charge. Another promising porphyrin **YD2** (Scheme 1-6) based on design of **YD1** is reported by the same group with the *tert*-butyl groups were replaced by hexyl chains in the diphenylamine donor. The device performance of **YD2** was improved to $\eta = 6.8\%$. The electron donating nature of the amino substituents in **YD1** and **YD2** appears to be accountable for their higher open-circuit voltage (V_{oc}).



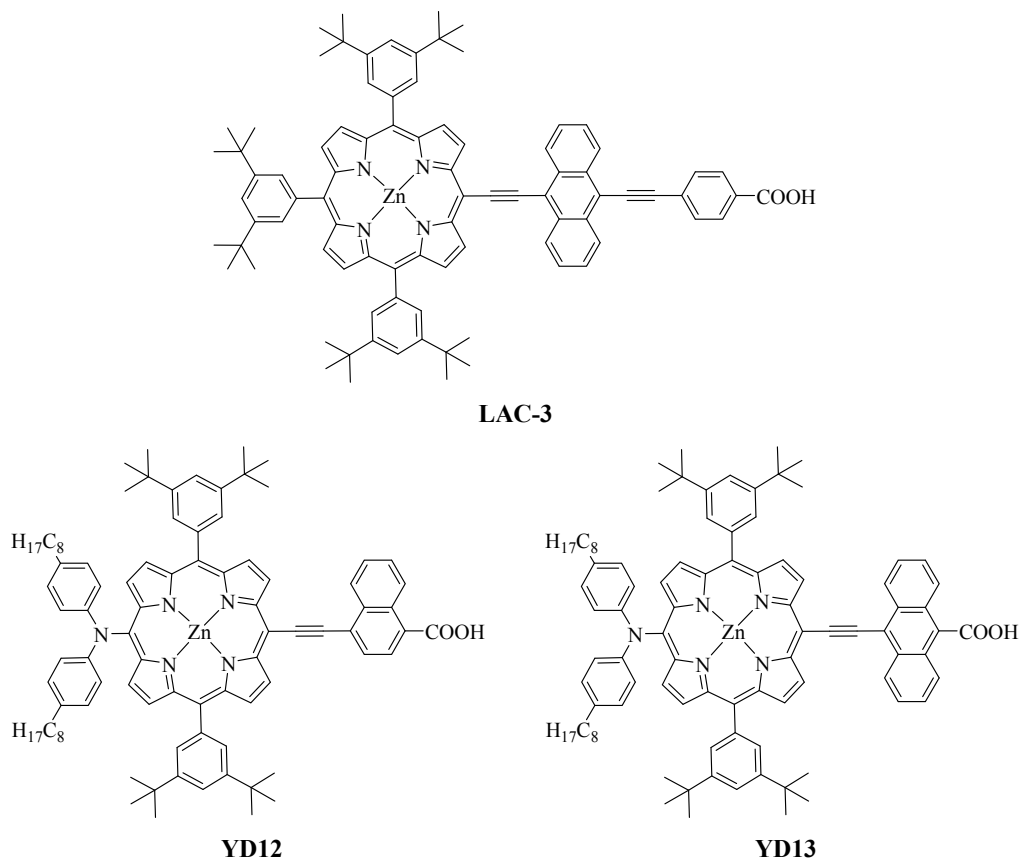
Scheme 1-6. Molecular structures of *meso*-substituted porphyrins YD1 and YD2.

Mozer and co-workers, using **GD2** as an example noted that the lower V_{oc} of porphyrins compared with the Ru sensitizers is due to the significantly decreased electron lifetime related to the rapid recombination of electrons with electrolyte.^[120] In 2010, performance of the device based on **YD2** was further improved by Grätzel and coworkers,^[121] giving $\eta = 10.9\%$ supported by $J_{sc}/\text{mA cm}^{-2} = 18.6$, $V_{oc}/V = 0.77$, $FF = 0.764$.

c) Porphyrins coupled with π -extended chromophores

The best practical way to enhance J_{sc} is to harvest a broader region of the solar spectrum. In general, porphyrins show a *Soret* band at 400–450 nm and Q bands at 500–650 nm. To extend the absorption of porphyrin dyes to the NIR region, the energy gap between the HOMO and the LUMO levels must be reduced. There are two approaches to achieve this: first is to couple a highly conjugated π -extended chromophore with the porphyrin ring, and second is to synthesize fused or dimeric porphyrins. As seen from the previous section the best strategy to extend the π -conjugation is through functionalize the porphyrin at *meso*-positions. The acene family is most suitable for these purpose, in which the π -conjugation can be effectively increased with increasing number of aromatic rings. Lin and co-workers^[122] prepared porphyrins coupled with acenes, from benzene to pentacene as π -extended chromophores, through ethynyl bond. Among these porphyrins, the anthracene substituted porphyrin **LAC-3** (Scheme 1-7) displayed the best performance reaching 80% of the **N3** dye under the similar conditions. Based on the backbone structure of **YD2**, Yeh and co-workers^[123] designed three acenyl-ethynyl substituted porphyrins **YD11-YD13**. The bridge between ethyne and carboxyl group is varied from phenylene for **YD11** (Scheme 1-7), naphthylene for **YD12** (Scheme 1-7) and to anthracenylene for **YD13**. Among these dyes, **YD11** and **YD12** both exhibited superior performance relative to **N719** dye with J_{sc} of these two porphyrin-based devices being significantly greater than that of **N719** device. Without an added scattering layer the overall power conversion efficiencies of **YD11** ($\eta = 6.7\%$) and **YD12** ($\eta = 6.8\%$) outperforms that of **N719** device ($\eta = 6.1\%$). When the TiO_2 films were covered with an additional scattering layer for light penetration, the cell performance of **N719** pointedly improved to $\eta = 7.3\%$, whereas the performances of the porphyrin dyes increased only slightly ($\eta = 6.8\%$ and 7.0% for **YD11** and **YD12**, respectively).^[123] These results indicate that a substantial increase in J_{sc} for the **N719** device is a crucial factor for the enhancement of the cell performance with the addition of a scattering layer.^[124] Based on those observations, the participation of the partially allowed triplet metal-to-ligand charge transfer (MLCT) states of ruthenium complexes was found to be responsible for the enhanced

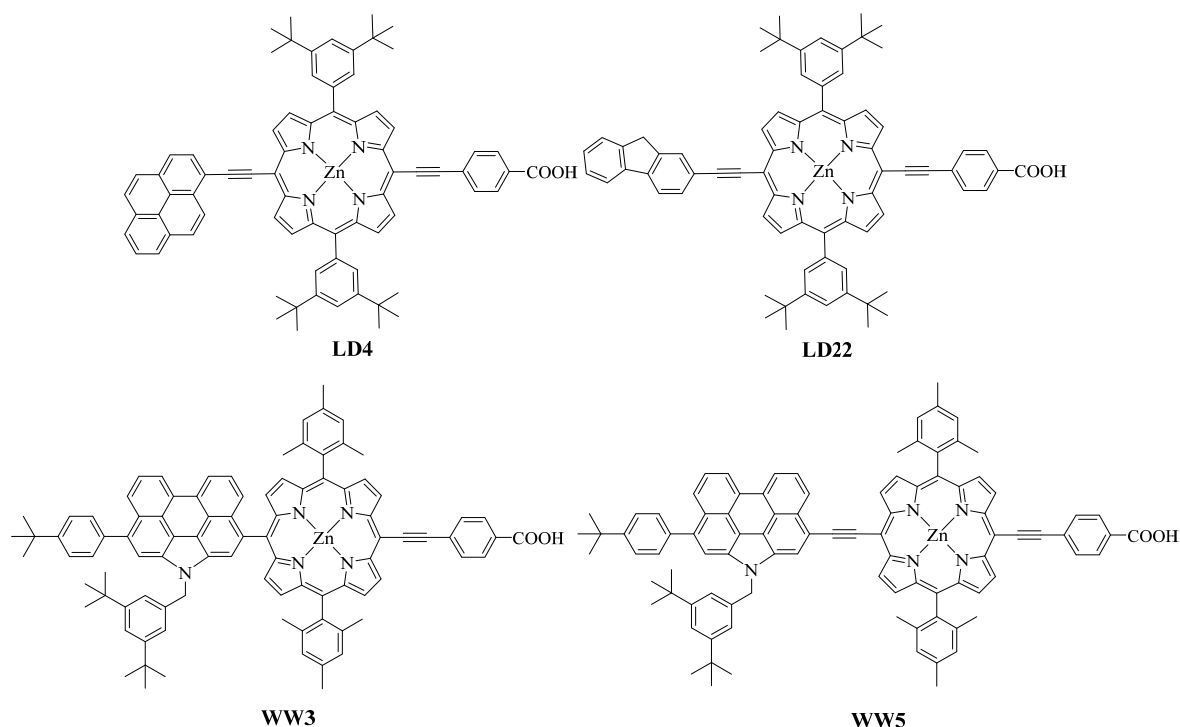
efficiency in the red shoulder of the IPCE spectrum of **N719**, whereas the spin-orbit coupling in zinc porphyrins has insufficient effect for the S_0 - T_1 transitions to occur; the additional scattering layer provided no improvement in the IPCE spectra of **YD11**–**YD13** beyond the Q band absorptions.^[123]



Scheme 1-7. Molecular structures of *meso*-substituted porphyrins.

Functionalized chromophore anthracene plays an important role to extend the π -conjugation in **LAC-3** for an improved overall device performance,^[122] but the same anthracene group in **YD13** with a link shorter than that in **LAC-3** exhibited a notable effect to deteriorate significantly the device performance of **YD13**.^[123] Results obtained from femtosecond measurements of fluorescence decay indicate that the presence of the anthracene group in the bridge from **YD13** to TiO_2 did not hamper the rate of interfacial electron transfer for the observed small injection yield of **YD13**; rather, it was the anthracene-induced rapid relaxation of intermolecular energy due to dye aggregation that gave the poor device performance of **YD13**, which was also evident in experiments in the absence and presence of co-adsorbent CDCA.^[123] Lin and co-workers further designed cyclic aromatic substituents attached at the porphyrinic *meso*-position opposite to the anchoring group.^[125-126] Among

these dyes the fluorene-modified porphyrin **LD22** (Scheme 1-8) displayed the device performance $\eta = 8.1\%$,^[125] and the pyrene-substituted porphyrin **LD4** (Scheme 1-8) attained an impressive efficiency of $\eta = 10.1\%$,^[126] and was superior to that of a **N719** dye ($\eta = 9.3\%$) under the same conditions. The superior photovoltaic performance of the **LD4**-based porphyrin-sensitized solar cell (PSSC) was attributed to its enhanced ability to harvest light with the IPCE action spectrum covering the entire visible spectral region and extending beyond 800 nm. Also V_{oc} of **LD4** device was much smaller than that of the **N719** device, which might be because of a much smaller electron lifetime of porphyrin-based solar cells than that of **N719** cells.^[120]



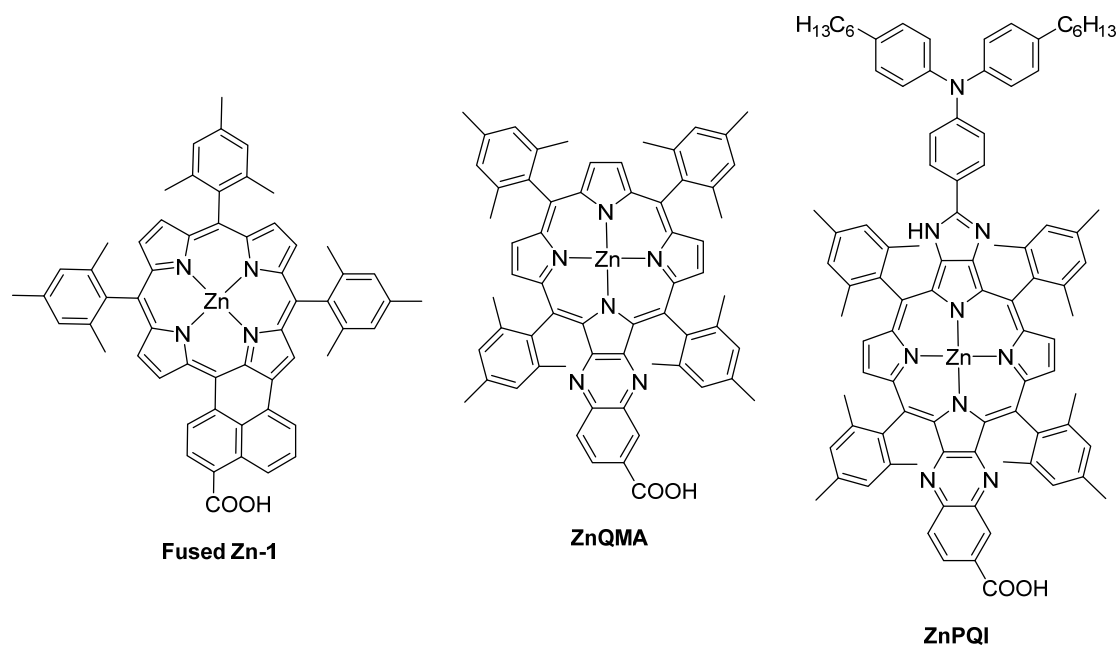
Scheme 1-8. Molecular structures of *meso*-substituted porphyrins.

V_{oc} of **LD4** was even smaller than that of **LD22**, which might be rationalized due to efficient electron interception for **LD4** than for **LD22** because of improved charge separation for the latter.^[127] Wang and Wu,^[128] reported another porphyrin dyes **WW3** and **WW5** (Scheme 1-8) coupled with *N*-annulated perylene (NP) which works as an efficient electron donor and also helps to push the absorption to higher wavelengths. The only difference between **WW3** and **WW5** was that the incorporation of an ethynylene group between the porphyrin and NP units, which would help to extend the π -conjugation and decrease the HOMO-LUMO gap, thus giving a longer-wavelength absorption spectrum. When tested for the photovoltaic performance, **WW3** showed a moderate power conversion efficiency of 5.6%. While, when

WW5 was employed, an impressive broad IPCE action spectrum covering the panchromatic visible region and part of the NIR region was achieved. The most distinct character is that the onset of IPCE action spectrum was further red-shifted to 815 nm for **WW5** cell, as a result, a high J_{sc} of 18.4 mA cm^{-2} was achieved corresponding to $\eta = 10.3\%$.

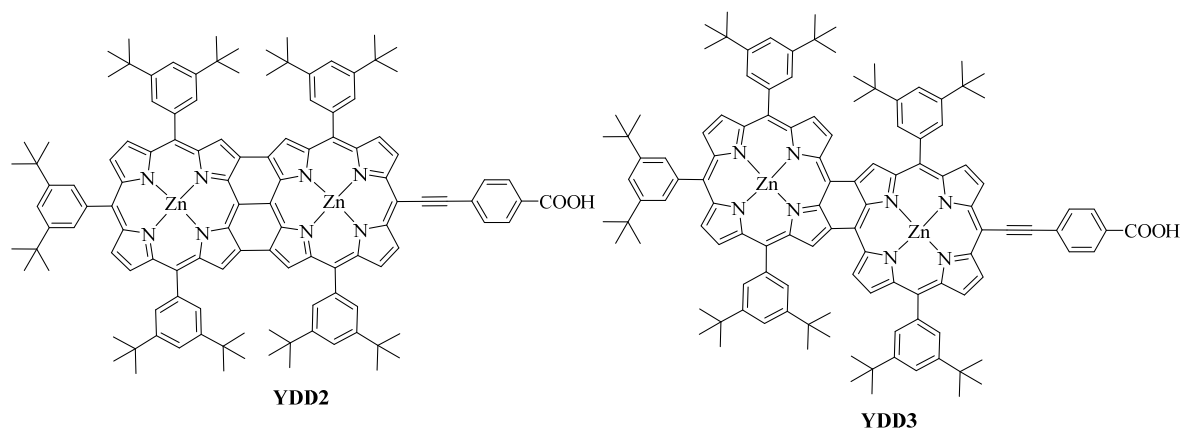
d) Fused Porphyrins

According to above mentioned examples, porphyrins are promising photosensitizers for DSSC due to their intense absorption in the *Soret* and Q bands to harvest solar energy efficiently over a broad spectral region, but the presence of a wide dip between the *Soret* and Q bands in porphyrins limits their DSSC performance. To improve the light-harvesting ability of the porphyrins, another useful strategy is fusion of a chromophore with porphyrin for π -elongation. Feasibility of this idea was first proved by Imahori and co-workers, when they reported a *meso*- β edge naphthalene fused zinc porphyrin **fused-Zn-1** (Scheme 1-9) which obtained $\eta = 4.1\%$, which was improved to 5.0% under co-sensitization relative to the reference cell with an unfused porphyrin.^[129-130] The same group^[131] reported the unsymmetrically π -elongated quinoxaline-based β - β' -edge fused zinc porphyrins, out of which a fused porphyrin with one anchoring group **ZnQMA** (Scheme 1-9) exhibited $\eta = 5.2\%$, attaining 80% performance of a **N719** device under the same conditions.



Scheme 1-9. Molecular structures of fused porphyrins.

Since these perylene fused porphyrins suffer from dye aggregation, the IPCE values did not exceed 30%, which was unable to attain a notable performance ($\eta \sim 1.3\%$). The same group later in 2014,^[128] reported another porphyrin dye fused with *N*-annulated perylene (NP) which works as an efficient electron donor and also helps to push the absorption to higher wavelengths. The absorption of the NP-fused porphyrin dye **WW4** was much more red-shifted to 792 nm due to the efficient π -extension after fusion. Two intense absorption bands at 444 nm and 540 nm were also observed. In spite of the red shifted absorption dye **WW4** exhibited poorer performance due to its low lying LUMO energy level and non-disjoint HOMO/LUMO profile indicating that its driving force for electron injection was not sufficient. A very weak photocurrent response was observed for **WW4**, although its absorption is extended to the NIR region up to 920 nm. Both the J_{sc} and V_{oc} gave very disappointing results (3.00 mA cm^{-2} and 0.500 V , respectively) corresponding to the overall $\eta = 0.3\%$ revealing that the fusion at opposite side of the anchoring group is less effective. Yeh and Diau^[134] proposed another strategy, the fusion of two porphyrins, to extend the π -conjugation. They designed and synthesized two fused porphyrins **YDD2** and **YDD3** (Scheme 1-11), but both of them exhibited poor DSSC performance. For **YDD2**, the absorption spectrum extends even beyond 1200 nm, but no photocurrent was observed because the energy level of LUMO was substantially lower than the conduction band edge of TiO_2 indicating that its driving force for electron injection was not sufficient.



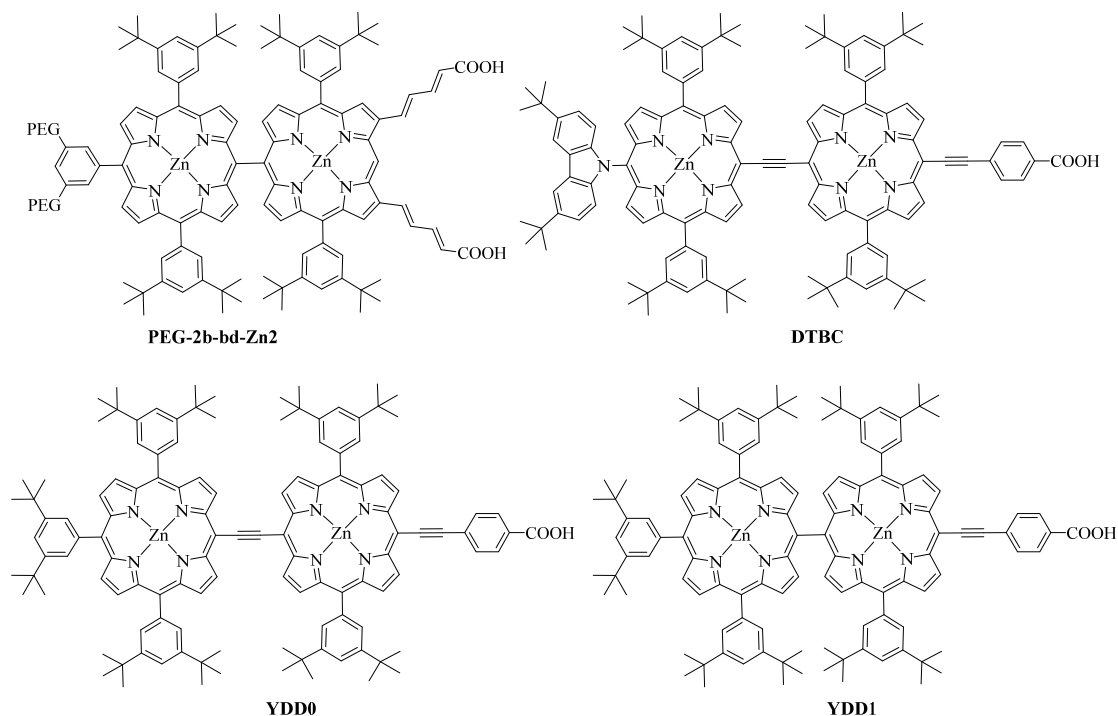
Scheme 1-11. Molecular structures of fused porphyrins.

For **YDD3**, although a small response was observed in the IPCE action spectrum corresponding to the contribution of broad bands I and II of the fused porphyrin, nearly no response was observed for the broad band III in region 700–900 nm. **WW2**, **WW4** and

YDD3 are, nevertheless, three interesting panchromatic porphyrin sensitizers with the potential to extend the light-harvesting ability toward the near-infrared region for PSSC. From all the example mentioned above, it is clear that the fusion at the acceptor part of the porphyrin is much more effective than the fusion at the donor part.

e) Porphyrin Dimers

Combination of two porphyrin moieties through a chemical bond is another useful strategy to improve light-harvesting ability of the sensitizer. The first attempt to use dimeric porphyrins as sensitizers for DSSC was made in 2009 by Officer and co-workers.^[135] The device based on dimeric porphyrin dyes exhibited light-harvesting efficiencies slightly improved relative to the corresponding monomeric porphyrin. The effect of π -conjugation for the red shift of the IPCE spectra due to porphyrin dimerization was small as the link between the two porphyrins was made at the β -position. The first effort to link the two porphyrins at the *meso*-position was made in 2009 by Kim and Osuka.^[136] Their polyethanediol (PEG)-modified dimer **PEG-2b-bd-Zn2** (Scheme 1-12) with two β -substituted linkers showed the best device performance of the various dimers, giving an overall efficiency $\eta = 4.2\%$. Yeh and Diau^[134] designed two porphyrin dimers, **YDD0** and **YDD1** (Scheme 1-12).



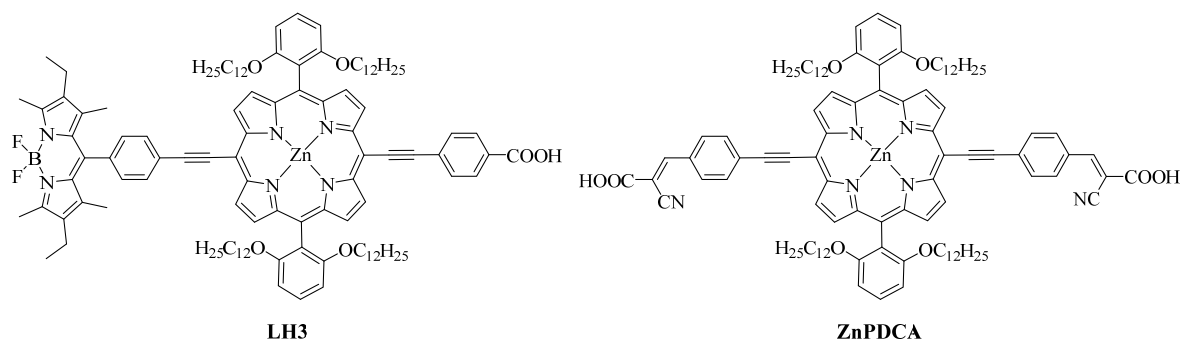
Scheme 1-12. Molecular structures of dimeric porphyrins.

Similar to the results of Kim and Osuka,^[136] the absorption spectrum of **YDD1** exhibited slight red-shift relative to that of the monomeric porphyrin **YD0**. Also because of effective excitonic coupling between the two nearly perpendicular porphyrin units in **YDD1**, the gap shown in the IPCE spectrum of **YD0** was completely filled in the spectrum of **YDD1**, making J_{sc} of its device become much better resulting in slightly higher $\eta = 5.23\%$. With the ethynyl linkage between the two porphyrin units, **YDD0** showed split *Soret* bands in the range of 400-500 nm, and red shifts and broadening of the Q bands extending to nearly 800 nm. The broad IPCE spectrum of **YDD0** showed much smaller efficiency of $\eta = 4.07\%$ than those of **YD0** and **YDD1** because of the co-planar structure which results in severe dye aggregation. Similar to the structural design of **YDD0**, Segawa and co-workers^[137] added an electron donating carbazole unit at the *meso*-position of the porphyrin edge to form a push-pull porphyrin dimer, **DTBC** (Scheme 1-12). **DTBC** has an absorption spectrum similar to that of **YDD0**, but its IPCE spectrum showed much greater efficiency than that of **YDD0**. In the absence of a TBP additive, the **DTBC** device exhibited IPCE values up to 80%, yielding a remarkable $J_{sc}/\text{mA cm}^{-2} = 18.2$ but also causing a poor $V_{oc}/V \sim 0.4$. The poor V_{oc} was significantly improved in the presence of TBP to attain an optimized device performance $\eta = 5.2\%$.

f) Enveloping porphyrins with long alkoxy chains

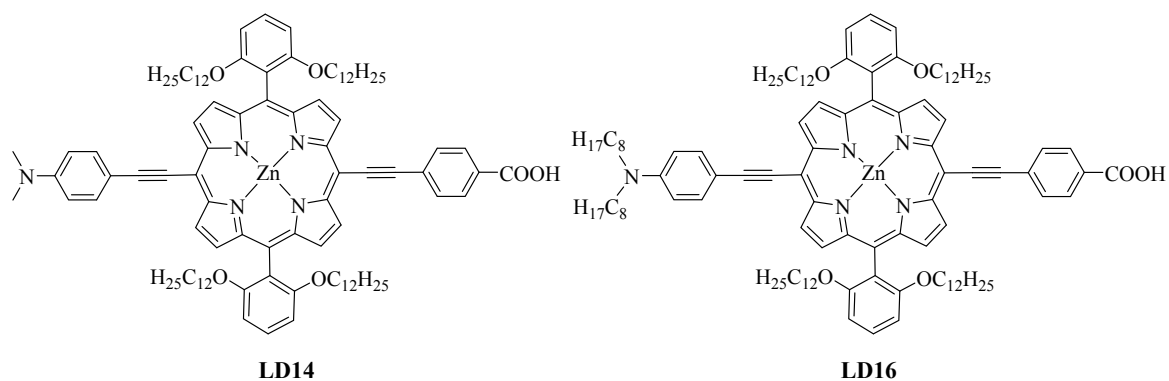
The superior performance of some of the above mentioned porphyrins such as **YD2**,^[121] **LD4**^[126] and **WW5**^[128] was due to their higher light-harvesting ability resulted mainly by the introduction of an electron donating group or a π -extended chromophore at the *meso*-position of the porphyrin ring. However V_{oc} of these highly efficient porphyrin dyes was significantly less than that of the commonly used ruthenium dyes. The considerably reduced electron lifetime was described to be responsible for the smaller V_{oc} of porphyrins, and the positively charged zinc center of the porphyrin core might attract the I_3^- ions in the electrolyte causing effectual electron interception from the TiO_2 surface.^[120] In case of the organic dyes, Tian and co-workers concluded that V_{oc} can be improved by decreasing the charge recombination and increasing the efficiency of electron injection.^[138] To solve this problem of aggregation in porphyrins, a new concept was introduced to design a zinc-porphyrin sensitizer with long alkoxy chains to protect the porphyrin core for retarded charge recombination and also to decrease effectively the dye aggregation for an efficient electron injection. Such a molecular design were first introduced in 2010 by Hupp and co-workers.^[139] They reported porphyrin

sensitizers with two phenyl groups attached at the 5,15-*meso*-positions bearing two dodecoxyl ($-\text{OC}_{12}\text{H}_{25}$) chains at the *ortho*-position of each phenyl group.



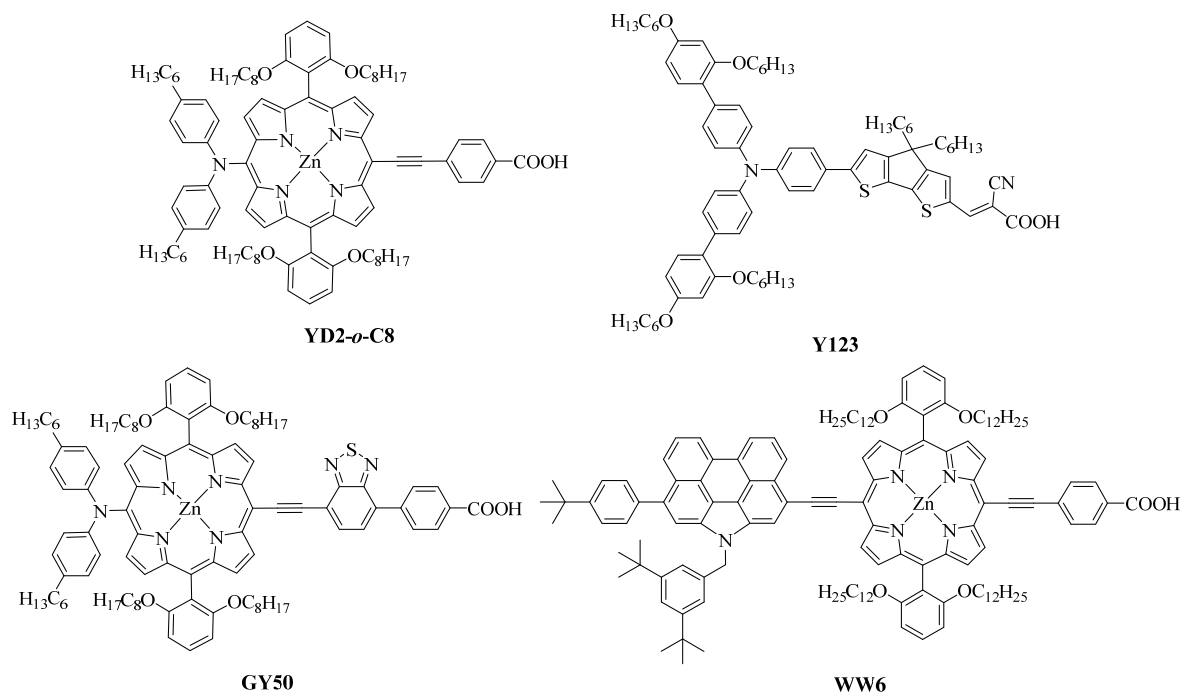
Scheme 1-13. Molecular structures of LH3 and ZnPDCA.

Among those *ortho*-substituted porphyrins, **LH3** (Scheme 1-13)^[139] and **ZnPDCA** (Scheme 1-13)^[140] displayed the best performance of each series attaining $\eta = 1.5\%$ and 5.5% respectively. Lin and co-workers^[141-142] reported a series of *ortho*-substituted porphyrins **LD14** and **LD16** as shown in Scheme 1-14. The photovoltaic measurement results indicate that J_{sc} was significantly improved on incorporation of the π -conjugated electron donating group while V_{oc} of those *ortho*-substituted porphyrins was significantly greater than that of a *para*- or *meta*-substituted counterpart. The best devices made from **LD14** and **LD16** attained power conversion efficiencies higher than 10%. The density functional theory studies revealed that the porphyrin core was fully enveloped by the four dodecoxyl chains to provide more effective insulation resulting in diminished molecular aggregation and increased solubility in non-coordinating organic solvents. The transient photoelectric results indicate that the upward shift of the TiO_2 potential and the charge recombination are two important factors for the enhanced V_{oc} of the *ortho*-substituted porphyrins.^[141]



Scheme 1-14. Molecular structures of LD dyes.

The long alkoxy chains thus play a key role to prevent the approach of I_3^- in the electrolyte to the surface of TiO_2 so as to retard the electron interception at the electrolyte/ TiO_2 interface. Based on a similar molecular design of **YD2**, an *ortho*-substituted push-pull zinc porphyrin **YD2-*o*-C8** (Scheme 1-15) was reported in 2011 by Grätzel and co-workers.^[25] When evaluated in DSSC, the **YD2-*o*-C8** dye attained $\eta = 11.9\%$. When **YD2-*o*-C8** was co-sensitized with an organic dye **Y123** (Scheme 1-15) in a cobalt-based redox electrolyte, the optimized performance of the device under AM1.5 one-sun irradiation was found as follow, $J_{sc}/mA\ cm^{-2} = 17.7$, $V_{oc}/V = 0.935$, $FF = 0.74$, and $\eta = 12.3\%$. Light induced photoelectric measurements of the **YD2-*o*-C8** devices revealed that the enhanced V_{oc} of the *ortho*-substituted devices was resulted by the upward shift of the TiO_2 conduction band and the enhanced electron lifetimes. The long alkoxy chains in these *ortho*-substituted porphyrins thus play an important role to effectively diminish the degree of dye aggregation for an improved device performance.



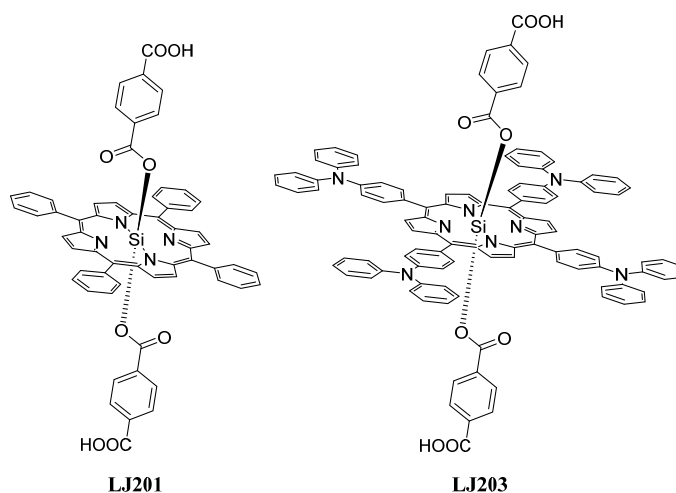
Scheme 1-15. Molecular structures of *ortho*-substituted porphyrins.

In 2014, the similar group reported the design and synthesis of **GY50** (Scheme 1-15), in which they applied a new strategy of introducing 2,1,3-benzothiadiazole (BTD) as a π -conjugated linker between the anchoring group and the porphyrin chromophore to broaden the absorption spectra to fill the valley between the *Soret* and Q bands. In the dye **GY50**, the electronic coupling is weakened due to the lack of planarity between the BTD and phenyl

rings. The device based on **GY50** sensitizer resulted in a J_{sc} value of 18.3 mA cm^{-2} , V_{oc} value of 0.885 V and a fill-factor of 0.77 corresponding to the overall solar-to-electric power-conversion efficiency (PCE) of 12.75% .^[143] In the same year, Wang and Wu^[128] reported) *ortho* alkoxy substituted porphyrin dye **WW6** (Scheme 1-15) coupled with an efficient electron donor, *N*-annulated perylene (NP). In **WW6** the introduction of an ethynylene spacer between the NP unit and the porphyrin core leads to an efficient π -conjugation which consequently red-shifted the absorption spectrum and thus improve their light-harvesting properties. The **WW6** based cell showed a panchromatic IPCE action spectrum with the onset reaching 785 nm , which is in consistence with its absorption spectra. For the device based on **WW6**, the J_{sc} value obtained was 17.69 mA cm^{-2} , the V_{oc} was 0.809 V , and the power conversion efficiency was as high as 10.5% , which is the similar to the **YD2-*o*-C8** cell ($\eta = 10.5\%$) under same irradiation conditions. Under a lower irradiance condition at $G = 50 \text{ mW cm}^{-2}$, the η value of the **WW6** cell ($\eta = 11.3\%$) was even higher than that of **YD2-*o*-C8** cell ($\eta = 10.8\%$).

g) Porphyrins with axial anchors

Sun and Yang^[144] reported two new silicon porphyrin-based sensitizers, **LJ201** and **LJ203** (Scheme 1-16), in order to provide a promising way to surmount the problem related to the charge recombination.

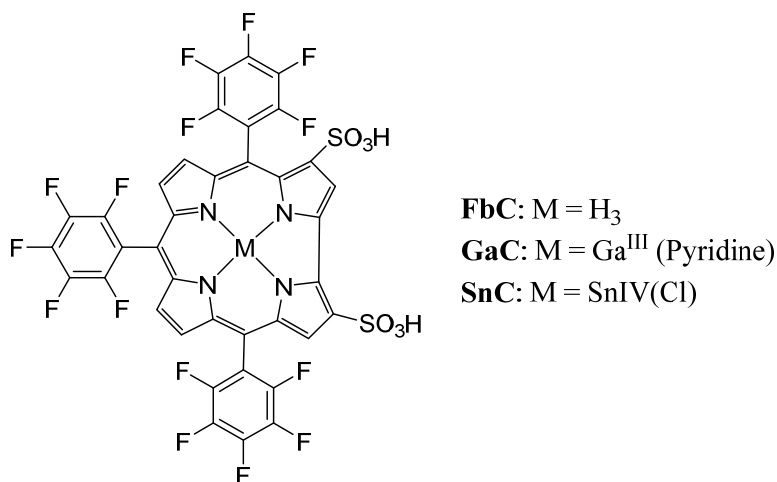


Scheme 1-16. Molecular structures of axial porphyrins.

Under the optimized fabrication conditions, **LJ203** achieved a η of 3.0% , with a J_{sc} of 8.24 mA cm^{-2} , a V_{oc} of 486 mV , and a FF of 0.74 . The η value of the **LJ203**-sensitized solar cell was two times that of the cell using **LJ201** ($\eta = 1.0\%$, $J_{sc} = 3.28 \text{ mA cm}^{-2}$, $V_{oc} = 436 \text{ mV}$, $FF = 0.72$).

1.5.3.3 Corroles

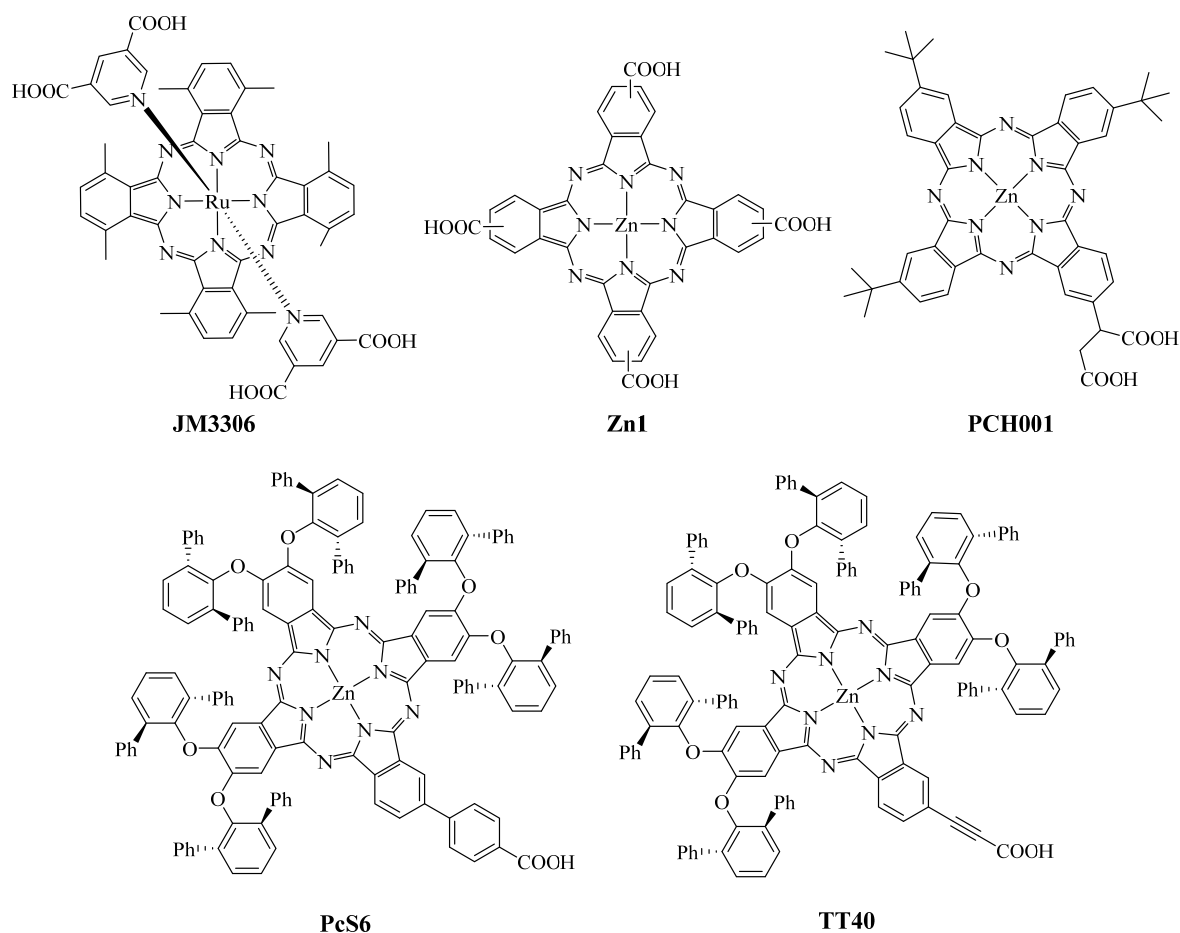
Corroles are contracted porphyrinoid derivatives, having one less *meso*-carbon than porphyrin on the aromatic macrocycle. Presently there are only two literature references dealing with their application in a DSSC, reported by Gross and coworkers.^[145-146] They synthesized a series of β -disulfonated corroles with *meso*-pentafluorophenyl groups as shown in Scheme 1-17. When evaluated in DSSCs, the best device based on **GaC**, gave an η of 1.6%, approximately half the efficiency of **N3** dye tested under similar conditions.^[145] The lower J_{sc} obtained for these corrole based DSSCs may be due to poor electron injection dynamics between the corrole LUMO and the conduction band of the TiO₂, possibly brought on by the use of sulfonyl binding groups rather than the more usual carboxyl groups.



Scheme 1-17. Molecular structures of Corroles.

1.5.3.4 Phthalocyanine and Subphthalocyanine sensitizers

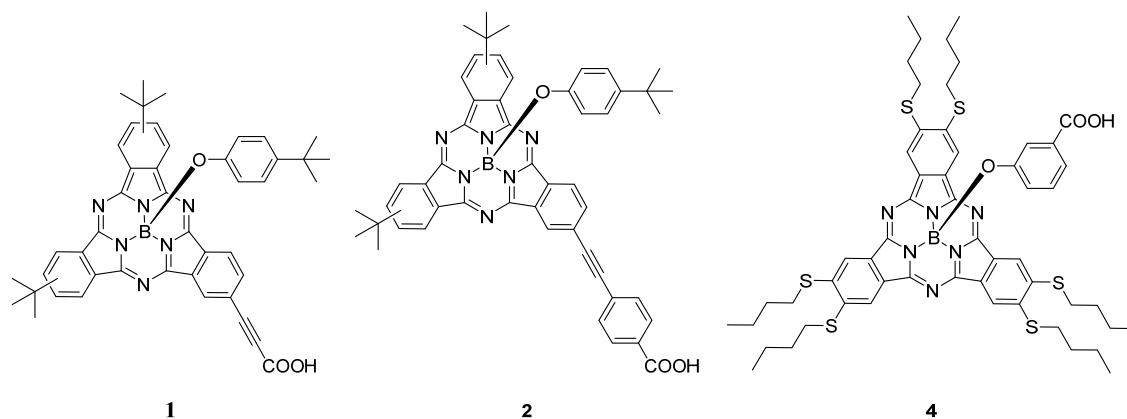
Phthalocyanines are suitable sensitizers for DSSCs due to their intense and tunable absorption in the red and NIR region as well as their promising electrochemical, photochemical and thermal properties. They possess very high molar extinction coefficients ($\epsilon > 100000 \text{ M}^{-1}\text{cm}^{-1}$).^[147-148] Though they have some disadvantages like low solubility, tendency to aggregate on the semiconductor surface, which can be minimized by structural optimization and using a co-absorber. In a pioneering work, Grätzel and co-workers used a Ru phthalocyanine sensitizer **JM3306** (Scheme 1-18) to achieve a high IPCE value more than 60%. The main feature of this result is that, they attached phthalocyanines to the semiconductor surface through axially attached pyridine ligands. They also reported a Zn phthalocyanine dye **Zn1** (Scheme 1-18), which obtained high IPCE of 45% in the NIR region and gives efficiency of 1%.^[149-150]



Scheme 1-18. Phthalocyanine Sensitizers.

Nazeeruddin and co-workers developed first unsymmetrical phthalocyanine sensitizer **PCH001** (Scheme 1-18) for DSSC application to get an IPCE value of 75% and conversion efficiency of 3.1% under AM 1.5 in liquid electrolyte cell.^[87, 151-152] Recently Mori et.al, reported a unsymmetrical phthalocyanine sensitizer **PcS6** (Scheme 1-18) having benzoic acid on one side of the macrocycle and six bulky electron donating 2,6-diphenyl-4-methoxyphenol units on other three sides. This three dimensional (3D) enlargement of the molecular structure, prevents the cofacial aggregation on the TiO₂ surface and offers the efficiency of 5.3% in liquid electrolyte cell under standard global AM 1.5 solar conditions. The similar dye when co-sensitized with an organic dye gives PCE of 6.2%.^[153-154] During the same period, Torres and Grätzel, developed a Zn^{II}Pc dye **TT40** (Scheme 1-18), having C-C triple bond as a spacer between the conjugated core and the anchoring COOH group. From the structure-function relationship studies it is revealed that the anchoring group should be electronically attached to the Zn^{II}Pc to facilitate the charge transfer from the LUMO of the dye to the Ti 3d orbital.^[155] The Zn^{II}Pc dye **TT40** sensitized solar cell without use of any co-adsorbent yielded

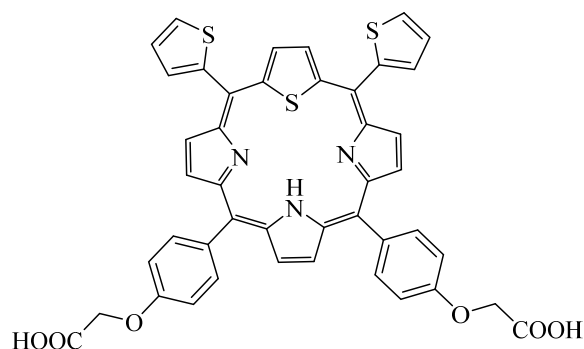
a PCE of 5.5% and 6.1% under 100 (1 sun irradiation) and 9.5 mWcm^{-2} , respectively.^[156] Torres and coworkers^[157] very recently reported the first use of subphthalocyanine in liquid DSSCs. They designed and prepared a series of subphthalocyanines functionalized with carboxylate group either at periphery or axial position as displayed in Scheme 1-19. The best device based on SubPc **1** attained overall conversion efficiency of 1.32% while the device based on SubPc **2** achieved η of 1.12%. However the device based on axial SubPc **4** obtained η of 0.38%. Due to complexity in the synthesis, phthalocyanine dyes remains substandard to the Ru and porphyrin dyes. As porphyrin sensitizers reached 12% PCE, there is still a big gap to fill up for phthalocyanines.



Scheme 1-19. Subphthalocyanine Sensitizers.

1.5.3.5 Core-modified porphyrins

Different molecular designs have been conducted to extend the absorption wavelengths of porphyrins to the near-infrared region in order to subsequently increase their overall photon-to-current conversion efficiencies. As described in above sections, two mostly explored routes to modify peripheral substituents of the porphyrin core are through either extending π -conjugation system over *meso*- or β -positions or fusing porphyrins with aromatic chromophores. Alternatively, the replacement of one or more pyrrolic nitrogens on the porphyrin central core with heteroatoms is another important but less explored approach to push the absorption of porphyrins towards red region. Tremendous efforts have been made to investigate the photovoltaic properties of regular porphyrins. Comparatively, only one example to investigate the performance of core-modified porphyrin in DSSC has been reported in the literature.^[158] Qiao and co-workers reported a series of monothia and dithia porphyrins to study the structural effects of core-modified porphyrins on efficiency in DSSCs. The best PCE, 0.19% is obtained for dye depicted in Scheme 1-20.



Scheme 1-20. Core-modified porphyrin sensitizers.

Though this result is not promising compared with the regular porphyrins, there is still a lot of scope to design novel sensitizers with core-modification.

1.6 Scope of present thesis

The brief introduction on various type of sensitizers presented in the previous sections offers a platform for the new research to screen other porphyrinoid sensitizers for DSSC application in this thesis. Porphyrinoids other than porphyrins like corroles, phthalocyanines, chlorins and bacteriochlorins have been successfully utilized as sensitizers in DSSCs. Although core atom modification induces red-shifted absorption wavelengths, their use is limited to synthetic methodologies, metal complexes and photo-dynamic therapy (PDT).

The aim of this thesis is to assess the performance of these core-modified porphyrins in DSSCs and try to push the efficiencies of these dyes to highest possible value through structural modification. For this purpose we prepared three novel porphyrins with *meso*-ethynylphenyl substitution N4, N3S, and N3O and check their performance in DSSCs. We have also prepared five novel thiaporphyrins with A₃B pattern having ethynylphenyl linker and cyanoacrylic acid anchor along with without ethynylphenyl linker and A₂B₂ pattern having different donors and two carboxylic acid group as anchor. With this molecular design we hope we can push the efficiencies of these thiaporphyrins further to a higher value. We also aim to apply the expanded porphyrins for the first time in DSSCs and develop new, efficient core-modified porphyrin sensitizers. For this purpose we developed boron oxasmaragdyrin dyes. We prepared five boron oxasmaragdyrins and applied them as sensitizers in DSSCs. We also add alkoxy chains with varied lengths to reduce the dye aggregation in this series of compounds. Later we engineered the molecular structure of these boron oxasmaragdyrins in an attempt to improve the device performance. We used different donors and linker and also different number and position of anchoring groups for comparison.

We also prepared two trithiasapphyrin derivatives with one or two carboxylic anchoring group and applied them in DSSCs, for the first time. Apart from the core-modified porphyrins and expanded porphyrins, we also experimented a co-sensitization method for regular porphyrins. We prepared mixed porphyrin DSSCs combining a free-base porphyrin and a zinc porphyrin having complementary absorption spectrum. Also we examined the efficiency of oxadiazole ring as electron transporter in DSSCs. We prepared three oxadiazole based dyes for this purpose.

1.7 References

- [1] BP Statistical Review of World Energy, June 2012, BP London, **2012**.
- [2] Renewables Global Status Report, Update 2012, Renewable Energy Policy Network, for the 21st Century, Paris, **2009**.
- [3] K. H. Neelson, P. G. Conrad, *Phil. Trans. R. Soc. Lond. B* **1999**, 354, 1923-1939.
- [4] Steger U, Nutzinger HG, Z. T, *Sustainable development and innovation in the energy sector* **2005**.
- [5] Raven PH, Evert RF, Eichhorn SE, *Biology of Plants, (7th ed.)*. New York: W.H. Freeman and Company Publishers. pp. 124–127. ISBN 0-7167-1007-2, **2005**.
- [6] K. Miyamoto, "Chapter 1 – Biological energy production". *Renewable biological systems for alternative sustainable energy production (FAO Agricultural Services Bulletin – 128)*. Food and Agriculture Organization of the United Nations. Retrieved 2009-01-04.
- [7] Govindjee, *What is photosynthesis?*
- [8] E. Bequerel., *Comptes rendus hebdomadaires des seances de l'Academie des Sciences* **1839**, 9, 145-149.
- [9] A. Einstein., *Annalen der Physik* **1905**, 17, 132-148.
- [10] M. Planck., *Annalen der Physik* **1901**, 4, 553-563.
- [11] European Photovoltaic Industry Association (2012), "Market Report" **2011**.
- [12] Sharp Develops Solar Cell with World's Highest Conversion Efficiency of 35.8%, *Physorg.com* **October 22, 2009**.
- [13] "SunPower TM 318 Solar Panel Data Sheet", *SunPower* **February, 2010**.
- [14] H. Gerischer, M. Michel-Beyerle, E Rebentrost, H Tributsch, *Electrochim. Acta* **1968**, 13, 1509–1515.
- [15] H. Tributsch, M. Calvin, *Photochemistry and Photobiology* **1971**, 14, 95-112.
- [16] H. Tributsch, *Photochemistry and Photobiology* **1972**, 16, 261-269.

- [17] N. R. E. L. Efficiency chart, (USA).
- [18] M. Matsumura, S. Matsudaira, H. Tsubomura, M. Takata, H. Yanagida, *Industrial & Engineering Chemistry Product Research and Development* **1980**, *19*, 415-421.
- [19] A. J. Bard, *J. Phys. Chem.* **1982**, *86*, 172-177.
- [20] A. Hagfeldt, M. Graetzel, *Chem. Rev.* **1995**, *95*, 49-68.
- [21] C. A. Bignozzi, R. Argazzi, C. J. Kleverlaan, *Chem. Soc. Rev.* **2000**, *29*, 87-96.
- [22] M. Grätzel, *Philosophical transactions. Series A, Mathematical, physical, and engineering sciences* **2007**, *365*, 993-1005.
- [23] B. O'Regan, M. Gratzel, *Nature* **1991**, *353*, 737-740.
- [24] L. Han, A. Islam, H. Chen, C. Malapaka, B. Chiranjeevi, S. Zhang, X. Yang, M. Yanagida, *Energy Environ. Sci.* **2012**, *5*, 6057-6060.
- [25] A. Yella, H.-W. Lee, H. N. Tsao, C. Yi, A. K. Chandiran, M. K. Nazeeruddin, E. W.-G. Diao, C.-Y. Yeh, S. M. Zakeeruddin, M. Grätzel, *Science* **2011**, *334*, 629-634.
- [26] M. A. Green, K. Emery, Y. Hishikawa, W. Warta, E. D. Dunlop, *Progress in Photovoltaics: Research and Applications* **2012**, *20*, 606-614.
- [27] R. Jose, V. Thavasi, S. Ramakrishna, *J. Am. Ceram. Soc.* **2009**, *92*, 289-301.
- [28] C. A. Bignozzi, J. R. Schoonover, F. Scandola, *Progr. Inorg. Chem.* **1997**, *44*, 1-95.
- [29] A. Hagfeldt, G. Boschloo, L. Sun, L. Kloo, H. Pettersson, *Chem. Rev.* **2010**, *110*, 6595-6663.
- [30] H. Imahori, T. Umeyama, S. Ito, *Acc. Chem. Res.* **2009**, *42*, 1809-1818.
- [31] M. V. Martinez-Diaz, G. de la Torre, T. Torres, *Chem. Comm.* **2010**, *46*, 7090-7108.
- [32] A. Mishra, M. K. R. Fischer, P. Bäuerle, *Angew. Chem. Int. Ed.* **2009**, *48*, 2474-2499.
- [33] Y. Ooyama, Y. Harima, *Eur. J. Org. Chem.* **2009**, *2009*, 2903-2934.
- [34] S. Anderson, E. C. Constable, M. P. Dare-Edwards, J. B. Goodenough, A. Hamnett, K. R. Seddon, R. D. Wright, *Nature Publishing Group* **1979**.
- [35] J. Desilvestro, M. Graetzel, L. Kavan, J. Moser, J. Augustynski, *J. Am. Chem. Soc.* **1985**, *107*, 2988-2990.
- [36] M. K. Nazeeruddin, A. Kay, I. Rodicio, R. Humphry-Baker, E. Mueller, P. Liska, N. Vlachopoulos, M. Graetzel, *J. Am. Chem. Soc.* **1993**, *115*, 6382-6390.
- [37] M. K. Nazeeruddin, F. De Angelis, S. Fantacci, A. Selloni, G. Viscardi, P. Liska, S. Ito, B. Takeru, M. Grätzel, *J. Am. Chem. Soc.* **2005**, *127*, 16835-16847.
- [38] M. Nazeeruddin, S. Zakeeruddin, R. Humphry-Baker, M. Jirousek, P. Liska, N. Vlachopoulos, V. Shklover, C.-H. Fischer, M. Grätzel, *Inorg. Chem.* **1999**, *38*, 6298-6305.

- [39] Q. Wang, S. Ito, M. Grätzel, F. Fabregat-Santiago, I. Mora-Seró, J. Bisquert, T. Bessho, H. Imai, *J. Phys. Chem. B* **2006**, *110*, 25210-25221.
- [40] M. K. Nazeeruddin, P. Pechy, M. Gratzel, *Chem. Comm.* **1997**, 1705-1706.
- [41] P. Péchy, T. Renouard, S. M. Zakeeruddin, R. Humphry-Baker, P. Comte, P. Liska, L. Cevey, E. Costa, V. Shklover, L. Spiccia, G. B. Deacon, C. A. Bignozzi, M. Grätzel, *J. Am. Chem. Soc.* **2001**, *123*, 1613-1624.
- [42] Y. Chiba, A. Islam, R. K. Y. Watanabe, N. Koide and L. Han, *Jpn. J. Appl. Phys.*, **2006**, *45*, L638
- [43] F. Gao, Y. Wang, D. Shi, J. Zhang, M. Wang, X. Jing, R. Humphry-Baker, P. Wang, S. M. Zakeeruddin, M. Grätzel, *J. Am. Chem. Soc.* **2008**, *130*, 10720-10728.
- [44] Y. Cao, Y. Bai, Q. Yu, Y. Cheng, S. Liu, D. Shi, F. Gao, P. Wang, *J. Phys. Chem. C* **2009**, *113*, 6290-6297.
- [45] D. Kim, J. K. Lee, S. O. Kang, J. Ko, *Tetrahedron* **2007**, *63*, 1913-1922.
- [46] N. Koumura, Z.-S. Wang, M. Miyashita, Y. Uemura, H. Sekiguchi, Y. Cui, A. Mori, S. Mori, K. Hara, *J. Mater. Chem.* **2009**, *19*, 4829-4836.
- [47] Z.-S. Wang, N. Koumura, Y. Cui, M. Takahashi, H. Sekiguchi, A. Mori, T. Kubo, A. Furube, K. Hara, *Chem. Mater.* **2008**, *20*, 3993-4003.
- [48] K. Hara, Y. Dan-oh, C. Kasada, Y. Ohga, A. Shinpo, S. Suga, K. Sayama, H. Arakawa, *Langmuir* **2004**, *20*, 4205-4210.
- [49] K. Hara, K. Miyamoto, Y. Abe, M. Yanagida, *J. Phys. Chem. B* **2005**, *109*, 23776-23778.
- [50] K. Hara, Z.-S. Wang, T. Sato, A. Furube, R. Katoh, H. Sugihara, Y. Dan-oh, C. Kasada, A. Shinpo, S. Suga, *J. Phys. Chem. B* **2005**, *109*, 15476-15482.
- [51] Z.-S. Wang, Y. Cui, Y. Dan-oh, C. Kasada, A. Shinpo, K. Hara, *J. Phys. Chem. C* **2007**, *111*, 7224-7230.
- [52] H. Choi, C. Baik, S. O. Kang, J. Ko, M.-S. Kang, M. K. Nazeeruddin, M. Grätzel, *Angew. Chem. Int. Ed.* **2008**, *47*, 327-330.
- [53] S. Kim, H. Choi, C. Baik, K. Song, S. O. Kang, J. Ko, *Tetrahedron* **2007**, *63*, 11436-11443.
- [54] S. Kim, J. K. Lee, S. O. Kang, J. Ko, J. H. Yum, S. Fantacci, F. De Angelis, D. Di Censo, M. K. Nazeeruddin, M. Grätzel, *J. Am. Chem. Soc.* **2006**, *128*, 16701-16707.
- [55] H. Qin, S. Wenger, M. Xu, F. Gao, X. Jing, P. Wang, S. M. Zakeeruddin, M. Grätzel, *J. Am. Chem. Soc.* **2008**, *130*, 9202-9203.

- [56] Z.-S. Wang, F.-Y. Li, C.-H. Huang, L. Wang, M. Wei, L.-P. Jin, N.-Q. Li, *J. Phys. Chem. B* **2000**, *104*, 9676-9682.
- [57] Q.-H. Yao, F.-S. Meng, F.-Y. Li, H. Tian, C.-H. Huang, *J. Mater. Chem.* **2003**, *13*, 1048-1053.
- [58] Q.-H. Yao, L. Shan, F.-Y. Li, D.-D. Yin, C.-H. Huang, *New J. Chem.* **2003**, *27*, 1277-1283.
- [59] D. Cao, J. Peng, Y. Hong, X. Fang, L. Wang, H. Meier, *Org. Lett.* **2011**, *13*, 1610-1613.
- [60] K. M. Karlsson, X. Jiang, S. K. Eriksson, E. Gabrielsson, H. Rensmo, A. Hagfeldt, L. Sun, *Chem. Eur. J.* **2011**, *17*, 6415-6424.
- [61] H. Tian, X. Yang, R. Chen, Y. Pan, L. Li, A. Hagfeldt, L. Sun, *Chem. Comm.* **2007**, 3741-3743.
- [62] H. Tian, X. Yang, J. Cong, R. Chen, J. Liu, Y. Hao, A. Hagfeldt, L. Sun, *Chem. Comm.* **2009**, 6288-6290.
- [63] C.-J. Yang, Y. J. Chang, M. Watanabe, Y.-S. Hon, T. J. Chow, *J. Mater. Chem.* **2012**, *22*, 4040-4049.
- [64] T. Horiuchi, H. Miura, K. Sumioka, S. Uchida, *J. Am. Chem. Soc.* **2004**, *126*, 12218-12219.
- [65] S. Ito, H. Miura, S. Uchida, M. Takata, K. Sumioka, P. Liska, P. Comte, P. Pechy, M. Gratzel, *Chem. Comm.* **2008**, 5194-5196.
- [66] S. Ito, S. M. Zakeeruddin, R. Humphry-Baker, P. Liska, R. Charvet, P. Comte, M. K. Nazeeruddin, P. Péchy, M. Takata, H. Miura, S. Uchida, M. Grätzel, *Adv. Mater.* **2006**, *18*, 1202-1205.
- [67] K. Sayama, S. Tsukagoshi, K. Hara, Y. Ohga, A. Shinpou, Y. Abe, S. Suga, H. Arakawa, *J. Phys. Chem. B* **2002**, *106*, 1363-1371.
- [68] S. Ferrere, B. A. Gregg, *New J. Chem.* **2002**, *26*, 1155-1160.
- [69] C. Li, J.-H. Yum, S.-J. Moon, A. Herrmann, F. Eickemeyer, N. G. Pschirer, P. Erk, J. Schöneboom, K. Müllen, M. Grätzel, M. K. Nazeeruddin, *ChemSusChem* **2008**, *1*, 615-618.
- [70] D. W. Chang, H. J. Lee, J. H. Kim, S. Y. Park, S.-M. Park, L. Dai, J.-B. Baek, *Org. Lett.* **2011**, *13*, 3880-3883.
- [71] K. Pei, Y. Wu, W. Wu, Q. Zhang, B. Chen, H. Tian, W. Zhu, *Chem. Eur. J.* **2012**, *18*, 8190-8200.
- [72] A. Burke, L. Schmidt-Mende, S. Ito, M. Gratzel, *Chem. Comm.* **2007**, 234-236.

- [73] T. Geiger, S. Kuster, J.-H. Yum, S.-J. Moon, M. K. Nazeeruddin, M. Grätzel, F. Nüesch, *Adv. Funct. Mater.* **2009**, *19*, 2720-2727.
- [74] S. Paek, H. Choi, C. Kim, N. Cho, S. So, K. Song, M. K. Nazeeruddin, J. Ko, *Chem. Comm.* **2011**, *47*, 2874-2876.
- [75] J. Park, C. Barolo, F. Sauvage, N. Barbero, C. Benzi, P. Quagliotto, S. Coluccia, D. Di Censo, M. Gratzel, M. K. Nazeeruddin, G. Viscardi, *Chem. Comm.* **2012**, *48*, 2782-2784.
- [76] Y. Shi, R. B. M. Hill, J.-H. Yum, A. Dualeh, S. Barlow, M. Grätzel, S. R. Marder, M. K. Nazeeruddin, *Angew. Chem. Int. Ed.* **2011**, *50*, 6619-6621.
- [77] J.-H. Yum, P. Walter, S. Huber, D. Rentsch, T. Geiger, F. Nüesch, F. De Angelis, M. Grätzel, M. K. Nazeeruddin, *J. Am. Chem. Soc.* **2007**, *129*, 10320-10321.
- [78] S. Hwang, J. H. Lee, C. Park, H. Lee, C. Kim, C. Park, M.-H. Lee, W. Lee, J. Park, K. Kim, N.-G. Park, C. Kim, *Chem. Comm.* **2007**, 4887-4889.
- [79] G. Li, K.-J. Jiang, Y.-F. Li, S.-L. Li, L.-M. Yang, *J. Phys. Chem. C* **2008**, *112*, 11591-11599.
- [80] W.-H. Liu, I. C. Wu, C.-H. Lai, C.-H. Lai, P.-T. Chou, Y.-T. Li, C.-L. Chen, Y.-Y. Hsu, Y. Chi, *Chem. Comm.* **2008**, 5152-5154.
- [81] H. Im, S. Kim, C. Park, S.-H. Jang, C.-J. Kim, K. Kim, N.-G. Park, C. Kim, *Chem. Comm.* **2010**, *46*, 1335-1337.
- [82] Y. Bai, J. Zhang, D. Zhou, Y. Wang, M. Zhang, P. Wang, *J. Am. Chem. Soc.* **2011**, *133*, 11442-11445.
- [83] W. Zeng, Y. Cao, Y. Bai, Y. Wang, Y. Shi, M. Zhang, F. Wang, C. Pan, P. Wang, *Chem. Mater.* **2010**, *22*, 1915-1925.
- [84] G. Zhang, H. Bala, Y. Cheng, D. Shi, X. Lv, Q. Yu, P. Wang, *Chem. Comm.* **2009**, 2198-2200.
- [85] T. Hasobe, H. Imahori, P. V. Kamat, T. K. Ahn, S. K. Kim, D. Kim, A. Fujimoto, T. Hirakawa, S. Fukuzumi, *J. Am. Chem. Soc.* **2005**, *127*, 1216-1228.
- [86] I. Radivojevic, A. Varotto, C. Farley, C. M. Drain, *Energy Environ. Sci.* **2010**, *3*, 1897-1909.
- [87] M. G. Walter, A. B. Rudine, C. C. Wamser, *J. Porphyrins Phthalocyanines* **2010**, *14*, 759-792.
- [88] M. J. Griffith, K. Sunahara, P. Wagner, K. Wagner, G. G. Wallace, D. L. Officer, A. Furube, R. Katoh, S. Mori, A. J. Mozer, *Chem. Comm.* **2012**, *48*, 4145-4162.

- [89] H. Imahori, T. Umeyama, K. Kurotobi, Y. Takano, *Chem. Comm.* **2012**, *48*, 4032-4045.
- [90] M. K. Panda, K. Ladomenou, A. G. Coutsolelos, *Coord. Chem. Rev.* **2012**, *256*, 2601-2627.
- [91] A. Kay, M. Graetzel, *J. Phys. Chem.* **1993**, *97*, 6272-6277.
- [92] A. Kay, R. Humphry-Baker, M. Graetzel, *J. Phys. Chem.* **1994**, *98*, 952-959.
- [93] Y. Amao, T. Komori, *Biosens. Bioelectron.* **2004**, *19*, 843-847.
- [94] Y. Amao, Y. Yamada, *Langmuir* **2005**, *21*, 3008-3012.
- [95] M. Ikegami, M. Ozeki, Y. Kijitori, T. Miyasaka, *Electrochemistry* **2008**, *76*, 140-143.
- [96] X.-F. Wang, J. Xiang, P. Wang, Y. Koyama, S. Yanagida, Y. Wada, K. Hamada, S.-i. Sasaki, H. Tamiaki, *Chem. Phys. Lett.* **2005**, *408*, 409-414.
- [97] X.-F. Wang, A. Matsuda, Y. Koyama, H. Nagae, S.-i. Sasaki, H. Tamiaki, Y. Wada, *Chem. Phys. Lett.* **2006**, *423*, 470-475.
- [98] X.-F. Wang, Y. Koyama, Y. Wada, S.-i. Sasaki, H. Tamiaki, *Chem. Phys. Lett.* **2007**, *439*, 115-120.
- [99] X.-F. Wang, C.-H. Zhan, T. Maoka, Y. Wada, Y. Koyama, *Chem. Phys. Lett.* **2007**, *447*, 79-85.
- [100] X.-F. Wang, Y. Koyama, H. Nagae, Y. Wada, S.-i. Sasaki, H. Tamiaki, *J. Phys. Chem. C* **2008**, *112*, 4418-4426.
- [101] X.-F. Wang, O. Kitao, H. Zhou, H. Tamiaki, S.-i. Sasaki, *J. Phys. Chem. C* **2009**, *113*, 7954-7961.
- [102] X.-F. Wang, O. Kitao, H. Zhou, H. Tamiaki, S.-i. Sasaki, *Chem. Comm.* **2009**, 1523-1525.
- [103] X.-F. Wang, Y. Koyama, O. Kitao, Y. Wada, S.-i. Sasaki, H. Tamiaki, H. Zhou, *Biosens. Bioelectron.* **2010**, *25*, 1970-1976.
- [104] X.-F. Wang, H. Tamiaki, L. Wang, N. Tamai, O. Kitao, H. Zhou, S.-i. Sasaki, *Langmuir* **2010**, *26*, 6320-6327.
- [105] M. K. Nazeeruddin, R. Humphry-Baker, D. L. Officer, W. M. Campbell, A. K. Burrell, M. Grätzel, *Langmuir* **2004**, *20*, 6514-6517.
- [106] T. Ma, K. Inoue, H. Noma, K. Yao, E. Abe, *J. Photochem. Photobiol., A* **2002**, *152*, 207-212.
- [107] R. B. M. Koehorst, G. K. Boschloo, T. J. Savenije, A. Goossens, T. J. Schaafsma, *J. Phys. Chem. B* **2000**, *104*, 2371-2377.

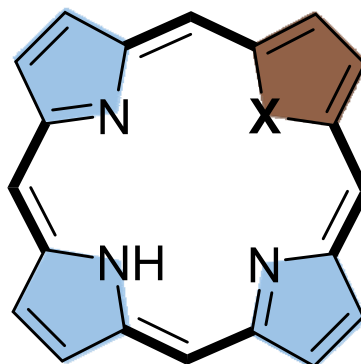
- [108] F. Odobel, E. Blart, M. Lagree, M. Villieras, H. Boujtita, N. El Murr, S. Caramori, C. Alberto Bignozzi, *J. Mater. Chem.* **2003**, *13*, 502-510.
- [109] L. Giribabu, C. V. Kumar, P. Y. Reddy, *J. Porphyrins Phthalocyanines* **2006**, *10*, 1007-1016.
- [110] Q. Wang, W. M. Campbell, E. E. Bonfantani, K. W. Jolley, D. L. Officer, P. J. Walsh, K. Gordon, R. Humphry-Baker, M. K. Nazeeruddin, M. Grätzel, *J. Phys. Chem. B* **2005**, *109*, 15397-15409.
- [111] W. M. Campbell, K. W. Jolley, P. Wagner, K. Wagner, P. J. Walsh, K. C. Gordon, L. Schmidt-Mende, M. K. Nazeeruddin, Q. Wang, M. Grätzel, D. L. Officer, *J. Phys. Chem. C* **2007**, *111*, 11760-11762.
- [112] J. K. Park, H. R. Lee, J. Chen, H. Shinokubo, A. Osuka, D. Kim, *J. Phys. Chem. C* **2008**, *112*, 16691-16699.
- [113] M. Ishida, S. W. Park, D. Hwang, Y. B. Koo, J. L. Sessler, D. Y. Kim, D. Kim, *J. Phys. Chem. C* **2011**, *115*, 19343-19354.
- [114] M. Ishida, D. Hwang, Y. B. Koo, J. Sung, D. Y. Kim, J. L. Sessler, D. Kim, *Chem. Comm.* **2013**, *49*, 9164-9166.
- [115] G. Di Carlo, A. Orbelli Biroli, M. Pizzotti, F. Tessore, V. Trifiletti, R. Ruffo, A. Abboto, A. Amat, F. De Angelis, P. R. Mussini, *Chem. Eur. J.* **2013**, *19*, 10723-10740.
- [116] T. E. O. Screen, K. B. Lawton, G. S. Wilson, N. Dolney, R. Ispasoiu, T. Goodson Iii, S. J. Martin, D. D. C. Bradley, H. L. Anderson, *J. Mater. Chem.* **2001**, *11*, 312-320.
- [117] V. Lin, S. DiMagno, M. Therien, *Science* **1994**, *264*, 1105-1111.
- [118] S. Cherian, C. C. Wamser, *J. Phys. Chem. B* **2000**, *104*, 3624-3629.
- [119] C.-W. Lee, H.-P. Lu, C.-M. Lan, Y.-L. Huang, Y.-R. Liang, W.-N. Yen, Y.-C. Liu, Y.-S. Lin, E. W.-G. Diau, C.-Y. Yeh, *Chem. Eur. J.* **2009**, *15*, 1403-1412.
- [120] A. J. Mozer, P. Wagner, D. L. Officer, G. G. Wallace, W. M. Campbell, M. Miyashita, K. Sunahara, S. Mori, *Chem. Comm.* **2008**, 4741-4743.
- [121] T. Bessho, S. M. Zakeeruddin, C.-Y. Yeh, E. W.-G. Diau, M. Grätzel, *Angew. Chem. Int. Ed.* **2010**, *49*, 6646-6649.
- [122] C.-Y. Lin, Y.-C. Wang, S.-J. Hsu, C.-F. Lo, E. W.-G. Diau, *J. Phys. Chem. C* **2009**, *114*, 687-693.
- [123] H.-P. Lu, C.-L. Mai, C.-Y. Tsia, S.-J. Hsu, C.-P. Hsieh, C.-L. Chiu, C.-Y. Yeh, E. W.-G. Diau, *PCCP* **2009**, *11*, 10270-10274.

- [124] S. Ito, T. N. Murakami, P. Comte, P. Liska, C. Grätzel, M. K. Nazeeruddin, M. Grätzel, *Thin Solid Films* **2008**, *516*, 4613-4619.
- [125] C.-H. Wu, T.-Y. Pan, S.-H. Hong, C.-L. Wang, H.-H. Kuo, Y.-Y. Chu, E. W.-G. Diau, C.-Y. Lin, *Chem. Comm.* **2012**, *48*, 4329-4331.
- [126] C.-L. Wang, Y.-C. Chang, C.-M. Lan, C.-F. Lo, E. Wei-Guang Diau, C.-Y. Lin, *Energy Environ. Sci.* **2011**, *4*, 1788-1795.
- [127] H.-P. Lu, C.-Y. Tsai, W.-N. Yen, C.-P. Hsieh, C.-W. Lee, C.-Y. Yeh, E. W.-G. Diau, *J. Phys. Chem. C* **2009**, *113*, 20990-20997.
- [128] J. Luo, M. Xu, R. Li, K.-W. Huang, C. Jiang, Q. Qi, W. Zeng, J. Zhang, C. Chi, P. Wang, J. Wu, *J. Am. Chem. Soc.* **2013**, *136*, 265-272.
- [129] M. Tanaka, S. Hayashi, S. Eu, T. Umeyama, Y. Matano, H. Imahori, *Chem. Comm.* **2007**, 2069-2071.
- [130] S. Hayashi, M. Tanaka, H. Hayashi, S. Eu, T. Umeyama, Y. Matano, Y. Araki, H. Imahori, *J. Phys. Chem. C* **2008**, *112*, 15576-15585.
- [131] S. Eu, S. Hayashi, T. Umeyama, Y. Matano, Y. Araki, H. Imahori, *J. Phys. Chem. C* **2008**, *112*, 4396-4405.
- [132] H. Hayashi, A. S. Touchy, Y. Kinjo, K. Kurotobi, Y. Toude, S. Ito, H. Saarenpää, N. V. Tkachenko, H. Lemmetyinen, H. Imahori, *ChemSusChem* **2013**, *6*, 508-517.
- [133] C. Jiao, N. Zu, K.-W. Huang, P. Wang, J. Wu, *Org. Lett.* **2011**, *13*, 3652-3655.
- [134] C.-L. Mai, W.-K. Huang, H.-P. Lu, C.-W. Lee, C.-L. Chiu, Y.-R. Liang, E. W.-G. Diau, C.-Y. Yeh, *Chem. Comm.* **2010**, *46*, 809-811.
- [135] A. J. Mozer, M. J. Griffith, G. Tsekouras, P. Wagner, G. G. Wallace, S. Mori, K. Sunahara, M. Miyashita, J. C. Earles, K. C. Gordon, L. Du, R. Katoh, A. Furube, D. L. Officer, *J. Am. Chem. Soc.* **2009**, *131*, 15621-15623.
- [136] J. K. Park, J. Chen, H. R. Lee, S. W. Park, H. Shinokubo, A. Osuka, D. Kim, *J. Phys. Chem. C* **2009**, *113*, 21956-21963.
- [137] Y. Liu, H. Lin, J. T. Dy, K. Tamaki, J. Nakazaki, D. Nakayama, S. Uchida, T. Kubo, H. Segawa, *Chem. Comm.* **2011**, *47*, 4010-4012.
- [138] Z. Ning, Y. Fu, H. Tian, *Energy Environ. Sci.* **2010**, *3*, 1170-1181.
- [139] C. Y. Lee, J. T. Hupp, *Langmuir* **2009**, *26*, 3760-3765.
- [140] C. Y. Lee, C. She, N. C. Jeong, J. T. Hupp, *Chem. Comm.* **2010**, *46*, 6090-6092.
- [141] C.-L. Wang, C.-M. Lan, S.-H. Hong, Y.-F. Wang, T.-Y. Pan, C.-W. Chang, H.-H. Kuo, M.-Y. Kuo, E. W.-G. Diau, C.-Y. Lin, *Energy Environ. Sci.* **2012**, *5*, 6933-6940.

- [142] Y.-C. Chang, C.-L. Wang, T.-Y. Pan, S.-H. Hong, C.-M. Lan, H.-H. Kuo, C.-F. Lo, H.-Y. Hsu, C.-Y. Lin, E. W.-G. Diau, *Chem. Comm.* **2011**, 47, 8910-8912.
- [143] A. Yella, C.-L. Mai, S. M. Zakeeruddin, S.-N. Chang, C.-H. Hsieh, C.-Y. Yeh, M. Grätzel, *Angew. Chem. Int. Ed.* **2014**, 53, 2973-2977.
- [144] J. Liu, X. Yang, L. Sun, *Chem. Comm.* **2013**, 49, 11785-11787.
- [145] Z. Gross, H. B. Gray, A. Zaban, J. R. Winkler, B. S. Brunshwig, A. Mahammed, S. Chappel, D. Walker, *J. Porphyrins Phthalocyanines* **2006**, 10, 1259-1262.
- [146] I. Aviv, Z. Gross, *Chem. Comm.* **2007**, 1987-1999.
- [147] G. de la Torre, C. G. Claessens, T. Torres, *Chem. Comm.* **2007**, 2000-2015.
- [148] J. Mack, N. Kobayashi, *Chem. Rev.* **2010**, 111, 281-321.
- [149] M. K. Nazeeruddin, R. Humphry-Baker, M. Grätzel, B. A. Murrer, *Chem. Comm.* **1998**, 719-720.
- [150] M. K. Nazeeruddin, R. Humphry-Baker, M. Grätzel, D. Wöhrle, G. Schnurpfeil, G. Schneider, A. Hirth, N. Trombach, *J. Porphyrins Phthalocyanines* **1999**, 03, 230-237.
- [151] P. Y. Reddy, L. Giribabu, C. Lyness, H. J. Snaith, C. Vijaykumar, M. Chandrasekharam, M. Lakshmikantam, J.-H. Yum, K. Kalyanasundaram, M. Grätzel, M. K. Nazeeruddin, *Angew. Chem. Int. Ed.* **2007**, 46, 373-376.
- [152] J.-J. Cid, J.-H. Yum, S.-R. Jang, M. K. Nazeeruddin, E. Martínez-Ferrero, E. Palomares, J. Ko, M. Grätzel, T. Torres, *Angew. Chem. Int. Ed.* **2007**, 46, 8358-8362.
- [153] M. Kimura, H. Nomoto, N. Masaki, S. Mori, *Angew. Chem. Int. Ed.* **2012**, 51, 4371-4374.
- [154] S. Mori, M. Nagata, Y. Nakahata, K. Yasuta, R. Goto, M. Kimura, M. Taya, *J. Am. Chem. Soc.* **2010**, 132, 4054-4055.
- [155] J.-J. Cid, M. García-Iglesias, J.-H. Yum, A. Forneli, J. Albero, E. Martínez-Ferrero, P. Vázquez, M. Grätzel, M. K. Nazeeruddin, E. Palomares, T. Torres, *Chem. Eur. J.* **2009**, 15, 5130-5137.
- [156] M.-E. Ragoussi, J.-J. Cid, J.-H. Yum, G. de la Torre, D. Di Censo, M. Grätzel, M. K. Nazeeruddin, T. Torres, *Angew. Chem. Int. Ed.* **2012**, 51, 4375-4378.
- [157] M. Ince, A. Medina, J.-H. Yum, A. Yella, C. G. Claessens, M. V. Martínez-Díaz, M. Grätzel, M. K. Nazeeruddin, T. Torres, *Chem. Eur. J.* **2014**, 20, 2016-2021.
- [158] Y. Xie, P. Joshi, M. Ropp, D. Galipeau, L. Zhang, H. Fong, Y. You, Q. Qiao, *J. Porphyrins Phthalocyanines* **2009**, 13, 903-909.

Section I

Heteroporphyrins



X = O, S

2. Effects of core-modification of porphyrin sensitizers to the efficiency of dye-sensitized solar cell

2.1 Introduction

The term “heteroporphyrin”, in the strict sense refers to the class of so-called core-modified porphyrins. Replacement of one or more pyrrolic nitrogen with other group 16 heteroatoms like oxygen, sulphur, selenium and tellurium in a porphyrin ring leads to the heteroatom substituted core-modified porphyrins as shown in Figure 2-1.^[1-3] This core perturbation results in significant changes in the optical, photophysical, electrical, magnetic and metal binding properties retaining the aromatic character. Although these exciting properties of core-modified porphyrins triggered enormous research in finding various synthetic methods to prepare functionalized heteroporphyrins, but until now, very few applications of these heteroporphyrins are reported, like new complexing agents for unusual metal oxidation states and photosensitizers for photodynamic therapy and sensitizers in DSSCs.^[4-9]

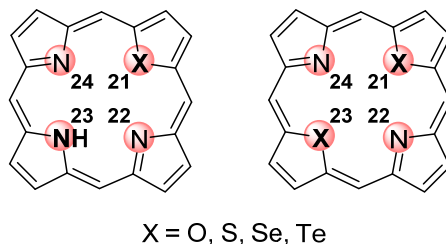
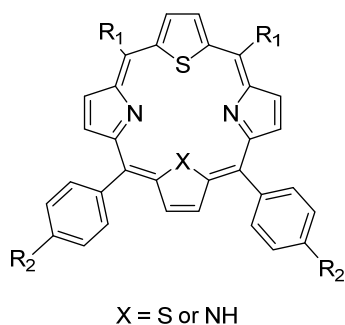


Figure 2-1. General structure and numbering of heteroporphyrins.

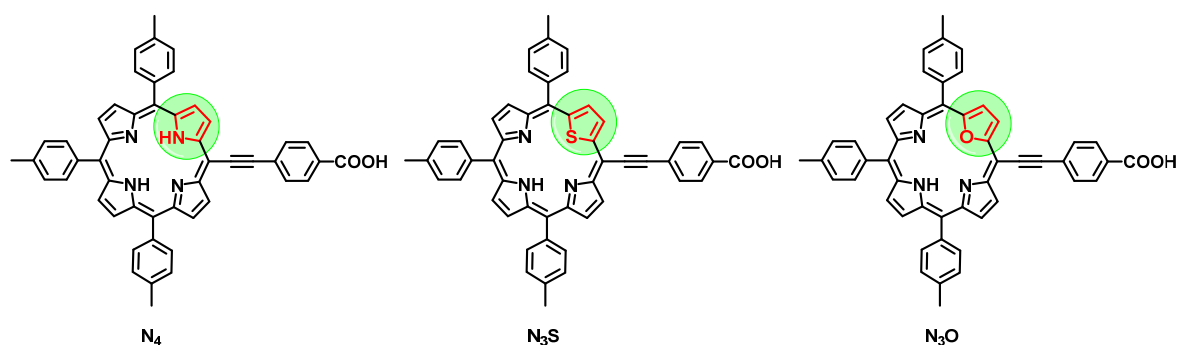
While these heteroporphyrins were established as complexing agents and PDT sensitizers, surprisingly, use of these core-modified porphyrins as sensitizers in DSSCs is very rare. The only example which demonstrates the use of core-modified porphyrins as a sensitizing dye in DSSC is reported by Xie *et al.*^[10] In this article a series of mono and dithiaporphyrins were utilized as a dye in DSSCs. The 21-thiaporphyrin with two *meso*-2-thienyl substituents adjacent to the porphyrinic thiophene obtained the highest efficiency of 0.19% (Scheme 2-1). There is no report till date, comparing the photophysical, electrochemical and photovoltaic properties of regular and core-modified porphyrins. The literature survey suggests that there is still a lot of scope to search for more efficient heteroporphyrin sensitizers with absorption in the NIR region. One of the reasons for the low efficiency of reported thiaporphyrin dyes in DSSCs would be the lack of effective electronic coupling between the porphyrin ring and the anchoring group which is essential for the effective charge transfer from dye to TiO₂ semiconductor. In most of the highly efficient porphyrin dyes, ethynylphenyl group is used as a linker to couple

the porphyrin ring and the anchoring carboxyl group.^[11-12] In this chapter, we discussed the synthesis of novel core-modified porphyrins **N3S** and **N3O** with ethynylphenyl group as a linker as shown in Scheme 2-2 to check the effects of core atom modification compared to the regular **N4** porphyrin, on the photovoltaic properties when applied in DSSC.



Group	Porphyrin	R ₁	R ₂	X	Efficiency (%)
A	1	thiophenyl	-OCH ₂ COOH	NH	0.19
	2	thiophenyl	-OCH ₂ COOEt	NH	0.02
	3	thiophenyl	-OCH ₂ COOEt	S	0.019
	4	biphenyl	-OCH ₃	S	0.14
B	5	biphenyl	-OH	S	0.10
	6	biphenyl	-OCH ₂ COOEt	S	0.043
	7	4'-dimethylaminophenyl	-OCH ₂ COOH	S	0.11
C	8	4'- <i>tert</i> -butylphenyl	-OCH ₂ COOH	S	0.10
	9	4'-methylphenyl	-OCH ₂ COOH	S	0.08

Scheme 2-1. General structures and efficiency of nine core-modified porphyrins with different *meso* aryl groups (R₁), anchoring groups (R₂) and core atoms (X) reported in literature.



Scheme 2-2. Molecular structures of the studied porphyrin dyes.

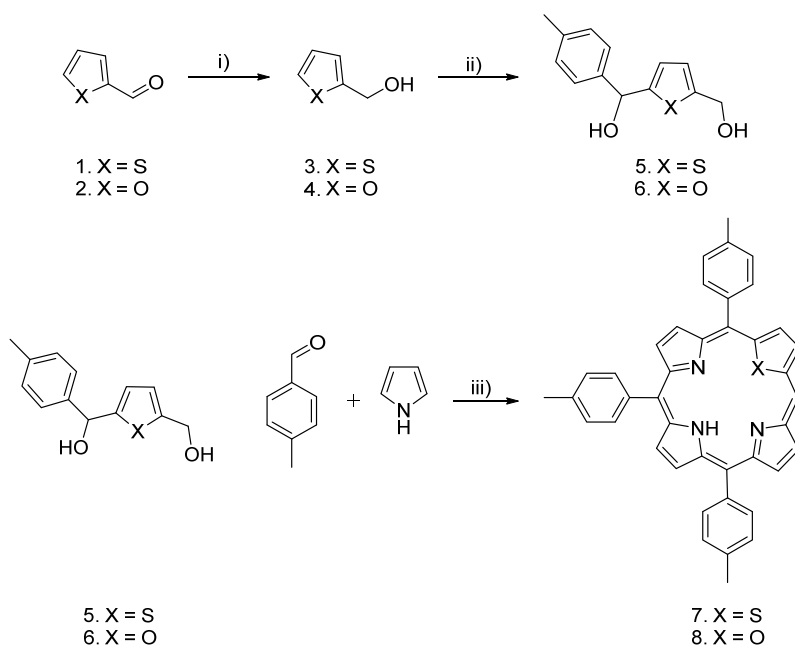
This systematic study, well supported by optical spectroscopy, cyclic voltammetry, DFT and TD-DFT calculations and photovoltaic measurements elucidates the significant influence of core atom replacement on the electronic structure, photophysical and photovoltaic properties. Our study revealed that the replacement of pyrrolic nitrogen with oxygen or sulfur resulted in

the red-shift of absorption of these porphyrins as compared to the regular porphyrins. The photovoltaic study reveals that in spite of the extended absorption wavelengths of core-modified porphyrins, the overall IPCEs of these porphyrins are much lower than the regular porphyrins.

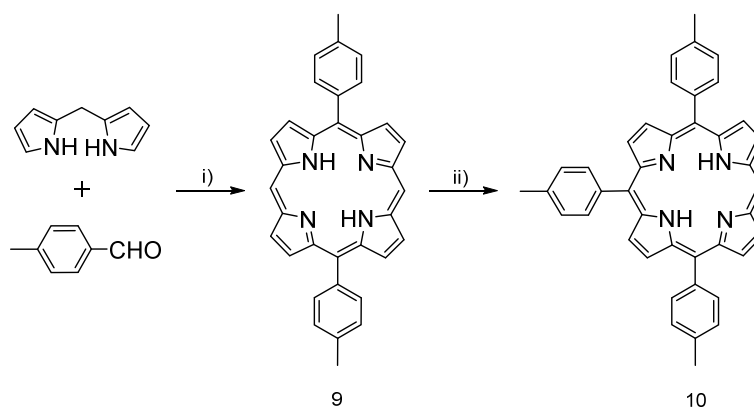
2.2 Results and Discussion

2.2.1 Syntheses

The thiaporphyrin (7) and oxaporphyrin (8) were prepared by condensation of thiophene and furan diol with two equivalents of *p*-tolualdehyde and three equivalents of pyrrole in the presence of catalytic amount of borontrifluoride etherate ($\text{BF}_3 \cdot \text{OEt}_2$) as displayed in Scheme 2-3. Porphyrin (9) was prepared by condensation dipyrromethane with *p*-tolualdehyde in presence of trifluoro acetic acid (TFA). The mono *meso*-unsubstituted free base porphyrin (10) was prepared from porphyrin (9) by coupling with tolyl lithium which was prepared *in-situ* by treating 4-bromotoluene with *n*-butyl lithium as shown in Scheme 2-4. The synthetic route to the porphyrins used in this study is depicted in Scheme 2-5. These mono *meso*-unsubstituted porphyrins were treated with N-bromosuccinimide (NBS) in dry dichloromethane to give 5-bromoporphyrins in 70-78% yield. The *m/z* peaks in mass spectra and the disappearance of the *meso* proton signal in ^1H NMR spectra confirmed the identity of the bromoporphyrins.

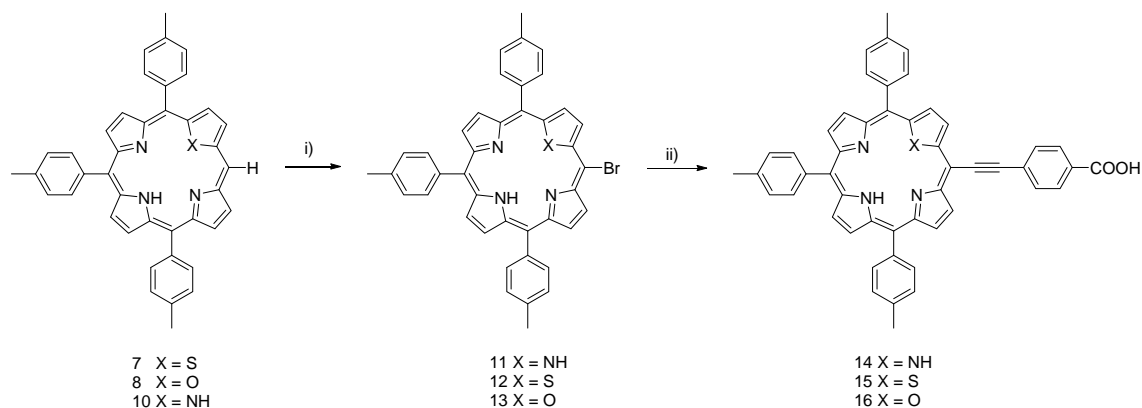


Scheme 2-3. Synthesis of N3S (7) and N3O (8) porphyrins. Reagents and conditions: i) NaBH_4 , MeOH; ii) *n*-BuLi, TMEDA, *p*-tolualdehyde, Hexane/THF; iii) $\text{BF}_3 \cdot \text{OEt}_2$, DDQ, DCM.



Scheme 2-4. Synthesis of N4 (10) porphyrin. Reagents and conditions: i) TFA, DDQ, DCM; ii) *p*-bromotoluene, *n*-BuLi, DDQ, Ether/THF.

These bromoporphyrins were further coupled with 4-ethynylbenzoic acid in tetrahydrofuran and triethylamine at room temperature through Sonogashira coupling in presence of tris(dibenzylideneacetone)dipalladium(0) and triphenylarsine to obtain the desired 4-ethynylbenzoic acid substituted porphyrins (14)-(16) in moderate yields. The downfield shifts of the β -pyrrolic protons and the inner NH in the heteroporphyrins **N3S** (15) and **N3O** (16) compared to **N4** porphyrin (14) confirms the core perturbation effect on porphyrin ring. The introduction of ethynyl bond between the porphyrin ring and the benzoic acid acceptor helps to maintain the planarity of the molecule assuring the effective electron coupling.



Scheme 2-5. Synthesis of N4, N3S and N3O porphyrin. Reagents and conditions: i) NBS, DCM, RT; ii) 4-Ethynylbenzoic acid, Pd(dba)₃, AsPh₃, THF, NEt₃, RT.

2.2.2 Optical Spectroscopy

The UV-Visible peak positions of the *Soret* and Q bands and the molar absorption coefficients (ϵ) of N4, N3S and N3O in THF are summarized in Table 2-1. The UV-Visible spectra of the

studied porphyrins as displayed in Figure 2-2 (a), show typical free base features, a strong *Soret* band around 450 nm and four weak Q bands around 520-700 nm. The core atom alteration results in slight red-shift in the *Soret* as well as Q bands extending the absorption maximum beyond 700 nm. The molar absorption coefficients of **N3S** thiaporphyrin and **N3O** oxaporphyrin are slightly higher than regular **N4** porphyrin.

Table 2-1. Optical and Electrochemical data of N4, N3S and N3O porphyrin in THF

Dye	$\lambda_{\text{abs}}/\text{nm}^a$ ($\epsilon/10^3\text{M}^{-1}\text{cm}^{-1}$)	$\lambda_{\text{em}}/\text{nm}^b$	Φ^c	E_{ox}/V^d	$E_{(0,0)}/\text{eV}^e$	$E_{\text{ox}}^*/\text{V}^f$
N4	433 (245), 534 (11), 575 (31), 610 (4.5), 668 (11)	673	0.11	0.93	1.85	-0.92
N3S	442 (257), 529 (17), 571 (37), 633 (5), 696 (9)	704	0.02	0.96	1.77	-0.81
N3O	436 (247), 525 (9), 565 (19), 629 (3), 691 (5)	695	0.06	0.97	1.79	-0.83

^aAbsorption maximum of porphyrins in THF. ^bEmission maximum measured in THF by exciting at *Soret* band. ^cRelative quantum yields of the porphyrins were calculated with reference to TPP ($\Phi = 0.11$ in toluene) ^doxidation potentials approximated from E_{ox}^* and $E_{(0,0)}$. ^e $E_{(0,0)}$ values were estimated from the intersection of the absorption and emission spectra. ^fFirst reduction potentials vs. NHE determined by Cyclic Voltammetry in THF and referenced to a ferrocene redox couple.^[13-15]

To obtain the absorption spectra of the thin film, the TiO₂ films with coating thickness of ~ 3 μm were immersed in THF solution of the porphyrins for 2 h at 40 °C and rinsed with THF to remove unadsorbed dye. The absorption spectra were recorded by reflectance measurements using an integrating sphere and shown in Figure 2-2 (b).

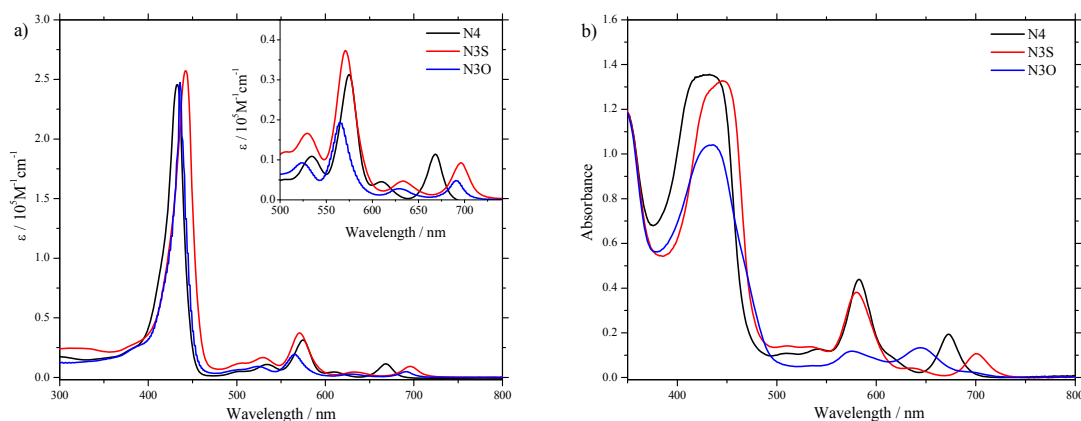


Figure 2-2. (a) UV-Visible spectra of N4, N3S and N3O in THF. Inset shows enlarged spectra for Q band region. (b) UV-Visible spectra of dyes/TiO₂ immersed in THF solution of porphyrins for 2 h. The thickness of the TiO₂ films is ~ 3 μm .

The examination on the *Soret* band region of spectra for dyes adsorbed on TiO₂ observed peak broadening for all compounds in comparison with the corresponding monomer spectra in THF, which reflects significant degree of *J*-aggregation on TiO₂.^[16-17] Noticeably, in the Q band region, the broadening of N3O/TiO₂ is more dramatic than that of N4/TiO₂ or N3S/TiO₂, which implies a higher degree of aggregation for **N3O** than **N4** and **N3S** porphyrins when adsorbed on TiO₂. The steady-state fluorescence spectra of all the core-modified porphyrins measured in THF by excitation at the *Soret* band wavelengths display the similar red-shifting as UV-Visible spectra (Figure 2-3). These bathochromic shifts in the absorption and emission spectra of heteroporphyrins may be attributed either to the structural distortion of porphyrin π -system or to the electronic effect of heteroatoms. From the density functional theory studies we observed negligible deviation from the planarity for the heteroporphyrins. Therefore the red-shifts in the absorption spectra are more likely caused by the electronic effects of the heteroatoms.^[18] We measured the relative quantum yields of all three porphyrins in THF with reference to the value of tetraphenylporphyrin (TPP) and the results are depicted in Table 2-1.

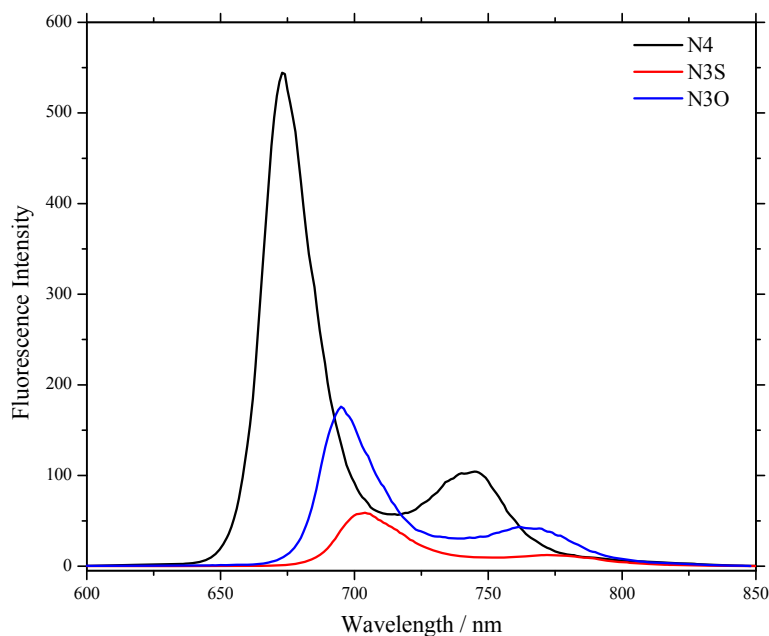


Figure 2-3. Fluorescence spectra of porphyrin dyes in THF.

The decreased quantum yields for **N3O** and **N3S** suggest that the non-radiative decay rates of the internal conversion or the intersystem crossing are much faster for the heteroporphyrins compared to the regular porphyrin **N4**. The much lower quantum yield for **N3S** than those of **N4** and **N3O** porphyrins indicates that the heavy atom effect of sulfur accelerates intersystem crossing rate.^[19]

2.2.3 Cyclic Voltammetry

The cyclic voltammetry measurements of the porphyrins were carried out in degassed THF containing 0.1 M [Bu₄N]PF₆ as the supporting electrolyte to obtain the first reduction potentials. The reduction couples of the studied porphyrins show reversible redox processes under a scan rate of 50 mV/sec and are stable over multiple scans. As depicted in Table 2-1, the reduction potential of the thiaporphyrin **N3S** (− 0.81 V vs NHE) shifts positively by 110 mV and the oxaporphyrin **N3O** (− 0.83 V vs NHE) is also positively shifts by 90 mV as compared to regular **N4** porphyrin (− 0.92 V vs NHE) making them easier to be reduced. The zero-zero excitation energies, $E_{(0,0)}$ were calculated from the intersection of the normalized absorption and emission spectra at the Q(0,0) band (Figure 2-4) and were found to be 1.85, 1.77 and 1.79 eV for N4, N3S and N3O porphyrins, respectively. The oxidation potentials were estimated from the reduction potentials and the zero-zero excitation energies and are listed in Table 2-1.

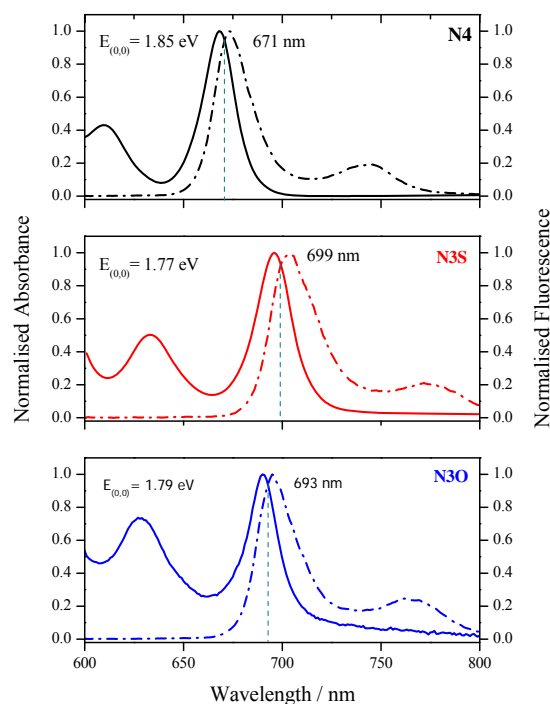


Figure 2-4. Normalized absorption (solid lines) and fluorescence (dash-dot lines) spectra in THF. The intersection wavelength is calculated for $E_{(0,0)}$ which is equal to $1240/\lambda$ nm.

The energy level diagram for these porphyrins as displayed in the Figure 2-5. As shown in the figure, the LUMOs of the porphyrins are more negative than the TiO₂ conduction band and thus ensure the enough driving force for the electron injection from LUMO energy level of the

dye to the TiO₂ conduction band. The HOMOs of all the porphyrins are more positive than the redox electrolyte which confirm the efficient dye regeneration.

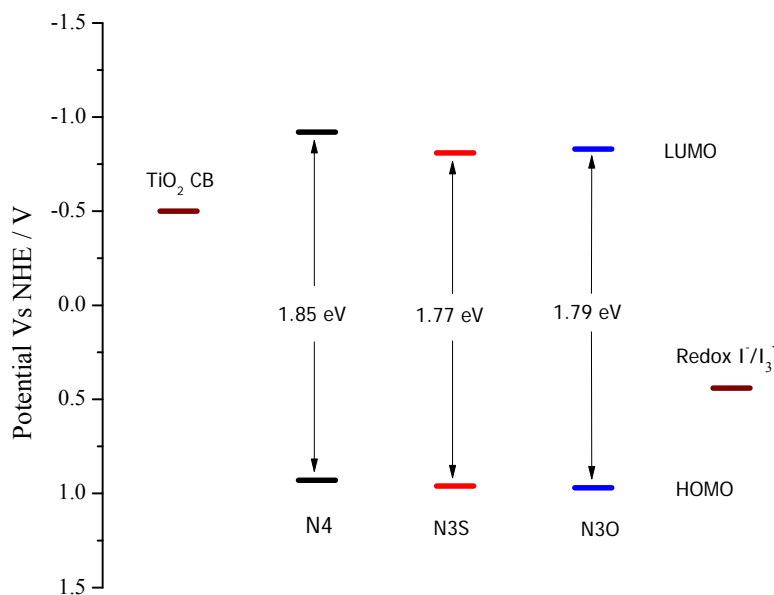


Figure 2-5. Energy level diagram for porphyrin dyes under study.

2.2.4 DFT Calculations

To correlate the molecular structures of the dyes with the performance of DSSCs, DFT as well as TD-DFT calculations were carried out. The results from quantum chemical calculations show planar macrocycles for all the porphyrins as shown in Figure 2-6. In HOMO of all the porphyrins, the majority of the electron density is localized on the porphyrin ring however a small portion is also extended over the ethynylphenyl group, while in the LUMO the electron density is populated equally on the porphyrin ring and the ethynylbenzoic acid. The increased electron density populating on the anchoring group in the LUMO facilitates efficient charge transfer from the excited state of the porphyrins to the TiO₂ conduction band. Interestingly in the LUMO+2, the electron density is extensively located on the ethynylbenzoic acid acceptor suggesting that the electron injection from higher excited states involving LUMO+2 might be more efficient than LUMO. It is evident from TD-DFT calculations that the calculated wavelengths registered in Table 2-2 are in good agreement with the experimental values. Pointedly the dipole moments obtained from calculations for the studied porphyrins are in order, **N4** > **N3S** > **N3O**. This trend is similar with the overall photon-to-current conversion efficiencies of these porphyrins. The higher polarizability is advantageous to facilitate intramolecular photoinduced electron transfer.

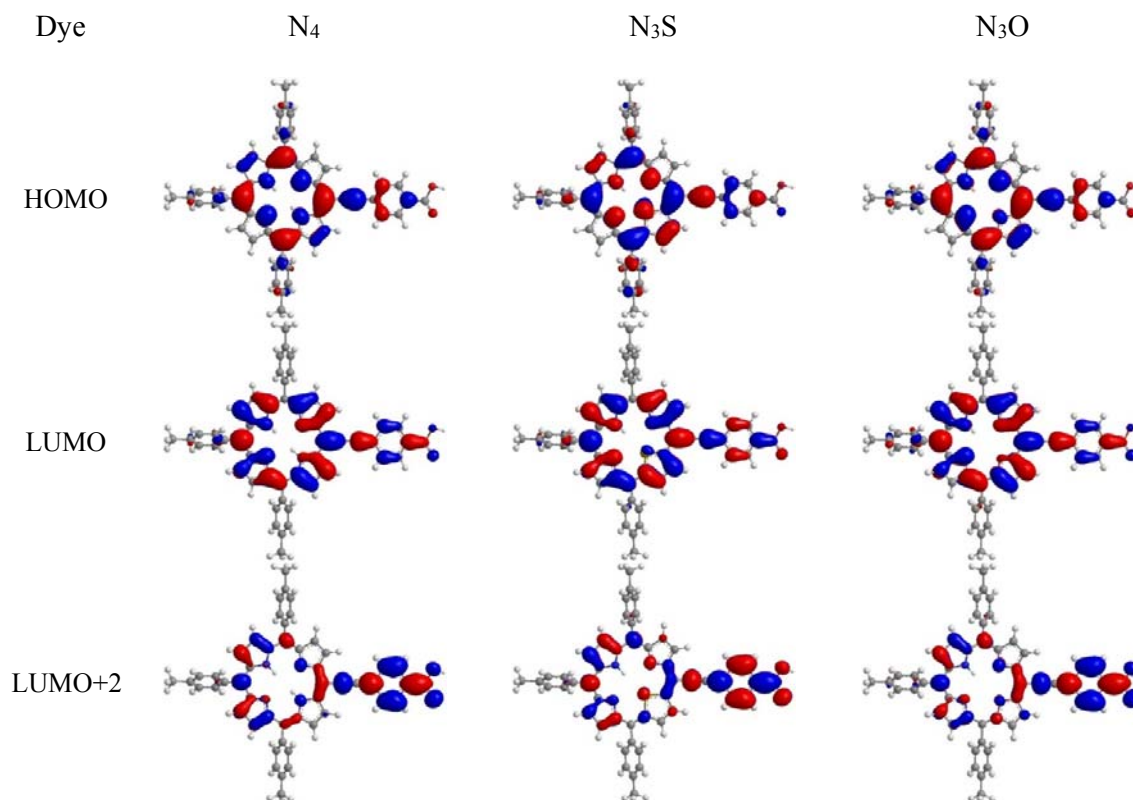


Figure 2-6. Molecular orbital diagrams of N4, N3S and N3O obtained from DFT calculations.

Table 2-2. Calculated TD-DFT composition in terms of frontier molecular orbitals, excitation energy, and the oscillator strengths of N4, N3S, and N3O.

Dyes	State	Composition (%)	E (eV)	λ (nm)	f	D(Debye)
N4	S1	H-1→L (12)	2.05	603.18	0.2321	4.72
		H-1→L+1 (12)				
		H→L (53)				
		H→L+1 (22)				
S2	S2	H-1→L (24)	2.20	563.23	0.2144	
		H-1→L+1 (6)				
		H→L (29)				
		H→L+1 (41)				
S3	S3	H-1→L+1 (37)	2.97	417.78	1.1369	
		H→L (9)				
		H→L+2 (46)				
S4	S4	H-2→L (59)	3.19	388.66	0.2144	
		H-1→L+1 (8)				
		H→L+2 (17)				
N3S	S1	H-1→L (13)	1.99	620.08	0.1509	4.57
		H-1→L+1 (11)				
		H→L (46)				

		H→L+1 (28)				
	S2	H-1→L (20)	2.18	567.41	0.276	
		H-1→L+1 (7)				
		H→L (35)				
		H→L+1 (37)				
	S3	H-4→L (10)	2.91	425.58	0.9903	
		H-1→L+1 (42)				
		H→L (9)				
		H→L+2 (24)				
	S4	H-4→L (59)	3.13	396.39	0.3169	
		H-2→L (24)				
N3O	S1	H-1→L (16)	2.02	613.44	0.1412	4.04
		H-1→L+1 (9)				
		H→L (39)				
		H→L+1 (34)				
	S2	H-1→L (18)	2.19	565.7	0.2903	
		H-1→L+1 (9)				
		H→L (42)				
		H→L+1 (30)				
	S3	H-3→L (6)	2.94	422.15	1.0362	
		H-1→L (9)				
		H-1→L+1 (38)				
		H→L (7)				
		H→L+2 (30)				
	S4	H-4→L (10)	3.11	398.48	0.0522	
		H-2→L (56)				
		H-2→L+1 (22)				

H=HOMO, L=LUMO, H-1=HOMO-1, H-2=HOMO-2, H-3=HOMO-3, H-4=HOMO-4
L+1=LUMO+1, L+2=LUMO+2.

2.2.5 Dye Loading Measurements

To better comprehend the adsorption behavior and measure the amount of adsorbed dye, we performed the measurements of porphyrin densities (Γ) adsorbed on TiO₂ surface. The porphyrin densities (Γ) were determined by measuring the concentrations of the porphyrin solutions desorbed from the dye-coated TiO₂ films after being immersed in 0.1 M KOH solution in THF. The saturated Γ values of the porphyrins under study were found as 360 ± 30 , 180 ± 30 , and 62 ± 10 nmol cm⁻² for **N4**, **N3S** and **N3O** porphyrins, respectively. The dye loading values are consistent with the overall conversion efficiencies obtained for the studied porphyrins, reported below. We attribute the difference of dye loading to the different affinity of the dye to the TiO₂ surface. The oxaporphyrin which is more electron-rich porphyrin, might decrease the acidity of the carboxylic acid and decrease the affinity of **N3O** to TiO₂ surface.

2.2.6 Photovoltaic Measurements

DSSCs based on liquid electrolytes were fabricated using the porphyrins **N4**, **N3S** and **N3O** and tested under AM 1.5 conditions. The photovoltaic parameters for the porphyrins under study are summarized in Table 2-3 and the I-V curves of the devices assembled using the porphyrins and measured under standard AM 1.5 G simulated solar conditions are shown in Figure 2-7(a).

Table 2-3. Photovoltaic parameters of N4, N3S and N3O dyes

Dye	J_{sc} (mA cm ⁻²)	V_{oc} (V)	FF (%)	η (%)
N4	8.82	0.57	73	3.66
N3S	0.83	0.45	58	0.22
N3O	0.06	0.24	50	0.01

As seen from the I-V curves, the device using regular free-base porphyrin **N4** outperformed the heteroporphyrin-based devices. It obtained the highest efficiency of 3.66% with photocurrent density of 8.82 mA cm⁻², open-circuit voltage 0.57 V and fill factor 73%. The thiaporphyrin **N3S** gave the photocurrent density of 0.83 mA cm⁻², open-circuit voltage 0.45 V and fill factor 58%. The oxaporphyrin **N3O** obtained the photocurrent density of 0.06 mA cm⁻², the open-circuit voltage of 0.24 and fill factor 50. These parameters gained the overall conversion efficiencies of 0.22% for **N3S** and 0.01% for **N3O**. The enhanced non-radiative internal conversion or intersystem crossing for the heteroporphyrins compared to regular porphyrin might decrease the lifetimes of excited state and decrease the efficiency of electron injection from the dye molecules to the conduction bands of TiO₂. The heavy atom effect of sulfur atom which causes faster intersystem crossing rates can be the main reason for the low efficiency of **N3S**.^[20] The incident photon-to-current conversion efficiency spectra (Figure 2-7b) for all the porphyrins are in good agreement with the corresponding absorption spectra on TiO₂ which displays the characteristic intense absorption in the *Soret* region. The IPCE maximum for regular **N4** porphyrin is found to be 50% in between 400-500 nm region and those for **N3S** and **N3O** are found to be 12% and less than 1%, respectively. The IPCE values for **N4** porphyrins are noticeable in the Q band region while those for **N3S** are surprisingly small and for **N3O** it is almost negligible in the Q band region. With this insignificant IPCE values, the minute performance of oxaporphyrin is understandable. The I-V curves under standard AM 1.5 G illumination are in qualitative agreement with the photo-action spectra.

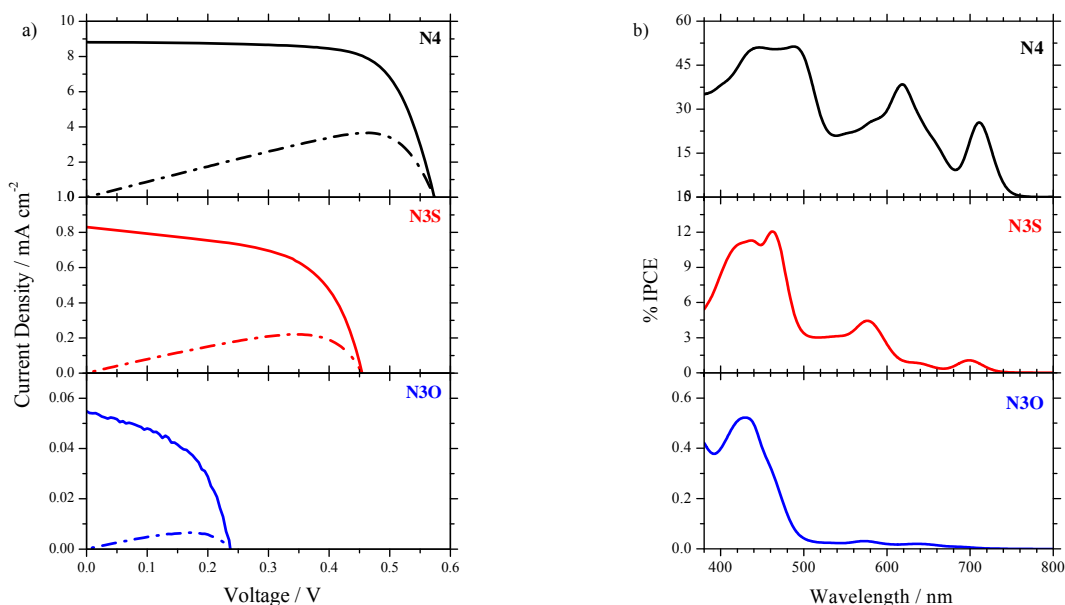


Figure 2-7. (a) I-V curves and (b) IPCE spectra of the DSSCs fabricated with N4, N3S and N3O.

2.2.7 TCSPC Measurements

As shown in Figure 2-8, the time-correlated single photon counting (TCSPC) data of **N4**, **N3O** and **N3S** adsorbed on Al₂O₃ or TiO₂ films allow the study of excited state lifetimes when these dyes were excited at Q(0,0) bands. Because of the complicated relaxation processes at the excited state, the lifetimes have been deconvoluted into two or three components using an iterative non-linear deconvolution fitting method and the mean lifetimes (τ_{av}), as shown in Table 2-4, are obtained from the weighted average of τ_1 and τ_2 , two main decaying components present in the data of all dyes. The mean relaxation lifetime of **N4** on non-injecting Al₂O₃ film is similar to that of **N3S**, and is longer than that of **N3O**.

Table 2-4. Fluorescence lifetimes and their fractional weights (A_i , normalized to 100%) of emission decays of porphyrin dyes adsorbed on either Al₂O₃ or TiO₂

Dye	τ_1 /ns (A_1 %)	τ_2 /ns (A_2 %)	τ_3 /ns (A_3 %)	Average (τ_{av} /ns) ¹
N4/TiO ₂	0.194(91)	0.522(9)	-	0.223
N4/Al ₂ O ₃	0.275(71)	0.87(25)	2.258(4%)	0.413
N3S/TiO ₂	0.234(85)	0.606(15)	-	0.290
N3S/Al ₂ O ₃	0.354(87)	0.894(13)	-	0.424
N3O/TiO ₂	0.08(96)	0.465(3)	1.534(1%)	0.091
N3O/Al ₂ O ₃	0.12(95)	0.697(4)	3.216(1%)	0.142

¹ Average = ($\tau_1 \times A_1\%$) + ($\tau_2 \times A_2\%$)

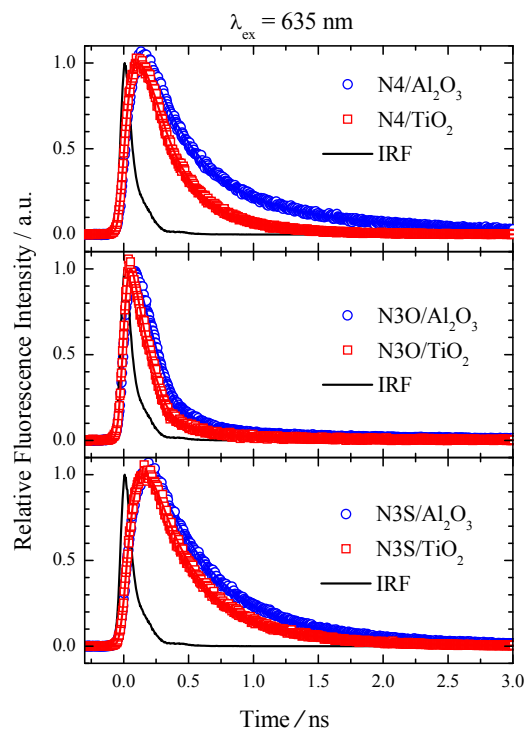


Figure 2-8. Picosecond fluorescence transients of the porphyrin sensitizers adsorbed on either TiO₂ or Al₂O₃; the fitted lifetimes are summarized in Table 2-4 (The black curve is instrument response function from picosecond laser source).

The short excited lifetime for **N30** on AlO₃ implies an extremely fast internal conversion and/or intermolecular energy transfer processes caused by dye-aggregations. As expected the fast electron injections into the TiO₂ conduction band after the photo-excitation significantly decrease the fluorescence lifetimes for the dyes adsorbed on TiO₂ films and the relative lifetimes reflect the efficiencies of electron injection. It is interesting to note that the difference of fluorescence transients between TiO₂ and Al₂O₃ are more obvious for **N4** than for **N30** and **N3S**. The intrinsic rapid fluorescence quenching of **N30** as observed on Al₂O₃ film leads to near static lifetimes between **N30** adsorbed on TiO₂ and Al₂O₃. Overall, the TCSPC data agree with the trend of efficiencies of electron injection as **N4** > **N3S** >> **N30**.

2.3 Conclusion

In summary, three novel free-base porphyrin sensitizers **N4**, **N3S**, and **N3O** were synthesized by simple and short routes. It is observed that the alteration of the core atom by group 16 heteroatoms has significant effect on the photophysical as well as photovoltaic properties of the studied porphyrins. The UV-Visible spectrum of the heteroporphyrins suggest that core-atom modification results in bathochromic enhancement of the absorption bands with the absorption onset reaching the NIR region. The steady-state fluorescence spectra displays that the heteroatom substitution on one of the pyrrolic nitrogens results in faster internal conversion or intersystem crossing which accelerates the non-radiative decay rates. The I-V curves suggest that the photocurrent density and the open-circuit voltage decrease substantially in DSSCs using core-modified porphyrins as sensitizers. The overall conversion efficiencies of the devices display the order **N4** (3.66%) \gg **N3S** (0.22%) $>$ **N3O** (0.01%). Noticeably, although lower dye loading can decrease the photo-current of **N3O** based DSSC, the fluorescence lifetimes suggest that poor electron injection caused by rapid excited-state relaxation is the main reason for the poor performance of **N3O** dye.

2.4 Experimental Section

2.4.1 General Techniques and Materials

All chemicals were obtained from commercial sources and used without further purification. All the reactions were carried out under nitrogen atmosphere. Solvents used in reactions were dried by PureSolv MD 5 system (Innovative Technology, Inc). Flash chromatography was carried out by using basic alumina (63-200 μm , Merck) and silica gel (40-63 μm , Merck). Analytical thin layer chromatography (TLC) was performed on Merck silica gel plates. ^1H and ^{13}C NMR spectra were recorded on a Bruker Avance 400 FT spectrometer. NMR samples were prepared in CDCl_3 and THF as *d*-solvents and chemical shifts were reported in δ scale. The standard abbreviations s, d, t, q, m and bs refer to singlet, doublet, triplet, quartet, multiplet and broad singlet respectively. Coupling constant (*J*) values are reported in Hertz (Hz). The ESI ion trap mass spectra were measured by a Finnigan MAT LCQ mass spectrometer. The HR-FAB spectra were conducted on a JMS-700 double focusing mass spectrometer. Transmittance and reflection UV-visible absorption spectra of the porphyrins in THF and adsorbed on TiO_2 electrodes, were recorded on a JASCO V-670 UV-vis/NIR spectrophotometer. Steady-state fluorescence spectra were acquired by using a Varian Cary Eclipse fluorescence spectrophotometer. The cyclic voltammetry measurements of the porphyrins were carried out on CHI 621B electrochemical analyzer (CH Instruments, Austin, TX, USA) in degassed THF containing 0.1 M tetrabutylammonium hexafluorophosphate (Bu_4NPF_6) as the supporting electrolyte. The cell assembly consists of a glossy carbon as the working electrode, a silver wire as the pseudo-reference electrode, and a platinum wire as the auxiliary electrode. The scan rate for all measurements was fixed at 50 mV/sec. A ferrocene^{+1/0} redox couple was used as the internal standard and the potential values obtained in reference to the silver electrode were converted to the vacuum scale. The density functional theory (DFT) and time-dependent density functional (TD-DFT) calculations were performed with Gaussian 09 package to study the electron distribution of the frontier molecular orbitals and the photoexcitation transitions. All ground state geometries of studied porphyrins were optimized in the gas phase by the hybrid B3LYP functional and the 6-31G basis set, and the TD-DFT calculation were based on the same functional and basis set. The molecular orbitals were visualized by the Chemoffice software.

2.4.2 Syntheses

2-(α -Hydroxymethyl)thiophene (3): 2-thiophenecarboxaldehyde (1) (5 ml, 53.50 mmol) was dissolved in 40 ml of distilled methanol in 250 ml round-bottomed flask. After stirring at 0 °C for 10 min, NaBH₄ (2.84 g, 74.90 mmol) was added very slowly and the stirring was continued for 15 min. Reaction progress was monitored by TLC. After the reaction was complete, reaction mixture washed with water and dichloromethane. The solvent was removed on a rotary evaporator to collect the mono-ol (3) as a yellow oil (4.15 g, 68%). ¹H NMR (400 MHz, CDCl₃) δ : 2.15 (s, 1H, OH), 4.81 (s, 2H, CH₂), 6.99 (m, 2H, thiophene) 7.28 (m, 1H, thiophene) ppm.

2-(α -Hydroxymethyl)furan (4): The reduction of 2-furancarboxaldehyde (2) (5.1 ml, 59.84 mmol) with NaBH₄ (3.18 g, 83.77 mmol) under the same experimental conditions as for (3) gave the furan mono-ol (4) as yellow oil (4.11 g, 70%). ¹H NMR (400 MHz, CDCl₃) δ : 2.81 (s, 1H, OH), 4.56 (s, 2H, CH₂), 6.26 (d, J = 2.97 Hz, 1H, furan), 6.32 (m, 1H, furan), 7.38 (d, J = 1.32 Hz, 1H, furan) ppm.

2-(Hydroxymethyl)-5-(hydroxy(*p*-tolyl)methyl)thiophene (5): Anhydrous hexane (40 ml) was added to a 250 ml three-necked round-bottomed flask equipped with rubber septum, gas inlet and gas outlet tube. A positive pressure of N₂ was maintained and after purging N₂ gas for 5 min, TMEDA (5.9 ml, 39.42 mmol) and *n*-BuLi (24.6 ml of 1.6 M solution in hexane) were added sequentially to the stirring solution at 0 °C. The mono-ol (3) (2 ml, 15.77 mmol) was then added and the solution was stirred at 0 °C for 1 h. An ice cold solution of *p*-tolualdehyde (4.6 ml, 39.42 mmol) in dry THF (20 ml) was then added to the stirring solution. The resulting reaction mixture was stirred at 0 °C for 15 min and then brought up to room temperature. The reaction was quenched by adding cold saturated NH₄Cl solution (50 ml). The organic layer was washed with brine and dried over anhydrous MgSO₄. The solvent was removed on a rotary evaporator under reduced pressure to afford the crude compound. TLC analysis showed three spots corresponding to the unreacted *p*-tolualdehyde, mono-ol (3) and the desired diol (5). The crude product was further purified by silica gel column chromatography (eluent: 25% ethyl acetate in hexanes) to collect desired diol (5) as white solid (1.5 g, 41%). ¹H NMR (400 MHz, CDCl₃) δ : 1.85 (s, 1H, OH), 2.35 (s, 3H, CH₃), 2.48 (s, 1H, OH), 4.73 (s, 2H, CH₂), 5.96 (s, 1H, *meso*), 6.74 (dd, J = 1.4 Hz, 1H, thiophene), 6.82 (d, J = 3.5 Hz, 1H, thiophene), 7.17 (d, J = 7.92 Hz, 2H, *m*-tolyl), 7.32 (d, J = 8.04 Hz, 2H, *o*-tolyl) ppm; ¹³C NMR (100 MHz, CDCl₃) δ : 21.14, 60.18, 72.41, 124.47, 125.06, 126.18, 129.22, 137.82, 140.07, 143.87, 148.66 ppm.

2-(Hydroxymethyl)-5-(hydroxy(*p*-tolyl)methyl)furan (6): In a three necked 250 ml round-bottomed flask, the furan mono-ol (4) (2 ml, 23.14 mmol) in dry hexane (30 ml) was treated with *p*-tolualdehyde (6.8 ml, 57.85 mmol) in the presence *n*-BuLi (36 ml of 1.6 M solution in hexane) of TMEDA (8.7 ml, 57.85 mmol) under the same experimental conditions as for (5) to afford the furan-diol (6) as a yellow solid (2.1 g, 42%). ¹H NMR (400 MHz, CDCl₃) δ: 2.32 (s, 3H, CH₃), 2.82 (s, 1H, OH), 3.28 (s, 1H, OH), 4.46 (s, 2H, CH₂), 5.68 (s, 1H, *meso*), 5.94 (d, *J* = 3.24 Hz, 1H, furan), 6.13 (d, *J* = 3.18 Hz, 1H, furan), 7.13 (d, *J* = 8.04 Hz, 2H, *m*-tolyl), 7.26 (d, *J* = 8.07 Hz, 2H, *o*-tolyl) ppm; ¹³C NMR (100 MHz, CDCl₃) δ: 21.18, 57.28, 69.85, 108.19, 108.34, 126.6, 129.12, 137.74, 153.93, 156.18 ppm.

10,15,20-Tris(*p*-tolyl)-21-thiaporphyrin (7): In a 250 ml one-necked round-bottomed flask fitted with a N₂ gas bubbler, a solution of the thiophene diol (5) (335 mg, 1.43 mmol), pyrrole (320 μl, 4.70 mmol) and *p*-tolualdehyde (350 μl, 2.91 mmol) in DCM (150 ml) was taken. Resulting reaction mixture was purged with N₂ for 15 min and then a catalytic amount of BF₃•OEt₂ (100 μl) was added at room temperature. After stirring for 1 h, DDQ (240 mg, 1.07 mmol) was added and the reaction mixture was stirred at room temperature in air for 1 h. The solvent was removed on a rotary evaporator. The crude product was purified by silica gel column chromatography using Hexanes/DCM (1:1) as eluent to afford the desired porphyrin (7) as purple solid. (62 mg, 7%). ¹H NMR (400 MHz, CDCl₃) δ: -2.82 (s, 1H, NH), 2.72 (s, 9H, CH₃), 7.54-7.67 (m, 6H, *m*-tolyl), 8.07-8.19 (m, 6H, *o*-tolyl), 8.64 (d, 1H, *J* = 4.44 Hz; β-pyrrole), 8.74 (m, 2H, β-pyrrole), 8.99 (s, 2H, β-pyrrole), 9.05 (d, 1H, *J* = 4.32 Hz; β-pyrrole), 9.89 (d, 1H, *J* = 5.12 Hz; β-thiophene), 10.02 (d, 1H, *J* = 5.04 Hz; β-thiophene), 10.67 (s, 1H, *meso*) ppm; HRMS-ESI: *m/z* calcd for C₄₁H₃₂N₃S: 598.2317, found 598.2318 [M+H]⁺.

10,15,20-Tris(*p*-tolyl)-21-oxaporphyrin (8): In a 250 ml one-necked round-bottomed flask fitted with a N₂ gas bubbler, a solution of the furandiol (500 mg, 2.29 mmol), pyrrole (500 μl, 7.31 mmol) and *p*-tolualdehyde (590 μl, 5.06 mmol) in DCM (200 ml) was taken. After purging with N₂ for 15 min, condensation of the diol, aldehyde and pyrrole was initiated at room temperature by addition of a catalytic amount of BF₃•OEt₂ (60 μl, 0.23 mmol). After stirring for 1 h, DDQ (520 mg, 2.32 mmol) was added and the reaction mixture was stirred at room temperature in air for an additional hour. The solvent was removed on a rotary evaporator. The crude product was purified by basic alumina column chromatography using Hexanes/DCM (1:1) and then DCM as eluent to afford a purple solid (67 mg, 5%). ¹H NMR (400 MHz, CDCl₃) δ: 2.74 (s, 9H, CH₃), 7.60 (m, 6H, *m*-tolyl), 8.12 (m, 6H, *o*-tolyl), 8.68 (d, 1H, β-pyrrole), 8.89 (s, 1H, β-pyrrole), 8.95 (d, 2H, β-pyrrole), 9.15 (s, 1H, β-pyrrole), 9.39 (s, 1H, β-furan), 9.71

(s, 1H, β -furan), 10.17 (s, 1H, *meso*) ppm; HRMS-ESI: m/z calcd for $C_{41}H_{32}N_3O$: 582.2545, found 582.2542 $[M+H]^+$.

5,15-Bis(*p*-tolyl)porphyrin (9): A solution of dipyrromethane (500 mg, 3.42 mmol) and *p*-tolualdehyde (403 μ l, 3.42 mmol) in DCM (350 ml) was stirred for 3 h under N_2 in the presence of TFA (153 μ l, 0.6 mmol). The reaction mixture was quenched by the addition of DDQ (1.56g, 2.05 mmol) and stirring continued for 0.5 h. The mixture was neutralized with triethylamine (NEt_3) and passed through a short silica column. The solvent was removed under pressure to give the title compound (9) as a purple solid (817 mg, 48%). 1H NMR (400 MHz, $CDCl_3$) δ : -3.09 (s, 2H, NH), 2.74 (s, 6H, CH_3), 7.62 (d, 4H, $J = 7.76$ Hz; *m*-tolyl), 8.16 (m, 6H, $J = 7.84$ Hz; *o*-tolyl), 9.11 (d, 4H, $J = 4.52$ Hz; β -pyrrole), 9.39 (d, 4H, $J = 4.56$ Hz; β -pyrrole), 10.31 (s, 2H, *meso*) ppm.

10,15,20-Tris(*p*-tolyl)porphyrin (10): A 1L 3-necked round bottom flask was charged with *p*-bromotoluene (5 g, 29.25 mmol, 14 equiv.) in dry diethyl ether (100 ml) under N_2 . *n*-Butyllithium (14 ml, 35.1 mmol, 17.2 equiv.) was added slowly at -70 $^{\circ}C$ over 30 min. After the addition was complete, the reaction mixture was warmed up to -20 $^{\circ}C$ and was stirred for 1 h (color change to white). Next, 5,15-bis(4-methylphenyl)porphyrin (1 g, 2.04 mmol, 1 equiv.) dissolved in THF (50 ml) was cannulated to the reaction mixture at -20 $^{\circ}C$ under N_2 . The combined reaction mixture was warmed up to room temperature and stirred for 1 h (color change to brown), then water (5 ml, color change to emerald green) and DDQ (2.1 g, 9.25 mmol, 4 equiv.) were added (color change to red). After 1 h, the crude product was filtered through a layer of silica gel and recrystallized from DCM/MeOH. The desired porphyrin (10) was obtained as purple solid (1.08 g, 91%). 1H NMR (400 MHz, $CDCl_3$) δ : -2.95 (s, 2H, NH), 2.73 (s, 3H, CH_3), 2.74(s, 6H, CH_3), 7.58 (m, 6H, *m*-tolyl), 8.13 (m, 6H, *o*-tolyl), 8.92 (d, 2H, $J = 4.76$ Hz; β -pyrrole), 8.95 (d, 2H, $J = 4.8$ Hz; β -pyrrole), 9.05 (d, 2H, $J = 4.52$ Hz; β -pyrrole), 9.32 (d, 2H, $J = 4.56$ Hz; β -pyrrole), 10.12 (s, 1H, *meso*) ppm; HRMS-ESI: m/z calcd for $C_{41}H_{33}N_4$: 581.2705, found 581.2706 $[M+H]^+$.

10,15,20-tris(*p*-tolyl)-5-bromoporphyrin (11): To a stirred solution of 10,15,20-tris(*p*-tolyl)porphyrin (10) (200 mg, 0.34 mmol) in chloroform (50 ml) at room temperature, NBS (73 mg, 0.41 mmol) was added. The progress of the reaction was monitored by TLC and absorption spectroscopy. After complete consumption of the porphyrin as confirmed by TLC, the reaction was quenched with acetone (10 ml) and the solvent was removed on a rotary evaporator under vacuum. The crude reaction mixture was purified by silica gel column chromatography with Hexanes/DCM (70:30) as eluent and the pure bromoporphyrin were

obtained as a purple solid (157 mg, 70%). ^1H NMR (400 MHz, CDCl_3) δ : -2.74 (s, 2H, NH), 2.69 (s, 3H, CH_3), 2.71 (s, 6H, CH_3), 7.53-7.58 (m, 6H, *m*-tolyl), 8.05-8.08 (m, 6H, *o*-tolyl), 8.81 (s, 4H, β -pyrrole), 8.91 (d, 2H, $J = 4.7$ Hz, β -pyrrole), 9.65 (d, 2H, $J = 4.8$ Hz, β -pyrrole) ppm; HRMS-ESI: m/z calcd for $\text{C}_{41}\text{H}_{32}\text{N}_4\text{Br}$: 659.1810, found 659.1806 $[\text{M}+\text{H}]^+$.

5-Bromo-10,15,20-tris(*p*-tolyl)-21-thiaporphyrin (12): To a solution of thiaporphyrin (7) (137 mg, 0.23 mmol) in dry dichloromethane (25 ml) in a 50 ml round-bottomed flask was added NBS (49 mg, 0.28 mmol) at 0 °C and then the reaction mixture was stirred at room temperature for 30 min. The progress of the reaction was monitored by TLC. After complete consumption of the thiaporphyrin as confirmed by TLC, the reaction was quenched with acetone and the solvent was removed with a rotary evaporator under vacuum. The crude compound was subjected to silica gel column chromatography with Hexanes/DCM (2:1) as eluent and the desired bromoporphyrin (12) was afforded as a purple solid (118 mg, 77%). ^1H NMR (400 MHz, CDCl_3) δ : -2.59 (s, 1H, NH), 2.70 (s, 9H, CH_3), 7.52-7.65 (m, 6H, *m*-tolyl), 8.03-8.13 (m, 6H, *o*-tolyl), 8.58 (d, 1H, $J = 4.52$ Hz; β -pyrrole), 8.64 (m, 2H, β -pyrrole), 8.91 (d, 2H, $J = 1.80$ Hz; β -pyrrole), 9.30 (d, 1H, $J = 4.56$ Hz; β -pyrrole), 9.83 (d, 1H, $J = 5.24$ Hz; β -thiophene), 10.19 (d, 1H, $J = 5.28$ Hz; β -thiophene) ppm; HRMS-ESI: m/z calcd for $\text{C}_{41}\text{H}_{31}\text{BrN}_3\text{S}$: 676.1422, found 676.1417 $[\text{M}+\text{H}]^+$.

5-Bromo-10,15,20-tris(*p*-tolyl)-21-oxaporphyrin (13): To a solution of oxaporphyrin (8) (58 mg, 0.1 mmol) in dry dichloromethane (10 ml) in a 50 ml round-bottomed flask was added NBS (22 mg, 0.12 mmol) at 0 °C and then the reaction mixture was stirred at room temperature for 30 min. The progress of the reaction was monitored by TLC. After complete consumption of the oxaporphyrin as confirmed by TLC, the reaction was quenched with acetone and the solvent was removed with a rotary evaporator under vacuum. The crude compound was subjected to silica gel column chromatography with Acetone/DCM (1:9) as eluent and the desired bromoporphyrin (13) was afforded as purple solid (52 mg, 78%). ^1H NMR (400 MHz, CDCl_3) δ : 2.71 (m, 9H, CH_3), 7.54-7.58 (m, 6H, *m*-tolyl), 8.03-8.07 (m, 6H, *o*-tolyl), 8.52 (d, 1H, $J = 4.64$ Hz; β -pyrrole), 8.59 (d, 1H, $J = 4.64$ Hz; β -pyrrole), 8.70 (d, 1H, $J = 4.68$ Hz; β -pyrrole), 8.86 (s, 2H, β -pyrrole), 9.31 (d, 1H, $J = 4.88$ Hz; β -pyrrole), 9.51 (d, 1H, $J = 4.68$ Hz; β -furan), 10.06 (d, 1H, $J = 4.92$ Hz; β -furan) ppm; HRMS-ESI: m/z calcd for $\text{C}_{41}\text{H}_{31}\text{BrN}_3\text{O}$: 660.1650, found 660.1652 $[\text{M}+\text{H}]^+$.

5-(4-Ethynylbenzoic acid)-10,15,20-tris(*p*-tolyl) porphyrin (14) [N4]: A mixture of 4-ethynylbenzoic acid (55 mg, 0.38 mmol) and bromoporphyrin (11) (50 mg, 0.076 mmol) in dry THF (5 ml) and NEt_3 (5 ml) was degassed with N_2 for 10 min, and then $\text{Pd}_2(\text{dba})_3$ (27 mg, 0.03

mmol) and AsPh₃ (58 mg, 0.19 mmol) were added to the mixture. The solution was stirred at room temperature for 12 h under N₂. The solvent was removed in *vacuo*, and the residue was purified by silica gel column chromatography with DCM/methanol (9/1) as eluent to give purple solid (31 mg, 56%). Mp > 300°C; ¹H NMR (400 MHz, THF-*d*₈) δ: -2.22 (s, 2H, NH), 2.68 (s, 3H, CH₃), 2.71 (s, 6H, CH₃), 7.57-7.63 (m, 6H, *m*-tolyl), 8.04-8.11 (m, 6H, *o*-tolyl), 8.16 (d, 2H, *J* = 8.3 Hz, Ph), 8.24 (d, 2H, *J* = 8.4 Hz, Ph), 8.76 (s, 4H, β-pyrrole), 8.94 (d, 2H, *J* = 4.7 Hz, β-pyrrole), 9.78 (d, 2H, *J* = 4.7 Hz, β-pyrrole) ppm; IR (Neat, cm⁻¹): 3312, 1684, 1603, 1424, 1312, 1292, 1174, 965, 794; UV-vis (THF) λ_{max}/nm (ε / 10³ M⁻¹cm⁻¹) = 433 (245), 534 (11), 575 (31), 610 (4), 668 (11); HRMS-ESI: *m/z* calcd for C₅₀H₃₇N₄O₂: 725.2917, found 725.2919 [M+H]⁺.

5-(4-Ethynylbenzoic acid)-10,15,20-tris(*p*-tolyl)-21-thiaporphyrin (15) [N3S]:

Bromothiaporphyrin (12) (100 mg, 0.15 mmol), Pd₂(dba)₃ (55 mg, 0.06 mmol), AsPh₃ (113 mg, 0.37 mmol) and 4-ethynylbenzoic acid (26 mg, 0.18 mmol) were added to a 100 ml round bottom flask and it is attached to high vacuum for 30 min. Then N₂ was flushed for 15 min and dry THF (40 ml) and triethylamine (10 ml) were added. The reaction mixture was stirred under N₂ at room temperature until completion of the reaction as monitored by TLC. The solvent was removed under pressure and the crude product was purified by column chromatography using 5% methanol/DCM as eluent to afford the pure product as a purple solid (99 mg, 90%). Mp > 300°C; ¹H NMR (400 MHz, DMSO-*d*₆) δ: -2.31 (s, 1H, NH) 2.67 (s, 9H, CH₃), 7.61-7.74 (m, 6H, *m*-tolyl), 8.04-8.16 (m, 6H, *o*-tolyl), 8.19 (d, 2H, Ph), 8.27 (d, 2H, Ph), 8.46 (d, 1H, β-pyrrole), 8.58 (m, 2H, β-pyrrole), 8.90 (s, 2H, β-pyrrole), 9.44 (d, 1H, β-pyrrole), 9.84 (d, 1H, β-thiophene), 10.48 (d, 1H, β-thiophene) ppm; IR (Neat, cm⁻¹): 3326, 1684, 1603, 1429, 1313, 1293, 1176, 967, 795; UV-vis (THF) λ_{max}/nm (ε / 10³ M⁻¹cm⁻¹) = 442 (257), 529 (17), 571 (37), 633 (5), 696 (9); HRMS-ESI: *m/z* calcd for C₅₀H₃₆N₃O₂S: 742.2528, found 742.2535 [M+H]⁺.

5-(4-Ethynylbenzoic acid)-10,15,20-tris(*p*-tolyl)-21-oxaporphyrin (16) [N3O]: Bromo oxaporphyrin (13) (52 mg, 0.08 mmol), Pd₂(dba)₃ (28 mg, 0.03 mmol), AsPh₃ (60 mg, 0.19 mmol) and 4-ethynylbenzoic acid (17 mg, 0.12 mmol) were added to a 100 ml round bottom flask and the flask is attached to high vacuum for 30 min. Then N₂ was flushed for 15 min and dry THF (20 ml) and triethylamine (5 ml) were added. The reaction mixture was stirred under N₂ at room temperature until completion of the reaction as monitored by TLC. The solvent was removed under pressure and the crude product was purified by silica gel column chromatography using 5% methanol/DCM as eluent to afford the pure product as a purple solid (29 mg, 51%). Mp > 300°C; ¹H NMR (400 MHz, THF-*d*₈) δ: 2.69 (m, 9H, CH₃), 7.56-7.62 (m,

6H, *m*-tolyl), 8.01-8.17 (m, 6H, *o*-tolyl), 8.15 (d, 2H, $J = 8.20$ Hz; Ph), 8.24 (d, 2H, $J = 8.24$ Hz; Ph), 8.38 (d, 1H, $J = 4.60$ Hz; β -pyrrole), 8.44 (d, 2H, $J = 4.56$ Hz; β -pyrrole), 8.64 (d, 1H, $J = 4.60$ Hz; β -pyrrole), 8.78 (s, 2H, β -pyrrole), 9.32 (d, 1H, $J = 4.80$ Hz; β -pyrrole), 9.56 (d, 1H, $J = 4.56$ Hz; β -furan), 10.15 (d, 1H, $J = 4.76$ Hz; β -furan) ppm; IR (Neat, cm^{-1}): 3233, 1707, 1603, 1462, 1376, 1258, 1181, 967, 798; UV-vis (THF) $\lambda_{\text{max}}/\text{nm}$ ($\epsilon / 10^3 \text{ M}^{-1}\text{cm}^{-1}$) = 436 (247), 525 (9), 565 (19), 629 (3), 691 (5); HRMS-ESI: m/z calcd for $\text{C}_{50}\text{H}_{36}\text{N}_3\text{O}_3$: 726.2757, found 726.2759 $[\text{M}+\text{H}]^+$.

2.4.6 Photovoltaic Measurements

To characterize the photovoltaic performance of the DSSC devices, fluorine-doped tin oxide glass (FTO; 6-8 Ω/sq , Pilkington Tec-7, USA, thickness 2.2 mm) plates were washed with soap solution in an ultrasonic bath for 10 min, and then rinsed with deionized (DI) water and methanol. The FTO glass plates were immersed in 40 mM aqueous TiCl_4 at 70 $^\circ\text{C}$ for 30 min and washed with DI water and methanol. A transparent nanocrystalline layer was prepared on the FTO glass plate by repeated screen printing with TiO_2 paste (Solaronix, 15-20 nm Ti-Nanoxide T/SP), then drying for 2 h at room temperature. The TiO_2 electrodes were gradually heated at 110 $^\circ\text{C}$ for 1 h and 450 $^\circ\text{C}$ for 1 h. The resulting layer was composed of a ~ 11 μm thickness, measured by DekTak 15 stylus profiler. Finally a scattering layer containing >100 nm anatase particles (Solaronix, Ti-Nanoxide R/SP) was deposited by screen printing and then dried at room temperature for 2 h. The FTO glass plates were again immersed in 40 mM aqueous TiCl_4 at 70 $^\circ\text{C}$ for 30 min and washed with DI water and methanol. The TiO_2 electrodes were gradually heated at 110 $^\circ\text{C}$ for 1 h and 450 $^\circ\text{C}$ for 1 h. The porphyrin/ TiO_2 layer was served as a working electrode (anode). We immersed the TiO_2 coated FTO (TiO_2 active size $0.4 \times 0.4 \text{ cm}^2$) films in a THF solution of porphyrins ($1 \times 10^{-4} \text{ M}$) at 40 $^\circ\text{C}$ for 2 h. The FTO glass plate used as cathode was coated with Pt particles by using the thermal platinum nano-cluster catalyst method. The Pt catalyst was deposited from a precursor solution composed of 5 mM solution of hexachloroplatinic acid in anhydrous isopropanol. The precursor solution was spin-coated on FTO glass ($10 \text{ L}/\text{cm}^2$) and dried in air for 3 min. Coated Pt electrode was placed in an oven and temperature was gradually increased to 360 $^\circ\text{C}$ and kept under 360 $^\circ\text{C}$ for 15 min. To fabricate the DSSC device, two electrodes were assembled into a sandwich type cell. The thin layer of electrolyte was introduced into the space between two electrodes. A typical redox electrolyte contained lithium iodide (LiI, 0.1 M), diiodine (I_2 , 0.05 M), 1,2-dimethyl-3-propylimidazolium iodide (DMII, 0.5 M), and 0.5 M 4-tert-butylpyridine in dry acetonitrile. The photoelectrochemical characterizations of the solar cells were carried out by using an Oriel

Class-A solar simulator (Oriel 91195A, Newport Corp.). Photocurrent and voltage curves were recorded with a potentiostat/galvanostat (CHI 650B, CH Instruments, Inc., USA) at a light intensity of one-sun irradiation calibrated by the Oriel reference solar cell (Oriel 91150, Newport Corp.). The IPCE measurements were carried out with a monochromator (Oriel 74100) at short circuit condition.

2.4.7 TCSPC Measurements

Fluorescence transients were recorded with a time-correlated single photon counting (TCSPC) system (FluoTime 200, PicoQuant) with the picosecond laser source for excitation at $\lambda_{\text{ex}} = 635$ nm. The excitation pulse was focused onto a rotating sample holder with a lens. A lens collected emission emitted from the sample at a right angle. An iris attenuated the intensity of the detected signal; the polarization of the detected emission relative to the excitation laser pulse was set at 54.7° with a polarizer. A double monochromator of a subtractive type compensated the group-velocity dispersion of emission and selected the detection wavelength; the resolution was 8 nm with a slit of width 1 mm. A micro-channel plate photomultiplier was connected to a computer with a TCSPC-module card (SPC-630, Becker & Hickl GmbH) for data acquisition. The full width at half maximum (FWHM) of the instrument response function (IRF) was typically 80 ps, measured with scattered light at the laser excitation wavelength.

2.5 References

- [1] P. J. Chmielewski, L. Latos-Grażyński, *Coord. Chem. Rev.* **2005**, *249*, 2510-2533.
- [2] I. Gupta, M. Ravikanth, *Coord. Chem. Rev.* **2006**, *250*, 468-518.
- [3] L. Arnold, K. Müllen, *J. Porphyrins Phthalocyanines* **2011**, *15*, 757-779.
- [4] P. Ziółkowski, K. Symonowicz, P. Chmielewski, L. Latos-Grażyński, G. Streckyte, R. Rotomskis, J. Rabczyński, *J. Cancer Res Clin Oncol* **1999**, *125*, 563-568.
- [5] D. G. Hilmey, M. Abe, M. I. Nelen, C. E. Stilts, G. A. Baker, S. N. Baker, F. V. Bright, S. R. Davies, S. O. Gollnick, A. R. Oseroff, S. L. Gibson, R. Hilf, M. R. Detty, *J. Med. Chem.* **2001**, *45*, 449-461.
- [6] Y. You, S. L. Gibson, R. Hilf, S. R. Davies, A. R. Oseroff, I. Roy, T. Y. Ohulchanskyy, E. J. Bergey, M. R. Detty, *J. Med. Chem.* **2003**, *46*, 3734-3747.
- [7] Y. You, S. L. Gibson, R. Hilf, T. Y. Ohulchanskyy, M. R. Detty, *Biorg. Med. Chem.* **2005**, *13*, 2235-2251.
- [8] E. J. Ngen, T. S. Daniels, R. S. Murthy, M. R. Detty, Y. You, *Biorg. Med. Chem.* **2008**, *16*, 3171-3183.

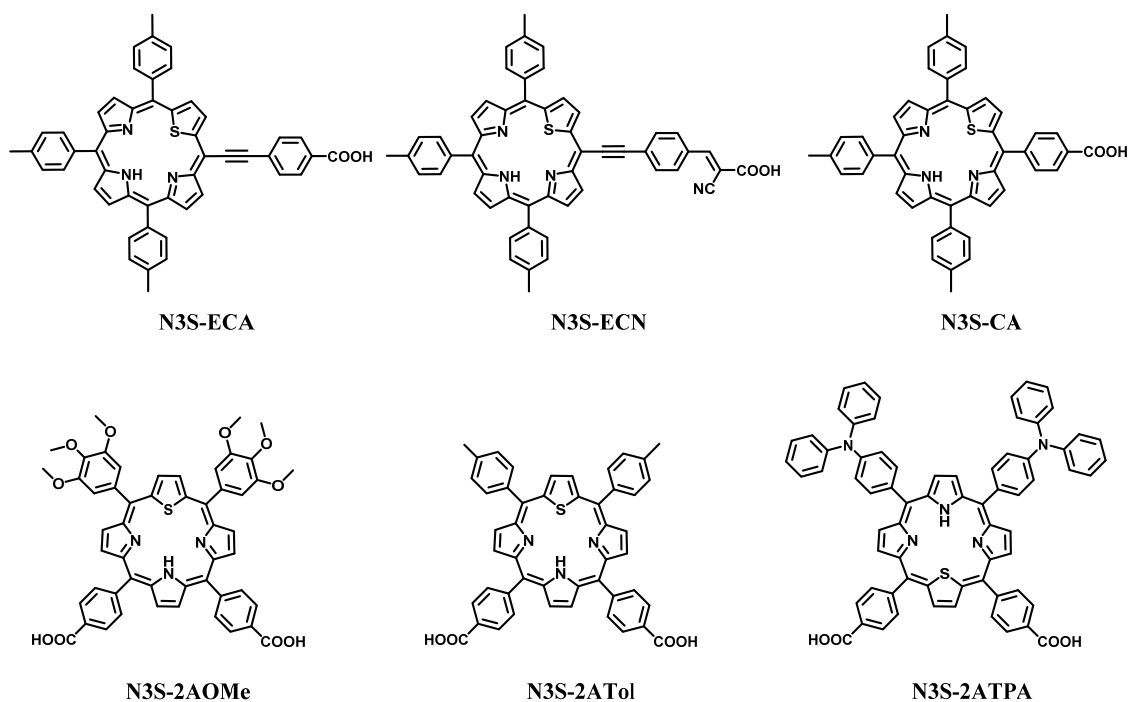
- [9] R. Minnes, H. Weitman, Y. You, M. R. Detty, B. Ehrenberg, *J. Phys. Chem. B* **2008**, *112*, 3268-3276.
- [10] Y. Xie, P. Joshi, M. Ropp, D. Galipeau, L. Zhang, H. Fong, Y. You, Q. Qiao, *J. Porphyrins Phthalocyanines* **2009**, *13*, 903-909.
- [11] T. Bessho, S. M. Zakeeruddin, C.-Y. Yeh, E. W.-G. Diau, M. Grätzel, *Angew. Chem. Int. Ed.* **2010**, *49*, 6646-6649.
- [12] A. Yella, H.-W. Lee, H. N. Tsao, C. Yi, A. K. Chandiran, M. K. Nazeeruddin, E. W.-G. Diau, C.-Y. Yeh, S. M. Zakeeruddin, M. Grätzel, *Science* **2011**, *334*, 629-634.
- [13] V. V. Pavlishchuk, A. W. Addison, *Inorg. Chim. Acta* **2000**, *298*, 97-102.
- [14] G. Boschloo, A. Hagfeldt, *Acc. Chem. Res.* **2009**, *42*, 1819-1826.
- [15] T. Daeneke, T.-H. Kwon, A. B. Holmes, N. W. Duffy, U. Bach, L. Spiccia, *Nat. Chem.* **2011**, *3*, 211-215.
- [16] C.-F. Lo, L. Luo, E. W.-G. Diau, I. J. Chang, C.-Y. Lin, *Chem. Commun.* **2006**, 1430-1432.
- [17] Y. Arai, H. Segawa, *Chem. Commun.* **2010**, *46*, 4279-4281.
- [18] L. Latos-Grazynski, *The Porphyrin Handbook Vol.2*, Academic Press, New York, 2010
- [19] J.-H. Ha, S. Ko, C.-H. Lee, W.-y. Lee, Y.-R. Kim, *Chem. Phys. Lett.* **2001**, *349*, 271-278.
- [20] R. Ambre, K.-B. Chen, C.-F. Yao, L. Luo, E. W.-G. Diau, C.-H. Hung, *J. Phys. Chem. C* **2012**, *116*, 11907-11916.

3. Synthesis of carboxylate functionalized A₃B and A₂B₂ thiaporphyrins and their application in dye-sensitized solar cells

3.1 Introduction

In the previous chapter, we have discussed the effects of the core atom modification on the efficiency of the porphyrins in DSSCs. We have shown that the π elongation through ethynylphenyl group at the *meso*-position of core-modified porphyrin is an effective approach to extend the absorption of the heteroporphyrin dyes towards the NIR region. Although, we obtained minute efficiencies for these heteroporphyrin sensitizers compared to the regular N4 porphyrins, this preliminary result will help us and other researchers to design the efficient heteroporphyrin sensitizers in DSSCs. Even though the efficiencies for the thiaporphyrin sensitizers are poorer than regular porphyrins, they have shown promise to some extent with efficiencies of 0.22% which are better than the reported efficiencies (0.19%) for thiaporphyrins in the literature.^[1] It is also evident from these results that, π elongation through ethynylphenyl group is beneficial for the heteroporphyrin sensitizers to achieve higher efficiencies.

In this chapter we concentrated our efforts to design and modify the structure of thiaporphyrins in order to improve their performance in DSSCs. For this purpose we prepared novel A₃B and A₂B₂ thiaporphyrins decorated by carboxyphenyl groups with various linker and acceptor groups as displayed in Scheme 3-1. In the A₃B type thiaporphyrins, we added electron withdrawing cyano group to the ethynylphenyl carboxyl linker *i.e.* **N3S-ECN** and directly attached a carboxyphenyl group at *meso*-position *i.e.* **N3S-CA** for comparison. In the A₂B₂ type of thiaporphyrins, we prepared porphyrins with two carboxyphenyl anchoring group to get the improved stability along with the efficiency. We compared performance of these thiaporphyrins with reference to **N3S-ECA**. It is evident from the UV-visible spectra that ethynylphenyl linker bathochromatically shifts the absorption spectra compared to the other dyes. With the support of photophysical and photovoltaic studies it is found that, although the dual anchoring groups can bind strongly to the TiO₂ surface, the presence of ethynylphenyl linker and moreover the electron withdrawing cyano group on anchor seems to be the pivotal factors to achieve higher efficiencies. Amongst the thiaporphyrins, **N3S-ECN** which has ethynylphenyl linker and cyanoacrylic acid as an anchor obtained the highest overall conversion efficiency of 1.69%, with $J_{sc} = 5.12 \text{ mA cm}^{-2}$, $V_{oc} = 0.49 \text{ V}$ and $FF = 67\%$.

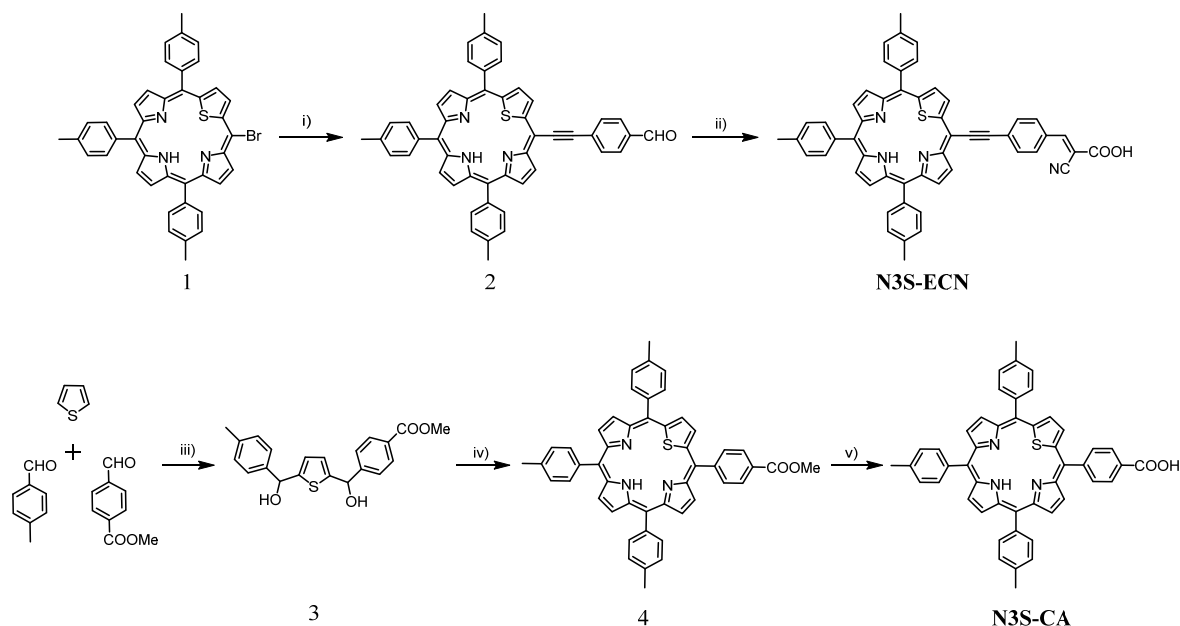


Scheme 3-1. Chemical structures of the A₃B and A₂B₂ Thiaporphyrin dyes.

3.2 Results and discussion

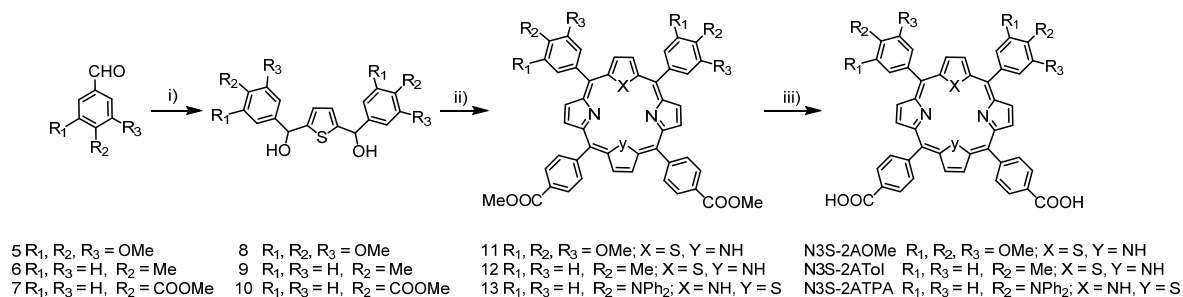
3.2.1 Synthesis

The A₃B thiaporphyrin dyes were synthesized according to the stepwise synthetic protocol depicted in Scheme 3-2. The synthesis of **N3S-ECA** was previously reported in Ch 1.^[2] **N3S-ECN** was prepared from N3S-Br (1) and 4-ethynylbenzaldehyde through Sonogashira coupling in the presence of a palladium catalyst. Compound (2) was further condensed with cyanoacetic acid following Knoevenagel protocol to obtain **N3S-ECN**. The presence of acrylic proton in the downfield region at 8.39 ppm in ¹H NMR spectrum of **N3S-ECN** confirmed the formation of cyano derivative. The presence of the cyano group is further confirmed by the presence of CN stretching frequency around 2224 cm⁻¹ in the IR spectrum. In order to prepare **N3S-CA**, thiophene was treated with *p*-tolualdehyde and methyl-4-formylbenzoate in presence of *n*-BuLi to get unsymmetrical diol (3) as shown in Scheme 3-2. The mixed condensation of this unsymmetrical diol (3) with *p*-tolualdehyde and pyrrole in the presence of boron trifluoride-diethyl etherate as a catalyst, followed by consequent oxidation by 2,3-dichloro-5,6-dicyanobenzoquinone (DDQ) gave monoester compound (4). This monoester compound (4) was further hydrolysed by aqueous solution of KOH to yield **N3S-CA**.



Scheme 3-2. Synthesis of A₃B thiaporphyrins. Reagents and conditions: i) 4-ethynylbenzaldehyde, Pd₂(dba)₃, AsPh₃, THF/NEt₃; ii) cyanoacetic acid, piperidine, CHCl₃; iii) *n*-BuLi, TMEDA, hexane/THF; iv) *p*-tolualdehyde, pyrrole, BF₃•OEt₂, DDQ, CH₂Cl₂; v) KOH_(aq), THF.

The A₂B₂ thiaporphyrin dyes were synthesized according to the stepwise synthetic protocol depicted in Scheme 3-3. Thiophene was treated with corresponding aldehydes in the presence of *n*-BuLi to get the desired symmetrical thiophene diols. The mixed-condensation of these symmetrical diols with appropriate aldehydes and pyrrole in the presence of borontrifluoride-diethyl etherate as catalyst, followed by subsequent oxidation by DDQ gave diester compounds.



Scheme 3-3. Synthesis of A₂B₂ thiaporphyrins. Reagents and conditions: i) Thiophene, *n*-BuLi, TMEDA, Hex/THF; ii) aldehyde, pyrrole, BF₃•OEt₂, DDQ, CH₂Cl₂; iii) KOH_(aq), THF.

The diester compounds were purified by column chromatography and the subsequent hydrolysis by KOH_(aq) yielded analytically pure thiaporphyrins. The carbonyl stretching peaks around 1680-1700 cm⁻¹ in the final carboxylic acid substituted compounds are slightly shifted to lower energy compared with their ester derivatives due to the intermolecular hydrogen bonding.

3.2.2 Optical Properties

The UV-Visible peak positions of the *Soret* and Q bands and the molar absorption coefficients (ϵ) of thiaporphyrins in THF are summarized in Table 3-1. The UV-Visible spectra of the studied porphyrins as displayed in Figure 3-1a, show typical free-base porphyrin features including a strong *Soret* band around 430 nm and four Q bands around 510-700 nm. The absorption wavelengths of these thiaporphyrins depend mainly on the nature of the substituents. The introduction of ethynylphenyl linker at a *meso*-carbon of the porphyrin ring significantly shifts the absorption wavelength towards low energy region as shown in **N3S-ECA** and **N3S-ECN** compared to **N3S-CA**. The UV-Visible spectrum of **N3S-ECN**, having a cyanoacrylic acid as the terminal anchoring group shows the largest red-shift in the *Soret* band as well as Q bands, extending the absorption onset beyond 700 nm. The electron donating triphenylamine substituents on *meso*-positions in **N3S-2ATPA** result in the broadening of *Soret* band as compared to **N3S-2ATol** and **N3S-2AOMe**. The extinction coefficient of **N3S-CA** is the highest amongst the thiaporphyrins. Although the extinction coefficient is not high for **N3S-ECN** and **N3S-2ATPA**, the IPCE might be compensated by the broadened absorption and increased electron injection resulting in a higher overall conversion efficiency. (*vide infra*)

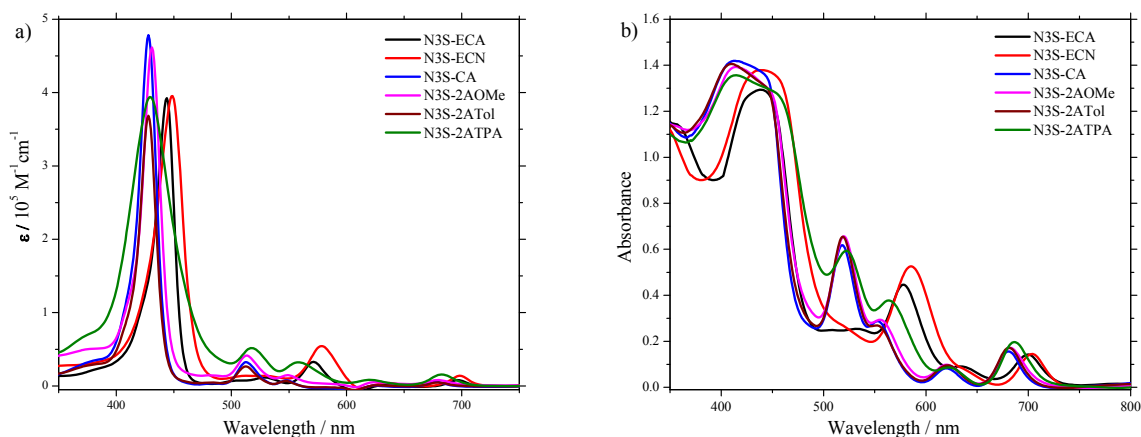


Figure 3-1. UV-Visible spectra of thiaporphyrin dyes a) in THF and b) adsorbed on TiO₂.

Table 3-1. Optical and Electrochemical data of thiaporphyrin dyes

Dye	$\lambda_{\text{abs}}/\text{nm}^a$ ($\epsilon/10^3\text{M}^{-1}\text{cm}^{-1}$)	$\lambda_{\text{em}}/\text{nm}^b$	E_{ox}/V^c	$E_{(0,0)}/\text{eV}^d$	$E_{\text{ox}}^*/\text{V}^e$
N3S-ECA	444 (393), 530 (13), 571 (34), 634 (3), 697 (9)	702 777	0.96	1.77	- 0.81
N3S-ECN	449 (396), 526 (15), 579 (55), 637 (5), 698(15)	705 779	0.97	1.77	- 0.80
N3S-CA	428 (504), 513 (35), 548 (9), 625 (1), 678 (7)	684 751	0.91	1.82	- 0.91
N3S-2AOMe	431 (438), 513 (39), 549 (14), 625 (5), 679(8)	688 755	0.94	1.81	- 0.87
N3S-2ATol	428 (369), 512 (28), 547 (8), 624 (2), 679 (6)	686 754	0.93	1.82	- 0.89
N3S-2ATPA	429 (394), 518 (52), 558 (32), 621 (8), 682 (16)	693 757	0.90	1.80	- 0.90

^aAbsorption maximum of porphyrins in THF. ^bEmission maximum measured in THF by exciting at *Soret* band. ^cOxidation potentials approximated from E_{ox}^* and $E_{(0,0)}$. ^d $E_{(0,0)}$ values were estimated from the intersection of the absorption and emission spectra. ^eFirst reduction potentials vs. NHE determined for A₃B by cyclic voltammetry and for A₂B₂ by square wave voltammetry in THF and referenced to a ferrocene redox couple.

The absorption spectra of these thiaporphyrins as thin films were studied to understand their adsorption behaviour on TiO₂. To obtain the absorption spectra on TiO₂ films, the films with thickness of approximately 3 μm were dipped in 0.1 mM THF solution of thiaporphyrins for 8 h at room temperature. The adsorption spectra were recorded by reflectance measurements using an integrated sphere and the results are displayed in Figure 3-1b. The spectra shows significant broadening and slightly red-shifts compared to its absorption spectrum in THF with threshold of absorption around 750 nm.^[3-4] Particularly, the UV-Visible spectrum of N3S-ECN/TiO₂ and N3S-2ATPA/TiO₂ shows obvious broadening and bathochromic shifts. This broadening in the UV-Visible spectra after adsorption on TiO₂ films suggest that higher charge collection is possible in Q band region which will ultimately help to attain higher efficiency when applied in DSSC. The steady-state fluorescence spectra of all the porphyrins were measured in THF by excitation at the *Soret* band and displayed in Figure 3-2. It exhibited a trend similar to the absorption spectra, with a significant redshift upon addition of ethynylphenyl linker. Not only the redshift but also higher fluorescence intensity of **N3S-ECA** and **N3S-ECN** suggests that the conjugation through ethynylphenyl linker is more effective than non ethynylphenyl linkers which might result in better electron communication between porphyrin core and the anchoring group.

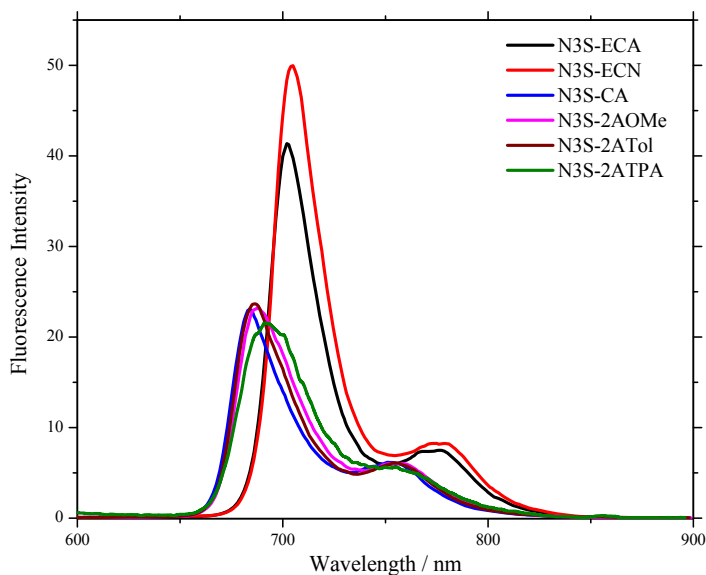


Figure 3-2. Fluorescence spectra of thiaporphyrin dyes in THF.

3.2.3 Electrochemical Properties

For the efficient electron injection into TiO₂ and faster regeneration of the oxidized dyes, appropriate tuning of HOMO with iodide/triiodide couple and the LUMO with TiO₂ conduction band is necessary. The cyclic voltammetry measurements of all the thiaporphyrins were carried out in degassed THF containing 0.1 M [Bu₄N]PF₆ as the supporting electrolyte to obtain the first reduction potentials as depicted in Figure 3-3.

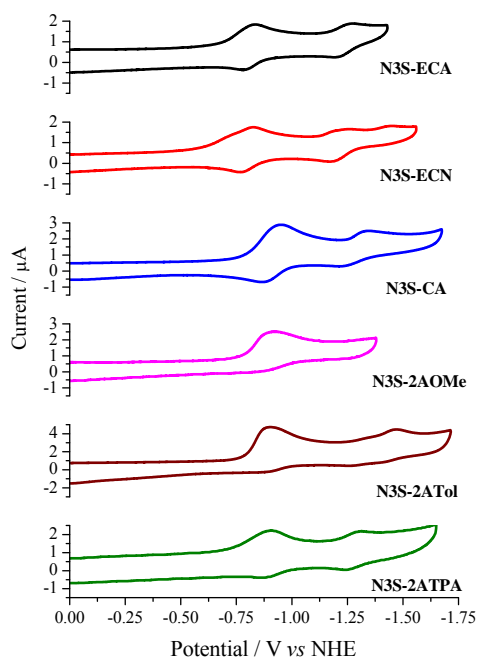


Figure 3-3. Cyclic Voltammograms of thiaporphyrin dyes in THF.

The first reduction couples of N3S-ECA, N3S-ECN and N3S-CA show quasi-reversible redox processes under a scan rate of 50 mV/s while irreversible processes of the first reduction couple were observed for thiaporphyrins with dual carboxyphenyl substituents, **N3S-2AOMe**, **N3S-2ATol** and **N3S-2ATPA**. The reduction potentials for thiaporphyrins with a meso ethynylphenyl substituent are less negative than the rest thiaporphyrins. The zero-zero excitation energies, $E_{(0,0)}$ were calculated from the intersection of the normalized absorption and emission spectra at the Q(0,0) band and were found to be 1.77, 1.77, 1.82, 1.81, 1.82 and 1.80 eV for **N3S-ECA**, **N3S-ECN**, **N3S-CA**, **N3S-2AOMe**, **N3S-2ATol** and **N3S-2ATPA** porphyrins, respectively. The oxidation potentials were estimated from the first reduction potentials and the $E_{(0,0)}$ and are listed in Table 3-1. The systematic energy level diagram for these thiaporphyrins is displayed in the Figure 3-4. As evident from the energy level diagram, the ethynylphenyl substitution results in the smaller HOMO and LUMO band gaps and consequently red-shifting the absorption, compared to those thiaporphyrins without an ethynylphenyl linkage. For A₂B₂ thiaporphyrins, the $E_{(0,0)}$ decreases with increasing electron donating ability of the thiaporphyrins. The LUMO of the thiaporphyrins are more negative than the TiO₂ conduction band (> 0.3 V) and thus ensure the adequate driving force for the electron injection from dye to the TiO₂ conduction band. The HOMO of all the porphyrins are more positive (> 0.5 V) than the redox electrolyte which confirms the efficient dye regeneration.

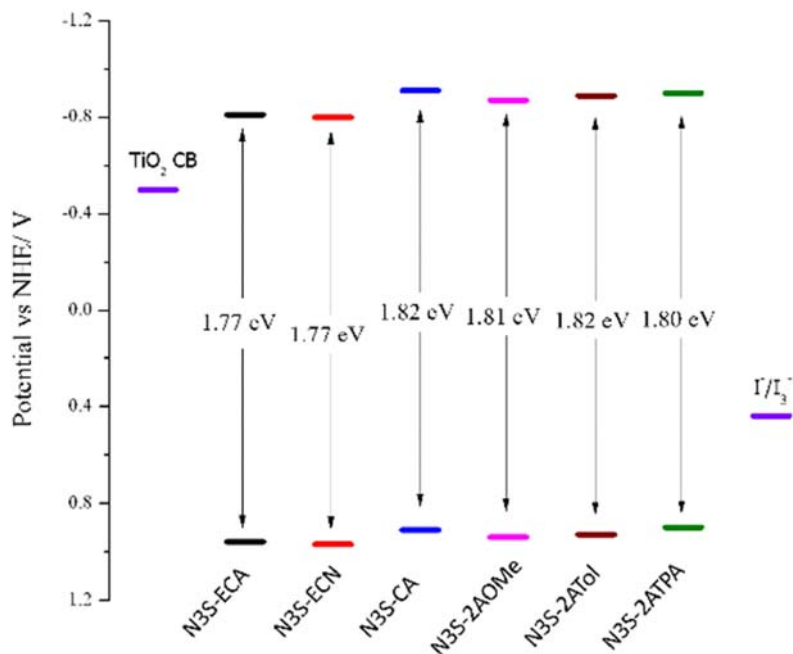


Figure 3-4. Energy level diagram for thiaporphyrin dyes under study.

3.2.4 DFT Calculations

The ground state geometries of studied thiaporphyrins were optimized in the gas phase by DFT calculations using the hybrid B3LYP functional and the 6-31G basis set. As presented in Figure 3-5, results from the quantum chemical calculations show planar macrocycles for the studied thiaporphyrins. The planar ring ensures the effective electron coupling between the porphyrin ring and the anchoring group. The HOMO-LUMO energy gaps for all the thiaporphyrins are consistent with the absorption energy obtained from UV-Visible spectra. In **N3S-ECA** and **N3S-ECN**, the majority of the π electron density is localized on the porphyrin ring however a small portion is also extended over the carboxylic anchoring group in HOMO. In the LUMO of **N3S-ECA**, the electron density is distributed equally on the porphyrin ring, the ethynylphenyl linker and carboxylic acid anchor. In the LUMO of **N3S-ECN**, more π electron density is localized on the ethynylphenyl linker and anchoring cyanoacrylic acid group than on the porphyrin core, which highlights the electron withdrawing effect of the cyano group.

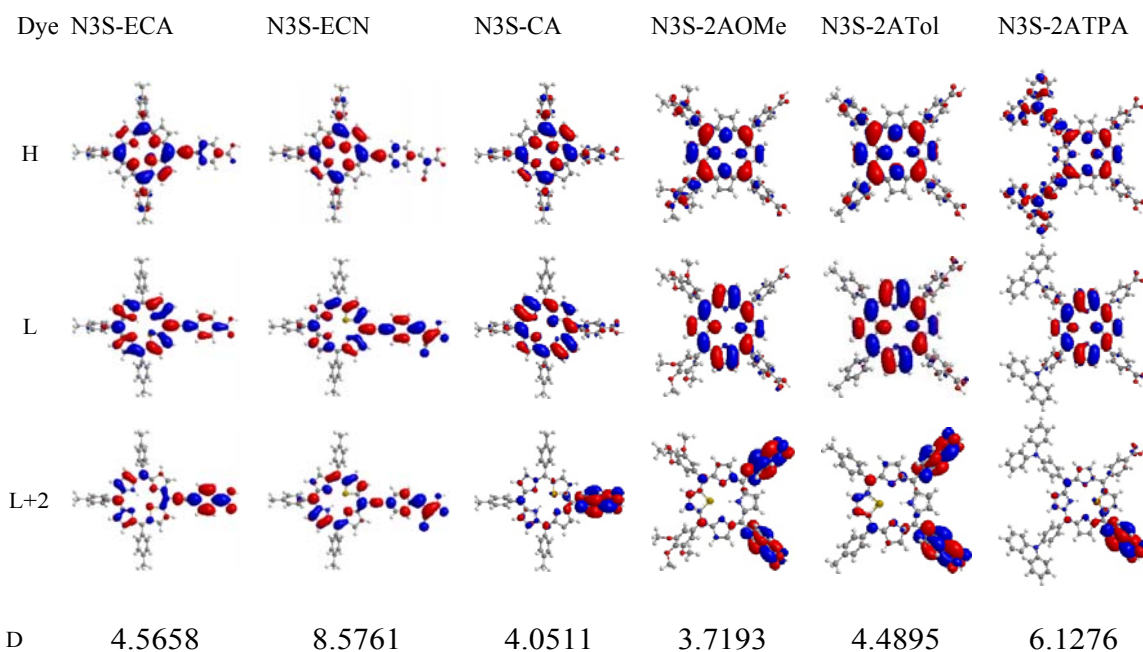


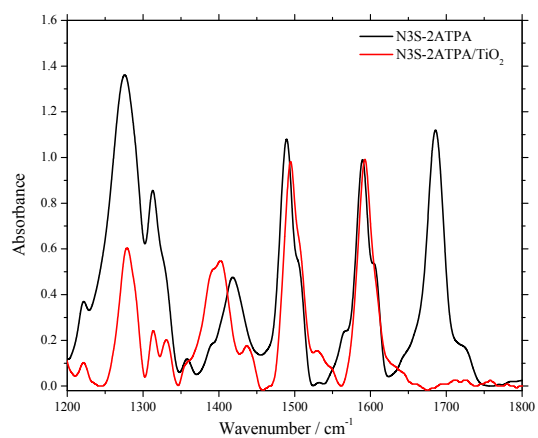
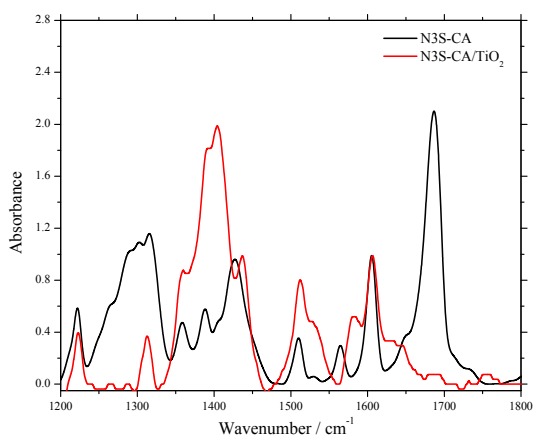
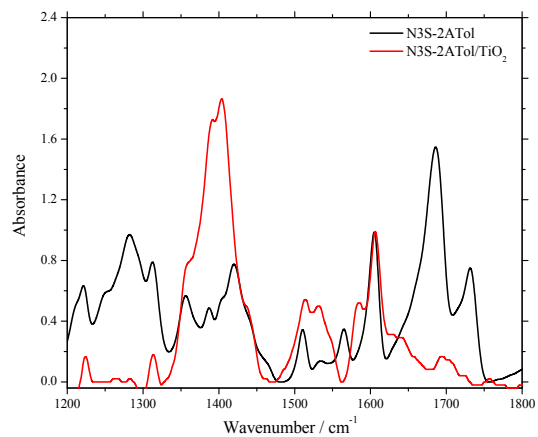
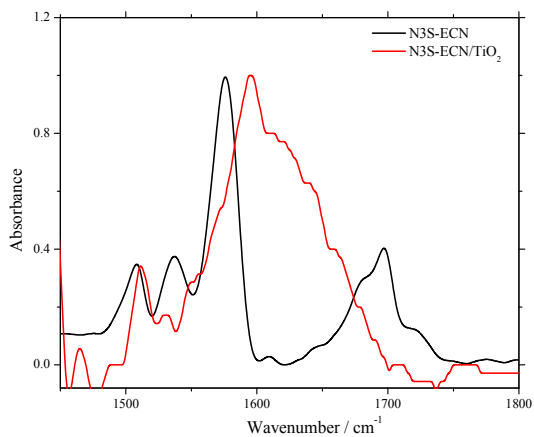
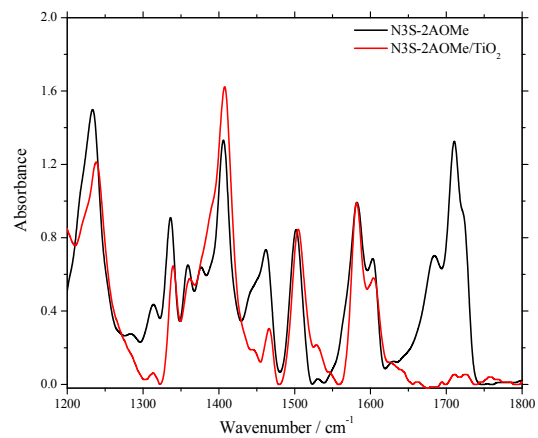
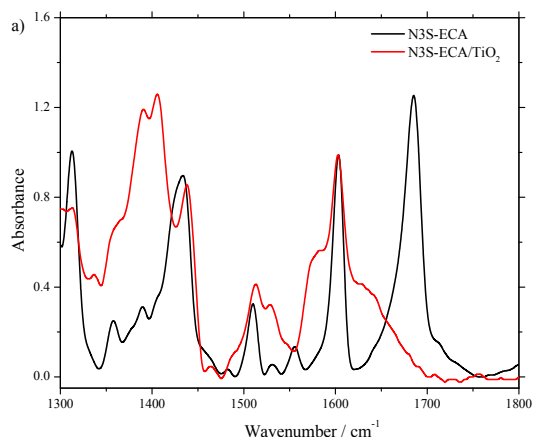
Figure 3-5. The molecular orbital diagrams for thiaporphyrin dyes.

For **N3S-CA**, **N3S-2AOMe**, **N3S-2ATol** and **N3S-2ATPA**, the majority of the electron density in HOMO as well as LUMO is located on the porphyrin ring suggesting that the charge transfer in these porphyrins might be less efficient than the *meso* ethynylphenyl substituted derivatives. Thus based on the theoretical calculations, it is evidenced that the

ethynylphenyl linker is highly beneficial for an efficient electron transfer from the porphyrin core to the electron withdrawing anchoring group. This effective electron distribution, especially in the case of **N3S-ECN** facilitates efficient charge transfer from the excited state of the porphyrins to the TiO₂ conduction band. Interestingly in the LUMO+2, the electron density is extensively located on the carboxylic acid acceptor suggesting that the electron injection from higher excited states involving LUMO+2 might be possible. The dipole moments for thiaporphyrins under study were estimated from theoretical calculations and displayed in Figure 3-5. The dipole moments decrease in the order **N3S-ECN** > **N3S-2ATPA** > **N3S-ECA** > **N3S-2ATol** > **N3S-CA** > **N3S-2AOMe**. The trend of dipole moments is consistent with the overall conversion efficiency for these thiaporphyrins except for **N3S-ECA**. **N3S-ECA** might have higher dipole moment (4.56 D) than **N3S-CA** due the presence of ethynyl linker. The highest dipole moment of 8.57 D is observed for **N3S-ECN**, highlighting the effectiveness of electron withdrawing cyanoacrylic anchoring group. The higher polarizability is advantageous to expedite intramolecular photoinduced electron transfer.

3.2.5 ATR-FTIR measurements

ATR-FTIR spectroscopy measurements have been utilized as one of the imperative tools for probing the number and mode of carboxylate groups anchored onto TiO₂.^[5-8] The ATR-FTIR spectra of neat thiaporphyrins contrasted with spectra of thiaporphyrins adsorbed on TiO₂. Comparative spectra of representative samples are shown in Figure 3-6. The spectra of neat **N3S-CA** and **N3S-2ATol** show strong $\nu(\text{C}=\text{O})$ stretches at 1687 and 1686 cm⁻¹, respectively, whereas $\nu_{\text{sym}}(\text{COO}^-)$ and $\nu_{\text{asym}}(\text{COO}^-)$ stretches are likely to be observed at about 1400 and 1600 cm⁻¹, respectively. In the comparative spectra of **N3S-CA/TiO₂** and **N3S-2ATol/TiO₂**, the $\nu(\text{C}=\text{O})$ stretches completely disappeared, accompanied by a noticeable rise in the stretching peaks of $\nu_{\text{sym}}(\text{COO}^-)$ and $\nu_{\text{asym}}(\text{COO}^-)$ at about 1400 and 1600 cm⁻¹, respectively. The observation noted above indicates that for **N3S-CA** bonding on to TiO₂ is achieved through one carboxyl group while in **N3S-2ATol**, both *p*-carboxyphenyl groups at the *cis*-positions are used for bonding onto TiO₂. Similar observations are found for the remaining thiaporphyrins, that is, **N3S-ECA**, **N3S-ECN**, **N3S-2AOMe** and **N3S-2ATPA**. Based on the above analyses, the single anchoring mode for A₃B thiaporphyrins and dual anchoring mode for A₂B₂ thiaporphyrins is proposed for the attachment of the porphyrins onto TiO₂.



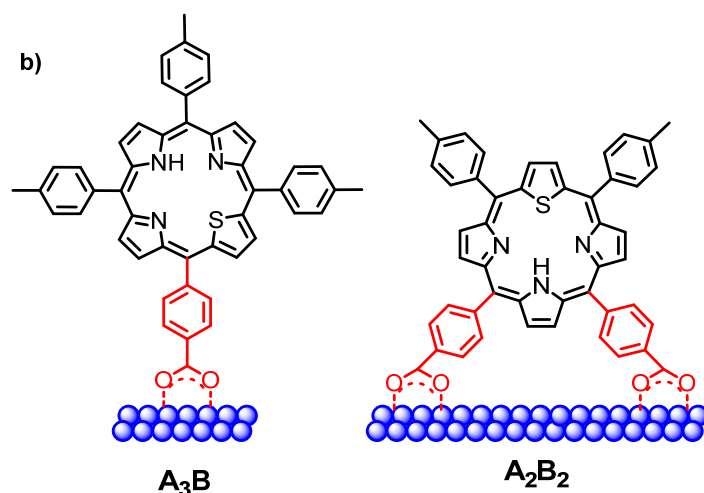


Figure 3-6. ATR-FTIR spectra of a) dye and dye/TiO₂; the ATR-FTIR spectra of the thiaporphyrins on TiO₂ are normalized for comparison. b) Possible modes of attachment of thiaporphyrins onto TiO₂. For demonstration purpose only, the relative sizes of the molecules and nanoparticles are not correlated in real dimensions.

3.2.6 Dye Loading Measurements

To better comprehend the adsorption behavior and measure the amount of adsorbed dye, we calculated the dye densities adsorbed on TiO₂ surface. The porphyrin densities (Γ) were determined by measuring the absorbance of the porphyrins desorbed from the sensitized TiO₂ films after being immersed in 0.1 M KOH solution in THF. The saturated Γ values of the thiaporphyrins under study were found as 141 ± 13 , 144 ± 11 , 100 ± 8 , 85 ± 5 , 116 ± 3 and 54 ± 8 nmol cm⁻² for **N3S-ECA**, **N3S-ECN**, **N3S-CA**, **N3S-2AOMe**, **N3S-2ATol** and **N3S-2ATPA** porphyrins, respectively. The dye loading values for A₂B₂ thiaporphyrins are inversely proportional to the steric bulkiness of the substituents. More bulky the substituent, less is the dye loading. Comprehensively, the dye loading amounts for A₂B₂ thiaporphyrins are lower than that of the A₃B thiaporphyrins. This can be explained with the help of dye attachment mode on the TiO₂ surface. As seen from the ATR-FTIR studies, A₂B₂ thiaporphyrins binds through dual anchoring mode while A₃B thiaporphyrins binds through the single anchoring carboxylic group to the TiO₂ surface. It is obvious that higher dye loading is observed for **N3S-ECA** and **N3S-ECN** as compared to other thiaporphyrins. The trends in the dye loading amounts mentioned above is not consistent with the overall conversion efficiencies with an exception of **N3S-ECN**, which has both, higher dye loading as well as higher efficiency. Regardless of low dye loading, **N3S-2ATPA** gave superior performance with higher current density.

3.2.7 Photovoltaic Measurements

Devices assembled with thiaporphyrin sensitizers using liquid electrolytes were tested under standard AM 1.5 illumination conditions. The photovoltaic parameters for the thiaporphyrins under study are summarized in Table 3-2 and the current-voltage characteristics of the devices are shown in Figure 3-7a. As evident from the I-V curve the **N3S-ECN** give the best performance with the overall photon to current conversion efficiency of 1.69%, supported by short-circuit current of 5.12 mA cm⁻², open-circuit voltage of 0.49 V and fill factor of 0.67. It is well reinforced by DFT calculations and photophysical studies that the electron withdrawing cyanoacrylic acid terminal group enhances the charge transfer from porphyrin ring towards the anchoring group. Also due to the electron withdrawing cyano group, the LUMO level of **N3S-ECN** is closer to the TiO₂ conduction band compared to other thiaporphyrins, which may facilitate the electron injection. The higher electron injection from the dye to the TiO₂ conduction band is well reflected by the much higher short-circuit current.

Table 3-2: Photovoltaic parameters of thiaporphyrin dyes

Dye	J_{sc} (mA cm ⁻²)	V_{oc} (V)	FF (%)	η (%)
N3S-ECA	0.89	0.41	0.55	0.20
N3S-ECN	5.12	0.49	0.67	1.69
N3S-CA	1.29	0.48	0.64	0.40
N3S-2AOMe	0.67	0.45	0.57	0.17
N3S-2ATol	1.52	0.47	0.65	0.46
N3S-2ATPA	2.84	0.48	0.63	0.86

Although the V_{oc} values are all alike, other A₃B and A₂B₂ thiaporphyrins have low J_{sc} values and therefore, inferior power conversion efficiencies. Noticeably, **N3S-ECA** only obtained short-circuit current of 0.89 mA cm⁻², open-circuit voltage of 0.41 V and fill factor 0.55 corresponding to photon-to-current conversion efficiency of 0.20%. It suggests that carboxylic acid alone is not sufficient to pull more electrons from the porphyrin core towards the anchor which results in the lower performance of **N3S-ECA**. Interestingly **N3S-CA**, without a *meso* ethynylphenyl linker, achieved higher efficiency of 0.40% with short-circuit current of 1.29 mA cm⁻², open-circuit voltage of 0.48 V and fill factor of 0.64. The A₂B₂ thiaporphyrin, **N3S-2ATol** with two anchoring carboxylic groups obtained the overall photon-to-current conversion efficiency of 0.46% with photo current density of 1.52 mA/cm², open-circuit voltage of 0.47 V and fill factor of 0.65, which is slightly higher than single arm

anchoring dye, **N3S-CA**. Among the thiaporphyrins, **N3S-2AOMe** gave the least conversion efficiency of 0.17% with short-circuit current of 0.67 mA cm⁻², open-circuit voltage of 0.45 V and fill factor of 0.57. This might be due to lower dye loadings as compared to other thiaporphyrins. Thiaporphyrin substituted with triphenylamine donor, **N3S-2ATPA** gave the highest efficiency among A₂B₂ thiaporphyrins. It obtained the overall conversion efficiency of 0.86%, with $J_{sc} = 2.84$ mA cm⁻², $V_{oc} = 0.48$ V and FF of 0.63.

The trend of J_{sc} in this series can be understood from the variation of the incident photon-to-current conversion efficiency spectra as displayed in Figure 3-7b and are in good agreement with the corresponding absorption spectra of the dyes on TiO₂ which display intense absorption bands in the *Soret* region. The I-V curves under standard AM 1.5 G illumination are in qualitative agreement with the photo-action spectra of these thiaporphyrins. For **N3S-ECN** the IPCE maximum is around 17% in the *Soret* region, while around 12% in the 550-600 nm region and 6% in the 700 nm region. This indicates that **N3S-ECN** shows panchromatic absorption behaviour covering whole visible region. This increased photon collection explicates the higher short-circuit current for this compound. In case of **N3S-ECA** and **N3S-CA**, there is insignificant IPCE in Q band region which is one of the reasons for their inferior performance compared to **N3S-ECN**. Even though the IPCE values are higher for **N3S-2AOMe** than **N3S-ECA** and **N3S-CA**, the lower dye density triggered by bulky methoxy groups might be the reason for its low efficiency.

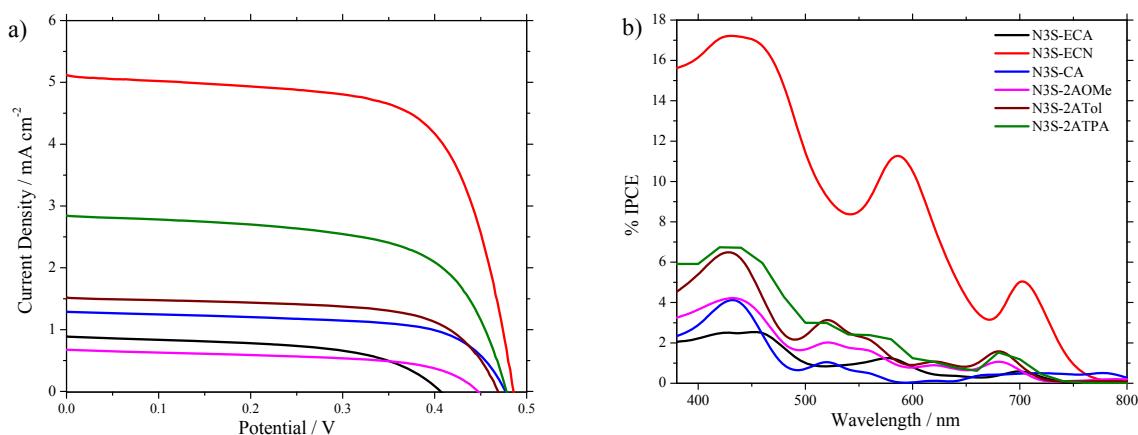


Figure 3-7. (a) I-V curves and (b) IPCE spectra for thiaporphyrin dyes.

3.2.8 Electrochemical Impedance Spectroscopy

To further study the correlation between the charge transfer processes and photovoltaic properties in the DSSC devices with different thiaporphyrin sensitizers, electrochemical impedance spectroscopy (EIS) studies were carried out under illumination applied with an open-circuit voltage with a frequency range of 1 Hz to 1 kHz. Figure 3-8 shows the EIS Nyquist plots (i.e. the minus imaginary part of the impedance Z'' vs. the real part of the impedance Z' when sweeping the frequency) for DSSCs based on thiaporphyrins. One semicircle was observed for all the thiaporphyrins in the Nyquist plots. This semicircle corresponds to the charge transfer processes at the TiO_2 -dye-electrolyte interface *i.e.* electron transport resistance.^[9] A smaller radius of the semicircle in the Nyquist plot corresponds to the lower electron transport resistance, in other words higher electron transfer. The radius of the semicircle in the Nyquist plot decreases in the order **N3S-2AOMe** > **N3S-2ATol** > **N3S-CA** > **N3S-ECA** > **N3S-2ATPA** > **N3S-ECN**. This trend is roughly consistent with the DSSC performance of the thiaporphyrin sensitizers. The DSSC based on **N3S-ECN** exhibited smaller interfacial charge transfer resistance at the dye- TiO_2 -electrolyte interface compared to other dyes indicating improved charge generation and transport, which is well reflected in its higher photocurrent density.

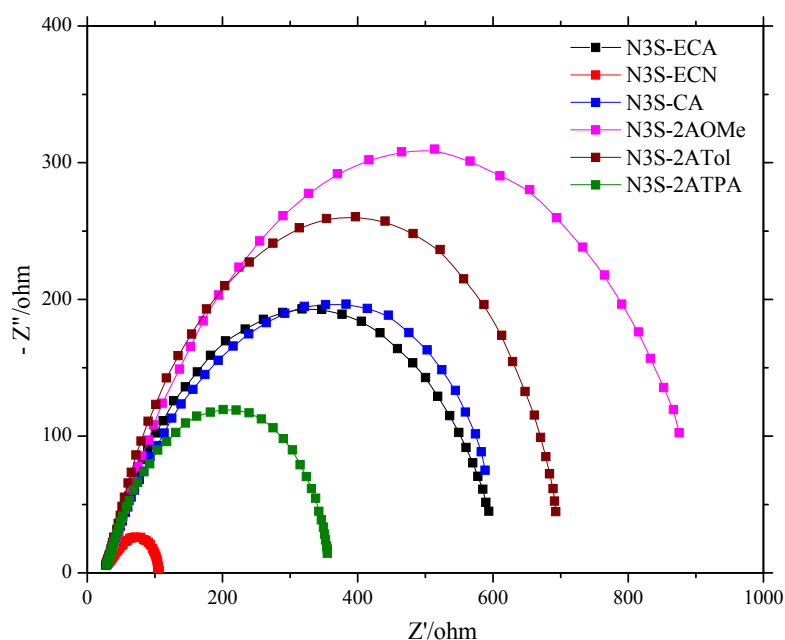


Figure 3-8. Impedance spectra (Nyquist plots) of DSSCs based on thiaporphyrins measured under illumination.

3.3 Conclusions

In summary, we have prepared novel mono- and di-carboxylate functionalized A₃B and A₂B₂ thiaporphyrins. With the support of the photophysical and photovoltaic data, it is revealed that these thiaporphyrins, after systematic structural modification can be applied efficiently to DSSCs. The UV-Visible spectra of these thiaporphyrins displayed that ethynyl phenyl linker effectively enhances the absorption towards NIR region. DFT calculations shows that, higher π electron density is localized on the cyanoacrylic acid anchor in LUMO of **N3S-ECN** compared to other thiaporphyrins; consequently, more electrons are available in LUMO of the dye for injection into the conduction band of TiO₂. As seen from the electrochemical properties and energy level diagram, the HOMO-LUMO energy levels of the thiaporphyrins are suitable for application as a sensitizer in DSSC. The best conversion efficiency of 1.69% with high photocurrent density of 5.12 mA cm⁻² is obtained for **N3S-ECN** owing to their superior photophysical properties. To the best of our knowledge this is the highest efficiency for thiaporphyrin-based DSSCs. These results suggests that the thiaporphyrins, core-modified derivatives of porphyrins, can serve as effective sensitizers for future DSSC applications.

3.4 Experimental

3.4.1 General Methods

All chemicals were obtained from commercial sources and used as received without further purification. All the reactions were carried out under nitrogen atmosphere. Solvents used in reactions were dried by PureSolv MD 5 system (Innovative Technology, Inc). Flash chromatography was carried out by using silica gel (40-63 μm , Merck). Analytical TLC was performed on Merck silica gel plates. ^1H NMR spectra were recorded on a Bruker 400 MHz spectrometer and performed in CDCl_3 ($\delta = 7.26$ ppm), $\text{THF-}d_8$ ($\delta = 1.73, 3.58$ ppm) or $\text{DMSO-}d_6$ ($\delta = 2.50$ ppm) solutions. ^{13}C NMR spectra were performed in CDCl_3 ($\delta = 7.26$ ppm) $\text{DMSO-}d_6$ ($\delta = 40.0$ ppm) solutions. Chemical shifts are reported in ppm. Coupling constants (J) are reported in Hz. The signals are described as s: singlet; d: doublet; dd: doublet of doublet. The ESI ion trap mass spectra were measured by a Finnigan MAT LCQ mass spectrometer. The HR-FAB spectra were conducted on a JMS-700 double focusing mass spectrometer. Transmittance and reflection UV-visible absorption spectra of the thiaporphyrins in THF and adsorbed on TiO_2 electrodes, respectively, were recorded on a JASCO V-670 UV-Vis/NIR spectrophotometer. Steady-state fluorescence spectra were acquired by using a Varian Cary Eclipse fluorescence spectrophotometer. The cyclic voltammetry measurements of all thiaporphyrins were carried out on CHI 621B electrochemical analyser (CH Instruments, Austin, TX, USA) in degassed THF containing 0.1 M tetrabutylammonium hexafluorophosphate (Bu_4NPF_6) as the supporting electrolyte. The cell assembly consists of a glossy carbon as the working electrode, a silver wire as the pseudo-reference electrode, and a platinum wire as the auxiliary electrode. The scan rate for all measurements was fixed at 50 mV/sec. A ferrocene^{+1/0} redox couple was used as the internal standard and the potential values obtained in reference to the silver electrode were converted to the vacuum scale. DFT calculations were performed using Gaussian 09 package.^[10] The molecular orbitals were visualized by the Chemoffice software.

3.4.2 Synthesis

The synthesis of 5-bromo-10,15,20-tris(*p*-tolyl)-21-thiaporphyrin (1) and N3S-ECA were reported in the previous chapter.

5-(4-Ethynylbenzaldehyde)-10,15,20-tris(*p*-tolyl)-21-thiaporphyrin (2):

Bromothiaporphyrin, N3S-Br (1) (100 mg, 0.15 mmol), $\text{Pd}_2(\text{dba})_3$ (55 mg, 0.06 mmol), AsPh_3 (113 mg, 0.37 mmol) and 4-ethynylbenzaldehyde (25 mg, 0.18 mmol) were added to a

100 ml round bottom flask and the flask is attached to high vacuum for 30 min. Then N₂ was flushed for 15 min and anhydrous THF (40 ml) and triethylamine (10 ml) were added. The reaction mixture was stirred under N₂ at room temperature for 12 h. After completion of the reaction as confirmed by TLC, the solvent was removed under pressure and the crude product was purified by column chromatography using hexanes/DCM (2/1) as eluent to afford the desired porphyrin (2) as a purple solid (76 mg, 70%). ¹H NMR (400 MHz, CDCl₃) δ: -2.18 (s, 1H, NH) 2.70 (s, 3H, CH₃), 2.72 (s, 6H, CH₃), 7.53-7.66 (m, 6H, *m*-tolyl), 8.03-8.09 (m, 6H, *o*-tolyl), 8.16 (m, 4H, Ar), 8.54 (d, 1H, *J* = 4.48 Hz; β-pyrrole), 8.61 (d, 1H, *J* = 4.52 Hz; β-pyrrole), 8.66 (d, 1H, *J* = 4.48 Hz; β-pyrrole), 8.86 (s, 2H, β-pyrrole), 9.34 (d, 1H, *J* = 4.48 Hz; β-pyrrole), 9.83 (d, 1H, *J* = 5.16 Hz; β-thiophene), 10.14 (s, 1H, CHO), 10.32 (d, 1H, *J* = 5.16 Hz; β-thiophene) ppm; ¹³C NMR (100 MHz, CDCl₃) δ: 21.53, 94.56, 97.69, 108.52, 124.99, 126.02, 127.39, 127.48, 128.46, 128.75, 129.38, 129.92, 130.07, 131.64, 132.25, 132.98, 133.08, 134.17, 134.25, 134.33, 135.20, 135.67, 135.82, 136.13, 137.67, 137.77, 137.90, 139.00, 139.30, 139.77, 146.23, 150.34, 154.41, 154.49, 157.96, 158.87, 191.41 ppm; HRMS-ESI: *m/z* calcd for C₅₀H₃₆N₃OS: 726.2579, found 726.2582 [M+H]⁺.

N3S-ECN: To a mixture of N3S-CHO (2) (100 mg, 0.13 mmol) in CHCl₃ (25 ml) and piperidine (128 μl, 1.3 mmol) was added cyanoacetic acid (46 mg, 0.52 mmol) and the reaction mixture is refluxed for 12 h under N₂. To this mixture 50 ml CHCl₃ and 100 ml water were added and transferred to a separation funnel. The pH value of this mixture is adjusted to approximately 2 with 2 M H₃PO₄. The CHCl₃ was removed by azeotropic distillation using acetonitrile in *vacuo*. Precipitation from the resulting acetonitrile solution (50 ml) using H₂O gave N3S-ECN purple solid (90 mg, 87%). ¹H NMR (400 MHz, THF-*d*8) δ: -2.08 (s, 1H, NH) 2.68 (s, 3H, CH₃), 2.70 (s, 6H, CH₃), 7.59 (m, 4H, *m*-tolyl), 7.69 (d, 2H, *J* = 7.8 Hz; *m*-tolyl), 8.06 (m, 4H, *o*-tolyl), 8.15 (d, 2H, *J* = 7.84 Hz; *o*-tolyl), 8.25 (d, 2H, *J* = 8.36 Hz; Ar), 8.30 (d, 2H, *J* = 8.40 Hz; Ph), 8.39 (s, 1H, acryl), 8.48 (d, 1H, *J* = 4.56 Hz; β-pyrrole), 8.56 (d, 1H, *J* = 4.56 Hz; β-pyrrole), 8.62 (d, 1H, *J* = 4.48 Hz; β-pyrrole), 8.87 (s, 2H, β-pyrrole), 9.39 (d, 1H, *J* = 4.44 Hz; β-pyrrole), 9.83 (d, 1H, *J* = 5.20 Hz; β-thiophene), 10.38 (d, 1H, *J* = 5.16 Hz; β-thiophene) ppm; ¹³C NMR (100 MHz, DMSO-*d*6) δ: 21.01, 45.39, 91.88, 98.87, 108.54, 114.12, 119.00, 124.58, 124.65, 125.44, 127.48, 127.55, 128.60, 129.06, 129.57, 129.84, 131.92, 132.25, 132.49, 133.04, 133.85, 133.93, 135.29, 135.75, 135.86, 136.61, 137.56, 137.71, 138.01, 138.15, 138.38, 138.78, 145.23, 146.66, 149.04, 153.49, 153.61, 157.03, 157.85, 162.88 ppm; IR (Neat, cm⁻¹): 3327, 2923, 2860, 2224, 2184, 1697, 1576, 1537, 1422, 1283, 1179, 941, 796, 704; UV-Vis (THF) λ_{max}/nm (ε/10³ M⁻¹ cm⁻¹)

= 449 (396), 526 (15), 579 (55), 637 (5), 698 (15); HRMS-ESI: m/z calcd for C₅₃H₃₇N₄O₂S: 793.2637, found 793.2635 [M+H]⁺.

Mixed diol (3): Anhydrous hexane (60 ml) was added to a 500 ml three-necked round-bottomed flask equipped with rubber septum, gas inlet and gas outlet tube. A positive pressure of N₂ was maintained and after purging N₂ gas for 5 min, TMEDA (11.5 ml, 75 mmol) and *n*-BuLi (62 ml of 1.6 M solution in hexane) were added sequentially to the stirring solution at room temperature. Thiophene (2 ml, 25 mmol) was then added and the solution was refluxed for 1 h. As the reaction progressed, a white turbid solution formed indicating the formation of the 2,5-dilithiated salt of thiophene. The reaction mixture was cooled with ice bath and an ice cold solution of *p*-tolualdehyde (2.95 ml, 25 mmol) and methyl-4-formylbenzoate (4.1 g, 25 mmol) in dry THF (60 ml) was then cannulated to the stirring solution. The resulting reaction mixture was stirred at 0 °C for 15 min and then brought up to room temperature. The reaction was quenched by adding cold saturated NH₄Cl solution (50 ml). The organic layer was washed with brine and dried over anhydrous MgSO₄. The solvent was removed on a rotary evaporator under reduced pressure to afford the crude compound. The crude product was further purified by silica gel column chromatography (eluent: 30% ethyl acetate in hexanes) to collect desired diol (3) as yellow solid (1.76 g, 19%). ¹H NMR (400 MHz, CDCl₃) δ: 2.34 (s, 3H, CH₃), 2.46 (d, 1H, *J* = 3.88 Hz; OH), 2.61 (d, 1H, *J* = 3.76 Hz; OH), 3.90 (s, 3H, OMe), 5.91 (s, 1H, *meso*), 5.99 (d, 1H, *meso*), 6.69 (m, 2H, *m*-tolyl), 7.15 (d, 2H, *J* = 8.00 Hz; Ph), 7.29 (m, 2H, *o*-tolyl), 7.49 (d, 2H, *J* = 2.67 Hz; β-thiophene), 8.00 (d, 2H, *J* = 8.16 Hz; Ph) ppm; ¹³C NMR (100 MHz, CDCl₃) δ: 21.13, 52.11, 71.94, 72.41, 124.29, 124.78, 126.13, 129.22, 129.81, 137.85, 139.88, 147.01, 147.10, 147.67, 148.86, 148.95, 166.85 ppm.

N3S-CE (4) : In a 500 ml one-necked round-bottomed flask fitted with a N₂ gas bubbler, a solution of the mixed thiophene diol (9) (737 mg, 2 mmol), pyrrole (411 μl, 6 mmol) and *p*-tolaldehyde (471 μl, 4 mmol) in DCM (400 ml) was taken. Resulting reaction mixture was purged with N₂ for 15 min and then a catalytic amount of BF₃•OEt₂ (25 μl, 0.2 mmol) was added at room temperature. After stirring for 1 h, DDQ (908 mg, 4 mmol) was added and the reaction mixture was stirred at room temperature in air for 1 h. The solvent was removed on a rotary evaporator. The crude product was purified by silica gel column chromatography using hexanes/DCM (1:1) as eluent to afford the desired porphyrin (4) as purple solid. (290 mg, 20%). ¹H NMR (400 MHz, CDCl₃) δ: -2.65 (s, 1H, NH), 2.71 (s, 9H, CH₃), 4.12 (s, 3H, OMe), 7.56 (d, 4H, *J* = 7.80 Hz; *m*-tolyl), 7.63 (d, 2H, *J* = 7.80 Hz; *m*-tolyl), 8.09 (m, 4H, *o*-

tolyl), 8.15 (d, 2H, $J = 7.88$ Hz; *o*-tolyl), 8.35 (d, 2H, $J = 8.12$ Hz; Ph), 8.51 (d, 2H, $J = 8.24$ Hz; Ph), 8.64 (m, 3H, β -pyrrole), 8.71 (d, 1H, $J = 4.60$ Hz, β -pyrrole), 8.97 (d, 2H, $J = 1.72$ Hz, β -pyrrole), 9.68 (d, 1H, $J = 5.28$ Hz, β -thiophene), 9.79 (d, 1H, $J = 5.32$ Hz, β -thiophene) ppm; ¹³C NMR (100 MHz, CDCl₃) δ : 21.50, 52.34, 124.11, 124.38, 127.35, 128.32, 128.69, 128.91, 129.03, 129.38, 129.54, 131.86, 132.51, 133.08, 133.55, 134.17, 134.36, 134.67, 135.58, 135.81, 137.61, 137.99, 139.11, 139.25, 139.46, 145.92, 146.75, 146.92, 154.54, 156.65, 157.62, 167.34 ppm; HRMS-ESI: m/z calcd for C₄₉H₃₈N₃O₂S: 732.2685, found 732.2684 [M+H]⁺.

N3S-CA: Thiaporphyrin ester (4) (200 mg, 0.27 mmol) was dissolved in 50 ml THF. To this mixture, 20 equivalent of KOH mixed in 10 ml water was added and the reaction mixture was refluxed for 12 h. After cooling, the organic solvent was removed under pressure. 50 ml water was added to the reaction mixture and the solution was treated slowly with 1 N HCl. The precipitation formed were filtered off and washed with distilled water. The residue remained is dissolved in methanol and dried in vacuum to yield the desired porphyrin as purple solid (175 mg, 90%). ¹H NMR (400 MHz, DMSO-*d*₆) δ : -2.82 (s, 1H, NH), 2.64 (s, 9H, CH₃), 7.62 (m, 6H, *m*-tolyl), 8.08 (m, 6H, *o*-tolyl), 8.34 (d, 2H, $J = 8.12$ Hz; Ph), 8.42 (d, 2H, $J = 8.16$ Hz; Ph), 8.53 (m, 2H, β -pyrrole), 8.62 (m, 2H, β -pyrrole), 8.97 (d, 2H, $J = 1.56$ Hz, β -pyrrole), 9.74 (d, 1H, $J = 5.28$ Hz, β -thiophene), 9.78 (d, 1H, $J = 5.20$ Hz, β -thiophene), 13.29 (bs, 1H, COOH) ppm; ¹³C NMR (100 MHz, DMSO-*d*₆) δ : 21.04, 124.11, 124.88, 127.53, 128.01, 128.57, 128.71, 129.35, 129.68, 130.41, 131.62, 132.97, 133.22, 133.87, 134.00, 134.42, 135.08, 135.81, 137.08, 137.52, 138.25, 138.40, 138.55, 139.16, 144.43, 145.98, 146.06, 153.75, 156.08, 156.80, 167.41 ppm; IR (neat, cm⁻¹): 3327, 2917, 2866, 1687, 1608, 1427, 1316, 1222, 1183, 968, 799, 717; UV-Vis (THF) λ_{\max}/nm ($\epsilon/10^3$ M⁻¹cm⁻¹) = 428 (504), 513 (35), 548 (9), 625 (5), 679 (8); HRMS-ESI: m/z calcd for C₄₈H₃₆N₃O₂S: 718.2528, found 718.2534 [M+H]⁺.

2,5-Bis(3,4,5-trimethoxyphenylmethanol)thiophene (8): Anhydrous hexane (40 ml) was added to a 250 ml three-necked round bottomed flask equipped with rubber septum, gas inlet and gas outlet tube. A positive pressure of N₂ was maintained and after purging N₂ gas for 5 min, TMEDA (4.7 ml, 31.25 mmol) and *n*-BuLi (13 ml of 2.5 M solution in hexane) were added sequentially to the stirring solution at room temperature. Thiophene (1 ml, 12.5 mmol) was then added and the solution was refluxed for 1 h. As the reaction progressed, a white turbid solution formed indicating the formation of the 2,5-dilithiated salt of thiophene. The reaction mixture was cooled with ice bath and an ice-cold solution of 3,4,5-

trimethoxybenzaldehyde (6.13 g, 31.25 mmol) in dry THF (20 ml) was then cannulated to the stirring solution. The resulting reaction mixture was stirred at 0 °C for 15 min and then brought up to room temperature. The reaction was quenched by adding cold saturated NH₄Cl solution (20 ml). The organic layer was washed with brine and dried over anhydrous MgSO₄. The solvent was removed on a rotary evaporator under reduced pressure to afford the crude compound. The crude product was further purified by silica gel column chromatography (eluent: 25% ethyl acetate in hexanes) to collect desired diol (8) as yellow solid (2.91 g, 49%). ¹H NMR (400 MHz, CDCl₃) δ: 2.57 (s, 1H, OH), 2.58 (s, 1H, OH), 3.83 (s, 18H, OCH₃), 5.89 (d, 2H, *J* = 3.48 Hz; *meso*), 6.61 (s, 4H, Ph), 6.71 (d, *J* = 3.36 Hz, 2H, β-thiophene) ppm; ¹³C NMR (100 MHz, CDCl₃) δ: 56.12, 60.81, 72.59, 103.28, 103.30, 103.84, 124.39, 124.43, 137.60, 138.50, 147.88, 147.97, 153.27 ppm.

2,5-Bis(*p*-tolylmethanol)thiophene (9): Anhydrous hexane (40 ml) was added to a 250 ml three-necked round-bottomed flask equipped with rubber septum, gas inlet and gas outlet tube. A positive pressure of N₂ was maintained and after purging N₂ gas for 5 min, TMEDA (10.6 ml, 71 mmol) and *n*-BuLi (45 ml of 1.6 M solution in hexane) were added sequentially to the stirring solution at room temperature. Thiophene (1.9 ml, 23.7 mmol) was then added and the solution was refluxed for 1 h. As the reaction progressed, a white turbid solution formed indicating the formation of the 2,5-dilithiated salt of thiophene. The reaction mixture was cooled with ice bath and an ice-cold solution of *p*-tolaldehyde (7 ml, 59.25 mmol) in dry THF (50 ml) was then cannulated to the stirring solution. The resulting reaction mixture was stirred at 0 °C for 15 min and then brought up to room temperature. The reaction was quenched by adding cold saturated NH₄Cl solution (50 ml). The organic layer was washed with brine and dried over anhydrous MgSO₄. The solvent was removed on a rotary evaporator under reduced pressure to afford the crude compound. The crude product was further purified by silica gel column chromatography (eluent: 30% ethyl acetate in hexanes) to collect desired diol (9) as yellow solid (6 g, 78%). ¹H NMR (400 MHz, CDCl₃) δ: 2.35 (s, 6H, CH₃), 2.38 (s, 1H, OH), 2.39 (s, 1H, OH), 5.92 (d, 2H, *J* = 3.60 Hz, *meso*), 6.69 (d, *J* = 2.6 Hz, 2H, β-thiophene), 7.16 (d, *J* = 7.92 Hz, 4H, *m*-tolyl), 7.30 (d, *J* = 6.84 Hz, 4H, *o*-tolyl) ppm; ¹³C NMR (100 MHz, CDCl₃) δ: 21.13, 72.42, 124.28, 126.22, 129.18, 137.73, 139.99, 148.19 ppm.

Dimethyl 4,4'-[thiophene-2,5-diylbis(hydroxymethylene)] dibenzoate (10): Anhydrous hexane (40 ml) was added to a 250 ml three-necked round-bottomed flask equipped with rubber septum, gas inlet and gas outlet tube. A positive pressure of N₂ was maintained and

after purging N₂ gas for 5 min, TMEDA (4.7 ml, 31.25 mmol) and *n*-BuLi (20 ml of 1.6 M solution in hexane) were added sequentially to the stirring solution at room temperature. Thiophene (1 ml, 12.5 mmol) was then added and the solution was refluxed for 1 h. As the reaction progressed, a white turbid solution formed indicating the formation of the 2,5-dilithiated salt of thiophene. The reaction mixture was cooled with ice bath and an ice cold solution of methyl-4-formylbenzoate (4 g, 25 mmol) in dry THF (20 ml) was then cannulated to the stirring solution. The resulting reaction mixture was stirred at 0 °C for 15 min and then brought up to room temperature. The reaction was quenched by adding cold saturated NH₄Cl solution (20 ml). The organic layer was washed with brine and dried over anhydrous MgSO₄. The solvent was removed on a rotary evaporator under reduced pressure to afford the crude compound. The crude product was further purified by silica gel column chromatography (eluent: 3:7, ethyl acetate/hexanes) to collect desired diol (10) as yellow solid (4.3 g, 84%). ¹H NMR (400 MHz, CDCl₃) δ: 2.55 (s, 1H, OH), 2.56 (s, 1H, OH), 3.9 (s, 6H, OCH₃), 6.01 (d, 2H, *J* = 3.72 Hz; *meso*), 6.72 (s, 2H, β-thiophene), 7.49 (m, 4H, Ph), 8.01 (d, *J* = 8.28 Hz, Ph) ppm; ¹³C NMR (100 MHz, CDCl₃) δ: 52.14, 71.97, 124.81, 126.12, 129.77, 129.88, 147.52, 147.74, 166.79 ppm.

N3S-2EOMe (11): In a 250 ml one-necked round-bottomed flask fitted with a N₂ gas bubbler, a solution of the thiophene diol (8) (476 mg, 1 mmol), pyrrole (205 μl, 3 mmol) and methyl-4-formylbenzoate (328 mg, 2 mmol) in DCM (200 ml) was taken. Resulting reaction mixture was purged with N₂ for 15 min and then a catalytic amount of BF₃•OEt₂ (15 μl, 0.1 mmol) was added at room temperature. After stirring for 1 h, DDQ (681 mg, 3 mmol) was added and the reaction mixture was stirred at room temperature in air for 1 h. The solvent was removed on a rotary evaporator. The crude product was purified by silica gel column chromatography using hexanes/DCM (1:1) as eluent to afford the desired porphyrin (11) as purple solid. (379 mg, 20%). ¹H NMR (400 MHz, CDCl₃) δ: -2.69 (s, 1H, NH), 4.02 (s, 12H, OCH₃), 4.12 (s, 6H, OCH₃), 4.18 (s, 6H, OMe), 7.49 (s, 4H, Ph), 8.28 (d, 4H, *J* = 8.16 Hz; *o*-Ph), 8.45 (d, 4H, *J* = 8.16 Hz; *m*-Ph), 8.56 (d, 2H, *J* = 4.60 Hz; β-pyrrole), 8.80 (d, 2H, *J* = 4.48 Hz; β-pyrrole), 8.89 (d, 2H, *J* = 1.72 Hz; β-pyrrole), 9.87 (s, 2H, β-thiophene) ppm; ¹³C NMR (100 MHz, CDCl₃) δ: 52.45, 56.46, 61.27, 112.22, 12.45, 127.91, 128.76, 129.89, 131.80, 133.62, 134.31, 134.69, 135.17, 136.24, 138.19, 138.38, 147.00, 147.55, 152.31, 154.05, 157.52, 167.19 ppm; HRMS-ESI: *m/z* calcd for C₅₄H₄₆N₃O₁₀S: 928.2904, found 928.2901 [M+H]⁺.

N3S-2ETol (12): In a 250 ml one-necked round-bottomed flask fitted with a N₂ gas bubbler, a solution of the thiophene diol (9) (500 mg, 1.54 mmol), pyrrole (316 μ l, 4.62 mmol) and methyl-4-formylbenzoate (506 mg, 3.08 mmol) in DCM (200 ml) was taken. Resulting reaction mixture was purged with N₂ for 15 min and then a catalytic amount of BF₃•OEt₂ (20 μ l, 0.15 mmol) was added at room temperature. After stirring for 1 h, DDQ (699 mg, 3.08 mmol) was added and the reaction mixture was stirred at room temperature in air for 1 h. The solvent was removed on a rotary evaporator. The crude product was purified by silica gel column chromatography using hexanes/DCM (1:1) as eluent to afford the desired porphyrin (12) as purple solid. (268 mg, 22%). ¹H NMR (400 MHz, CDCl₃) δ : -2.70 (s, 1H, NH), 2.72 (s, 6H, CH₃), 4.12 (s, 6H, OMe), 7.64 (d, 4H, *J* = 7.76 Hz; *m*-tolyl), 8.15 (d, 4H, *J* = 7.76 Hz; *o*-tolyl), 8.29 (d, 4H, *J* = 8.08 Hz; *o*-Ph), 8.44 (d, 4H, *J* = 8.04 Hz; *m*-Ph), 8.55 (d, 2H, *J* = 4.60 Hz; β -pyrrole), 8.74 (d, 2H, *J* = 4.52 Hz; β -pyrrole), 8.89 (d, 2H, *J* = 1.4 Hz; β -pyrrole), 9.81 (s, 2H, β -thiophene) ppm; ¹³C NMR (100 MHz, CDCl₃) δ : 21.49, 52.42, 122.03, 127.85, 128.35, 128.60, 129.76, 132.15, 133.73, 134.20, 134.34, 134.73, 134.96, 137.77, 137.88, 138.26, 147.19, 147.68, 153.94, 157.64, 167.24 ppm; HRMS-ESI: *m/z* calcd for C₅₀H₃₈N₃O₄S: 776.2583, found 776.2584 [M+H]⁺.

N3S-2ETPA (13): In a 250 ml one-necked round-bottomed flask fitted with a N₂ gas bubbler, a solution of the thiophene diol (10) (413 mg, 1 mmol), pyrrole (205 μ l, 3 mmol) and 4-(diphenylamino)benzaldehyde (546 mg, 2 mmol) in DCM (200 ml) was taken. Resulting reaction mixture was purged with N₂ for 15 min and then a catalytic amount of BF₃•OEt₂ (38 μ l, 0.3 mmol) was added at room temperature. After stirring for 1 h, DDQ (681 mg, 3 mmol) was added and the reaction mixture was stirred at room temperature in air for 1 h. The solvent was removed on a rotary evaporator. The crude product was purified by silica gel column chromatography using hexanes/DCM (1:1) as eluent to afford the desired porphyrin (13) as purple solid. (80 mg, 7%). ¹H NMR (400 MHz, CDCl₃) δ : -2.59 (s, 1H, NH), 4.12 (s, 6H, OMe), 7.15 (m, 4H, Ph), 7.42 (m, 20H, Ph), 8.05 (d, 4H, *J* = 8.44 Hz; Ph), 8.34 (d, 4H, *J* = 8.20 Hz; Ph), 8.50 (d, 4H, *J* = 8.24 Hz; Ph), 8.64 (d, 2H, *J* = 4.60 Hz; β -pyrrole), 8.77 (d, 2H, *J* = 4.64 Hz; β -pyrrole), 9.13 (d, 2H, *J* = 1.76 Hz; β -pyrrole), 9.67 (s, 2H, β -thiophene) ppm; ¹³C NMR (100 MHz, CDCl₃) δ : 52.44, 120.98, 123.47, 124.7, 125.03, 128.76, 129.19, 129.54, 129.67, 129.86, 132.59, 134.02, 134.18, 135.52, 135.83, 135.97, 145.71, 146.54, 147.74, 147.83, 154.68, 156.85, 167.30 ppm; HRMS-FAB⁺: *m/z* calcd for C₇₂H₅₂N₅O₄S: 1082.3740, found 1082.3738 [M+H]⁺.

N3S-2AOMe: Thiaporphyrin ester (11) (50 mg, 54 μ mol) was dissolved in 40 ml THF. To this mixture, 20 equivalent of KOH mixed in 2 ml water was added and the reaction mixture was refluxed for 12 h. After cooling, the organic solvent was removed under pressure. An amount of 20 ml water was added to the reaction mixture and the solution was treated slowly with 1 N HCl. The precipitation formed were filtered off and washed with distilled water. The residue remained is dissolved in methanol and dried in vacuum to yield desired porphyrin as purple solid (48 mg, 98%). ¹H NMR (400 MHz, DMSO-*d*₆) δ : -2.82 (s, 1H, NH), 3.96 (s, 12H, OCH₃), 3.99 (s, 6H, OCH₃), 7.56 (s, 4H, Ph), 8.33 (d, 4H, *J* = 8.16 Hz; *o*-Ph), 8.39 (d, 4H, *J* = 8.24 Hz; *m*-Ph), 8.52 (d, 2H, *J* = 4.64 Hz; β -pyrrole), 8.80 (d, 2H, *J* = 4.48 Hz; β -pyrrole), 8.96 (d, 2H, *J* = 2.04 Hz; β -pyrrole), 9.95 (s, 2H, β -thiophene) ppm; ¹³C NMR (100 MHz, DMSO-*d*₆) δ : 56.26, 60.38, 112.24, 122.39, 127.81, 129.22, 130.67, 131.69, 133.94, 134.19, 135.29, 135.40, 137.62, 145.82, 146.65, 152.09, 153.33, 156.83, 167.42 ppm; IR (Neat, cm⁻¹): 3327, 2923, 2853, 1711, 1684, 1603, 1582, 1502, 1462, 1406, 1336, 1234, 1122, 942, 792, 715; UV-Vis (THF) $\lambda_{\text{max}}/\text{nm}$ ($\epsilon/10^3 \text{ M}^{-1} \text{ cm}^{-1}$) = 431 (438), 513 (39), 549 (14), 625 (5), 679 (8); HRMS-ESI: *m/z* calcd for C₅₄H₄₂N₃O₁₀S: 900.2591, found 900.2585 [M+H]⁺.

N3S-2ATol: N3S-2Etol (12) (250 mg, 0.32 mmol) was dissolved in 60 ml THF. To this mixture, 20 equivalent of KOH mixed in 10 ml water was added and the reaction mixture was refluxed for 12 h. After cooling, the organic solvent was removed under pressure. An amount of 50 ml water was added to the reaction mixture and the solution was treated slowly with 1 N HCl. The precipitation formed were filtered off and washed with distilled water. The residue remained is dissolved in methanol and dried in vacuum to yield porphyrin as purple solid (215 mg, 90%). ¹H NMR (400 MHz, DMSO-*d*₆) δ : -2.87 (s, 1H, NH), 2.67 (s, 6H, CH₃), 7.70 (d, 4H, *J* = 7.60 Hz; *m*-tolyl), 8.14 (d, 4H, *J* = 7.64 Hz; *o*-tolyl), 8.33 (d, 4H, *J* = 8.04 Hz; *o*-Ph), 8.38 (d, 4H, *J* = 8.04 Hz; *m*-Ph), 8.52 (d, 2H, *J* = 4.64 Hz; β -pyrrole), 8.67 (d, 2H, *J* = 4.60 Hz; β -pyrrole), 8.97 (d, 2H, *J* = 1.84 Hz; β -pyrrole), 9.81 (s, 2H, β -thiophene) ppm; ¹³C NMR (100 MHz, DMSO-*d*₆) δ : 21.03, 122.29, 124.89, 127.78, 128.59, 129.28, 130.68, 131.78, 133.69, 133.93, 134.23, 135.08, 135.33, 137.04, 137.67, 145.79, 146.60, 153.31, 156.77, 167.41 ppm; IR (Neat, cm⁻¹): 3325, 2920, 2854, 1732, 1686, 1608, 1420, 1313, 1282, 967, 795, 710; UV-vis (THF) $\lambda_{\text{max}}/\text{nm}$ ($\epsilon/10^3 \text{ M}^{-1} \text{ cm}^{-1}$) = 428 (369), 512 (28), 547 (8), 624 (2), 679 (6); HRMS-ESI: *m/z* calcd for C₄₈H₃₄N₃O₄S: 748.2270, found 748.2267 [M+H]⁺.

N3S-2ATPA: Thiaporphyrin ester (13) (50 mg, 46 μ mol) was dissolved in 30 ml THF. To this solution, 20 equivalent of KOH mixed in 2 ml water was added and the reaction mixture was refluxed for 12 h. After cooling, the organic solvent was removed under pressure. An amount of 20 ml water was added to the reaction mixture and was treated slowly with 1 N HCl. The precipitation formed were filtered off and washed with distilled water. The residue remained is dissolved in methanol and dried in vacuum to yield desired porphyrin as purple solid (48 mg, 98%). ¹H NMR (400 MHz, DMSO-*d*₆) δ : -2.72 (s, 1H, NH), 7.19 (m, 4H, Ph), 7.37 (m, 12H, Ph), 7.47 (m, 8H, Ph), 8.08 (d, 4H, *J* = 8.20 Hz; Ph), 8.36 (d, 4H, *J* = 8.00 Hz; Ph), 8.44 (d, 4H, *J* = 8.04 Hz; Ph), 8.64 (d, 2H, *J* = 4.44 Hz; β -pyrrole), 8.71 (d, 2H, *J* = 4.52 Hz; β -pyrrole), 9.15 (s, 2H, β -pyrrole), 9.74 (s, 2H, β -thiophene), 13.30 (br s, 2H, COOH) ppm; ¹³C NMR (100 MHz, DMSO-*d*₆) δ : 120.25, 123.76, 124.40, 124.88, 128.74, 129.50, 129.82, 129.94, 130.45, 132.89, 134.14, 134.78, 135.49, 136.04, 138.62, 144.33, 145.76, 147.08, 147.39, 153.90, 156.20, 167.41 ppm; IR (Neat, cm⁻¹): 3332, 2918, 2867, 1686, 1590, 1489, 1418, 1313, 1276, 1173, 968, 797, 695; UV-Vis (THF) $\lambda_{\text{max}}/\text{nm}$ ($\epsilon/10^3 \text{ M}^{-1} \text{ cm}^{-1}$) = 429 (394), 518 (52), 558 (32), 621 (8), 682 (16); HRMS-ESI: *m/z* calcd for C₇₀H₄₈N₅O₄S: 1054.3427, found 1054.3433 [M+H]⁺.

3.4.3 Photovoltaic Measurements

TiO₂ photoanode films and Pt counter electrodes were purchased from Yingkou Opvtech New Energy Co. Ltd. Liaoning, China. The films, which were prepared by using the screen-printing method, were composed of a transparent layer (thickness \approx 12 μ m), a scattering layer (thickness \approx 4 μ m), and a working area of 0.4 \times 0.4 cm² and were used as received. The films were pretreated according to the following activation procedures before use: heating at 100 $^{\circ}$ C for 22 min, at 110 $^{\circ}$ C for 60 min, at 450 $^{\circ}$ C for 68 min, at 500 $^{\circ}$ C 60 min, at 250 $^{\circ}$ C for 60 min, cooling at 80 $^{\circ}$ C and keeping at 80 $^{\circ}$ C before immersion. The TiO₂ films were immersed in a 1 \times 10⁻⁴ M solution of the porphyrin in THF for 6-8 h at 25 $^{\circ}$ C. The dye-sensitized TiO₂ films were washed with THF, dried in hot air, and used as the working electrode. To fabricate the DSSC device, the two electrodes were tightly clipped together into a sandwich-type cell that was spaced by a 40 μ m film spacer. A thin layer of electrolyte, which contained 0.05 M I₂, 0.1 M lithium iodide (LiI), 0.6 M dimethyl-propyl-benzimidazole iodide (DMPII), and 0.6 M 4-tert-butylpyridine (TBP) in dry CH₃CN, was introduced into the space between the two electrodes. The photo-electrochemical characterizations of the solar cells were performed on an Oriel Class A solar simulator (Oriel 91195A, Newport Corp.). Photocurrent–voltage characteristics of the DSSCs were recorded on a potentiostat/galvanostat (CHI650B, CH

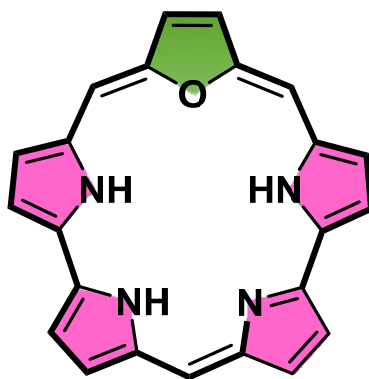
Instruments, Inc.) at a light intensity of 100 mWcm⁻² and calibrated to an Oriel reference solar cell (Oriel 91150, Newport Corp.). The monochromatic quantum efficiency was recorded on a monochromator (Oriel 74100, Newport Corp.) under short-circuit conditions. The intensity of each wavelength was within the range 1–3 mWcm⁻². The EIS measurements were carried on CHI 621B electrochemical impedance analyser (CH Instruments, Austin, TX, USA), under applied AC voltage and bias potential on the cells and measured the corresponding current and voltage under the white LED lamp with various neutral density filters for white light intensity in order to change the Fermi level of DSSCs. The data was analyzed using Zview software.

3.5 References:

- [1] Y. Xie, P. Joshi, M. Ropp, D. Galipeau, L. Zhang, H. Fong, Y. You, Q. Qiao, *J. Porphyrins Phthalocyanines* **2009**, *13*, 903-909.
- [2] S. B. Mane, L. Luo, G.-F. Chang, E. W.-G. Diao, C.-H. Hung, *J. Chin. Chem. Soc.* **2014**, *61*, 545-555.
- [3] C.-F. Lo, L. Luo, E. W.-G. Diao, I. J. Chang, C.-Y. Lin, *Chem. Commun.* **2006**, 1430-1432.
- [4] Y. Arai, H. Segawa, *Chem. Commun.* **2010**, *46*, 4279-4281.
- [5] R. Ambre, K.-B. Chen, C.-F. Yao, L. Luo, E. W.-G. Diao, C.-H. Hung, *J. Phys. Chem. C* **2012**, *116*, 11907-11916.
- [6] R. B. Ambre, G.-F. Chang, C.-H. Hung, *Chem. Commun.* **2014**, *50*, 725-727.
- [7] R. B. Ambre, G.-F. Chang, M. R. Zanwar, C.-F. Yao, E. W.-G. Diao, C.-H. Hung, *Chem. Asian J.* **2013**, *8*, 2144-2153.
- [8] A. Abboto, N. Manfredi, C. Marinzi, F. De Angelis, E. Mosconi, J.-H. Yum, Z. Xianxi, M. K. Nazeeruddin, M. Gratzel, *Energy Environ. Sci.* **2009**, *2*, 1094-1101.
- [9] C.-J. Yang, Y. J. Chang, M. Watanabe, Y.-S. Hon, T. J. Chow, *J. Mater. Chem.* **2012**, *22*, 4040-4049.
- [10] M. J. Frisch, Gaussian 09, Revision A.1, *Gaussian, Inc., Wallingford CT* **2009**.

Section II

Core-modified Expanded Porphyrins

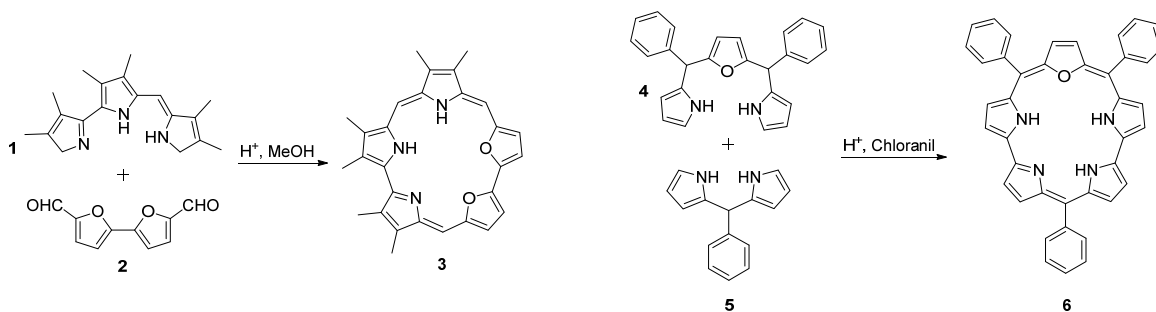


4. Novel expanded porphyrin sensitized solar cell using boryl oxasmaragdyrin as the sensitizer

4.1 Introduction

Expanded porphyrins and expanded core-modified porphyrins are synthetic analogues of porphyrins and core-modified porphyrins, respectively, containing more than 18 π -electrons in the conjugated systems either due to an increased number of heterocyclic rings or due to multiple *meso* carbon bridges.^[1] Expanded porphyrin is a rich class of porphyrin offering enlarged π conjugated systems with the number of π -electrons ranging from 22 up to 56 (dodecaphyrin). From the spectroscopic point of view, the expanded porphyrins offer a broad range of compounds with absorption energies down to infrared regions.^[2] Due to their enlarged cavity sizes and unique properties in association with extended π -conjugation, expanded porphyrins with more than four pyrrole subunits in the porphyrinic macrocycle have been widely used in a variety of applications including anion and metal sensors,^[3] NIR sensing dyes,^[4] two-photon absorption materials,^[5] MRI agents and photodynamic therapy^[6] as depicted in Figure 4-1. ‘Smaragdyrin or norsapphyrin’ is [22] pentaphyrin (1.1.0.1.0)^[7] that has only three *meso* carbons which bears a structural relationship with sapphyrins as corrole does to porphyrin.

The dioxasmaragdyrin (3) is the first reported smaragdyrin, prepared by the 3+2 condensation of a pyrrolyl bipyrrrole (1) and diformyl bifuranan (2), as shown in Scheme 4-1. Recently, Chandrashekar and coworkers^[8] reported facile and efficient synthesis of stable *meso*-aryl oxasmaragdyrin (6), by an oxidative coupling of tripyrrane (4) and dipyrromethane (5) (Scheme 4-1). The oxasmaragdyrins showed very interesting spectral, electrochemical and photophysical properties. Chandrashekar and co-workers exploited the oxasmaragdyrins for metallation as well as anion binding studies.



Scheme 4-1. Synthesis of core-modified oxasmaragdyrins

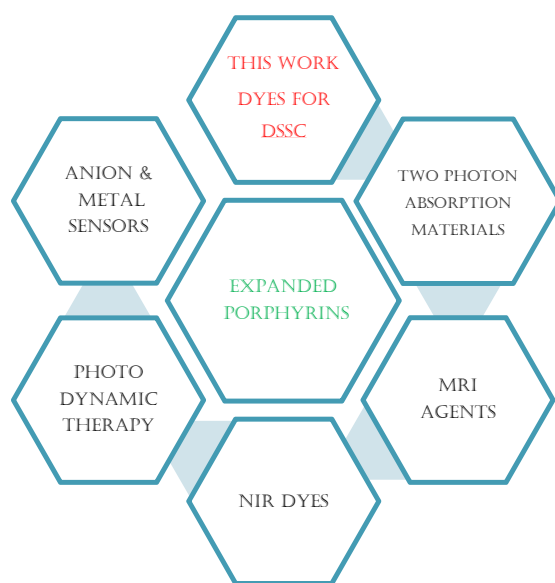
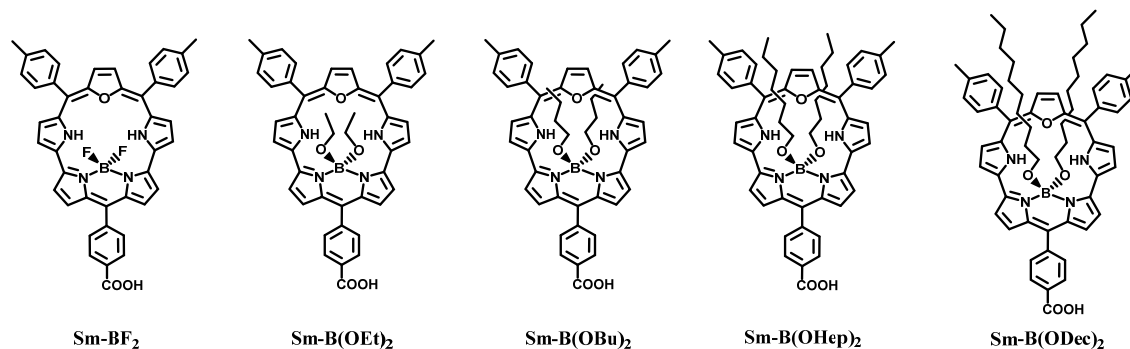


Figure 4-1. Various applications of expanded porphyrins.

Although enormous literature is available on porphyrin-sensitized solar cells^[9] and red-shifted absorption bands of expanded porphyrins match well with the demands for a low energy sensitizer, surprisingly an expanded porphyrin has never been used as the sensitizer for DSSCs. To uncover the potential of applying expanded porphyrins to DSSC studies, herein we report the syntheses, photophysical and photovoltaic properties of boron chelated oxasmaragdyrins, a class of aromatic core-modified expanded porphyrin with a 22 π -electron conjugation. The oxasmaragdyrin boron complexes Sm-BR₂ with structures depicted in Scheme 4-2, demonstrate panchromatic incident photon-to-current efficiencies, high short-circuit photocurrent densities, and moderate-to-good overall efficiencies revealing an opportunity to develop expanded porphyrin-based highly efficient sensitizers for DSSCs.

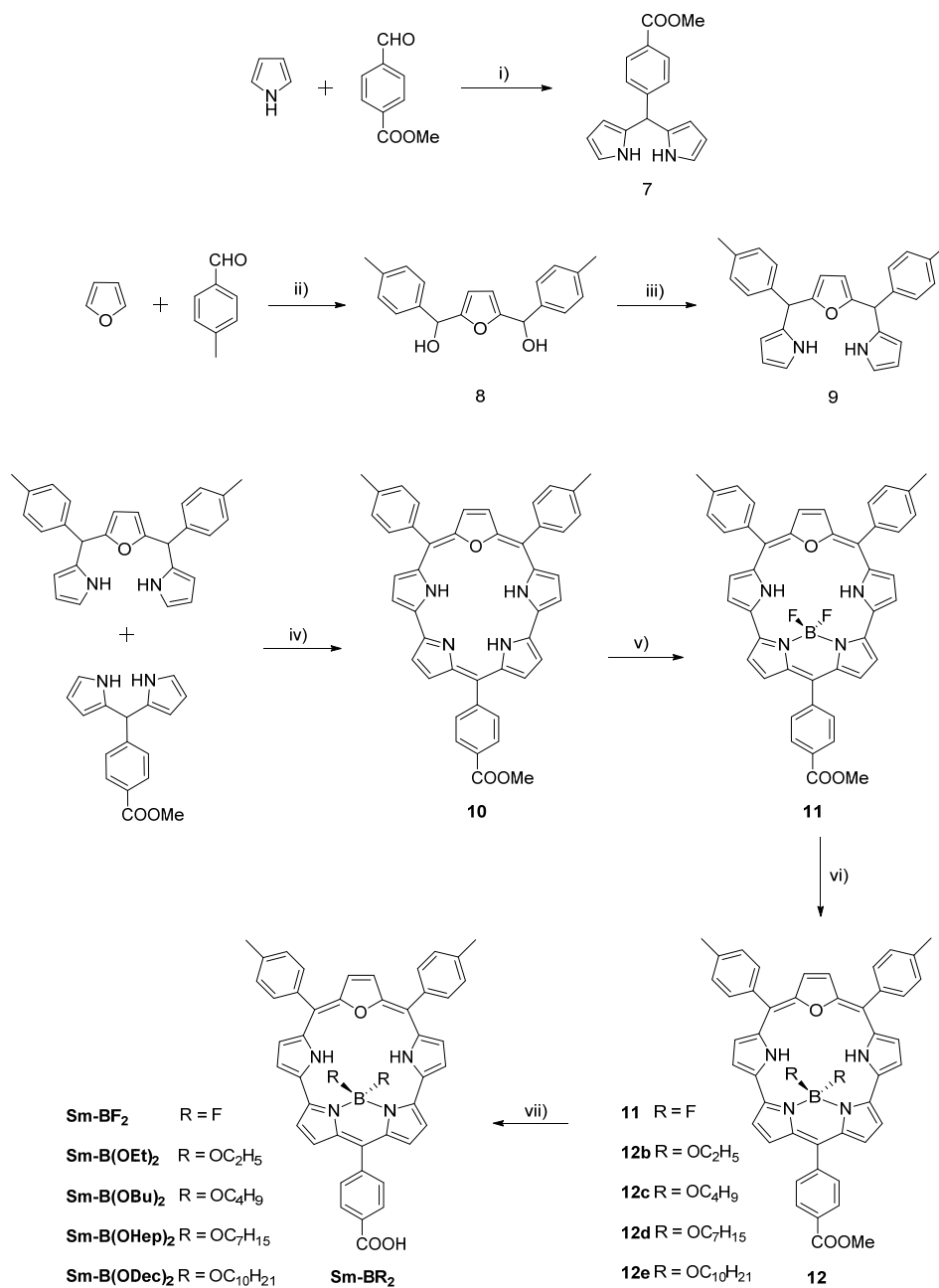


Scheme 4-2. Molecular structures of oxasmaragdyrin dyes.

4.2 Results and Discussion

4.2.1 Syntheses

The desired oxasmaragdyrin complexes Sm-BR₂, were prepared in four steps in decent yields under mild reaction conditions from the readily available starting compounds dipyrromethane and oxatripyrrane as depicted in Scheme 4-3.



Scheme 4-3. Synthesis of oxasmaragdyrins Sm-BR₂. Reagents and Conditions: i) TFA; ii) *n*-BuLi, TMEDA, Hexanes/THF; iii) pyrrole, BF₃•OEt₂; iv) TFA, DDQ, DCM; v) BF₃•OEt₂, NEt₃, DCM; vi) AlCl₃, alcohol, dry DCM; vii) KOH(aq), THF.

Methyl-4-formylbenzoate was treated with excess pyrrole in presence of trifluoroacetic acid (TFA) at 55 °C for 3 hours to yield the desired *meso*-(4-methoxyphenyl)dipyrromethane (7). To synthesize the 16-oxatripyrrane (9), furan was reacted with *p*-tolualdehyde in the presence of *n*-BuLi to get the symmetric diol (8), which was further treated with excess pyrrole under mild acidic condition at room temperature to obtain the 16-oxatripyrrane (9). The oxasmaragdyrin ring (10) was assembled by a McDonald type '3+2' condensation of *meso*-(4-methoxyphenyl)dipyrromethane (7) and a 16-oxatripyrrane (9) in DCM in the presence of 0.1 equivalents of TFA followed by oxidation with DDQ.^[8] Column chromatographic purification on basic alumina afforded the oxasmaragdyrin (10) as dark green solid in 38% yield. The BF₂ chelated complex (11) was prepared by treating oxasmaragdyrin (10) with 40 equivalents of triethylamine followed by 50 equivalents of BF₃•OEt₂ in DCM at room temperature for 30 min. The progress of the reaction was monitored by TLC analysis and absorption spectroscopy. The reaction progress was also clearly evident in the colour change of the reaction mixture from dark green to light green. After standard work-up and chromatographic purification on silica, the BF₂ complex was isolated as green powder in 62% yield. The HR-MS mass spectra confirmed the formation of BF₂ complex. The complex (11) was characterized in detail by ¹H, ¹³C, ¹⁹F and ¹¹B NMR spectra. The alkoxy substituted B(OR)₂-oxasmaragdyrin complexes were prepared by treating BF₂-oxasmaragdyrin (11) with appropriate alcohols in excess amount in the presence of AlCl₃ in DCM at refluxing temperature for 10 min.^[10] The crude compounds were purified by column chromatographic on silica to afford B(OR)₂-oxasmaragdyrin complexes in 60-90% yields. The final oxasmaragdyrins Sm-BR₂ were isolated in moderate yields by hydrolysis of the precursors (11) and (12b)-(12e) with aqueous KOH in THF at reflux conditions. After acid work-up the precipitate was filtered through buckner funnel and dried under vacuum to yield analytically pure carboxyphenyl substituted Sm-BR₂ complexes. In our design, alkoxy groups with long chains from C₂ to C₁₀ are introduced to shield oxasmaragdyrins from aggregation and to increase their solubility.

4.2.2 Optical properties

The UV-Visible peak positions of *Soret* band and Q band, and molar absorption coefficient (ϵ) of oxasmaragdyrins Sm-BR₂ in THF are listed in Table 4-1. The absorption spectra of the studied oxasmaragdyrins Sm-BR₂ display two well separated split *Soret* bands in 400-500 nm and Q bands in 550-750 nm region as shown in Figure 4-2 (a). Markedly, the split *Soret* band covers a broader range of absorption wavelengths than regular porphyrins. The most interesting feature of BF₂ complexes is the strong absorption band at ~706 nm.

Table 4-1. Photophysical and Electrochemical data for oxasmaragdyrin dyes

Dye	$\lambda_{\text{abs}}/\text{nm}^a$ ($\epsilon / 10^3 \text{M}^{-1} \text{cm}^{-1}$)	$\lambda_{\text{em}}/\text{nm}^b$	E_{ox}/V^c	$E_{(0,0)}/\text{eV}^d$	$E_{\text{ox}}^*/\text{V}^e$
Sm-BF ₂	446 (278), 474 (113), 706 (36)	716	0.86	1.75	-0.89
Sm-B(OEt) ₂	450 (303), 479 (121), 711 (41)	724	0.69	1.73	-1.04
Sm-B(OBu) ₂	450 (291), 479 (117), 711 (38)	724	0.71	1.73	-1.02
Sm-B(OHep) ₂	450 (242), 480 (98), 710 (32)	723	0.72	1.73	-1.01
Sm-B(ODec) ₂	450 (188), 480 (79), 710 (29)	722	0.71	1.73	-1.02

^a In THF. ^b Emission maximum measured in THF by exciting at *Soret* band. ^cFirst oxidation potentials vs. NHE in THF calibrated by Fc/Fc⁺ couple.^[11] ^dEstimated from the intersection of the absorption and emission spectra. ^e approximated from E_{ox} and $E_{(0,0)}$.

This Q band is three times more intense than the absorption band of free-base oxasmaragdyrin present in the same region. The alkoxy chain substitution in **Sm-B(OR)₂** on boron atom slightly red shifted the absorption spectra compared to the BF₂ chelated oxasmaragdyrin **Sm-BF₂** which is supposed to be caused by the inductive effect of the alkoxy chains. Additionally, the Q bands, which are more intense than typical zinc or free base porphyrins and are mainly contributed from the HOMO to LUMO transition (Table 4-2) give the highest extinction coefficient (ϵ) at 710 nm, a shift of almost 100 nm into the NIR region compared to Zn(TPP). Figure 4-2 (b) displays absorption spectra of oxasmaragdyrins Sm-BR₂ adsorbed on TiO₂ film, illustrating the adsorption behavior of oxasmaragdyrins on TiO₂.

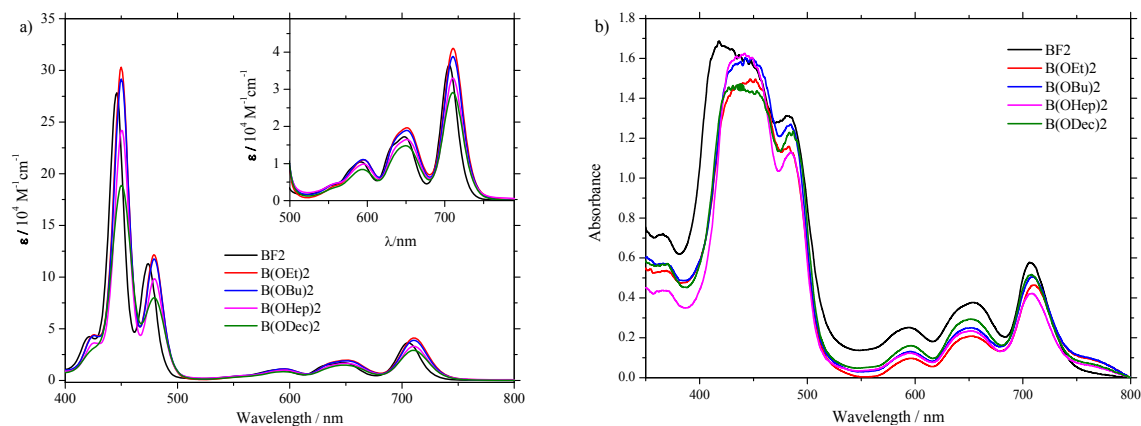


Figure 4-2. Absorption spectra of oxasmaragdyrins: (a) in THF, (inset: expansion of Q bands) and (b) adsorbed on TiO₂.

After adsorption on TiO_2 the absorption onset of the oxasmaragdyrins reached 800 nm, indicating that these dyes can act as NIR sensitizers. It is obvious that the *Soret* as well as Q bands are broadened after adsorption on TiO_2 which will ensure the collection of more photons when exposed to sunlight and consequently might result in higher efficiencies. We used the multi-gaussian functions to fit the absorption spectra in the Q band region ($1300\text{-}1800\text{ cm}^{-1}$). The absorption bands of oxasmaragdyrins on TiO_2 films are red-shifted as compared to the absorption in THF as shown in Figure 4-3. It also shows the packing modes of oxasmaragdyrins on TiO_2 are *J*-type aggregation. However, the alkyl chains attached on boron atom can protect the dye molecules from intermolecular aggregation. The energies of red-shifts at lowest band are 125.8 , 56.0 , and 27.9 cm^{-1} for **Sm-BF₂**, **Sm-B(OEt)₂**, and **Sm-B(ODec)₂**, respectively. The red-shift energies of **Sm-B(OBu)₂**, **Sm-B(OHep)₂** and **Sm-BF₂** are similar.

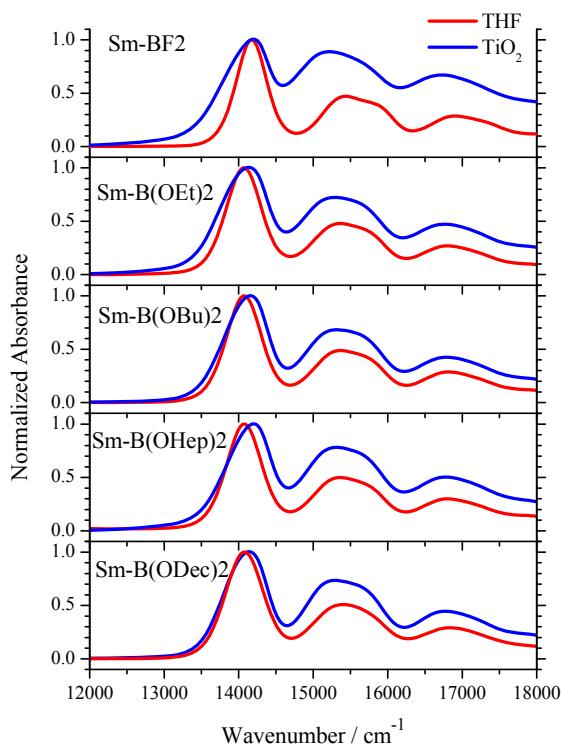


Figure 4-3. Absorption spectra of oxasmaragdyrins Sm-BR_2 in THF and on TiO_2 films.

The steady-state fluorescence spectra of all oxasmaragdyrins were measured in THF by excitation at *Soret* band and displayed in Figure 4-4. It revealed a similar pattern to the UV-Visible spectra, with slight red-shift due to alkoxy chain substitution but with considerably decreased intensity. The chain length has no effect on the fluorescence properties of these oxasmaragdyrins.

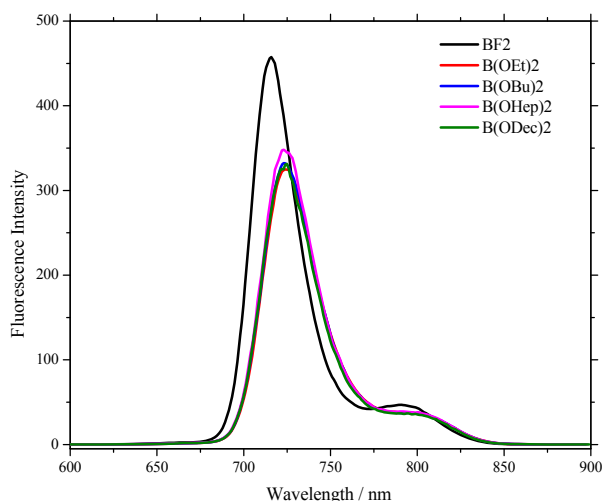


Figure 4-4. Fluorescence spectra of oxasmaragdyrins Sm-BR₂.

4.2.3 Cyclic Voltammetry Studies

The cyclic voltammetry (CV) measurements of all oxasmaragdyrins Sm-BR₂ observed two reversible oxidations and one reversible reduction couples as depicted in Figure 4-5. The static potentials and currents under multiple scans suggest high stability and reversibility of these compounds. The data in Table 4-1 show that the oxidation potentials of alkoxy substituted oxasmaragdyrins, shifted towards less positive by 140 to 170 mV resulting in elevated HOMO levels compared to BF₂ chelated oxasmaragdyrin. The reduction potentials of **Sm-B(OR)₂** shifted toward more negative by approximately 120 mV than Sm-BF₂ complex.

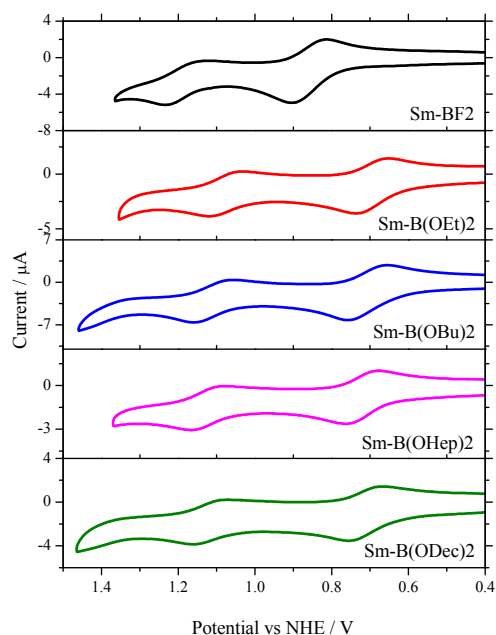


Figure 4-5. CV spectra of Sm-BR₂ oxasmaragdyrins.

From the intersection of the normalized absorption and emission spectra at Q(0,0) band, the zero-zero excitation energies $E_{(0,0)}$ for Sm-BR₂ were determined and listed in Table 4-1. Based on $E_{(0,0)}$ and the first oxidation potential obtained from CV, the ground state oxidation potentials (E_{ox}) and excited state oxidation potentials (E_{ox}^*) were calculated as listed in Table 4-1. The ground state oxidation potentials (E_{ox}) and excited state oxidation potentials (E_{ox}^*) are plotted along with TiO₂ conduction band and iodide/triiodide redox potential to gain an insight into the electron injection and dye regeneration dynamics (Figure 4-6). For an efficient electron injection from the excited state of the dye into the conduction band of TiO₂ and a faster regeneration of the oxidized dyes, appropriate tuning of HOMO with iodide/triiodide couple and the LUMO with TiO₂ conduction band is necessary. Although the red-shifting in absorption band of oxasmaragdyrins stands for smaller band gap between HOMO and LUMO levels, the electrochemical data confirm the high driving force for electron injection from the oxidized dye to the conduction band of TiO₂.

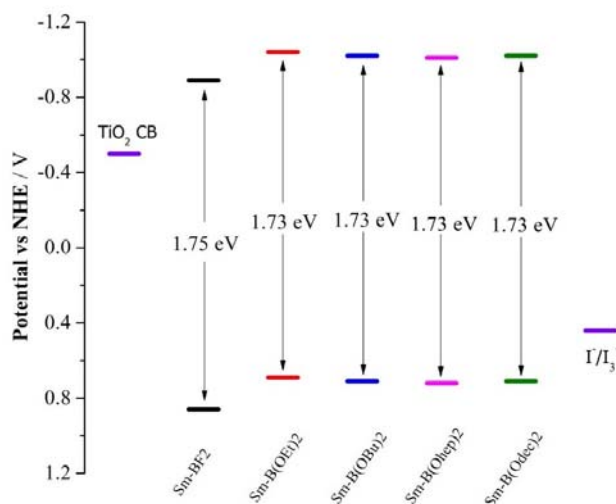


Figure 4-6. Energy level diagram of oxasmaragdyrins Sm-BR₂.

For all of the oxasmaragdyrin boryl complexes, E_{ox}^* are more negative than the conduction band edge of the TiO₂ electrode, indicating suitable driving force for efficient electron injection. The difference between the iodine/triiodide redox potential and the ground state oxidation potentials of the oxasmaragdyrin **Sm-BF₂** is 0.42V while it is 0.25 V for **Sm-B(OEt)₂**, 0.27 V for **Sm-B(OBu)₂**, 0.28 for **Sm-B(OHep)₂** and 0.27 for **Sm-B(ODec)₂**. The potential difference for oxasmaragdyrin **Sm-BF₂** is sufficient for effectual dye regeneration while it is insufficient for **Sm-B(OR)₂** (< 0.3 eV), which can also be seen from the high efficiency of the dye **Sm-BF₂**. It can be suggested from this difference that the dye regeneration for the alkoxide

substituted dyes **Sm-B(OR)₂** is not as efficient as **Sm-BF₂**. This might be one of the reason for the inferior efficiencies of former dyes compared to the later.

4.2.4 Density Functional Theory calculations

The quantum-mechanical calculations for structural optimization were performed for all the oxasmaragdyrins Sm-BR₂ using the density functional theory (DFT) with B3LYP functional and the 6-31G basis set. The results show planar macrocycles for all studied dyes (Figure 4-7).

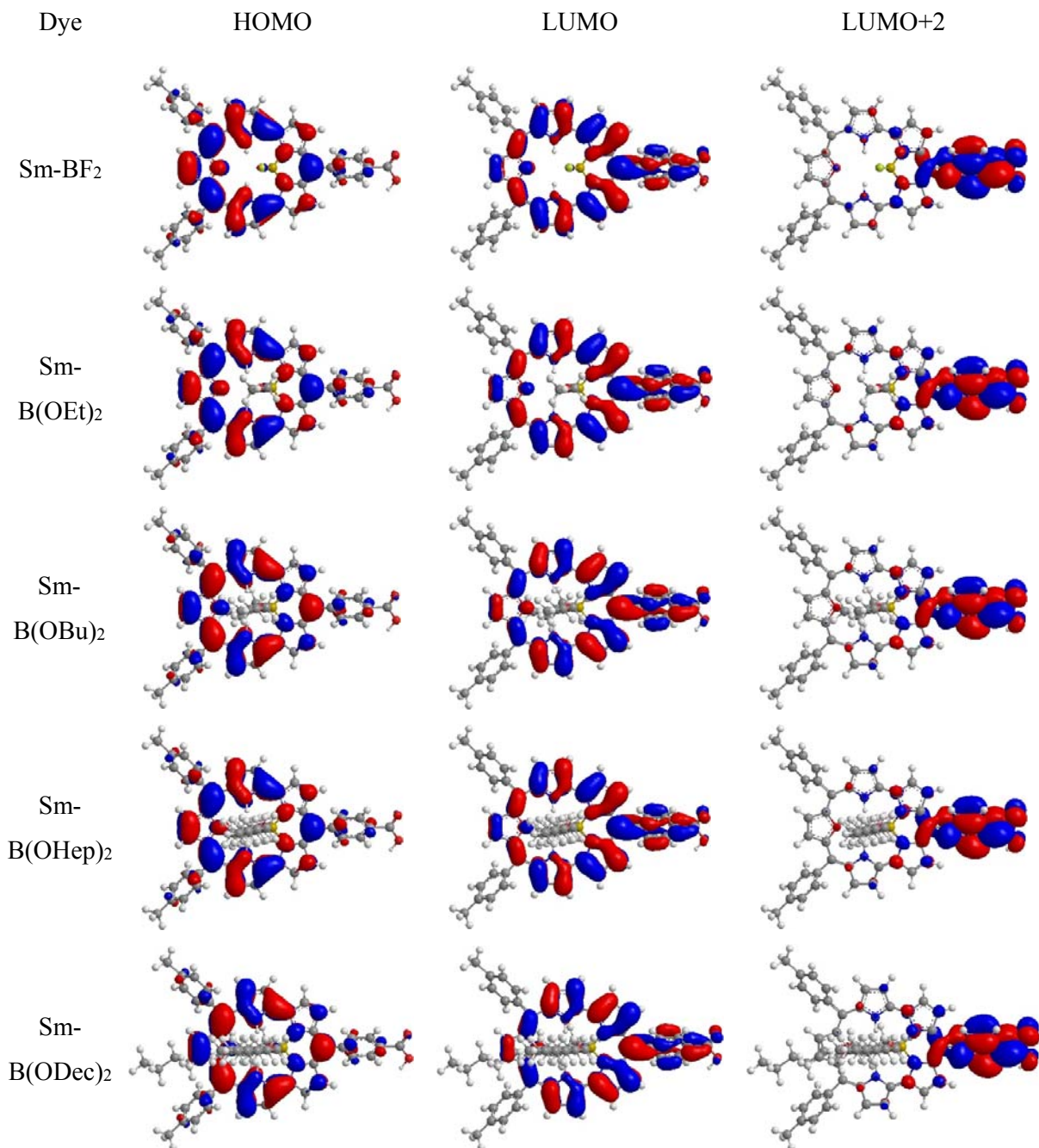


Figure 4-7. Molecular orbital diagrams of oxasmaragdyrins obtained from DFT calculations.

The planar ring ensures the effective transfer of the electrons from the donor to the acceptor groups. Two alkoxide long chains lay on opposite sides of the oxasmaragdyrin plane and extended over to shield the furanan ring. These alkoxy chains laying on the opposite side of the oxasmaragdyrin plane act as molecular separator and may help to reduce the aggregation of these dyes. The calculations indicate that in the HOMO and HOMO–1 orbitals, majority of the electron density localizes on the macrocyclic π -system of oxasmaragdyrin ring whereas in the LUMO orbitals, electron densities delocalized further to the *meso*-carboxyphenyl anchoring group. In LUMO+2 orbitals the electron density is extensively localized over the *meso*-carboxyphenyl anchoring group suggesting that the electron injection from higher excited states might also be possible. The effective electron density redistribution should facilitate efficient electron injection from the excited state of oxasmaragdyrin to the conduction band of TiO₂. Time-dependent density functional theory (TD-DFT) were also performed at B3LYP functional and the 6-31G basis set using Gaussian 9 software. For all the oxasmaragdyrins, the lowest energy transition ($S_0 \rightarrow S_1$) is approximately 80% of the HOMO \rightarrow LUMO transition, thus confirming its donor to acceptor charge-transfer character. Significantly, TD-DFT calculations also revealed a higher molecular dipole moment (8.60 D) for the BF₂ chelated oxasmaragdyrin than an average of 7.86 D for B(OR)₂ chelated oxasmaragdyrins as shown in Table 4-2. The higher polarizability is beneficial to facilitate intramolecular photoinduced electron transfer.

Table 4-2. Calculated TD-DFT compositions in terms of frontier molecular orbitals, excitation energy, and the oscillator strengths of Sm-BR₂

Dyes	State	Composition (%)	E (eV)	λ (nm)	f	Dipole Moment (Debye)
Sm-BF ₂	S1	H-1 \rightarrow L+1 (21) H \rightarrow L (79)	1.96	633.6	0.2646	8.5998
	S2	H-1 \rightarrow L+1 (29) H \rightarrow L (8) H \rightarrow L+2 (62)	2.86	434.0	0.6798	
	S3	H-1 \rightarrow L (36) H-1 \rightarrow L+2 (18) H \rightarrow L+1 (46)	2.95	420.3	0.8786	
	S4	H-1 \rightarrow L+1 (47) H \rightarrow L (13) H \rightarrow L+2 (37)	3.17	391.4	1.0674	
Sm-B(OEt) ₂	S1	H-1 \rightarrow L+1 (18) H \rightarrow L (82)	1.93	642.3	0.2906	7.9118
	S2	H-1 \rightarrow L+1 (24) H \rightarrow L (5) H \rightarrow L+2 (70)	2.78	446.2	0.4747	

	S3	H-1→L (34) H-1→L+2 (19) H→L+1 (48)	2.87	432.1	0.7172	
	S4	H-1→L+1 (54) H→L (13) H→L+2 (29)	3.11	399.0	1.0445	
Sm-B(OBu) ₂	S1	H-1→L+1 (18) H→L (82)	1.93	642.8	0.2848	7.8298
	S2	H-1→L+1 (25) H→L (6) H→L+2 (69)	2.78	445.7	0.4837	
	S3	H-1→L (34) H-1→L+2 (18) H→L+1 (48)	2.87	432.6	0.7114	
	S4	H-1→L+1 (54) H→L (13) H→L+2 (30)	3.10	399.7	0.9871	
Sm-B(OHep) ₂	S1	H-1→L+1 (18) H→L (82)	1.93	642.1	0.2829	7.9740
	S2	H-1→L+1 (24) H→L (5) H→L+2 (70)	2.78	446.1	0.4643	
	S3	H-1→L (34) H-1→L+2 (19) H→L+1 (48)	2.87	432.2	0.6939	
	S4	H-1→L+1 (54) H→L (13) H→L+2 (29)	3.10	399.4	0.999	
Sm-B(ODec) ₂	S1	H-1→L+1 (18) H→L (82)	1.93	641.9	0.2822	7.6389
	S2	H-1→L+1 (25) H→L (5) H→L+2 (69)	2.78	446.0	0.4699	
	S3	H-1→L (34) H-1→L+2 (18) H→L+1 (48)	2.87	432.3	0.6794	
	S4	H-1→L+1 (54) H→L (13) H→L+2 (30)	3.10	399.9	0.9761	
H=HOMO, L=LUMO, H-1=HOMO-1, L+1=LUMO+1, L+2=LUMO+2.						

4.2.5 Dye Loading Measurements

To better comprehend the adsorption behavior and measure the amount of adsorbed dye, we calculated the dye densities (Γ) adsorbed on TiO₂ surface. The oxasmaragdyrin densities (Γ) were determined by measuring the absorbance of the oxasmaragdyrins desorbed from the sensitized TiO₂ films after being immersed in 0.1 M KOH solution in THF. The saturated Γ

values of the oxasmaragdyrins under study were found to be 184, 110, 119, 146 and 194 nmol cm⁻² for **Sm-BF₂**, **Sm-B(OEt)₂**, **Sm-B(OBu)₂**, **Sm-B(OHep)₂** and **Sm-B(ODec)₂** oxasmaragdyrins, respectively. We expected that with the increasing length of the alkoxy chain the dye loading should be decrease. But the higher dye loadings for longer alkoxy substituted oxasmaragdyrins could be credited to their higher solubility in organic solvents. The trend of the dye loading is almost consistent with the overall efficiency pattern for these oxasmaragdyrins. The lower efficiencies of the devices for **Sm-B(OEt)₂** and **Sm-B(OBu)₂** can be partly attributed to the lower dye loading (DL) as shown in Table 4-3. In spite of having lower DL of 119 nmol compared to 146 nmol for **Sm-B(OHep)₂**, the superior performance of device based on **Sm-B(OBu)₂** is due to the higher short-circuit photocurrent density and open-circuit photovoltage. The same hypothesis is applicable for **Sm-BF₂** vs **Sm-B(ODec)₂**.

4.2.6 Photovoltaic Measurements

The Sm-BR₂ oxasmaragdyrins were fabricated into the solar cell devices in presence of CDCA as a co-adsorbent according to the procedures detailed in general techniques and evaluated for the photovoltaic performance under standard AM 1.5 G simulated solar conditions. The best photovoltaic performances of each oxasmaragdyrins are summarized in Table 4-3, where *J*_{sc} is short-circuit photocurrent density, *V*_{oc} is open-circuit photovoltage, *FF* is fill factor and *η* is solar to electrical conversion efficiency. The optimized I-V characteristics of the devices are displayed in Figure 4-8(a).

Table 4-3. Photovoltaic properties of devices with Sm-BR₂ dyes.

Dye	DL (nmol cm ⁻²)	<i>J</i> _{sc} (mA cm ⁻²)	<i>V</i> _{oc} (V)	<i>FF</i> (%)	<i>η</i> (%)
Sm-BF ₂	184	13.71	0.591	703	5.70
Sm-B(OEt) ₂	110	6.60	0.535	695	2.45
Sm-B(OBu) ₂	119	8.12	0.558	690	3.13
Sm-B(OHep) ₂	146	7.51	0.534	679	2.72
Sm-B(ODec) ₂	194	10.22	0.581	682	4.05

^aImmersion in EtOH at room temperature for 6-8 h.

As observed for the I-V curve, the DSSCs sensitized with oxasmaragdyrin BF₂ complex **Sm-BF₂** exhibited the best performance with a short-circuit photocurrent density of 13.71 mA cm⁻², an open-circuit voltage of 0.591 V, and a fill factor of 0.703, corresponding to an overall power conversion efficiency (*η*) of 5.70%. The oxasmaragdyrins **Sm-B(OR)₂** had the efficiencies lower than that of the **Sm-BF₂** complex, with a typical trend of an improved device

performance as increasing the length of alkoxy chains with an exception of the **Sm-B(OHep)₂** which has lower efficiency than **Sm-B(OBu)₂**. With the support of J_{sc} , 6.60 mA cm⁻², V_{oc} of 0.53 V and fill factor of 0.69, the **Sm-B(OEt)₂** achieved the overall photon-to-current conversion efficiency of 2.45%. The device assembled with **Sm-B(OBu)₂** obtained the efficiency of 3.13% well reinforced by J_{sc} of 8.12 mA cm⁻², V_{oc} of 0.56 V and fill factor of 0.69. The overall efficiency of 2.72% for **Sm-B(OHep)₂** is supported by J_{sc} of 7.51 mA cm⁻², V_{oc} of 0.53 V and fill factor of 0.68. The second best overall efficiency of 4.05% was obtained for **Sm-B(ODec)₂** with J_{sc} of 10.22 mA cm⁻², V_{oc} of 0.58 V and fill factor of 0.68.

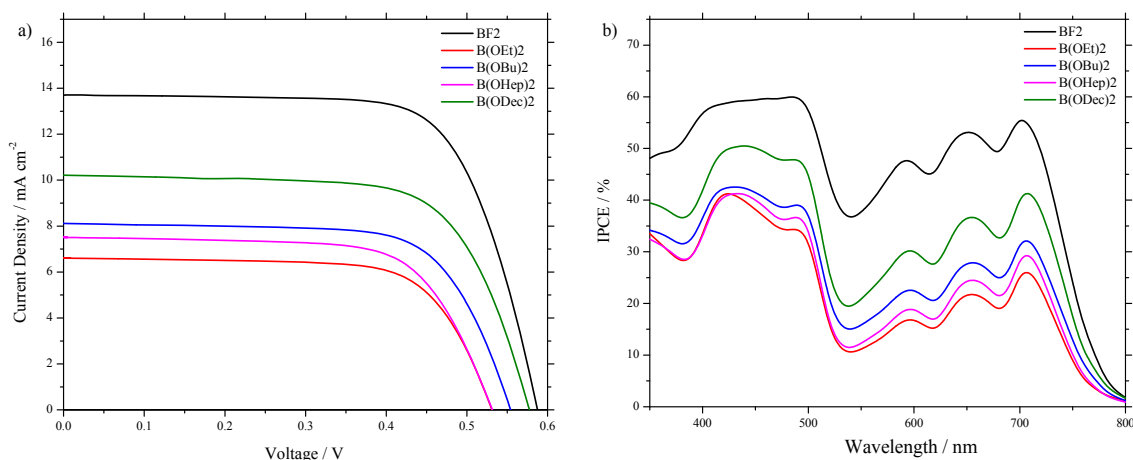


Figure 4-8 (a) IV characteristics and (b) IPCE spectra of DSSCs fabricated with oxasmaragdyrins Sm-BR₂ under 100% sun (AM 1.5 G).

The trend of J_{sc} in this series can be understood from the variation of IPCE spectra of these oxasmaragdyrins as shown in Figure 4-8(b). IPCE spectra of all the oxasmaragdyrins are in qualitative agreement with the corresponding absorption spectra of the dyes adsorbed on TiO₂. We note that the IPCE values corresponding to the absorption region of the *Soret* band of device **Sm-BF₂** reached 60%, and that of the Q band are around 50%. Also the dip between 500-600 nm is much higher (around 40%) for **Sm-BF₂** device compared to the devices based on oxasmaragdyrins **Sm-B(OR)₂**. From the IPCE spectra it is clear that the oxasmaragdyrin **Sm-BF₂** has panchromatic absorption feature covering whole visible region and a part of the near IR region.

4.2.7 Transient photoelectric and Charge-Extraction Measurements

To understand the key factors accounting for the IPCE values observed herein, we carried out transient photoelectric and charge-extraction (CE) measurements for the five devices under

investigation. The charge densities (N_e) of the devices under a certain bias light irradiation at an open-circuit condition were determined *via* CE measurements when the circuit of the system was switched to the short-circuit condition.^[12] The CE results show that the extracted charge densities were much smaller than those of highly efficient devices reported elsewhere.^[12] As a result, transient photovoltage decay (ΔV_{oc} vs. time) was performed using the small-amplitude approach based on seven white-light intensities (power densities in the range 7-102 mW cm⁻²) as bias irradiation under open-circuit conditions.^[12] Decay curves of ΔV_{oc} vs. time for the five devices were fitted according to a single exponential function to determine time coefficients for charge recombination (τ_R). Figure 4-9(a) and (b) show the plots of τ_R vs. N_e and V_{oc} vs. N_e , respectively. The plots of V_{oc} vs. N_e show that the potentials were down-shifted upon increasing the length of the alkoxy chains, and this trend is against the variation of V_{oc} showing the opposite trend (Table 4-3).

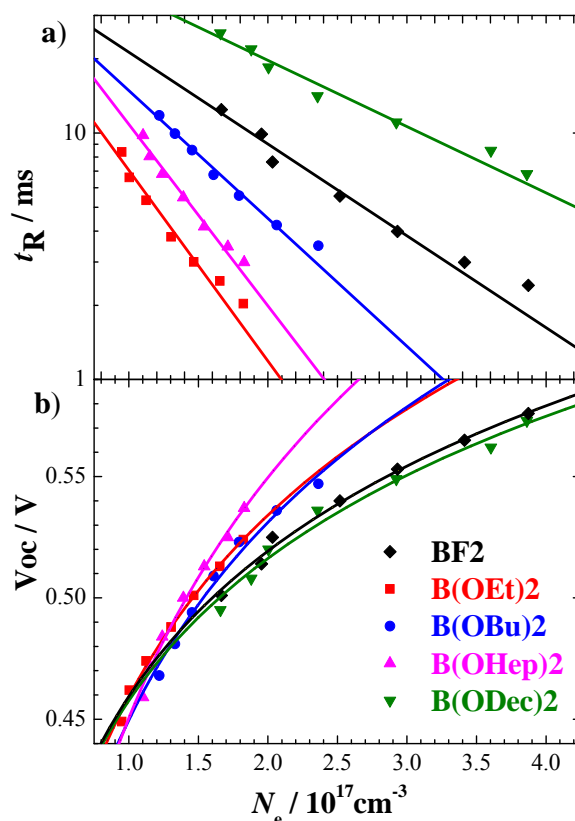


Figure 4-9. Plots of (a) charge recombination time coefficient (τ_R) vs. electron density (N_e) and (b) V_{oc} vs. N_e for DSSCs fabricated with Sm-BR₂.

On the other hand, we found that the values of τ_R in this series are much smaller than those reported for highly efficient dyes,^[12] confirming that the relatively poor device performances

of these oxasmaragdyrins are due to the effect of rapid charge recombination. This effect causes significant reduction of the charge densities in the conduction band of the TiO₂, and thus leads to a decrease in the performance for both J_{sc} and V_{oc} . The plots of τ_R vs. N_e shown in Figure 4-9a display a systematic trend of τ_R for B(OR)₂ complexes with **Sm-B(ODec)**₂ > **Sm-B(OBu)**₂ > **Sm-B(OHep)**₂ > **Sm-B(OEt)**₂, consistent with the variation of V_{oc} in this series. These results indicate that the two alkoxy chains attached to the boron center could help in retarding the charge recombination. Typically, a longer alkoxy chain would have a better retardation effect to repel the approach of triiodide anion species toward the surface of TiO₂ for a larger τ_R and a higher V_{oc} , but an exception for the **Sm-B(OHep)**₂ complex with heptoxyl chains was observed. Interestingly, we observed that the τ_R values of **Sm-B(ODec)**₂ were significantly greater than those of **Sm-BF**₂, which cannot explain the fact that V_{oc} of **Sm-BF**₂ was slightly larger than that of **Sm-B(ODec)**₂. We expect that the electron injection efficiency of the **Sm-BF**₂ device should be greater than that of the **Sm-B(ODec)**₂ device so as to generate more injected electrons in the CB of TiO₂ to give a larger fermi level for the observed higher V_{oc} for the former than for the latter. The effect of electron injection can also be applied to rationalize for the observed trend of J_{sc} , which is higher for **Sm-BF**₂ than for **Sm-B(ODec)**₂.^[13]

4.2.8 Femtosecond Transient Absorption studies

The transient absorption spectra of **Sm-BF**₂ and **Sm-B(OR)**₂ dyes on TiO₂ with excitation at 640 nm and monitored at 4800 nm are displayed in Figure 4-10. Since the transient absorption signal of electrons on TiO₂ conduction band is at ~4.8 μm , the transient absorption signal at 4800 nm directly displays the kinetics of the electron injection on TiO₂. As the excitation photon excites the smaragdyrin molecules to the first singlet excited state, the excited electron inject into the conduction band of TiO₂, and the absorption signal at 4.8 μm shows the rising behavior. The rising lifetime of all the smaragdyrin dyes demonstrates same electron injection lifetime around 50 femtosecond (fs). However, the transient absorption spectrum of **N719** on TiO₂ shows the double injection processes, the first at 50 fs and the second around 500 ps. The two injection processes for **N719** could be attributed to the injection from the singlet and triplet excited states. Compared with **N719**, the excited oxasmaragdyrins only inject electron from the S₁ state of the dye to TiO₂ CB. Although the energy gap between the LUMO and TiO₂ conduction band edge is the smallest for **Sm-BF**₂, the electron injection kinetics for oxasmaragdyrins on TiO₂ does not affect by the energy gap due to the highly conjugated linker. In addition, the transient absorption spectra also show the back electron transfer from TiO₂ to the dye cation.

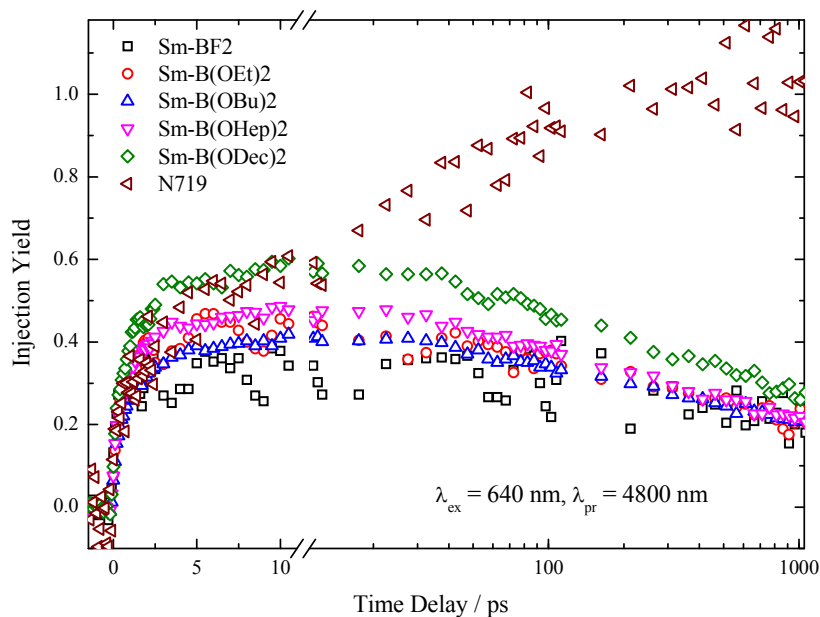


Figure 4-10. The transient absorption spectra of Sm-BR₂ dyes.

The length of alkoxy chain on boron atom in the oxasmaragdyrin is systemically increased from **B(OEt)₂** to **B(ODec)₂**, but it has negligible impact on the back electron transfer rate. Although the electron withdrawing strength of fluoride atoms is stronger than that of alkoxy groups, the back electron transfer rate is not influenced by it. Based on the femtosecond transient absorption spectra of oxasmaragdyrins, the rates of electron injection and back electron transfer of oxasmaragdyrins with excitation at the S₁ state are almost the same. They are mainly caused by the electronic densities at LUMO and LUMO+1 of oxasmaragdyrin molecules.

4.3 Conclusions

In conclusion, we are able to demonstrate for the first time that boron complexes of oxasmaragdyrin, a class of core-modified expanded porphyrin, can be applied as efficient photosensitizers for DSSC. Five novel oxasmaragdyrin boron complexes were prepared in four steps with 18% overall yield. Without exhausted coupling reactions to add electron donating groups, the plain oxasmaragdyrin boron chelated complex has already reached 5.7% power conversion efficiency. We demonstrated that the HOMO and LUMO energy levels of these dyes match quite well with the redox potential of I⁻/I₃⁻ electrolyte and with the TiO₂ conducting band. Boron chelated oxasmaragdyrins provide desired redox potentials, high absorption coefficients, high stability, and higher power conversion efficiencies suitable for an effective sensitizer in DSSCs. More importantly, broad absorption spreading the entire visible region

and its lower energy Q band covering part of the NIR region make this class of compounds an optimistic candidate for being one of the future selections of porphyrin-sensitized solar cells. By appending alkoxy substituents with different lengths, we are able to show that the alkyl chains extended from the central core can shield the molecules from aggregation while maintaining high degree of dye loading. Our current charge extraction measurements revealed faster charge recombination in comparison with the highest efficiency porphyrin dyes and provided an important direction to further improve the power conversion efficiency of these oxasmaragdyrin based expanded porphyrin dyes. We hope that this pioneer work can provide new insights and can inspire broad explorations on using diverse expanded porphyrins as NIR dyes for DSSC or on developing new suitable assemblies to take full advantage of expanded porphyrins to absorb NIR/IR light.

4.4 Experimental Section

4.4.1 General Techniques and Materials

All chemicals were obtained from commercial sources and used as received without further purification. All the reactions were carried out under nitrogen atmosphere. Solvents used in reactions were dried by PureSolv MD 5 system (Innovative Technology, Inc). Flash chromatography was carried out by using basic alumina (63-200 μm , Merck) and silica gel (40-63 μm , Merck). Analytical TLC was performed on Merck silica gel plates. ^1H , ^{13}C , ^{11}B and ^{19}F NMR spectra were recorded on a Bruker Avance 400 FT and DRX 500 spectrometer. NMR samples were prepared in CDCl_3 and THF as *d*-solvents and chemical shifts were reported in δ scale. The standard abbreviations s, d, t, q, m and bs refer to singlet, doublet, triplet, quartet, multiplet and broad singlet respectively. Coupling constant (J) values are reported in Hertz. The ESI ion trap mass spectra were measured by a Finnigan MAT LCQ mass spectrometer. The HR-FAB spectra were conducted on a JMS-700 double focusing mass spectrometer. Transmittance and reflection UV–visible absorption spectra of the oxasmaragdyrins in THF and adsorbed on TiO_2 electrodes, respectively, were recorded on a JASCO V-670 UV-vis/NIR spectrophotometer. Steady-state fluorescence spectra were acquired by using a Varian Cary Eclipse fluorescence spectrophotometer. The cyclic voltammetry measurements of all oxasmaragdyrins were carried out on CHI 621B electrochemical analyzer (CH Instruments, Austin, TX, USA) in degassed THF containing 0.1 M tetrabutylammonium hexafluorophosphate (Bu_4NPF_6) as the supporting electrolyte. The cell assembly consists of a glossy carbon as the working electrode, a silver wire as the pseudo-reference electrode, and a platinum wire as the auxiliary electrode. The scan rate for all measurements was fixed at 50 mV/sec. A ferrocene^{+1/0} redox couple was used as the internal standard and the potential values obtained in reference to the silver electrode were converted to the vacuum scale. The density functional theory (DFT) and time-dependent density functional (TD-DFT) calculations were performed with Gaussian 09 package to study the electron distribution of the frontier molecular orbitals and the photoexcitation transitions. All ground state geometries of oxasmaragdyrins Sm-BR₂ were optimized in the gas phase by the hybrid B3LYP functional and the 6-31G basis set, and the TD-DFT calculation were based on the same functional and basis set.^[14] The molecular orbitals were visualized by the Chemoffice software.

4.4.2 Synthesis

5(*p*-Methoxycarbonylphenyl)dipyrromethane (7)

A mixture of methyl-4-formylbenzoate (3.28 g, 0.02 mol) and pyrrole (137 ml, 2 mol) was degassed with N₂ for 15 min. at room temperature. TFA (150 μl, 0.002 mol) was then added and the mixture was stirred at room temperature for 3 hrs. After completion of the reaction, NaOH (2.4 g, 0.06 mol) was added and mixture was stirred for 1 h and then filtered. The filtrate was concentrated and pyrrole was removed under vacuum. The crude obtained after removing pyrrole was subjected to silica gel column chromatography using DCM/hexanes (4:6, R_f = 0.2) as eluting solvent to obtain the dipyrromethane (4.8 g, 86% Yield). ¹H NMR (400 MHz, CDCl₃) δ: 3.91 (s, 3H, CH₃), 5.53 (s, 1H, *meso* CH), 5.89 (s, 2H, β-pyrrole), 6.16 (m, 2H, β-pyrrole), 6.72 (m, 2H, α-pyrrole), 7.28 (m, 2H, Ph), 7.98, (m, 4H, Ph, NH) ppm; ¹³C NMR (100 MHz, CDCl₃) δ: 43.97, 52.08, 107.50, 108.57, 117.54, 128.41, 129.91, 131.58, 147.34 ppm.

2,5-Bis(*p*-tolylmethanol)furan (8)

Furan (1 ml, 13.75 mmol) was added to a solution of *n*-BuLi (22 ml, 34.37 mmol) and TMEDA (5.15 ml, 34.37 mmol) in 40 ml dry hexane under N₂. The reaction mixture was heated at reflux temperature for 1 h and then cooled to 0 °C. To this suspension, a pre-cooled solution of *p*-tolualdehyde (3.48 ml, 29.5 mmol) in 40 ml dry THF was added drop wise. After the addition was complete, the mixture was warmed to room temperature while stirring for 30 minutes. Saturated NH₄Cl solution was added to quench the reaction. The organic phase was extracted with H₂O, brine and then dried over MgSO₄. The crude product was subjected to silica gel column chromatography using EA/hexanes (3:7, R_f = 0.2) as eluting solvent to get furan diol (2.47 g, 58% Yield). ¹H NMR (400 MHz, CDCl₃) δ: 2.36 (s, 6H, Me), 2.42 (bs, 2H, OH), 5.75 (d, 2H, *meso* CH), 5.96 (d, β-furan), 7.16 (d, 4H, Ar), 7.30 (d, 4H, Ar) ppm; ¹³C NMR (100 MHz, CDCl₃) δ: 21.15, 69.99, 108.04, 108.11, 126.61, 129.12, 137.83, 156.20 ppm.

5,10-Ditolyl-16-oxatripyrrane (9)

Furan-diol (8) (1 g, 3.25 mmol) was dissolved in pyrrole (8.9 ml, 130 mmol) under N₂. To this solution BF₃•OEt₂ (0.41 ml, 3.25 mmol) was added. The mixture was stirred for 30 min. at room temperature. After completion of reaction as confirmed by TLC, the reaction was quenched by adding aqueous NaOH (0.1 N, 50 ml). The mixture was extracted with DCM and washed with water. The organic layer was dried over MgSO₄ and excess pyrrole was removed under vacuum. The crude oil was purified by column chromatography on silica using DCM/Hexanes (1:1, R_f = 0.4) as eluting solvent to get pure oxatripyrrane (800 mg, 60% Yield). ¹H NMR (400 MHz, CDCl₃) δ: 2.37 (s, 6H, Me), 5.39 (s, 2H, *meso* CH), 5.94 (s, 2H, β-pyrrole),

5.98 (d, 2H, β -furan), 6.16 (m, 2H, β -pyrrole), 6.65 (s, 2H, α -pyrrole), 7.13 (m, 8H, Ar), 7.98 (bs, 2H, NH) ppm; ^{13}C NMR (100 MHz, CDCl_3): δ = 21.01, 43.83, 107.01, 107.76, 108.11, 117.12, 128.17, 129.16, 131.21, 136.57, 137.74, 155.03 ppm.

19-(4-Methoxycarbonylphenyl)-5,10-di(*p*-tolyl)-25-oxasmaragdyrin (10)

5(*p*-methoxycarbonylphenyl)dipyrromethane (7) (513 mg, 1.26 mmol) and 5,10-ditolyl-16-oxatripyrrane (10) (354 mg, 1.26 mmol) were dissolved in 750 ml of DCM and stirred under nitrogen for 5 min. The reaction was initiated by adding TFA (10 μl , 0.126 mmol) and the stirring was continued for 90 min. DDQ (860 mg, 3.79 mmol) was then added and the reaction mixture was stirred in open air for additional 90 min. The solvent was removed and crude compound was purified by basic alumina column chromatography eluted with DCM/hexanes (3:7, R_f = 0.35) to get the desired oxasmaragdyrin as a green solid (325 mg, 38% yield). ^1H NMR (400 MHz, CDCl_3) δ : 2.72 (s, 6H; CH_3), 4.12 (s, 3H; OCH_3), 7.62 (d, 4H, J = 7.76 Hz; Ph), 8.10 (d, 4H, J = 7.8 Hz; Ph), 8.49 (m, 6H; Ph and β -pyrrole), 8.83 (s, 2H; β -furan), 8.95 (d, 2H, J = 4.32 Hz, β -pyrrole), 9.43 (d, 2H, J = 4.28 Hz; β -pyrrole), 9.52 (d, 2H, J = 4.28 Hz; β -pyrrole) ppm; HRMS-FAB $^+$: m/z calcd for $\text{C}_{45}\text{H}_{35}\text{N}_4\text{O}_3$: 679.2709, found 679.2708 $[\text{M}+\text{H}]^+$.

BF_2 -[19-(4-Methoxycarbonylphenyl)-5,10-di(*p*-tolyl)-25-oxasmaragdyrin] (11)

Oxasmaragdyrin (9) (700 mg, 1.03 mmol) was dissolved in DCM (100 ml) and triethylamine (5.72 ml, 41.2 mmol) was added at room temperature. After 10 min $\text{BF}_3 \cdot \text{OEt}_2$ (6.53 ml, 51.5 mmol) was added and the stirring was continued for 30 min. Completion of the reaction was confirmed by TLC. The reaction mixture was washed thoroughly with 0.1 M NaOH solution and water. The combined organic layers were dried over MgSO_4 , filtered and the solvent was removed under reduced pressure. The crude compound was purified by silica gel column chromatography, using DCM/hexanes (3:7, R_f = 0.27) to afford the desired compound (11) as green solid (464 mg, 62% yield). ^1H NMR (400 MHz, CDCl_3) δ : -3.97 (t, 2H; NH), 2.8 (s, 6H; Tol), 4.13 (s, 3H; OCH_3), 7.71 (d, 4H, J = 7.76 Hz; Ph), 8.31 (d, 4H, J = 7.8 Hz; Ph), 8.64 (d, 2H, J = 8.28 Hz; Ph), 8.71 (d, 2H, J = 8.28 Hz; Ph), 9.04 (dd, 2H, 1J = 4.34, 2J = 1.68; β -pyrrole), 9.52 (s, 2H; β -furan), 9.58 (d, 2H, J = 4.52 Hz, β -pyrrole), 10.24 (dd, 2H, 1J = 4.36, 2J = 1.84; β -pyrrole), 10.34 (d, 2H, J = 4.48 Hz; β -pyrrole) ppm; ^{11}B NMR (160.4 MHz, CDCl_3) δ : -12.79 (br s) ppm; ^{19}F NMR (470.5 MHz, CDCl_3) δ : -149.22 (br s) ppm; ^{13}C NMR (100 MHz, CDCl_3) δ : 167.45, 149.87, 144.02, 139.50, 137.95, 134.82, 134.28, 131.41, 130.68, 130.44, 129.56, 129.47, 128.30, 125.03, 123.90, 123.78, 122.14, 120.96, 120.43, 117.08, 107.10, 52.46, 21.64 ppm; HRMS-FAB $^+$: m/z calcd for $\text{C}_{45}\text{H}_{33}\text{BF}_2\text{N}_4\text{O}_3$: 726.2614, found 726.2617 $[\text{M}]^+$.

B(OC₂H₅)₂-[19-(4-Methoxycarbonylphenyl)-5,10-di(*p*-tolyl)-25-oxasmaragdyrin] (12b)

BF₂-Oxasmaragdyrin (11) (218 mg, 0.3 mmol) was dissolved in dry DCM (100 ml) in the presence of aluminum chloride (240 mg, 1.8 mmol) under nitrogen. The resulting mixture was refluxed for 10 min and then ethanol (10 ml) was added. The reaction mixture was stirred for additional 10 min at the same temperature. The reaction mixture was concentrated and purified by column chromatography on silica gel using hexanes/dichloromethane (1:1, R_f = 0.4) to get the desired product (12b) as green solid (210 mg, 90% yield). ¹H NMR (400 MHz, CDCl₃) δ: -3.91 (t, 6H, *J* = 7.36 Hz; CH₃), -3.59 (q, 4H, *J* = 7.16 Hz; OCH₂), -1.17 (s, 2H; NH), 2.78 (s, 6H; Tol), 4.16 (s, 3H; OCH₃), 7.67 (d, 4H, *J* = 7.64 Hz; Ph), 8.31 (d, 4H, *J* = 7.56 Hz; Ph), 8.63 (d, 2H, *J* = 7.72 Hz; Ph), 8.72 (d, 2H, *J* = 8.32 Hz; Ph), 8.78 (dd, 2H, ¹*J* = 3.26, ²*J* = 2.24; β-pyrrole), 9.39 (s, 2H; β-furan), 9.44 (d, 2H, *J* = 3.92 Hz, β-pyrrole), 9.98 (dd, 2H, ¹*J* = 3.54, ²*J* = 2.04; β-pyrrole), 10.17 (d, 2H, *J* = 4.48 Hz; β-pyrrole) ppm; ¹¹B NMR (160.4 MHz, CDCl₃) δ: -12.67 (br s); ¹³C NMR (125 MHz, CDCl₃) δ: 167.58, 149.51, 144.65, 140.1, 137.42, 134.94, 134.34, 132.25, 131.64, 130.05, 129.26, 128.97, 128.05, 124.62, 124.31, 122.97, 121.36, 119.38, 118.85, 117.17, 106.64, 52.48, 48.68, 21.63, 11.45 ppm; HRMS-FAB⁺: *m/z* calcd for C₄₉H₄₃BN₄O₅ : 778.3327, found 778.3333 [M]⁺.

B(OC₄H₉)₂-[19-(4-Methoxycarbonylphenyl)-5,10-di(*p*-tolyl)-25-oxasmaragdyrin] (12c)

BF₂-Oxasmaragdyrin (11) (218 mg, 0.3 mmol) was dissolved in dry DCM (100 ml) in the presence of aluminum chloride (240 mg, 1.8 mmol) under nitrogen. The resulting mixture was refluxed for 10 min and then 1-butanol (10 ml) was added. The reaction mixture was stirred for additional 10 min. The reaction mixture was concentrated and purified by column chromatography on silica gel using hexanes/DCM (6:4, R_f = 0.4) to get the desired product (12c) as green solid (221 mg, 88% yield). ¹H NMR (400 MHz, CDCl₃) δ: -3.73 (m, 4H; OCH₂), -3.53 (m, 8H; CH₂), -1.79 (m, 6H; CH₃), -1.26 (s, 2H; NH), 2.78 (s, 6H; Tol), 4.16 (s, 3H; OCH₃), 7.67 (d, 4H, *J* = 7.72 Hz; Ph), 8.28 (d, 4H, *J* = 7.76 Hz; Ph), 8.62 (d, 2H, *J* = 8.16 Hz; Ph), 8.71 (d, 2H, *J* = 8.16 Hz; Ph), 8.75 (dd, 2H, ¹*J* = 3.9, ²*J* = 1.96; β-pyrrole), 9.36 (s, 2H; β-furan), 9.44 (d, 2H, *J* = 4.36 Hz, β-pyrrole), 9.97 (dd, 2H, ¹*J* = 4.22, ²*J* = 1.6; β-pyrrole), 10.16 (d, 2H, *J* = 4.40 Hz; β-pyrrole) ppm; ¹¹B NMR (160.4 MHz, CDCl₃) δ: -12.47 (br s) ppm; ¹³C NMR (125 MHz, CDCl₃) δ: 167.53, 149.57, 144.77, 140.3, 137.46, 134.89, 134.31, 132.49, 131.75, 130.34, 129.22, 128.05, 124.52, 124.45, 122.9, 121.31, 119.36, 118.83, 117.24, 106.82, 52.53, 52.35, 30.84, 27.96, 21.59, 14.4, 10.62 ppm; HRMS-FAB⁺: *m/z* calcd for C₅₃H₅₁BN₄O₅: 834.3953, found 834.3957 [M]⁺.

B(OC₇H₁₅)₂-[19-(4-Methoxycarbonylphenyl)-5,10-di(*p*-tolyl)-25-oxasmaragdyrin] (12d)

BF₂-Oxasmaragdyrin (11) (218 mg, 0.3 mmol) was dissolved in dry DCM (100 ml) in the presence of aluminum chloride (240 mg, 1.8 mmol) under nitrogen. The resulting mixture was refluxed for 10 min and then 1-heptanol (10 ml) was added. The reaction mixture was stirred for additional 10 min. The reaction mixture was concentrated and purified by column chromatography on silica gel using hexanes/DCM (6:4, R_f = 0.43) to get the desired product (12d) as green solid (228 mg, 83% yield). ¹H NMR (400 MHz, CDCl₃) δ: -3.76 (m, 8H; OCH₂CH₂), -3.44 (m, 4H; CH₂), -1.56 (m, 4H; CH₂), -1.27 (s, 2H; NH), -0.69 (m, 4H; CH₂), 0.12 (m, 4H; CH₂), 0.31 (t, 6H; CH₃), 2.79 (s, 6H; Tol), 4.16 (s, 3H; OCH₃), 7.67 (d, 4H, *J* = 7.72 Hz; Ph), 8.28 (d, 4H, *J* = 7.76 Hz; Ph), 8.62 (d, 2H, *J* = 8.16 Hz; Ph), 8.71 (d, 2H, *J* = 8.12 Hz; Ph), 8.76 (dd, 2H, ¹*J* = 4.22, ²*J* = 1.96; β-pyrrole), 9.37 (s, 2H; β-furan), 9.43 (d, 2H, *J* = 4.36 Hz, β-pyrrole), 9.96 (dd, 2H, ¹*J* = 4.2, ²*J* = 1.72; β-pyrrole), 10.16 (d, 2H, *J* = 4.40 Hz; β-pyrrole) ppm; ¹¹B NMR (160.4 MHz, CDCl₃) δ: -12.52 (br s) ppm; ¹³C NMR (100 MHz, CDCl₃) δ: 167.58, 149.56, 144.8, 140.33, 137.46, 134.94, 134.37, 132.48, 131.72, 130.31, 129.25, 129.17, 128.06, 125.51, 124.55, 124.46, 122.9, 121.33, 119.42, 118.81, 117.22, 106.78, 52.92, 52.4, 30.32, 30.17, 26.28, 26.05, 21.6, 21.47, 13.58 ppm; HRMS-ESI: *m/z* calcd for C₅₉H₆₃BN₄O₅ : 918.4892, found 918.4886 [M]⁺.

B(OC₁₀H₂₁)₂-[19-(4-Methoxycarbonylphenyl)-5,10-di(*p*-tolyl)-25-oxasmaragdyrin] (12e)

BF₂-Oxasmaragdyrin (11) (165 mg, 0.23 mmol) was dissolved in dry DCM (100 ml) in the presence of aluminum chloride (181 mg, 1.36 mmol) under nitrogen. The resulting mixture was refluxed for 10 min and then 1-decanol (10 ml) was added. The reaction mixture was stirred for additional 10 min. The mixture was concentrated and purified by column chromatography on silica gel using hexanes/DCM (6:4, R_f = 0.48) to get the desired product (12e) as green solid (131 mg, 57% yield). ¹H NMR (400 MHz, CDCl₃) δ: -3.75 (m, 8H; OCH₂CH₂), -3.45 (m, 4H; CH₂), -1.58 (m, 4H; CH₂), -1.27 (s, 2H; NH), -0.69 (m, 4H; CH₂), 0.14 (m, 4H; CH₂), 0.66 (m, 4H; CH₂), 0.78 (t, 6H; CH₃), 0.89 (m, 4H; CH₂), 1.10 (m, 4H; CH₂), 2.79 (s, 6H; Tol), 4.16 (s, 3H; OCH₃), 7.67 (d, 4H, *J* = 7.68 Hz; Ph), 8.28 (d, 4H, *J* = 7.84 Hz; Ph), 8.62 (d, 2H, *J* = 8.08 Hz; Ph), 8.71 (d, 2H, *J* = 8.08 Hz; Ph), 8.76 (dd, 2H, ¹*J* = 4.14, ²*J* = 1.84; β-pyrrole), 9.36 (s, 2H; β-furan), 9.43 (d, 2H, *J* = 4.4 Hz, β-pyrrole), 9.96 (dd, 2H, ¹*J* = 4.26, ²*J* = 1.84; β-pyrrole), 10.16 (d, 2H, *J* = 4.44 Hz; β-pyrrole) ppm; ¹¹B NMR (160.4 MHz, CDCl₃) δ: -12.44 (br s) ppm; ¹³C NMR (125 MHz, CDCl₃) δ: 167.57, 149.56, 144.81, 140.33, 137.46, 134.93, 134.39, 132.48, 131.73, 130.31, 129.24, 129.18, 128.05, 124.55, 124.47, 122.9, 121.33, 119.43, 118.81, 117.22, 106.79, 52.91, 52.39, 31.6, 30.88, 28.86, 28.68,

28.02, 26.66, 26.05, 22.55, 21.62, 14.01 ppm; HRMS-FAB⁺: *m/z* calcd for C₆₅H₇₅BN₄O₅: 1002.5831, found 1002.5847 [M]⁺.

BF₂-[19-(4-Carboxyphenyl)-5,10-di(*p*-tolyl)-25-oxasmaragdyrin] (Sm-BF₂)

Oxasmaragdyrin (11) (125 mg, 0.17 mmol) was dissolved in 20 ml THF. To this mixture, KOH (193 mg, 3.4 mol) dissolved in 2 ml water was added and refluxed for 12 h. After cooling, the solvent was removed under vacuum. To the crude product DCM was added and extracted with 1 N HCl. The organic layer was dried over MgSO₄ and concentrated. Crude product was purified by silica gel column chromatography using DCM/MeOH (9.5:0.5, R_f = 0.1) as eluent to get the desired product **Sm-BF₂** as green solid (114 mg, 94% yield). ¹H NMR (400 MHz, THF-*d*8) δ: -3.88 (t, 2H; -NH), 2.78 (s, 6H; Tol), 7.73 (d, 4H, *J* = 7.64 Hz; Ph), 8.32 (d, 4H, *J* = 7.68 Hz; Ph), 8.66 (d, 2H, *J* = 7.96 Hz; Ph), 8.75 (d, 2H, *J* = 7.96 Hz; Ph), 9.01 (d, 2H, *J* = 4.12; β-pyrrole), 9.55 (s, 2H; β-furan), 9.64 (d, 2H, *J* = 4.40 Hz, β-pyrrole), 10.42 (dd, 2H, ¹*J* = 4.54, ²*J* = 1.44; β-pyrrole), 10.51 (d, 2H, *J* = 4.44 Hz; β-pyrrole) ppm; ¹¹B NMR (160.4 MHz, THF-*d*8) δ: -14.76 (br s) ppm; ¹⁹F NMR (470.5 MHz, THF-*d*8) δ: -151.35 (br s) ppm; ¹³C NMR (125 MHz, THF-*d*8) δ: 168.00, 152.74, 150.74, 144.47, 140.64, 138.9, 138.19, 135.8, 135.18, 132.44, 131.67, 131.42, 130.6, 129.23, 128.85, 125.96, 125.69, 124.98, 124.86, 123.37, 121.72, 121.69, 118.44, 107.83, 21.75 ppm; HRMS-FAB⁺: *m/z* calcd for C₄₄H₃₁BF₂N₄O₃: 712.2457, found 712.2449 [M]⁺.

B(OC₂H₅)₂-[19-(4-Carboxyphenyl)-5,10-di(*p*-tolyl)-25-oxasmaragdyrin] [Sm-B(OEt)₂]

Oxasmaragdyrin 12b (40 mg, 0.052 mmol) was dissolved in 10 ml THF. To this mixture, KOH (56 mg, 1.04 mol) dissolved in 2 ml water was added and refluxed for 12h. After cooling, the solvent was removed under vacuum. Residue was dissolved in DCM and extracted with 1 N HCl. The organic layer was dried over MgSO₄ and concentrated. Crude product was purified by silica gel column chromatography using DCM/MeOH (9.5:0.5, R_f = 0.16) as eluent to get the desired product **Sm-B(OEt)₂** as green solid (35 mg, 88% yield). ¹H NMR (400 MHz, CDCl₃) δ: -3.92 (t, 6H, *J* = 6.88 Hz; CH₃), -3.61 (q, 4H, *J* = 6.94 Hz; OCH₂), -1.22 (s, 2H; NH), 2.79 (s, 6H; Tol), 7.68 (d, 4H, *J* = 7.64 Hz; Ph), 8.31 (d, 4H, *J* = 7.64 Hz; Ph), 8.76 (m, 6H; β-pyrrole, Ph), 9.39 (s, 2H; β-furan), 9.48 (d, 2H, *J* = 2.96 Hz; β-pyrrole), 10.00 (d, 2H, *J* = 2.12 Hz; β-pyrrole), 10.2 (d, 2H, *J* = 4.28 Hz; β-pyrrole) ppm; ¹¹B NMR (160.4 MHz, CDCl₃) δ: -12.64 (br s) ppm; ¹³C NMR (125 MHz, CDCl₃) δ: 171.07, 149.7, 145.67, 140.28, 137.5, 135.1, 134.43, 132.43, 131.81, 130.27, 129.91, 128.09, 124.63, 122.96, 121.48, 119.51, 118.97, 117.03, 106.79, 48.75, 21.6, 11.43 ppm; HRMS- FAB⁺: *m/z* calcd for C₄₈H₄₁BN₄O₅: 764.3170, found 764.3169 [M]⁺.

B(OC₄H₉)₂-[19-(4-Carboxyphenyl)-5,10-di(*p*-tolyl)-25-oxasmaragdyrin] [Sm-B(OBu)₂]

Oxasmaragdyrin 12c (200 mg, 0.24 mmol) was dissolved in 50 ml THF. To this mixture, KOH (269 mg, 4.8 mol) dissolved in 5 ml water was added and refluxed for 12h. After cooling, the solvent was removed under vacuum. To the crude product DCM was added and extracted with 1 N HCl. The organic layer was dried over MgSO₄ and concentrated. Crude product was purified by silica gel column chromatography using DCM/MeOH (9.5:0.5, R_f = 0.15) as eluent to get the desired product **Sm-B(OBu)₂** as green solid (169 mg, 86% yield). ¹H NMR (400 MHz, CDCl₃) δ: -3.73 (t, 4H; OCH₂), -3.51 (m, 8H; CH₂), -1.8 (t, 6H; CH₃), -1.29 (s, 2H; NH), 2.8 (s, 6H; Tol), 7.69 (d, 4H, *J* = 7.5 Hz; Ph), 8.29 (d, 4H, *J* = 7.65 Hz; Ph), 8.78 (m, 6H; β-pyrrole, Ph), 9.38 (s, 2H; β-furan), 9.5 (s, 2H, β-pyrrole), 10.01 (d, 2H, *J* = 3.16, β-pyrrole), 10.21 (d, 2H, *J* = 4.35 Hz; β-pyrrole) ppm; ¹¹B NMR (160.4 MHz, CDCl₃) δ: -12.47 (br s) ppm; ¹³C NMR (125 MHz, CDCl₃) δ: 171.71, 149.61, 145.76, 143.13, 140.32, 137.51, 135.13, 134.37, 132.51, 131.72, 130.39, 129.92, 128.09, 125.51, 124.51, 122.92, 121.46, 119.51, 118.96, 117.02, 106.9, 52.56, 30.33, 27.98, 21.64, 14.43, 10.67 ppm; HRMS-FAB⁺: *m/z* calcd for C₅₂H₄₉BN₄O₅: 820.3796, found 820.3798 [M]⁺.

B(OC₇H₁₅)₂-[19-(4-Carboxyphenyl)-5,10-di(*p*-tolyl)-25-oxasmaragdyrin] [Sm-B(OHep)₂]

Oxasmaragdyrin 12d (200 mg, 0.22 mmol) was dissolved in 50 ml THF. To this mixture, KOH (244 mg, 4.36 mmol) dissolved in 5 ml water was added and refluxed for 12h. After cooling, the solvent was removed under vacuum. To the crude product DCM was added and extracted with 1N HCl. The organic layer was dried over MgSO₄ and concentrated. Crude product was purified by silica gel column chromatography using DCM/MeOH (9.5:0.5, R_f = 0.16) as eluent to get the desired product **Sm-B(OHep)₂** as green solid (188 mg, 94% yield). ¹H NMR (400 MHz, CDCl₃) δ: -3.74 (m, 8H; OCH₂CH₂), -3.43 (m, 4H; CH₂), -1.55 (m, 4H; CH₂), -1.28 (s, 2H; NH), -0.67 (m, 4H; CH₂), 0.14 (m, 4H; CH₂), 0.32 (t, 6H; CH₃), 2.79 (s, 6H; Tol), 7.69 (d, 4H, *J* = 7.76 Hz; Ph), 8.29 (d, 4H, *J* = 7.72 Hz; Ph), 8.79 (m, 6H; β-pyrrole, Ph), 9.39 (s, 2H; β-furan), 9.49 (d, 2H, *J* = 4.36 Hz, β-pyrrole), 9.99 (dd, 2H, ¹*J* = 4.14, ²*J* = 1.6; β-pyrrole), 10.2 (d, 2H, *J* = 4.36 Hz; β-pyrrole) ppm; ¹¹B NMR (160.4 MHz, CDCl₃) δ: -12.47 (br s) ppm; ¹³C NMR (100 MHz, CDCl₃) δ: 171.49, 149.58, 145.71, 140.34, 137.48, 135.13, 134.39, 132.47, 131.69, 130.34, 129.9, 128.33, 128.08, 124.57, 124.52, 122.9, 121.45, 119.52, 118.9, 116.98, 106.83, 52.93, 30.19, 26.29, 26.05, 21.61, 21.48, 13.6 ppm; HRMS-ESI: *m/z* calcd for C₅₈H₆₁BN₄O₅: 904.4735, found 904.4739 [M]⁺.

B(OC₁₀H₂₁)₂-[19-(4-Carboxyphenyl)-5,10-di(*p*-tolyl)-25-oxasmaragdyrin][Sm-B(ODec)₂]
 Oxasmaragdyrin 12e (131 mg, 0.13 mmol) was dissolved in 30 ml THF. To this mixture, KOH (145 mg, 2.61 mmol) dissolved in 5 ml water was added and refluxed for 12h. After cooling, the solvent was removed under vacuum. To the crude product DCM was added and extracted with 1N HCl. The organic layer was dried over MgSO₄ and concentrated. Crude product was purified by silica gel column chromatography using DCM/MeOH (9.5:0.5, R_f = 0.18) as eluent to get the desired product **Sm-B(ODec)₂** as green solid (112 mg, 91% yield). ¹H NMR (400 MHz, CDCl₃) δ: -3.75 (m, 8H; OCH₂CH₂), -3.45 (m, 4H; CH₂), -1.58 (m, 4H; CH₂), -1.3 (s, 2H; NH), -0.68 (m, 4H; CH₂), 0.15 (m, 4H; CH₂), 0.67 (m, 4H; CH₂), 0.79 (t, 6H; CH₃), 0.88 (m, 4H; CH₂), 1.10 (m, 4H; CH₂), 2.8 (s, 6H; Tol), 7.68 (d, 4H, *J* = 7.72 Hz; Ph), 8.29 (d, 4H, *J* = 7.68 Hz; Ph), 8.77 (m, 6H; β-pyrrole, Ph), 9.39 (s, 2H; β-furan), 9.49 (d, 2H, *J* = 4.08 Hz, β-pyrrole), 9.99 (d, 2H, *J* = 2.56; β-pyrrole), 10.19 (d, 2H, *J* = 3.92 Hz; β-pyrrole) ppm; ¹¹B NMR (160.4 MHz, CDCl₃) δ: -12.46 (br s) ppm; ¹³C NMR (100 MHz, CDCl₃) δ: 172.09, 149.57, 145.76, 140.34, 137.48, 135.15, 134.43, 132.47, 131.67, 130.33, 129.94, 128.07, 124.58, 124.53, 122.9, 121.46, 119.54, 118.91, 116.96, 106.84, 52.9, 31.63, 28.89, 28.71, 28.04, 26.67, 26.05, 22.58, 21.65, 21.57, 14.05 ppm; HRMS-FAB⁺: *m/z* calcd for C₆₄H₇₃BN₄O₅ : 988.5674, found 988.5676 [M]⁺.

4.4.3 Electrode preparation and Device fabrication

The devices were fabricated with a working electrode based on TiO₂ nanoparticles (NP) and a Pt-coated counter electrode reported elsewhere. For the working electrode, a paste composed of TiO₂ NP (particle size ~20 nm) prepared with a sol-gel method for the transparent nanocrystalline layer was coated on a TiCl₄-treated FTO glass substrate (TEC 7, Hartford, USA) to obtain the required thickness of the film with repetitive screen printing. To improve the performance of the device, an additional scattering layer (particle size ~300 nm) was added on the transparent active layer. The TiO₂ electrode was immersed in either of the following solutions containing (1) **Sm-BF₂** (0.1 mM) and CDCA (0.3 mM) in ethanol at 25 °C for 7 h; (2) **Sm-B(OEt)₂** (0.1 mM) and CDCA (0.3 mM) in ethanol at 25 °C for 6 h; (3) **Sm-B(OBu)₂** (0.1 mM) and CDCA (0.3 mM) in ethanol at 25 °C for 6 h; (4) **Sm-B(OHep)₂** (0.1 mM) and CDCA (0.3 mM) in ethanol at 25 °C for 5 h; (5) **Sm-B(ODec)₂** (0.1 mM) and CDCA (0.3 mM) in ethanol at 25 °C for 5h. Afterwards, the sensitized film was washed in absolute ethanol, dried in air. The working electrode was assembled with the counter electrode into a complete cell of sandwich type and sealed with a hot-melt film (SX1170, thickness 60 μm) at 120 °C. The

electrolyte solution containing LiI (0.1 M), I₂ (0.05 M), PMII (1.0 M), and 4-tert-butylpyridine (0.5 M) in a mixture of acetonitrile was introduced into the space between the two electrodes, so completing the fabrication of these DSSC devices.

4.4.4 Photovoltaic characterization

The current-voltage characteristics were determined with a digital source meter (Keithley 2400) with the device under one-sun AM-1.5G irradiation from a solar simulator (XES-502S, SAN-El) calibrated with a standard silicon reference cell (Oriel PN 91150V, VLSI standards). The efficiency (η) of conversion of light to electricity is obtained via $\eta = J_{sc} V_{oc} FF / P_{in}$, in which $J_{sc}/\text{mA cm}^{-2}$ is the current density measured at short circuit, and V_{oc}/V is the voltage measured at open circuit. P_{in} is the input radiation power (for one-sun illumination $P_{in} = 100 \text{ mW cm}^{-2}$) and FF is the filling factor. The spectra of the IPCE of the corresponding devices were recorded with a system comprising a Xe lamp (PTi A-1010, 150 W), a monochromator (PTi, 1200 gr mm^{-1} blazed at 500 nm), and a source meter (Keithley 2400). A standard Si photodiode (ThorLabs FDS1010) served as reference to calibrate the power density of the light source at each wavelength.

4.5 References

- [1] (a)J. L. W. Sessler, S. J., *Expanded, contracted and isomeric porphyrins (Oxford: Elsevier), and references therein. 1997*; (b)J. L. G. Sessler, A.; Weghorn, S. J., *Expanded porphyrins. In The porphyrin handbook (Eds) Kadish, K. M.; Smith, K. M.; Guillard, R. (New York: Academic Press). 2000*.
- [2] J. M. Lim, Z. S. Yoon, J.-Y. Shin, K. S. Kim, M.-C. Yoon, D. Kim, *Chem. Commun. 2009*, 261-273.
- [3] (a)B. Sridevi, S. J. Narayanan, R. Rao, T. K. Chandrashekar, U. Englisch, K. Ruhlandt-Senge, *Inorg. Chem. 2000*, 39, 3669-3677; (b)P. D. Beer, P. A. Gale, *Angew. Chem. Int. Ed. 2001*, 40, 486-516; (c)J. L. Sessler, S. Camiolo, P. A. Gale, *Coord. Chem. Rev. 2003*, 240, 17-55; (d)Y. Ikawa, M. Takeda, M. Suzuki, A. Osuka, H. Furanuta, *Chem. Commun. 2010*, 46, 5689-5691.
- [4] K. Naoda, H. Mori, N. Aratani, B. S. Lee, D. Kim, A. Osuka, *Angew. Chem. Int. Ed. 2012*, 51, 9856-9859.
- [5] (a)R. Misra, R. Kumar, V. PrabhuRaja, T. K. Chandrashekar, *J. Photochem. Photobiol., A 2005*, 175, 108-117; (b)R. Misra, R. Kumar, T. K. Chandrashekar, A. Nag, D. Goswami, *Org. Lett. 2006*, 8, 629-631.

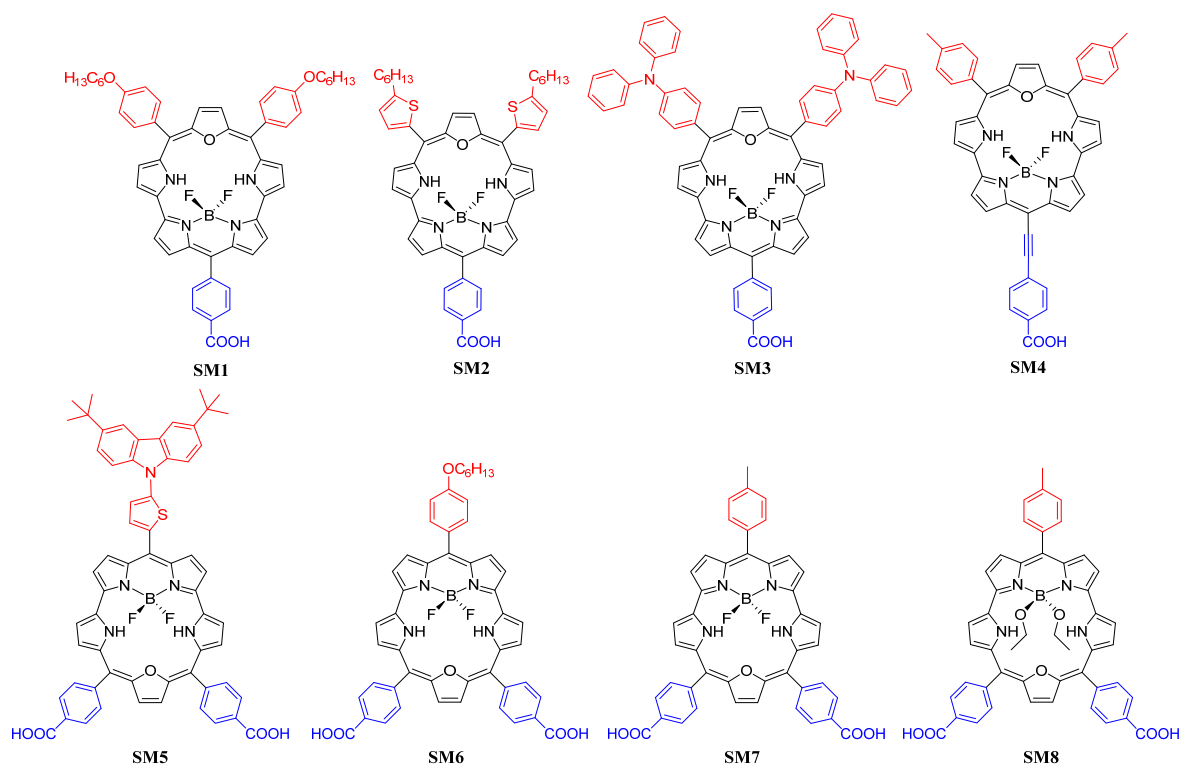
- [6] (a)A. Harriman, B. G. Maiya, T. Murai, G. Hemmi, J. L. Sessler, T. E. Mallouk, *J. Chem. Soc., Chem. Commun.* **1989**, 314-316; (b)M. M. Judy, J. L. Maithews, J. T. Newman, H. L. Skiles, R. L. Boriack, J. L. Sessler, M. Cyr, B. G. Maiya, S. T. Nichol, *Photochem. Photobiol.* **1991**, 53, 101-107; (c)Pushpan S. K., A. V. G. Venkatraman S., Sankar J., Parmeswaran D., Ganesan S., Chandrashekar T. K., *Curr Med Chem Anticancer Agents* **2002**, 2, 187-207; (d)J. Seenisamy, S. Bashyam, V. Gokhale, H. Vankayalapati, D. Sun, A. Siddiqui-Jain, N. Streiner, K. Shin-ya, E. White, W. D. Wilson, L. H. Hurley, *J. Am. Chem. Soc.* **2005**, 127, 2944-2959.
- [7] (a)M. J. Broadhurst, R. Grigg, A. W. Johnson, *J. Chem. Soc. D: Chem. Comm.* **1969**, 0, 1480-1482; (b)V. J. Bauer, D. L. J. Clive, D. Dolphin, J. B. Paine, F. L. Harris, M. M. King, J. Loder, S. W. C. Wang, R. B. Woodward, *J. Am. Chem. Soc.* **1983**, 105, 6429-6436.
- [8] S. J. Narayanan, B. Sridevi, T. K. Chandrashekar, U. Englisch, K. Ruhlandt-Senge, *Org. Lett.* **1999**, 1, 587-590.
- [9] L.-L. Li, E. W.-G. Diao, *Chem. Soc. Rev.* **2013**, 42, 291-304.
- [10] M. Rajeswara Rao, M. Ravikanth, *J. Org. Chem.* **2011**, 76, 3582-3587.
- [11] (a)V. V. Pavlishchuk, A. W. Addison, *Inorg. Chim. Acta* **2000**, 298, 97-102; (b)G. Boschloo, A. Hagfeldt, *Acc. Chem. Res.* **2009**, 42, 1819-1826; (c)T. Daeneke, T.-H. Kwon, A. B. Holmes, N. W. Duffy, U. Bach, L. Spiccia, *Nat. Chem.* **2011**, 3, 211-215.
- [12] L.-L. Li, Y.-C. Chang, H.-P. Wu, E. W.-G. Diao, *Int. Rev. Phys. Chem.* **2012**, 31, 420-467.
- [13] C. Y. Lee, C. She, N. C. Jeong, J. T. Hupp, *Chem. Commun.* **2010**, 46, 6090-6092.
- [14] M. J. Frisch, et al., *Gaussian 09 (Revision A.02)*

5. Molecular engineering of boryl oxasmaragdyrin sensitizers through peripheral modification: Effect of number and position of donor-acceptor groups

5.1 Introduction

The design, synthesis and first DSSC application of novel boryl oxasmaragdyrin dyes was discussed in the previous chapter. The photovoltaic studies revealed that these core-modified expanded porphyrins exhibited panchromatic IPCEs, high photo-current densities and moderate-to-good efficiencies. These excellent photovoltaic properties of core-modified expanded porphyrins advocates the fruitful application of these dyes in efficient DSSCs. The short synthetic route of 3-4 steps with high overall yields (15-18%) compared with the highly efficient porphyrin dyes (> 6 steps, overall yield < 5%) open up high chances of their practical application. We believed that molecular engineering of these oxasmaragdyrin dyes through peripheral substitutions like long alkoxy chains, different donor and linker groups and reversal of the electron flow by changing the position of carboxylic acid anchors shall lead to the improved performance in DSSCs. In an attempt to improve the solubility, decrease the molecular aggregation and efficiency of these expanded porphyrins, we introduced long alkoxy chains on the boron atom. In spite of the increased solubility the photovoltaic performance remain inferior to the BF₂ chelated oxasmaragdyrin as discussed in the previous chapter.

In this chapter we have devoted our efforts to modify the oxasmaragdyrin ring with long alkoxy chains on *meso*-position, different donor and linker groups and reversal of the electron flow by changing the position of carboxylic acid anchors. We have designed and synthesized eight oxasmaragdyrin molecules with various substituents on the periphery and their structures are presented in Scheme 5-1. The dyes **SM1** and **SM2** consists of *p*-hexyloxyphenyl and hexyl thiophene groups, while dye **SM3** is decorated with the electron donating triphenylamine (TPA) group along with one *p*-carboxyphenyl group on the *meso*-positions. In the dye **SM4** π -conjugation of the oxasmaragdyrin ring was extended with the coupling of ethynylphenyl linker group with carboxylic acid as anchoring group. The concept of reversal of electron flow was materialized with swapping the positions of donor and anchor groups in dye **SM1**. The dyes **SM5**, **SM6** and **SM7** were prepared with two *p*-carboxyphenyl groups as anchors and thiophene carbazole, *p*-hexyloxyphenyl and tolyl groups as donors on *meso*-positions. The possibility of upsurge in electron transport on replacing the electron withdrawing fluoride atoms with electron rich ethoxy groups on boron atom was examined in dye **SM8**.



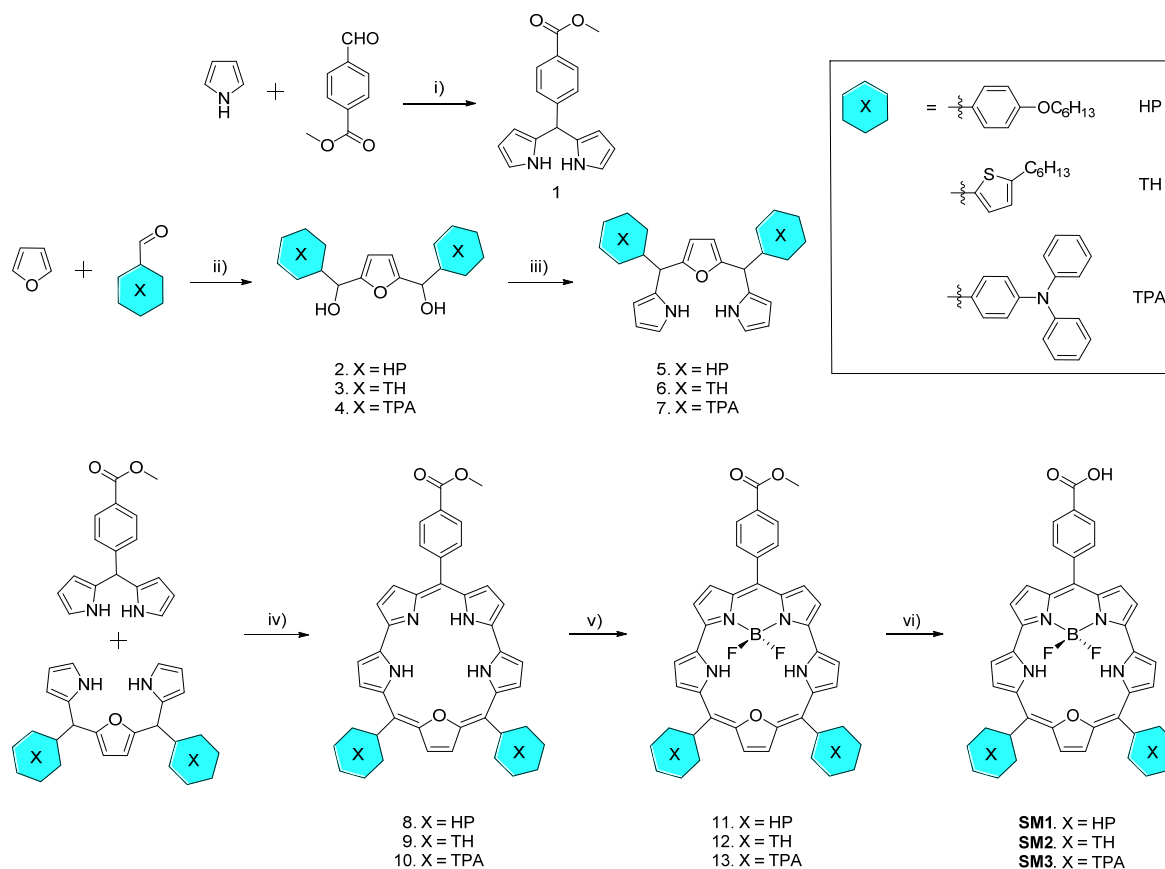
Scheme 5-1. Molecular structures of oxasmaragdyrin dyes.

5.2 Results and Discussion

5.2.1 Syntheses of SM dyes

SM dyes were synthesized in least possible steps with minimum application of tedious coupling reactions, starting with the key precursors dipyrromethane and 16-oxatripyrrane. The assembly of the oxasmaragdyrins **SM1-SM3** and its boron chelation is displayed in Scheme 5-2. One equivalent of methyl-4-formylbenzoate was treated with excess pyrrole in presence of TFA as acid catalyst to obtain the *meso*-(4-methoxyphenyl)dipyrromethane in good yields. For oxatripyrrane, furan was treated with corresponding aldehydes in presence of *n*-BuLi to get a symmetrical furan diols which were further reacted with excess pyrrole in presence boron trifluoride-diethyl etherate as catalyst to yield *meso*-aryl-16-oxatripyrranes. The oxasmaragdyrins were prepared by the 3+2 MacDonald-type condensation of *meso*-(4-methoxyphenyl)dipyrromethane with *meso*-aryl-16-oxatripyrrane under mild acidic condition followed by subsequent oxidation with 2,3-dichloro-5,6-dicyano-1,4-benzoquinone (DDQ) to afford the *meso* substituted oxasmaragdyrins as major product. These free base oxasmaragdyrins were further treated with excess triethylamine (NEt₃) followed by boron trifluoride-diethyl etherate (BF₃•OEt₂) at room temperature to give boron chelated

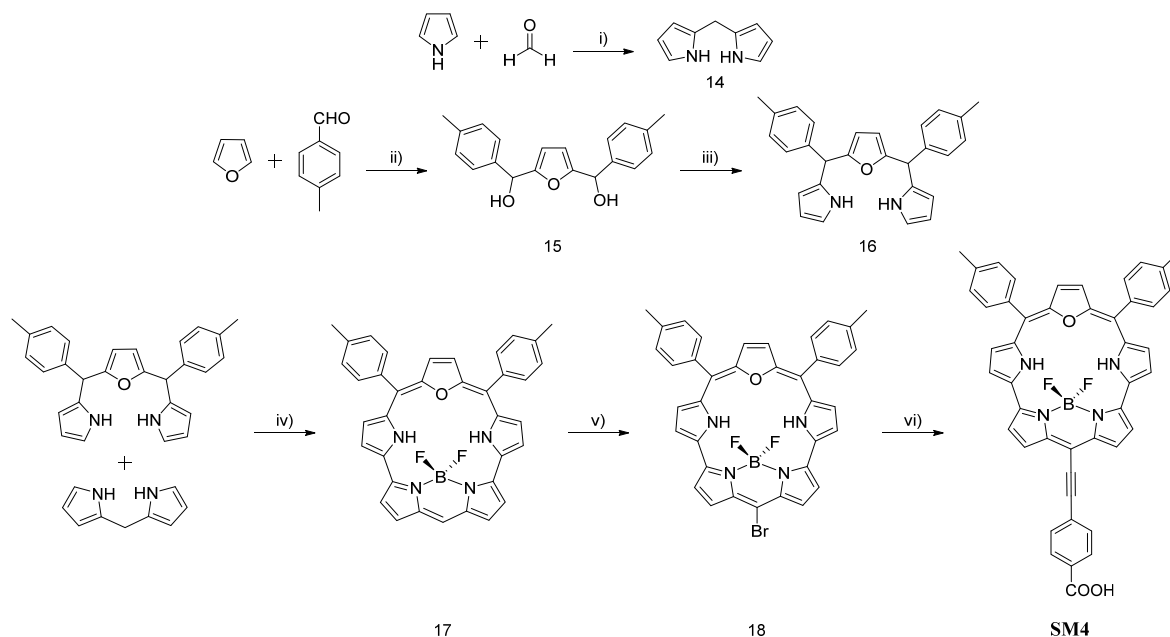
oxasmaragdyrins. After basic workup the oxasmaragdyrins were chromatographed to the purest possible form at this stage so as to avoid the purification in the last step. These mono ester oxasmaragdyrins were hydrolyzed with aqueous solution of KOH to yield analytically pure oxasmaragdyrins as green solids in decent yields.



Scheme 5-2. Synthesis of oxasmaragdyrin dyes SM1-SM3. Reagents and Conditions: i) TFA; ii) *n*-BuLi, TMEDA, Hexane/THF; iii) Pyrrole, $\text{BF}_3 \cdot \text{OEt}_2$; iv) TFA, DDQ, DCM; v) NEt_3 , $\text{BF}_3 \cdot \text{OEt}_2$, DCM; vi) KOH (aq.), THF.

To prepare **SM4** (Scheme 5-3), one equivalent of paraformaldehyde was treated with excess pyrrole in presence of TFA to obtain the *meso*-unsubstituted dipyrromethane **14**. The *meso*-tolyl-16-oxatripyrrane was prepared following the synthetic path for oxatripyrrane **16**. The *meso*-unsubstituted oxasmaragdyrin is assembled under acidic conditions followed by subsequent oxidation with DDQ which was further treated with excess NEt_3 and $\text{BF}_3 \cdot \text{OEt}_2$ at room temperature to give boron chelated oxasmaragdyrin **17** in 3% yield as shown in Scheme 5-3. After standard workup and chromatographic purification, the oxasmaragdyrin was isolated as green solid. This *meso*-unsubstituted oxasmaragdyrin **17**, is then brominated with *N*-

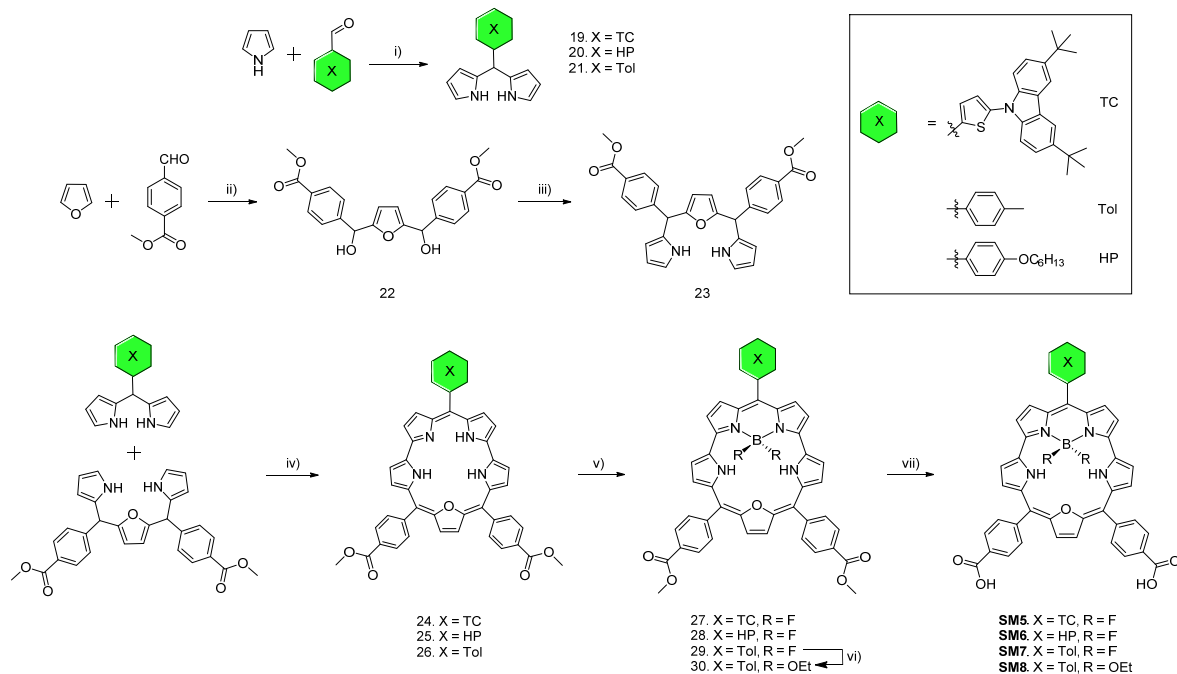
bromosuccinamide (NBS) at low temperature to get the oxasmaragdyrin **18**. This *meso*-bromooxasmaragdyrin was reacted with 4-ethynylbenzoic acid at 60 °C under Sonogashira coupling protocol to obtain the desired **SM4** in good yield.



Scheme 5-3. Synthesis of oxasmaragdyrin dyes **SM4**. Reagents and Conditions: i) TFA; ii) *n*-BuLi, TMEDA, Hexane/THF; iii) Pyrrole, $\text{BF}_3 \cdot \text{OEt}_2$; iv) a. TFA, DDQ, DCM; b. NEt_3 , $\text{BF}_3 \cdot \text{OEt}_2$, DCM; v) NBS, THF; vi) 4-ethynylbenzoic acid, $\text{Pd}_2(\text{dba})_3$, AsPh_3 , Toulene/ NEt_3 .

The boryl oxasmaragdyrins **SM5-SM8** were prepared following the same synthetic path used for **SM1-SM3** and is presented in Scheme 5-4. The *meso*-aryldipyrromethanes were prepared in decent yields by treating one equivalent of corresponding aldehydes with excess pyrrole in presence of TFA as catalyst. Furan was treated with methyl-4-formylbenzoate in presence of *n*-BuLi to get a symmetrical diol which was further reacted with excess pyrrole in presence of $\text{BF}_3 \cdot \text{OEt}_2$ to yield *meso*-(4-methoxyphenyl)-16-oxatripyrrane. The oxasmaragdyrins were prepared by following the 3+2 MacDonald-type condensation protocol of *meso*-aryldipyrromethanes with the 16-oxatripyrrane under mild acidic conditions followed by succeeding oxidation with DDQ to afford the dicarboxylate substituted oxasmaragdyrins. These free-base oxasmaragdyrins were further treated with excess NEt_3 and $\text{BF}_3 \cdot \text{OEt}_2$ at room temperature to give boron chelated oxasmaragdyrins. After regular workup the oxasmaragdyrins were purified by column chromatography to afford the pure products. These diester oxasmaragdyrins were hydrolyzed with aqueous solution of KOH to yield analytically pure oxasmaragdyrins as green solids in decent yields. All these boryl oxasmaragdyrins along

with their intermediates were thoroughly characterized with the help of common analytical techniques such as ^1H , ^{13}C , ^{11}B , ^{19}F NMR spectroscopy, UV-Visible spectroscopy, cyclic voltammetry, and HRMS spectroscopy.



Scheme 5-4. Synthesis of oxasmaragdyrin dyes SM5-SM8. Reagents and Conditions: i) TFA; ii) *n*-BuLi, TMEDA, Hexane/THF; iii) Pyrrole, $\text{BF}_3 \cdot \text{OEt}_2$; iv) TFA, DDQ, DCM; v) NEt_3 , $\text{BF}_3 \cdot \text{OEt}_2$, DCM; vi) EtOH, AlCl_3 , DCM; vii) KOH (aq.), THF.

5.2.2 Optical properties

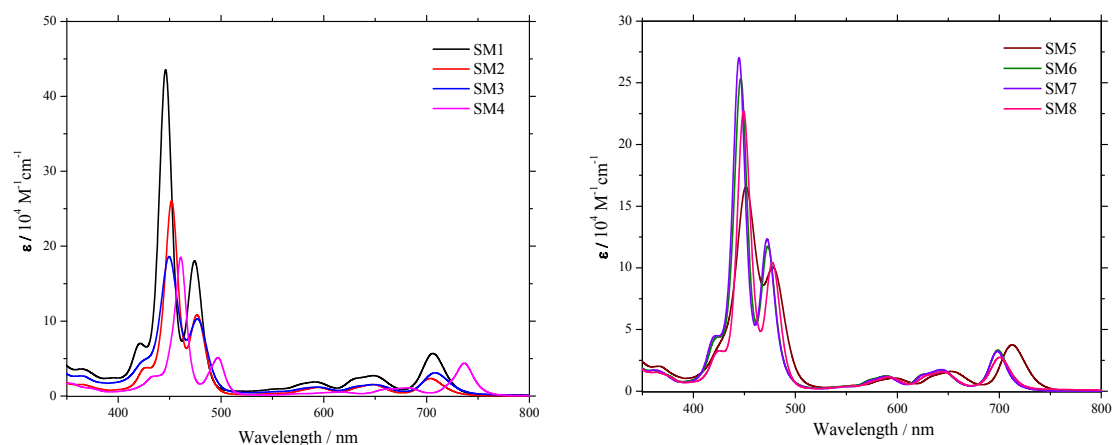
The UV-Visible peak positions of the *Soret* and Q bands and the molar extinction coefficients (ϵ) of the oxasmaragdyrins in THF are summarized in Table 5-1. The absorption spectra of these oxasmaragdyrins display split *Soret* bands in the 445-500 nm region and Q bands in the 550–750 nm region as shown in Figure 5-1. Evidently, the split *Soret* band covers a broader range of absorption wavelengths than regular porphyrins and BODIPY dyes. Additionally, the Q bands, which are more intense than those for typical porphyrins are mainly contributed from the HOMO to LUMO transition. The absorption wavelengths of these oxasmaragdyrins depend largely on the nature of the substituents. In monocarboxylic acid substituted oxasmaragdyrins, the addition of electron donating hexylthiophene group in **SM2** and triphenylamine group in **SM3** red-shifted the absorption wavelengths by 3-6 nm compared to **SM1**, while the coupling of ethynylphenyl linker in **SM4** observed the highest bathochromic shift of 15 nm for the *Soret* band compared to **SM1**.

Table 5-1. Photophysical and electrochemical data for SM dyes.

Dye	$\lambda_{\text{abs}}/\text{nm}^a$ ($\epsilon/10^3\text{M}^{-1}\text{cm}^{-1}$)	$\lambda_{\text{em}}/\text{nm}^b$	E_{ox}/V^c	$E_{(0,0)}/\text{eV}^d$	$E_{\text{ox}}^*/\text{V}^e$
SM1	446 (438), 474 (181), 706 (57)	719	0.82	1.75	-0.93
SM2	452 (261), 477 (108), 704 (23)	719	0.88	1.75	-0.87
SM3	449 (186), 477 (103), 708 (31)	723	0.86	1.74	-0.88
SM4	461 (186), 497 (51), 737 (44)	743	0.88	1.68	-0.80
SM5	452 (165), 478 (100), 712 (38)	726	0.90	1.72	-0.82
SM6	446 (254), 473 (118), 699 (33)	705	0.87	1.77	-0.90
SM7	445 (271), 472 (124), 698 (32)	705	0.88	1.77	-0.89
SM8	449 (228), 477 (104), 700 (27)	710	0.73	1.76	-1.03

^aIn THF. ^bEmission maximum measured in THF by exciting at *Soret* band. ^cFirst oxidation potentials vs. NHE in THF calibrated with Fc/Fc⁺ couple. ^dEstimated from the intersection of the absorption and emission spectra. ^eApproximated from E_{ox} and $E_{(0,0)}$.

The absorption onset in dye **SM4** reached beyond 750 nm, indicating the light harvesting for this dye might be higher in visible as well as in near infra-red (NIR) region. In dicarboxylic acid substituted oxasmaragdyrins, the substitution of electron donating thiophene carbazole unit on the oxasmaragdyrin ring in **SM5**, bathochromically shifted the absorption in *Soret* as well as Q band region, extending the absorption onset beyond 750 nm. The broadened absorption is beneficial as increased light harvesting can improve the photocurrent density. Changing the number and position of the hexyloxyphenyl and carboxylic acid in **SM6** compared to **SM1** did not have any effect on the absorption spectrum. Ethoxy substitution on the boron atom in case of dye **SM8** as compared to dye **SM7** slightly red-shifted the absorption spectrum.

**Figure 5-1.** UV-Visible spectra of SM dyes in THF.

This suggests that the electron donating nature of ethoxy group has negligible influence on the optical properties of this dye. The higher molar extinction coefficients ($1.65\text{--}4.38 \times 10^5 \text{ M}^{-1} \text{ cm}^{-1}$) for **SM1-SM8** also supports the proposition of a good light harvesting nature of these dyes. To better comprehend the adsorption behavior of the dyes on TiO_2 , absorption spectra of these dyes as thin films were studied and the results are displayed in Figure 5-2.

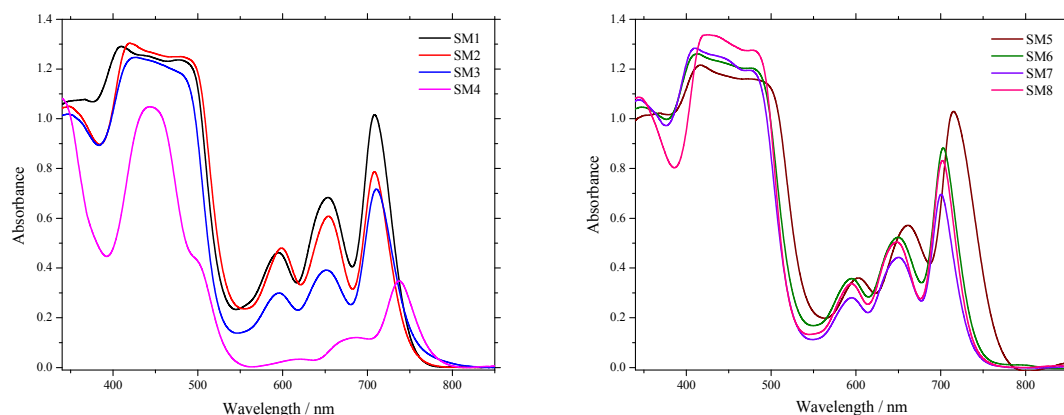


Figure 5-2. UV-visible spectra of SM dyes in adsorbed on TiO_2 .

To obtain the absorption spectra on TiO_2 films, the films with $\sim 3 \mu\text{m}$ thickness were immersed in 0.1 mM THF solution of the SM dyes at room temperature. The adsorption spectra were recorded by reflectance measurements using an integrated sphere. The absorption spectra of dyes show significant broadening and slight red-shifts upon adsorption on the TiO_2 surface compared to their UV-Visible spectra in THF with threshold of absorption around 800 nm. This broadening and significant red-shifts in the UV-Visible spectra after adsorption on TiO_2 films suggests that more charge collection is possible in *Soret* and Q band region which in turn may result in higher efficiency in DSSCs.

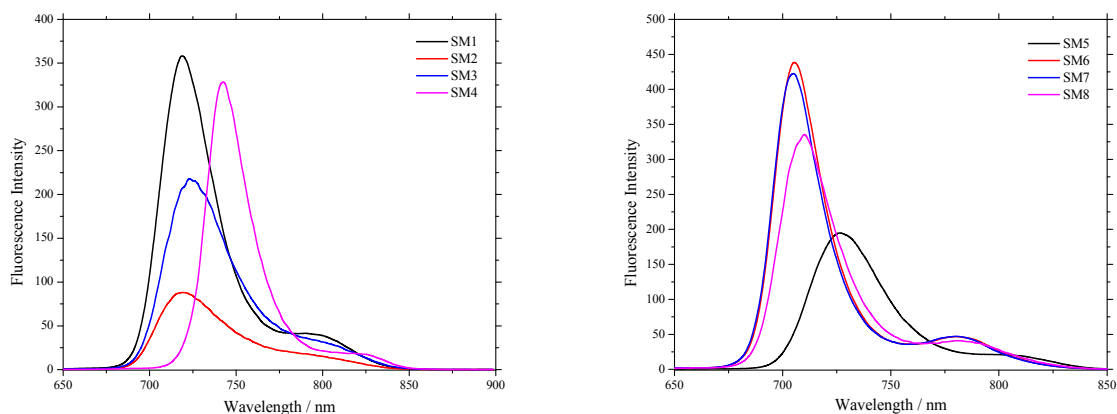


Figure 5-3. Fluorescence spectra of SM dyes.

The steady-state fluorescence spectra of these dyes were measured in THF by excitation at *Soret* band. As displayed in Figure 5-3, it revealed a similar trend to the UV-Visible spectra, with slight red-shift in the wavelengths due to the increased π -conjugation through donor and linker variations.

5.2.3 Electrochemical properties

Suitable matching of highest occupied molecular orbital (HOMO) with the electrolyte for a faster regeneration of the oxidized dye and the lowest unoccupied molecular orbital (LUMO) with the conduction band of semiconductor for an efficient electron injection is important. The cyclic voltammetry measurements of all the oxasmaragdyrins were carried out in degassed THF containing 0.1 M tetrabutyl ammonium hexafluorophosphate ($[\text{Bu}_4\text{N}]\text{PF}_6$) as the supporting electrolyte under a scan rate of 50 mV to obtain the first oxidation potentials as depicted in Figure 5-4. As seen from the CV spectra, two reversible oxidation couples and one reversible reduction couple were observed for **SM1**, **SM2** and **SM5** whereas one reversible oxidation and one reversible reduction couple was observed for **SM3**, **SM4**, **SM6**, **SM7** and **SM8**.

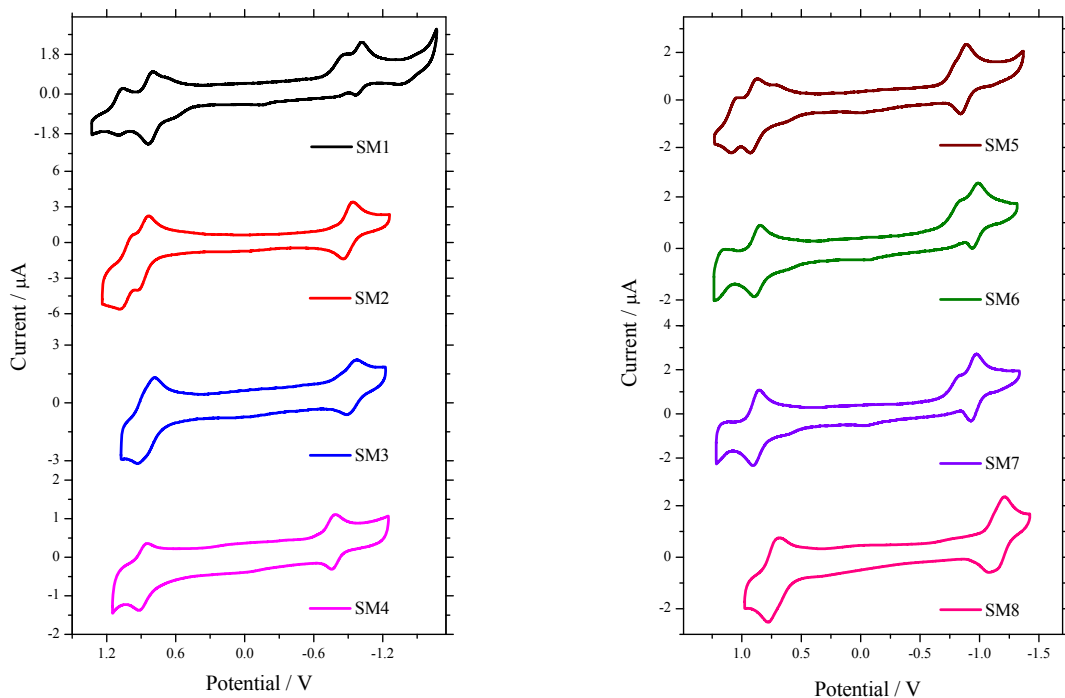


Figure 5-4. Cyclic voltammograms of SM dyes.

The first oxidation couple in **SM1**, **SM2** and **SM5** corresponds to the oxasmaragdyrin ring. In monocarboxylic acid substituted oxasmaragdyrins, the oxidation potentials for **SM2**, **SM3** and

SM4 are more positive than that of the **SM1** indicating that they are harder to be oxidized. The oxidation potentials in the dicarboxylic acid substituted oxasmaragdyrins **SM5**, **SM6** and **SM7** are larger by 50-80 mV and for **SM8**, it is smaller by 90 mV than that of **SM1**. The ethoxy substitution on boron center in **SM8** resulted in a negative shift in the oxidation potential by 150 mV than **SM7**. The zero-zero excitation energies, $E_{(0,0)}$ were calculated from the intersection of the normalized absorption and emission spectra at the Q (0,0) band and were depicted in Table 5-1. The excited state oxidation potentials were estimated from the first oxidation potentials and the zero-zero excitation energies and are listed in Table 5-1. The systematic energy level diagram for the studied oxasmaragdyrin dyes is displayed in the Figure 5-5. As evident from the energy level diagram, for the monocarboxylic acid substituted oxasmaragdyrins, the addition of hexylthiophene group did not change the band gap, while TPA (**SM3**) donor unit lowers the band gap than **SM1**. Obvious decrease in the band gap is observed for **SM4** due to the increased conjugation through ethynylphenyl linker. However in dicarboxylic acid substituted oxasmaragdyrins, incorporation of electron rich thiophene-carbazole unit reduced the energy gap compared to other derivatives. It is also observed from the energy level diagram that the difference between the ground state oxidation potential of **SM8** and the redox potential of the electrolyte is 0.29 V which is not enough to regenerate the oxidized dye. The LUMO of the oxasmaragdyrins are more negative than the TiO₂ conduction band (> 0.3 V) and thus ensure the adequate driving force for the electron injection from dye to the TiO₂ conduction band. The HOMO of all the oxasmaragdyrins except **SM8** are more positive (> 0.3 V) than the redox electrolyte which confirms the efficient dye regeneration. This might be one of the reason for the inferior efficiency of dye **SM8**. Overall, the band gap analysis suggests, the energy gaps and the HOMO-LUMO potentials of these dyes are suitable for the DSSC application.

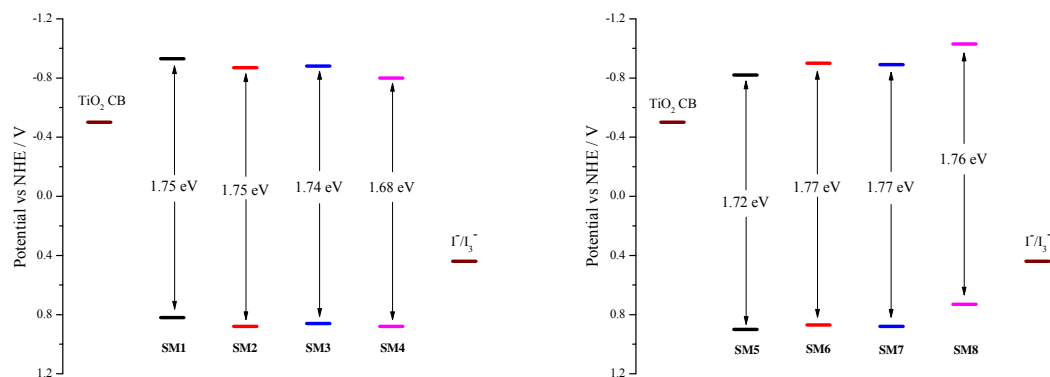


Figure 5-5. Energy level diagram for SM dyes.

5.2.4 DFT calculations

To correlate the molecular structures of dyes with the performance of DSSCs, we carried out density functional theory (DFT) as well as time-dependent DFT (TD-DFT) calculations at the B3LYP/6-31G level of theory using a suite of Gaussian 9 software. The results from theoretical calculations show planar macrocycles for all studied dyes as depicted in Figure 5-6.

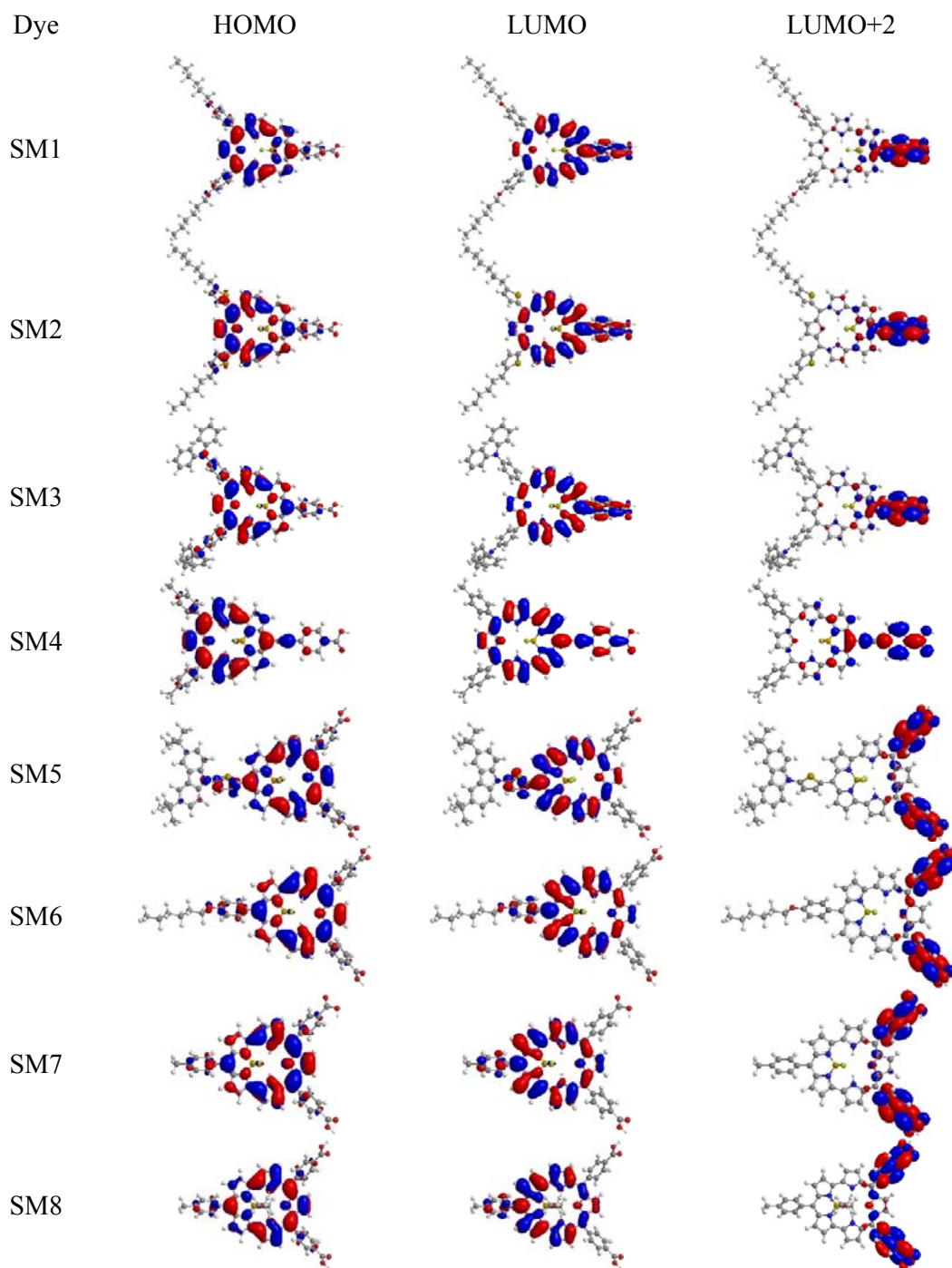


Figure 5-6. The molecular orbital diagrams for SM dyes.

The fluoride atoms lie on opposite sides of the oxasmaragdyrin ring and has no effect on the electron distribution along the ring. The planar ring ensures the effective coupling of the electron between the donor and acceptor groups. In the HOMO of all the SM dyes, majority of the electron density is largely located on the oxasmaragdyrin ring, while a small part of it is distributed over donor unit. This indicates the insignificant influence of the donor groups on the π -conjugation of the oxasmaragdyrin ring. In the LUMO of the monocarboxylic acid substituted oxasmaragdyrins **SM1-SM4**, the electron density is equally distributed over the oxasmaragdyrin ring and the carboxyphenyl anchor revealing the charge separation in these molecules is effective. Whereas in the LUMO of the dicarboxylic acid substituted oxasmaragdyrins **SM5-SM8**, the electron density still remain located over the oxasmaragdyrin ring which suggests the charge separation is less efficient. No charge delocalization in LUMO orbital, even with the push-pull system in dyes **SM5-SM8**, suggests inefficient electron injection. In LUMO+2 of all the SM dyes, the electron density is completely localized on the carboxyphenyl anchoring group highlighting the probability of electron injection from higher excited states involving LUMO+2. These quantum mechanical calculations again emphasized that, the importance of the molecular design with two donors and one anchoring group is more effective than the reverse, with two anchoring groups and one donor. Form the comparison between the oxasmaragdyrins with and without ethynylphenyl, it is observed that the population of electron density on the carboxyphenyl acceptor group is decreased when the distance between the oxasmaragdyrin ring and the acceptor group is increased. Time-dependent density functional theory (TD-DFT) were also performed at B3LYP functional and 6-31G basis set using Gaussian 9 software. For all the compounds, the lowest energy transition ($S_0 \rightarrow S_1$) is approximately 72-85 % of the HOMO \rightarrow LUMO transition, thus confirming its donor to acceptor charge-transfer character. The dipole moments for the oxasmaragdyrins under study were estimated from the theoretical calculations and listed in Table 5-2. Significantly higher molecular dipole moment was observed for **SM1** than the rest of the dyes. The higher polarizability is expedient to accelerate the intramolecular photo induced charge transfer.

Table 5-2. Calculated TD-DFT composition in terms of frontier molecular orbitals, excitation energies, oscillator strengths and dipole moments.

Dye	State	Composition (%)	E (eV)	λ (nm)	f	Dipole moment (D)
SM1	S1	H-1 \rightarrow L+1 (23) H \rightarrow L (77)	1.97	629.57	0.2293	6.6132
	S2	H-1 \rightarrow L+1 (30)	2.84	436.63	0.7636	

		H→L (10)				
		H→L+2 (59)				
	S3	H-1→L (37)	2.94	422.27	0.8955	
		H-1→L+2 (20)				
	S4	H→L+1 (44)				
		H-2→L (5)	3.15	394.03	0.9841	
		H-1→L+1 (40)				
		H→L (12)				
		H→L+2 (39)				
SM2	S1	H-1→L+1 (22)	1.95	635.05	0.2282	5.1484
		H→L (77)				
	S2	H-1→L+1 (43)	2.82	439.85	0.9935	
		H→L (13)				
	S3	H→L+2 (42)				
		H-1→L (39)	2.90	428.14	0.9976	
		H-1→L+2 (14)				
	S4	H→L+1 (48)				
		H-1→L+1 (29)	3.10	400.41	0.5893	
		H→L (8)				
		H→L+2 (56)				
SM3	S1	H-1→L+1 (20)	1.93	642.11	0.2553	5.2209
		H→L (79)				
	S2	H-3→L+1 (54)	2.71	456.84	0.5769	
		H-1→L (16)				
	S3	H→L+1 (27)				
		H-2→L+1 (66)	2.77	447.46	0.5322	
		H-1→L+1 (20)				
	S4	H-2→L+1 (25)	2.88	430.57	0.5648	
		H-1→L+1 (17)				
		H→L (7)				
		H→L+2 (46)				
SM4	S1	H-1→L+1 (16)	1.85	671.22	0.5806	6.5527
		H→L (85)				
	S2	H-1→L+1 (39)	2.76	448.88	1.2021	
		H→L (9)				
	S3	H→L+2 (51)				
		H-1→L (34)	2.80	441.81	0.7477	
		H-1→L+2 (15)				
	S4	H→L+1 (53)				
		H-2→L (41)	3.01	411.79	0.9121	
		H-1→L+1 (23)				
		H→L (6)				
		H→L+2 (29)				
SM5	S1	H-1→L+1 (22)	1.92	644.38	0.2997	3.9259
		H→L (78)				
	S2	H-2→L (89)	2.40	516.23	0.2101	
		H-1→L+1 (7)				
	S3	H-2→L+1 (9)	2.70	458.75	0.5994	
		H-1→L (29)				
		H→L+1 (36)				

	S4	H→L+3 (25) H-2→L (6) H-1→L+1 (31) H→L (9) H→L+2 (49)	2.79	444.12	0.8743	
SM6	S1	H-1→L+1 (28) H→L (71)	2.01	618.54	0.1533	4.7692
	S2	H-1→L (19) H→L+1 (23) H→L+3 (58)	2.72	455.83	0.4124	
	S3	H-1→L+1 (18) H→L (7) H→L+2 (72)	2.78	445.11	0.58	
	S4	H-1→L+1 (42) H-1→L+3 (13) H→L (15) H→L+2 (26)	2.88	431.17	0.7649	
SM7	S1	H-1→L+1 (27) H→L (72)	2.01	615.65	0.1476	6.0501
	S2	H-1→L (24) H→L+1 (24) H→L+3 (49)	2.74	453.32	0.4972	
	S3	H-1→L+1 (11) H→L+2 (81)	2.76	449	0.3794	
	S4	H-1→L+1 (54) H-1→L+3 (12) H→L (19) H→L+2 (15)	2.90	427.81	0.9246	
SM8	S1	H-1→L+1 (26) H→L (73)	1.975	627.76	0.144	5.5281
	S2	H-1→L (29) H→L+1 (31) H→L+3 (39)	2.67	464.2	0.559	
	S3	H-1→L+1 (23) H→L (8) H→L+2 (67)	2.72	455.7	0.5918	
	S4	H-1→L+1 (44) H-1→L+3 (10) H→L (14) H→L+2 (31)	2.82	439.4	0.5616	
H=HOMO, L=LUMO, H-1=HOMO-1, H-2=HOMO-2, H-3=HOMO-3, H-4=HOMO-4 L+1=LUMO+1, L+2=LUMO+2.						

5.2.5 Dye loading measurements

To better comprehend the adsorption behavior and measure the amount of adsorbed dye, we calculated the dye densities adsorbed on TiO₂ surface. The oxasmaragdyrin densities (Γ) were determined by measuring the absorbance of the oxasmaragdyrins desorbed from the sensitized

TiO₂ films after being immersed in 0.1 M KOH solution in THF. The saturated Γ values of the oxasmaragdyrins under study were listed in Table 5-3. The dye densities for two carboxyphenyl substituted oxasmaragdyrins were higher than one carboxyphenyl counterparts. For one acceptor series, the dye loading were found as 109 ± 3 , 113 ± 6 , 153 ± 8 and 119 ± 3 nmol/cm² for **SM1**, **SM2**, **SM3** and **SM4** respectively. Even though **SM1** has lower dye loading compared to other three derivatives, the better solubility and the larger charge separation due to higher dipole moment may be accountable for its increased short circuit current density and consequently the higher overall conversion efficiency. Whereas for **SM3**, the higher dye loading was observed, but the lower dipole moment and high molecular aggregation may decrease its efficiency. For two acceptor series, the dye densities were found as 168 ± 9 , 183 ± 7 , 173 ± 6 and 114 ± 4 nmol cm⁻² for **SM5**, **SM6**, **SM7** and **SM8** respectively. Even though **SM7** has higher dipole moment than **SM6**, its higher solubility due to alkoxy chain and dye loading may be responsible for its increased short-circuit current density and consequently the higher overall conversion efficiency. The dye loading trend in this two acceptor series is alike to the overall efficiency with higher dye loading resulting in increased conversion efficiency.

5.2.6 Photovoltaic measurement results

The boryl oxasmaragdyrins shown in Scheme 5-1 were evaluated as sensitizers in DSSC devices, assembled with the opaque active TiO₂ layer on FTO glass as photoanode using iodide/triiodide as electrolyte and tested under standard AM 1.5 illumination conditions. The detail information about the device preparation were depicted in general techniques. The best photovoltaic performances for each oxasmaragdyrin dye are summarized in Table 5-3.

Table 5-3. Photovoltaic characteristics of DSSCs incorporating oxasmaragdyrin dyes.

Dye	DL (nmol cm ⁻²)	<i>J</i> _{sc} (mAcm ⁻²)	<i>V</i> _{oc} (V)	<i>FF</i> (%)	η (%)
SM1	109	10.91	0.59	68	4.36
SM2	113	7.16	0.56	67	2.74
SM3	153	5.16	0.52	65	1.79
SM4	119	4.65	0.49	66	1.49
SM5	168	3.95	0.53	71	1.48
SM6	183	6.22	0.54	69	2.33
SM7	173	5.67	0.53	68	2.05
SM8	114	2.32	0.47	61	0.66

The J_{sc} refers to short-circuit photo-current density, V_{oc} is open-circuit photo-voltage, FF is fill factor and η is solar-to-electrical conversion efficiency. The optimized I-V characteristics of the devices measured under standard AM 1.5 G simulated solar conditions are displayed in Figure 5-7. As seen from the I-V curves, the device prepared with **SM1** obtained highest short-circuit current of 10.91 mA cm^{-2} , in combination with open circuit voltage of 0.59 V and fill factor of 68, collectively corresponding to the best photon-to-current conversion efficiency of 4.36%. The cell assembled with **SM2** attained the overall conversion efficiency of 2.74%, well reinforced by J_{sc} of 7.16 mA cm^{-2} , V_{oc} of 0.56 V and fill factor of 67.

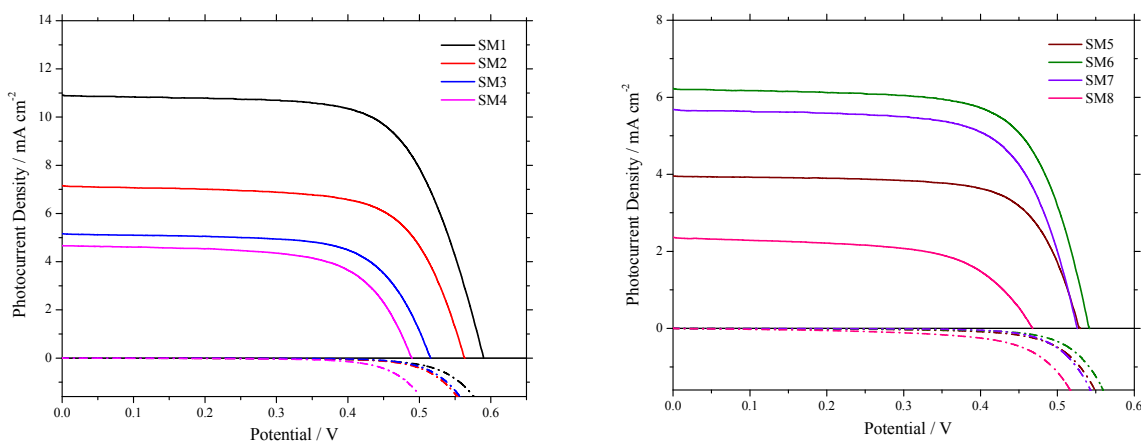


Figure 5-7. I-V curves of the DSSCs based on the oxasmaragdyrin dyes

The DSSC assembled with **SM3** exhibited the efficiency of 1.79% with J_{sc} of 5.16 mA cm^{-2} , V_{oc} of 0.52 V and fill factor of 65. The donor TPA group substitution resulted in inferior J_{sc} and V_{oc} values beckoning insignificant effect on the efficiency in **SM3** compared with **SM1**. In **SM4**, incorporation of the ethynylphenyl linker between the oxasmaragdyrin ring and the acceptor group did not show any improvement in the DSSC performance, which might be due to the increased distance of the acceptor from the oxasmaragdyrin ring. The red-shifted absorption profile and the near equal dipole moments compared with **SM1** were also not helpful for the efficiency improvement for **SM4**, which gained overall efficiency of 1.49% supported with J_{sc} of 4.65 mA cm^{-2} , V_{oc} of 0.49 V and fill factor of 66.

The two acceptor derivatives with the reversed molecular design were evaluated for the DSSC performance and compared with **SM1**. We assumed that the direction of electron flow away from the boron center with aid of two acceptor and the strong π -conjugation of the oxasmaragdyrin ring shall contribute to enhance the photovoltaic performance. To our disappointment the best performance of these two acceptor dyes reached merely half of the

SM1 device performance. The finest photovoltaic performance among the two acceptor series was displayed by **SM6**, with overall photon-to-current conversion efficiency of 2.33% along with J_{sc} of 6.22 mA cm^{-2} , V_{oc} of 0.54 V and fill factor of 69. The effect of electron donating thiophenecarbazole group is well evident in the optical spectrum of **SM5** but the dipole moments is only 3.9 D, telling that the electron donors near the boron center are not much effective. Also the same effect is observed from the dipole moments of other oxasmaragdyrins **SM6** (4.7 D) and **SM7** (6 D). The electron donating power of the substituents is inversely proportional to the dipole moment. The dye **SM5** provided the overall photon-to-current conversion efficiency of 1.48% along with J_{sc} of 3.95 mA cm^{-2} , V_{oc} of 0.53 V and fill factor of 71, while the oxasmaragdyrin **SM7** achieved the photon-to-current conversion efficiency of 2.05% alongside the J_{sc} of 5.67 mA cm^{-2} , V_{oc} of 0.53 V and fill factor of 68. Superior solubility due to the addition of long alkoxy chains and higher dye loading of **SM6** might be responsible for its increased photovoltaic conversion than dye **SM7**, in spite of having higher dipole moment. We also tuned the electronic environment near the boron center to check its consequences on the photovoltaic performance with replacement of the electron withdrawing fluoride atoms attached to boron with electron donating ethoxy groups. This alteration resulted in decreased device performance for dye **SM8**, which attained minute efficiency of 0.66% with J_{sc} of 2.32 mA cm^{-2} , V_{oc} of 0.47 V and fill factor of 61.

The trends in the J_{sc} for these oxasmaragdyrins can be witnessed from the variation of incident photon-to-current conversion efficiency (IPCE) plots of these dyes as shown in Figure 5-8. The IPCE spectra of all the dyes are in qualitative agreement with the corresponding absorption spectra of the dyes on TiO_2 which shows intense absorption in both *Soret* as well as Q band region.

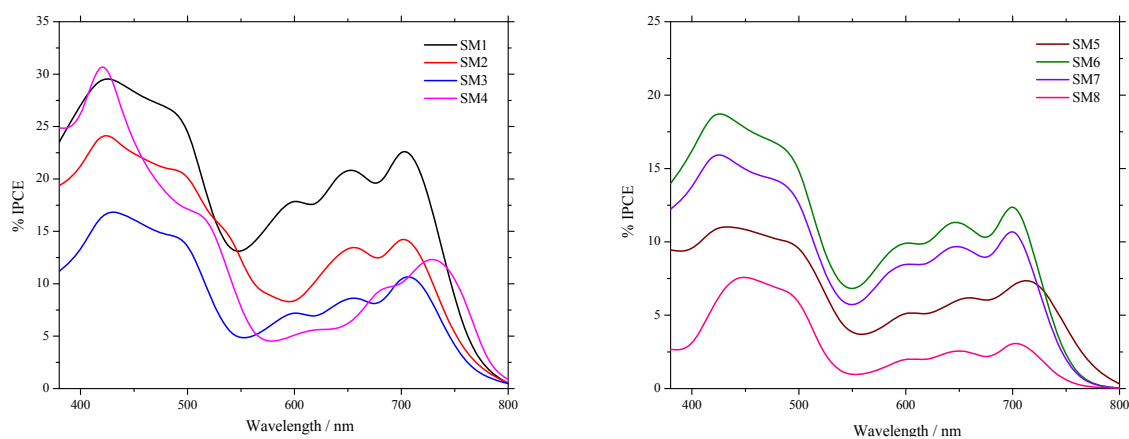


Figure 5-8. IPCE plots of the DSSCs based on the oxasmaragdyrin dyes.

The superior performance of **SM1** can be understood from its IPCE spectrum, which exhibits a high plateau in the 380 to 550 nm region, with IPCE reaching 30% at 425 nm, whereas it also displayed another intense peak in the 550 to 750 nm region with the IPCE value of 25% at 703 nm. The intensity of the dip between 550-600 nm is still higher than other oxasmaragdyrins with IPCE value of 15%. The dye **SM1** shows panchromatic absorption feature covering whole 380-750 nm region. The other oxasmaragdyrins follow the parallel pattern in the IPCE spectra but with inferior IPCE values. The IPCE spectrum for oxasmaragdyrin **SM6** exhibits a high plateau in the 380 to 550 nm region, with IPCE reaching 19% at 425 nm, whereas it also displayed another intense peak in the 550 to 750 nm region with the IPCE value of 12% at 700 nm. The other oxasmaragdyrins follow the similar pattern in the IPCE spectra with lower IPCE values. Interestingly, the IPCE spectra of **SM5** covers extended absorption region with the onset reaching around 800 nm as compared to other dyes, but its lower IPCE values in the higher energy region results in lower conversion efficiency.

5.3 Conclusions

To conclude, we have engineered the molecular structure of oxasmaragdyrin in an attempt to enhance their photovoltaic performances. We have synthesized eight novel oxasmaragdyrins decorated with different number and position of donor and anchor groups and evaluated their performance as sensitizers in DSSCs. All eight oxasmaragdyrins displayed good absorption feature in both *Soret* as well as Q band region. Although the substitution of electron donating groups and extension of π -conjugation through ethynylphenyl group obviously resulted in red shifted and broadened absorption wavelengths, it has insignificant effect on their photovoltaic performance. The reversed position and increased number of anchoring group also exhibited very minor influence on their DSSC outcomes. Cyclic voltammetry measurements and DFT calculations confirmed the viability of electron injection and intramolecular charge transfer. Among these dyes, one anchor dye **SM1** sensitized cell gave the finest DSSC performance with overall photon-to-current conversion efficiency of 4.36%, while the device made from two anchor dye **SM6** obtained efficiency of 2.33%. From these photovoltaic results it is clear that the molecular design of **SM1** still prevails all other modification.

5.4 Experimental Section

5.4.1 General Techniques and Materials

All chemicals were obtained from commercial sources and used as received without further purification. All the reactions were carried out under nitrogen atmosphere. Solvents used in reactions were dried by PureSolv MD 5 system (Innovative Technology, Inc). Flash chromatography was carried out by using basic alumina (63-200 μm , Merck) and silica gel (40-63 μm , Merck). Analytical TLC was performed on Merck silica gel plates. ^1H and ^{13}C NMR spectra were recorded on a Bruker 400 MHz spectrometer and performed in CDCl_3 ($\delta = 7.26$ ppm) and THF-D_8 ($\delta = 1.73, 3.58$ ppm) solutions. ^{11}B and ^{19}F NMR spectra were recorded on a DRX 500 MHz spectrometer. Chemical shifts are reported in ppm. Coupling constants J are reported in Hz. The signals are described as s: singlet; d: doublet; dd: doublet of doublet. The ESI ion trap mass spectra were measured by a Finnigan MAT LCQ mass spectrometer. The HR-FAB spectra were conducted on a JMS-700 double focusing mass spectrometer. MALDI-mass spectra were conducted on an Applied Biosystems 4800 Proteomics Analyzer (Applied Biosystem, Foster City) equipped with an Nd/YAG laser (335nm). Transmittance and reflection UV–visible absorption spectra of the oxasmaragdyrins in THF and adsorbed on TiO_2 electrodes, respectively, were recorded on a JASCO V-670 UV–Vis/NIR spectrophotometer. Steady-state fluorescence spectra were acquired by using a Varian Cary Eclipse fluorescence spectrophotometer. The cyclic voltammetry measurements of all oxasmaragdyrins were carried out on CHI 621B electrochemical analyser (CH Instruments, Austin, TX, USA) in degassed THF containing 0.1 M tetrabutylammonium hexafluorophosphate (Bu_4NPF_6) as the supporting electrolyte. The cell assembly consists of a glossy carbon as the working electrode, a silver wire as the pseudo-reference electrode, and a platinum wire as the auxiliary electrode. The scan rate for all measurements was fixed at 50 mV/sec. A ferrocene $^{+1/0}$ redox couple was used as the internal standard and the potential values obtained in reference to the silver electrode were converted to the vacuum scale. The density functional theory (DFT) and time-dependent density functional (TD-DFT) calculations were performed with Gaussian 09 package to study the electron distribution of the frontier molecular orbitals and the photoexcitation transitions. All ground state geometries of oxasmaragdyrins were optimized in the gas phase by the hybrid B3LYP functional and the 6-31G basis set, and the TD-DFT calculation were based on the same functional and basis set. The molecular orbitals were visualized by the Chem-office software. The EIS instrument involves the chemical electric impedance analyser (CHI 621B electrochemical analyser) with applied ac voltage and bias potential on the cells and measured

the corresponding current and voltage under the white LED lamp with various neutral density filters to change the illumination white light intensity in order to change the fermi level of DSCs. In addition, we used the Z-view program to analyze the data.

5.4.2 Synthesis

5-(*p*-methoxycarbonylphenyl) dipyrromethane (1)

A mixture of methyl-4-formylbenzoate (3.28 g, 0.02 mol) and pyrrole (137 ml, 2 mol) was degassed with N₂ for 15 min. at room temperature. TFA (150 μ l, 0.002 mol) was then added and the mixture was stirred at room temperature for 3 hrs. After completion of the reaction, NaOH (2.4 g, 0.06 mol) was added and mixture was stirred for 1 h and then filtered. The filtrate was concentrated and pyrrole was removed under vacuum. The crude obtained after removing pyrrole was subjected to silica gel column chromatography using DCM/Hexanes (4:6, R_f = 0.2) as eluting solvent to obtain the dipyrromethane (4.8 g, 86% Yield). ¹H NMR (400 MHz, CDCl₃) δ : 3.91 (s, 3H, CH₃), 5.53 (s, 1H, *meso* CH), 5.89 (s, 2H, β -pyrrole), 6.16 (m, 2H, β -pyrrole), 6.72 (m, 2H, α -pyrrole), 7.28 (m, 2H, Ph), 7.98, (m, 4H, Ph, NH) ppm; ¹³C NMR (100 MHz, CDCl₃) δ : 43.97, 52.08, 107.50, 108.57, 117.54, 128.41, 129.91, 131.58, 147.34 ppm.

2,5-bis(*p*-hexyloxyphenyl)furandiol (2)

Furan (2 ml, 27.62 mmol) was added to a solution of *n*-BuLi (43 ml, 69.05 mmol) and TMEDA (10.35 ml, 69.05 mmol) in 40 ml dry hexane under N₂. The reaction mixture was heated at reflux temperature for 1 hour and then cooled to 0 °C. To this suspension, a pre-cooled solution of *p*-hexyloxybenzaldehyde (14.3 ml, 69.05 mmol) in 40 ml dry THF was added drop wise. After the addition was complete, the mixture was warmed to room temperature while stirring for 30 minutes. Saturated NH₄Cl solution was added to quench the reaction. The organic phase was extracted with H₂O, brine and then dried over MgSO₄. The crude product was subjected to silica gel column chromatography using EA/Hexanes (3:7, R_f = 0.22) as eluting solvent to get furan diol (8.68 g, 65% Yield). ¹H NMR (400 MHz, CDCl₃) δ : 0.91 (m, 6H, CH₃), 1.34 (m, 8H, CH₂), 1.45 (m, 4H, CH₂), 1.78 (m, 4H, CH₂), 2.66 (bs, 2H, -OH), 3.95 (m, 4H, -OCH₂), 5.72 (s, 2H, *meso*-CH), 5.94 (d, 2H, *J* = 3.84 Hz, β -furan), 6.87 (m, 4H, Ar), 7.31 (m, 4H, Ar) ppm; ¹³C NMR (100 MHz, CDCl₃) δ : 14.01, 22.58, 25.70, 29.21, 31.57, 68.04, 69.73, 107.94, 107.99, 114.36, 127.95, 132.59, 156.24, 158.99 ppm.

2,5-bis(5-hexylthiophene-2-yl)furandiol (3)

Furan (2 ml, 27.6 mmol) was added to a solution of *n*-BuLi (43 ml, 69 mmol) and TMEDA (11 ml, 69 mmol) in 40 ml dry hexane under N₂. The reaction mixture was heated at reflux

temperature for 1 hour and then cooled to 0 °C. To this suspension, a pre-cooled solution of 5-hexylthiophene-2-carbaldehyde (11 ml, 61 mmol) in 60 ml dry THF was added drop wise. After the addition was complete, the mixture was warmed to room temperature while stirring for 30 minutes. Saturated NH₄Cl solution was added to quench the reaction. The organic phase was extracted with H₂O, brine and then dried over MgSO₄. The crude product was subjected to silica gel column chromatography using EA/Hexanes (3:7, R_f = 0.21) as eluting solvent to get furan diol (9.95 g, 78% Yield). ¹H NMR (400 MHz, CDCl₃) δ: 0.89 (m, 6H, CH₃), 1.33 (m, 12H, CH₂), 1.65 (m, 4H, CH₂), 2.77 (m, 4H, CH₂), 2.85 (bs, 2H, -OH), 5.93 (s, 2H, *meso*-CH), 6.22 (s, 2H, β-furan), 6.62 (m, 2H, Ar), 6.81 (m, 2H, Ar) ppm; ¹³C NMR (100 MHz, CDCl₃) δ: 14.02, 22.53, 28.76, 30.18, 31.52, 31.56, 66.38, 107.98, 108.00, 123.44, 123.46, 125.21, 141.23, 141.26, 146.54, 155.09 ppm.

2,5-bis[4-(diphenylamino)phenyl]furandiol (4)

Furan (2 ml, 27.6 mmol) was added to a solution of *n*-BuLi (43 ml, 69 mmol) and TMEDA (11ml, 69 mmol) in 40 ml dry hexane under N₂. The reaction mixture was heated at reflux temperature for 1 hour and then cooled to 0 °C. To this suspension, a pre-cooled solution of triphenylamine benzaldehyde (16.67 g, 61 mmol) in 60 ml dry THF was added drop wise. After the addition was complete, the mixture was warmed to room temperature while stirring for 30 minutes. Saturated NH₄Cl solution was added to quench the reaction. The organic phase was extracted with H₂O, brine and then dried over MgSO₄. The crude product was subjected to silica gel column chromatography using EA/Hexanes (3:7, R_f = 0.32) as eluting solvent to get furan diol (3.86 g, 23% Yield). ¹H NMR (400 MHz, CDCl₃) δ: 5.77 (s, 2H, *meso*-CH), 6.10 (d, 2H, *J* = 2.84 Hz, β-furan), 7.07 (m, 20H, Ar), 7.28 (m, 8H, Ar) ppm; ¹³C NMR (100 MHz, CDCl₃) δ: 69.89, 108.03, 122.97, 123.47, 124.42, 127.71, 129.26, 134.53, 147.66, 147.78, 156.24 ppm.

5,10-di(*p*-hexyloxyphenyl)-16-oxatripyrrane (5)

Furan-diol (**2**, 2 g, 4.16 mmol) was dissolved in pyrrole (11.5 ml, 166 mmol) under N₂. To this solution BF₃•OEt₂ (0.53 ml, 4.16 mmol) was added. The mixture was stirred for 30 min. at room temperature. After completion of reaction as confirmed by TLC, the reaction was quenched by adding aq.NaOH (0.1 N, 20 ml). The mixture was extracted with dichloromethane and washed with water. The organic layer was dried over MgSO₄ and excess pyrrole was removed under vacuum. The crude oil was purified by column chromatography on silica using DCM/Hexanes (3:7, R_f = 0.28) as eluting solvent to get pure oxatripyrrane (1.4 g, 58% Yield). ¹H NMR (400 MHz, CDCl₃) δ: 0.91 (m, 6H, CH₃), 1.34 (m, 8H, CH₂), 1.46 (m, 4H, CH₂), 1.77

(m, 4H, CH₂), 3.93 (m, 4H, -OCH₂), 5.34 (s, 2H, *meso*-CH), 5.89 (m, 2H, β -pyrrole), 5.93 (d, 2H, $J = 2.12$ Hz, β -furan), 6.12 (m, 2H, β -pyrrole), 6.63 (m, 2H, α -pyrrole), 6.82 (m, 4H, Ar), 7.09 (m, 4H, Ar), 7.97 (br s, 2H, NH) ppm; ¹³C NMR (100 MHz, CDCl₃) δ : 14.02, 22.59, 25.73, 29.25, 31.58, 43.48, 68.04, 106.99, 107.69, 108.16, 114.45, 117.11, 129.31, 131.48, 132.61, 155.22, 158.17 ppm; HRMS-ESI⁻: m/z calcd for C₃₈H₄₅N₂O₃: 577.3430, found 577.3434 [M-H]⁻.

5,10-di(5-hexylthiophen-2-yl)-16-oxatripyrrane (6)

Furan-diol (**3**, 2.3 g, 5 mmol) was dissolved in pyrrole (13.6 ml, 200 mmol) under N₂. To this solution BF₃•OEt₂ (0.63 ml, 5 mmol) was added. The mixture was stirred for 30 min. at room temperature. After completion of reaction as confirmed by TLC, the reaction was quenched by adding aq.NaOH (0.1 N, 20 ml). The mixture was extracted with dichloromethane and washed with water. The organic layer was dried over MgSO₄ and excess pyrrole was removed under vacuum. The crude oil was purified by column chromatography on silica using DCM/Hexanes (2:8, R_f = 0.32) as eluting solvent to get pure oxatripyrrane (1.28 g, 46% Yield). ¹H NMR (400 MHz, CDCl₃) δ : 0.91 (m, 6H, CH₃), 1.34 (m, 12H, CH₂), 1.65 (m, 4H, CH₂), 2.75 (m, 4H, -CH₂), 5.60 (s, 2H, *meso*-CH), 6.05 (s, 2H, β -pyrrole), 6.09 (d, 2H, β -furan), 6.15 (m, 2H, β -pyrrole), 6.60 (m, 4H, β -thiophene), 6.67 (m, 2H, α -pyrrole), 8.16 (br s, 2H, NH) ppm; ¹³C NMR (100 MHz, CDCl₃) δ : 14.05, 22.54, 28.82, 30.20, 31.53, 31.59, 39.69, 106.80, 107.52, 108.15, 108.19, 117.35, 123.34, 125.03, 125.09, 130.57, 141.34, 141.54, 145.41, 154.27, 154.35 ppm.

5,10-di[4-(diphenylamino)phenyl]-16-oxatripyrrane (7)

Furan-diol (**4**, 1.3 g, 2 mmol) was dissolved in pyrrole (5.5 ml, 80 mmol) under N₂. To this solution BF₃•OEt₂ (0.25 ml, 2 mmol) was added. The mixture was stirred for 30 min. at room temperature. After completion of reaction as confirmed by TLC, the reaction was quenched by adding aq.NaOH (0.1 N, 20 ml). The mixture was extracted with dichloromethane and washed with water. The organic layer was dried over MgSO₄ and excess pyrrole was removed under vacuum. The crude oil was purified by column chromatography on silica using DCM/Hexanes (1:1, R_f = 0.26) as eluting solvent to get pure oxatripyrrane (0.65 g, 46% Yield). ¹H NMR (400 MHz, CDCl₃) δ : 5.37 (s, 2H, *meso*-CH), 5.95 (s, 2H, β -pyrrole), 6.01 (s, 2H, β -furan), 6.15 (m, 2H, β -pyrrole), 6.67 (m, 2H, α -pyrrole), 7.00 (m, 8H, Ar), 7.06 (m, 12H, Ar), 7.23 (m, 8H, Ar), 8.05 (br s, 2H, NH) ppm; ¹³C NMR (100 MHz, CDCl₃) δ : 43.66, 107.10, 107.81, 108.22, 117.24, 122.77, 123.82, 124.19, 128.99, 129.21, 131.14, 134.84, 146.68, 147.70, 154.99 ppm.

19-(*p*-methoxycarbonylphenyl)-5,10-di(*p*-hexyloxyphenyl)-25-oxasmaragdyrin (8)

5-(*p*-methoxycarbonylphenyl)dipyrromethane (280 mg, 1 mmol) and 5,10-di(*p*-hexyloxyphenyl)-16-oxatripyrrane (579 mg, 1 mmol) were dissolved in 700 ml of dichloromethane and stirred under nitrogen for 10 min. The reaction was initiated by adding TFA (8 μ l, 0.1 mmol) and the stirring was continued for 90 min. DDQ (681 mg, 3 mmol) was then added and the reaction mixture was stirred in open-air for additional 90 min. The solvent was removed and crude compound was purified by basic alumina column chromatography eluted with DCM/Hexanes (3:7, $R_f = 0.31$) to get the desired oxasmaragdyrin as a green solid (350 mg, 41% yield). ^1H NMR (400 MHz, CDCl_3) δ : 1.01 (m, 6H, CH_3), 1.48 (m, 8H, CH_2), 1.66 (m, 4H, CH_2), 2.01 (m, 4H, CH_2), 4.11 (s, 3H, -OMe), 4.28 (m, 4H, -OCH $_2$), 7.33 (d, 4H, $J = 8.24$ Hz, Ar), 8.11 (d, 4H, $J = 8.20$ Hz, Ar), 8.50 (m, 6H, Ar, β -pyrrole), 8.84 (s, 2H, β -furan), 8.94 (d, 2H, $J = 4.28$ Hz, β -pyrrole), 9.43 (d, 2H, $J = 4.28$, β -pyrrole), 9.58 (d, 2H, $J = 4.24$ Hz, β -pyrrole) ppm; ^{13}C NMR (100 MHz, CDCl_3) δ : 14.13, 22.72, 25.94, 29.51, 31.74, 52.37, 68.38, 105.01, 113.67, 115.74, 118.98, 119.72, 123.30, 124.21, 124.98, 127.56, 128.75, 129.29, 129.75, 134.40, 134.70, 135.70, 138.09, 145.23, 149.25, 159.18, 167.50 ppm; HRMS-ESI: m/z calcd for $\text{C}_{55}\text{H}_{55}\text{N}_4\text{O}_5$: 851.4172, found 851.4169 $[\text{M}+\text{H}]^+$.

19-(*p*-methoxycarbonylphenyl)-5,10-di(5-hexylthiophen-2-yl)-25-oxasmaragdyrin (9)

5-(*p*-methoxycarbonylphenyl)dipyrromethane (281 mg, 1 mmol) and 5,10-di(5-hexylthiophen-2-yl)-16-oxatripyrrane (560 mg, 1 mmol) were dissolved in 700 ml of dichloromethane and stirred under nitrogen for 10 min. The reaction was initiated by adding TFA (8 μ l, 0.1 mmol) and the stirring was continued for 90 min. DDQ (681 mg, 3 mmol) was then added and the reaction mixture was stirred in open-air for additional 90 min. The solvent was removed and crude compound was purified by basic alumina column chromatography eluted with DCM/Hexanes (3:7, $R_f = 0.31$) to get the desired oxasmaragdyrin as a green solid (250 mg, 30% yield). This pure oxasmaragdyrin was used for the next reaction without further delay and data collection.

19-(*p*-methoxycarbonylphenyl)-5,10-di[4-(diphenylamino)phenyl]-25-oxasmaragdyrin (10)

5-(*p*-methoxycarbonylphenyl) dipyrromethane (281 mg, 1 mmol) and 5,10-di[4-(diphenylamino)phenyl]-16-oxatripyrrane (713 mg, 1 mmol) were dissolved in 700 ml of dichloromethane and stirred under nitrogen for 10 min. The reaction was initiated by adding TFA (8 μ l, 0.1 mmol) and the stirring was continued for 90 min. DDQ (681 mg, 3 mmol) was then added and the reaction mixture was stirred in open-air for additional 90 min. The solvent

was removed and crude compound was purified by basic alumina column chromatography eluted with DCM/Hexanes (3:7, $R_f = 0.34$) to get the desired oxasmaragdyrin as a green solid (270 mg, 27% yield). This pure oxasmaragdyrin was used for the next reaction without further delay and data collection.

BF₂-[19-(*p*-methoxycarbonylphenyl)-5,10-di(*p*-hexyloxyphenyl)-25-oxasmaragdyrin]

(11)

Oxasmaragdyrin (**8**, 749 mg, 0.88 mmol) was dissolved in CH₂Cl₂ (80 ml) and triethylamine (4.91 ml, 35.2 mmol) was added at room temperature. After 10 min BF₃•OEt₂ (5.57 ml, 44 mmol) was added and the stirring was continued for 30 min. Completion of the reaction was confirmed by TLC. The reaction mixture was washed thoroughly with 0.1 M NaOH solution and water. The organic layers were combined, dried over MgSO₄, filtered and the solvent was removed. The crude compound was purified by silica gel column chromatography, using dichloromethane/hexanes (3:2, $R_f = 0.42$) to afford the desired compound as green solid (508 mg, 64% yield). ¹H NMR (400 MHz, CDCl₃) δ: -3.96 (t, 2H, -NH), 1.03 (m, 6H, CH₃), 1.51 (s, 8H, CH₂), 1.68 (m, 4H, CH₂), 2.04 (m, 4H, CH₂), 4.17 (s, 3H, OMe), 4.32 (m, 4H, OCH₂), 7.41 (d, 4H, $J = 7.48$ Hz, Ar), 8.30 (d, 4H, $J = 7.40$ Hz, Ar), 8.64 (d, 2H, $J = 7.56$ Hz, Ar), 8.70 (d, 2H, $J = 7.68$ Hz, Ar), 9.05 (d, 2H, β-pyrrole), 9.54 (s, 2H, β-furan), 9.57 (d, 2H, β-pyrrole), 10.24 (d, 2H, β-pyrrole), 10.33 (d, 2H, β-pyrrole) ppm; ¹¹B NMR (160.4 MHz, CDCl₃) δ: -12.78 (br s) ppm; ¹⁹F NMR (470.5 MHz, CDCl₃) δ: -149.22 (br s) ppm; ¹³C NMR (125 MHz, CDCl₃) δ: 14.14, 22.74, 25.96, 29.52, 31.76, 52.46, 68.43, 106.82, 113.56, 117.01, 120.43, 120.95, 122.14, 123.80, 123.87, 125.04, 129.47, 129.56, 130.41, 130.94, 131.41, 134.55, 134.82, 135.36, 144.04, 150.12, 159.37, 167.45 ppm; HRMS-FAB+: m/z calcd for C₅₅H₅₃BF₂N₄O₅: 898.4077, found 898.4084 [M]⁺.

BF₂-[19-(*p*-methoxycarbonylphenyl)-5,10-di(5-hexylthiophene-2-yl)-25-oxasmaragdyrin] (12)

Oxasmaragdyrin (**9**, 446 mg, 0.55 mmol) was dissolved in CH₂Cl₂ (100 ml) and triethylamine (3 ml, 22 mmol) was added at room temperature. After 10 min BF₃•OEt₂ (3.5 ml, 27.5 mmol) was added and the stirring was continued for 30 min. Completion of the reaction was confirmed by TLC. The reaction mixture was washed thoroughly with 0.1 M NaOH solution and water. The organic layers were combined, dried over MgSO₄, filtered and the solvent was removed. The crude compound was purified by silica gel column chromatography, using dichloromethane/hexanes (3:2, $R_f = 0.42$) to afford the desired compound as green solid (300 mg, 62% yield). ¹H NMR (400 MHz, CDCl₃) δ: -3.85 (t, 2H, NH), 1.03 (m, 6H, CH₃), 1.51 (s,

8H, CH₂), 1.67 (m, 4H, CH₂), 2.05 (m, 4H, CH₂), 3.23 (m, 4H, CH₂), 4.17 (s, 3H, OMe), 7.31 (d, 2H, *J* = 3.28 Hz, β -thiophene), 7.95 (d, 2H, *J* = 3.24 Hz, β -thiophene), 8.64 (d, 2H, *J* = 8.20 Hz, Ar), 8.68 (d, 2H, *J* = 8.24 Hz, Ar), 9.05 (m, 2H, β -pyrrole), 9.55 (d, 2H, *J* = 4.48 Hz, β -pyrrole), 9.82 (s, 2H, β -furan), 10.23 (m, 2H, β -pyrrole), 10.30 (d, 2H, *J* = 4.44 Hz, β -pyrrole) ppm; ¹¹B NMR (160.4 MHz, CDCl₃) δ : -12.59 (br s) ppm; ¹⁹F NMR (470.5 MHz, CDCl₃) δ : -149.04 (br s) ppm; ¹³C NMR (125 MHz, CDCl₃) δ : 14.18, 22.72, 29.08, 30.63, 31.74, 31.94, 52.47, 99.89, 117.65, 120.52, 120.97, 122.35, 123.58, 123.97, 124.28, 125.24, 129.50, 129.72, 130.89, 131.07, 131.63, 133.01, 134.76, 140.56, 143.83, 148.83, 150.59, 167.41 ppm; HRMS-MALDI: *m/z* calcd for C₅₁H₄₉BF₂N₄O₃S₂: 878.3307, found 878.3331 [M]⁺.

BF₂-[19-(*p*-methoxycarbonylphenyl)-5,10-di[4-(diphenylamino)phenyl]-25-oxasmaragdyrin] (13)

Oxasmaragdyrin (**10**, 562 mg, 0.57 mmol) was dissolved in CH₂Cl₂ (100 ml) and triethylamine (3.18 ml, 22.8 mmol) was added at room temperature. After 10 min BF₃•OEt₂ (3.61 ml, 28.5 mmol) was added and the stirring was continued for 30 min. Completion of the reaction was confirmed by TLC. The reaction mixture was washed thoroughly with 0.1 M NaOH solution and water. The organic layers were combined, dried over MgSO₄, filtered and the solvent was removed. The crude compound was purified by silica gel column chromatography, using dichloromethane/hexanes (1:1, R_f = 0.47) to afford the desired compound as green solid (380 mg, 64% yield). ¹H NMR (400 MHz, CDCl₃) δ : -3.93 (t, 2H, NH), 4.18 (s, 3H, OMe), 7.21 (m, 4H, Ar), 7.50 (m, 16H, Ar), 7.58 (d, 4H, *J* = 8.32 Hz, Ar), 8.24 (d, 4H, *J* = 8.36 Hz, Ar), 8.64 (d, 2H, *J* = 8.28 Hz, Ar), 8.68 (d, 2H, *J* = 8.28 Hz, Ar), 9.15 (dd, 2H, *J* = 1.80 Hz, β -pyrrole), 9.56 (d, 2H, *J* = 4.48 Hz, β -pyrrole), 9.64 (s, 2H, β -furan), 10.24 (dd, 2H, *J* = 1.91, β -pyrrole), 10.32 (d, 2H, *J* = 4.44 Hz, β -pyrrole) ppm; ¹¹B NMR (160.4 MHz, CDCl₃) δ : -12.62 (br s) ppm; ¹⁹F NMR (470.5 MHz, CDCl₃) δ : -149.12 (br s) ppm; ¹³C NMR (125 MHz, CDCl₃) δ : 52.45, 106.92, 117.12, 120.44, 120.90, 122.01, 122.17, 123.42, 123.91, 125.01, 129.47, 129.58, 130.47, 130.73, 131.46, 134.81, 135.23, 136.08, 144.01, 147.91, 147.97, 150.04, 167.43 ppm; HRMS-MALDI: *m/z* calcd for C₆₇H₄₇BF₂N₆O₃: 1032.3771, found 1032.3798 [M]⁺.

BF₂-[19-(*p*-carboxyphenyl)-5,10-di(*p*-hexyloxyphenyl)-25-oxasmaragdyrin] (SM1)

BF₂-oxasmaragdyrin (**11**, 200 mg, 0.22 mmol) was dissolved in 50 ml THF. To this mixture, KOH (250 mg, 4.45 mmol) dissolved in 1 ml water was added and refluxed for 12 h. After cooling, the solvent was removed under vacuum. To the crude product dichloromethane was added and extracted with 1N HCl. The organic layer was dried over MgSO₄ and concentrated.

Crude product was purified by silica gel column chromatography using CH₂Cl₂/MeOH (9.5:0.5, R_f = 0.2) as eluent to get the desired product as green solid (177 mg, 91% yield). ¹H NMR (400 MHz, THF-*d*8) δ: -3.92 (t, 2H, NH), 1.03 (m, 6H, CH₃), 1.53 (m, 12H, CH₂), 2.04 (m, 4H, CH₂), 4.35 (m, 4H, OCH₂), 7.47 (d, 4H, *J* = 8.44 Hz, Ar), 8.33 (d, 4H, *J* = 8.36 Hz, Ar), 8.66 (d, 2H, *J* = 7.88 Hz, Ar), 8.76 (d, 2H, *J* = 7.96 Hz, Ar), 9.04 (d, 2H, *J* = 3.84 Hz, β-pyrrole), 9.59 (s, 2H, β-furan), 9.65 (d, 2H, *J* = 4.44 Hz, β-pyrrole), 10.44 (d, 2H, *J* = 3.16 Hz, β-pyrrole), 10.53 (d, 2H, *J* = 4.32 Hz, β-pyrrole) ppm; ¹¹B NMR (160.4 MHz, THF-*d*8) δ: -12.69 (br s) ppm; ¹⁹F NMR (470.5 MHz, THF-*d*8) δ: -149.47 (br s) ppm; ¹³C NMR (125 MHz, THF-*d*8) δ: 14.57, 23.75, 27.05, 30.60, 32.84, 69.08, 107.71, 114.49, 118.41, 121.60, 121.72, 123.29, 124.91, 124.96, 125.73, 130.60, 131.61, 131.72, 131.83, 132.51, 135.77, 136.24, 144.55, 151.12, 160.76, 168.04 ppm; UV-vis (THF) λ_{max}/nm (ε/10³ M⁻¹cm⁻¹) = 446 (438), 474 (181), 706 (57); HRMS-FAB⁺: *m/z* calcd for C₅₄H₅₁BF₂N₅O₅: 884.3921, found 884.3917 [M]⁺.

BF₂-[19-(*p*-carboxyphenyl)-5,10-di(5-hexylthiophene-2-yl)-25-oxasmaragdyrin] (SM2)

BF₂-oxasmaragdyrin (**12**, 200 mg, 0.22 mmol) was dissolved in 50 ml THF. To this mixture, KOH (250 mg, 4.45 mmol) dissolved in 1 ml water was added and refluxed for 12 h. After cooling, the solvent was removed under vacuum. To the crude product dichloromethane was added and extracted with 1N HCl. The organic layer was dried over MgSO₄ and concentrated. Crude product was purified by silica gel column chromatography using CH₂Cl₂/MeOH (9.5:0.5, R_f = 0.2) as eluent to get the desired product as green solid (177 mg, 91% yield). ¹H NMR (400 MHz, THF-*d*8) δ: -3.79 (t, 2H, NH), 1.03 (m, 6H, CH₃), 1.52 (m, 8H, CH₂), 1.69 (m, 4H, CH₂), 2.07 (m, 4H, CH₂), 3.26 (m, 4H, CH₂), 7.38 (d, 2H, *J* = 3.24 Hz, β-thiophene), 7.99 (d, 2H, *J* = 3.32 Hz, β-thiophene), 8.66 (d, 2H, *J* = 8.00 Hz, Ar), 8.74 (d, 2H, *J* = 8.00 Hz, Ar), 9.28 (d, 2H, *J* = 3.96 Hz, β-pyrrole), 9.63 (d, 2H, *J* = 4.40 Hz, β-pyrrole), 9.83 (s, 2H, β-furan), 10.42 (d, 2H, *J* = 3.16 Hz, β-pyrrole), 10.51 (d, 2H, *J* = 4.48 Hz, β-pyrrole) ppm; ¹¹B NMR (160.4 MHz, THF-*d*8) δ: -10.79 (br s) ppm; ¹⁹F NMR (470.5 MHz, THF-*d*8) δ: -147.53 (br s) ppm; ¹³C NMR (125 MHz, THF-*d*8) δ: 14.56, 23.67, 30.08, 31.36, 32.77, 33.08, 100.51, 119.14, 121.71, 123.58, 124.76, 125.10, 125.38, 125.85, 130.59, 131.79, 132.17, 132.73, 134.15, 135.69, 141.61, 144.24, 149.61, 151.46, 167.98 ppm; UV-vis (THF) λ_{max}/nm (ε/10³ M⁻¹cm⁻¹) = 452 (261), 477 (108), 704 (23); HRMS-MALDI: *m/z* calcd for C₅₀H₄₇BF₂N₄O₃S₂: 864.3151, found 864.3176 [M]⁺.

**BF₂-[19-(*p*-carboxyphenyl)-5,10-di[4-(diphenylamino)phenyl]-25-oxasmaragdyrin]
(SM3)**

BF₂-oxasmaragdyrin (**13**, 103 mg, 0.1 mmol) was dissolved in 20 ml THF. To this mixture, KOH (112 mg, 2 mmol) dissolved in 1 ml water was added and refluxed for 12 h. After cooling, the solvent was removed under vacuum. To the crude product dichloromethane was added and extracted with 1N HCl. The organic layer was dried over MgSO₄ and concentrated. Crude product was purified by silica gel column chromatography using CH₂Cl₂/MeOH (9.5:0.5, R_f = 0.35) as eluent to get the desired product as green solid (62 mg, 61% yield). ¹H NMR (400 MHz, CDCl₃) δ: -3.97 (t, 2H, NH), 7.20 (m, 4H, Ar), 7.49 (m, 16H, Ar), 7.60 (d, 4H, *J* = 8.28 Hz, Ar), 8.28 (d, 4H, *J* = 8.32 Hz, Ar), 8.76 (s, 4H, Ar), 9.18 (d, 2H, *J* = 3.52 Hz, β-pyrrole), 9.62 (d, 2H, *J* = 4.36 Hz, β-pyrrole), 9.68 (s, 2H, β-furan), 10.29 (dd, 2H, *J* = 2.96, β-pyrrole), 10.38 (d, 2H, *J* = 4.44 Hz, β-pyrrole) ppm; ¹¹B NMR (160.4 MHz, CDCl₃) δ: -12.72 (br s) ppm; ¹⁹F NMR (470.5 MHz, CDCl₃) δ: -149.19 (br s) ppm; ¹³C NMR (100 MHz, CDCl₃) δ: 106.98, 116.84, 120.54, 121.02, 122.01, 122.30, 123.44, 123.93, 125.03, 128.60, 129.59, 130.14, 130.43, 130.78, 131.45, 135.01, 135.26, 136.08, 144.96, 147.92, 148.01, 150.07, 170.96 ppm; UV-vis (THF) λ_{max}/nm (ε/10³ M⁻¹cm⁻¹) = 449 (186), 477 (103), 708 (31); HRMS-MALDI: *m/z* calcd for C₆₆H₄₅BF₂N₆O₃: 1018.3615, found 1018.3642 [M]⁺.

di(1H-pyrrol-2-yl)methane (14)

A mixture of paraformaldehyde (600 mg, 0.02 mol) and pyrrole (137 ml, 2 mol) was degassed with N₂ for 15 min. at room temperature. The mixture was then heated at 50 °C for 10 min under N₂ to get a clear solution. TFA (149 μl, 0.002 mmol) was then added and the mixture was stirred at 50 °C for 3 h. The heat source was removed and NaOH (730 mg, 18.27 mmol) was added and mixture was stirred for 1 h and then filtered. The filtrate was concentrated and pyrrole was removed under vacuum. The crude obtained after removing pyrrole was subjected to silica gel column chromatography using DCM/Hexanes (1:1, R_f = 0.34) as eluting solvent to obtain the dipyrromethane (1.8 g, 62% Yield). ¹H NMR (400 MHz, CDCl₃) δ: 3.97 (s, 2H, *meso* CH₂), 6.05 (s, 2H, β-pyrrole), 6.16 (s, 2H, β-pyrrole), 6.65 (s, 2H, α-pyrrole), 7.80 (bs, 2H, -NH) ppm; ¹³C NMR (100 MHz, CDCl₃) δ: 26.38, 106.33, 106.39, 117.21, 129.01 ppm.

2,5-bis(*p*-tolyl)furandiol (15)

Furan (1 ml, 13.75 mmol) was added to a solution of *n*-BuLi (22 ml, 34.37 mmol) and TMEDA (5.15 ml, 34.37 mmol) in 40 ml hexane under N₂. The reaction mixture was heated at reflux temperature for 1 hour and then cooled to 0 °C. To this suspension, a pre-cooled solution of *p*-tolaldehyde (3.48 ml, 29.5 mmol) in 40 ml dry THF was added drop wise. After the addition

was complete, the mixture was warmed to room temperature while stirring for 30 minutes. Saturated NH_4Cl solution was added to quench the reaction. The organic phase was extracted with H_2O , brine and then dried over MgSO_4 . The crude product was subjected to silica gel column chromatography using EA/Hexanes (3:7, $R_f = 0.2$) as eluting solvent to get furan diol (2.47 g, 58% Yield). ^1H NMR (400 MHz, CDCl_3) δ : 2.36 (s, 6H, Me), 2.42 (bs, 2H, OH), 5.75 (d, 2H, *meso* CH), 5.96 (d, β -furan), 7.16 (d, 4H, Ar), 7.30 (d, 4H, Ar) ppm; ^{13}C NMR (100 MHz, CDCl_3) δ : 21.15, 69.99, 108.04, 108.11, 126.61, 129.12, 137.83, 156.20 ppm.

5,10-di(*p*-tolyl)-16-oxatripyrrane (16)

Furan-diol (**15**, 1 g, 3.25 mmol) was dissolved in pyrrole (8.9 ml, 130 mmol) under N_2 . To this solution $\text{BF}_3 \cdot \text{OEt}_2$ (0.41 ml, 3.25 mmol) was added. The mixture was stirred for 30 min. at room temperature. After completion of reaction as confirmed by TLC, the reaction was quenched by adding aq. NaOH (0.1 N, 50 ml). The mixture was extracted with DCM and washed with water. The organic layer was dried over MgSO_4 and excess pyrrole was removed under vacuum. The crude oil was purified by column chromatography on silica using DCM/Hexanes (1:1, $R_f = 0.4$) as eluting solvent to get pure oxatripyrrane (800 mg, 60% Yield). ^1H NMR (400 MHz, CDCl_3) δ : 2.37 (s, 6H, Me), 5.39 (s, 2H, *meso* CH), 5.94 (s, 2H, β -pyrrole), 5.98 (d, 2H, β -furan), 6.16 (m, 2H, β -pyrrole), 6.65 (s, 2H, α -pyrrole), 7.13 (m, 8H, Ar), 7.98 (bs, 2H, NH) ppm; ^{13}C NMR (100 MHz, CDCl_3): $\delta = 21.01, 43.83, 107.01, 107.76, 108.11, 117.12, 128.17, 129.16, 131.21, 136.57, 137.74, 155.03$ ppm.

***meso*-Free BF_2 -Oxasmaragdyrin (17)**

Dipyrromethane (**14**, 146 mg, 1 mol) and 5,10-di(*p*-tolyl)-16-oxatripyrrane (406 mg, 1 mol) were dissolved in 400 ml of dichloromethane and stirred under nitrogen for 10 min. The reaction was initiated by adding TFA (8 μl , 0.1 mol) and the stirring was continued for 90 min. DDQ (681 mg, 3 mmol) was then added and the reaction mixture was stirred in open-air for additional 90 min. The solvent was removed and crude compound was purified by basic alumina column chromatography eluted with DCM/Hexanes (3:7, $R_f = 0.35$) to get the desired oxasmaragdyrin as a green solid. The oxasmaragdyrin was dissolved in CH_2Cl_2 (60 ml) and triethylamine (5.6 ml, 40 mmol) was added at room temperature. After 10 min $\text{BF}_3 \cdot \text{OEt}_2$ (6.3 ml, 50 mmol) was added and the stirring was continued for 30 min. Completion of the reaction was confirmed by TLC. The reaction mixture was washed thoroughly with 0.1 M NaOH solution and water. The organic layers were combined, dried over MgSO_4 , filtered and the solvent was removed. The crude compound was purified by silica gel column chromatography, using dichloromethane/hexanes (1:1, $R_f = 0.52$) to afford the desired compound as green solid

(18 mg, 3% yield). ^1H NMR (400 MHz, CDCl_3) δ : – 4.20 (t, 2H, NH), 2.80 (s, 6H, Tol), 7.70 (d, 4H, $J = 7.72$ Hz, Ar), 8.30 (d, 4H, $J = 7.80$ Hz, Ar), 9.05 (m, 2H, β -pyrrole), 9.54 (s, 2H, β -furan), 9.77 (d, 2H, $J = 4.36$ Hz, β -pyrrole), 10.28 (m, 2H, β -pyrrole), 10.37 (d, 2H, $J = 4.36$ Hz, β -pyrrole), 10.65 (s, 1H, *meso*-H) ppm; ^{11}B NMR (160.4 MHz, CDCl_3) δ : –12.80 (br s) ppm; ^{19}F NMR (470.5 MHz, CDCl_3) δ : –149.33 (br s) ppm; ^{13}C NMR (125 MHz, CDCl_3) δ : 21.66, 102.75, 106.74, 120.31, 120.80, 121.84, 123.46, 124.15, 124.84, 128.27, 130.43, 132.25, 134.31, 137.89, 139.70, 149.67 ppm; HRMS-FAB $^+$: m/z calcd for $\text{C}_{37}\text{H}_{27}\text{BF}_2\text{N}_4\text{O}$: 592.2246, found 592.2238 $[\text{M}]^+$.

***meso*-Bromo BF_2 -Oxasmaragdyrin (18)**

A solution of BF_2 -oxasmaragdyrin (**18**, 60 mg, 0.1 mmol) in dry THF (20 ml) was treated with N-bromosuccinimide (18 mg, 0.1 mmol), and the reaction mixture was allowed to stir at -78 °C for 30 min initially and continued stirring for additional 1 h at room temperature. The solvent was removed on a rotary evaporator under a vacuum. The crude compound was purified by silica gel column chromatography using hexanes/dichloromethane (7:3) and afforded pure compound as green solid (32 mg, 78% yield). ^1H NMR (400 MHz, CDCl_3) δ : – 4.05 (t, 2H, NH), 2.80 (s, 6H, Tol), 7.70 (d, 4H, $J = 7.72$ Hz, Ar), 8.28 (d, 4H, $J = 7.80$ Hz, Ar), 9.04 (m, 2H, β -pyrrole), 9.52 (s, 2H, β -furan), 9.89 (d, 2H, $J = 4.48$ Hz, β -pyrrole), 10.25 (m, 2H, β -pyrrole), 10.34 (d, 2H, $J = 4.40$ Hz, β -pyrrole) ppm; ^{11}B NMR (160.4 MHz, CDCl_3) δ : –12.90 (br s) ppm; ^{19}F NMR (470.5 MHz, CDCl_3) δ : –149.25 (br s) ppm; ^{13}C NMR (100 MHz, CDCl_3) δ : 21.66, 97.78, 107.37, 120.77, 121.29, 122.34, 123.73, 124.18, 125.28, 128.34, 130.60, 130.89, 131.76, 134.29, 138.05, 139.42, 150.08 ppm; HRMS-MALDI: m/z calcd for $\text{C}_{37}\text{H}_{26}\text{BBrF}_2\text{N}_4\text{O}$: 670.1351, found 670.1368 $[\text{M}]^+$.

***meso*-4-Ethynylcarboxyphenyl BF_2 -Oxasmaragdyrin (SM4)**

To a solution of *meso*-bromo BF_2 -oxasmaragdyrin (**18**, 40 mg 0.06 mmol) in toluene/triethylamine (3:1), 4-ethynylbenzoic acid (11 mg, 0.07 mmol) was added, and the mixture was stirred for 15 min under N_2 atmosphere. The coupling was initiated by addition of catalytic amounts of $\text{Pd}_2(\text{dba})_3$ (27 mg, 0.03 mmol) and AsPh_3 (64 mg, 0.21 mmol). The reaction mixture was stirred at 60 °C for 4 h. The solvent was removed on rotary evaporator under a vacuum. The crude product was subjected to silica gel column chromatographic purification using methanol/dichloromethane (5%) to afforded pure compound as green solid (13 mg, 30% yield). ^1H NMR (400 MHz, $\text{THF-}d_8$) δ : – 4.27 (t, 2H, NH), 2.79 (s, 6H, Tol), 7.75 (d, 4H, $J = 7.72$ Hz, Ar), 8.34 (d, 8H, $J = 7.92$ Hz, Ar), 9.04 (d, 2H, $J = 4.16$ Hz, β -pyrrole), 9.65 (s, 2H, β -furan), 10.15 (d, 2H, $J = 4.40$ Hz, β -pyrrole), 10.54 (m, 2H, β -pyrrole), 10.65 (d,

2H, $J = 4.44$ Hz, β -pyrrole) ppm; ^{11}B NMR (128.4 MHz, THF- d_8) δ : -13.11 (br s) ppm; ^{19}F NMR (376.5 MHz, THF- d_8) δ : -149.03 (br s) ppm; ^{13}C NMR (100 MHz, THF- d_8) δ : 21.73, 92.43, 96.75, 99.07, 108.57, 122.38, 123.00, 123.19, 123.68, 125.90, 129.22, 130.11, 130.96, 131.70, 131.89, 132.64, 135.02, 135.27, 139.05, 140.56, 151.10, 167.24 ppm; UV-vis (THF) $\lambda_{\text{max}}/\text{nm}$ ($\epsilon/10^3 \text{ M}^{-1}\text{cm}^{-1}$) = 461 (186), 497 (51), 737 (44); HRMS-FAB+: m/z calcd for $\text{C}_{46}\text{H}_{31}\text{BF}_2\text{N}_4\text{O}_3$: 736.2457, found 736.2466 [M] $^+$.

5-(5-*t*BuCarbazolethiophen-2-yl)dipyrromethane (19)

A mixture of 5-*t*BuCarbazole thiophene aldehyde (1 g, 2.57 mmol) and pyrrole (17.6 ml, 257 mmol) was degassed with N_2 for 15 min. at room temperature. TFA (19 μl , 0.26 mmol) was then added and the mixture was stirred at room temperature for 3 hrs. After completion of the reaction, NaOH (308 mg, 7.71 mmol) was added and mixture was stirred for 1 h and then filtered. The filtrate was concentrated and pyrrole was removed under vacuum. The crude obtained after removing pyrrole was subjected to silica gel column chromatography using DCM/Hexanes (1:1, $R_f = 0.31$) as eluting solvent to obtain the dipyrromethane (1.1 g, 85% Yield). ^1H NMR (400 MHz, CDCl_3) δ : 1.48 (s, 18H, *t*Bu), 5.76 (s, 1H, *meso*-CH), 6.13 (m, 2H, β -pyrrole), 6.22 (m, 2H, β -pyrrole), 6.75 (m, 2H, α -pyrrole), 6.90 (d, 1H, β -thiophene), 7.02 (d, 1H, β -thiophene), 7.43 (dd, 2H, $J = 4.36$ Hz, Ar), 7.50 (dd, 2H, $J = 3.51$ Hz, Ar), 8.05 (bs, 2H, -NH), 8.11 (d, 2H, $J = 1.56$ Hz, Ar); ^{13}C NMR (100 MHz, CDCl_3) δ : 31.97, 34.73, 39.78, 107.33, 108.57, 109.62, 116.14, 117.70, 123.42, 123.60, 123.82, 124.18, 131.45, 138.28, 140.17, 143.52; HRMS-ESI $^-$: m/z calcd for $\text{C}_{33}\text{H}_{34}\text{N}_3\text{S}$: 504.2473, found 504.2478 [M-H] $^-$.

5-(*p*-hexyloxyphenyl) dipyrromethane (20)

A mixture of 4-hexyloxybenzaldehyde (4.2 ml, 0.02 mol) and pyrrole (137 ml, 2 mol) was degassed with N_2 for 15 min. at room temperature. TFA (150 μl , 0.002 mol, 0.1 eq) was then added and the mixture was stirred at room temperature for 3 hrs. After completion of the reaction, NaOH (2.4 g, 0.06 mol) was added and mixture was stirred for 1 h and then filtered. The filtrate was concentrated and pyrrole was removed under vacuum. The crude obtained after removing pyrrole was subjected to silica gel column chromatography using DCM/Hexanes (1:1, $R_f = 0.2$) as eluting solvent to obtain the dipyrromethane (5.57 g, 86% Yield). ^1H NMR (400 MHz, CDCl_3) δ : 0.95 (t, 3H, -CH $_3$), 1.38 (m, 4H, -CH $_2$), 1.49 (m, 2H, -CH $_2$), 1.80 (m, 2H, -CH $_2$), 3.96 (t, 2H, -OCH $_2$), 5.41 (s, 1H, *meso*-CH), 5.93 (m, 2H, β -pyrrole), 6.18 (m, 2H, β -pyrrole), 6.68 (m, 2H, α -pyrrole), 6.87 (d, 2H, Ar), 7.13 (d, 2H, Ar), 7.87 (bs, 2H, -NH) ppm; ^{13}C NMR (100 MHz, CDCl_3) δ : 13.99, 22.56, 25.69, 29.22, 31.55, 43.09, 68.02, 107.00,

108.32, 114.53, 117.03, 129.30, 132.89, 133.93, 158.07 ppm; HRMS-ESI⁻: m/z calcd for C₂₁H₂₅N₂O: 321.1967, found 321.1958 [M-H]⁻.

5-(*p*-tolyl)dipyrromethane (21)

A mixture of *p*-tolylaldehyde (2.4 ml, 0.02 mol) and pyrrole (137 ml, 2 mol) was degassed with N₂ for 15 min. at room temperature. TFA (150 μ l, 0.002 mol) was then added and the mixture was stirred at room temperature for 3 hrs. After completion of the reaction, NaOH (2.4 g, 0.06 mol) was added and mixture was stirred for 1 h and then filtered. The filtrate was concentrated and pyrrole was removed under vacuum. The crude obtained after removing pyrrole was subjected to silica gel column chromatography using DCM/Hexanes (4:6, R_f = 0.18) as eluting solvent to obtain the dipyrromethane (4.1 g, 86% Yield). ¹H NMR (400 MHz, CDCl₃) δ : 2.34 (s, 3H, -CH₃), 5.44 (s, 1H, *meso*-CH), 5.93 (s, 2H, β -pyrrole), 6.16 (m, 2H, β -pyrrole), 6.69 (m, 2H, α -pyrrole), 7.12 (m, 4H, tolyl), 7.92, (bs, 2H, -NH) ppm; ¹³C NMR (100 MHz, CDCl₃) δ : 21.00, 43.57, 107.05, 108.37, 117.07, 128.25, 129.31, 132.68, 136.57, 139.03 ppm; HRMS-FAB⁺: m/z calcd for C₁₆H₁₆N₂: 236.1313, found 236.1313 [M]⁺.

2,5-bis(*p*-methoxycarbonylphenyl)furandiol (22)

Furan (1 ml, 13.75 mmol) was added to a solution of *n*BuLi (22 ml, 34.37 mmol) and TMEDA (5.15 ml, 34.37 mmol) in 40 ml Hexane under N₂. The reaction mixture was heated at reflux temperature for 1 hour and then cooled to 0 °C. To this suspension, a pre-cooled solution of Methyl-4-formylbenzoate (4.51 g, 27.5 mmol) in 40 ml dry THF was added drop wise. After the addition was complete, the mixture was warmed to room temperature while stirring for 30 minutes. Saturated NH₄Cl solution was added to quench the reaction. The organic phase was extracted with H₂O, brine and then dried over MgSO₄. The crude product was subjected to silica gel column chromatography using EA/Hexanes (3:7, R_f = 0.21) as eluting solvent to get furan diol (820 mg, 15% Yield). ¹H NMR (400 MHz, CDCl₃) δ : 2.74 (bs, 2H, -OH), 3.91 (s, 6H, -OMe), 5.84 (s, 2H, *meso*-CH), 5.97 (d, J = 6.28 Hz, β -Furan), 7.48 (d, 4H, J = 8.24 Hz, Ar), 8.02 (d, 4H, J = 8.24 Hz, Ar) ppm; ¹³C NMR (100 MHz, CDCl₃) δ : 52.17, 69.54, 108.57, 108.64, 126.52, 129.77, 129.89, 145.29, 155.64, 166.82 ppm.

5,10-di(*p*-methoxycarbonylphenyl)-16-oxatripyrrane (23)

Furan-diol (1.37 g, 3.45 mmol) was dissolved in pyrrole (9.5 ml, 138 mmol) under N₂. To this solution BF₃•OEt₂ (0.44 ml, 3.45 mmol) was added. The mixture was stirred for 30 min. at room temperature. After completion of reaction as confirmed by TLC, the reaction was quenched by adding aq. NaOH (0.1 N, 20 ml). The mixture was extracted with dichloromethane and washed with water. The organic layer was dried over MgSO₄ and excess pyrrole was

removed under vacuum. The crude oil was purified by column chromatography on silica using DCM/Hexanes (1:1, $R_f = 0.3$) as eluting solvent to get pure oxatripyrrane (992 mg, 58% Yield). ^1H NMR (400 MHz, CDCl_3) δ : 3.91 (s, 6H, -OMe), 5.45 (s, 2H, meso -CH), 5.89 (s, 2H, β -pyrrole), 6.00 (d, 2H, β -Furan), 6.14 (m, 2H, β -pyrrole), 6.67 (m, 2H, α -pyrrole), 7.25 (m, 4H, Ar), 7.96 (m, 4H, Ar) ppm; ^{13}C NMR (100 MHz, CDCl_3) δ : 44.25, 52.11, 107.58, 108.42, 117.69, 128.31, 129.05, 129.87, 129.96, 145.78, 154.43, 166.82 ppm; HRMS-ESI $^-$: m/z calcd for $\text{C}_{30}\text{H}_{25}\text{N}_2\text{O}_5$: 493.1763, found 493.1760 $[\text{M}-\text{H}]^-$.

19-(5-*t*BuCarbazolethiophen-2-yl)-5,10-di(*p*-methoxycarbonylphenyl)-25-oxasmaragdyrin (24)

5(5-*t*BuCarbazolethiophen-2-yl) dipyrromethane (506 mg, 1 mmol) and 5,10-di(*p*-methoxycarbonylphenyl)-16-oxatripyrrane (495 mg, 1 mmol) were dissolved in 700 ml of dichloromethane and stirred under nitrogen for 10 min. The reaction was initiated by adding TFA (8 μl , 0.1 mmol) and the stirring was continued for 90 min. DDQ (681 mg, 3 mmol) was then added and the reaction mixture was stirred in open-air for additional 90 min. The solvent was removed and crude compound was purified by basic alumina column chromatography eluted with DCM/Hexanes (3:7, $R_f = 0.32$) to get the desired oxasmaragdyrin as a green solid (338 mg, 34% yield). ^1H NMR (400 MHz, CDCl_3) δ : 1.55 (s, 18H, *t*Bu), 4.12 (s, 6H, -OMe), 7.68 (d, 2H, $J = 8.40$ Hz, Ar), 7.71 (d, 1H, $J = 3.68$ Hz, β -thiophene), 7.90 (d, 2H, $J = 8.64$ Hz, Ar), 8.13 (d, 1H, $J = 4.12$ Hz, β -thiophene), 8.23 (s, 2H, Ar), 8.31 (d, 4H, $J = 7.84$ Hz, Ar), 8.43 (d, 2H, $J = 4.24$ Hz, β -pyrrole), 8.49 (d, 4H, $J = 7.84$ Hz, Ar), 8.75 (s, 2H, β -furan), 9.43 (d, 2H, $J = 4.32$ Hz, β -pyrrole), 9.47 (d, 2H, $J = 4.28$ Hz, β -pyrrole), 9.52 (d, 2H, $J = 4.24$, β -pyrrole) ppm; HRMS-ESI $^-$: m/z calcd for $\text{C}_{63}\text{H}_{52}\text{N}_5\text{O}_5\text{S}$: 990.3689, found 990.3698 $[\text{M}-\text{H}]^-$.

19-(*p*-hexyloxyphenyl)-5,10-di(*p*-methoxycarbonylphenyl)-25-oxasmaragdyrin (25)

5-(*p*-hexyloxyphenyl) dipyrromethane (322 mg, 1 mmol) and 5,10-di(*p*-methoxycarbonylphenyl)-16-oxatripyrrane (495 mg, 1 mmol) were dissolved in 700 ml of dichloromethane and stirred under nitrogen for 10 min. The reaction was initiated by adding TFA (8 μl , 0.1 mmol) and the stirring was continued for 90 min. DDQ (681 mg, 3 mmol) was then added and the reaction mixture was stirred in open-air for additional 90 min. The solvent was removed and crude compound was purified by basic alumina column chromatography eluted with DCM/Hexanes (3:7, $R_f = 0.36$) to get the desired oxasmaragdyrin as a green solid (322 mg, 20% yield). ^1H NMR (500 MHz, CDCl_3) δ : 1.01 (t, 3H, -CH $_3$), 1.48 (m, 4H, -CH $_2$), 1.65 (m, 2H, -CH $_2$), 2.01 (m, 2H, -CH $_2$), 4.11 (s, 6H, -OMe), 4.28 (t, 2H, -OCH $_2$), 7.38 (d, 2H, $J = 7.38$ Hz, Ar), 8.27 (m, 8H, Ar, β -pyrrole), 8.46 (s, 4H, Ar), 8.62 (s, 2H, β -furan), 8.92 (s,

2H, β -pyrrole), 9.28 (s, 2H, β -pyrrole), 9.37 (s, 2H, β -pyrrole) ppm; HRMS-MALDI: m/z calcd for $C_{51}H_{44}N_4O_6$: 808.3260, found 808.3278 $[M]^+$.

19-(*p*-tolyl)-5,10-di(*p*-methoxycarbonylphenyl)-25-oxasmaragdyrin (26)

5-(*p*-tolyl) dipyrromethane (236 mg, 1 mmol) and 5,10-di(*p*-methoxycarbonylphenyl)-16-oxatripyrrane (495 mg, 1 mmol) were dissolved in 700 ml of dichloromethane and stirred under nitrogen for 10 min. The reaction was initiated by adding TFA (8 μ l, 0.1 mmol) and the stirring was continued for 90 min. DDQ (681 mg, 3 mmol) was then added and the reaction mixture was stirred in open-air for additional 90 min. The solvent was removed and crude compound was purified by basic alumina column chromatography eluted with DCM/Hexanes (3:7, R_f = 0.34) to get the desired oxasmaragdyrin as a green solid (434 mg, 30% yield). 1H NMR (400 MHz, $CDCl_3$) δ : 2.73 (s, 3H, -CH₃), 4.09 (s, 6H, -OMe), 7.66 (d, 2H, J = 7.52 Hz, tolyl), 8.27 (m, 8H, Ar, tolyl, β -pyrrole), 8.44 (d, 4H, J = 7.72 Hz, Ar), 8.64 (s, 2H, β -furan), 8.92 (d, 2H, J = 4.00 Hz, β -pyrrole), 9.28 (d, 2H, J = 4.04, β -pyrrole), 9.36 (d, 2H, J = 3.80 Hz, β -pyrrole) ppm; HRMS- ESI⁻: m/z calcd for $C_{46}H_{33}N_4O_5$: 721.2451, found 721.2452 $[M-H]^-$.

BF₂-[19-(5-*t*BuCarbazolethiophen-2-yl)-5,10-di(*p*-methoxycarbonylphenyl)-25-oxasmaragdyrin] (27)

Oxasmaragdyrin (**24**, 338 mg, 0.34 mmol) was dissolved in CH_2Cl_2 (60 ml) and triethylamine (1.91 ml, 13.7 mmol) was added at room temperature. After 10 min $BF_3 \cdot OEt_2$ (2.15 ml, 17 mmol) was added and the stirring was continued for 30 min. Completion of the reaction was confirmed by TLC. The reaction mixture was washed thoroughly with 0.1 M NaOH solution and water. The organic layers were combined, dried over $MgSO_4$, filtered and the solvent was removed. The crude compound was purified by silica gel column chromatography, using dichloromethane/hexanes (6:4, R_f = 0.34) to afford the desired compound as green solid (170 mg, 48% yield). 1H NMR (400 MHz, $CDCl_3$) δ : -3.77 (t, 2H, -NH), 1.58 (s, 18H, *t*Bu), 4.18 (s, 6H, -OMe), 7.71 (d, 2H, J = 8.68 Hz, Ar), 7.79 (d, 1H, J = 3.44 Hz, β -thiophene), 7.96 (d, 2H, J = 8.64 Hz, Ar), 8.29 (d, 3H, J = 4.20 Hz, Ar, β -thiophene), 8.50 (d, 4H, J = 7.46 Hz, Ar), 8.60 (d, 4H, J = 7.52 Hz, Ar), 8.95 (d, 2H, J = 4.24 Hz, β -pyrrole), 9.43 (s, 2H, β -furan), 9.99 (d, 2H, J = 4.08 Hz, β -pyrrole), 10.23 (d, 2H, J = 4.04, β -pyrrole), 10.34 (d, 2H, J = 4.04 Hz, β -pyrrole) ppm; ^{11}B NMR (160.4 MHz, $CDCl_3$) δ : -12.58 (br s) ppm; ^{19}F NMR (470.5 MHz, $CDCl_3$) δ : -149.04 (br s) ppm; ^{13}C NMR (125 MHz, $CDCl_3$) δ : 32.08, 34.90, 52.49, 106.33, 110.03, 111.35, 116.47, 120.74, 120.81, 122.41, 123.97, 124.22, 124.76, 128.88, 129.83, 130.24, 130.78, 131.12, 132.05, 134.45, 137.19, 140.29, 143.76, 144.08, 147.09,

149.10, 167.29 ppm; HRMS-FAB⁺: m/z calcd for C₆₃H₅₂BF₂N₅O₅S: 1039.3750, found 1039.3752 [M]⁺.

BF₂-[19-(*p*-hexyloxyphenyl)-5,10-di(*p*-methoxycarbonyl phenyl)-25-oxasmaragdyrin] (28)

Oxasmaragdyrin (**25**, 256 mg, 0.32 mmol) was dissolved in CH₂Cl₂ (40 ml) and triethylamine (1.8 ml, 12.7 mmol) was added at room temperature. After 10 min BF₃•OEt₂ (2 ml, 16 mmol) was added and the stirring was continued for 30 min. Completion of the reaction was confirmed by TLC. The reaction mixture was washed thoroughly with 0.1 M NaOH solution and water. The organic layers were combined, dried over MgSO₄, filtered and the solvent was removed. The crude compound was purified by silica gel column chromatography, using dichloromethane/hexanes (4:6, R_f = 0.4) to afford the desired compound as green solid (150 mg, 55% yield). ¹H NMR (400 MHz, CDCl₃) δ: -3.38 (t, 2H, -NH), 1.02 (t, 3H, -CH₃), 1.50 (m, 4H, -CH₂), 1.68 (m, 2H, -CH₂), 2.04 (m, 2H, -CH₂), 4.16 (s, 6H, -OMe), 4.31 (t, 2H, -OCH₂), 7.49 (d, 2H, *J* = 8.56 Hz, Ar), 8.48 (m, 6H, Ar), 8.57 (d, 4H, *J* = 8.08 Hz, Ar), 8.84 (dd, 2H, *J* = 1.96 Hz, β-pyrrole), 9.32 (s, 2H, β-furan), 9.55 (d, 2H, *J* = 4.48 Hz, β-pyrrole), 10.13 (dd, 2H, *J* = 2.01, β-pyrrole), 10.21 (d, 2H, *J* = 4.40 Hz, β-pyrrole) ppm; ¹¹B NMR (160.4 MHz, CDCl₃) δ: -12.16 (br s) ppm; ¹⁹F NMR (470.5 MHz, CDCl₃) δ: -149.19 (br s) ppm; ¹³C NMR (125 MHz, CDCl₃) δ: 14.12, 22.72, 25.93, 29.47, 31.73, 52.47, 68.48, 105.97, 114.70, 119.92, 120.10, 120.85, 121.74, 123.81, 124.60, 125.20, 128.86, 129.59, 130.12, 130.83, 131.41, 132.16, 134.38, 135.77, 147.22, 148.99, 159.80, 167.33 ppm; HRMS-MALDI: m/z calcd for C₅₁H₄₄BF₂N₄O₆: 857.3322, found 857.3356 [M+H]⁺.

BF₂-[19-(*p*-tolyl)-5,10-di(*p*-methoxycarbonylphenyl)-25-oxasmaragdyrin] (29)

Oxasmaragdyrin (**26**, 391 mg, 0.54 mmol) was dissolved in CH₂Cl₂ (60 ml) and triethylamine (3 ml, 21.6 mmol) was added at room temperature. After 10 min BF₃•OEt₂ (3.42 ml, 27 mmol) was added and the stirring was continued for 30 min. Completion of the reaction was confirmed by TLC. The reaction mixture was washed thoroughly with 0.1 M NaOH solution and water. The organic layers were combined, dried over MgSO₄, filtered and the solvent was removed. The crude compound was purified by silica gel column chromatography, using dichloromethane/hexanes (1:1, R_f = 0.59) to afford the desired compound as green solid (120 mg, 30% yield). ¹H NMR (400 MHz, CDCl₃) δ: -3.48 (t, 2H, -NH), 2.78 (s, 3H, -CH₃), 4.17 (s, 6H, -OMe), 7.79 (d, 2H, *J* = 7.72 Hz, tolyl), 8.49 (d, 6H, *J* = 8.08 Hz, Ar, tolyl), 8.58 (d, 4H, *J* = 8.12 Hz, Ar), 8.86 (dd, 2H, *J* = 2.96 Hz, β-pyrrole), 9.34 (s, 2H, β-furan), 9.58 (d, 2H, *J* = 4.40 Hz, β-pyrrole), 10.16 (dd, 2H, *J* = 1.95, β-pyrrole), 10.24 (d, 2H, *J* = 4.40 Hz, β-

pyrrole) ppm; ^{11}B NMR (160.4 MHz, CDCl_3) δ : -12.39 (br s) ppm; ^{19}F NMR (470.5 MHz, CDCl_3) δ : -149.23 (br s) ppm; ^{13}C NMR (125 MHz, CDCl_3) δ : 21.57, 52.48, 105.99, 120.05, 120.22, 120.77, 121.85, 123.83, 124.61, 125.20, 128.87, 129.27, 129.61, 130.15, 131.36, 132.09, 134.41, 134.67, 135.84, 138.25, 147.24, 148.98, 167.34 ppm; HRMS-FAB $^+$: m/z calcd for $\text{C}_{46}\text{H}_{33}\text{BF}_2\text{N}_4\text{O}_5$: 770.2572, found 770.2529 $[\text{M}]^+$.

$\text{B}(\text{OC}_2\text{H}_5)_2$ -[19-(*p*-tolyl)-5,10-di(*p*-methoxycarbonylphenyl)-25-oxasmaragdyrin] (30)

BF_2 -Oxasmaragdyrin (**29**, 100 mg, 0.13 mmol) was dissolved in dry CH_2Cl_2 (50 ml) in the presence of aluminum chloride (104 mg, 0.78 mmol) under nitrogen. The resulting mixture was refluxed for 10 min and then ethanol (10 ml) was added. The reaction mixture was stirred for additional 10 min. The reaction mixture was concentrated and purified by column chromatography on silica gel using hexanes/dichloromethane (1:1, $R_f = 0.62$) to get the desired product as green solid (100 mg, 93% yield). ^1H NMR (400 MHz, CDCl_3) δ : -3.77 (t, 6H, $J = 6.96$ Hz; - CH_3), -3.39 (q, 4H, $J = 7.00$ Hz; - OCH_2), -0.65 (s, 2H; -NH), 2.77 (s, 3H; - CH_3), 4.16 (s, 6H; -OMe), 7.76 (d, 4H, $J = 7.84$ Hz; Ar), 8.49 (m, 6H, Ph), 8.55 (d, 2H, $J = 8.20$ Hz; Ar), 8.61 (m, 2H, β -pyrrole), 9.42 (s, 2H, β -furan), 9.42 (d, 2H, $J = 4.36$ Hz; β -pyrrole), 9.87 (m, 2H, β -pyrrole), 10.05 (d, 2H, $J = 4.40$ Hz; β -pyrrole) ppm; ^{11}B NMR (128.4 MHz, CDCl_3) δ : -12.00 (br s) ppm; ^{13}C NMR (100 MHz, CDCl_3) δ : 11.64, 21.54, 49.02, 52.42, 105.70, 118.50, 118.57, 121.05, 124.24, 124.50, 128.65, 129.02, 129.67, 132.68, 133.06, 134.54, 134.67, 136.39, 137.81, 148.01, 148.79, 167.47 ppm; HRMS-ESI: m/z calcd for $\text{C}_{50}\text{H}_{43}\text{BN}_4\text{O}_7$: 822.3225, found 822.3231 $[\text{M}+\text{H}]^+$.

BF_2 -[19-(5-*t*BuCarbazolethiophen-2-yl)-5,10-di(4-carboxylphenyl)-25-oxasmaragdyrin] (SM5)

BF_2 -oxasmaragdyrin (**27**, 150 mg, 0.14 mmol) was dissolved in 50 ml THF. To this mixture, KOH (162 mg, 2.8 mmol) dissolved in 1 ml water was added and refluxed for 12 h. After cooling, the solvent was removed under vacuum. To the crude product dichloromethane was added and extracted with 1N HCl. The organic layer was dried over MgSO_4 and concentrated. Crude product was purified by silica gel column chromatography using $\text{CH}_2\text{Cl}_2/\text{MeOH}$ (9.5:0.5, $R_f = 0.1$) as eluent to get the desired product as green solid (141 mg, 98% yield). ^1H NMR (400 MHz, THF- d_8) δ : -3.79 (t, 2H, -NH), 1.55 (s, 18H, *t*Bu), 7.71 (d, 2H, $J = 8.64$ Hz, Ar), 7.95 (d, 1H, $J = 3.72$ Hz, β -thiophene), 7.97 (d, 2H, $J = 8.64$ Hz, Ar), 8.33 (d, 2H, $J = 1.48$ Hz, Ar), 8.49 (d, 1H, $J = 3.72$ Hz, β -thiophene), 8.55 (d, 4H, $J = 8.12$ Hz, Ar), 8.61 (d, 4H, $J = 8.08$ Hz, Ar), 9.01 (dd, 2H, $J = 2.12$ Hz, β -pyrrole), 9.57 (s, 2H, β -furan), 10.11 (d, 2H, $J = 4.52$ Hz, β -pyrrole), 10.49 (dd, 2H, $J = 1.91$, β -pyrrole), 10.60 (d, 2H, $J = 4.48$ Hz; β -pyrrole)

ppm; ^{11}B NMR (160.4 MHz, THF-*d*8) δ : -12.86 (br s) ppm; ^{19}F NMR (470.5 MHz, THF-*d*8) δ : -149.34 (br s) ppm; ^{13}C NMR (125 MHz, THF-*d*8) δ : 32.47, 35.59, 107.46, 110.92, 111.81, 117.38, 121.74, 122.14, 123.66, 125.01, 125.16, 125.35, 125.51, 125.79, 125.97, 126.22, 129.97, 130.91, 131.87, 132.18, 132.55, 133.01, 135.33, 138.36, 141.44, 144.82, 147.74, 150.30, 167.94 ppm; UV-vis (THF) $\lambda_{\text{max}}/\text{nm}$ ($\epsilon/10^3 \text{ M}^{-1}\text{cm}^{-1}$): 452 (165), 478 (100), 712 (38); HRMS-FAB+: m/z calcd for $\text{C}_{61}\text{H}_{48}\text{BF}_2\text{N}_5\text{O}_5\text{S}$: 1011.3437, found 1011.3455 $[\text{M}]^+$.

BF₂-[19-(*p*-hexyloxyphenyl)-5,10-di(4-carboxylphenyl)-25-oxasmaragdyrin] (SM6)

BF₂-oxasmaragdyrin (**28**, 100 mg, 0.12 mmol) was dissolved in 50 ml THF. To this mixture, KOH (131 mg, 2.4 mmol) dissolved in 1 ml water was added and refluxed for 12 h. After cooling, the solvent was removed under vacuum. To the crude product dichloromethane was added and extracted with 1N HCl. The organic layer was dried over MgSO₄ and concentrated. Crude product was purified by silica gel column chromatography using CH₂Cl₂/MeOH (9.5:0.5, $R_f = 0.14$) as eluent to get the desired product as green solid (95 mg, 92% yield). ^1H NMR (400 MHz, THF-*d*8) δ : -3.38 (t, 2H, -NH), 1.03 (t, 3H, -CH₃), 1.52 (m, 6H, -CH₂), 2.03 (m, 2H, -CH₂), 4.35 (t, 2H, -OCH₂), 7.56 (d, 2H, $J = 8.48$ Hz, Ar), 8.55 (m, 10H, Ar), 8.89 (dd, 2H, $J = 2.12$ Hz, β -pyrrole), 9.44 (s, 2H, β -furan), 9.60 (d, 2H, $J = 4.40$ Hz, β -pyrrole), 10.34 (dd, 2H, $J = 2.16$, β -pyrrole), 10.42 (d, 2H, $J = 4.40$ Hz, β -pyrrole) ppm; ^{11}B NMR (160.4 MHz, THF-*d*8) δ : -14.00 (br s) ppm; ^{19}F NMR (470.5 MHz, THF-*d*8) δ : -151.36 (br s) ppm; ^{13}C NMR (125 MHz, THF-*d*8) δ : 14.56, 23.74, 27.00, 30.81, 32.81, 69.13, 107.05, 115.62, 120.87, 121.32, 121.59, 122.89, 124.90, 125.56, 125.88, 125.98, 129.96, 130.62, 131.82, 132.02, 132.50, 133.09, 135.24, 136.76, 147.89, 150.15, 161.12, 167.91; UV-vis (THF) $\lambda_{\text{max}}/\text{nm}$ ($\epsilon/10^3 \text{ M}^{-1}\text{cm}^{-1}$): 446 (254), 473 (118), 699 (33); HRMS-FAB+: m/z calcd for $\text{C}_{49}\text{H}_{39}\text{BF}_2\text{N}_4\text{O}_6$: 828.2931, found 828.2927 $[\text{M}]^+$.

BF₂-[19-(*p*-tolyl)-5,10-di(4-carboxylphenyl)-25-oxasmaragdyrin] (SM7)

BF₂-oxasmaragdyrin (**29**, 100 mg, 0.13 mmol) was dissolved in 50 ml THF. To this mixture, KOH (146 mg, 2.6 mmol) dissolved in 1 ml water was added and refluxed for 12 h. After cooling, the solvent was removed under vacuum. To the crude product dichloromethane was added and extracted with 1N HCl. The organic layer was dried over MgSO₄ and concentrated. Crude product was purified by silica gel column chromatography using CH₂Cl₂/MeOH (9.5:0.5, $R_f = 0.12$) as eluent to get the desired product as green solid (95 mg, 98% yield). ^1H NMR (400 MHz, THF-*d*8) δ : -3.52 (t, 2H, -NH), 2.77 (s, 3H, -CH₃), 7.82 (d, 2H, $J = 7.76$ Hz, tolyl), 8.53 (d, 6H, $J = 8.07$ Hz, Ar, tolyl), 8.59 (d, 4H, $J = 8.12$ Hz, Ar), 8.92 (dd, 2H, $J = 2.16$ Hz, β -pyrrole), 9.48 (s, 2H, β -furan), 9.61 (d, 2H, $J = 4.40$ Hz, β -pyrrole), 10.37 (dd, 2H, $J =$

1.97, β -pyrrole), 10.44 (d, 2H, $J = 4.52$ Hz; β -pyrrole) ppm; ^{11}B NMR (160.4 MHz, THF-*d*8) δ : -14.20 (br s) ppm; ^{19}F NMR (470.5 MHz, THF-*d*8) δ : -151.36 (br s) ppm; ^{13}C NMR (125 MHz, THF-*d*8) δ : 21.64, 107.09, 121.02, 121.32, 121.47, 123.03, 124.94, 125.58, 125.80, 129.95, 130.16, 130.65, 132.04, 132.42, 132.99, 135.27, 135.67, 137.03, 139.11, 147.89, 150.14, 167.91 ppm; UV-vis (THF) $\lambda_{\text{max/nm}}$ ($\epsilon/10^3 \text{ M}^{-1}\text{cm}^{-1}$) = 445 (271), 472 (124), 698 (32); HRMS-FAB+: m/z calcd for $\text{C}_{44}\text{H}_{29}\text{BF}_2\text{N}_4\text{O}_5$: 742.2199, found 742.2197 [M] $^+$.

B(OC₂H₅)₂-[19-(*p*-tolyl)-5,10-di(4-carboxylphenyl)-25-oxasmaragdyrin] (SM8)

B(OEt)₂-oxasmaragdyrin (**30**, 100 mg, 0.12 mmol) was dissolved in 50 ml THF. To this mixture, KOH (136 mg, 2.4 mmol) dissolved in 1 ml water was added and refluxed for 12 h. After cooling, the solvent was removed under vacuum. To the crude product dichloromethane was added and extracted with 1N HCl. The organic layer was dried over MgSO₄ and concentrated. Crude product was purified by silica gel column chromatography using CH₂Cl₂/MeOH (9.5:0.5, $R_f = 0.14$) as eluent to get the desired product as green solid (83 mg, 87% yield). ^1H NMR (400 MHz, CDCl₃) δ : -3.85 (t, 6H, $J = 6.68$ Hz; -CH₃), -3.50 (q, 4H, $J = 6.85$ Hz; -OCH₂), -0.89 (s, 2H; -NH), 2.75 (s, 3H; -CH₃), 7.79 (d, 4H, $J = 7.44$ Hz; Ar), 8.49 (m, 6H, Ph), 8.56 (d, 2H, $J = 7.20$ Hz; Ar), 8.61 (d, 2H, $J = 4.16$ Hz; β -pyrrole), 9.33 (s, 2H, β -furan), 9.44 (d, 2H, $J = 4.32$ Hz; β -pyrrole), 10.05 (d, 2H, $J = 4.16$ Hz; β -pyrrole), 10.23 (d, 2H, $J = 4.36$ Hz; β -pyrrole) ppm; ^{11}B NMR (128.4 MHz, CDCl₃) δ : -13.97 (br s) ppm; ^{13}C NMR (100 MHz, CDCl₃) δ : 12.03, 21.60, 49.67, 106.88, 119.67, 119.96, 121.47, 122.23, 124.88, 125.12, 125.62, 125.95, 129.83, 130.12, 131.64, 133.66, 134.12, 135.34, 135.58, 137.62, 138.68, 148.63, 149.92, 167.96 ppm; UV-vis (THF) $\lambda_{\text{max/nm}}$ ($\epsilon/10^3 \text{ M}^{-1}\text{cm}^{-1}$) = 449 (228), 477 (104), 700 (27); HRMS-ESI: m/z calcd for $\text{C}_{48}\text{H}_{39}\text{BN}_4\text{O}_7$: 794.2912, found 794.2919 [M] $^+$.

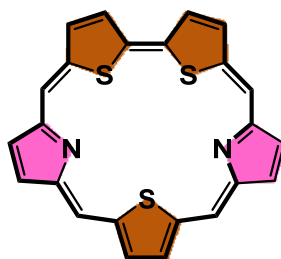
5.4.3 Photovoltaic Measurements

TiO₂ photoanode films and Pt counter electrodes were purchased from Yingkou Opvtech New Energy Co. Ltd. Liaoning, China. The films, which were prepared by using the screen-printing method, were composed of a transparent layer (thickness $\approx 12 \mu\text{m}$), a scattering layer (thickness $\approx 4 \mu\text{m}$), and a working area of $0.4 \times 0.4 \text{ cm}^2$ and were used as received. The films were pretreated according to the following activation procedures before use: heating at 100 °C for 22 min, at 110 °C for 60 min, at 450 °C for 68 min, at 500 °C 60 min, at 250 °C for 60 min, cooling at 80 °C and keeping at 80 °C before immersion. The TiO₂ films were immersed in a solution of $1 \times 10^{-4} \text{ M}$ oxasmaragdyrin and $3 \times 10^{-4} \text{ M}$ CDCA in THF at 30 °C and for a designated time as 8 h for SM1, SM2 and SM3, 6 h for SM4 (at 40 °C), 4 h for SM5 and SM6,

8 h for SM7 and 6 h for SM8. The dye-sensitized TiO₂ films were washed with THF, dried in hot air, and used as the working electrode. To fabricate the DSSC device, the two electrodes were tightly clipped together into a sandwich-type cell that was spaced by a 40 μm film spacer. A thin layer of electrolyte, which contained 0.05 M I₂, 0.1 M lithium iodide (LiI), 0.6 M dimethyl-propyl-benzimidazole iodide (DMPII), and 0.6 M 4-tert-butylpyridine (TBP) in dry CH₃CN, was introduced into the space between the two electrodes. The photo-electrochemical characterizations of the solar cells were performed on an Oriel Class A solar simulator (Oriel 91195A, Newport Corp.). Photocurrent–voltage characteristics of the DSSCs were recorded on a potentiostat/galvanostat (CHI650B, CH Instruments, Inc.) at a light intensity of 100 mW/cm² and calibrated to an Oriel reference solar cell (Oriel 91150, Newport Corp.). The monochromatic quantum efficiency was recorded on a monochromator (Oriel 74100, Newport Corp.) under short-circuit conditions. The intensity of each wavelength was within the range 1–3 mWcm⁻².

Section II

Core-modified Expanded Porphyrins

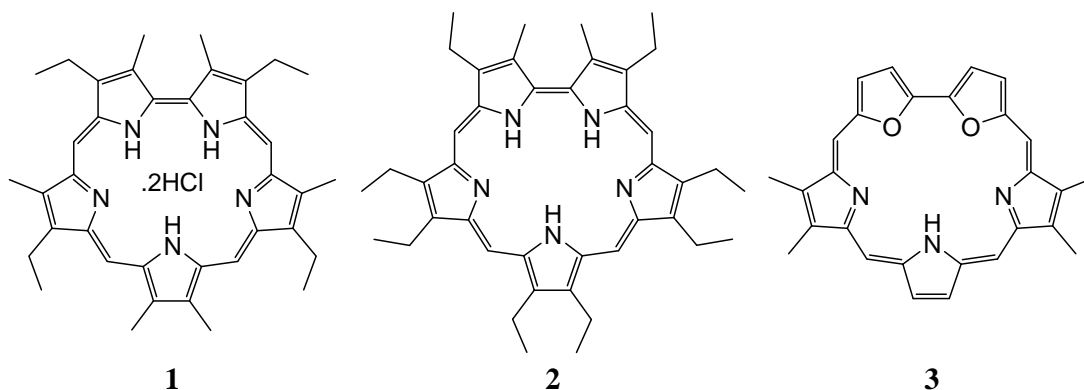


6. Novel carboxylate functionalized N₂S₃ Sapphyrins: Synthesis, Photophysical and Photovoltaic properties

6.1 Introduction

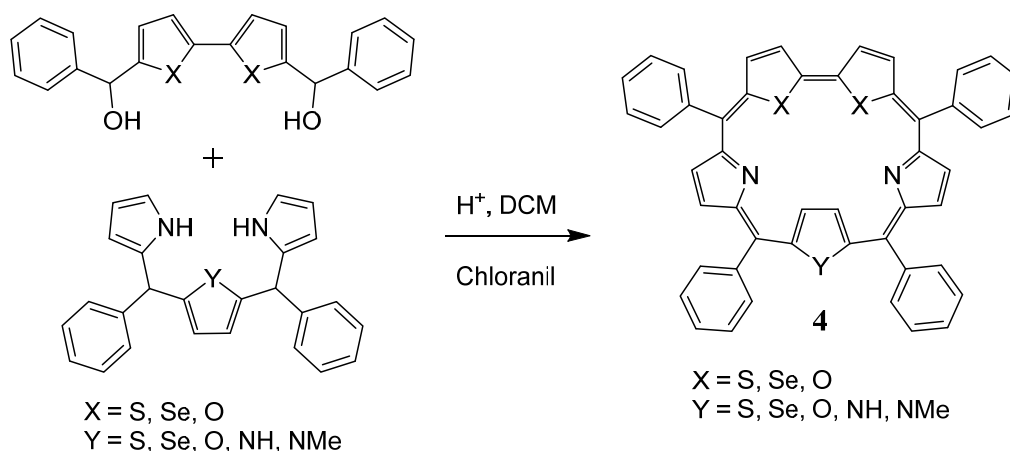
Expanded porphyrins containing a larger central core than the regular porphyrin possess novel spectral and electronic properties, exciting and often exceptional cation-coordination features, anion binding and in favorable cases anion transport, as sensitizers for photodynamic therapy (PDT),^[1-4] as contrasting agents in magnetic resonance imaging (MRI),^[5-6] as radiation therapy enhancer,^[7] as nonlinear optical materials^[8-10] and for studying fundamental issues related to aromaticity. The number of π -electrons in the ring can be increased either by increasing the number of conjugated double bonds between the pyrrole rings or by increasing the number of pyrrole rings. Accordingly, 22π sapphyrins, 26π rubyrins, 30π heptaphyrins, 34π octaphyrins and higher cyclic polypyrrole analogues containing 40π , 48π , 64π , 80π and 96π systems have recently been reported in the literature. These macrocycles show rich structural diversity where normal and different kinds of inverted structures have been identified. Sapphyrins are [22] pentaphyrins (1.1.1.1.0), which are aromatic and are the first expanded porphyrins to be reported. R. B. Woodward and coworkers^[11] serendipitously isolated in 1966 and named as 'sapphyrin' for this macrocycle due to its intense blue green color in organic solvent. Sapphyrin **1** (Scheme 6-1) was obtained in the 4+1 condensation reaction between the linear tetrapyrrolic precursor, bipyrrrolyl dipyrromethane and 2,5-diformyl-3,4-dimethyl pyrrole in acidic medium. Later, Woodward's group^[12] and Johnson and coworkers^[13] independently tried a 3+2 condensation involving a bipyrrrole dialdehyde with a tripyrrane with acid catalysis followed by air oxidation to get sapphyrin **2** (Scheme 1). Alternately, Woodward and coworkers, by using 3+2 condensation of pyrrolyl bipyrrrole and diformyl dipyrromethane, synthesized sapphyrin **2** in 35% yield. However, the difficulty in precursor synthesis limited the utility of the above methods.

Substitution of one or more pyrrolic units with other heterocycles such as furan, thiophene and selenophene leads to hetero expanded porphyrins. The core-modification leads to changes in size of the inner cavity and nature of the electronic structure. There are only limited reports on the syntheses and characterization of core-modified expanded porphyrins in the literature. Johnson and coworkers^[14] developed the first example of such a sapphyrin system when they tried to generate dioxa sapphyrin **3** of corroles by condensing diformylbifuran and dipyrromethane.



Scheme 6-1. Structures of sapphyrins 1-3.

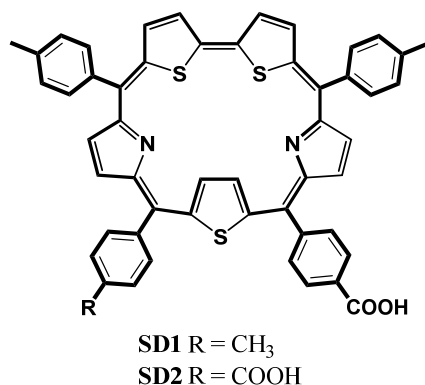
Sessler and coworkers^[15-16] have synthesized a series of β -substituted sapphyrins containing one or more heteroatoms by 3+2 methodology using appropriate precursors. Chandrashekar and coworkers^[17-19] have reported a series of *meso*-aryl sapphyrins **4** where O, S and Se substituted in place of two or three core nitrogens by an easy and efficient MacDonald 3+2 condensation involving tripyrromethanes and diols in high yield (Scheme 6-2).



Scheme 6-2. Synthesis of sapphyrin 4.

The synthesis of mono-functionalized core-modified sapphyrins and their application in the formation of covalently linked porphyrin-expanded porphyrin dyads is well reported in the literature.^[20-22] Even though a variety of functionalized core-modified porphyrins have been published in the literature, the synthesis of carboxylate substituted core-modified sapphyrins and their application in dye-sensitized solar cells is not yet reported. As these free-base sapphyrins are less basic than the free-base oxasamaragdyrins, we can easily manipulate the substituents on the periphery to modify the structure and check their efficacy in DSSCs. These sapphyrins also possess very good absorption features with a strong *Soret* band around 507 nm and two Q bands in the 600-740 nm and thus can be utilized as individual sensitizer or as a co-

sensitizer along with complementary porphyrin or organic dyes. With this purpose in mind, we have prepared two carboxylate functionalized N_2S_3 sapphyrins in least possible steps and evaluated them in DSSCs. The sapphyrin **SD1** with three tolyl and one carboxyl substituent and sapphyrin **SD2** with two tolyl and two carboxyl group substituents were prepared. The general structures of these sapphyrin sensitizers are depicted in Scheme 6-3.

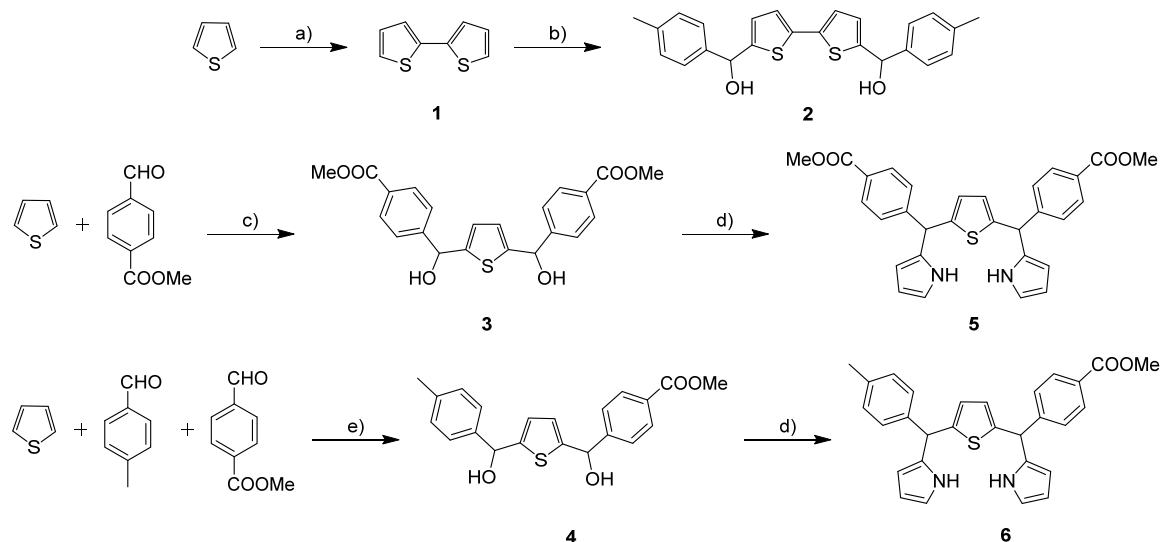


Scheme 6-3. General structure of sapphyrin dyes.

6.2 Results and Discussion

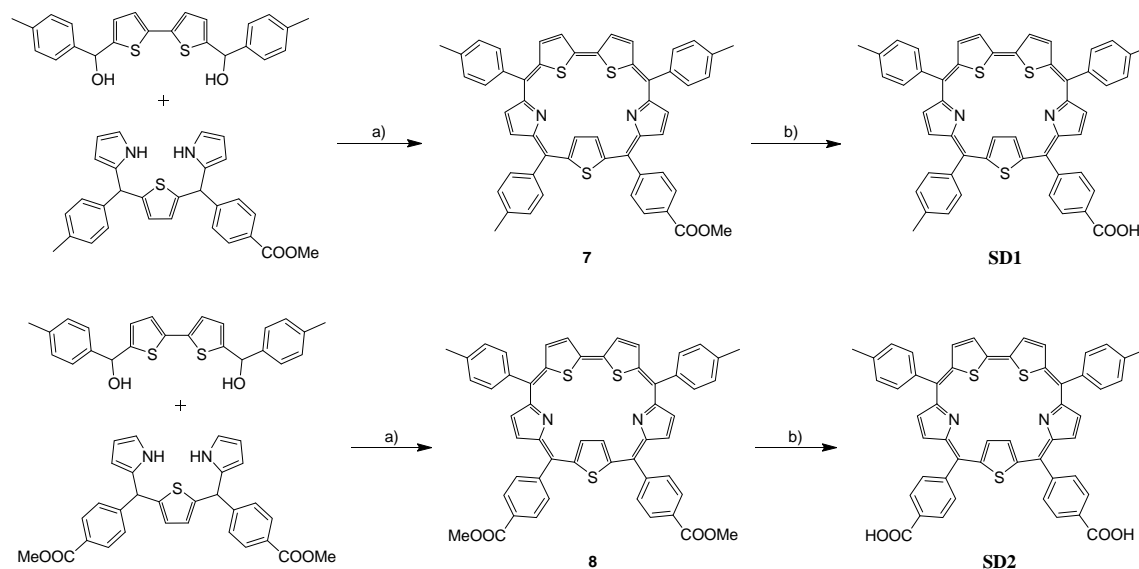
6.2.1 Syntheses

The synthesis of the starting compounds required for the assembly of the sapphyrin ring is described in Scheme 6-4. To prepare bithiophene **1**, thiophene is treated with *n*-BuLi and CuCl₂ at low temperature.



Scheme 6-4. Synthesis of intermediate diols and tripyrranes. Reagents and conditions: a) *n*-BuLi, CuCl₂, Ether/THF; b) *p*-tolualdehyde, *n*-BuLi, TMEDA, Hex/THF; c) *n*-BuLi, TMEDA, Hex/THF; d) Pyrrole, BF₃•OEt₂; e) *n*-BuLi, TMEDA, Hex/THF.

This bithiophene was further treated with *n*-BuLi and tetramethyl ethylenediamine (TMEDA) followed by *p*-tolualdehyde to obtain bithiophene diol **2**. For the synthesis of another starting compound, thiophene was treated with *n*-BuLi followed by methyl-4-formylbenzoate to get the thiophene diol **3**, which was treated with pyrrole under acidic condition to yield the thiatripyrrane **5**. The mixed condensation of thiophene with equimolar amount of *p*-tolualdehyde and methyl-4-formylbenzoate in presence of *n*-BuLi yielded the mixed thiophene diol **4**, which on further treatment with excess pyrrole under Lewis acidic condition resulted in the formation of another starting compound, the thiatripyrrane **6**. The condensation of the bithiophene diol **2** and the 16-thiatripyrrane **6**, was initiated with trifluoroacetic acid (TFA) followed by aerobic oxidation with 2,3-dichloro-5,6-dicyano-1,4-benzoquinone (DDQ) to assemble the sapphyrin ring **7**, which was saponificated in the presence of aq. KOH to yield the final sapphyrin **SD1** as shown in the Scheme 6-5. The sapphyrin ring **8**, was assembled following the similar sequence of acidic condensation with subsequent aerobic oxidation and it is further hydrolyzed with aq. KOH to obtain the sapphyrin dye **SD2** as presented in the Scheme 6-5. All the sapphyrins along with the intermediate compounds are thoroughly characterized by ^1H , ^{13}C NMR and HRMS spectroscopy. The interesting feature of these sapphyrins is the presence of the two β -thiophene protons in the up field region as evident from the ^1H NMR spectrum.



Scheme 6-5. Synthesis of the sapphyrin dyes SD1 and SD2. Reagents and conditions: a) TFA, DDQ, DCM; b) aq. KOH, THF.

It indicates that the thiophene ring at the opposite position of the bithiophene is inverted and due to the influence of the large ring currents the protons at the β -position are shifted towards

the up field region. These sapphyrin dyes can be prepared from the readily available bithiophene diol and 16-thiatripyrrane in just two steps.

6.2.2 Optical properties

The UV-Visible peak positions of the *Soret* and Q bands and the molar absorption coefficients (ϵ) of sapphyrins in THF are summarized in Table 6-1. The UV-Visible spectra of the studied sapphyrins as displayed in Figure 6-1(a), shows typical porphyrin features including a strong *Soret* band at 507 nm and two Q bands around 600-700 nm. The *Soret* band for sapphyrins is red-shifted and broader than that of the porphyrins covering the wavelengths in the region of 430-550 nm. The molar extinction coefficient for dye **SD1** is slightly higher than that of the dye **SD2**.

Table 6-1. Optical and electrochemical properties of sapphyrin dyes.

Dye	$\lambda_{\text{abs}} / \text{nm}^a$ ($\epsilon / 10^3 \text{M}^{-1} \text{cm}^{-1}$)	$E_{\text{ox}} / \text{V}^b$	$E_{(0,0)} / \text{eV}^c$	$E_{\text{ox}}^* / \text{V}^d$
SD1	507 (145), 621 (8.8), 676 (18.7)	0.99	1.71	-0.72
SD2	507 (121), 623 (9.5), 675(15.8)	1.07	1.67	-0.60

^aRecorded in THF at 298K, ^bFirst oxidation potentials vs. NHE determined for SD1 by cyclic voltammetry and for SD2 by square wave voltammetry in THF and referenced to a ferrocene redox couple, ^cThe band gap, $E_{(0,0)}$, was derived from peak separation of the cathodic and anodic waves, ^dThe excited state oxidation potential versus a normal hydrogen electrode (NHE).

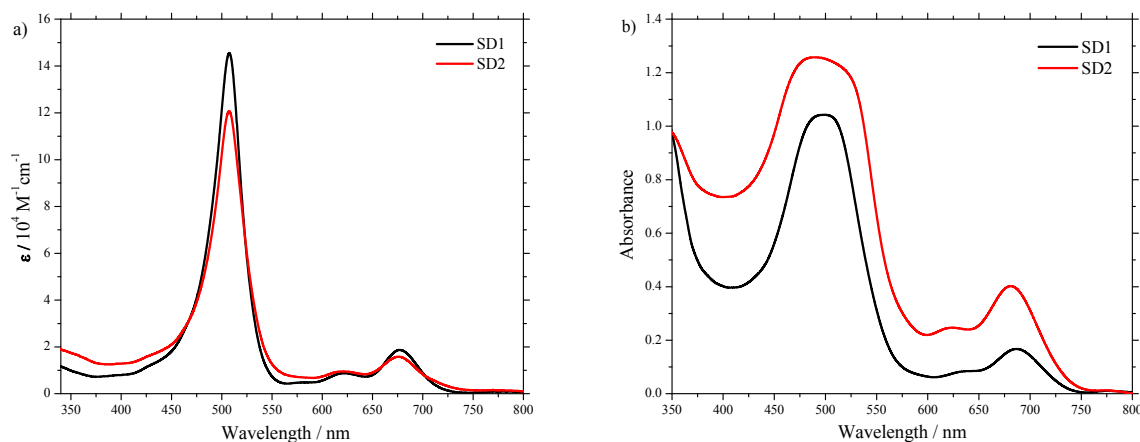


Figure 6-1. Absorption spectra of sapphyrins a) measured in THF, b) adsorbed on TiO_2 .

The absorption spectra of these sapphyrins as thin films were studied to understand their adsorption behavior on TiO_2 . To obtain the absorption spectra on TiO_2 films, the films with

thickness of approximately 3 μm were dipped in 0.1 mM THF solution of sapphyrins for 4 h at room temperature. The adsorption spectra were recorded by reflectance measurements using an integrated sphere and the results are displayed in Figure 6-1(b). As observed from the Figure 6-1(b), the *Soret* as well as Q band are slightly red-shifted and broadened considerably. These red-shifted absorption onset towards 750 nm and broadening of the absorption spectra suggest that these sapphyrins can serve as sensitizers for DSSCs. Noticeably, we did not observe any fluorescence for these sapphyrins, which might be due the presence of three thiophene units in the sapphyrin ring. The presence of more number of sulfur atoms, which might cause a heavy atom effect to accelerate the intersystem crossing rate considerably.

6.2.3 Electrochemical properties

The cyclic voltammetry measurements of the sapphyrin dyes were carried out in degassed THF containing 0.1 M $[\text{Bu}_4\text{N}]\text{PF}_6$ as the supporting electrolyte and a scan rate of 50 mV/sec to obtain the first oxidation and reduction potentials and the resulted spectra were depicted in Figure 6-2. The relevant electrochemical data is summarized in Table 6-1. The sapphyrin **SD1** show one reversible oxidation and two reversible reduction couples, while in case of the sapphyrin **SD2** one quasi-reversible oxidation and two quasi-reversible reduction couples were observed. As the reduction couples for **SD2** were not clear from the CV measurement we utilized square wave voltammetry to obtain the reduction potential for **SD2**. The oxidation potential of **SD2** is shifted towards more positive by 80 mV and the reduction potential towards less negative by 120 mV compared to **SD1**, making it harder to oxidize and easier to reduce.

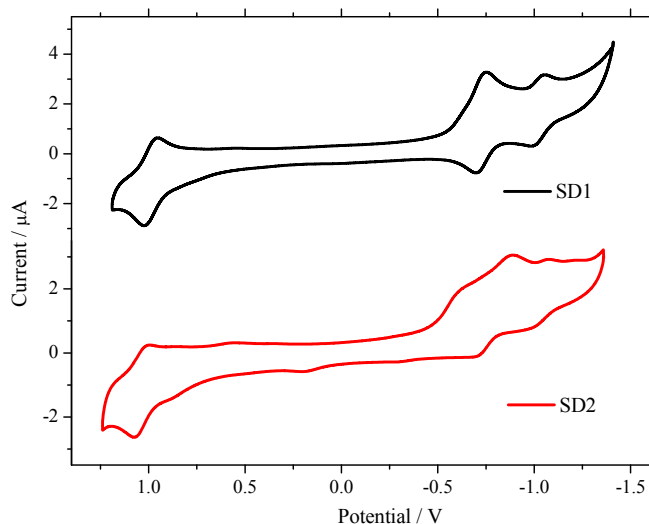


Figure 6-2. Cyclic voltammograms of sapphyrins measured in THF at a scan rate of 50 mV/sec.

The band gap, $E_{(0,0)}$, was derived from peak separation of the cathodic and anodic waves in the CV spectra and are listed in Table 6-1. The oxidation potentials and the excited state oxidation potential versus a normal hydrogen electrode (NHE) were also determined from the CV spectra and are listed in Table 6-1. The ground state oxidation potentials (E_{ox}) and the excited state oxidation potentials (E_{ox}^*) of the sapphyrins are plotted along with TiO_2 conduction band and Iodine/Iodide redox potential to gain an insight into the electron injection and dye regeneration dynamics as shown in Figure 6-3. The energy gap for dye **SD1** is marginally larger than that of the dye **SD2**. As shown in the Figure 6-3, the difference between the excited state oxidation potentials of the sapphyrin **SD1** and the conduction band (CB) of the TiO_2 is 0.22 V and that for **SD2** is 0.10 V. This potential difference is less than the minimum requirement (0.3 V) and is not sufficient for the effective electron injection from the dye to the CB of the TiO_2 . The ground state oxidation potentials are more positive (> 0.5 V) than the redox potential of the electrolyte, certifying the efficient dye regeneration. Although, the red-shifted absorption matches well with the requirement of the efficient sensitizer, the electrochemical data reveals that the inefficient electron injection from dye to CB of the TiO_2 is going to be a major drawback for these sapphyrin dyes for the application as a sensitizer in the DSSCs.

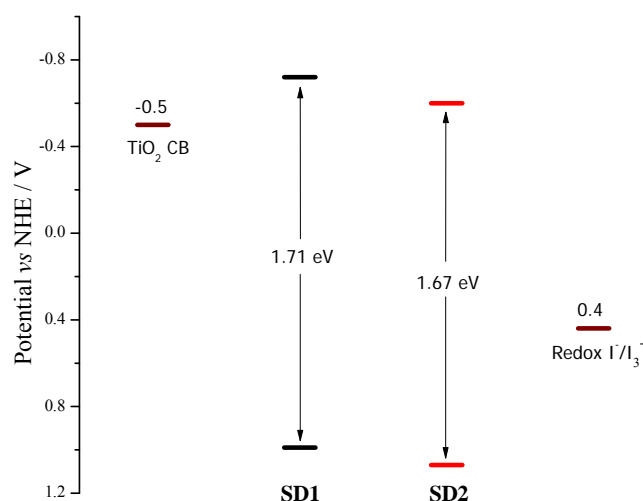


Figure 6-3. Energy level diagram for sapphyrin dyes.

6.2.4 DFT calculation results

The ground state geometries of studied thiaporphyrins were optimized in the gas phase by DFT calculations using the hybrid B3LYP functional and the 6-31G basis set. As presented in Figure 6-4, results from the quantum chemical calculations of these SD dyes show that, the thiophene

ring is twisted out of the sapphyrin plane while bithiophene and two pyrrole rings remain coplanar. The twist angle between two planes is approximately 15° . Due to this considerable deviation from the planarity, the conjugation might get disturbed and the electron flow may be perturbed. In HOMO of all the sapphyrins, the majority of the electron density is localized on the porphyrin ring however a small portion is also extended over the tolyl and carboxyphenyl group, while in the LUMO the electron density is populated majorly on the sapphyrin ring and few part of it is extended over the carboxylic acid group. The enlarged electron density population on the sapphyrin ring in both the HOMO and LUMO suggests that the charge transfer in these sapphyrins might be less efficient. Interestingly in the LUMO+2, the electron density is comprehensively located on the carboxylic acid acceptor suggesting that the electron injection from higher excited states involving LUMO+2 might be more efficient than LUMO. Significantly, DFT calculations also revealed a higher molecular dipole moment (7.39 D) for the **SD2** than for **SD1** (5.12 D) as shown in Figure 6-4.

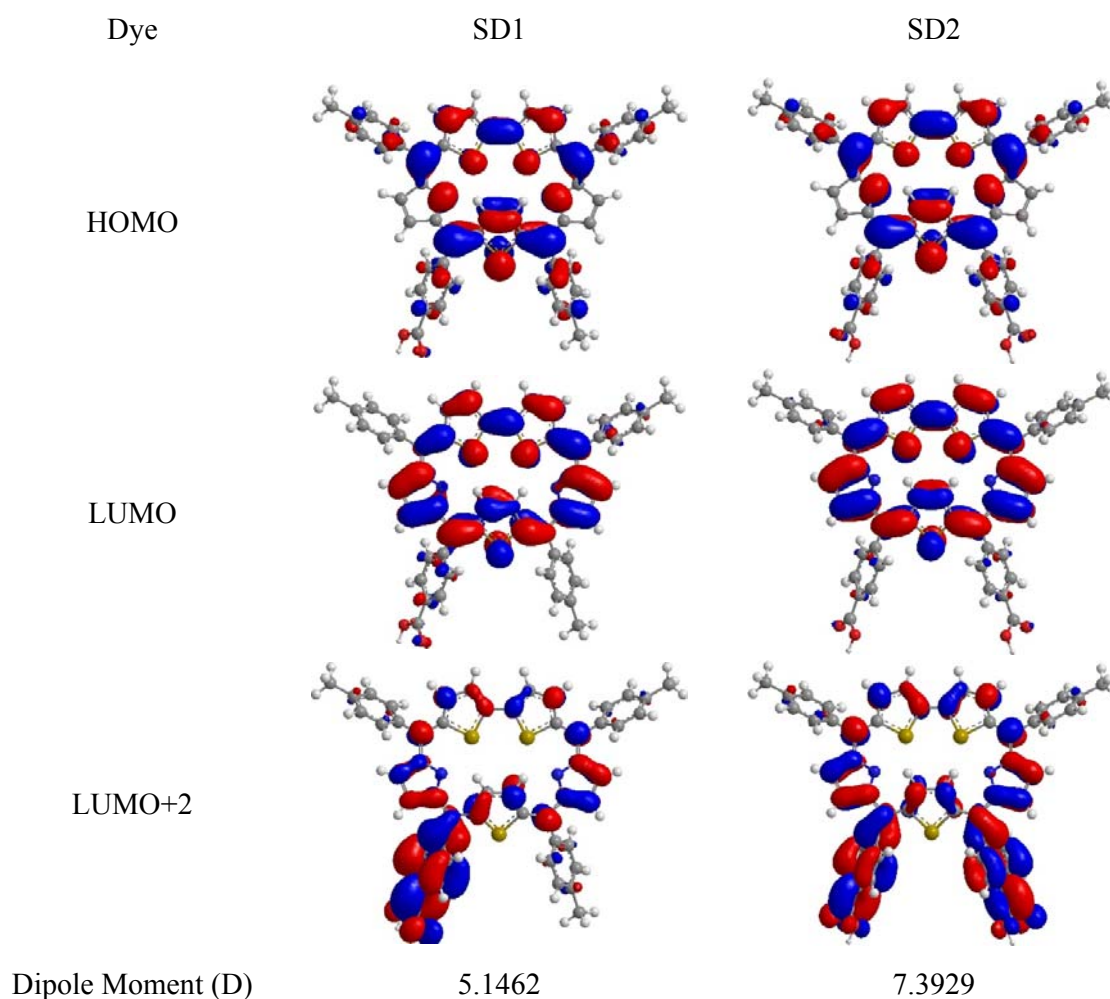


Figure 6-4. The molecular orbital diagrams for thiasapphyrins.

6.2.5 Photovoltaic properties

Devices assembled with sapphyrin sensitizers using liquid electrolytes were tested under standard AM 1.5 illumination conditions. The photovoltaic parameters for the sapphyrins **SD1** and **SD2** under study are summarized in Table 6-2 and the current-voltage characteristics of the devices are shown in Figure 6-5(a).

Table 6-2: Photovoltaic parameters of thiasapphyrin dyes

Dye	J_{sc} (mA cm ⁻²)	V_{oc} (V)	FF (%)	$\eta \times 10^{-1}$ (%)
SD1	0.11	0.31	0.44	0.15
SD2	0.10	0.25	0.44	0.11

As evident from the I-V curve the **SD1** give the overall photon-to-current conversion efficiency of 0.015 %, supported by short-circuit current (J_{sc}) of 0.11 mA cm⁻², open-circuit voltage (V_{oc}) of 0.31 V and fill factor of 0.44. The device assembled with dye **SD2** obtained the overall conversion efficiency of 0.011%. It was evident from the energy level diagram that, due to the LUMO levels of these sapphyrins were very close to the TiO₂ conduction band and therefore the driving force for the electron injection from the oxidized dye into the TiO₂ conduction band is insufficient which might result in low short-circuit current density. Also the presence of three heavy sulfur atoms inside the sapphyrin core might considerably accelerate the intersystem crossing rate, consequently lowering the number of electrons available in the excited state of the dye for injection into the conduction band of semiconductor as is the case for thiaporphyrins.

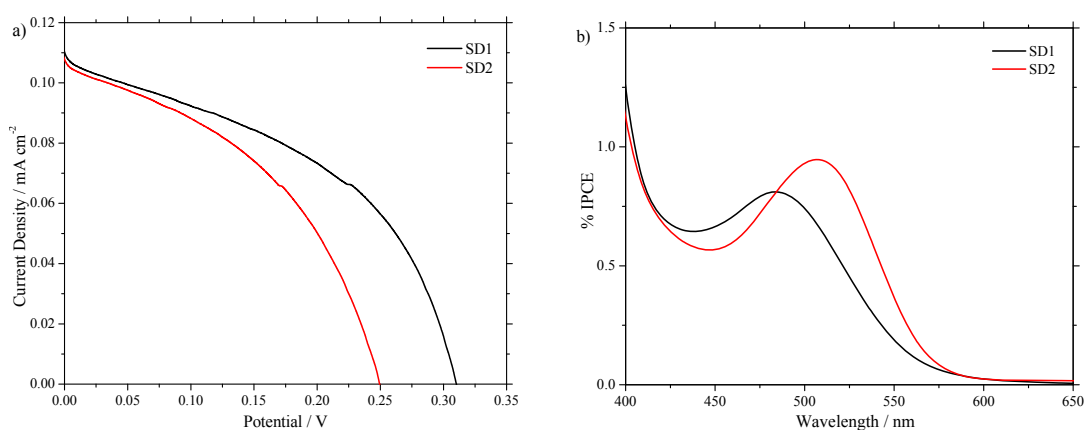


Figure 6-5. (a) I-V curves and (b) IPCE spectra for thiasapphyrin dyes.

The trend of J_{sc} in this series can be understood from the variation of the incident photon-to-current conversion efficiency spectra as displayed in Figure 6-5(b) and are not in agreement

with the corresponding absorption spectra of the dyes on TiO_2 which display intense absorption bands in the *Soret* region. The IPCE value of approximately 1% was observed in the *Soret* band region, highlighting the electron injection problem for these dyes.

6.2.6 EIS studies

Electrochemical impedance spectroscopy (EIS) was carried out under dark at bias voltage of -0.55 V and under illumination at applied open-circuit voltage with a frequency range of 1 Hz to 100 kHz to elucidate information about electron injection and recombination at the TiO_2 /dye/electrolyte interface. Figure 6-6 shows the EIS Nyquist plots (i.e. the minus imaginary part of the impedance Z'' vs. the real part of the impedance Z' when sweeping the frequency) for DSSCs based on thiasapphyrins. In the dark condition, one semicircle was observed for both the thiasapphyrins in the Nyquist plot which corresponds to the resistance of recombination between the electrons on the TiO_2 surface and the oxidized electrolyte. Larger the recombination resistance (semicircle), slower the recombination rate. The recombination rate of **SD1** is slower than that of **SD2**, which means more electrons are available for injection into TiO_2 conduction band. Upon illumination of the cell under open-circuit voltage conditions, the intermediate frequency semicircle in the Nyquist plot reflects charge or electron transport resistance.^[23] A smaller radius of the semicircle in the Nyquist plot corresponds to the lower electron transport resistance, in other words higher electron transfer. The charge transport resistance of **SD1** is smaller than that of **SD2**.

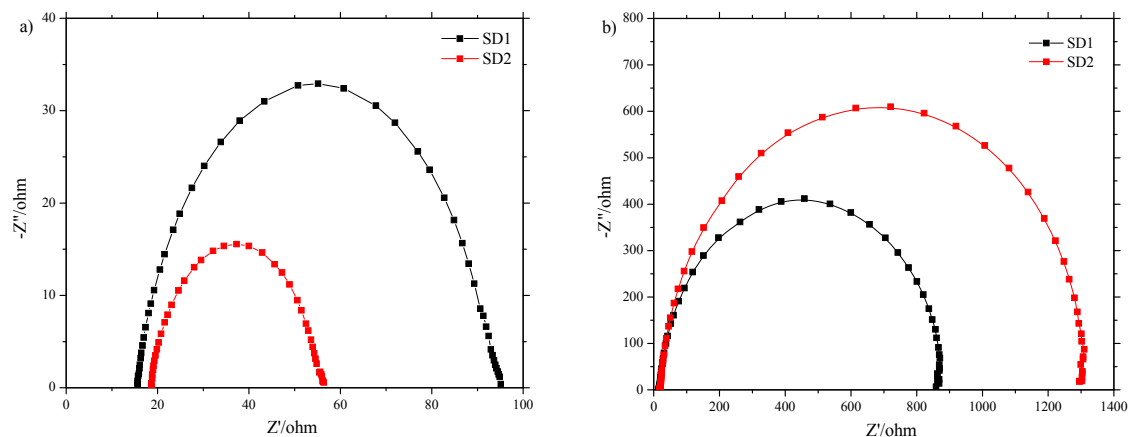


Figure 6-6. Electrochemical impedance spectra (Nyquist plots) of the DSSC devices with saphyrin dyes measured a) in the dark under -0.55 V bias and b) under illumination at V_{oc} .

6.3 Conclusion

In conclusion, novel core-modified sapphyrins, substituted with mono or di-carboxylate groups are synthesized and for the first time applied in dye-sensitized solar cells. The dyes **SD1** and **SD2** are synthesized in two steps from the readily available starting compounds. Optical properties as well as density functional theory calculations suggest that these dyes are well suitable for the application as a sensitizer in DSSCs. The electrochemical results shows that the potential difference between the excited state oxidation potential and the conduction band of TiO₂ is not sufficient for effective electron injection, thus indicating that low electron injection is the major drawback of these dyes. Though the results are not satisfactory, this strategy of applying novel expanded thiasapphyrin dyes in DSSCs will serve as a useful guideline for future molecular designs of efficient expanded porphyrins dyes.

6.4 Experimental Section

6.4.1 General techniques

All chemicals were obtained from commercial sources and used as received without further purification. All the reactions were carried out under nitrogen atmosphere. Solvents used in reactions were dried by PureSolv MD 5 system (Innovative Technology, Inc). Flash chromatography was carried out by using silica gel (40-63 μm , Merck). Analytical TLC was performed on Merck silica gel plates. ^1H and ^{13}C NMR spectra were recorded on a Bruker 400 MHz spectrometer and performed in CDCl_3 ($\delta = 7.26$ ppm), $\text{THF-}d_8$ ($\delta = 1.73, 3.58$ ppm) or $\text{DMSO-}d_6$ ($\delta = 2.50$ ppm) solutions. Chemical shifts are reported in ppm. Coupling constants (J) are reported in Hz. The signals are described as s: singlet; d: doublet; dd: doublet of doublet. MALDI-mass spectra were conducted on an Applied Biosystems 4800 Proteomics Analyzer (Applied Biosystem, Foster City) equipped with an Nd/YAG laser (335nm). Transmittance and reflection UV-visible absorption spectra of the thiaporphyrins in THF and adsorbed on TiO_2 electrodes, respectively, were recorded on a JASCO V-670 UV-Vis/NIR spectrophotometer. Steady-state fluorescence spectra were acquired by using a Varian Cary Eclipse fluorescence spectrophotometer. The cyclic voltammetry measurements of all thiaporphyrins were carried out on CHI 621B electrochemical analyser (CH Instruments, Austin, TX, USA) in degassed THF containing 0.1 M tetrabutylammonium hexafluorophosphate (Bu_4NPF_6) as the supporting electrolyte. The cell assembly consists of a glossy carbon as the working electrode, a silver wire as the pseudo-reference electrode, and a platinum wire as the auxiliary electrode. The scan rate for all measurements was fixed at 50 mV/sec. A ferrocene $^{+1/0}$ redox couple was used as the internal standard and the potential values obtained in reference to the silver electrode were converted to the vacuum scale. DFT calculations were performed using Gaussian 09 package. The molecular orbitals were visualized by the chemoffice software. Electrochemical impedance spectra were recorded for DSSCs under illumination at an open-circuit voltage (V_{oc}) or in the dark at -0.55 V at room temperature. The frequencies explored ranged from 10 mHz to 100 kHz. The data was analyzed using Zview software.

6.4.2 Synthesis

Thiophene diols (3) and (4) were prepared following the procedure reported in Ch 3. The bithiophene (1) and bithiophene diol (2) were prepared by literature procedures.^[20]

2,2'-bithiophene (1)

To a solution of thiophene (1.8 ml, 23 mmol) in 1:1 mixture of dry diethyl ether (20 ml) and dry THF (20 ml), *n*-BuLi (16.8 ml, 27 mmol) was added at -70 °C and allowed to stir for 2 h at the same temperature. CuCl₂ (5.76 g, 40 mmol) was added to the reaction mixture and stirring was continued for an additional 2 h maintaining the temperature at -70 °C. The reaction was quenched by the addition of saturated ice cold solution of NH₄Cl. This mixture was then extracted several times with ethyl acetate. The combined organic layers were concentrated and the crude product was subjected to silica gel column chromatography eluted with hexanes to get the required bithiophene as pale yellow oil in 47% yield (1.8 g). ¹H NMR (400 MHz, CDCl₃) δ: 7.02 (dd, 2H, β-thiophene), 7.18 (dd, 2H, β-thiophene), 7.21 (dd, 2H, α-thiophene) ppm; ¹³C NMR (100 MHz, CDCl₃) δ: 123.75, 124.34, 127.74, 137.40 ppm.

5,5'-Bis(*p*-tolyl)hydroxymethyl]-2,2'-bithiophene (2)

To a 500 ml three-neck round-bottom flask containing 2,2'-bithiophene (1.8 g, 10.8 mmol) equipped with a glass inlet tube, a reflux condenser and a rubber septum dry hexane (40 ml) was added. N,N,N',N'-Tetramethyl ethylenediamine (4 ml, 27 mmol) and *n*-BuLi (17 ml, of 1.6 M solution in hexane) were injected into the stirred solution and the solution was refluxed gently for 1 h. The reaction mixture was then allowed to attain room temperature. The ice cold solution of *p*-tolualdehyde (3.18 ml, 27 mmol) in dry THF (40 ml) was added slowly to the reaction flask. After the addition was complete, the reaction mixture was allowed to attain room temperature, saturated ammonium chloride solution was added and the reaction mixture was extracted with ethyl acetate. The organic layers were combined, washed with brine and dried over anhydrous MgSO₄. The crude compound was subjected to silica gel column chromatography using hexanes / ethyl acetate (7:3) to obtain the desired diol as a white solid in 70% yield (3 g). ¹H NMR (400 MHz, CDCl₃) δ: 2.34 (bs, 2H, OH), 2.35 (s, 6H, CH₃), 5.96 (d, 2H, CH), 6.75 (d, 2H, *J* = 3.68 Hz; β-thiophene), 6.92 (d, 2H, *J* = 3.56 Hz; β-thiophene), 7.18 (d, 4H, *J* = 7.92 Hz; Ph), 7.34 (d, 4H, *J* = 8.04 Hz; Ph) ppm; ¹³C NMR (100 MHz, CDCl₃) δ: 21.14, 72.42, 123.07, 125.39, 126.24, 129.28, 137.37, 137.93, 139.93, 147.33 ppm.

Dimethyl 4,4'-(thiophene-2,5-diylbis(hydroxymethylene)) dibenzoate (3)

Anhydrous hexane (40 ml) was added to a 250 ml three-necked round-bottomed flask equipped with rubber septum, gas inlet and gas outlet tube. A positive pressure of N₂ was maintained and after purging N₂ gas for 5 min, TMEDA (4.7 ml, 31.25 mmol) and *n*-BuLi (20 ml of 1.6 M solution in hexane) were added sequentially to the stirring solution at room temperature. Thiophene (1 ml, 12.5 mmol) was then added and the solution was refluxed for 1 h. As the

reaction progressed, a white turbid solution formed indicating the formation of the 2,5-dilithiated salt of thiophene. The reaction mixture was cooled with ice bath and an ice-cold solution of methyl-4-formylbenzoate (4 g, 25 mmol) in dry THF (20 ml) was then cannulated to the stirring solution. The resulting reaction mixture was stirred at 0 °C for 15 min and then brought up to room temperature. The reaction was quenched by adding cold saturated NH₄Cl solution (20 ml). The organic layer was washed with brine and dried over anhydrous MgSO₄. The solvent was removed on a rotary evaporator under reduced pressure to afford the crude compound. The crude product was further purified by silica gel column chromatography (eluent: 3:7, ethyl acetate/hexane) to collect desired diol as yellow solid (4.3 g, 84%). ¹H NMR (400 MHz, CDCl₃) δ: 2.55 (s, 1H, OH), 2.56 (s, 1H, OH), 3.9 (s, 6H, COOCH₃), 6.01 (d, 2H, *J* = 3.72 Hz; *meso*), 6.72 (s, 2H, β-thiophene), 7.49 (m, 4H, Ph), 8.01 (d, *J* = 8.28 Hz, Ph) ppm; ¹³C NMR (100 MHz, CDCl₃) δ: 52.14, 71.97, 124.81, 126.12, 129.77, 129.88, 147.52, 147.74, 166.79 ppm.

Methyl-4-(hydroxy(5-(hydroxy(*p*-tolyl)methyl)thiophen-2-yl)methyl)benzoate (4)

Dry hexane (60 ml) was added to a 500 ml three-necked round-bottomed flask equipped with rubber septum, gas inlet and gas outlet tube. A positive pressure of N₂ was maintained and after purging N₂ gas for 5 min, TMEDA (11.5 ml, 75 mmol) and *n*-BuLi (62 ml of 1.6 M solution in hexane) were added sequentially to the stirring solution at room temperature. Thiophene (2 ml, 25 mmol) was then added and the solution was refluxed for 1 h. As the reaction progressed, a white turbid solution formed indicating the formation of the 2,5-dilithiated salt of thiophene. The reaction mixture was cooled with ice bath and an ice-cold solution of *p*-tolualdehyde (2.95 ml, 25 mmol) and methyl-4-formylbenzoate (4.1 g, 25 mmol) in dry THF (60 ml) was then cannulated to the stirring solution. The resulting reaction mixture was stirred at 0 °C for 15 min and then brought up to room temperature. The reaction was quenched by adding cold saturated NH₄Cl solution (50 ml). The organic layer was washed with brine and dried over anhydrous MgSO₄. The solvent was removed on a rotary evaporator under reduced pressure to afford the crude compound. The crude product was further purified by silica gel column chromatography (eluent: 30% ethyl acetate in hexane) to collect desired diol (3) as yellow solid (1.76 g, 19%). ¹H NMR (400 MHz, CDCl₃) δ: 2.34 (s, 3H, CH₃), 2.46 (d, 1H, *J* = 3.88 Hz; OH), 2.61 (d, 1H, *J* = 3.76 Hz; OH), 3.90 (s, 3H, OMe), 5.91 (s, 1H, *meso*), 5.99 (d, 1H, *meso*), 6.69 (m, 2H, *m*-tolyl), 7.15 (d, 2H, *J* = 8.00 Hz; Ph), 7.29 (m, 2H, *o*-tolyl), 7.49 (d, 2H, *J* = 2.67 Hz; β-thiophene), 8.00 (d, 2H, *J* = 8.16 Hz; Ph) ppm; ¹³C NMR (100 MHz, CDCl₃) δ: 21.13, 52.11,

71.94, 72.41, 124.29, 124.78, 126.13, 129.22, 129.81, 137.85, 139.88, 147.01, 147.10, 147.67, 148.86, 148.95, 166.85 ppm.

5,10-di-(4-Methoxycarbonylphenyl)-16-thiatripyrrane (5)

Thiophene-diol (**3**, 650 mg, 1.57 mmol) was dissolved in pyrrole (7 ml, 102 mmol) under N₂. To this solution BF₃•OEt₂ (0.2 ml, 1.57 mmol) was added. The mixture was stirred for 30 min. at room temperature. After completion of reaction as confirmed by TLC, the reaction was quenched by adding aq. NaOH (0.1 N, 30 ml). The mixture was extracted with DCM and washed with water. The organic layer was dried over MgSO₄ and excess pyrrole was removed under vacuum. The crude oil was purified by column chromatography on silica using DCM/Hexanes (1:1) as eluting solvent to get pure thiatripyrrane (480 mg, 60% Yield). ¹H NMR (400 MHz, CDCl₃) δ: 3.90 (s, 6H, OMe), 5.61 (s, 2H, *meso* CH), 5.89 (s, 2H, β-pyrrole), 6.14 (m, 2H, β-pyrrole), 6.61 (s, 2H, β-thiophene), 6.71 (s, 2H, α-pyrrole), 7.30 (d, 4H, *J* = 7.88 Hz; Ph), 7.94 (bs, 2H, NH), 7.97 (d, 4H, *J* = 8.20 Hz; Ph) ppm; ¹³C NMR (100 MHz, CDCl₃) δ: 45.93, 52.10, 107.86, 108.48, 117.62, 125.69, 128.38, 129.01, 129.94, 131.95, 145.29, 147.65, 166.81 ppm.

5-(4-Methoxycarbonylphenyl)-10-(*p*-tolyl)-16-thiatripyrrane (6)

Thiophene-diol (**4**, 1.6 g, 4.3 mmol) was dissolved in pyrrole (19 ml, 279 mmol) under N₂. To this solution BF₃•OEt₂ (0.55 ml, 4.3 mmol) was added. The mixture was stirred for 30 min. at room temperature. After completion of reaction as confirmed by TLC, the reaction was quenched by adding aq. NaOH (0.1 N, 30 ml). The mixture was extracted with DCM and washed with water. The organic layer was dried over MgSO₄ and excess pyrrole was removed under vacuum. The crude oil was purified by column chromatography on silica using DCM/Hexanes (1:1) as eluting solvent to get pure thiatripyrrane (1.4 g, 70% Yield). ¹H NMR (400 MHz, CDCl₃) δ: 2.34 (s, 3H, CH₃), 3.91 (s, 3H, OMe), 5.53 (s, 1H, *meso* CH), 5.61 (s, 1H, *meso* CH), 5.90 (s, 1H, β-pyrrole), 5.93 (s, 1H, β-pyrrole), 6.15 (m, 2H, β-pyrrole), 6.62 (m, 2H, β-thiophene), 6.69 (m, 2H, α-pyrrole), 7.14 (s, 4H, Ph), 7.32 (d, 4H, *J* = 8.28 Hz; Ph) 7.89 (bs, 1H, NH), 7.95 (bs, 1H, NH), 7.98 (d, 4H, *J* = 8.12 Hz; Ph) ppm; ¹³C NMR (100 MHz, CDCl₃) δ: 21.01, 45.60, 45.89, 52.06, 107.41, 107.76, 108.25, 108.39, 117.17, 117.53, 125.26, 125.57, 128.18, 128.39, 128.86, 129.28, 129.86, 132.08, 133.05, 136.71, 139.55, 144.59, 146.67, 147.84, 166.86 ppm.

5-(4-Methoxycarbonylphenyl)-10,15,20-tritoly-25,27,29-trithiasapphyrin (7)

In a 250 ml one necked round bottom flask fitted with nitrogen bubbler, diol **2** (407 mg, 1 mmol) and 16-thiatripyrrane **6** (467 mg, 1 mmol) were dissolved in 400 ml of CH₂Cl₂. After

purging nitrogen for 10 min, the condensation of diol **2** with tripyrrane **6** was initiated by adding TFA (75 μ l, 1 mmol). The reaction mixture was stirred at room temperature for 1 h. DDQ (227 mg, 1 mmol) was then added and the reaction mixture was stirred in air for additional 1 h. TLC analysis indicated the formation of one brown spots of the desired N₂S₃ sapphyrin. The crude compound was subjected to silica gel column chromatography using hexanes/dichloromethane (40:60) to afford the desired N₂S₃ sapphyrin as a greenish brown solid (138 mg, 17%). ¹H NMR (400 MHz, CDCl₃) δ : -0.66 (s, 2H, β -thiophene), 2.63 (s, 3H, CH₃), 2.74 (s, 6H, CH₃), 4.07 (s, 3H, OMe), 7.59 (d, 2H, J = 7.92 Hz; Ph), 7.68 (d, 4H, J = 7.80 Hz; Ph), 8.19 (d, 4H, J = 7.04 Hz; Ph), 8.24 (d, 2H, J = 7.88 Hz; Ph), 8.44 (s, 2H, Ph), 8.47 (d, 1H, J = 4.44 Hz; β -pyrrole), 8.54 (d, 1H, J = 4.40 Hz; β -pyrrole), 8.65 (t, 2H, β -pyrrole), 9.74 (d, 2H, J = 4.32 Hz; β -thiophene), 10.13 (d, 2H, J = 4.56 Hz; β -thiophene) ppm; ¹³C NMR (100 MHz, CDCl₃): δ = 21.53, 52.34, 125.14, 128.61, 129.41, 129.53, 129.72, 132.43, 132.74, 133.25, 133.49, 133.83, 134.21, 134.56, 135.64, 137.35, 137.38, 137.53, 137.74, 138.05, 138.21, 138.38, 138.69, 139.95, 144.80, 145.13, 146.54, 153.86, 154.23, 157.37, 157.75, 167.18 ppm; HRMS-MALDI: m/z calcd for C₅₃H₃₉N₂O₂S₃: 831.2168, found 831.2159 [M+H].

5,10-di(4-Methoxycarbonylphenyl)-15,20-ditolyl-25,27,29-trithiasapphyrin (8)

In a 250 ml one necked round bottom flask fitted with nitrogen bubbler, diol **2** (407 mg, 1 mmol) and 16-thiatripyrrane **5** (511 mg, 1 mmol) were dissolved in 400 ml of CH₂Cl₂. After purging nitrogen for 10 min, the condensation of diol **2** with tripyrrane **5** was initiated by adding TFA (75 μ l, 1 mmol). The reaction mixture was stirred at room temperature for 1 h. DDQ (227 mg, 1 mmol) was then added and the reaction mixture was stirred in air for additional 1 h. TLC analysis indicated the formation of one brown spots of the desired N₂S₃ sapphyrin. The crude compound was subjected to silica gel column chromatography using hexanes/dichloromethane (40:60) to afford the desired N₂S₃ sapphyrin as a greenish brown solid (142 mg, 16%). ¹H NMR (400 MHz, CDCl₃) δ : -0.53 (s, 2H, β -thiophene), 2.73 (s, 6H, CH₃), 4.06 (s, 6H, OMe), 7.68 (d, 4H, J = 7.56 Hz; Ph), 8.18 (d, 4H, J = 7.92 Hz; Ph), 8.42 (m, 10H, Ph, β -pyrrole), 8.63 (d, 2H, J = 4.60 Hz; β -pyrrole), 9.73 (d, 2H, J = 4.52 Hz; β -thiophene), 10.12 (d, 2H, J = 4.60 Hz; β -thiophene) ppm; ¹³C NMR (100 MHz, CDCl₃) δ : 21.54, 52.34, 125.21, 128.66, 129.65, 129.81, 130.16, 132.65, 134.04, 134.20, 135.15, 135.88, 137.20, 137.84, 138.05, 138.39, 138.64, 145.40, 146.28, 153.71, 157.65, 167.10 ppm; HRMS-MALDI: m/z calcd for C₅₄H₃₉N₂O₄S₃: 875.2066, found 875.2069 [M+H].

5-(4-carboxyphenyl)-10,15,20-tritoyl-25,27,29-trithiasapphyrin (SD1)

Trithiasapphyrin **7** (100 mg, 0.12 mmol) was dissolved in 20 ml THF. To this mixture, KOH (135 mg, 4.4 mmol) dissolved in 2 ml water was added and refluxed for 12 h. After cooling, the solvent was removed under vacuum. To this crude mixture 0.1N KOH was added and then precipitated with the help of 1 N HCl. The solid compound was filtered, washed with water and dried in air to get the desired product as brown solid (92 mg, 94% yield). ¹H NMR (400 MHz, CDCl₃) δ: -0.99 (s, 2H, β-thiophene), 2.57 (s, 3H, CH₃), 2.70 (s, 6H, CH₃), 7.63 (d, 2H, *J* = 7.92 Hz; Ph), 7.75 (d, 4H, *J* = 7.76 Hz; Ph), 8.10 (d, 2H, *J* = 7.92 Hz; Ph), 8.19 (d, 4H, *J* = 7.72 Hz; Ph), 8.30 (d, 2H, *J* = 8.12 Hz; Ph), 8.35 (d, 2H, *J* = 8.32 Hz; Ph), 8.43 (m, 2H, β-pyrrole), 8.58 (m, 2H, β-pyrrole), 9.79 (m, 2H, β-thiophene), 10.58 (d, 2H, *J* = 4.64 Hz; β-thiophene) ppm; UV-vis (THF) λ_{max}/nm (ε/10³ M⁻¹cm⁻¹): 507 (145), 621 (8.8), 676 (18.7); HRMS-MALDI: *m/z* calcd for C₅₂H₃₇N₂O₂S₃: 817.2011, found 817.2015 [M+H].

5,10-di(4-carboxyphenyl)-15,20-ditoyl-25,27,29-trithiasapphyrin (SD2)

Trithiasapphyrin **8** (100 mg, 0.11 mmol) was dissolved in 20 ml THF. To this mixture, KOH (128 mg, 2.3 mol) dissolved in 2 ml water was added and refluxed for 12 h. After cooling, the solvent was removed under vacuum. To this crude mixture 0.1N KOH was added and then precipitated with the help of 1 N HCl. The solid compound was filtered, washed with water and dried in air to get the desired product as brown solid (89 mg, 96% yield). ¹H NMR (400 MHz, CDCl₃) δ: -0.78 (s, 2H, β-thiophene), 2.70 (s, 6H, CH₃), 7.77 (d, 4H, *J* = 7.72 Hz; Ph), 8.22 (d, 4H, *J* = 7.68 Hz; Ph), 8.38 (m, 8H, Ph), 8.43 (d, 2H, *J* = 4.40 Hz; β-pyrrole), 8.60 (d, 2H, *J* = 4.36 Hz; β-pyrrole), 9.82 (d, 2H, *J* = 4.56 Hz; β-thiophene), 10.63 (d, 2H, *J* = 4.56 Hz; β-thiophene) ppm; UV-vis (THF) λ_{max}/nm (ε/10³ M⁻¹cm⁻¹): 507 (121), 623 (9.5), 675 (15.8); HRMS-MALDI: *m/z* calcd for C₅₂H₃₅N₂O₄S₃: 847.1753, found 847.1751 [M+H].

6.4.3 Photovoltaic Measurements

TiO₂ photoanode films and Pt counter electrodes were purchased from Yingkou Opvtech New Energy Co. Ltd. Liaoning, China. The films, which were prepared by using the screen-printing method, were composed of a transparent layer (thickness ≈ 12 μm), a scattering layer (thickness ≈ 4 μm), and a working area of 0.4×0.4 cm² and were used as received. The films were pretreated according to the following activation procedures before use: heating at 100 °C for 22 min, at 110 °C for 60 min, at 450 °C for 68 min, at 500 °C 60 min, at 250 °C for 60 min, cooling at 80 °C and keeping at 80 °C before immersion. The TiO₂ films were immersed in a 1×10⁻⁴ M solution of the sapphyrin in THF for 6 h at 25 °C. The dye-sensitized TiO₂ films were

washed with THF, dried in hot air, and used as the working electrode. To fabricate the DSSC device, the two electrodes were tightly clipped together into a sandwich-type cell that was spaced by a 40 μm film spacer. A thin layer of electrolyte, which contained 0.05 M I_2 , 0.1 M lithium iodide (LiI), 0.6 M dimethyl-propyl-benzimidazole iodide (DMPII), and 0.6 M 4-tert-butylpyridine (TBP) in dry CH_3CN , was introduced into the space between the two electrodes. The Photoelectrochemical characterizations on the solar cells were performed by using an Oriel Class AAA solar simulator (Oriel 94043A, Newport Corp.). Photocurrent–voltage characteristics of the DSSCs were recorded with a potentiostat/galvanostat (CHI650B, CH Instruments, Inc.) at a light intensity of 100 mWcm^{-2} calibrated by an Oriel reference solar cell (Oriel 91150, Newport Corp.). The monochromatic quantum efficiency was recorded through a monochromator (Oriel 74100, Newport Corp.) under short-circuit condition. The intensity of each wavelength was in the range of 1 to 3 mWcm^{-2} . Electrochemical impedance spectra were recorded for DSSCs under illumination at an open-circuit voltage (V_{oc}) or in the dark at -0.55 V at room temperature. The frequencies explored ranged from 10 mHz to 100 kHz. The data was analysed using Zview software.

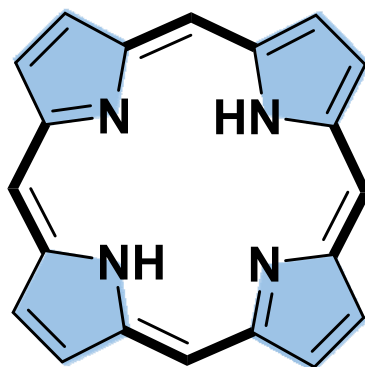
6.5 References

- [1] A. Harriman, B. G. Maiya, T. Murai, G. Hemmi, J. L. Sessler, T. E. Mallouk, *J. Chem. Soc., Chem. Commun.* **1989**, 314-316.
- [2] M. M. Judy, J. L. Maithews, J. T. Newman, H. L. Skiles, R. L. Boriack, J. L. Sessler, M. Cyr, B. G. Maiya, S. T. Nichol, *Photochemistry and Photobiology* **1991**, *53*, 101-107.
- [3] Pushpan S. K., A. V. G. Venkatraman S., Sankar J., Parmeswaran D., Ganesan S., Chandrashekar T. K., *Curr Med Chem Anticancer Agents* **2002**, *2*, 187-207.
- [4] J. Seenisamy, S. Bashyam, V. Gokhale, H. Vankayalapati, D. Sun, A. Siddiqui-Jain, N. Streiner, K. Shin-ya, E. White, W. D. Wilson, L. H. Hurley, *J. Am. Chem. Soc.* **2005**, *127*, 2944-2959.
- [5] Y. Ni, *Current Medical Imaging Reviews* **2008**, *4*, 96-112.
- [6] H. Ali, Lier, Johan Evan, *In Handbook of Porphyrin Science; Karl Kadish, Kevin Smith and Roger Guilard; World Scientific Publishing Co. Pte. Ltd.* **2010**.
- [7] R. K. Pandey, Zheng, G., *In Porphyrin Handbook; Kadish, K. M., Smith, K. M., Guilard, R., Eds.; Academic Press: San Diego; Vol. VI, Chapter 43.* **1999**.

- [8] J. H. Chou, Nalwa, H. S., Kosal, M. E., Rakow, N. A., Suslick, K. S., *In Porphyrin Handbook; Kadish, K. M., Smith, K. M., Guillard, R., Eds.; Academic Press: San Diego; Vol. VI, Chapter 41* **1999**.
- [9] R. Misra, R. Kumar, T. K. Chandrashekar, A. Nag, D. Goswami, *Org. Lett.* **2006**, *8*, 629-631.
- [10] R. Misra, R. Kumar, V. PrabhuRaja, T. K. Chandrashekar, *J. Photochem. Photobiol., A* **2005**, *175*, 108-117.
- [11] R. B. Woodward, *Aromaticity Conference, Sheffield, UK* **1966**.
- [12] V. J. Bauer, D. L. J. Clive, D. Dolphin, J. B. Paine, F. L. Harris, M. M. King, J. Loder, S. W. C. Wang, R. B. Woodward, *J. Am. Chem. Soc.* **1983**, *105*, 6429-6436.
- [13] J. L. Sessler, M. R. Johnson, V. Lynch, *J. Org. Chem.* **1987**, *52*, 4394-4397.
- [14] M. J. Broadhurst, R. Grigg, A. W. Johnson, *J. Chem. Soc.D, Chem. Commun.* **1969**, 23-24.
- [15] J. L. Sessler, M. Cyr, A. K. Burrell, *Tetrahedron* **1992**, *48*, 9661-9672.
- [16] J. L. Sessler, M. C. Hoehner, A. Gebauer, A. Andrievsky, V. Lynch, *J. Org. Chem.* **1997**, *62*, 9251-9260.
- [17] A. Srinivasan, A. V. G, S. J. Narayanan, S. K. Pushpan, M. R. Kumar, T. K. Chandrashekar, K.-i. Sugiura, Y. Sakata, *J. Org. Chem.* **1999**, *64*, 8693-8697.
- [18] A. Srinivasan, S. K. Pushpan, M. Ravi Kumar, S. Mahajan, T. K. Chandrashekar, R. Roy, P. Ramamurthy, *J. Chem. Soc., Perkin Trans. 2* **1999**, 961-968.
- [19] A. Srinivasan, S. Mahajan, S. K. Pushpan, M. Ravikumar, T. K. Chandrashekar, *Tetrahedron Lett.* **1998**, *39*, 1961-1964.
- [20] M. Rajeswara Rao, M. Ravikanth, *Eur. J. Org. Chem.* **2011**, *2011*, 1335-1345.
- [21] Y. Pareek, M. Ravikanth, *Eur. J. Org. Chem.* **2011**, *2011*, 5390-5399.
- [22] R. R. Malakalappalli, R. Mangalampalli, *Tetrahedron* **2012**, *68*, 1306-1314.
- [23] C.-J. Yang, Y. J. Chang, M. Watanabe, Y.-S. Hon, T. J. Chow, *J. Mater. Chem.* **2012**, *22*, 4040-4049.

Section III

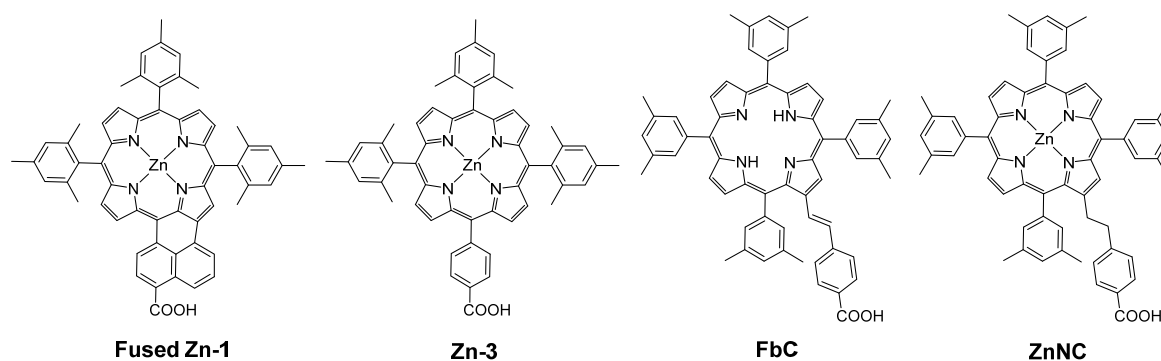
Miscellaneous dyes



7. Co-sensitization of free-base and Zinc porphyrins: An effective approach to improve the photon-to-current conversion efficiency in DSSCs.

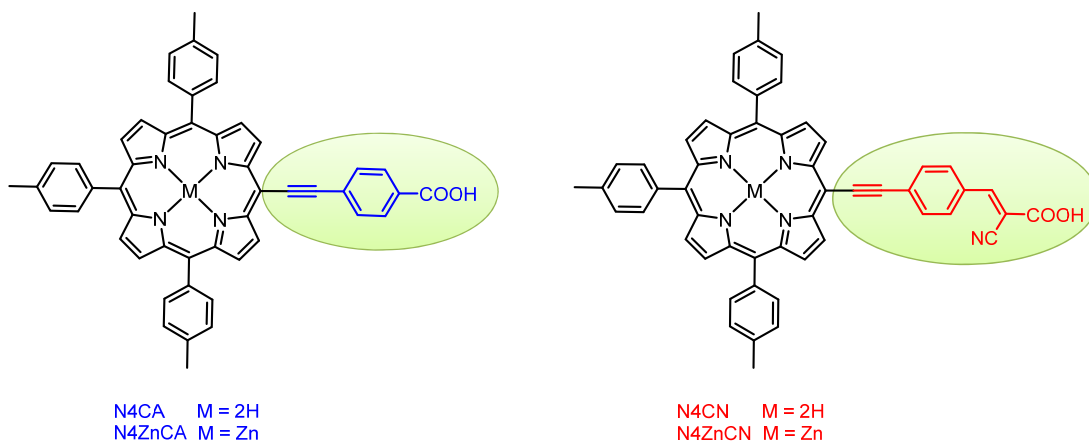
7.1 Introduction

Co-sensitization of two or more dyes with complementary absorption spectra on TiO₂ film is a very effective approach to obtain the panchromatic sensitization in order to enhance the light harvesting ability of dyes so as to improve the photocurrents of the devices in dye-sensitized solar cells (DSSCs). Several co-sensitization systems, such as ruthenium complex with organic dye,^[1-4] metal-free organic dye,^[5-8] phthalocyanine with organic dye,^[9-12] dye co-sensitization in separate layers,^[2, 13-14] and porphyrins co-sensitized with organic dyes^[15-21] have been described in the literature to show enhanced photovoltaic performance relative to their individual single-dye systems. Based on the organic dye systems, Robertson stated that co-sensitization with strongly absorbing dyes would give sufficient space on the surface of TiO₂ to allow absorption of other dyes with a complementary absorption spectrum.^[10] Porphyrin sensitizers are hence perfect candidates to improve the device performance through co-sensitization. Although porphyrins co-sensitized with various organic dyes have been studied widely, surprisingly porphyrins co-sensitized with other free-base or zinc porphyrins has been scarcely explored. From the vast literature survey it is observed that, there are only two examples of such kind has been reported.^[22-24] Imahori and coworkers showed that co-sensitization of the porphyrins with dissimilar absorption features is also an interesting approach to increase the overall performance of the DSSC.^[22] The TiO₂ cell sensitized with the naphthyl-fused-porphyrin **Fused Zn-1**(4.1%) exhibited improved power conversion efficiency of 5.0% when it is co-sensitized with the porphyrin **Zn-3**(4.6%). Even though it achieved moderate efficiencies of 5%, the overall improvement from individual performance of 4.1 or 4.6% is not so remarkable. Recently Griffith and co-workers reported an outstanding synergetic effect in mixed porphyrin DSSC. In this report they mixed free base (**FbC**) and zinc porphyrin (**ZnNC**) as shown in Scheme 7-1, having different structure to get 300% efficiency enhancement. They found that this enhancement is mainly due to the corresponding increase in the short circuit current.^[23-24] The solar-to-electrical power conversion efficiency of mixture surpassed that of either dye individually, increasing from 0.4% for **FbC** and 0.7% for **ZnNC** to 2.1% for the best mixture. Even though the increase in the efficiency is as high as 300%, still for the best mixture it is only around 2%.



Scheme 7-1. Molecular structures of the co-sensitized porphyrins in literature.

One of the reasons for this low efficiency might be the use of unconjugated anchor in ZnNC which might give low efficiency due to ineffective charge transfer. To the best of our knowledge this is the only report in the literature stating about the mixture of free base and zinc porphyrins. It has been proved that the ethynylphenyl linker is much more efficient for effective charge transfer compared to the non-ethynylphenyl linkers or non-conjugated linkers. Also the positive effect of electron withdrawing cyanoacrylic acid acceptor on the efficiency has been documented in the literature. Therefore in order to check the combined effect of the ethynylphenyl linker and the cyanoacrylic acid acceptor we designed four novel free base and zinc porphyrin sensitizers as depicted in Scheme 7-2. From the IV curves and IPCE spectra of the co-sensitized DSSCs it is obvious that the enhancement in the power conversion efficiency is due to the increase in the short circuit current.

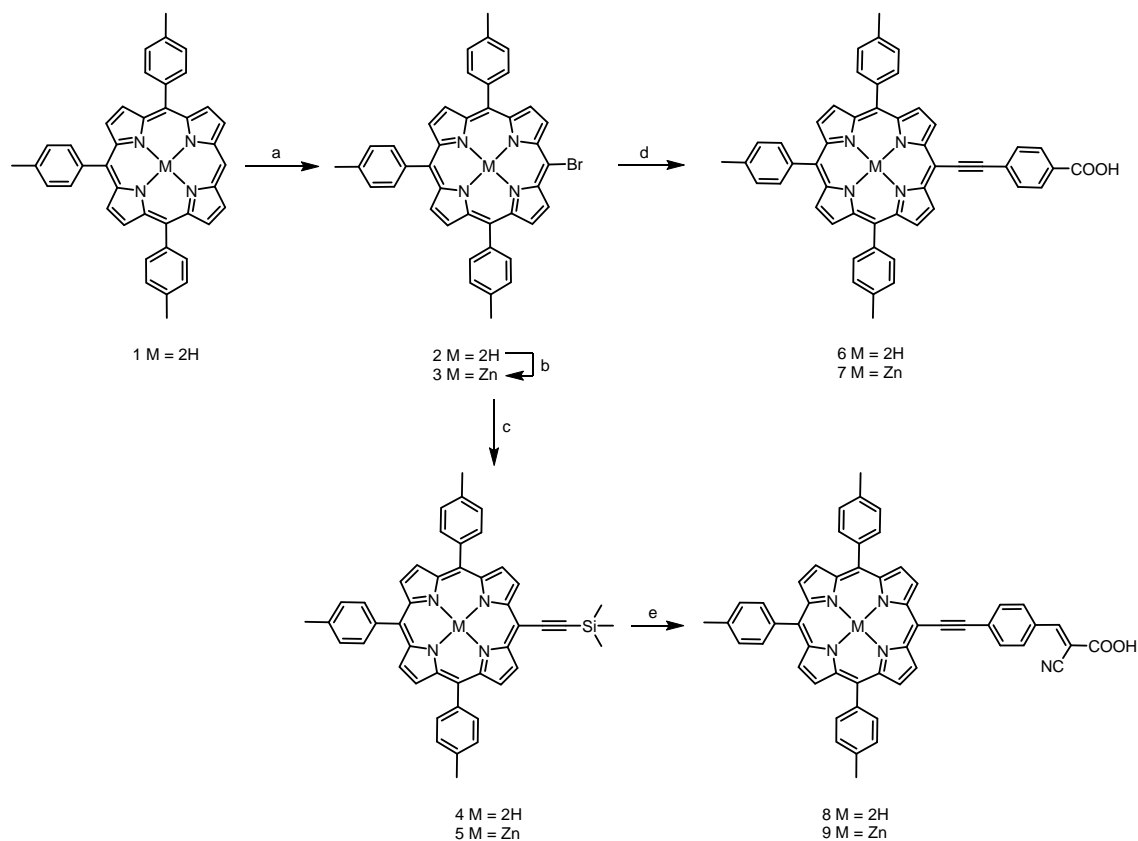


Scheme 7-2. Molecular structures of the porphyrins under study.

7.2 Results and Discussion

7.2.1 Synthesis

4-ethynylbenzoic acid,^[25] 2-cyano-3-(4-iodophenyl)acrylic acid^[26] and 5,10,15-Tris(*p*-tolyl)porphyrin **1**^[27] were prepared following the literature procedure. The synthetic route to the porphyrins under study is depicted in Scheme 7-3. The carboxylic acid derivatives were prepared in three steps and the cyanoacrylic acid derivatives were prepared in four steps from the starting porphyrin **1**. The mono *meso*-unsubstituted porphyrin **1** was subjected to bromination with N-bromosuccinamide in dichloromethane at room temperature to obtain the bromoporphyrin **2** which was further metalized with zinc chloride in dichloromethane and methanol mixture at room temperature to get the zinc bromoporphyrin **3**.



Scheme 7-3. Synthesis of free-base and zinc porphyrins. Reagents and conditions: a) NBS, DCM; b) ZnCl₂, DCM/MeOH; c) TMSA, Pd(dba)₃, AsPh₃, THF/NEt₃; d) 4-ethynylbenzoic acid, Pd(dba)₃, AsPh₃, THF/NEt₃; e) TBAF, 2-cyano-3-(4-iodophenyl)acrylic acid, Pd(dba)₃, AsPh₃, THF/NEt₃.

Formation of the desired porphyrin was confirmed by both the ¹H NMR spectrum, as it shows complete disappearance of the *meso* proton at 10.19 ppm and inner NH protons at -2.95 ppm

and the HR mass spectra. The free-base bromoporphyrin **2** and zinc bromoporphyrin **3** were treated with trimethylsilylacetylene in presence of palladium (0) catalyst in tetrahydrofuran and triethylamine mixture solvent to yield the trimethylsilylacetylene derivatives **4** and **5**. The elevated temperature is essential for zinc porphyrin to get complete conversion as the conversion was not completed even after 48 h stirring at room temperature. The free-base porphyrin **2** was reacted with 4-ethynylbenzoic acid under typical Sonogashira conditions at room temperature to achieve **N4CA** (**6**) porphyrin in good yield. Similarly the zinc bromoporphyrin **3** was reacted with 4-ethynylbenzoic acid under Sonogashira conditions at 40 °C to get **N4ZnCA** (**7**) porphyrin. The trimethylsilylacetylene derivatives **4** and **5** were first treated with tetrabutylammonium fluoride in tetrahydrofuran at room temperature for 30 minutes in order to remove the trimethylsilyl group and the crude product from this reaction was used as such without further purification for the Sonogashira coupling reaction with 2-cyano-3-(4-iodophenyl)acrylic acid under palladium catalysis to get the cyanoacrylic acid porphyrins **N4CN** (**8**) and **N4ZnCN** (**9**). All the final porphyrins and their intermediates were characterized by NMR spectroscopy and high resolution mass spectroscopy.

7.2.2 Optical properties

The UV-Visible peaks values and the molar absorption coefficients (ϵ) of **N4CA**, **N4CN**, **N4ZnCA** and **N4ZnCN** are given in Table 7-1. The UV-Visible spectra of **N4CA** and **N4CN** displayed typical free-base features, a strong *Soret* band around 435 nm and four Q bands around 520-700 nm as shown in Figure 7-1(a). The zinc porphyrins **N4ZnCA** and **N4ZnCN** showed the characteristic metal porphyrin properties with a strong *Soret* band around 445 nm and two Q bands around 570-640 nm. The substitution of the cyano group at the anchoring carboxylic unit shifted the absorption slightly towards red region compared to the carboxylic units. The attachment of the electron withdrawing cyano group lowers the molar extension coefficients but has broad absorption in *Soret* region, for both free-base and zinc porphyrins, **N4CN** and **N4ZnCN** compared to the **N4CA** and **N4ZnCA**. To examine the adsorption behavior of the porphyrins on the thin films, the TiO₂ films with coating thickness of 1 μm were immersed in THF solution of the porphyrins for 2 h at 40 °C and rinsed with THF to remove unabsorbed dye. The absorption spectra of the porphyrins adsorbed on TiO₂ films are shown in Figure 7-1(b). For all the porphyrins the absorption spectra is broadened on adsorption on TiO₂ with absorption onset reaching 700 nm. This widening of the spectrum shows that these dyes can absorb more solar radiation which in turn can increase the power conversion efficiency of these porphyrins. As seen from the UV-vis spectra both in solution

and adsorbed on TiO₂, it is obvious that the zinc porphyrins have broader absorption spectra in the *Soret* band region compared to the free-base porphyrins and in the Q band region the absorption region is complementary to each other with zinc porphyrins covering the dip visible for free-base porphyrins in the 650 nm region.

Table 7-1. Optical and electrochemical properties of porphyrins under study.

Dye	$\lambda_{\text{abs}}/\text{nm}^a$ ($\epsilon/10^3\text{M}^{-1}\text{cm}^{-1}$)	$\lambda_{\text{em}}/\text{nm}^b$	E_{ox}/V^c	$E_{(0,0)}/\text{eV}^d$	$E_{\text{ox}}^*/\text{V}^e$
N4CA	433 (245), 534 (11), 575 (31), 610 (4.5), 668 (11)	673	1.24	1.85	-0.61
N4CN	438 (136), 537 (6), 581 (22), 612 (4), 671 (10)	676	1.25	1.84	-0.59
N4ZnCA	443 (281), 574 (9), 625 (20)	632	1.05	1.98	-0.93
N4ZnCN	449 (116), 575 (7), 634 (21)	643	1.06	1.94	-0.88

^aAbsorption maximum of porphyrins in THF. ^bEmission maximum measured in THF by exciting at *Soret* band. ^coxidation potentials vs. NHE determined by cyclic voltammetry in THF and referenced to a ferrocene redox couple.^[28-30] ^d $E_{(0,0)}$ values were estimated from the intersection of the absorption and emission spectra. ^eFirst reduction potentials approximated from E_{ox} and $E_{(0,0)}$.

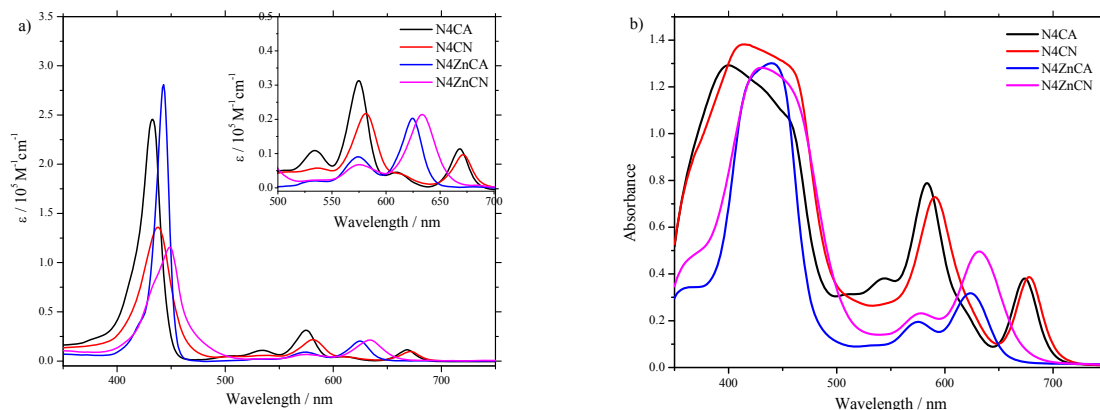


Figure 7-1. UV-Visible spectra of porphyrin dyes a) in THF, Inset shows enlarged spectra for Q band region and b) on TiO₂.

As seen from the UV-vis spectra both in solution and adsorbed on TiO₂, it is obvious that the zinc porphyrins have broader absorption spectra in the *Soret* band region compared to the free-base porphyrins and in the Q band region the absorption region is complementary to each other with zinc porphyrins covering the dip visible for free-base porphyrins in the 650 nm region. This feature indicates that these free-base and zinc porphyrins can be used as co-sensitizing dyes complementary to each other for improved short-circuit current to achieve

higher efficiencies in DSSCs. The steady state fluorescence spectra of all the porphyrins are measured in THF by excitation at the Soret band and depicted in Figure 7-2. The cyano group substitution on the anchoring unit red shifted the emission spectra of cyano derivatives compared to carboxylic acid derivatives.

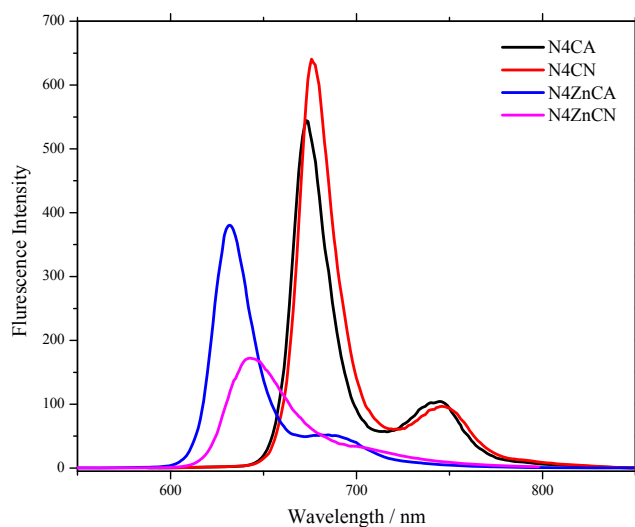


Figure 7-2. Fluorescence spectra of free-base and zinc porphyrins in THF.

7.2.3 Cyclic Voltammetry

The cyclic voltammetry (CV) and differential pulse voltammetry (DPV) measurements of the free-base and zinc porphyrins under study were carried out in degassed THF containing 0.1 M $[\text{Bu}_4\text{N}]\text{PF}_6$ as the supporting electrolyte to obtain the first oxidation potentials calibrated with ferrocene as internal standard and the resulting spectra are displayed in Figure 7-3. The oxidation couples of the zinc porphyrins show reversible redox processes and are stable over multiple scans. The oxidation features for the free-base porphyrins are quite indistinguishable in CV measurements therefore DPV is used to measure oxidation potentials. As shown in Table 7-1, the free-base porphyrins have higher oxidation potentials than the zinc porphyrins which make them harder to oxidize than the later. The zero-zero excitation energies, $E_{(0,0)}$ were calculated from the intersection of the normalized absorption and emission spectra at the Q(0,0) band and found to be 1.85 and 1.84 for free-base porphyrins **N4CA** and **N4CN**, 1.98 and 1.94 for zinc porphyrins **N4ZnCA** and **N4ZnCN**. The excited state oxidation potentials were estimated from the ground state oxidation potentials and the zero-zero excitation energies and are listed in Table 7-1. The excited state oxidation potentials for the free-base porphyrins are much lower than their zinc counterparts. The energy level diagram for these porphyrins is shown in Figure 7-4.

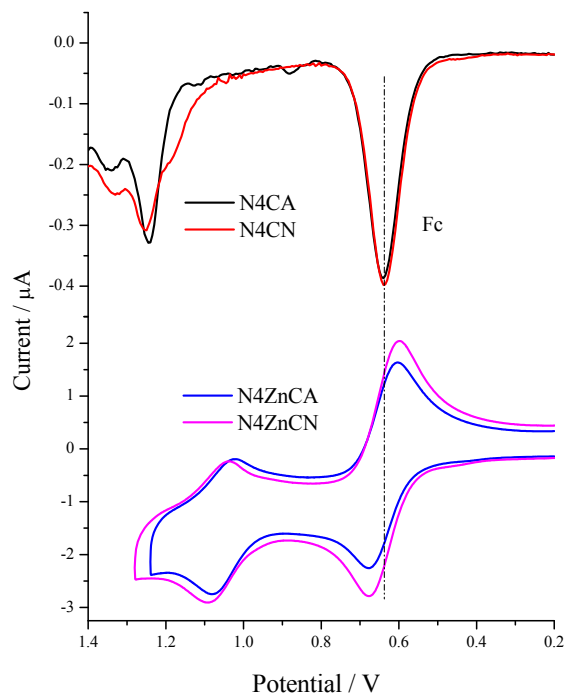


Figure 7-3. CV spectra for free-base and Zinc porphyrins calibrated with ferrocene.

The difference between the potentials of TiO_2 conduction band and the lowest unoccupied molecular orbitals (LUMO) of the free-base porphyrins is less than 0.3 volts which might be one of the reason for the lower efficiencies of free-base porphyrins compared to the zinc porphyrins as there is no sufficient driving force for electron injection from dye to TiO_2 conduction band.

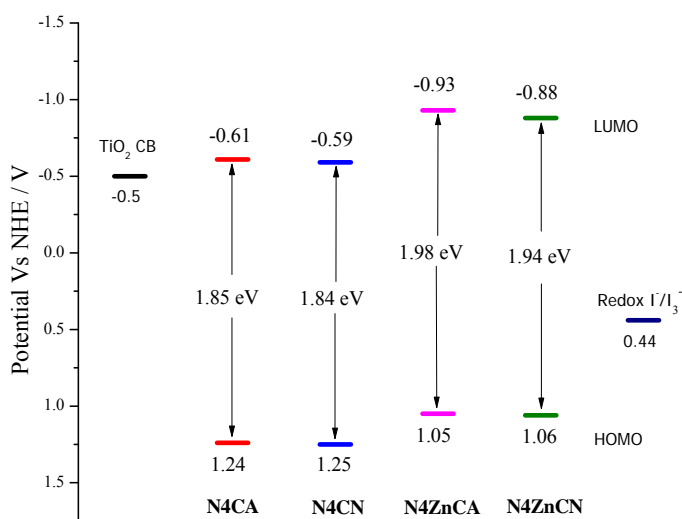


Figure 7-4. Energy level diagram for porphyrins.

As shown in the Figure 7-4, LUMO of the zinc porphyrins are more negative than the TiO₂ conduction band which ensures sufficient driving force for the electron injection from the dye to the TiO₂ conduction band. The highest occupied molecular orbitals (HOMO) of all the porphyrins are more positive than the redox electrolyte ensuring the efficient dye regeneration.

7.2.4 DFT calculations

To gain insight into the equilibrium geometry and electronic structures for the frontier molecular orbitals of the porphyrins, quantum chemical calculations using density functional theory (DFT) and time-dependent density functional theory (TD-DFT) were performed. The calculated structures do not show negative frequencies, confirming that the optimized geometry has attained the global energy minimum. The calculation result show planar macrocycles for all the porphyrins as described in Figure 7-5.

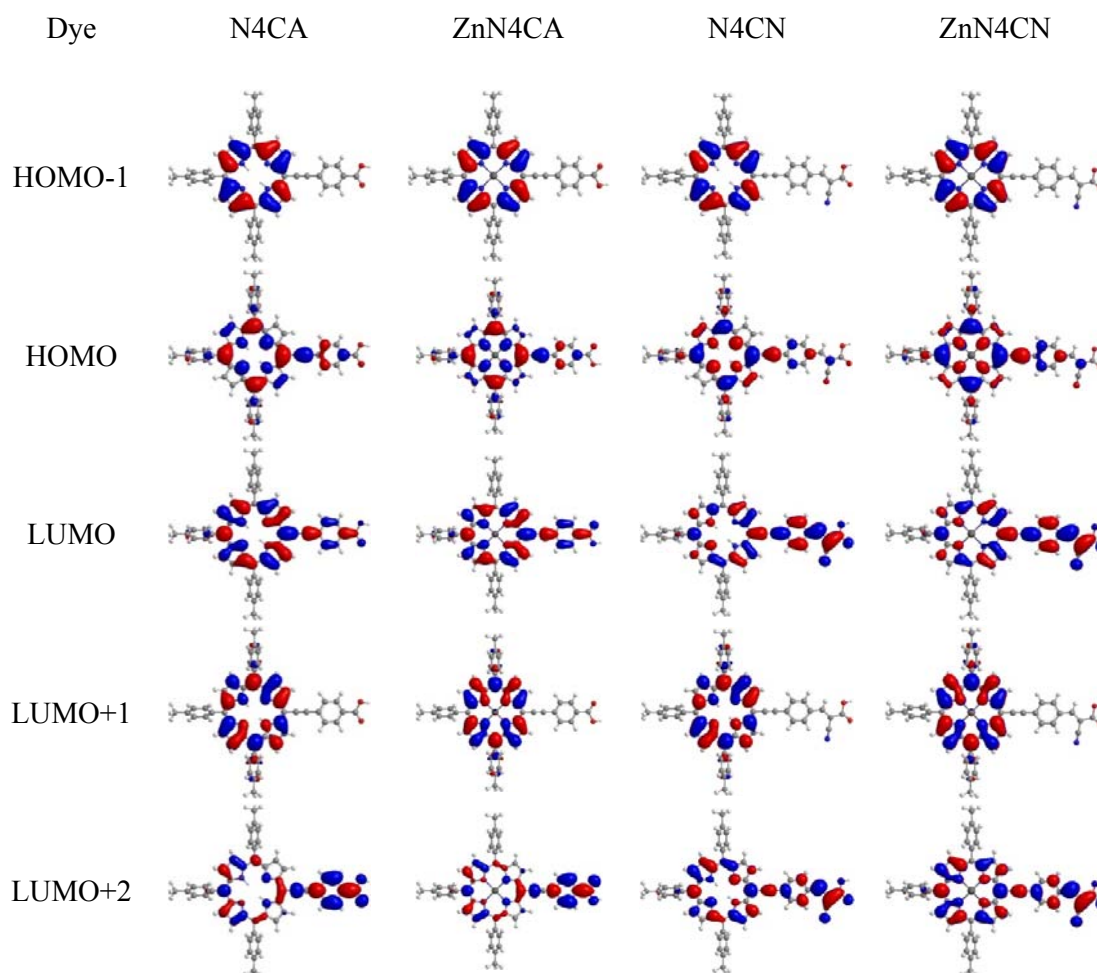


Figure 7-5. Frontier molecular orbitals for porphyrins under study.

The ethynylphenyl carboxylic acid and ethynylphenyl cyanoacrylic acid moieties are coplanar with the porphyrin ring, which makes sure that the conjugation between the porphyrin ring and anchoring group is effective. In HOMO of all the studied porphyrins, majority of the electron density is localized on the porphyrin ring as well as a small portion is also distributed over the anchoring group. In LUMO of the **N4CA** and **N4ZnCA**, the electron density is localized equally on the porphyrin ring and the ethynylphenyl carboxylic acid group while for the **N4CN** and **N4ZnCN**, the electron density is localized more on the ethynylphenyl cyanoacrylic acid group guaranteeing more effective charge separation. This effective electron distribution facilitates effective charge transfer from the excited state of the porphyrins to the TiO₂ conduction band. Interestingly in the LUMO+2, the electron density is localized extensively on the anchoring group. The nature of the electronic transitions involved in various absorption bands for the studied porphyrins can be understood by the TD-DFT calculations. The results are listed in Table 7-2. The dipole moments computed for cyano derivatives are relatively higher than the carboxylic acid derivatives. The polarizability is inversely proportional to the intramolecular photoinduced electron transfer. The theoretical wavelengths listed in Table 7-2 are in good agreement with the experimental values. For all the compounds, the lowest energy transition ($S_0 \rightarrow S_1$) is approximately 50-90% of the HOMO \rightarrow LUMO transition, thus confirming its charge-transfer character (D to A). The dipole moments for the porphyrins under study were estimated from the theoretical calculations and displayed in Table 7-2. The dipole moments decrease in the order **N4ZnCN** (9.51 D) > **N4CN** (8.23 D) > **N4ZnCA** (5.12 D) > **N4CA** (4.72 D). This trend is nearly consistent with the overall conversion efficiencies for these dyes except for the **N4CN**.

Table 7-2. Calculated TD-DFT composition in terms of frontier molecular orbitals, excitation energies, oscillator strengths and dipole moments.

Dye	State	Composition (%)	E (eV)	λ (nm)	f	Dipole Moment (Debye)
N4CA	S1	H-1 \rightarrow L (12)	2.05	603.18	0.2321	4.72
		H-1 \rightarrow L+1 (12)				
		H \rightarrow L (53)				
		H \rightarrow L+1 (22)				
	S2	H-1 \rightarrow L (24)	2.20	563.23	0.2144	
		H-1 \rightarrow L+1 (6)				
		H \rightarrow L (29)				
	S3	H \rightarrow L+1 (41)	2.97	417.78	1.1369	
		H-4 \rightarrow L (2)				
		H-1 \rightarrow L+1 (37)				
		H \rightarrow L (9)				
		H \rightarrow L+2 (46)				

	S4	H-4→L (2) H-4→L+1 (2) H-1→L (54) H-1→L+2 (4) H→L+1 (27) H→L+2 (7)	3.03	408.65	0.8168	
N4ZnCA	S1	H-1→L+1 (21) H→L (78)	2.17	572.26	0.385	5.12
	S2	H-2→L (19) H-1→L+1 (33) H→L (11) H→L+2 (34)	2.94	421.32	1.0096	
	S3	H-2→L (77) H-1→L+1 (7) H→L (3) H→L+2 (10)	2.96	419.42	0.2872	
	S4	H-1→L (50) H-1→L+2 (10) H→L+1 (37)	2.99	413.31	0.7717	
N4CN	S1	H-1→L (3) H-1→L+1 (7) H→L (84) H→L+1 (5)	1.92	645.3	0.78	8.23
	S2	H-1→L (39) H-1→L+2 (4) H→L (9) H→L+1 (48)	2.10	590.18	0.1514	
	S3	H-1→L (46) H-1→L+1 (3) H-1→L+2 (26) H→L+1 (22) H→L+2 (3)	2.57	482.77	0.1754	
	S4	H-4→L (8) H-3→L (3) H-2→L (58) H-1→L+1 (18) H-1→L+2 (3) H→L+2 (3)	2.95	419.55	0.6865	
N4ZnCN	S1	H-1→L+1 (8) H→L (91)	2.03	609.18	0.8952	9.51
	S2	H-1→L+1 (23) H→L (4) H→L+2 (71)	2.49	497.72	0.1554	
	S3	H-1→L (34) H-1→L+2 (34) H→L+1 (31)	2.60	476.72	0.1297	
	S4	H-2→L (50) H-1→L+1 (33) H→L (3) H→L+2 (10)	3.04	407.37	1.4136	

H=HOMO, L=LUMO, H-1=HOMO-1, H-2=HOMO-2, H-3=HOMO-3, H-4=HOMO-4
L+1=LUMO+1, L+2=LUMO+2.

7.2.5 Dye loading measurements

To thoroughly understand the adsorption behavior and measure the amount of adsorbed dye, we calculated the dye densities adsorbed on TiO₂ surface. The porphyrin densities (Γ) were determined by measuring the absorbance of the porphyrins desorbed from the sensitized TiO₂ films after being immersed in 0.1 M KOH solution in THF. The saturated Γ values of the porphyrins under study were found as 161 ± 4 , 121 ± 2 , 153 ± 6 and 128 ± 3 nmol cm⁻² for **N4CA**, **N4ZnCA**, **N4CN** and **N4ZnCN** respectively. The dye loadings of the free-base porphyrins are higher than that of the zinc porphyrins. The dye loading trend is similar to the overall efficiency pattern for these porphyrins dyes with higher dye loading resulting in increased conversion efficiency.

7.2.6 Photovoltaic Measurements

DSSCs based on liquid electrolytes were fabricated using the porphyrins and tested under standard AM 1.5 G illumination conditions and the photovoltaic parameters are summarized in **Table 7-3**. The I-V characteristics and the IPCE action spectra of the devices assembled using porphyrins are displayed in **Figure 7-6**. The TiO₂ films with thickness of approximately 12 μ m were immersed in dye solution for the time mentioned for each dye in the experimental section at 40 °C.

Table 7-3. Photovoltaic parameters of N4CA, N4CN, N4ZnCA and N4ZnCN dyes

Dye	J_{sc} (mA cm ⁻²)	V_{oc} (V)	FF (%)	η (%)
N4CA	6.47	0.57	73	2.71
N4ZnCA	7.41	0.57	73	3.09
Mix-1^a	7.38	0.61	73	3.28
N4CN	4.86	0.55	72	1.94
N4ZnCN	8.33	0.58	73	3.52
Mix-2^b	10.4	0.56	72	4.18

^aMix1 = N4CA+N4ZnCA (1:1); ^bMix2 = N4CN+N4ZnCN (1:1)

The device prepared with the free-base porphyrin **N4CA** obtained the overall conversion efficiency of 2.71%, with short-circuit current (J_{sc}) of 6.47 mA cm⁻², open circuit voltage (V_{oc}) of 0.57 V and the fill factor (FF) of 0.73. The cell assembled with **N4ZnCA** achieved the efficiency of 3.09% based on the J_{sc} of 7.41 mA cm⁻², V_{oc} of 0.57 V and the FF of 0.73.

To check the co-sensitization effect of free-base and zinc porphyrin we mixed the free-base **N4CA** porphyrin with zinc porphyrin **N4ZnCA** in equimolar ratio in THF to prepare **Mix-1** and evaluated the performance of this mixture in DSSC. The TiO_2 films were immersed in this solution for 2 h at 40 °C. **Mix-1** achieves the efficiency of 3.28% supported by the J_{sc} of 7.38 mA cm^{-2} , V_{oc} of 0.61 V and the FF of 0.73, which is higher than the both individual dyes. The short-circuit current and the fill factor for **Mix-1** are same while the open-circuit voltage is higher by 40 mV than the individual porphyrins.

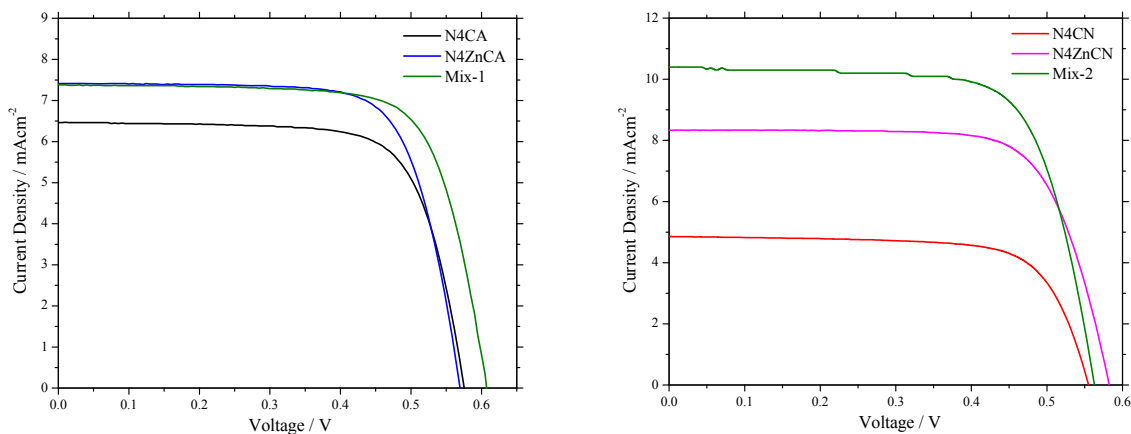


Figure 7-6. I-V curves of the DSSCs fabricated with porphyrins N4CA, N4ZnCA, Mix-1 and N4CN, N4ZnCN, Mix-2.

The solar cell fabricated with the cyanoacrylic acid substituted free-base porphyrin **N4CN** obtained overall photon-to-current conversion efficiency of 1.94%, with short-circuit current of 4.86 mA cm^{-2} , open-circuit voltage of 0.55 V and the fill factor of 0.72. The device prepared using its zinc derivative **N4ZnCN** achieved the overall conversion efficiency of 3.52% reinforced by J_{sc} of 8.33 mA cm^{-2} , V_{oc} of 0.58 V and the FF of 0.73. **Mix-2** composed of the free-base **N4CN** along with zinc metalized porphyrin **N4ZnCN** in same molar ratio (1:1) is also tested in the DSSCs. **Mix-2** sensitized cell exhibit the highest solar cell performance with overall conversion efficiency of 4.18% based on the J_{sc} of 10.4 mA cm^{-2} , V_{oc} of 0.56 V and the FF of 0.72. The obvious difference seen from the I-V curve is the short-circuit current of the **Mix-2** sensitized solar cell is much higher than the individual free-base or zinc porphyrins, while the open-circuit voltage for **Mix-2** is slightly higher than the free-base porphyrin and lower than that of the zinc porphyrin sensitized cell. The prominent difference between these two mixtures is the current density. **Mix-2** has much higher current density (10.4 mA cm^{-2}) than **Mix-1** (7.38 mA cm^{-2}), while the open-circuit voltage for the former (0.56 V) is slightly lower (0.61 V) than the later. It is obvious from the higher current

density of **N4ZnCN** compared to **N4ZnCA** that, the electron withdrawing cyano group pulls more electrons towards the anchoring group and consequently more electrons might be injected to the TiO₂ conduction band. Interestingly similar assumption can't be applied for free-base porphyrins, where the **N4CA** obtained higher efficiency (2.71%) than the **N4CN** (1.94%).

The trends in the J_{sc} for these porphyrins can be understood from the variation of incident photon-to-current conversion efficiency (IPCE) plots of these dyes as shown in Figure 7-7. The IPCE spectra of all the dyes are in qualitative agreement with the corresponding absorption spectra of the dyes on TiO₂ which shows intense and broad absorption in both *Soret* as well as Q band region. It is clear from the IPCE spectra of the mixtures that, the mixture of the dyes covers broader region in the visible region compared to the single dye. **Mix-1** and **Mix-2** have higher IPCE values in the 500-600 nm region compensating the dip observed for the individual free-base or zinc porphyrins. The IPCE value for **Mix-2** in *Soret* band region reaches around 70% which is higher than that of **Mix-1** (65%). The IPCE value for **Mix-1** for the dip around 500-600 nm is significantly higher, its plateau reaching 40% at 580 nm. Also the dip around 550 nm is much higher for **Mix-2** corresponding to IPCE value of 25%, while its plateau reaching 40% in the Q band region is around. Collectively higher photon-to-current conversion over the panchromatic region ensures the higher current density for **Mix-2** giving prominent solar cell efficiency.

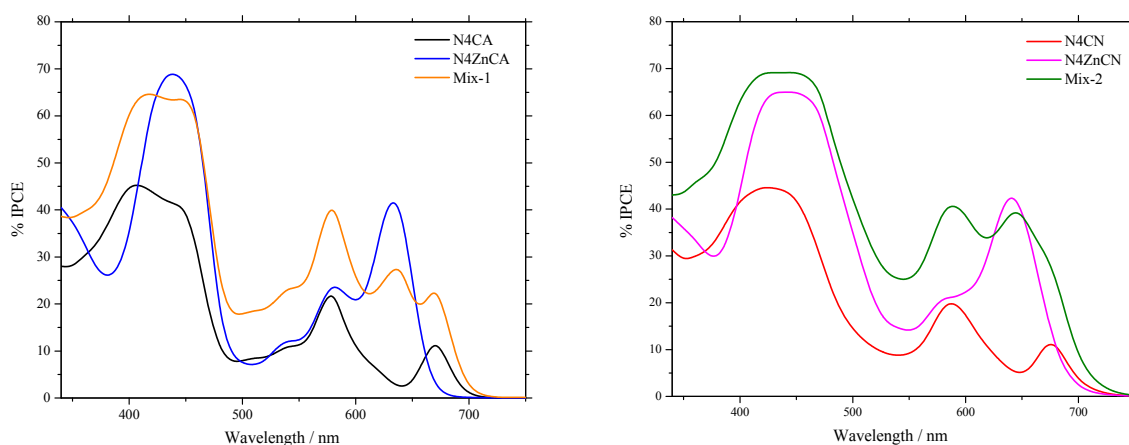


Figure 7-7. IPCE action spectra of the DSSCs fabricated with porphyrins N4CA, N4ZnCA, Mix-1, N4CN, N4ZnCN, and Mix-2.

7.3 Conclusions

In summary, we have prepared four novel free-base and zinc porphyrins and applied them as sensitizer in the DSSCs to evaluate their individual as well as co-sensitized performance. We have combined two discretely moderate dyes with complementary absorption spectra to construct a mixed porphyrin DSSC which shows a significant enhancement in short circuit current and consequently in the overall photon-to-current conversion efficiency. From photo-action spectra, it is evident that the incident photon collection for the mixed dyes is higher than the individual dyes due to the broader absorption. Without extensive fabrications on the substituents of dye and before exhausted device optimizations, we are able to show that the co-sensitization of free-base porphyrins and their zinc complexes is an effective strategy to improve the photon to current conversion efficiency of the DSSCs.

7.4 Experimental Section

7.4.1 General Techniques and Materials

All chemicals were obtained from commercial sources and used as received without further purification. All the reactions were carried out under nitrogen atmosphere. Solvents used in reactions were dried by PureSolv MD 5 system (Innovative Technology, Inc). Flash chromatography was carried out by using silica gel (40-63 μm , Merck). Analytical TLC was performed on Merck silica gel plates. ^1H and ^{13}C NMR spectra were recorded on a Bruker Avance 400 FT spectrometer. NMR samples were prepared in CDCl_3 and THF as *d*-solvents and chemical shifts were reported in δ scale using tetramethylsilane (TMS) as internal standard. The standard abbreviations s, d, t, q, m and bs refer to singlet, doublet, triplet, quartet, multiplet and broad singlet respectively. Coupling constant (J) values are reported in Hertz. The ESI ion trap mass spectra were measured by a Finnigan MAT LCQ mass spectrometer. The HR-FAB spectra were conducted on a JMS-700 double focusing mass spectrometer. Transmittance and reflection UV-visible absorption spectra of the porphyrins in tetrahydrofuran (THF) and adsorbed on TiO_2 electrodes, respectively, were recorded on a JASCO V-670 UV-vis/NIR spectrophotometer. Steady-state fluorescence spectra were acquired by using a Varian Cary Eclipse fluorescence spectrophotometer. The cyclic voltammetry measurements of the porphyrins were carried out on CHI 621B electrochemical analyzer (CH Instruments, Austin, TX, USA) in degassed THF containing 0.1 M tetrabutylammonium hexafluorophosphate (Bu_4NPF_6) as the supporting electrolyte. The cell assembly consists of a glossy carbon as the working electrode, a silver wire as the pseudo-reference electrode, and a platinum wire as the auxiliary electrode. The scan rate for all measurements was fixed at 50 mV/sec. A ferrocene^{+1/0} redox couple was used as the internal standard and the potential values obtained in reference to the silver electrode were converted to the vacuum scale. The density functional theory (DFT) and time-dependent density functional (TD-DFT) calculations were performed with Gaussian 09 package to study the electron distribution of the frontier molecular orbitals and the photoexcitation transitions. All ground state geometries of studied porphyrins were optimized in the gas phase by the hybrid B3LYP functional and the 6-31G basis set, and the TD-DFT calculation were based on the same functional and basis set. The molecular orbitals were visualized by the Chemoffice software.

7.4.2 Synthesis

5,10,15-Tris(*p*-tolyl)-20-bromoporphyrin (2)

To a stirred solution of 5,10,15-Tris(*p*-tolyl)porphyrin (1) (200 mg, 0.34 mmol) in chloroform (50 ml) at room temperature, *N*-bromosuccinimide (73 mg, 0.41 mmol) was added. The progress of the reaction was monitored by TLC and absorption spectroscopy. After complete consumption of the starting porphyrin as confirmed by TLC, the reaction was quenched by adding acetone (10 ml) and the solvent was removed on a rotary evaporator under vacuum. The crude reaction mixture was purified by silica gel column chromatography with hexanes/CH₂Cl₂ (70:30) as the eluent and the pure bromoporphyrin (2) was obtained as a purple solid in 70% yield (157 mg). ¹H NMR (400 MHz, CDCl₃) δ: 9.65 (d, 2H, *J* = 4.8 Hz, β-pyrrole), 8.91 (d, 2H, *J* = 4.7 Hz, β-pyrrole), 8.81 (s, 4H, β-pyrrole), 8.06 (m, 6H, Ph), 7.55 (m, 6H, Ph), 2.72 (s, 6H, Tol), 2.70 (s, 3H, Tol), -2.75 (s, 2H, NH) ppm; HRMS-ESI: *m/z* calcd for C₄₁H₃₂N₄Br: 659.1810, found 659.1806 [M+H]⁺.

Zinc (II) 5,10,15-Tris(*p*-tolyl)-20-bromoporphyrin (3)

In a 100 ml round bottom flask porphyrin (2) (100 mg, 0.15 mmol) was dissolved in 50 ml CH₂Cl₂/MeOH (3:2). To this solution molar excess of anhydrous zinc chloride (20 equiv) was added and the reaction mixture was stirred at room temperature. Reaction progress was monitored by TLC and UV-Visible spectroscopy. After the completion of reaction, solvent was removed under reduced pressure. Water was added to the residue and extracted with CH₂Cl₂. The organic layer was concentrated and dried with anhydrous MgSO₄ and evaporated to dryness to give Zn(II) porphyrin (3) as a purple solid in 96% yield (104 mg). ¹H NMR (400 MHz, CDCl₃) δ: 9.75 (d, 2H, *J* = 4.68 Hz, β-pyrrole), 9.01 (d, 2H, *J* = 4.72 Hz, β-pyrrole), 8.92 (s, 4H, β-pyrrole), 8.06 (m, 6H, Ph), 7.55 (m, 6H, Ph), 2.72 (s, 6H, Tol), 2.70 (s, 3H, Tol) ppm; HRMS-FAB⁺: *m/z* calcd for C₄₁H₃₀BrN₄Zn: 721.0945, found 721.0955 [M+H]⁺.

5,10,15-Tris(*p*-tolyl)-20-trimethylsilylethynylporphyrin (4)

To a 50 ml two neck round bottom flask bromoporphyrin (2) (50 mg, 0.076 mmol), Pd₂(dba)₃ (21 mg, 0.022 mmol) and AsPh₃ (58 mg, 0.19 mmol) were added and flushed with N₂ for 20 min. To this dry THF (20 ml) and dry NEt₃ (5 ml) were added and flushed with N₂ again for 15 min. Then trimethylsilyl acetylene (TMSA) (22 μl, 0.152 mmol) was added and the reaction mixture was stirred under N₂ at room temperature for 12 h. After completion of the reaction as confirmed by the TLC, the solvents were removed under reduced pressure and the crude compound is purified by silica gel column chromatography using CH₂Cl₂/hexanes =

2/8 as eluent to give trimethylsilylethynyl porphyrin in 52% yield (27 mg). ^1H NMR (400 MHz, CDCl_3) δ : 9.69 (d, 2H, $J = 4.7$ Hz, β -pyrrole), 8.95 (d, 2H, $J = 4.68$ Hz, β -pyrrole), 8.82 (s, 4H, β -pyrrole), 8.09 (m, 6H, Ph), 7.56 (m, 6H, Ph), 2.73 (s, 6H, Tol), 2.71 (s, 3H, Tol), 0.66 (s, 9H, 3 CH_3), -2.35 (s, 2H, NH) ppm; HRMS-ESI: m/z calcd for $\text{C}_{46}\text{H}_{41}\text{N}_4\text{Si}$: 677.3101, found 677.3101 $[\text{M}+\text{H}]^+$.

Zinc (II) 5,10,15-Tris(*p*-tolyl)-20-trimethylsilylethynylporphyrin (5)

To a 25 ml two neck round bottom flask porphyrin (3) (100 mg, 0.14 mmol), $\text{Pd}(\text{PPh}_3)_2\text{Cl}_2$ (20 mg, 0.028 mmol) and CuI (8 mg, 0.042 mmol) were added and flushed with N_2 for 20 min. To this dry THF (7 ml) and dry NEt_3 (3 ml) were added and flushed with N_2 again for 15 min. Then TMSA (393 μl , 2.8 mmol) was added and the reaction mixture was stirred at under N_2 at 40 $^\circ\text{C}$ for 12 h. After completion of the reaction as confirmed by the TLC, the solvents were removed under reduced pressure and the crude compound is purified by silica gel column chromatography using $\text{CH}_2\text{Cl}_2/\text{Hex} = 2/8$ as eluent to give porphyrin (5) in 78% yield (81 mg). ^1H NMR (400 MHz, CDCl_3) δ : 9.75 (d, 2H, $J = 4.52$ Hz, β -pyrrole), 9.01 (d, 2H, $J = 4.68$ Hz, β -pyrrole), 8.89 (s, 4H, β -pyrrole), 8.07 (m, 6H, Ph), 7.56 (m, 6H, Ph), 2.73 (s, 6H, Tol), 2.71 (s, 3H, Tol), 0.63 (s, 9H, 3 CH_3); HRMS-FAB $^+$: m/z calcd for $\text{C}_{46}\text{H}_{39}\text{N}_4\text{SiZn}$: 739.2235, found 739.2246 $[\text{M}+\text{H}]^+$.

N_4CA (6)

A mixture of porphyrin (2) (50 mg, 0.069 mmol) and 4-ethynylbenzoic acid (12 mg, 0.083 mmol) in dry THF (30 ml) and NEt_3 (6 ml) was degassed with N_2 for 10 min. Then $\text{Pd}_2(\text{dba})_3$ (27 mg, 0.03 mmol) and AsPh_3 (58 mg, 0.19 mmol) were added to the mixture. The solution was stirred at room temperature for 12 h under N_2 . The solvent was removed in *vacuo*, and the residue was purified by column chromatography (silica gel) using $\text{CH}_2\text{Cl}_2/\text{methanol} = 9.5/0.5$ as eluent to give porphyrin (6) in 62% yield (20 mg). ^1H NMR (400 MHz, THF-*d*8) δ : 9.79 (d, 2H, $J = 4.61$ Hz, β -pyrrole), 8.94 (d, 2H, $J = 4.54$ Hz, β -pyrrole), 8.76 (s, 4H, β -pyrrole), 8.24 (d, 2H, $J = 8.21$ Hz, Ph), 8.16 (d, 2H, $J = 8.26$ Hz, Ph), 8.07 (m, 6H, Ph), 7.59 (m, 6H, Ph), 2.71 (s, 6H, Tol), 2.68 (s, 3H, Tol), -2.22 (s, 2H, NH) ppm; UV-Visible (THF) $\lambda_{\text{max}}/\text{nm}$ ($\epsilon/10^3 \text{ M}^{-1}\text{cm}^{-1}$) = 433 (245), 534 (11), 575 (31), 613 (4), 668 (11); HRMS-ESI: m/z calcd for $\text{C}_{50}\text{H}_{37}\text{N}_4\text{O}_2$: 725.2917, found 725.2919 $[\text{M}+\text{H}]^+$.

N_4ZnCA (7)

A mixture of 4-ethynylbenzoic acid (12 mg, 0.083 mmol) and porphyrin (7) (50 mg, 0.069 mmol) in dry THF (30 ml) and NEt_3 (6 ml) was degassed with N_2 for 10 min. Then $\text{Pd}_2(\text{dba})_3$ (27 mg, 0.03 mmol) and AsPh_3 (58 mg, 0.19 mmol) were added to the mixture. The solution

was refluxed for 12 h under N₂. The solvent was removed in *vacuo*, and the residue was purified by column chromatography (silica gel) using CH₂Cl₂/methanol = 9.5/0.5 as eluent to give porphyrin (7) in 62% yield (20 mg). ¹H NMR (400 MHz, THF-*d*₈) δ: 9.79 (d, 2H, *J* = 4.64 Hz, β-pyrrole), 8.94 (d, 2H, *J* = 4.52 Hz, β-pyrrole), 8.76 (s, 4H, β-pyrrole), 8.23 (d, 2H, *J* = 8.16 Hz, Ph), 8.14 (d, 2H, *J* = 8.28 Hz, Ph), 8.05 (m, 6H, Ph), 7.56 (m, 6H, Ph), 2.70 (s, 6H, Tol), 2.68 (s, 3H, Tol) ppm; UV-Visible (THF) λ_{max}/nm (ε/10³ M⁻¹cm⁻¹) = 443 (281), 574 (9), 625 (20); HRMS-FAB⁺: *m/z* calcd for C₅₀H₃₅N₄O₂Zn: 787.2051, found 787.2064 [M+H]⁺.

N₄CN (8)

To a solution of porphyrin (20 mg, 0.033 mmol) in dry THF (10 ml) was added *tetra*-butyl ammonium fluoride (TBAF) and the reaction mixture was stirred at room temperature for 30 min under N₂. After completion of the reaction as confirmed by the TLC, the reaction was quenched with water and extracted with CH₂Cl₂. The organic layer was dried over MgSO₄ and concentrated under reduced pressure. The crude compound and 2-cyano-3-(4-iodophenyl)acrylic acid (15 mg, 0.049 mmol) were dissolved in a mixture of dry THF/NEt₃ (12/3 ml, v/v) and flushed with N₂ for 15 min. To this solution Pd₂(dba)₃ (12 mg, 0.013 mmol), AsPh₃ (25 mg, 0.082 mmol) were added and the reaction mixture was stirred at room temperature under N₂ for 12 h. The solvent was removed in *vacuo* and the residue was purified by column chromatography (silica gel) using CH₂Cl₂/MeOH 9.5/0.5 as eluent to give porphyrin (8) in 46% yield (12 mg). ¹H NMR (400 MHz, DMSO-*d*₆) δ: 9.83 (d, 2H, *J* = 4.60 Hz, β-pyrrole), 8.91 (d, 2H, *J* = 4.57 Hz, β-pyrrole), 8.75 (s, 4H, β-pyrrole), 8.26 (d, 2H, *J* = 8.1 Hz, Ph), 8.14 (d, 2H, *J* = 8.0 Hz, Ph), 8.07 (m, 6H, Ph), 8.04 (s, 1H, Acrylic H), 7.63 (m, 6H, Ph), 2.68 (s, 6H, Tol), 2.66 (s, 3H, Tol), -2.45 (s, 2H, NH) ppm; UV-Visible (THF) λ_{max}/nm (ε /10³ M⁻¹cm⁻¹) = 438 (136), 537 (6), 581 (22), 612 (4), 671 (10); HRMS-FAB⁺: *m/z* calcd for C₅₃H₃₈O₂N₅: 776.3026, found 776.3030 [M+H]⁺.

N₄ZnCN (9)

To a solution of porphyrin **9** (40 mg, 0.05 mmol) in dry THF (10 ml) was added TBAF and the reaction mixture was stirred at room temperature for 30 min under N₂. After completion of the reaction as confirmed by the TLC, the reaction was quenched with water and extracted with CH₂Cl₂. The organic layer was dried over MgSO₄ and concentrated under reduced pressure. The crude compound and 2-cyano-3-(4-iodophenyl)acrylic acid (30 mg, 0.1 mmol) were dissolved in a mixture of dry THF/NEt₃ (12/3, v/v ml) and flushed with N₂ for 15 min. To this solution Pd₂(dba)₃ (18 mg, 0.02 mmol) and AsPh₃ (38 mg, 0.12 mmol) were added

and the reaction mixture was refluxed for 6 h. The solvent was removed in *vacuo*, and the residue was purified on a column chromatograph (silica gel) using CH₂Cl₂/methanol (9/1) as eluent to give porphyrin (**10**) in 90% yield (38 mg, 0.027 mmol). ¹H NMR (400 MHz, *d8*-THF) δ : 9.31 (d, 2H, $J = 4.52$ Hz, β -pyrrole), 8.47 (d, 2H, $J = 4.56$ Hz, β -pyrrole), 8.28 (t, 4H, β -pyrrole), 7.84 (s, 1H, Acrylic H), 7.77 (d, 2H, $J = 8.00$ Hz, Ph), 7.70 (d, 2H, $J = 8.24$ Hz, Ph), 7.57 (m, 6H, Ph), 7.08 (m, 6H, Ph), 2.22 (s, 6H, Tol), 2.20 (s, 3H, Tol) ppm; UV-Visible (THF) $\lambda_{\text{max}}/\text{nm}$ ($\epsilon/10^3 \text{ M}^{-1}\text{cm}^{-1}$) = 449 (116), 575 (7), 634 (21); HRMS-FAB⁺: m/z calcd for C₅₃H₃₆N₅O₂Zn: 838.2159, found 838.2176 [M+H]⁺.

7.4.3 Photovoltaic Measurements

To characterize the photovoltaic performance of the DSSC devices, fluorine-doped tin oxide glass (FTO; 6-8 Ω/sq , Pilkington Tec-7, USA, thickness 2.2 mm) plates were washed with a soap solution in an ultrasonic bath for 10 min, and then rinsed with DI water and methanol. The FTO glass plates were immersed in 40 mM aqueous TiCl₄ at 70 °C for 30 min and washed with DI water and methanol. A transparent nanocrystalline layer was prepared on the FTO glass plate by repeated screen printing with TiO₂ paste (Solaronix, 15-20 nm Ti-Nanoxide T/SP), then drying for 2 h at room temperature. The TiO₂ electrodes were gradually heated at 110 °C for 1 h and 450 °C for 1 h. The resulting layer was composed of a $\sim 11 \mu\text{m}$ thickness, measured by DekTak 150 stylus profiler. Finally a scattering layer containing $>100 \text{ nm}$ anatase particles (Solaronix, Ti-Nanoxide R/SP) was deposited by screen printing and then dried at room temperature for 2 h. The FTO glass plates were again immersed in 40 mM aqueous TiCl₄ at 70 °C for 30 min and washed with DI water and methanol. The TiO₂ electrodes were gradually heated at 110 °C for 1 h and 450 °C for 1 h. The porphyrin/TiO₂ layer was served as a working electrode (anode). We immersed the TiO₂ coated FTO (TiO₂ active size $0.4 \times 0.4 \text{ cm}^2$) films in a THF solution containing porphyrins ($1 \times 10^{-4} \text{ M}$) at 40 °C for 2 h. The FTO glass plate used as cathode was coated with Pt particles by using the thermal platinum nano-cluster catalyst method. The Pt catalyst was deposited from a precursor solution composed of 5 mM solution of hexachloroplatinic acid in anhydrous isopropanol. The precursor solution was spin-coated on FTO glass (10 L/cm²) and dried in air for 3 min. Coated Pt electrode was placed in an oven and temperature was gradually increased to 360 °C and kept under 360 °C for 15 min. To fabricate the DSSC device, the two electrodes were assembled into a sandwich type cell. The thin layer of electrolyte was introduced into the space between the two electrodes. A typical redox electrolyte contained lithium iodide (LiI, 0.1 M), diiodine (I₂, 0.05 M), 1,2-dimethyl-3-propylimidazolium iodide

(DMII, 0.5 M), and 0.5 M 4-tert-butylpyridine in dry MeCN. The photoelectrochemical characterizations of the solar cells were carried out by using an Oriel Class-A solar simulator (Oriel 91195A, Newport Corp.). Photocurrent and voltage curves were recorded with a potentiostat/galvanostat (CHI 650B, CH Instruments, Inc., USA) at a light intensity of one-sun irradiation calibrated by an Oriel reference solar cell (Oriel 91150, Newport Corp.). The incident photon-to-current conversion efficiency (IPCE) measurements were carried out with a monochromator (Oriel 74100) at short circuit condition.

7.5 References

- [1] P. Zuo, C. Li, Y.-S. Wu, X.-C. Ai, X.-S. Wang, B.-W. Zhang, J.-P. Zhang, *J. Photochem. Photobiol., A* **2006**, *183*, 138-145.
- [2] H. Choi, S. Kim, S. O. Kang, J. Ko, M.-S. Kang, J. N. Clifford, A. Forneli, E. Palomares, M. K. Nazeeruddin, M. Grätzel, *Angew. Chem. Int. Ed.* **2008**, *47*, 8259-8263.
- [3] R. Y. Ogura, S. Nakane, M. Morooka, M. Orihashi, Y. Suzuki, K. Noda, *Appl. Phys. Lett.* **2009**, *94*, -.
- [4] L. Han, A. Islam, H. Chen, C. Malapaka, B. Chiranjeevi, S. Zhang, X. Yang, M. Yanagida, *Energy Environ. Sci.* **2012**, *5*, 6057-6060.
- [5] A. Ehret, L. Stuhl, M. T. Spitler, *J. Phys. Chem. B* **2001**, *105*, 9960-9965.
- [6] Y. Chen, Z. Zeng, C. Li, W. Wang, X. Wang, B. Zhang, *New J. Chem.* **2005**, *29*, 773-776.
- [7] D. Kuang, P. Walter, F. Nüesch, S. Kim, J. Ko, P. Comte, S. M. Zakeeruddin, M. K. Nazeeruddin, M. Grätzel, *Langmuir* **2007**, *23*, 10906-10909.
- [8] J.-H. Yum, S.-R. Jang, P. Walter, T. Geiger, F. Nüesch, S. Kim, J. Ko, M. Grätzel, M. K. Nazeeruddin, *Chem. Commun.* **2007**, *0*, 4680-4682.
- [9] J.-J. Cid, J.-H. Yum, S.-R. Jang, M. K. Nazeeruddin, E. Martínez-Ferrero, E. Palomares, J. Ko, M. Grätzel, T. Torres, *Angew. Chem. Int. Ed.* **2007**, *46*, 8358-8362.
- [10] N. Robertson, *Angew. Chem. Int. Ed.* **2008**, *47*, 1012-1014.
- [11] J. N. Clifford, A. Forneli, H. Chen, T. Torres, S. Tan, E. Palomares, *J. Mater. Chem.* **2011**, *21*, 1693-1696.
- [12] M. Kimura, H. Nomoto, N. Masaki, S. Mori, *Angew. Chem. Int. Ed.* **2012**, *51*, 4371-4374.
- [13] F. Inakazu, Y. Noma, Y. Ogomi, S. Hayase, *Appl. Phys. Lett.* **2008**, *93*, 093304.

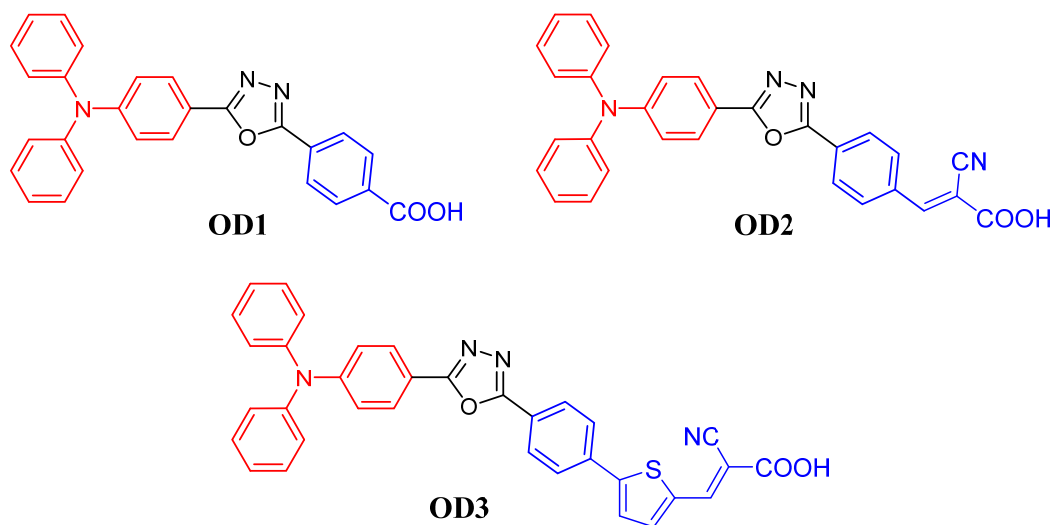
- [14] S. W. P. Kyungtae Lee, Min Jae Ko, Kyungkon Kim and Nam-Gyu Park, *Nat. Mater.* **2009**, *8*, 665-671.
- [15] T. Bessho, S. M. Zakeeruddin, C.-Y. Yeh, E. W.-G. Diau, M. Grätzel, *Angew. Chem. Int. Ed.* **2010**, *49*, 6646-6649.
- [16] T. D. Santos, A. Morandeira, S. Koops, A. J. Mozer, G. Tsekouras, Y. Dong, P. Wagner, G. Wallace, J. C. Earles, K. C. Gordon, D. Officer, J. R. Durrant, *J. Phys. Chem. C* **2010**, *114*, 3276-3279.
- [17] A. Yella, H.-W. Lee, H. N. Tsao, C. Yi, A. K. Chandiran, M. K. Nazeeruddin, E. W.-G. Diau, C.-Y. Yeh, S. M. Zakeeruddin, M. Grätzel, *Science* **2011**, *334*, 629-634.
- [18] C.-M. Lan, H.-P. Wu, T.-Y. Pan, C.-W. Chang, W.-S. Chao, C.-T. Chen, C.-L. Wang, C.-Y. Lin, E. W.-G. Diau, *Energy Environ. Sci.* **2012**, *5*, 6460-6464.
- [19] M. Shrestha, L. Si, C.-W. Chang, H. He, A. Sykes, C.-Y. Lin, E. W.-G. Diau, *J. Phys. Chem. C* **2012**, *116*, 10451-10460.
- [20] J. Warnan, Y. Pellegrin, E. Blart, F. Odobel, *Chem. Commun.* **2012**, *48*, 675-677.
- [21] H.-P. Wu, Z.-W. Ou, T.-Y. Pan, C.-M. Lan, W.-K. Huang, H.-W. Lee, N. M. Reddy, C.-T. Chen, W.-S. Chao, C.-Y. Yeh, E. W.-G. Diau, *Energy Environ. Sci.* **2012**, *5*, 9843-9848.
- [22] S. Hayashi, M. Tanaka, H. Hayashi, S. Eu, T. Umeyama, Y. Matano, Y. Araki, H. Imahori, *J. Phys. Chem. C* **2008**, *112*, 15576-15585.
- [23] A. J. M. Matthew J. Griffith, George Tsekouras, Ying Dong, Pawel Wagner, Klaudia Wagner, Gordon G. Wallace, Shogo Mori, and David. L. Officer, *Appl. Phys. Lett.* **2011**, *98*, 163502.
- [24] M. J. Griffith, K. Sunahara, P. Wagner, K. Wagner, G. G. Wallace, D. L. Officer, A. Furube, R. Katoh, S. Mori, A. J. Mozer, *Chem. Commun.* **2012**, *48*, 4145-4162.
- [25] A. T. Wright, J. D. Song, B. F. Cravatt, *J. Am. Chem. Soc.* **2009**, *131*, 10692-10700.
- [26] C. Y. Lee, C. She, N. C. Jeong, J. T. Hupp, *Chem. Commun.* **2010**, *46*, 6090-6092.
- [27] S. Horn, M. O. Senge, *Eur. J. Org. Chem.* **2008**, *2008*, 4881-4890.
- [28] V. V. Pavlishchuk, A. W. Addison, *Inorg. Chim. Acta* **2000**, *298*, 97-102.
- [29] G. Boschloo, A. Hagfeldt, *Acc. Chem. Res.* **2009**, *42*, 1819-1826.
- [30] T. Daeneke, T.-H. Kwon, A. B. Holmes, N. W. Duffy, U. Bach, L. Spiccia, *Nat. Chem.* **2011**, *3*, 211-215.

8. Novel D- π -A type organic dyes with oxadiazole ring as electron transporter for DSSC application

8.1 Introduction

The first example of 1,3,4-oxadiazoles as excellent electron transporters in organic multilayer electroluminescent diodes was reported in 1990.^[1-2] Followed by this pioneer work many researchers, by exploration of various derivatives revealed that the oxadiazole ring functions well as an electron-transport moiety. This survey of conjugated 1,3,4-oxadiazole-containing polymers and small molecules has led to a host of new materials advantageous for optoelectronics by offering not only improved balance of charge mobility but enhanced thermal and photostability as well. Having robust functionality and straightforward synthetic routes, 1,3,4-oxadiazoles have been applied in a variety of application like, Organic light emitting diodes (OLEDs),^[3-6] Signaling components in molecular sensory systems^[7-10] and Molecular logic gates and Fluorescent Switches.^[11]

Although these oxadiazole rings possessed promising charge carrier properties, they have not been employed as π -conjugate linkers in photovoltaic systems. We designed three novel oxadiazole dyes based on donor- π conjugate linker-acceptor (D- π -A) molecular design, in which the triphenylamine group was utilized as donor and cyanoacrylic acid group as acceptor. The molecular structures of these dyes are displayed in Scheme 8-1.



Scheme 8-1. Molecular structures of the Oxadiazole dyes.

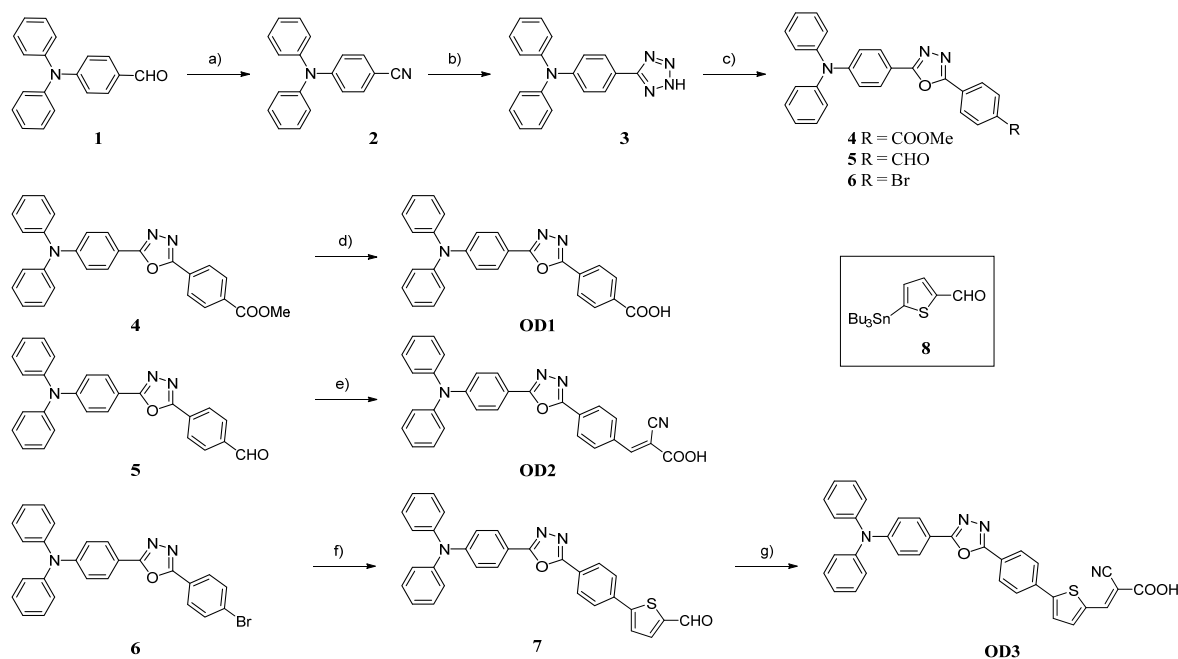
Dye **OD1** comprised of carboxylic acid anchor, while dye **OD2** consist of cyanoacrylic acid as anchoring group. The dye **OD3** was embraced with thiophene group to enhance the π -

conjugation and cyanoacrylic acid as anchor. These oxadiazole dyes demonstrate good absorption features in visible region, good charge transfer ability upon excitation and suitable redox potentials, which collectively suggests that these dyes shall work as efficient sensitizers in dye-sensitized solar cells.

8.2 Results and Discussion

8.2.1 Syntheses

The new oxadiazole-based (**OD1-OD3**) push-pull dyes are shown in Scheme 8-1 and the main synthetic pathways are depicted in Scheme 8-2. The starting compounds (4)-(6) were prepared following literature procedures. The triphenylamine (TPA) aldehyde (**1**) was readily converted into nitrile (**2**) in the presence of hydroxylamine hydrochloride and acetic acid, which was further treated with sodium azide to obtain TPA tetrazole (**3**). This TPA tetrazole was reacted with corresponding acid chlorides to yield the compounds (4)-(5).



Scheme 8-2. Synthetic pathways of **OD** dyes. Reagents and Conditions: a) $\text{NH}_2\text{OH}\cdot\text{HCl}$, AcOH, Pyridine; b) NaN_3 , NH_4Cl ; c) RPhCOCl , Pyridine; d) KOH (aq.); e) CNCH_2COOH , NH_4OAc , AcOH; f) Comp. 8, $\text{Pd}(\text{PPh}_3)_4$; g) CNCH_2COOH , NH_4OAc , AcOH.

The ester group in compound (**4**) was converted to carboxylic acid by saponification in the presence of aq. KOH to get the desired dye **OD1**. The dye **OD2** was obtained via Knoevenagel

condensation of compound (5) with cyanoacetic acid. Compound (6) was treated with compound (8) under Stille coupling protocol to achieve intermediate compound (7) which was further condensed with cyanoacetic acid under Knoevenagel condensation conditions to obtain the **OD3** dye. All the final compounds were thoroughly characterized with the help of NMR, HRMS, UV and CV studies.

8.2.2 Optical properties

The UV-Visible absorption spectra of these **OD** dyes measured in ethanol are displayed in Figure 8-1(a) and the related photophysical data are summarized in Table 8-1. The characteristic features of the absorption spectra are composed of two broad peaks in the range of 260-500 nm. The bands at the wavelength below 400 nm are attributed to the π - π^* transition of the conjugated molecules, and that in the longer wavelength region (480-600 nm) are accredited to intramolecular charge transfer (ICT) with π - π^* transition character respectively. The spectral coverage of these dyes follow the order of **OD3** > **OD2** > **OD1**, anticipating the phenomena of more extended π -conjugation displays lower energy absorptions and larger spectral coverage. The steady-state emission maxima also follows the similar trend as the absorption spectra with more π -conjugated molecules displaying red-shifted emission. The absorption spectra of all dyes adsorbed on a transparent TiO₂ film are depicted in Figure 8-1(b). Compared to the absorption spectra measured in ethanol, apparent bathochromic shifts and broadening of the peaks were observed for all the dyes. This bathochromic shifts after adsorption on TiO₂ might be due to the coordination of the carboxylate group to the surface of Ti⁴⁺, which lowers the π^* level of the organic dyes.^[12]

Table 8-1. Optical and Electrochemical data of OD dyes in EtOH.

Dye	$\lambda_{\text{abs}}/\text{nm}^a$ ($\epsilon/10^3\text{M}^{-1}\text{cm}^{-1}$)	$\lambda_{\text{em}}/\text{nm}^b$	E_{ox}/V^c	$E_{(0,0)}/\text{eV}^d$	$E_{\text{ox}}^*/\text{V}^e$
OD1	364 (25.4), 281 (18)	473	1.14	3.00	-1.86
OD2	375 (24.3), 299 (23)	475	1.31	2.91	-1.60
OD3	406 (32), 289 (13)	535	1.36	2.72	-1.36

^aAbsorption maximum of dyes in EtOH, ^bEmission maximum measured in EtOH by exciting at lower energy band, ^cFirst oxidation potentials *vs.* NHE determined by differential pulse voltammetry in THF and referenced to a ferrocene redox couple, ^d $E_{(0,0)}$ values were estimated from the intersection of the absorption and emission spectra. ^ereduction potentials approximated from E_{ox}^* and $E_{(0,0)}$.

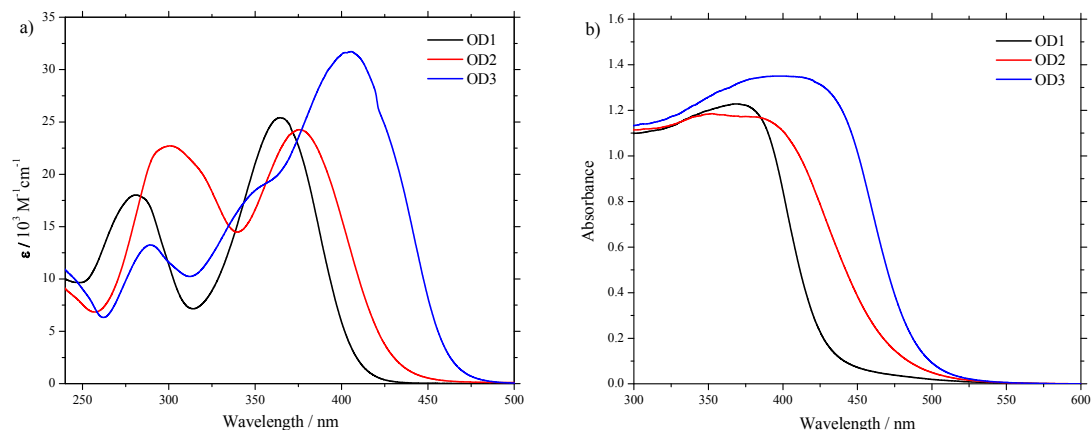


Figure 8-1. a) Absorption spectra measured in EtOH and b) absorption spectra measured with dyes adsorbed on TiO_2 surface.

The amount of dye loadings on the TiO_2 surface were estimated by measuring the absorbance of the dyes desorbed from the sensitized TiO_2 films after being immersed in 0.1M KOH solution in THF. The saturated dye densities for the **OD** dyes were found to be 367, 218 and 388 nmol cm^{-2} for **OD1**, **OD2** and **OD3** respectively. It is quite interesting that in spite of having lower dye loading, the dye **OD2** outperforms dye **OD1**. Although the difference in the dye loading is not considerable, performance of dye **OD3** is far superior to that of dye **OD1**.

8.2.3 Cyclic voltammetry results

The cyclic voltammograms of the dyes were acquired by differential pulse voltammetry and are shown in Figure 8-2. The relevant electrochemical data are summarized in Table 8-1. All of the dyes exhibit one oxidation potential, which is attributed to the oxidation of arylamine and decreases in the order **OD3** > **OD2** > **OD1**.

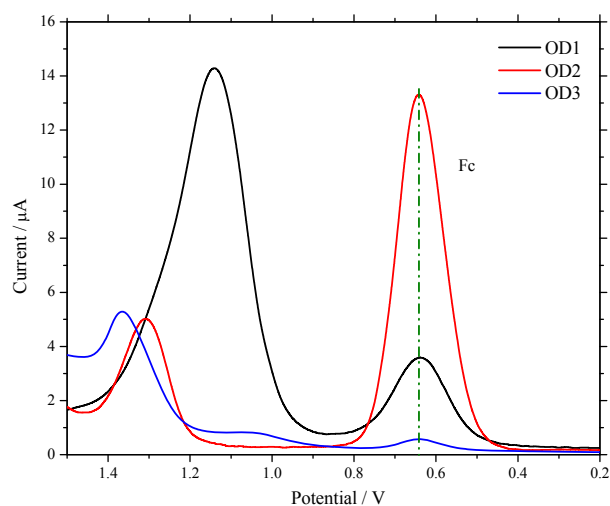


Figure 8-2. DPV spectra for OD dyes.

The excited state potential (E_{ox}^*) of the sensitizer was estimated from the difference between the first oxidation potential and the zero-zero excitation energy $E_{(0,0)}$, where the zero-zero excitation energy was estimated from the intersection of absorption and emission spectra. The systematic energy level diagram for the studied **OD** dyes is displayed in the Figure 8-3. As evident from the energy level diagram, the increase in the π -conjugation results in the smaller HOMO and LUMO band gaps and consequently red-shifting the absorption. The more negative excited state oxidation potential of the **OD** dyes (E_{ox}^* , -1.36 to -1.86 V vs. NHE) than the conduction band-edge level of the TiO_2 electrode (-0.5 V vs. NHE), ensures effective electron injection into the conduction band of TiO_2 . The first oxidation potential of the dyes is more positive than that of I^-/I_3^- redox couple (0.4 V vs. NHE), indicating that regeneration of the dyes (1.14 to 1.36 V vs. NHE) is energetically favorable.

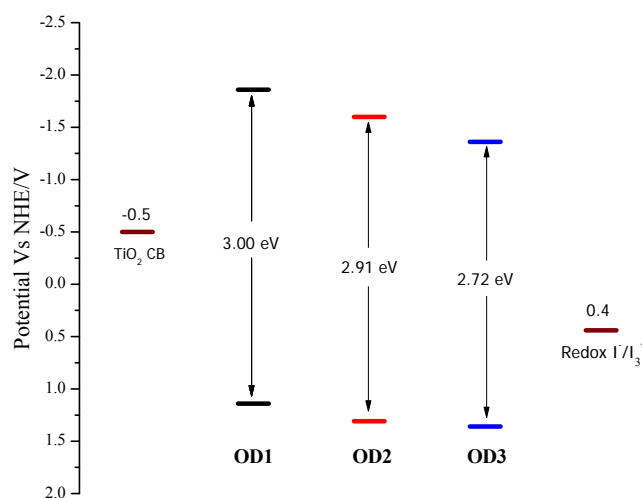


Figure 8-3. Energy level diagram for OD dyes.

8.2.4 DFT calculations

Theoretical studies based on density functional theory (DFT) calculations using Gaussian 09 program at the B3LYP/6-31G* level of theory were carried out for optimization of the **OD** dyes to gain an insight into the geometric electronic structures. The frontier molecular orbitals for the three dyes are depicted in Figure 8-4. It is clearly seen from the Figure 8-4 that the electron density of the highest occupied molecular orbitals (HOMO) is predominantly localized on the triphenylamine donor moiety and diffusively distributed over the π -conjugation onto the oxadiazole ring. In contrast, the electron density of the lowest unoccupied molecular orbitals (LUMO) is extended over the oxadiazole and acceptor acid groups. It is noteworthy from the frontier MOs that the dye **OD2** and **OD3** exhibit more localized electron density distribution

than dye **OD1** which denotes a prominent charge separation upon photoexcitation. This effective electron density redistribution should assist effective electron injection from the excited state of dye to the conduction band of TiO₂. This elusive difference, along with other photophysical parameters, may contribute to the superior performance of dyes **OD2** and **OD3** over dye **OD1**.

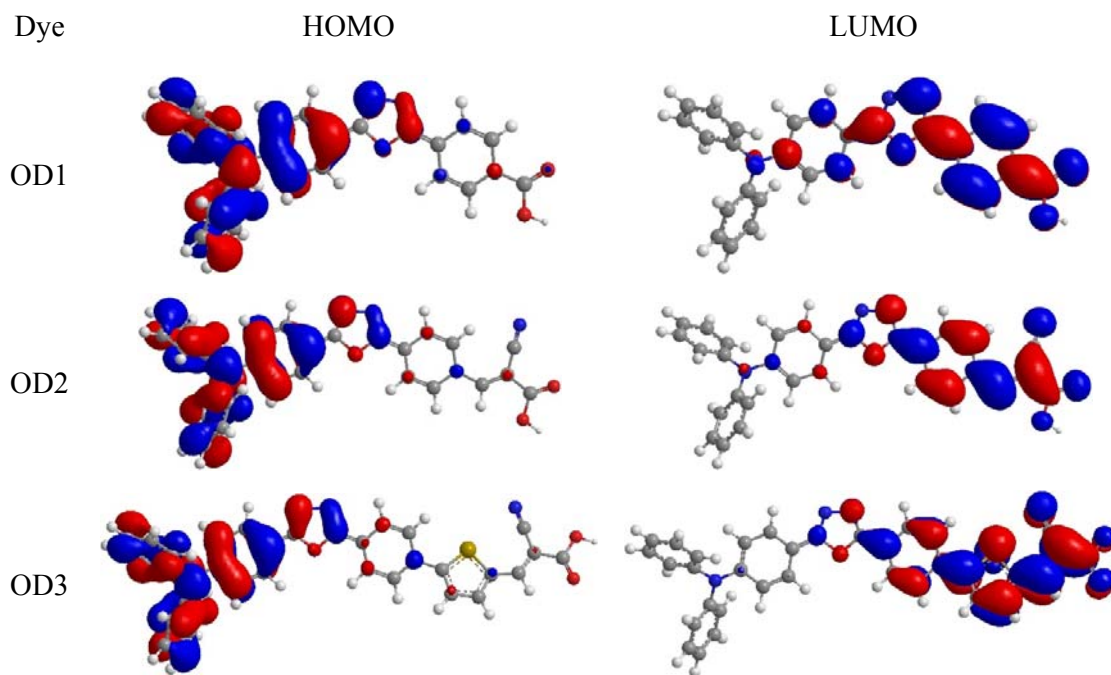


Figure 8-4. Selected frontier molecular orbitals of OD dyes.

Time-dependent density functional theory (TD-DFT) calculations were also performed at B3LYP functional and the 6-31G* basis set using Gaussian 9 software. For all the dyes, the lowest energy transition ($S_0 \rightarrow S_1$) is about 99% of the HOMO \rightarrow LUMO transition. Whereas the $S_0 \rightarrow S_2$ transition for all the OD dyes mainly composed of the HOMO \rightarrow LUMO+1 transition, thus confirming its donor to acceptor charge-transfer character. Significantly, TD-DFT calculations also revealed a higher molecular dipole moment (11.54 D) for the **OD3** than for **OD2** (8.87 D) and **OD1** (6.83 D) dyes as shown in Table 8-2. The higher dipole moments are beneficial to facilitate efficient intramolecular photoinduced electron transfer.

Table 8-2. Calculated TD-DFT composition in terms of frontier molecular orbitals, excitation energy, the oscillator strengths and the dipole moments of OD dyes.

Dyes	State	Composition (%)	E (eV)	(nm)	f	Dipole Moment (D)
OD1	S1	H \rightarrow L (99)	2.74	453.26	0.4481	

	S2	H-1→L (4) H→L+1 (93)	3.61	343.75	0.6135	6.83
OD2	S1	H→L (99)	2.14	579.61	0.331	
	S2	H-1→L (47) H→L+1 (52)	3.29	376.86	1.3325	8.87
OD3	S1	H→L (99)	2.18	569.15	0.2627	
	S2	H-1→L (71) H→L+1 (27)	3.04	408.35	1.6419	11.54

H=HOMO, L=LUMO, H-1=HOMO-1, L+1=LUMO+1.

8.2.5 Photovoltaic studies

The I-V curves and the action spectrum of the incident photon-to-current conversion efficiency (IPCE) for the DSSCs based on the dyes studied in this work under AM 1.5 illumination are depicted in Figure 8-5. The best device performance and the relative data of the assembled DSSC devices are summarized in Table 8-3. Chenodeoxycholic acid (CDCA) is used as a co-adsorbent to reduce the molecular aggregation. The detailed conditions for device preparation are given in the experimental section. The term J_{sc} refers to short-circuit current, V_{oc} to open-circuit voltage, FF to fill factor and η to the power conversion efficiency. The overall power conversion efficiencies are in the order of **OD1** (0.8%) < **OD2** (1.76%) < **OD3** (2.72%).

Table 8-3 Photovoltaic properties of devices with OD dyes.

Dye	J_{sc} (mA cm ⁻²)	V_{oc} (V)	FF (%)	η (%)
OD1	1.82	0.62	71	0.80
OD2	3.88	0.64	71	1.76
OD3	6.87	0.58	68	2.72

The inferior performance of the dye **OD1** compared to other dyes is due to the lower short-circuit current of 1.82 mA cm⁻². Although it has higher dye loadings than the other **OD** dyes, molecular aggregation on the TiO₂ surface might be the reason for its lower currents. It is observed from the absorption spectrum and the I-V curves that, higher the π -conjugation, higher is the photocurrent density and consequently higher is the overall conversion efficiency. Higher J_{sc} of 3.88 mA cm⁻² and V_{oc} of 0.64 V obtained for device based on dye **OD2** compared to the dye **OD1** resulted in its superior photovoltaic performance of 1.76%. The best overall photon-to-current conversion efficiency (η) of 2.72% was observed for dye **OD3**, with J_{sc} of

6.87 mA cm⁻², V_{oc} of 0.58 V and fill factor of 68. The V_{oc} of the dye **OD3** is least among all three dyes indicating that the charge recombination might be higher for this dye.

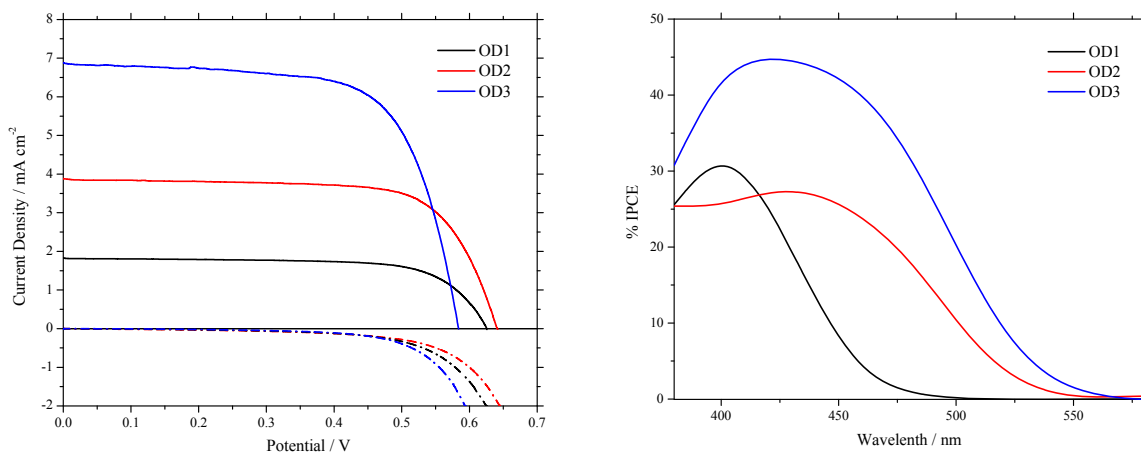


Figure 8-5. a) I-V curves and b) IPCE spectrum for the devices based on **OD** dyes.

The trend of the IPCE spectra is consistent with the I-V curves. The broad spectral coverage of the IPCE plots are consistent with the trend of the π -conjugation of the organic dyes, matching well with the absorption spectra of dyes adsorbed on the TiO₂ surface. The device based on dye **OD3** produced maximum IPCE values of approximately 45% at 450 nm and maintained 40% or higher in the range of 400 nm to 460 nm. The IPCE value for dye **OD1** is around 30% at 400 nm and that for dye **OD2** is 25% at 400 nm but it covers broader area up to 550 nm. The higher IPCE of the DSSC based on dye **OD3** is probably due to the combined effects of a particularly high surface dye loading, a large driving force from the LUMO level of the dye to the conduction band edge of TiO₂, a high molar extinction coefficient, and the efficient charge separation that led to a greater electron injection efficiency and higher light-harvesting efficiency (LHE) than DSSCs based on the other **OD** dyes.

8.2.6 Electrochemical Impedance Spectroscopy results

Faster charge recombination from the TiO₂ film with the oxidized electrolyte corresponds to the larger dark currents. The I-V curves of the devices under dark conditions are displayed in Figure 8-5(a) and the values decrease in the order of **OD2** > **OD1** > **OD3**. This trend is roughly consistent with the electrochemical impedance studies. Electrochemical impedance spectra (EIS) was measured in the dark as well as under the illumination conditions to explicate the information about electron injection and the recombination at the TiO₂/dye/electrolyte

interface. The Nyquist plot recorded in the dark under a forward bias of -0.55 V are depicted in Figure 8-6(a).

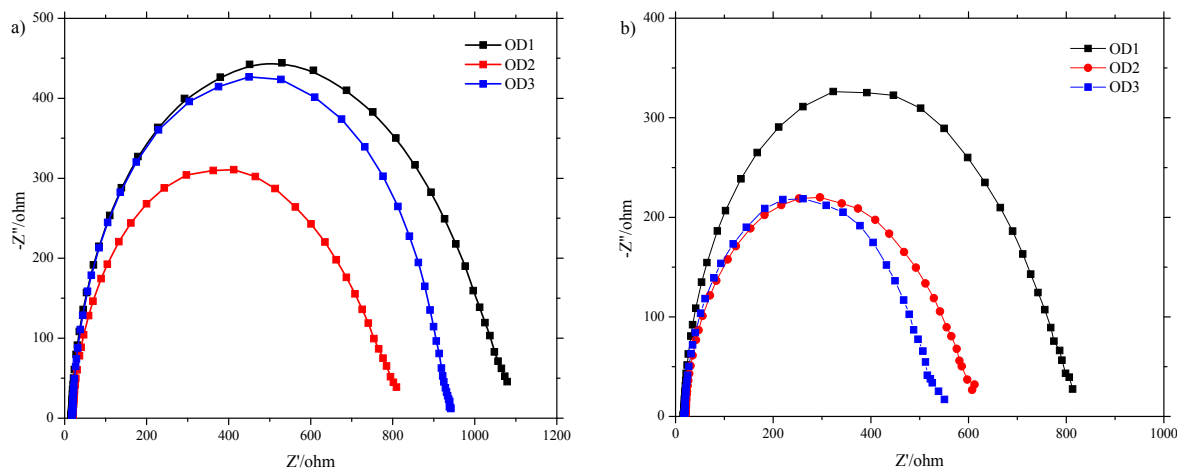


Figure 8-6. EIS spectra (Nyquist plots) a) under dark and b) under illumination of DSSCs based on OD dyes.

For all the dyes one semicircle is observed which is related to the recombination resistance between the TiO_2 surface and the oxidized electrolyte. The radius of the semicircle is inversely proportional to the recombination resistance i_e . Larger the semicircle smaller is the recombination resistance. From Figure 8-6(a), it is observed that the recombination rate decrease in the order of **OD1** > **OD3** > **OD2**. As presented in Figure 8-6(b), under illumination condition with applied open-circuit voltage, the intermediate frequency semicircle in the Nyquist plot reflects charge-transfer resistance at the semiconductor-dye-electrolyte interface. The radius of the semicircle decrease in the order of **OD1** > **OD2** > **OD3** indicating that the dye **OD3** has least electron transport resistance which implies higher electron transport than the dyes **OD2** and **OD1**. This trend is consistent with the DSSC performance of the **OD** dyes.

8.3 Conclusion

Three metal-free dipolar organic dyes (**OD1-OD3**) with D- π -A structure, having oxadiazole moiety as an electron transporter incorporated within the π -framework, with triphenylamine donor and carboxylic acid or cyanoacrylic acid as acceptor were designed and synthesized for DSSC application. DFT and TD-DFT studies confirm the bipolar nature of these dyes suggesting that these dyes can serve as efficient sensitizers in DSSCs. The electrochemical studies shown that the HOMO-LUMO potentials for these dyes were well matched with TiO_2 conduction band and the electrolyte redox potential. The photovoltaic experiments revealed

that the dye with oxadiazole linker incorporated with thiophene exhibit superior photon-to-current conversion efficiencies. This study expands the scope to use oxadiazole ring as electron transporter in DSSCs which might be beneficial for future design of efficient organic sensitizers.

8.4 Experimental section

8.4.1 General Techniques and Materials

All chemicals were obtained from commercial sources and used as received without further purification. All the reactions were carried out under nitrogen atmosphere. Solvents used in reactions were dried by PureSolv MD 5 system (Innovative Technology, Inc). Flash chromatography was carried out by using silica gel (40-63 μm , Merck). Analytical TLC was performed on Merck silica gel plates. ^1H and ^{13}C NMR spectra were recorded on a Bruker Avance 400 FT spectrometer. NMR samples were prepared in CDCl_3 and $\text{DMSO-}d_6$ as *d*-solvents and chemical shifts were reported in δ scale. The standard abbreviations s, d, t, q, m and bs refer to singlet, doublet, triplet, quartet, multiplet and broad singlet respectively. Coupling constant (*J*) values are reported in Hertz. The ESI ion trap mass spectra were measured by a Finnigan MAT LCQ mass spectrometer. The HR-FAB spectra were conducted on a JMS-700 double focusing mass spectrometer. Transmittance and reflection UV–visible absorption spectra of the oxasmaragdyrins in THF and adsorbed on TiO_2 electrodes, respectively, were recorded on a JASCO V-670 UV-vis/NIR spectrophotometer. Steady-state fluorescence spectra were acquired by using a Varian Cary Eclipse fluorescence spectrophotometer. The cyclic voltammetry measurements of all oxasmaragdyrins were carried out on CHI 621B electrochemical analyzer (CH Instruments, Austin, TX, USA) in degassed THF containing 0.1 M tetrabutylammonium hexafluorophosphate (Bu_4NPF_6) as the supporting electrolyte. The cell assembly consists of a glossy carbon as the working electrode, a silver wire as the pseudo-reference electrode, and a platinum wire as the auxiliary electrode. The scan rate for all measurements was fixed at 50 mV/sec. A ferrocene $^{+1/0}$ redox couple was used as the internal standard and the potential values obtained in reference to the silver electrode were converted to the vacuum scale. The density functional theory (DFT) and time-dependent density functional (TD-DFT) calculations were performed with Gaussian 09 package to study the electron distribution of the frontier molecular orbitals and the photoexcitation transitions. All ground state geometries of oxasmaragdyrins Sm-BR $_2$ were optimized in the gas phase by the hybrid B3LYP functional and the 6-31G basis set, and the TD-DFT calculation were based

on the same functional and basis set.^[13] The molecular orbitals were visualized by the Chemoffice software.

8.4.2 Syntheses

The intermediate oxadiazole compounds (4)-(6) were synthesized by following literature procedures with slight variations.^[3]

4-Cyanotriphenylamine (2): A mixture of *N,N*-diphenylaminobenzaldehyde (1.5 g, 5.49 mmol), hydroxylamine hydrochloride (0.46 g, 6.62 mmol), acetic acid (1.13 g, 18.83 mmol), pyridine (0.65 g, 8.21 mmol) and DMF (4 ml) was stirred and heated at 150 °C for 2.5 h. The product was purified by column chromatography (developing solvent: toluene) and recrystallized from *n*-hexane. Yield 1.28 g (86%). ¹H NMR (400 MHz, CDCl₃) δ: 6.96 (d, 2H, *J* = 8.76 Hz; Ph), 7.16 (m, 6H, Ph), 7.33 (t, 4H, *J* = 7.80 Hz; Ph), 7.41 (d, 2H, *J* = 8.80 Hz; Ph) ppm; ¹³C NMR (100 MHz, CDCl₃) δ: 102.50, 119.70, 125.13, 126.17, 129.78, 133.17, 145.97, 151.61 ppm; HRMS-FAB+: *m/z* calcd for C₁₉H₁₄N₂: 270.1157, found 270.1161 [M]⁺.

4-Tetrazolyltriphenylamine (3): A mixture of 4-cyanotriphenylamine (**2**, 0.7 g, 2.59 mmol), sodium azide (2.7 g, 41.5 mmol), ammonium chloride (2.22 g, 41.5 mmol), and dry DMF (20 ml) was refluxed for 24 h. The cooled solution was then added to aqueous hydrochloric acid. The precipitate was collected and washed with water. Recrystallization from toluene gave the desired product as creamy solid (0.49 g, 60%). ¹H NMR (400 MHz, CDCl₃) δ: 7.10 (d, 2H, *J* = 8.20 Hz; Ph), 7.17 (d, 6H, *J* = 7.40 Hz; Ph), 7.38 (t, 4H, *J* = 7.50 Hz; Ph), 7.97 (d, 2H, *J* = 8.16 Hz; Ph) ppm; ¹³C NMR (100 MHz, CDCl₃) δ: 117.92, 122.27, 125.34, 126.53, 129.11, 130.66, 147.86, 151.53, 206.21 ppm; HRMS-ESI: *m/z* calcd for C₁₉H₁₄N₅: 312.1254, found 312.1249 [M-H]⁻.

Methyl-4-(5-(4-(diphenylamino)phenyl)-1,3,4-oxadiazol-2-yl)benzoate (4): 4-tetrazolyl triphenyl amine (**3**, 500 mg, 1.6 mmol) and methyl-4-(chlorocarbonyl) benzoate (476 mg, 2.4 mmol) were mixed with pyridine (10 ml). The resulting mixture was refluxed under N₂ for 12 h. After the completion of reaction the solvent was evaporated and the crude product was purified by column chromatography to get the desired compound as faint yellow solid. (536 mg, 75%). ¹H NMR (400 MHz, CDCl₃) δ: 3.96 (s, 3H, OCH₃), 7.14 (m, 8H, Ph), 7.33 (t, 4H, *J* = 7.78 Hz; Ph), 7.94 (d, 2H, *J* = 8.68 Hz; Ph), 8.18 (s, 4H, Ph) ppm; ¹³C NMR (100 MHz, CDCl₃) δ: 52.40, 115.51, 120.85, 124.50, 125.75, 126.62, 127.89, 128.11, 129.60, 130.20, 132.50, 146.51, 151.17, 163.17, 165.08, 166.13 ppm.

4-(5-(4-(diphenylamino)phenyl)-1,3,4-oxadiazol-2-yl)benzaldehyde (5):

4-tetrazolyltriphenyl amine (**3**, 500 mg, 1.6 mmol) and 4-formylbenzoyl chloride (1 g, 5.9 mmol) in pyridine (15 ml) were refluxed under N₂ for 18 h. After completion of reaction, the solvent was removed under vacuum and the crude product was extracted with DCM, dried over MgSO₄ and concentrated. The crude product was purified by flash chromatography using DCM as eluent to get the titled compound as yellow solid (420 mg, 62%). ¹H NMR (400 MHz, CDCl₃) δ: 7.14 (m, 8H, Ph), 7.33 (t, 4H, *J* = 7.78 Hz; Ph), 7.94 (d, 2H, *J* = 8.68 Hz; Ph), 8.03 (d, 2H, *J* = 8.12 Hz; Ph), 8.29 (d, 2H, *J* = 8.12 Hz; Ph), 10.09 (s, 1H, CHO) ppm; ¹³C NMR (100 MHz, CDCl₃) δ: 115.32, 120.78, 124.57, 125.80, 127.23, 128.17, 129.12, 129.63, 130.21, 137.95, 146.48, 151.29, 162.96, 165.30, 191.24 ppm; HRMS-FAB+: *m/z* calcd for C₂₇H₂₀O₂N₃: 418.1556, found 418.1548 [M+H]⁺.

4-(5-(4-bromophenyl)-1,3,4-oxadiazol-2-yl)-N,N-diphenylaniline (6): A mixture of 4-tetrazolyltriphenylamine (500 mg, 1.6 mmol), 4-bromobenzoyl chloride (421 mg, 1.92 mmol) and dry toluene (20 ml) was stirred and heated under reflux for 8 h. After the mixture was cooled, the solvent was evaporated. The crude was subjected to column chromatography on silica gel with DCM as eluent to yield the title compound as yellow solid (458 mg, 61%). ¹H NMR (400 MHz, CDCl₃) δ: 7.14 (m, 8H, Ph), 7.33 (t, 4H, *J* = 7.86 Hz; Ph), 7.66 (d, 2H, *J* = 8.64 Hz; Ph), 7.93 (d, 2H, *J* = 8.80 Hz; Ph), 7.98 (d, 2H, *J* = 8.64 Hz; Ph) ppm; ¹³C NMR (100 MHz, CDCl₃) δ: 115.75, 120.98, 123.09, 124.47, 125.73, 126.73, 128.04, 128.16, 129.60, 132.35, 146.60, 151.11, 163.26, 164.80 ppm; HRMS-ESI: *m/z* calcd for C₂₆H₁₉N₃O₂Br: 468.0711, found 468.0701 [M+H]⁺.

5-(4-(5-(4-(diphenylamino)phenyl)-1,3,4-oxadiazol-2-yl)phenyl)thiophene-2-

carbaldehyde (7): A mixture of compound (**6**) (400 mg, 0.85 mmol) compound (**8**) (511 mg, 1.27 mmol) and Pd(PPh₃)₄ (104 mg, 0.09 mmol) in dry DMF was heated at 100 °C for 24 h. After the reaction was complete, the reaction mixture was extracted with water and NH₄Cl and then subjected to silica gel chromatography using DCM as eluent to get the titled compound as yellow solid (224 mg, 53%). ¹H NMR (400 MHz, CDCl₃) δ: 7.14 (m, 8H, Ph), 7.33 (t, 4H, *J* = 7.82 Hz; Ph), 7.52 (d, 1H, *J* = 4.00 Hz; β-thiophene), 7.78 (d, 1H, *J* = 3.96 Hz; β-thiophene), 7.82 (d, 2H, *J* = 8.44 Hz; Ph), 7.94 (d, 2H, *J* = 8.76 Hz; Ph), 8.18 (d, 2H, *J* = 8.44 Hz; Ph), 9.92 (s, 1H, CHO) ppm; ¹³C NMR (100 MHz, CDCl₃) δ: 115.71, 120.95, 124.49, 124.67, 125.06, 125.75, 126.88, 127.51, 128.08, 129.62, 135.76, 137.19, 143.36, 146.58, 151.12, 152.37, 163.33, 164.87, 182.72 ppm; HRMS-ESI: *m/z* calcd for C₃₁H₂₂O₂N₃S: 500.1433, found 500.1441 [M+H]⁺.

OD1: Methyl-4-(5-(4-(diphenylamino)phenyl)-1,3,4-oxadiazol-2-yl)benzoate (**4**, 150 mg, 0.34 mmol) was dissolved in THF/MeOH (3:1, v/v). To this aqueous KOH solution was added and the reaction mixture was refluxed under N₂ overnight. The solvent was removed under vacuum and crude is acidified with 1 N HCl. The precipitates were washed with water and collected by filtration to afford the desired product as pale yellow solid (135 mg, 92%). ¹H NMR (400 MHz, CDCl₃) δ: 7.14 (m, 8H, Ph), 7.33 (m, 4H, Ph), 7.95 (d, 2H, *J* = 8.84 Hz; Ph), 8.24 (m, 4H, Ph) ppm; ¹³C NMR (100 MHz, CDCl₃) δ: 115.42, 120.86, 124.58, 125.83, 126.77, 128.22, 128.57, 129.65, 130.86, 131.75, 146.54, 151.31, 163.15, 165.24, 169.78 ppm; HRMS-FAB+: *m/z* calcd for C₂₇H₂₀O₃N₃: 434.1505, found 434.1512 [M+H]⁺.

OD2: 4-(5-(4-(diphenylamino)phenyl)-1,3,4-oxadiazol-2-yl)benzaldehyde (300 mg, 0.72 mmol) and cyanoacetic acid (306 mg, 3.6 mmol) dissolved in acetic acid (10 ml) were condensed in the presence of ammonium acetate (5 mol%) for 12 h under N₂. After cooling to room temperature, the reaction mixture was poured into a crushed ice and solid obtained was washed thoroughly with water to remove excess of acetic acid and cyanoacetic acid. Finally, washed with hexane and 3% ethyl acetate/hexane to afford a fine yellow colored solid (280 mg, 80%). ¹H NMR (400 MHz, CDCl₃) δ: 7.03 (d, 2H, *J* = 8.28 Hz; Ph), 7.19 (m, 6H, Ph), 7.41 (t, 4H, *J* = 7.54 Hz; Ph), 7.99 (m, 3H, Ph), 8.07 (d, 2H, *J* = 8.00 Hz; Ph), 8.18 (d, 2H, *J* = 8.12 Hz; Ph) ppm; ¹³C NMR (100 MHz, CDCl₃) δ: 115.50, 116.35, 119.34, 120.62, 125.30, 126.20, 127.36, 128.66, 130.41, 130.51, 136.89, 146.21, 146.49, 151.14, 162.69, 163.41, 164.72 ppm; HRMS-ESI: *m/z* calcd for C₃₀H₁₉O₃N₄: 483.1457, found 483.1457 [M-H]⁺.

OD3: 5-(4-(5-(4-(diphenylamino)phenyl)-1,3,4-oxadiazol-2-yl)phenyl)thiophene-2-carbaldehyde (**7**) (50 mg, 0.1 mmol), cyanoacetic acid (43 mg, 0.5 mmol), ammonium acetate (12 mg) and acetic acid (10 ml) was heated at 100 °C for 12 h. The solution was cooled by pouring into crushed ice. The resulting solid was filtered, washed thoroughly with water, dried and further re-precipitated from dichloromethane by pouring into methanol to afford the titled compound as a reddish yellow solid (47 mg, 82%). ¹H NMR (400 MHz, CDCl₃) δ: 7.03 (d, 2H, *J* = 8.88 Hz; Ph), 7.19 (m, 6H, Ph), 7.41 (t, 4H, *J* = 7.84 Hz; Ph), 7.94 (d, 1H, *J* = 4.08 Hz; β-thiophene), 7.99 (d, 2H, *J* = 8.80 Hz; Ph), 8.04 (d, 2H, *J* = 8.48 Hz; Ph), 8.07 (d, 1H, *J* = 4.08 Hz; β-thiophene), 8.18 (d, 2H, *J* = 8.44 Hz; Ph), 8.54 (s, 1H, CH) ppm; ¹³C NMR (100 MHz, CDCl₃) δ: 115.00, 116.34, 120.12, 123.88, 124.82, 125.72, 126.48, 126.98, 127.45, 128.17, 129.93, 135.09, 135.69, 141.19, 145.99, 146.43, 150.61, 162.92, 163.38, 164.18 ppm; HRMS-ESI: *m/z* calcd for C₃₄H₂₁O₃N₄S: 565.1334, found 565.1339 [M-H]⁺.

8.4.3 Photovoltaic Measurements

TiO₂ photoanode films and Pt counter electrodes were purchased from Yingkou Opvtech New Energy Co. Ltd. Liaoning, China. The films, which were prepared by using the screen-printing method, were composed of a transparent layer (thickness $\approx 12 \mu\text{m}$), a scattering layer (thickness $\approx 4 \mu\text{m}$), and a working area of $0.4 \times 0.4 \text{ cm}^2$ and were used as received. The films were pretreated according to the following activation procedures before use: heating at 100 °C for 22 min, at 110 °C for 60 min, at 450 °C for 68 min, at 500 °C 60 min, at 250 °C for 60 min, cooling at 80 °C and keeping at 80 °C before immersion. The TiO₂ films were immersed in a $1 \times 10^{-4} \text{ M}$ solution of the dye **OD1** and **OD2** in EtOH for 6 h at 30 °C and dye **OD3** in EtOH for 1 h at 50 °C. A co-adsorbent (3 eq.) chenodeoxycholic acid (CDCA) was used in the same solution to reduce the molecular dye aggregation. The dye-sensitized TiO₂ films were washed with THF, dried in hot air, and used as the working electrode. To fabricate the DSSC device, the two electrodes were tightly clipped together into a sandwich-type cell that was spaced by a 40 μm film spacer. A thin layer of electrolyte, which contained 0.05 M I₂, 0.1 M lithium iodide (LiI), 0.6 M dimethyl-propyl-benzimidazole iodide (DMPII), and 0.6 M 4-tert-butylpyridine (TBP) in dry CH₃CN, was introduced into the space between the two electrodes. The Photoelectrochemical characterizations on the solar cells were performed by using an Oriel Class AAA solar simulator (Oriel 94043A, Newport Corp.). Photocurrent–voltage characteristics of the DSSCs were recorded with a potentiostat/galvanostat (CHI650B, CH Instruments, Inc.) at a light intensity of 100 mWcm^{-2} calibrated by an Oriel reference solar cell (Oriel 91150, Newport Corp.). The monochromatic quantum efficiency was recorded through a monochromator (Oriel 74100, Newport Corp.) under short-circuit condition. The intensity of each wavelength was in the range of 1 to 3 mWcm^{-2} . Electrochemical impedance spectra were recorded for DSSCs under illumination at an open-circuit voltage (V_{oc}) or in the dark at -0.55 V at room temperature. The frequencies explored ranged from 10 mHz to 100 kHz. The data was analysed using Zview software.

8.5 Reference

- [1] C. Adachi, T. Tsutsui, S. Saito, *Appl. Phys. Lett.* **1990**, *56*, 799-801.
- [2] C. Adachi, T. Tsutsui, S. Saito, *Appl. Phys. Lett.* **1990**, *57*, 531-533.
- [3] N. Tamoto, C. Adachi, K. Nagai, *Chem. Mater.* **1997**, *9*, 1077-1085.
- [4] W. Huang, H. Meng, W.-L. Yu, J. Gao, A. J. Heeger, *Adv. Mater.* **1998**, *10*, 593-596.

- [5] D. W. Lee, K.-Y. Kwon, J.-I. Jin, Y. Park, Y.-R. Kim, I.-W. Hwang, *Chem. Mater.* **2001**, *13*, 565-574.
- [6] Y. Tao, Q. Wang, Y. Shang, C. Yang, L. Ao, J. Qin, D. Ma, Z. Shuai, *Chem. Commun.* **2009**, 77-79.
- [7] Y. Liu, L. Zong, L. Zheng, L. Wu, Y. Cheng, *Polymer* **2007**, *48*, 6799-6807.
- [8] S. H. Mashraqui, S. Subramanian, A. C. Bhasikuttan, *Tetrahedron* **2007**, *63*, 1680-1688.
- [9] C. K. Kwak, C.-H. Lee, T. S. Lee, *Tetrahedron Lett.* **2007**, *48*, 7788-7792.
- [10] G. Zhou, Y. Cheng, L. Wang, X. Jing, F. Wang, *Macromolecules* **2005**, *38*, 2148-2153.
- [11] A.-F. Li, Y.-B. Ruan, Q.-Q. Jiang, W.-B. He, Y.-B. Jiang, *Chem. Eur. J.* **2010**, *16*, 5794-5802.
- [12] Z.-S. Wang, K. Hara, Y. Dan-oh, C. Kasada, A. Shinpo, S. Suga, H. Arakawa, H. Sugihara, *J. Phys. Chem. B* **2005**, *109*, 3907-3914.
- [13] M. J. Frisch, et al., *Gaussian 09 (Revision A.02)*

9. Concluding Remarks

Several porphynoids have proved their significance in DSSCs with moderate to high efficiencies such as Chlorins ($\eta = 8\%$) and Bacteriochlorins ($\eta = 6.6\%$), Porphyrins ($\eta = 12.7\%$), Phthalocyanines ($\eta = 6.1\%$), Subphthalocyanines ($\eta = 1.32\%$), Corroles ($\eta = 1.6\%$) and thiaporphyrins ($\eta = 0.19\%$). In this thesis we designed, synthesized and explored several core-modified porphyrins and expanded core-modified porphyrins for solar cell application. We carried out extensive photophysical and photovoltaic studies to optimize the DSSC performance of these dyes and finally bring out some conclusions for future molecular designs of efficient core-modified porphyrins.

✚ Three novel free-base porphyrins, **N4**, **N3S** and **N3O** were prepared and compared their photophysical and photovoltaic properties to study the effect of core-modification. Even though the heteroporphyrins observed bathochromic shift in the absorption and the onset reached 700 nm (near infrared region), the obtained efficiency order **N4** (3.66%) >>> **N3S** (0.22%) >> **N3O** (0.01%) underlined adverse effects of core perturbation on the photovoltaic properties of these porphyrins. The I-V curves suggested that the photocurrent density and the open-circuit voltage are the major factors in the substantial decrease in the performance of the porphyrins in DSSCs. The fluorescence lifetimes revealed that poor electron injection caused by rapid excited-state relaxation is the main reason for the poor performance of **N3O** dye.

✚ A series of mono- and di-carboxylate functionalized A₃B and A₂B₂ thiaporphyrins was prepared. The UV-Visible spectra of these thiaporphyrins displayed that ethynylphenyl linker effectively enhances the absorption wavelengths towards NIR region. DFT calculations shows that, higher π electron density is localized on the cyanoacrylic acid anchor in LUMO of **N3S-ECN** compared to other thiaporphyrins; consequently, more electrons are available in LUMO of the dye for injection into the conduction band of TiO₂. With aid of accurate molecular design, we were able to improve the overall photon-to-current conversion efficiency of thiaporphyrins from 0.2% for **N3S-ECA** to 1.69% for **N3S-ECN**. This is highest efficiency for thiaporphyrin-based DSSCs.

✚ The results from previous two chapters explicated that the performance of these free-base thiaporphyrins is confined within the limit of 2%. Inspired by this small success in the efficient molecular design, we diverted our focus to expanded core-modified porphyrins. Extensive literature survey expressed us that an expanded porphyrin has never been used

as the sensitizer for DSSCs. To uncover the potential of applying expanded porphyrins to DSSC studies, we prepared five novel boron chelated oxasmaragdyrins in just 3-4 steps with 18% overall yield. Without exhausted coupling reactions to add electron donating groups, the plain oxasmaragdyrin boron chelated complex has already reached 5.7% power conversion efficiency. These oxasmaragdyrins provide desired redox potentials, high absorption coefficients, high stability, and higher power conversion efficiencies suitable for an effective sensitizer in DSSCs. More importantly, broad absorption spreading the entire visible region and its lower energy Q band covering part of the NIR region make this class of compounds an optimistic candidate for being one of the future selections of porphyrin-sensitized solar cells.

- ✚ The encouraging results from the previous chapter inspired us to engineer the molecular design of these oxasmaragdyrins for improved performance. A series of eight novel oxasmaragdyrins decorated with different number and position of donor and anchor groups was synthesized and evaluated their performance as sensitizers in DSSCs. Although the substitution of electron donating groups and extension of π -conjugation through ethynylphenyl group obviously resulted in red shifted and broadened absorption wavelengths, it has insignificant effect on their photovoltaic performance. The reversed position and increased number of anchoring group also exhibited very minor influence on their DSSC outcomes. Among these dyes, one anchor dye **SM1** sensitized cell gave the finest DSSC performance with overall photon-to-current conversion efficiency of 4.36%, while the device made from two anchor dye **SM6** obtained efficiency of 2.33%. From these photovoltaic results it is clear that the molecular design of SM1 still prevails all other modification.
- ✚ Novel core-modified sapphyrins, substituted with mono- or di-carboxylate groups were synthesized and for the first time applied in dye-sensitized solar cells. Optical properties as well as density functional theory calculations suggests that these dyes were well suitable for the application as a sensitizer in DSSCs. The electrochemical results explained that the potential difference between the excited state oxidation potential and the conduction band of TiO₂ is not sufficient for effective electron injection, thus indicating that low electron injection is the major drawback of these dyes. Though the results were not satisfactory (0.01%), this strategy of applying novel expanded trithiasapphyrin dyes in DSSCs will serve as a useful guideline for future molecular designs of efficient expanded porphyrins dyes.

- ✚ Four novel regular porphyrins were prepared. Zinc porphyrins gave superior performance than their free-base analogs in terms of efficiency. The cyanoacrylic acid derivative N4ZnCN gave the best photovoltaic results with conversion efficiency of 3.52%. When we combined two individually poor free-base porphyrins with their corresponding zinc counterparts to construct a mixed porphyrin DSSC, significant enhancement in short circuit current and consequently in the overall photon to current conversion efficiency was observed. The mixture of cyano acrylic acid derivatives, achieved highest overall efficiency of 4.18%. We have shown that the co-sensitization of free-base porphyrins and their zinc complexes is an effective strategy to improve the photon to current conversion efficiency of the DSSCs.
- ✚ Three metal-free dipolar organic dyes (**OD1-OD3**) with D- π -A structure, having oxadiazole moiety as an electron transporter incorporated within the π -framework, with triphenylamine donor and carboxylic acid or cyanoacrylic acid as acceptor were designed and synthesized for DSSC application. DFT and TD-DFT studies confirm the bipolar nature of these dyes suggesting that these dyes can serve as efficient sensitizers in DSSCs. The electrochemical studies shown that the HOMO-LUMO potentials for these dyes were well matched with TiO₂ conduction band and the electrolyte redox potential. The dye **OD3** with oxadiazole linker incorporated with thiophene ring exhibit superior photon-to-current conversion efficiencies of 2.72%. This study expands the scope to use oxadiazole ring as electron transporter in DSSCs which might be beneficial for future design of efficient organic sensitizers.

We hope that the efficient molecular design for core-modified porphyrins and the pioneer work on expanded core-modified porphyrins with comparable photovoltaic performance with some of the porphyrinoids mention above shall provide new insights and inspire broad explorations on using diverse expanded porphyrins as NIR dyes for DSSCs or on developing new suitable assemblies to take full advantage of expanded porphyrins to absorb NIR/IR light.

Appendix 1: Publications

ARTICLE

Synthesis of Carboxylate Functionalized A₃B and A₂B₂ Thiaporphyrins and Their Application in Dye-Sensitized Solar Cells

Cite this: DOI: 10.1039/x0xx00000x

Sandeep B. Mane^{a, b} and Chen-Hsiung Hung^{a*}Received 00th January 2012,
Accepted 00th January 2012

DOI: 10.1039/x0xx00000x

www.rsc.org/

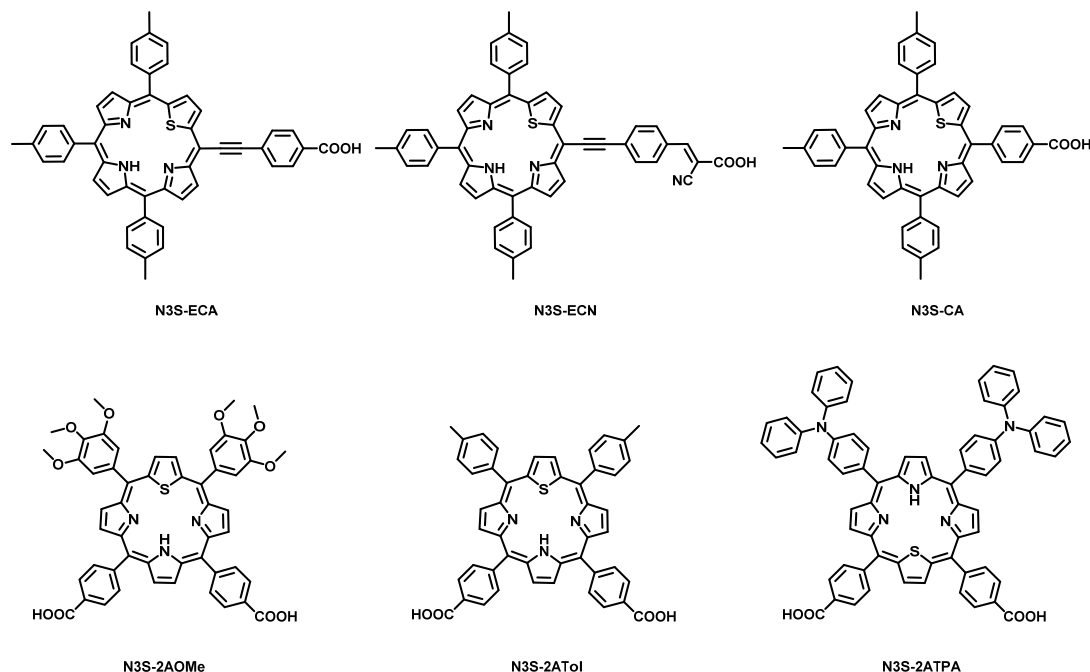
A series of novel A₃B and A₂B₂ thiaporphyrins consisting of mono or dual anchoring groups with different linkers has been synthesized and effectively applied in dye-sensitized solar cells (DSSCs). The presence of ethynylphenyl linker has pronounced effect on their optical, electrochemical and photovoltaic properties. The ethynylphenyl linker bathochromically shifted the absorption spectra. The density functional theory (DFT) studies revealed that attachment of ethynylphenyl linker through one of the *meso* position to the porphyrin core results in planar macrocycles which is essential for the active electron coupling of the porphyrin core with the anchor group in DSSCs. Although the dual anchoring groups can bind strongly to the TiO₂ surface, the presence of ethynylphenyl linker and moreover the electron withdrawing cyano group on the anchoring group proved to be the pivotal factors to achieve higher efficiency. Among these dyes, N3S-ECN having ethynylphenyl linker and a cyano acrylic acid as the anchor, achieved the highest efficiency of 1.69%, with $J_{sc} = 5.12 \text{ mA cm}^{-2}$, $V_{oc} = 0.49 \text{ V}$ and FF = 67%. To the best of our knowledge this is the highest efficiency obtained for thiaporphyrins.

Introduction

Developing renewable energy resources to replace the depleting fossil fuel reserves is the biggest challenge for civilization. Since the pioneer work from Grätzel *et al.* in 1991, dye-sensitized solar cell (DSSC) has been an apparent choice over conventional silicon solar cells owing to their affordable production cost, light fabrication and relatively high solar to current conversion efficiencies.¹⁻² DSSCs assembled with ruthenium complexes as sensitizers gave excellent performance with efficiencies of 11%.³ Although ruthenium dyes featured advantages like broad absorption, suitable energy levels and higher efficiencies, the drawbacks of moderate extinction coefficients, restricted availability, and higher purification cost hampers their practical application. Nature utilizes chlorophyll in plants as antennae to harvest light for solar energy conversion in photosynthesis. The porphyrins regarded as artificial chlorophylls, gained huge attention in recent years due to their strong absorption in visible region, high absorption coefficients, better thermal and photo-stability and appropriate energy levels. Moreover their optical and electrochemical properties can be fine-tuned through varying substituents on four *meso* and eight *beta* positions. A glimpse of better performance of porphyrins was displayed in 2007, when officer *et al.* reported *beta*-substituted zinc porphyrins with 7.1% efficiency.⁴ This result was further bettered in 2010, with a

meso-linked zinc porphyrin with a push-pull framework with 11% solar conversion efficiency.⁵ In 2011, Yella *et al.* reported a Zn(II) porphyrin having long alkoxy chains to wrap the porphyrin core to suppress the aggregation with a D- π -A structure showing remarkable power conversion efficiency of 12.3% when combined with an organic dye in Co(II/III) tris(bipyridyl)-based redox electrolyte under standard AM 1.5G simulated sunlight.⁶ Extensive literature survey on porphyrin sensitized solar cells revealed that the design of the sensitizers is restricted to the regular free-base or zinc porphyrins.⁷⁻¹⁰ From the above mentioned examples of regular porphyrin sensitizers, it is estimated that the near-infrared (NIR) absorption and panchromatic spectral character might enhance the solar to current conversion efficiency of DSSCs. The bathochromic absorption enhancement is achieved through extension of π conjugation of these regular porphyrins either by substitutions on *meso*- and *beta*-positions or fusion with aromatic chromophores.⁹

Core modification of the porphyrin core by replacing one or more pyrrolic nitrogens in porphyrin ring with heteroatoms like oxygen, sulphur, selenium and tellurium is an alternative and effective approach to adjust the photophysical properties of porphyrins.¹¹⁻¹² This core alteration induces interesting variations in photophysical properties of porphyrins without affecting the aromaticity of the macrocycle.¹³ Based on these improved optical properties, core-modified porphyrins have



Scheme 1. Chemical structures of A_3B and A_2B_2 thiaporphyrin dyes.

been widely used as complexation agents for metal ions in unusual oxidation states¹¹ and as photosensitizers in photodynamic therapy.¹⁴⁻¹⁹ A variety of mono-functionalized thiaporphyrins have been reported in the literature,²⁰⁻²¹ but the synthesis of carboxyl functionalized thiaporphyrins are quite rare.²² Although these thiaporphyrins possess interesting optical properties, surprisingly their use in DSSCs is very uncommon.²³ Following our interest in thiaporphyrins and their metal complexes,²⁴⁻²⁵ we have recently shown that these heteroporphyrins can be successfully applied as sensitizers in DSSCs.²⁶⁻²⁷ Thiaporphyrin N3S-ECA with an ethynylphenyl linker at a *meso* position and a carboxylic acid as the terminal anchoring group, obtained minute efficiency with iodine/triiodide redox electrolyte.²⁷ As an attempt to improve the properties of thiaporphyrins-based DSSCs, we explored some possibilities of structural modification on *meso* substituents of thiaporphyrin in order to get higher light harvesting efficiency (LHE) in NIR region.

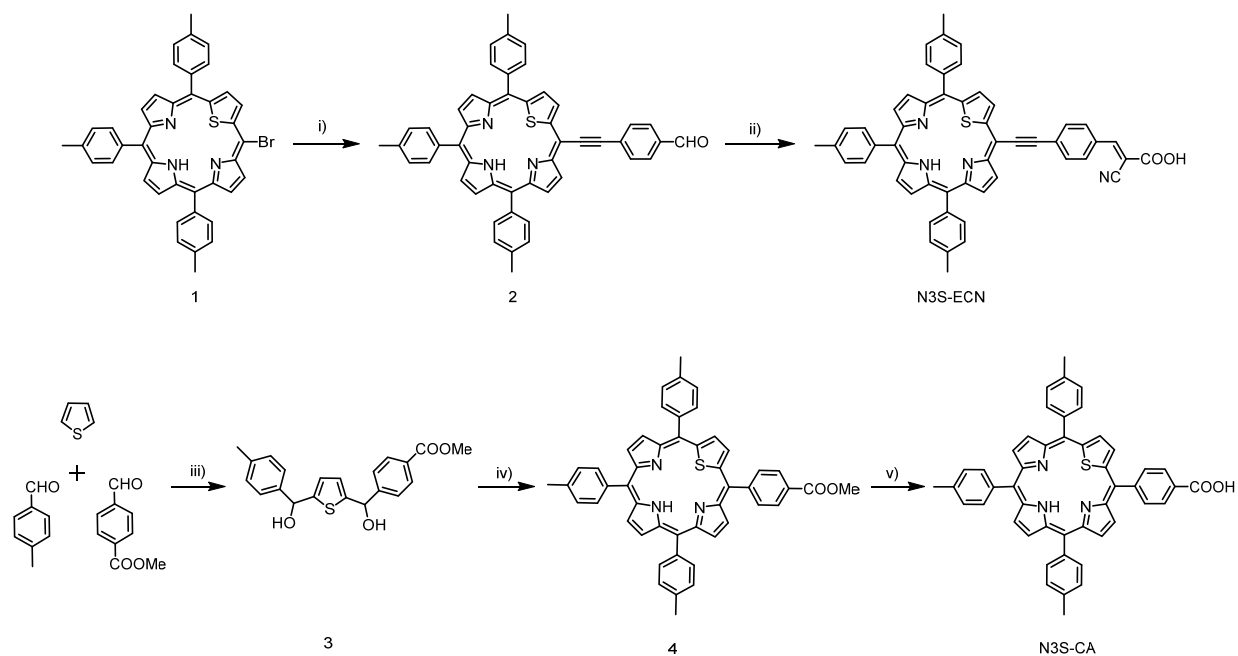
In this report, we designed and synthesized novel A_3B thiaporphyrins as shown in Scheme 1, with (N3S-ECA) or without (N3S-CA) ethynylphenyl linker along with using either simply carboxylic acid or cyanoacrylic acid (N3S-ECN) as the anchoring group. Also, A_2B_2 thiaporphyrins possessing two carboxylic acid anchors on *cis*-position in conjunction with donors like, 3,4,5-trimethoxy (N3S-2AOMe), tolyl (N3S-2ATol) and triphenylamine (N3S-2ATPA) are prepared for comparison. The effect of one anchor versus two anchors as well as the effect of ethynylphenyl linker and the electron withdrawing cyano group on the photophysical properties of the thiaporphyrins are studied. The systematic study, well supported by optical spectroscopy, CV measurements, DFT calculations, attenuated total reflectance Fourier transform

infrared spectroscopy (ATR-FTIR), and photovoltaic measurements revealed the marked significance of ethynylphenyl linker and electron-withdrawing cyano group to the overall photon conversion efficiencies.

Results and discussion

Syntheses

The A_3B thiaporphyrin dyes were synthesized according to the stepwise synthetic protocol depicted in Scheme 2. The synthesis of N3S-ECA was previously reported.²⁷ N3S-ECN was prepared from N3S-Br (1) and 4-ethynylbenzaldehyde through Sonogashira coupling in the presence of palladium catalyst. Compound (2) was further condensed with cyanoacetic acid following Knoevenagel protocol to obtain N3S-ECN. The presence of acrylic proton in the downfield region at 8.39 ppm in ¹H NMR spectrum of N3S-ECN confirmed the formation of cyano derivative. The presence of the cyano group is further confirmed by the presence of CN stretching frequency around 2224 cm^{-1} in the IR spectrum. In order to get N3S-CA, thiophene was treated with *p*-tolualdehyde and methyl-4-formylbenzoate in presence of *n*-BuLi to get unsymmetrical diol (3) as shown in Scheme 2. The mixed condensation of this unsymmetrical diol (3) with *p*-tolualdehyde and pyrrole in the presence of boron trifluoride-diethyl etherate as catalyst, followed by consequent oxidation by 2,3-dichloro-5,6-dicyanobenzoquinone (DDQ) gave monoester compound (4), which was further hydrolysed by aqueous solution of KOH to yield N3S-CA. The A_2B_2 thiaporphyrin dyes were synthesized according to the stepwise synthetic protocol depicted in Scheme 3.



Scheme 2. Synthesis of A₃B thiaporphyrins. Reagents and conditions: i) 4-ethynylbenzaldehyde, Pd₂(dba)₃, AsPh₃, THF/NEt₃; ii) cyanoacetic acid, piperidine, CHCl₃; iii) *n*-BuLi, TMEDA, Hexane/THF; iv) *p*-tolualdehyde, pyrrole, BF₃•OEt₂, DDQ, CH₂Cl₂; v) KOH_(aq), THF.

Thiophene was treated with corresponding aldehydes in the presence of *n*-BuLi to get the desired symmetrical thiophene diols. The mixed-condensation of these symmetrical diols with appropriate aldehydes and pyrrole in the presence of boron trifluoride-diethyl etherate as catalyst, followed by subsequent oxidation by DDQ gave diester compounds. The diester compounds were purified by column chromatography and subsequent hydrolysis by KOH_(aq) yielded analytically pure thiaporphyrins. The carbonyl stretching peaks around 1680-1700 cm⁻¹ in the final carboxylic acid substituted compounds are slightly shifted to lower energy compared with their ester derivatives due to the intermolecular hydrogen bonding.

Absorption and Emission properties

The UV-Visible peak positions of the *Soret* and Q-bands and the molar absorption coefficients (ϵ) of thiaporphyrins in THF are summarized in Table 1. The UV-Visible spectra of the studied porphyrins as displayed in Figure 1, shows typical free-base porphyrin features including a strong *Soret* band around 430 nm and four Q-bands around 510-700 nm. The absorption wavelengths of these thiaporphyrins depend mainly on the nature of the substituents. The introduction of ethynylphenyl linker at a *meso* carbon significantly shifts the absorption wavelength towards low energy region as shown in N3S-ECA and N3S-ECN compared to N3S-CA. The UV-Visible spectrum of N3S-ECN, having a cyanoacrylic acid terminal as the anchor shows the largest red-shift in the *Soret* band as well as Q-bands, extending the absorption onset beyond 700 nm. The electron donating triphenylamine substituents on *meso* positions in N3S-

2ATPA result in the broadening of *Soret* band as compared to N3S-2ATol and N3S-2AOMe. The extinction coefficient of N3S-CA is the highest amongst the thiaporphyrins. Although the ϵ is not high for N3S-ECN and N3S-2ATPA, the IPCE (incident photon-to-current efficiency) might be compensated by the broadened absorption and increased electron injection resulting in a higher overall conversion efficiency. (*vide infra*)

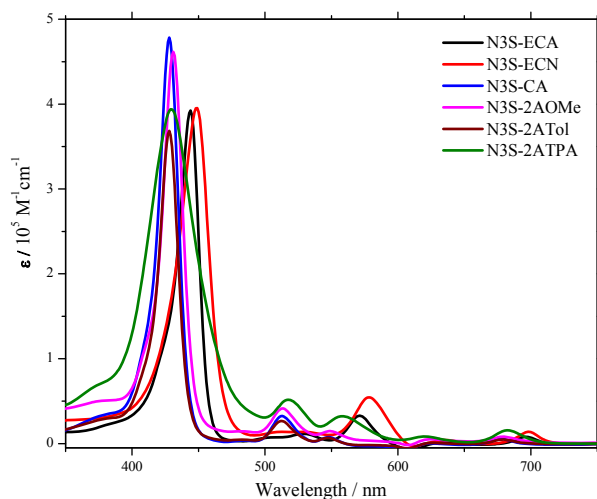
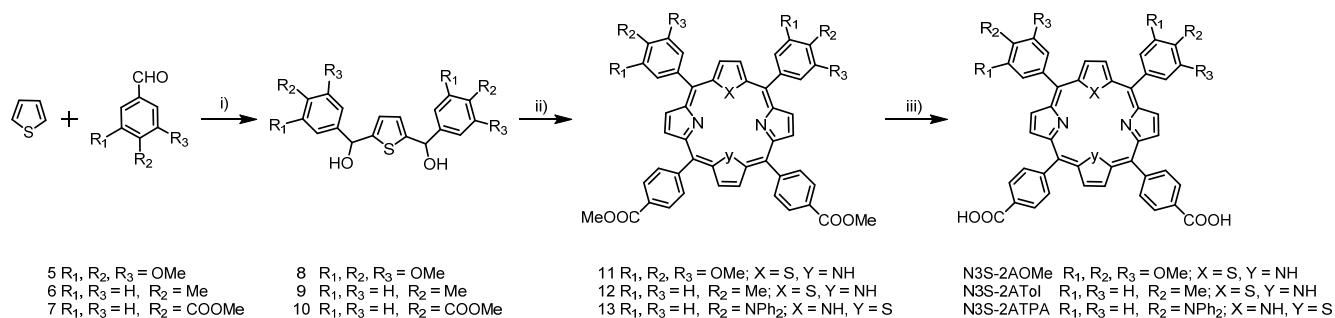


Figure 1. UV-Visible spectra of thiaporphyrin dyes in THF.

The absorption spectra of these thiaporphyrins as thin films were studied to understand their adsorption behaviour on TiO₂.



Scheme 3. Synthesis of A₂B₂ thiaporphyrins. Reagents and conditions: i) *n*-BuLi, TMEDA, hexane/THF; ii) aldehyde, pyrrole, BF₃·OEt₂, DDQ, CH₂Cl₂; iii) KOH(aq), THF.

Table 1. Optical and Electrochemical data of thiaporphyrin dyes

Dye	λ_{abs}^a [nm] ($\epsilon/10^3\text{M}^{-1}\text{cm}^{-1}$)	λ_{em}^b [nm]	E_{ox}^c [V]	$E_{(0,0)}^d$ [eV]	E_{ox}^{*e} [V]
N3S-ECA	444 (393), 530 (13), 571 (34), 634 (3), 697 (9)	702 777	0.96	1.77	-0.81
N3S-ECN	449 (396), 526 (15), 579 (55), 637 (5), 698(15)	705 779	0.97	1.77	-0.80
N3S-CA	428 (504), 513 (35), 548 (9), 625 (1), 678 (7)	684 751	0.91	1.82	-0.91
N3S-2AOMe	431 (438), 513 (39), 549 (14), 625 (5), 679(8)	688 755	0.94	1.81	-0.87
N3S-2ATol	428 (369), 512 (28), 547 (8), 624 (2), 679 (6)	686 754	0.93	1.82	-0.89
N3S-2ATPA	429 (394), 518 (52), 558 (32), 621 (8), 682 (16)	693 757	0.90	1.80	-0.90

^aAbsorption maximum of porphyrins in THF. ^bEmission maximum measured in THF by exciting at Soret band. ^cOxidation potentials approximated from E_{ox}^* and $E_{(0,0)}$. ^d $E_{(0,0)}$ values were estimated from the intersection of the absorption and emission spectra. ^eFirst reduction potentials vs. NHE determined for A₃B by cyclic voltammetry and for A₂B₂ by square wave voltammetry in THF and referenced to a ferrocene redox couple.

To obtain the absorption spectra on TiO₂ films, the films with thickness of approximately 3 μm were dipped in 0.1 mM THF solution of thiaporphyrins for 8 h at room temperature. The adsorption spectra were recorded by reflectance measurements using an integrated sphere and the results are displayed in Figure 2. The absorption spectra of dyes adsorbed on TiO₂ show significant broadening and slightly redshifts compared to its absorption spectrum in THF with threshold of absorption around 750 nm.²⁸⁻²⁹ Particularly, the UV-Visible spectrum of N3S-ECN/TiO₂ and N3S-2ATPA/TiO₂ shows obvious broadening and bathochromic shifts. This broadening in the UV-Vis spectra after adsorption on TiO₂ films suggests that

higher charge collection is possible in Q-band region which will ultimately help to attain higher efficiency when applied in DSSC. The steady-state fluorescence spectra of all the porphyrins were measured in THF by excitation at the Soret band and displayed in Figure 3.

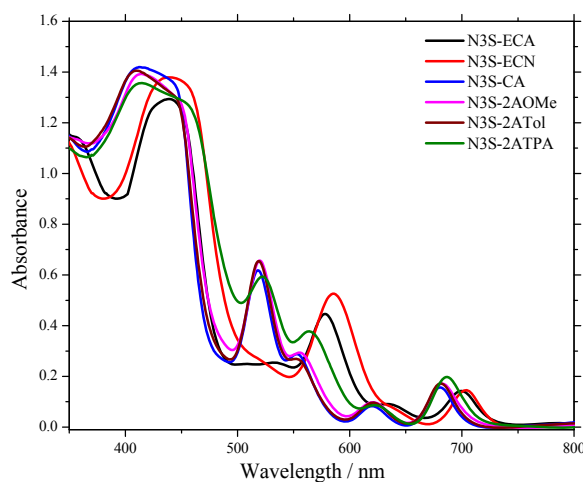


Figure 2. UV-Visible spectra of dyes/TiO₂

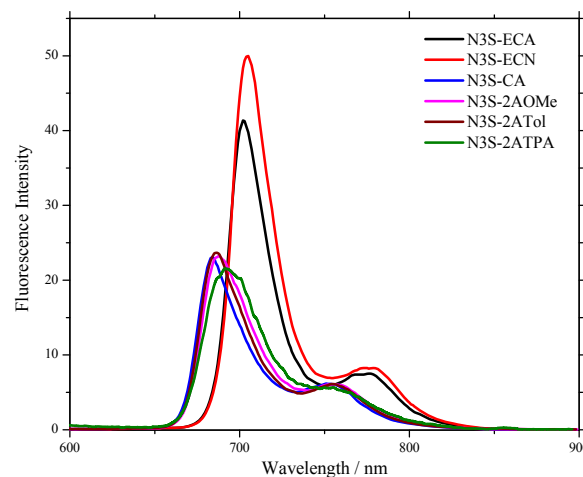


Figure 3. Fluorescence spectra of thiaporphyrin dyes in THF

It exhibited a trend similar to the absorption spectra, with a significant redshift upon addition of ethynylphenyl linker. Not only the redshift but also higher fluorescence intensity of N3S-ECA and N3S-ECN suggests that the conjugation through ethynylphenyl linker is more effective than direct phenyl substitution which might result in better electron communication between porphyrin core and the anchoring group.

Electrochemical studies

For the efficient electron injection into TiO₂ and faster regeneration of the oxidized dyes, appropriate tuning of highest occupied molecular orbitals (HOMO) with iodide/triiodide couple and the lowest unoccupied molecular orbitals (LUMO) with TiO₂ conduction band is necessary. The cyclic voltammetry measurements of all the thiaporphyrins were carried out in degassed THF containing 0.1 M [Bu₄N]PF₆ as the supporting electrolyte to obtain the first reduction potentials as depicted in Figure 4. The first reduction couples of N3S-ECA, N3S-ECN and N3S-CA show quasi-reversible redox processes under a scan rate of 50 mV/s while irreversible processes of the first reduction couple were observed for thiaporphyrins with dual carboxyphenyl substituents, N3S-2AOMe, N3S-2ATol and N3S-2ATPA. The reduction potentials for thiaporphyrins with a *meso* ethynylphenyl substituent are less negative than the rest thiaporphyrins. The zero-zero excitation energies, $E_{(0,0)}$ were calculated from the intersection of the normalized absorption and emission spectra at the Q (0,0) band and were found to be 1.77, 1.77, 1.82, 1.81, 1.82 and 1.80 eV for N3S-ECA, N3S-ECN, N3S-CA, N3S-2AOMe, N3S-2ATol and N3S-2ATPA porphyrins, respectively. The oxidation potentials were estimated from the first reduction potentials and the zero-zero excitation energies and are listed in Table 1.

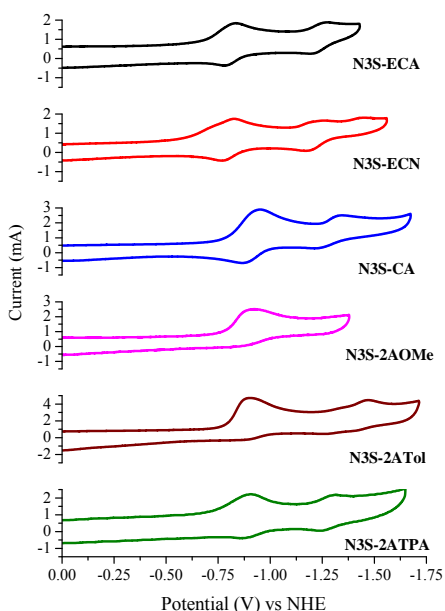


Figure 4. Cyclic Voltammograms of thiaporphyrin dyes in THF.

The systematic energy level diagram for the studied thiaporphyrins is displayed in the Figure 5. As evident from the energy level diagram, the ethynylphenyl substitution results in the smaller HOMO and LUMO band gaps and consequently red shifting the absorption for A₃B thiaporphyrins compared to those without an ethynylphenyl linkage. For A₂B₂ thiaporphyrins, the $E_{(0,0)}$ decreases with increasing electron donating ability of the thiaporphyrins. The LUMO of the thiaporphyrins are more negative than the TiO₂ conduction band (> 0.3 V) and thus ensure the adequate driving force for the electron injection from dye to the TiO₂ conduction band. The HOMO of all the porphyrins are more positive (> 0.5 V) than the redox electrolyte which confirms the efficient dye regeneration.

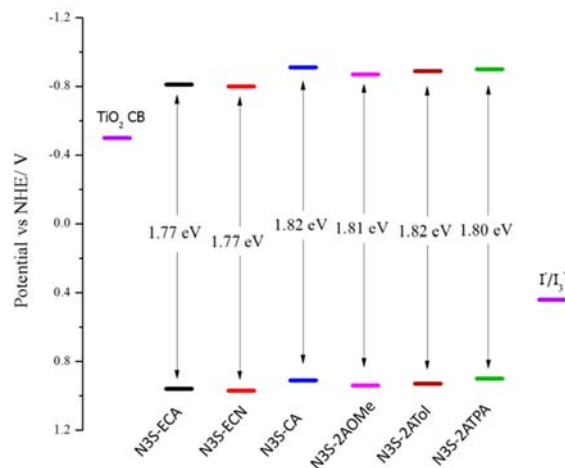


Figure 5. Energy level diagram for thiaporphyrin dyes under study.

DFT Calculation results

The ground state geometries of studied thiaporphyrins were optimized in the gas phase by DFT calculations using the hybrid B3LYP functional and the 6-31G basis set. As presented in Figure 6, result from the quantum chemical calculations show planar macrocycles for the studied thiaporphyrins. The planar ring ensures the effective electron coupling between the porphyrin ring and the anchoring group. The HOMO-LUMO energy gaps for all the thiaporphyrins are consistent with the absorption energy obtained from UV-Vis spectra. In N3S-ECA and N3S-ECN, the majority of the π electron density is localized on the porphyrin ring however a small portion is also extended over the anchoring group in HOMO. In the LUMO of N3S-ECA, the electron density is distributed equally on the porphyrin ring, the ethynylphenyl linker and carboxylic acid anchor. In the LUMO of N3S-ECN, more π electron density is localized on the ethynylphenyl linker and anchoring cyano acrylic acid group than on the porphyrin core, which highlights the electron withdrawing effect of the cyano group. For N3S-CA, N3S-2AOMe, N3S-2ATol and N3S-2ATPA, the majority of the electron density in HOMO as well as LUMO is located on the porphyrin ring suggesting that the charge transfer in

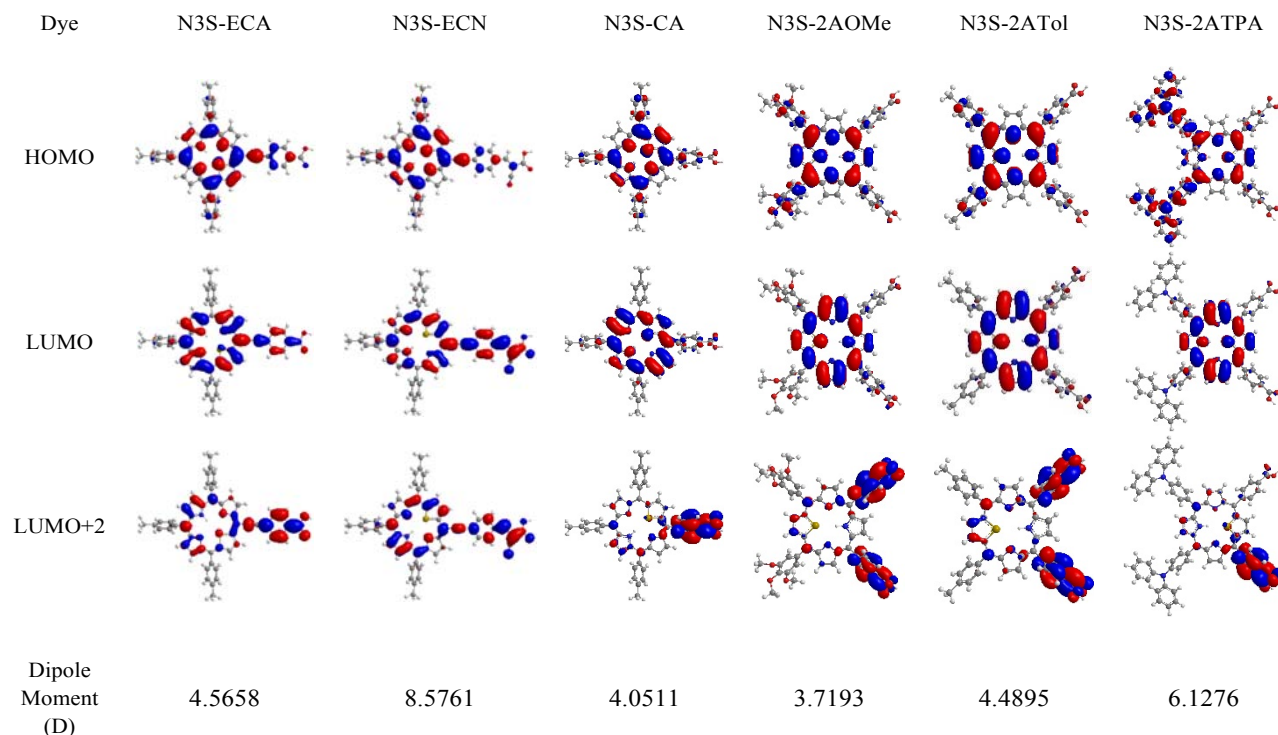


Figure 6. The molecular orbital diagrams for thiaporphyrin dyes.

these porphyrins might be less efficient than the *meso* ethynylphenyl substituted derivatives. Thus based on the theoretical calculations, it is evidenced that the ethynylphenyl linker is highly beneficial for an efficient electron transfer from the porphyrin core to the electron withdrawing anchoring group. This effective electron distribution, especially in the case of N3S-ECN facilitates efficient charge transfer from the excited state of the porphyrins to the TiO₂ conduction band. Interestingly in the LUMO+2, the electron density is extensively located on the carboxylic acid acceptor suggesting that the electron injection from higher excited states involving LUMO+2 might be possible. The dipole moments for thiaporphyrins under study were estimated from theoretical calculations and displayed in Figure 6. The dipole moments decrease in the order N3S-ECN > N3S-2ATPA > N3S-ECA > N3S-2ATol > N3S-CA > N3S-2AOMe. The trend of dipole moments is consistent with the overall conversion efficiency for these thiaporphyrins except for N3S-ECA. N3S-ECA might have higher dipole moment (4.56 D) than N3S-CA due the presence of ethynyl linker. The highest dipole moment of 8.57 D is observed for N3S-ECN, highlighting the effectiveness of electron withdrawing cyano acrylic anchoring group. The higher polarizability is advantageous to expedite intramolecular photoinduced electron transfer.

ATR-FTIR studies

ATR-FTIR spectroscopy measurements have been utilized as one of the imperative tools for probing the number and mode of carboxylate groups anchored onto TiO₂.³⁰⁻³³ The ATR-FTIR

spectra of neat thiaporphyrins contrasted with spectra of thiaporphyrins adsorbed on TiO₂. Comparative spectra of representative samples are shown in Figure 7. The spectra of neat N3S-CA and N3S-2ATol show strong $\nu(\text{C}=\text{O})$ stretches at 1687 and 1686 cm⁻¹, respectively, whereas $\nu_{\text{sym}}(\text{COO}^-)$ and $\nu_{\text{asym}}(\text{COO}^-)$ stretches are likely to be observed at about 1400 and 1600 cm⁻¹, respectively. In the comparative spectra of N3S-CA/TiO₂ and N3S-2ATol/TiO₂, the $\nu(\text{C}=\text{O})$ stretches completely disappeared, accompanied by a noticeable rise in the stretching peaks of $\nu_{\text{sym}}(\text{COO}^-)$ and $\nu_{\text{asym}}(\text{COO}^-)$ at about 1400 and 1600 cm⁻¹, respectively. The observation noted above indicates that for N3S-CA bonding on to TiO₂ is achieved through one carboxyl group while in N3S-2ATol, both *p*-carboxyphenyl groups at the *cis* positions are used for bonding onto TiO₂. Similar observations are found for the remaining thiaporphyrins, that is, N3S-ECA, N3S-ECN, N3S-2AOMe and N3S-2ATPA (ESI, Figure S1). Based on the above analyses, the single-anchoring mode for A₃B thiaporphyrins and dual-anchoring mode for A₂B₂ thiaporphyrins is proposed for the attachment of the porphyrins onto TiO₂.

Dye loading results

To better comprehend the adsorption behavior and measure the amount of adsorbed dye, we calculated the dye densities adsorbed on TiO₂ surface. The porphyrin densities (Γ) were determined by measuring the absorbance of porphyrins desorbed from the sensitized TiO₂ films after being immersed in 0.1 M KOH solution in THF.

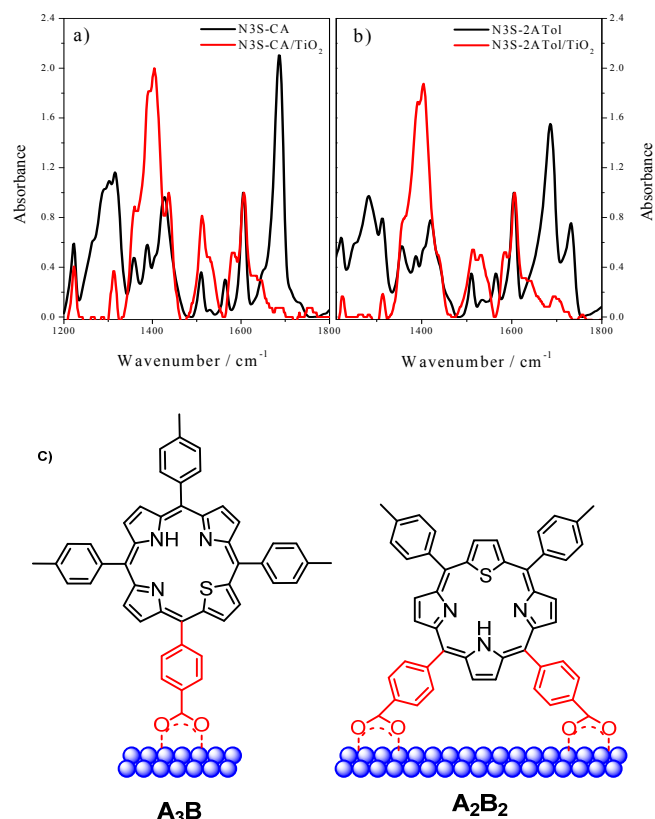


Figure 7. ATR-FTIR spectra of a) N3S-CA and N3S-CA/TiO₂ and b) N3S-2ATol and N3S-2ATol/TiO₂; the ATR-FTIR spectra of the thiaporphyrins on TiO₂ are normalized for comparison. c) Possible modes of attachment of thiaporphyrins onto TiO₂. For demonstration purpose only, the relative sizes of the molecules and nanoparticles are not correlated in real dimensions.

The saturated Γ values of A₃B thiaporphyrins under study were found as 141 ± 13 , 144 ± 11 and 100 ± 8 nmol cm⁻² for N3S-ECA, N3S-ECN and N3S-CA. Due to the ethynylphenyl substitution the thiaporphyrins N3S-ECA and N3S-ECN became planar compared to N3S-CA, giving dense packing on the TiO₂ surface resulting in higher dye loadings. The Γ values for A₂B₂ thiaporphyrins N3S-2AOMe, N3S-2ATol and N3S-2ATPA are found as 85 ± 5 , 116 ± 3 and 54 ± 8 nmol cm⁻², respectively. The dye loading values for A₂B₂ thiaporphyrins are inversely proportional to the steric bulkiness of the substituents. More bulky the substituent, less is the dye loading. Comprehensively, the dye loading amounts for A₂B₂ thiaporphyrins are lower than that of the A₃B thiaporphyrins. This can be explained with the help of dye attachment mode on the TiO₂ surface. As seen from the ATR-FTIR studies, A₂B₂ thiaporphyrins binds through dual anchoring mode while A₃B thiaporphyrins binds through the single anchoring carboxylic group to the TiO₂ surface. Thus A₂B₂ thiaporphyrins requires more space on the TiO₂ surface compared to the A₃B thiaporphyrins thus giving less dye loadings. It is obvious that higher dye loading is observed for N3S-ECA and N3S-ECN as

compared to other thiaporphyrins. The trends in the dye loading amounts mentioned above is not consistent with the efficiency with an exception of N3S-ECN, which has both, higher dye loading as well as higher efficiency. Regardless of low dye loading, N3S-2ATPA gave superior performance with higher current density.

Photovoltaic studies

Devices assembled with thiaporphyrin sensitizers using liquid electrolytes were tested under standard AM 1.5 illumination conditions. The photovoltaic parameters for the thiaporphyrins under study are summarized in Table 2 and the current-voltage characteristics of the devices are shown in Figure 8a.

Table 2: Photovoltaic parameters of thiaporphyrin dyes

Dye	J_{sc} (mA cm ⁻²)	V_{oc} (V)	ff (%)	η (%)
N3S-ECA	0.89	0.41	0.55	0.20
N3S-ECN	5.12	0.49	0.67	1.69
N3S-CA	1.29	0.48	0.64	0.40
N3S-2AOMe	0.67	0.45	0.57	0.17
N3S-2ATol	1.52	0.47	0.65	0.46
N3S-2ATPA	2.84	0.48	0.63	0.86

As evident from the I-V curve, the N3S-ECN give the best performance with the overall photon-to-current conversion efficiency of 1.69%, supported by short-circuit current (J_{sc}) of 5.12 mA cm⁻², open-circuit voltage (V_{oc}) of 0.49 V and fill factor (ff) of 0.67. It is well reinforced by DFT calculations and photophysical studies that the electron-withdrawing cyano acrylic acid terminal group enhances the charge transfer from porphyrin ring towards the anchoring group. Also due to the electron withdrawing cyano group, the LUMO level of N3S-ECN is closer to the TiO₂ conduction band compared to other thiaporphyrins, which may facilitate the electron injection. The higher electron injection from the dye to the TiO₂ conduction band is well reflected by the much higher short-circuit current for N3S-ECN. Although the V_{oc} values are all alike, other A₃B and A₂B₂ thiaporphyrins have low J_{sc} values and therefore, inferior power conversion efficiencies. Noticeably, N3S-ECA only obtained short-circuit current of 0.89 mA cm⁻², open-circuit voltage of 0.41 V and fill factor 0.55 corresponding to photon-to-current conversion efficiency of 0.20%. It suggests that carboxylic acid alone is not sufficient to pull more electrons from the porphyrin core towards the anchor which results in the lower performance of N3S-ECA. Interestingly N3S-CA, without a *meso* ethynylphenyl linker, achieved higher efficiency of 0.40% with short-circuit current of 1.29 mA cm⁻², open-circuit voltage of 0.48 V and fill factor of 0.64. The A₂B₂ thiaporphyrin, N3S-2ATol with two anchoring carboxylic groups obtained the overall photon-to-current conversion efficiency of 0.46% with photocurrent density of 1.52 mA cm⁻²,

open-circuit voltage of 0.47 V and fill factor of 0.65, which is slightly higher than single arm anchoring dye, N3S-CA. Among the thiaporphyrins, N3S-2AOMe gave the least conversion efficiency of 0.17% with short-circuit current of 0.67 mA cm^{-2} , open-circuit voltage of 0.45 V and fill factor of 0.57. This might be due to lower dye loadings as compared to other thiaporphyrins. Thiaporphyrin substituted with triphenylamine donor, N3S-2ATPA gave the highest efficiency among A_2B_2 thiaporphyrins. It obtained conversion efficiency of 0.86%, with $J_{sc} = 2.84 \text{ mA cm}^{-2}$, $V_{oc} = 0.48 \text{ V}$ and fill factor of 0.63. The trend of J_{sc} in this series can be understood from the variation of the IPCE spectra as displayed in Figure 8b and are in good agreement with the corresponding absorption spectra of the dyes on TiO_2 which display intense absorption bands in the *Soret* region.

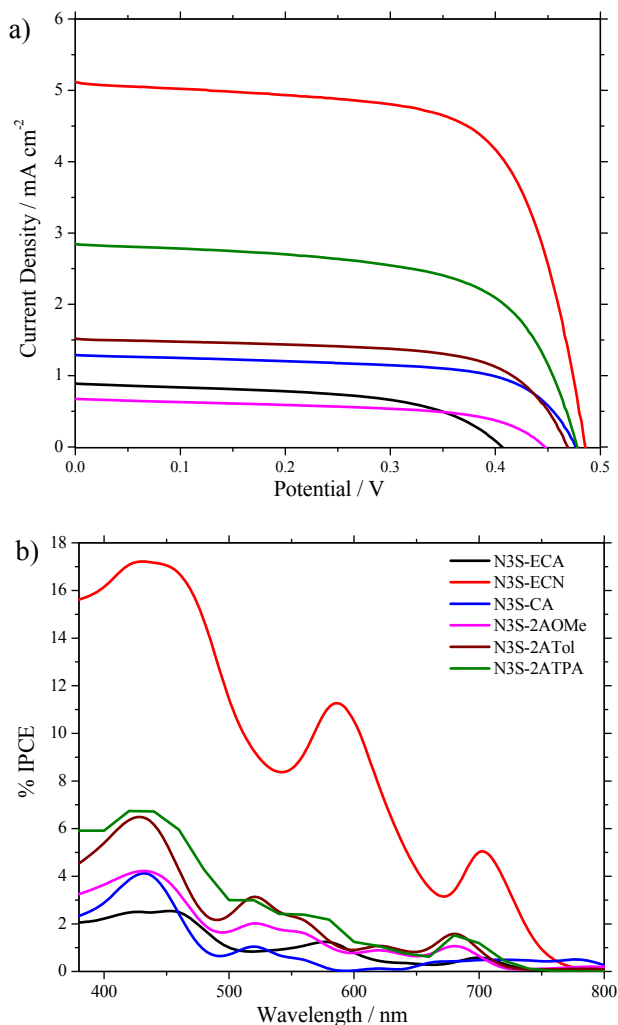


Figure 8. (a) I-V curves and (b) IPCE spectra for A_3B and A_2B_2 thiaporphyrin dyes.

The J - V curves under standard AM 1.5 G illumination are in qualitative agreement with the photo-action spectra of these thiaporphyrins. For N3S-ECN the IPCE maximum is around 17% in the *Soret* region, while around 12% in the 550-600 nm region and 6% in the 700 nm region. This indicates that N3S-

ECN shows panchromatic absorption behaviour covering whole visible region. This increased photon collection explicates the higher short-circuit current for this compound. In case of N3S-ECA and N3S-CA, there is insignificant IPCE in Q-band region which is one of the reasons for their inferior performance compared to N3S-ECN. Even though the IPCE values are higher for N3S-2AOMe than N3S-ECA and N3S-CA, the lower dye density triggered by bulky methoxy groups might be the reason for its low efficiency.

Electrochemical Impedance Spectroscopy results

To further study the correlation between the charge transfer processes and photovoltaic properties in the DSSC devices with different thiaporphyrin sensitizers, electrochemical impedance spectroscopy (EIS) was measured under illumination with an open-circuit voltage with a frequency range of 1 Hz to 1 kHz. Figure 9 shows the EIS Nyquist plots (i.e. the minus imaginary part of the impedance Z'' vs. the real part of the impedance Z' when sweeping the frequency) for DSSCs based on thiaporphyrins. One semicircle was observed for all the thiaporphyrins in the Nyquist plots. This semicircle corresponds to the charge transfer processes at the TiO_2 -dye-electrolyte interface i.e. electron transport resistance.³⁴ A smaller radius of the semicircle in the Nyquist plot corresponds to the lower electron transport resistance, in other words higher electron transfer. The radius of the semicircle in the Nyquist plot decreases in the order N3S-2AOMe > N3S-2ATol > N3S-CA > N3S-ECA > N3S-2ATPA > N3S-ECN. This trend is roughly consistent with the DSSC performance of the thiaporphyrin sensitizers. The DSSC based on N3S-ECN exhibited smaller interfacial charge transfer resistance at the dye- TiO_2 -electrolyte interface compared to other dyes indicating improved charge generation and transport, which is well reflected in its higher photocurrent density.

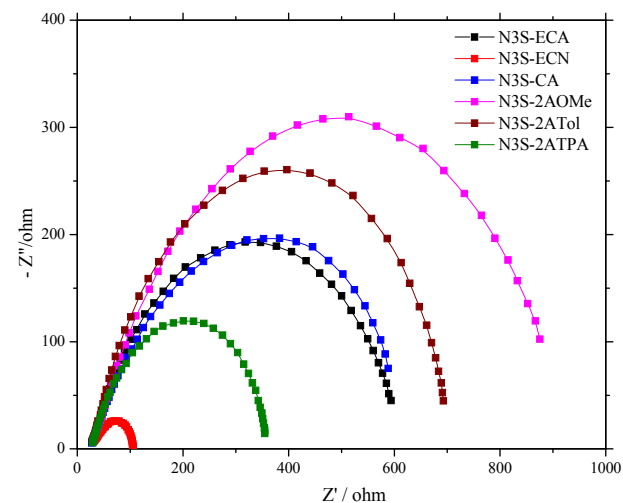


Figure 9. Impedance spectra (Nyquist plots) of DSSCs based on thiaporphyrins measured under illumination.

Conclusion

In summary, we have prepared novel mono- and di- carboxylate functionalized A₃B and A₂B₂ thiaporphyrins. With the support of the photophysical and photovoltaic data, it is revealed that these thiaporphyrins, after systematic structural modification can be applied in dye-sensitized solar cells. The UV-Visible spectra of these thiaporphyrins displayed that ethynyl phenyl linker effectively enhances the absorption wavelengths towards near infra-red region. Density functional theory calculations show that, higher π electron density is localized on the cyano acrylic acid anchor in lower unoccupied molecular orbital of N3S-ECN compared to other thiaporphyrins; consequently, more electrons are available for injection from the dye into the conduction band of TiO₂. As seen from the electrochemical properties and energy level diagram, the energy levels of the thiaporphyrins are suitable for application as a sensitizer in dye-sensitized solar cells. The best conversion efficiency of 1.69% with high photocurrent density of 5.12 mA cm⁻² is obtained for N3S-ECN owing to their superior photophysical properties. To the best of our knowledge this is the highest efficiency for thiaporphyrin-based dye-sensitized solar cells. These results suggests that the thiaporphyrins, core-modified derivatives of porphyrins, can serve as effective sensitizers for future dye-sensitized solar cell applications.

Experimental

General Methods

All chemicals were obtained from commercial sources and used as received without further purification. All the reactions were carried out under nitrogen atmosphere. Solvents used in reactions were dried by PureSolv MD 5 system (Innovative Technology, Inc). Flash chromatography was carried out by using silica gel (40-63 μ m, Merck). Analytical TLC was performed on Merck silica gel plates. ¹H NMR spectra were recorded on a Bruker 400 MHz spectrometer and performed in CDCl₃ (δ = 7.26 ppm), THF-D₈ (δ = 1.73, 3.58 ppm) or DMSO-D₆ (δ = 2.50 ppm) solutions. ¹³C NMR spectra were performed in CDCl₃ (δ = 7.26 ppm) DMSO-D₆ (δ = 40.0 ppm) solutions. Chemical shifts are reported in ppm. Coupling constants *J* are reported in Hz. The signals are described as s: singlet; d: doublet; dd: doublet of doublet. The ESI ion trap mass spectra were measured by a Finnigan MAT LCQ mass spectrometer. The HR-FAB spectra were conducted on a JMS-700 double focusing mass spectrometer. Transmittance and reflection UV-visible absorption spectra of the thiaporphyrins in THF and adsorbed on TiO₂ electrodes, respectively, were recorded on a JASCO V-670 UV-Vis/NIR spectrophotometer. Steady-state fluorescence spectra were acquired by using a Varian Cary Eclipse fluorescence spectrophotometer. The cyclic voltammetry measurements of all thiaporphyrins were carried out on CHI 621B electrochemical analyser (CH Instruments, Austin, TX, USA) in degassed THF containing 0.1 M tetrabutylammonium hexafluorophosphate (Bu₄NPF₆) as the supporting electrolyte. The cell assembly consists of a glossy carbon as the working electrode, a silver wire as the pseudo-

reference electrode, and a platinum wire as the auxiliary electrode. The scan rate for all measurements was fixed at 50 mV/sec. A ferrocene^{+1/0} redox couple was used as the internal standard and the potential values obtained in reference to the silver electrode were converted to the vacuum scale. DFT calculations were performed using Gaussian 09 package.³⁵ The molecular orbitals were visualized by the chem-office software.

Syntheses

The precursors 4-ethynylbenzaldehyde, thiophene diols,³⁶ 5-bromo-10,15,20-tris(*p*-tolyl)-21-thiaporphyrin (1)³⁷⁻³⁸ and N3S-ECA²⁷ were prepared by following the reported procedures.

5-(4-Ethynylbenzaldehyde)-10,15,20-tris(*p*-tolyl)-21-

thiaporphyrin (2): Bromothiaporphyrin, N3S-Br (1) (100 mg, 0.15 mmol), Pd₂(dba)₃ (55 mg, 0.06 mmol), AsPh₃ (113 mg, 0.37 mmol) and 4-ethynylbenzaldehyde (25 mg, 0.18 mmol) were added to a 100 ml round bottom flask and the flask is attached to high vacuum for 30 min. Then N₂ was flushed for 15 min and anhydrous THF (40 ml) and triethylamine (10 ml) were added. The reaction mixture was stirred under N₂ at room temperature for 12 h. After completion of the reaction as confirmed by TLC, the solvent was removed under pressure and the crude product was purified by column chromatography using Hexanes/DCM (2/1) as eluent to afford the desired porphyrin (2) as a purple solid (76 mg, 70%). ¹H NMR (400 MHz, CDCl₃) δ : -2.18 (s, 1H, NH) 2.70 (s, 3H, CH₃), 2.72 (s, 6H, CH₃), 7.53-7.66 (m, 6H, *m*-tolyl), 8.03-8.09 (m, 6H, *o*-tolyl), 8.16 (m, 4H, Ar), 8.54 (d, 1H, *J* = 4.48 Hz; β -pyrrole), 8.61 (d, 1H, *J* = 4.52 Hz; β -pyrrole), 8.66 (d, 1H, *J* = 4.48 Hz; β -pyrrole), 8.86 (s, 2H, β -pyrrole), 9.34 (d, 1H, *J* = 4.48 Hz; β -pyrrole), 9.83 (d, 1H, *J* = 5.16 Hz; β -thiophene), 10.14 (s, 1H, CHO), 10.32 (d, 1H, *J* = 5.16 Hz; β -thiophene) ppm; ¹³C NMR (100 MHz, CDCl₃) δ : 21.53, 94.56, 97.69, 108.52, 124.99, 126.02, 127.39, 127.48, 128.46, 128.75, 129.38, 129.92, 130.07, 131.64, 132.25, 132.98, 133.08, 134.17, 134.25, 134.33, 135.20, 135.67, 135.82, 136.13, 137.67, 137.77, 137.90, 139.00, 139.30, 139.77, 146.23, 150.34, 154.41, 154.49, 157.96, 158.87, 191.41 ppm; HRMS-ESI: *m/z* calcd for C₅₀H₃₆N₃OS: 726.2579, found 726.2582 [M+H]⁺.

N3S-ECN: To a mixture of thiaporphyrin-CHO (2) (100 mg, 0.13 mmol) in CHCl₃ (25 ml) and piperidine (128 μ l, 1.3 mmol) was added cyanoacetic acid (46 mg, 0.52 mmol) and the reaction mixture is refluxed for 12 h under N₂. To this mixture 50 ml CHCl₃ and 100 ml water were added and transferred to a separation funnel. The pH value of this mixture is adjusted to approximately 2 with 2 M H₃PO₄. The CHCl₃ was removed by azeotropic distillation using acetonitrile in vacuo. Precipitation from the resulting acetonitrile solution (50 ml) using H₂O gave N3S-ECN purple solid (90 mg, 87%). ¹H NMR (400 MHz, THF-*d*₈) δ : -2.08 (s, 1H, NH) 2.68 (s, 3H, CH₃), 2.70 (s, 6H, CH₃), 7.59 (m, 4H, *m*-tolyl), 7.69 (d, 2H, *J* = 7.8 Hz; *m*-tolyl), 8.06 (m, 4H, *o*-tolyl), 8.15 (d, 2H, *J* = 7.84 Hz; *o*-tolyl), 8.25 (d, 2H, *J* = 8.36 Hz; Ar), 8.30 (d, 2H, *J* = 8.40 Hz; Ph), 8.39 (s, 1H, acryl), 8.48 (d, 1H, *J* = 4.56 Hz; β -pyrrole), 8.56 (d, 1H, *J* =

4.56 Hz; β -pyrrole), 8.62 (d, 1H, $J = 4.48$ Hz; β -pyrrole), 8.87 (s, 2H, β -pyrrole), 9.39 (d, 1H, $J = 4.44$ Hz; β -pyrrole), 9.83 (d, 1H, $J = 5.20$ Hz; β -thiophene), 10.38 (d, 1H, $J = 5.16$ Hz; β -thiophene) ppm; ^{13}C NMR (100 MHz, DMSO- d_6) δ : 21.01, 45.39, 91.88, 98.87, 108.54, 114.12, 119.00, 124.58, 124.65, 125.44, 127.48, 127.55, 128.60, 129.06, 129.57, 129.84, 131.92, 132.25, 132.49, 133.04, 133.85, 133.93, 135.29, 135.75, 135.86, 136.61, 137.56, 137.71, 138.01, 138.15, 138.38, 138.78, 145.23, 146.66, 149.04, 153.49, 153.61, 157.03, 157.85, 162.88 ppm; IR (Neat): 3327, 2923, 2860, 2224, 2184, 1697, 1576, 1537, 1422, 1283, 1179, 941, 796, 704; UV-Vis (THF) $\lambda_{\text{max}}/\text{nm}$ ($\epsilon/10^3 \text{ M}^{-1} \text{ cm}^{-1}$) = 449 (396), 526 (15), 579 (55), 637 (5), 698 (15); HRMS-ESI: m/z calcd for $\text{C}_{53}\text{H}_{37}\text{N}_4\text{O}_2\text{S}$: 793.2637, found 793.2635 $[\text{M}+\text{H}]^+$.

Mixed diol (3): Anhydrous hexane (60 ml) was added to a 500 ml three-necked round-bottomed flask equipped with rubber septum, gas inlet and gas outlet tube. A positive pressure of N_2 was maintained and after purging N_2 gas for 5 min, TMEDA (11.5 ml, 75 mmol) and $n\text{-BuLi}$ (62 ml of 1.6 M solution in hexane) were added sequentially to the stirring solution at room temperature. Thiophene (2 ml, 25 mmol) was then added and the solution was refluxed for 1 h. As the reaction progressed, a white turbid solution formed indicating the formation of the 2,5-dilithiated salt of thiophene. The reaction mixture was cooled with ice bath and an ice-cold solution of p -tolualdehyde (2.95 ml, 25 mmol) and methyl-4-formylbenzoate (4.1 g, 25 mmol) in dry THF (60 ml) was then cannulated to the stirring solution. The resulting reaction mixture was stirred at 0 °C for 15 min and then brought up to room temperature. The reaction was quenched by adding cold saturated NH_4Cl solution (50 ml). The organic layer was washed with brine and dried over anhydrous MgSO_4 . The solvent was removed on a rotary evaporator under reduced pressure to afford the crude compound. The crude product was further purified by silica gel column chromatography using EA/Hexanes (3:7) as eluent to collect desired diol (3) as yellow solid (1.76 g, 19%). ^1H NMR (400 MHz, CDCl_3) δ : 2.34 (s, 3H, CH_3), 2.46 (d, 1H, $J = 3.88$ Hz; OH), 2.61 (d, 1H, $J = 3.76$ Hz; OH), 3.90 (s, 3H, OMe), 5.91 (s, 1H, *meso*), 5.99 (d, 1H, *meso*), 6.69 (m, 2H, *m*-tolyl), 7.15 (d, 2H, $J = 8.00$ Hz; Ph), 7.29 (m, 2H, *o*-tolyl), 7.49 (d, 2H, $J = 2.67$ Hz; β -thiophene), 8.00 (d, 2H, $J = 8.16$ Hz; Ph) ppm. ^{13}C NMR (100 MHz, CDCl_3) δ : 21.13, 52.11, 71.94, 72.41, 124.29, 124.78, 126.13, 129.22, 129.81, 137.85, 139.88, 147.01, 147.10, 147.67, 148.86, 148.95, 166.85 ppm.

N3S-CE (4): In a 500 ml one-necked round-bottomed flask fitted with a N_2 gas bubbler, a solution of the mixed thiophene diol (9) (737 mg, 2 mmol), pyrrole (411 μl , 6 mmol) and p -tolaldehyde (471 μl , 4 mmol) in DCM (400 ml) was taken. Resulting reaction mixture was purged with N_2 for 15 min and then a catalytic amount of $\text{BF}_3 \cdot \text{OEt}_2$ (25 μl , 0.2 mmol) was added at room temperature. After stirring for 1 h, DDQ (908 mg, 4 mmol) was added and the reaction mixture was stirred at room temperature in air for 1 h. The solvent was removed on a rotary evaporator. The crude product was purified by silica gel

column chromatography using Hexanes/DCM (1:1) as eluent to afford the desired porphyrin (4) as purple solid. (290 mg, 20%). ^1H NMR (400 MHz, CDCl_3) δ : -2.65 (s, 1H, NH), 2.71 (s, 9H, CH_3), 4.12 (s, 3H, OMe), 7.56 (d, 4H, $J = 7.80$ Hz; *m*-tolyl), 7.63 (d, 2H, $J = 7.80$ Hz; *m*-tolyl), 8.09 (m, 4H, *o*-tolyl), 8.15 (d, 2H, $J = 7.88$ Hz; *o*-tolyl), 8.35 (d, 2H, $J = 8.12$ Hz; Ph), 8.51 (d, 2H, $J = 8.24$ Hz; Ph), 8.64 (m, 3H, β -pyrrole), 8.71 (d, 1H, $J = 4.60$ Hz, β -pyrrole), 8.97 (d, 2H, $J = 1.72$ Hz, β -pyrrole), 9.68 (d, 1H, $J = 5.28$ Hz, β -thiophene), 9.79 (d, 1H, $J = 5.32$ Hz, β -thiophene) ppm. ^{13}C NMR (100 MHz, CDCl_3) δ : 21.50, 52.34, 124.11, 124.38, 127.35, 128.32, 128.69, 128.91, 129.03, 129.38, 129.54, 131.86, 132.51, 133.08, 133.55, 134.17, 134.36, 134.67, 135.58, 135.81, 137.61, 137.99, 139.11, 139.25, 139.46, 145.92, 146.75, 146.92, 154.54, 156.65, 157.62, 167.34 ppm. HRMS-ESI: m/z calcd for $\text{C}_{49}\text{H}_{38}\text{N}_3\text{O}_2\text{S}$: 732.2685, found 732.2684 $[\text{M}+\text{H}]^+$.

N3S-CA: Thiaporphyrin ester (4) (200 mg, 0.27 mmol) was dissolved in 50 mL THF. To this mixture, 20 equivalent of KOH mixed in 10 ml water was added and the reaction mixture was refluxed for 12 h. After cooling, the organic solvent was removed under pressure. 50 mL water was added to the reaction mixture and the solution was treated slowly with 1 N HCl. The precipitation formed were filtered off and washed with distilled water. The residue remained is dissolved in methanol and dried in vacuum to yield the desired porphyrin as purple solid (175 mg, 90%). ^1H NMR (400 MHz, DMSO- d_6) δ : -2.82 (s, 1H, NH), 2.64 (s, 9H, CH_3), 7.62 (m, 6H, *m*-tolyl), 8.08 (m, 6H, *o*-tolyl), 8.34 (d, 2H, $J = 8.12$ Hz; Ph), 8.42 (d, 2H, $J = 8.16$ Hz; Ph), 8.53 (m, 2H, β -pyrrole), 8.62 (m, 2H, β -pyrrole), 8.97 (d, 2H, $J = 1.56$ Hz, β -pyrrole), 9.74 (d, 1H, $J = 5.28$ Hz, β -thiophene), 9.78 (d, 1H, $J = 5.20$ Hz, β -thiophene), 13.29 (bs, 1H, COOH) ppm. ^{13}C NMR (100 MHz, DMSO- d_6) δ : 21.04, 124.11, 124.88, 127.53, 128.01, 128.57, 128.71, 129.35, 129.68, 130.41, 131.62, 132.97, 133.22, 133.87, 134.00, 134.42, 135.08, 135.81, 137.08, 137.52, 138.25, 138.40, 138.55, 139.16, 144.43, 145.98, 146.06, 153.75, 156.08, 156.80, 167.41 ppm; IR (neat): 3327, 2917, 2866, 1687, 1608, 1427, 1316, 1222, 1183, 968, 799, 717; UV-Vis (THF) $\lambda_{\text{max}}/\text{nm}$ ($\epsilon/10^3 \text{ M}^{-1} \text{ cm}^{-1}$) = 428 (504), 513 (35), 548 (9), 625 (5), 679 (8); HRMS-ESI: m/z calcd for $\text{C}_{48}\text{H}_{36}\text{N}_3\text{O}_2\text{S}$: 718.2528, found 718.2534 $[\text{M}+\text{H}]^+$.

2,5-Bis(3,4,5-trimethoxyphenylmethanol)thiophene (8): Anhydrous hexane (40 ml) was added to a 250 ml three-necked round bottomed flask equipped with rubber septum, gas inlet and gas outlet tube. A positive pressure of N_2 was maintained and after purging N_2 gas for 5 min, TMEDA (4.7 ml, 31.25 mmol) and $n\text{-BuLi}$ (13 ml of 2.5 M solution in hexane) were added sequentially to the stirring solution at room temperature. Thiophene (1 ml, 12.5 mmol) was then added and the solution was refluxed for 1 h. As the reaction progressed, a white turbid solution formed indicating the formation of the 2,5-dilithiated salt of thiophene. The reaction mixture was cooled with ice bath and an ice-cold solution of 3,4,5-trimethoxybenzaldehyde (6.13 g, 31.25 mmol) in dry THF (20 ml) was then cannulated to the stirring solution. The resulting reaction mixture was

stirred at 0 °C for 15 min and then brought up to room temperature. The reaction was quenched by adding cold saturated NH₄Cl solution (20 ml). The organic layer was washed with brine and dried over anhydrous MgSO₄. The solvent was removed on a rotary evaporator under reduced pressure to afford the crude compound. The crude product was further purified by silica gel column chromatography using EA/Hexanes (3:7) as eluent to collect desired diol (8) as yellow solid (2.91 g, 49%). ¹H NMR (400 MHz, CDCl₃) δ: 2.57 (s, 1H, OH), 2.58 (s, 1H, OH), 3.83 (s, 18H, OCH₃), 5.89 (d, 2H, *J* = 3.48 Hz; *meso*), 6.61 (s, 4H, Ph), 6.71 (d, *J* = 3.36 Hz, 2H, β-thiophene) ppm; ¹³C NMR (100 MHz, CDCl₃) δ: 56.12, 60.81, 72.59, 103.28, 103.30, 103.84, 124.39, 124.43, 137.60, 138.50, 147.88, 147.97, 153.27 ppm.

2,5-Bis(*p*-tolylmethanol)thiophene (9): Anhydrous hexane (40 ml) was added to a 250 ml three-necked round-bottomed flask equipped with rubber septum, gas inlet and gas outlet tube. A positive pressure of N₂ was maintained and after purging N₂ gas for 5 min, TMEDA (10.6 ml, 71 mmol) and *n*-BuLi (45 ml of 1.6 M solution in hexane) were added sequentially to the stirring solution at room temperature. Thiophene (1.9 ml, 23.7 mmol) was then added and the solution was refluxed for 1 h. As the reaction progressed, a white turbid solution formed indicating the formation of the 2,5-dilithiated salt of thiophene. The reaction mixture was cooled with ice bath and an ice-cold solution of *p*-tolaldehyde (7 ml, 59.25 mmol) in dry THF (50 ml) was then cannulated to the stirring solution. The resulting reaction mixture was stirred at 0 °C for 15 min and then brought up to room temperature. The reaction was quenched by adding cold saturated NH₄Cl solution (50 ml). The organic layer was washed with brine and dried over anhydrous MgSO₄. The solvent was removed on a rotary evaporator under reduced pressure to afford the crude compound. The crude product was further purified by silica gel column chromatography using EA/Hexanes (3:7) as eluent to collect desired diol (9) as yellow solid (6 g, 78%). ¹H NMR (400 MHz, CDCl₃) δ: 2.35 (s, 6H, CH₃), 2.38 (s, 1H, OH), 2.39 (s, 1H, OH), 5.92 (d, 2H, *J* = 3.60 Hz, *meso*), 6.69 (d, *J* = 2.6 Hz, 2H, β-thiophene), 7.16 (d, *J* = 7.92 Hz, 4H, *m*-tolyl), 7.30 (d, *J* = 6.84 Hz, 4H, *o*-tolyl) ppm. ¹³C NMR (100 MHz, CDCl₃) δ: 21.13, 72.42, 124.28, 126.22, 129.18, 137.73, 139.99, 148.19 ppm.

Dimethyl 4,4'-(thiophene-2,5-diylbis(hydroxymethylene)) dibenzoate (10): Anhydrous hexane (40 ml) was added to a 250 ml three-necked round-bottomed flask equipped with rubber septum, gas inlet and gas outlet tube. A positive pressure of N₂ was maintained and after purging N₂ gas for 5 min, TMEDA (4.7 ml, 31.25 mmol) and *n*-BuLi (20 ml of 1.6 M solution in hexane) were added sequentially to the stirring solution at room temperature. Thiophene (1 ml, 12.5 mmol) was then added and the solution was refluxed for 1 h. As the reaction progressed, a white turbid solution formed indicating the formation of the 2,5-dilithiated salt of thiophene. The reaction mixture was cooled with ice bath and an ice-cold solution of methyl-4-formylbenzoate (4 g, 25 mmol) in dry

THF (20 ml) was then cannulated to the stirring solution. The resulting reaction mixture was stirred at 0 °C for 15 min and then brought up to room temperature. The reaction was quenched by adding cold saturated NH₄Cl solution (20 ml). The organic layer was washed with brine and dried over anhydrous MgSO₄. The solvent was removed on a rotary evaporator under reduced pressure to afford the crude compound. The crude product was further purified by silica gel column chromatography using EA/Hexanes (3:7) as eluent to collect desired diol (10) as yellow solid (4.3 g, 84%). ¹H NMR (400 MHz, CDCl₃) δ: 2.55 (s, 1H, OH), 2.56 (s, 1H, OH), 3.9 (s, 6H, COOCH₃), 6.01 (d, 2H, *J* = 3.72 Hz; *meso*), 6.72 (s, 2H, β-thiophene), 7.49 (m, 4H, Ph), 8.01 (d, *J* = 8.28 Hz, Ph) ppm. ¹³C NMR (100 MHz, CDCl₃) δ: 52.14, 71.97, 124.81, 126.12, 129.77, 129.88, 147.52, 147.74, 166.79.

N3S-2EOME (11): In a 250 ml one-necked round-bottomed flask fitted with a N₂ gas bubbler, a solution of the thiophene diol (8) (476 mg, 1 mmol), pyrrole (205 μl, 3 mmol) and methyl-4-formylbenzoate (328 mg, 2 mmol) in DCM (200 ml) was taken. Resulting reaction mixture was purged with N₂ for 15 min and then a catalytic amount of BF₃•OEt₂ (15 μl, 0.1 mmol) was added at room temperature. After stirring for 1 h, DDQ (681 mg, 3 mmol) was added and the reaction mixture was stirred at room temperature in air for 1 h. The solvent was removed on a rotary evaporator. The crude product was purified by silica gel column chromatography using Hexanes/DCM (1:1) as eluent to afford the desired porphyrin (11) as purple solid. (379 mg, 20%). ¹H NMR (400 MHz, CDCl₃) δ: -2.69 (s, 1H, NH), 4.02 (s, 12H, OCH₃), 4.12 (s, 6H, OCH₃), 4.18 (s, 6H, OMe), 7.49 (s, 4H, Ph), 8.28 (d, 4H, *J* = 8.16 Hz; *o*-Ph), 8.45 (d, 4H, *J* = 8.16 Hz; *m*-Ph), 8.56 (d, 2H, *J* = 4.60 Hz; β-pyrrole), 8.80 (d, 2H, *J* = 4.48 Hz; β-pyrrole), 8.89 (d, 2H, *J* = 1.72 Hz; β-pyrrole), 9.87 (s, 2H, β-thiophene) ppm; ¹³C NMR (100 MHz, CDCl₃) δ: 52.45, 56.46, 61.27, 112.22, 12.45, 127.91, 128.76, 129.89, 131.80, 133.62, 134.31, 134.69, 135.17, 136.24, 138.19, 138.38, 147.00, 147.55, 152.31, 154.05, 157.52, 167.19 ppm; HRMS-ESI: *m/z* calcd for C₅₄H₄₆N₃O₁₀S: 928.2904, found 928.2901 [M+H]⁺.

N3S-2Etol (12): In a 250 mL one-necked round-bottomed flask fitted with a N₂ gas bubbler, a solution of the thiophene diol (9) (500 mg, 1.54 mmol), pyrrole (316 μl, 4.62 mmol) and methyl-4-formylbenzoate (506 mg, 3.08 mmol) in DCM (200 ml) was taken. Resulting reaction mixture was purged with N₂ for 15 min and then a catalytic amount of BF₃•OEt₂ (20 μl, 0.15 mmol) was added at room temperature. After stirring for 1 h, DDQ (699 mg, 3.08 mmol) was added and the reaction mixture was stirred at room temperature in air for 1 h. The solvent was removed on a rotary evaporator. The crude product was purified by silica gel column chromatography using Hexanes/DCM (1:1) as eluent to afford the desired porphyrin (12) as purple solid. (268 mg, 22%). ¹H NMR (400 MHz, CDCl₃) δ: -2.70 (s, 1H, NH), 2.72 (s, 6H, CH₃), 4.12 (s, 6H, OMe), 7.64 (d, 4H, *J* = 7.76 Hz; *m*-tolyl), 8.15 (d, 4H, *J* = 7.76 Hz; *o*-tolyl), 8.29 (d, 4H, *J* = 8.08 Hz; *o*-Ph), 8.44 (d, 4H, *J* = 8.04 Hz; *m*-Ph), 8.55

(d, 2H, $J = 4.60$ Hz; β -pyrrole), 8.74 (d, 2H, $J = 4.52$ Hz; β -pyrrole), 8.89 (d, 2H, $J = 1.4$ Hz; β -pyrrole), 9.81 (s, 2H, β -thiophene) ppm. ^{13}C NMR (100 MHz, CDCl_3) δ : 21.49, 52.42, 122.03, 127.85, 128.35, 128.60, 129.76, 132.15, 133.73, 134.20, 134.34, 134.73, 134.96, 137.77, 137.88, 138.26, 147.19, 147.68, 153.94, 157.64, 167.24 ppm. HRMS-ESI: m/z calcd for $\text{C}_{50}\text{H}_{38}\text{N}_3\text{O}_4\text{S}$: 776.2583, found 776.2584 $[\text{M}+\text{H}]^+$.

N3S-2ETPA (13): In a 250 ml one-necked round-bottomed flask fitted with a N_2 gas bubbler, a solution of the thiophene diol (10) (413 mg, 1 mmol), pyrrole (205 μl , 3 mmol) and 4-(diphenylamino)benzaldehyde (546 mg, 2 mmol) in DCM (200 ml) was taken. Resulting reaction mixture was purged with N_2 for 15 min and then a catalytic amount of $\text{BF}_3\cdot\text{OEt}_2$ (38 μl , 0.3 mmol) was added at room temperature. After stirring for 1 h, DDQ (681 mg, 3 mmol) was added and the reaction mixture was stirred at room temperature in air for 1 h. The solvent was removed on a rotary evaporator. The crude product was purified by silica gel column chromatography using Hexanes/DCM (1:1) as eluent to afford the desired porphyrin (13) as purple solid. (80 mg, 7%). ^1H NMR (400 MHz, CDCl_3) δ : -2.59 (s, 1H, NH), 4.12 (s, 6H, OMe), 7.15 (m, 4H, Ph), 7.42 (m, 20H, Ph), 8.05 (d, 4H, $J = 8.44$ Hz; Ph), 8.34 (d, 4H, $J = 8.20$ Hz; Ph), 8.50 (d, 4H, $J = 8.24$ Hz; Ph), 8.64 (d, 2H, $J = 4.60$ Hz; β -pyrrole), 8.77 (d, 2H, $J = 4.64$ Hz; β -pyrrole), 9.13 (d, 2H, $J = 1.76$ Hz; β -pyrrole), 9.67 (s, 2H, β -thiophene) ppm. ^{13}C NMR (100 MHz, CDCl_3) δ : 52.44, 120.98, 123.47, 124.7, 125.03, 128.76, 129.19, 129.54, 129.67, 129.86, 132.59, 134.02, 134.18, 135.52, 135.83, 135.97, 145.71, 146.54, 147.74, 147.83, 154.68, 156.85, 167.30. HRMS-FAB $^+$: m/z calcd for $\text{C}_{72}\text{H}_{52}\text{N}_5\text{O}_4\text{S}$: 1082.3740, found 1082.3738 $[\text{M}+\text{H}]^+$.

N3S-2AOMe: Thiaporphyrin ester (11) (50 mg, 54 μmol) was dissolved in 40 ml THF. To this mixture, 20 equivalent of KOH mixed in 2 ml water was added and the reaction mixture was refluxed for 12 h. After cooling, the organic solvent was removed under pressure. An amount of 20 ml water was added to the reaction mixture and the solution was treated slowly with 1 N HCl. The precipitation formed were filtered off and washed with distilled water. The residue remained is dissolved in methanol and dried in vacuum to yield desired porphyrin as purple solid (48 mg, 98%). ^1H NMR (400 MHz, $\text{DMSO}-d_6$) δ : -2.82 (s, 1H, NH), 3.96 (s, 12H, OCH_3), 3.99 (s, 6H, OCH_3), 7.56 (s, 4H, Ph), 8.33 (d, 4H, $J = 8.16$ Hz; o -Ph), 8.39 (d, 4H, $J = 8.24$ Hz; m -Ph), 8.52 (d, 2H, $J = 4.64$ Hz; β -pyrrole), 8.80 (d, 2H, $J = 4.48$ Hz; β -pyrrole), 8.96 (d, 2H, $J = 2.04$ Hz; β -pyrrole), 9.95 (s, 2H, β -thiophene) ppm. ^{13}C NMR (100 MHz, $\text{DMSO}-d_6$) δ : 56.26, 60.38, 112.24, 122.39, 127.81, 129.22, 130.67, 131.69, 133.94, 134.19, 135.29, 135.40, 137.62, 145.82, 146.65, 152.09, 153.33, 156.83, 167.42 ppm; IR (Neat): 3327, 2923, 2853, 1711, 1684, 1603, 1582, 1502, 1462, 1406, 1336, 1234, 1122, 942, 792, 715; UV-Vis (THF) $\lambda_{\text{max}}/\text{nm}$ ($\epsilon/10^3 \text{ M}^{-1} \text{ cm}^{-1}$) = 431 (438), 513 (39), 549 (14), 625 (5), 679 (8); HRMS-ESI: m/z calcd for $\text{C}_{54}\text{H}_{42}\text{N}_3\text{O}_{10}\text{S}$: 900.2591, found 900.2585 $[\text{M}+\text{H}]^+$.

N3S-2Atol: N3S-2Etol (12) (250 mg, 0.32 mmol) was dissolved in 60 ml THF. To this mixture, 20 equivalent of KOH mixed in 10 ml water was added and the reaction mixture was refluxed for 12 h. After cooling, the organic solvent was removed under pressure. An amount of 50 mL water was added to the reaction mixture and the solution was treated slowly with 1 N HCl. The precipitation formed were filtered off and washed with distilled water. The residue remained is dissolved in methanol and dried in vacuum to yield porphyrin as purple solid (215 mg, 90%). ^1H NMR (400 MHz, $\text{DMSO}-d_6$) δ : -2.87 (s, 1H, NH), 2.67 (s, 6H, CH_3), 7.70 (d, 4H, $J = 7.60$ Hz; m -tolyl), 8.14 (d, 4H, $J = 7.64$ Hz; o -tolyl), 8.33 (d, 4H, $J = 8.04$ Hz; o -Ph), 8.38 (d, 4H, $J = 8.04$ Hz; m -Ph), 8.52 (d, 2H, $J = 4.64$ Hz; β -pyrrole), 8.67 (d, 2H, $J = 4.60$ Hz; β -pyrrole), 8.97 (d, 2H, $J = 1.84$ Hz; β -pyrrole), 9.81 (s, 2H, β -thiophene) ppm. ^{13}C NMR (100 MHz, $\text{DMSO}-d_6$) δ : 21.03, 122.29, 124.89, 127.78, 128.59, 129.28, 130.68, 131.78, 133.69, 133.93, 134.23, 135.08, 135.33, 137.04, 137.67, 145.79, 146.60, 153.31, 156.77, 167.41 ppm; IR (Neat): 3325, 2920, 2854, 1732, 1686, 1608, 1420, 1313, 1282, 967, 795, 710; UV-vis (THF) $\lambda_{\text{max}}/\text{nm}$ ($\epsilon/10^3 \text{ M}^{-1} \text{ cm}^{-1}$) = 428 (369), 512 (28), 547 (8), 624 (2), 679 (6); HRMS-ESI: m/z calcd for $\text{C}_{48}\text{H}_{34}\text{N}_3\text{O}_4\text{S}$: 748.2270, found 748.2267 $[\text{M}+\text{H}]^+$.

N3S-2ATPA: Thiaporphyrin ester (13) (50 mg, 46 μmol) was dissolved in 30 ml THF. To this solution, 20 equivalent of KOH mixed in 2 ml water was added and the reaction mixture was refluxed for 12 h. After cooling, the organic solvent was removed under pressure. An amount of 20 mL water was added to the reaction mixture and was treated slowly with 1 N HCl. The precipitation formed were filtered off and washed with distilled water. The residue remained is dissolved in methanol and dried in vacuum to yield desired porphyrin as purple solid (48 mg, 98%). ^1H NMR (400 MHz, $\text{DMSO}-d_6$) δ : -2.72 (s, 1H, NH), 7.19 (m, 4H, Ph), 7.37 (m, 12H, Ph), 7.47 (m, 8H, Ph), 8.08 (d, 4H, $J = 8.20$ Hz; Ph), 8.36 (d, 4H, $J = 8.00$ Hz; Ph), 8.44 (d, 4H, $J = 8.04$ Hz; Ph), 8.64 (d, 2H, $J = 4.44$ Hz; β -pyrrole), 8.71 (d, 2H, $J = 4.52$ Hz; β -pyrrole), 9.15 (s, 2H, β -pyrrole), 9.74 (s, 2H, β -thiophene), 13.30 (br s, 2H, COOH) ppm. ^{13}C NMR (100 MHz, $\text{DMSO}-d_6$) δ : 120.25, 123.76, 124.40, 124.88, 128.74, 129.50, 129.82, 129.94, 130.45, 132.89, 134.14, 134.78, 135.49, 136.04, 138.62, 144.33, 145.76, 147.08, 147.39, 153.90, 156.20, 167.41 ppm; IR (Neat): 3332, 2918, 2867, 1686, 1590, 1489, 1418, 1313, 1276, 1173, 968, 797, 695; UV-Vis (THF) $\lambda_{\text{max}}/\text{nm}$ ($\epsilon/10^3 \text{ M}^{-1} \text{ cm}^{-1}$) = 429 (394), 518 (52), 558 (32), 621 (8), 682 (16); HRMS-ESI: m/z calcd for $\text{C}_{70}\text{H}_{48}\text{N}_5\text{O}_4\text{S}$: 1054.3427, found 1054.3433 $[\text{M}+\text{H}]^+$.

Photovoltaic Measurements

TiO_2 photoanode films and Pt counter electrodes were purchased from Yingkou Opvtech New Energy Co. Ltd. Liaoning, China. The films, which were prepared by using the screen-printing method, were composed of a transparent layer (thickness $\approx 12 \mu\text{m}$), a scattering layer (thickness $\approx 4 \mu\text{m}$), and a working area of $0.4 \times 0.4 \text{ cm}^2$ and were used as received. The films were pretreated according to the following activation

procedures before use: heating at 100 °C for 22 min, at 110 °C for 60 min, at 450 °C for 68 min, at 500 °C 60 min, at 250 °C for 60 min, cooling at 80 °C and keeping at 80 °C before immersion. The TiO₂ films were immersed in a 2×10⁻⁴ M solution of the porphyrin in THF for 6-8 h at 25 °C. The dye-sensitized TiO₂ films were washed with THF, dried in hot air, and used as the working electrode. To fabricate the DSSC device, the two electrodes were tightly clipped together into a sandwich-type cell that was spaced by a 40 μm film spacer. A thin layer of electrolyte, which contained 0.05 M I₂, 0.1 M lithium iodide (LiI), 0.6 M dimethyl-propyl-benzimidazole iodide (DMPII), and 0.6 M 4-tert-butylpyridine (TBP) in dry CH₃CN, was introduced into the space between the two electrodes. The photo-electrochemical characterizations of the solar cells were performed on an Oriel Class A solar simulator (Oriel 91195A, Newport Corp.). Photocurrent–voltage characteristics of the DSSCs were recorded on a potentiostat/galvanostat (CHI650B, CH Instruments, Inc.) at a light intensity of 100 mWcm⁻² and calibrated to an Oriel reference solar cell (Oriel 91150, Newport Corp.). The monochromatic quantum efficiency was recorded on a monochromator (Oriel 74100, Newport Corp.) under short-circuit conditions. The intensity of each wavelength was within the range 1–3 mWcm⁻². The EIS measurements were carried on CHI 621B electrochemical impedance analyser (CH Instruments, Austin, TX, USA), under applied AC voltage and bias potential on the cells and measured the corresponding current and voltage under the white LED lamp with various neutral density filters for white light intensity in order to change the Fermi level of DSSCs. The data was analysed using Zview software.

Acknowledgements

The authors greatly acknowledge financial support from the National Science Council (Taiwan) and the Academia Sinica. Mass spectroscopy analysis was performed by the Mass Spectrometry Facility of the Institute of Chemistry, Academia Sinica (Taiwan). Help from Dr. Jiann-T'suen Lin with the measurements and instrumentation is greatly appreciated.

Notes and references

^a Institute of Chemistry, Academia Sinica, Nankang Taipei, 115 Taiwan.

^b Department of Chemistry, National Taiwan Normal University, Taipei, 116 Taiwan.

Electronic Supplementary Information (ESI) available: [ATR-FTIR for N3S-ECA, N3S-ECN, N3S-2AOMe and N3S-2ATPA; ¹H, ¹³C NMR and HR-Mass spectra of thiaporphyrins]. See DOI: 10.1039/b000000x/

- B. O'Regan and M. Gratzel, *Nature*, 1991, **353**, 737-740.
- L. M. Goncalves, V. de Zea Bermudez, H. A. Ribeiro and A. M. Mendes, *Energy Environ. Sci.*, 2008, **1**, 655-667.
- L. Han, A. Islam, H. Chen, C. Malapaka, B. Chiranjeevi, S. Zhang, X. Yang and M. Yanagida, *Energy Environ. Sci.*, 2012, **5**, 6057-6060.
- W. M. Campbell, K. W. Jolley, P. Wagner, K. Wagner, P. J. Walsh, K. C. Gordon, L. Schmidt-Mende, M. K. Nazeeruddin, Q. Wang, M. Grätzel and D. L. Officer, *J. Phys. Chem. C*, 2007, **111**, 11760-11762.
- T. Bessho, S. M. Zakeeruddin, C.-Y. Yeh, E. W.-G. Diao and M. Grätzel, *Angew. Chem. Int. Ed.*, 2010, **49**, 6646-6649.
- A. Yella, H.-W. Lee, H. N. Tsao, C. Yi, A. K. Chandiran, M. K. Nazeeruddin, E. W.-G. Diao, C.-Y. Yeh, S. M. Zakeeruddin and M. Grätzel, *Science*, 2011, **334**, 629-634.
- A. Hagfeldt, G. Boschloo, L. Sun, L. Kloo and H. Pettersson, *Chem. Rev.*, 2010, **110**, 6595-6663.
- H. Imahori, T. Umeyama and S. Ito, *Acc. Chem. Res.*, 2009, **42**, 1809-1818.
- L.-L. Li and E. W.-G. Diao, *Chem. Soc. Rev.*, 2013, **42**, 291-304.
- M. V. Martinez-Diaz, G. de la Torre and T. Torres, *Chem. Commun.*, 2010, **46**, 7090-7108.
- P. J. Chmielewski and L. Latos-Grażyński, *Coord. Chem. Rev.*, 2005, **249**, 2510-2533.
- I. Gupta and M. Ravikanth, *Coord. Chem. Rev.*, 2006, **250**, 468-518.
- J.-H. Ha, S. Ko, C.-H. Lee, W.-y. Lee and Y.-R. Kim, *Chem. Phys. Lett.*, 2001, **349**, 271-278.
- P. Ziolkowski, K. Symonowicz, P. Chmielewski, L. Latos-Grażyński, G. Streckyte, R. Rotomskis and J. Rabczyński, *J. Cancer Res Clin Oncol*, 1999, **125**, 563-568.
- D. G. Hilmey, M. Abe, M. I. Nelen, C. E. Stilts, G. A. Baker, S. N. Baker, F. V. Bright, S. R. Davies, S. O. Gollnick, A. R. Oseroff, S. L. Gibson, R. Hilf and M. R. Detty, *J. Med. Chem.*, 2001, **45**, 449-461.
- R. Minnes, H. Weitman, Y. You, M. R. Detty and B. Ehrenberg, *J. Phys. Chem. B*, 2008, **112**, 3268-3276.
- E. J. Ngen, T. S. Daniels, R. S. Murthy, M. R. Detty and Y. You, *Bioorg. Med. Chem.*, 2008, **16**, 3171-3183.
- Y. You, S. L. Gibson, R. Hilf, S. R. Davies, A. R. Oseroff, I. Roy, T. Y. Ohulchanskyy, E. J. Bergey and M. R. Detty, *J. Med. Chem.*, 2003, **46**, 3734-3747.
- Y. You, S. L. Gibson, R. Hilf, T. Y. Ohulchanskyy and M. R. Detty, *Bioorg. Med. Chem.*, 2005, **13**, 2235-2251.
- I. Gupta and M. Ravikanth, *J. Org. Chem.*, 2004, **69**, 6796-6811.
- Y. Pareek and M. Ravikanth, *RSC Advances*, 2014, **4**, 7851-7880.
- S. Stute, K. Gloe and K. Gloe, *Tetrahedron*, 2005, **61**, 2907-2912.
- Y. Xie, P. Joshi, M. Ropp, D. Galipeau, L. Zhang, H. Fong, Y. You and Q. Qiao, *J. Porphyrins Phthalocyanines*, 2009, **13**, 903-909.
- C.-H. Hung, C.-K. Ou, G.-H. Lee and S.-M. Peng, *Inorg. Chem.*, 2001, **40**, 6845-6847.
- C.-H. Chuang, C.-K. Ou, S.-T. Liu, A. Kumar, W.-M. Ching, P.-C. Chiang, M. A. C. dela Rosa and C.-H. Hung, *Inorg. Chem.*, 2011, **50**, 11947-11957.
- S. B. Mane, J.-Y. Hu, Y.-C. Chang, L. Luo, E. W.-G. Diao and C.-H. Hung, *Chem. Commun.*, 2013, **49**, 6882-6884.
- S. B. Mane, L. Luo, G.-F. Chang, E. W.-G. Diao and C.-H. Hung, *J. Chin. Chem. Soc.*, 2014, DOI: 10.1002/jccs.201300525.
- C.-F. Lo, L. Luo, E. W.-G. Diao, I. J. Chang and C.-Y. Lin, *Chem. Commun.*, 2006, 1430-1432.
- Y. Arai and H. Segawa, *Chem. Commun.*, 2010, **46**, 4279-4281.
- R. Ambre, K.-B. Chen, C.-F. Yao, L. Luo, E. W.-G. Diao and C.-H. Hung, *J. Phys. Chem. C*, 2012, **116**, 11907-11916.
- R. B. Ambre, G.-F. Chang and C.-H. Hung, *Chem. Commun.*, 2014, **50**, 725-727.
- R. B. Ambre, G.-F. Chang, M. R. Zanwar, C.-F. Yao, E. W.-G. Diao and C.-H. Hung, *Chem. Asian J.*, 2013, **8**, 2144-2153.
- A. Abbotto, N. Manfredi, C. Marini, F. De Angelis, E. Mosconi, J.-H. Yum, Z. Xianxi, M. K. Nazeeruddin and M. Gratzel, *Energy Environ. Sci.*, 2009, **2**, 1094-1101.
- C.-J. Yang, Y. J. Chang, M. Watanabe, Y.-S. Hon and T. J. Chow, *J. Mater. Chem.*, 2012, **22**, 4040-4049.
- M. J. Frisch, Gaussian 09, Revision A.1, *Gaussian, Inc., Wallingford CT*, 2009.
- I. Gupta, N. Agarwal and M. Ravikanth, *Eur. J. Org. Chem.*, 2004, **2004**, 1693-1697.
- S. Punidha, N. Agarwal, R. Burai and M. Ravikanth, *Eur. J. Org. Chem.*, 2004, **2004**, 2223-2230.
- S. Punidha, N. Agarwal, I. Gupta and M. Ravikanth, *Eur. J. Org. Chem.*, 2007, **2007**, 1168-1175.

Effects of Core-modification on Porphyrin Sensitizers to the Efficiencies of Dye-sensitized Solar Cells

Sandeep B. Mane,^{a,b} Liyang Luo,^c Gao-Fong Chang,^a Eric Wei-Guang Diao^d and Chen-Hsiung Hung^{a,*}

^aInstitute of Chemistry, Academia Sinica, Nankang Taipei 115, Taiwan.

^bDepartment of Chemistry, National Taiwan Normal University, Taipei 116, Taiwan.

^cDepartment of Chemistry, Chung Yuan Christian University, Chung Li 320, Taiwan.

^dDepartment of Applied Chemistry, National Chiao Tung University, Hsinchu 300, Taiwan.

(Received: Oct. 17, 2013; Accepted: Dec. 10, 2013; Published Online: Feb. 17, 2014; DOI: 10.1002/jccs.201300525)

To study dye-sensitized solar cells (DSSCs) with core-modified porphyrins as the sensitizing dyes, three porphyrins with an ethynyl benzoic acid as an anchoring group are prepared. The properties of free-base regular porphyrin (N4), thiaporphyrin (N3S) and oxaporphyrin (N3O) were thoroughly studied by spectroscopic methods, DFT calculations, and photovoltaic measurements. Replacing one of the porphyrinic core nitrogen atoms by oxygen or sulfur considerably changes the absorption spectra. The *Soret* band of the N3O and N3S observed bathochromic shifts of 3–9 nm while the *Q* band reaches 700 nm to the near-infrared region. The overall conversion efficiencies of the DSSCs based on these porphyrins are in the order N4 (3.66%) >> N3S (0.22%) > N3O (0.01%). The time-correlated single photon counting observed short fluorescence lifetimes for N3O adsorbed both on TiO₂ and Al₂O₃ which explicates the poor efficiency of DSSC using N3O as the photosensitizer.

Keywords: Core-modified porphyrins; Dye-sensitized solar cells; Photovoltaics.

INTRODUCTION

Production of eco-friendly and cost-effective energy is one of the major challenges for scientific community. Among the known renewable energy sources, solar energy is the most likely choice as it is abundant and sustainable. Dye-sensitized solar cell (DSSC) made from a crystalline TiO₂ electrode coated with a layer of photosensitizing dye is one of the most promising contenders in recent quest for cheaper, cleaner and greener alternatives to fossil fuels.¹ The overall solar energy conversion efficiencies of dye molecules can be strongly influenced by light harvesting properties of the sensitizing dyes, electronic structure and photophysical properties of dyes,^{1c,2} anchoring group of the dyes,³ bridging distance between the dye and TiO₂,⁴ and type of the central metal.⁵ Amid these factors, light harvesting properties of the dye molecules are the most important. In recent years, a variety of sensitizers including ruthenium complexes, porphyrins, phthalocyanines, and organic dyes have been studied extensively to find a cost effective and highly efficient sensitizer.^{1c,2,6} The ruthenium sensitizers had achieved the best conversion efficiency of 11.4% but their commercial applications are limited owing to low absorption coefficients of ruthenium dyes and limited re-

sources of ruthenium metal.⁷ Porphyrinic dyes have attracted much attention owing to their structural relationship with chlorophylls of the photosystem antenna complexes and their unique optical properties along with their photochemical and thermal stability.⁶ In last decade, a wide variety of porphyrins has been extensively studied as sensitizers in DSSCs. The device based on the D- π -A push-pull zinc porphyrin sensitizer, YD2-*o*-C8, co-sensitized with an organic dye using a cobalt based redox electrolyte reached a benchmark efficiency of 12.3%.⁸ Different molecular designs have been conducted to extend the absorption wavelengths of porphyrins to the near-infrared region in order to subsequently increase their overall photon to current conversion efficiencies. Two mostly explored routes to modify peripheral substituents of the porphyrin core are through either extending π -conjugation system over β - or *meso*-positions or fusing porphyrins with aromatic chromophores.⁹ Alternatively, the replacement of one or more pyrrolic nitrogens on the porphyrin central core with heteroatoms is another important but less explored approach to push the absorption of porphyrins towards red region.¹⁰ Our lab is interested in the synthesis of core modified porphyrins and their metal complexes.¹¹ We

* Corresponding author. E-mail: chhung@chem.sinica.edu.tw

have recently shown that oxasmaragdyrin boron complexes, which are a class of expanded core-modified porphyrin with 22 π -electrons, can be used as efficient sensitizers for DSSCs.¹²

The replacement of one or more pyrrolic nitrogens with the Group 16 heteroatoms like oxygen, sulfur, selenium, and tellurium in a porphyrin ring leads to a heteroatom substituted core-modified porphyrin.¹³ This core perturbation results in significant changes in the optical, photophysical, electrochemical, magnetic, and metal binding properties while retains the aromatic character. Surprisingly, the application of the core-modified porphyrins in DSSC as a sensitizer is very rare. The only article which demonstrates the use of core-modified porphyrins as the sensitizing dye in DSSCs is reported by Xie *et al.* where *meso* 2-thienyl substituted mono- and di-thiaporphyrins were used as sensitizers to obtain the highest efficiency of 0.19%.¹⁴ There is no report comparing the photophysical, electrochemical, and photovoltaic properties of regular and core modified porphyrins thus far.

One of the reasons for the low efficiency of the reported thiaporphyrin dyes-based DSSCs would be due to the lack of an effective electronic coupling between the porphyrin ring and the anchoring group to ensure an efficient charge transfer from the dye to TiO₂ semiconductor. In most of the highly efficient porphyrin dyes, ethynylphenyl group is used as a linker to couple the porphyrin ring and the anchoring carboxyl group.^{8,9c} In this report, we have synthesized novel core-modified porphyrins, N3S and N3O, with an ethynylphenyl group as the anchoring group as shown in Scheme I to examine the effects of core atom modification on the photovoltaic properties in DSSCs. This systematic study elucidates the significant influence of core atom replacement on the electronic structure, photophysical, and photovoltaic properties. The photovoltaic study reveals that in spite of the broad absorption peaks of core-modified porphyrins covering some near-infrared region, the overall photon-to-current conversion efficiencies

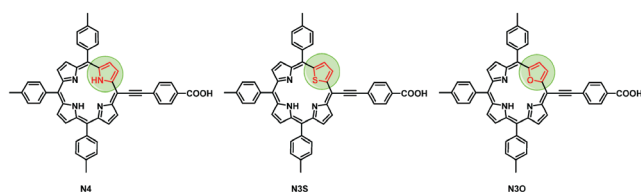
of these porphyrins are much lower than the regular porphyrins.

RESULTS AND DISCUSSION

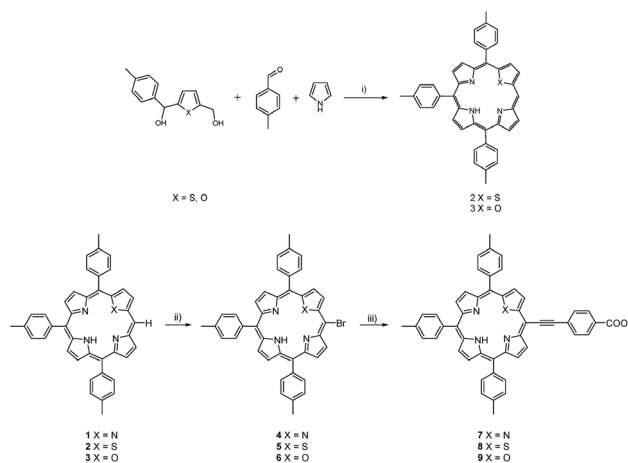
Synthesis

The free-base porphyrins, N4, N3S, and N3O, were synthesized from readily accessible starting materials in two steps. The mono *meso*-unsubstituted regular porphyrin (1) was prepared by literature procedures. The thiaporphyrin (2) and oxaporphyrin (3) were prepared by condensation of thiophene or furan diol with two equivalents of tolualdehyde and three equivalents of pyrrole in presence of catalytic amount of boron trifluoride etherate. As shown in Scheme II, these mono *meso*-unsubstituted porphyrins were then treated with N-bromosuccinimide in dry dichloromethane to give 5-bromo substituted porphyrins in 70–78% yields. The *m/z* peaks in mass spectra and the disappearance of the *meso* proton signal in ¹H NMR spectra confirmed the identity of the bromoporphyrins. These bromoporphyrins were further reacted with 4-ethynylbenzoic acid in tetrahydrofuran and triethylamine at room temperature by Sonogashira coupling in presence of Pd₂(dba)₃ as the catalyst to obtain the desired 4-ethynylbenzoic acid substituted porphyrins (7)–(9) with moderate yields. In the ¹H NMR spectra of N3S and N3O porphyrins, it is observed that β -thiophene and β -furan protons appeared as two doublets. The downfield shifts of the β -pyrrolic protons and the inner NH in the heteroporphyrins compared to

Scheme I Molecular structures of the studied porphyrin dyes



Scheme II Synthesis of N4, N3S and N3O porphyrin. Reagents and conditions: i) BF₃·OEt₂, DDQ, CH₂Cl₂; ii) NBS, CH₂Cl₂, room temp.; iii) 4-Ethynylbenzoic acid, Pd(dba)₃, AsPh₃, THF, NEt₃, room temp.



the N4 porphyrin confirms the core perturbation effect on porphyrin ring. The introduction of ethynyl bond between the porphyrin ring and the benzoic acid helps to maintain the planarity of the molecule assuring the effective electron coupling.

Optical Spectroscopy

The UV-visible peak positions of the *Soret* and *Q* bands and the molar absorption coefficients (ϵ) of N4, N3S and N3O in THF are listed in Table 1. The UV-visible spectra of the studied porphyrins as displayed in Figure 1, show typical features of free-base porphyrins, which consist of a strong *Soret* band around 450 nm and four *Q* bands around 520-700 nm. The core atom alteration results in slight red-shifts in the *Soret* as well as *Q* bands extending the absorption maximum beyond 700 nm. The molar absorption coefficients of N3S thiaporphyrin and N3O oxaporphyrin are slightly higher than regular N4 porphyrin.

To obtain the absorption spectra of the thin films, the TiO₂ films with coating thickness of 1 μm were immersed in THF solution of the porphyrins for 2 h at 40 °C and rinsed with THF to remove unadsorbed dye. The absorption spectra were recorded by reflectance measurements using an integrating sphere and the results are depicted in Figure 2. The examination on the *Soret* band region of spectra for dyes adsorbed on TiO₂ observed peak broadening for all compounds in comparison with the corresponding spectra in THF, which reflects significant degree of H-aggregation for all compounds on TiO₂. Noticeably, in the *Q* band region, the broadening of N3O/TiO₂ is more dramatic than that of N4/TiO₂ or N3S/TiO₂, which implies

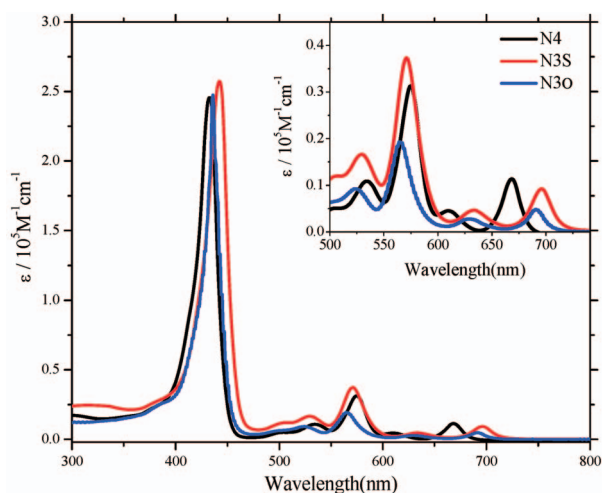


Fig. 1. UV-visible spectra of N4, N3S and N3O in THF. Inset shows enlarged spectra for *Q* band region.

Table 1. Optical and Electrochemical data of N4, N3S, and N3O porphyrin in THF

Dye	$\lambda_{\text{abs}}/\text{nm}^{[a]}$ ($\epsilon/10^3\text{M}^{-1}\text{cm}^{-1}$)	$\lambda_{\text{em}}/\text{nm}^{[b]}$	$\Phi^{[c]}$	$E_{\text{ox}}/\text{V}^{[d]}$	$E_{(0,0)}/\text{eV}^{[e]}$	$E_{\text{ox}}^*/\text{V}^{[f]}$
N4	433 (245), 534 (11), 575 (31), 610 (4.5), 668 (11)	673	0.11	0.93	1.85	-0.92
N3S	442 (257), 529 (5), 571 (37), 633 (9), 696 (9)	704	0.02	0.96	1.77	-0.81
N3O	436 (247), 525 (9), 565 (19), 629 (3), 691 (5)	695	0.06	0.97	1.79	-0.83

^[a] Absorption maximum of porphyrins in THF. ^[b] Emission maximum measured in THF by exciting at *Soret* band. ^[c] Relative quantum yields of the porphyrins were calculated with reference to TPP ($\Phi = 0.11$ in toluene). ^[d] Oxidation potentials approximated from E_{ox}^* and $E_{(0,0)}$. ^[e] $E_{(0,0)}$ values were estimated from the intersection of the absorption and emission spectra. ^[f] First reduction potentials vs. NHE determined by cyclic voltammetry in THF and referenced to the ferrocene redox couple.

a higher degree of aggregation for N3O than N4 and N3S when adsorbed on TiO₂.

The steady-state fluorescence spectra of all the core-modified porphyrins measured in THF by excitation at the *Soret* band wavelengths display the similar red-shifting as UV-vis spectra (Figure 3). These bathochromic shifts in the absorption and emission spectra of heteroporphyrins may be attributed to structural distortion of porphyrin π -system or the electronic effect of heteroatoms. From the density functional theory studies we observed negligible deviation from the planarity for the heteroporphyrins. Therefore, the red shifts in the spectra are more likely caused by the elec-

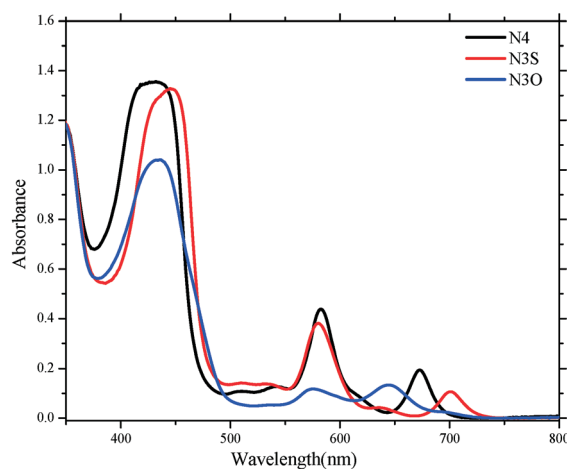


Fig. 2. UV-visible spectra of N4/TiO₂, N3S/TiO₂ and N3O/TiO₂.

tronic effects of the heteroatoms.¹⁰ We measured the relative quantum yields of all three porphyrins in THF with reference to the value of tetraphenylporphyrin and the results are depicted in Table 1. The decreased quantum yields for N3O and N3S suggest that the non-radiative decay rates of the internal conversion or the intersystem crossing are much faster for the heteroporphyrins compared to the regular porphyrins. The much lower quantum yield for N3S than those of N4 and N3O porphyrins indicates that the heavy atom effect of sulfur accelerates intersystem crossing rate.¹⁵

Cyclic Voltammetry

The cyclic voltammetry measurements of the porphyrins were carried out in degassed THF containing 0.1 M [Bu₄N]PF₆ as the supporting electrolyte to obtain the first reduction potentials. The reduction couples of the studied porphyrins show reversible redox processes under a scan rate of 50 mV/sec and are stable over multiple scans. As depicted in Table 1, the reduction potential of thiaporphyrin N3S (-0.81 V vs NHE) shifts positively by 110 mV and the oxaporphyrin N3O (-0.83 V vs NHE) also positively shifts by 90 mV as compared to regular N4 porphyrin (-0.92 V vs NHE) making them easier to be reduced. The zero-zero excitation energies, $E_{(0,0)}$ were calculated from the intersection of the normalized absorption and emission spectra at the $Q(0,0)$ band (See supporting information Figure S1) and were found to be 1.85, 1.77 and 1.79 eV for N4, N3S and N3O porphyrins, respectively. The oxidation potentials were estimated from the reduction potentials and the zero-zero excitation energies and are listed in Table 1. The energy level diagram for these porphyrins is displayed in

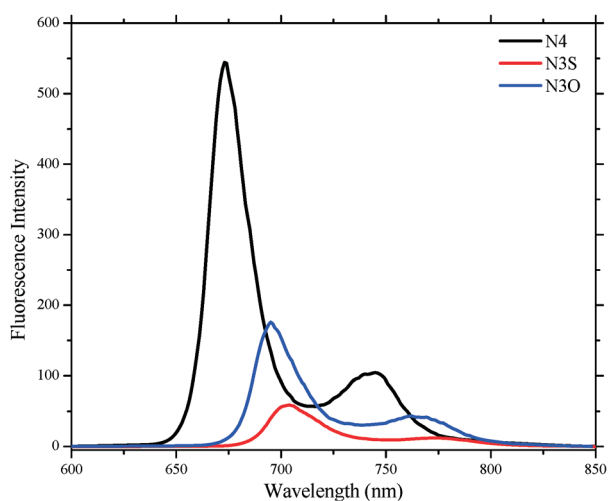


Fig. 3. Fluorescence spectra of porphyrin dyes in THF.

Figure 4. As shown in the figure, the lowest unoccupied molecular orbitals (LUMO) of the porphyrins are more negative than the TiO₂ conduction band and thus ensure enough driving force for the electron injection from the LUMO energy level of the dye to the TiO₂ conduction band. The highest occupied molecular orbitals (HOMO) of all the porphyrins are more positive than the redox electrolyte which confirms the efficient dye regeneration.

DFT Calculations

To correlate the molecular structures of the dyes with the performance of DSSCs, DFT as well as TD-DFT calculations were carried out. The results from quantum chemical calculations show planar macrocycles for all the porphyrins as shown in Figure 5. In HOMO of all the porphyrins, the majority of the electron density is localized on the porphyrin ring however a small portion is also extended over the ethynylphenyl group, while in the LUMO the elec-

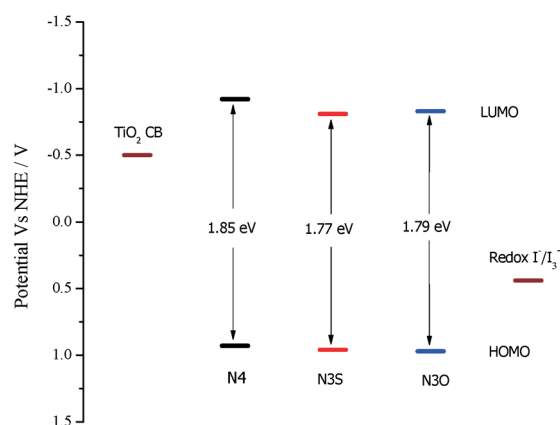


Fig. 4. Energy level diagram for the studied porphyrin dyes.

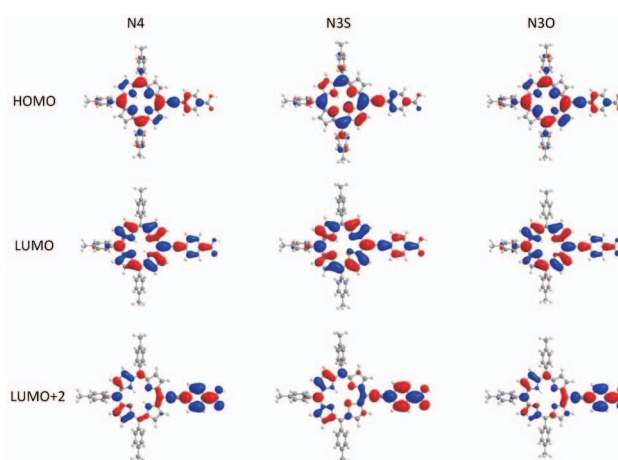


Fig. 5. Molecular orbital diagrams of N4, N3S and N3O obtained from DFT calculations.

tron density is populated equally on the porphyrin ring and the ethynylbenzoic acid acceptor. The increased electron density populating to the anchoring group in the LUMO facilitates efficient charge transfer from the excited state of the porphyrins to the TiO₂ conduction band. Interestingly in the LUMO+2, the electron density is extensively located on the ethynylbenzoic acid acceptor suggesting that the electron injection from the higher excited states involving LUMO+2 might be more efficient than LUMO.

It is evident from TD-DFT calculations that the calculated wavelengths given in Table 2 are in good agreement with the experimental values. Pointedly the calculations obtained dipole moments for the studied porphyrins in order, N4 > N3S > N3O. This trend is similar with the overall efficiencies of these porphyrins. The higher polarizability is advantageous to facilitate intramolecular photoinduced electron transfer.

Dye Loading Measurements

To better comprehend the adsorption behavior and measure the amount of the adsorbed dye, we performed the measurements of porphyrin densities (Γ) adsorbed on TiO₂ surface. The porphyrin densities were determined by measuring the concentrations of the porphyrin solutions desorbed from the dye-coated TiO₂ films after being immersed in 0.1 M KOH solution in THF. The saturated Γ values of the porphyrins under study were found as 360 ± 30 , 180 ± 30 and 62 ± 10 nmol cm⁻² for N4, N3S and N3O porphyrins respectively. The dye loadings values are consistent with the overall conversion efficiencies obtained for the studied porphyrins, reported below. We attribute the difference of dye-loading to the different affinity of the dye to the TiO₂ surface. The oxaporphyrin which is a more electron-rich porphyrin might decrease the acidity of carboxylic acid and decrease the affinity of N3O to TiO₂ surface.

Photovoltaic Measurements

DSSCs based on liquid electrolytes were fabricated using the porphyrins N4, N3S and N3O and tested under AM 1.5 conditions. The photovoltaic parameters for the porphyrins in this study are summarized in Table 3 and the I-V curves of the devices assembled using the porphyrins and measured under standard AM 1.5 G simulated solar conditions are shown in Figure 6.

As seen from the I-V curves, the device using regular free-base porphyrin N4 outperformed those heteroporphyrin-based devices. It obtained the highest efficiency of 3.66% with photocurrent density of 8.82 mA cm⁻², open-circuit voltage of 0.57 V, and fill factor of 73%. The thia-

Table 2. Calculated TD-DFT composition in terms of frontier molecular orbitals, excitation energy, and the oscillator strengths of N4, N3S, and N3O

Dyes	State	Composition (%)	<i>E</i> (eV)	λ (nm)	<i>f</i>	D (Debye)
N ₄	S1	H-1→L (12)	2.05	603.18	0.2321	4.72
		H-1→L+1 (12)				
		H→L (53)				
	S2	H→L+1 (22)	2.20	563.23	0.2144	
		H-1→L (24)				
		H-1→L+1 (6)				
	S3	H→L (29)	2.97	417.78	1.1369	
		H→L+1 (41)				
		H-1→L+1 (37)				
	S4	H→L (9)	3.19	388.66	0.2144	
		H→L+2 (46)				
		H-2→L (59)				
N ₃ S	S1	H-1→L+1 (8)	1.99	620.08	0.1509	4.57
		H→L+2 (17)				
		H-1→L (13)				
	S2	H-1→L+1 (11)	2.18	567.41	0.276	
		H→L (46)				
		H→L+1 (28)				
	S3	H-1→L (20)	2.91	425.58	0.9903	
		H-1→L+1 (7)				
		H→L (35)				
	S4	H→L+1 (37)	3.13	396.39	0.3169	
		H-4→L (10)				
		H-1→L+1 (42)				
N ₃ O	S1	H→L (9)	2.02	613.44	0.1412	4.04
		H→L+2 (24)				
		H-1→L (16)				
	S2	H-1→L+1 (9)	2.19	565.7	0.2903	
		H→L (39)				
		H→L+1 (34)				
	S3	H-1→L (18)	2.94	422.15	1.0362	
		H-1→L+1 (9)				
		H→L (42)				
	S4	H→L+1 (30)	3.11	398.48	0.0522	
		H-3→L (6)				
		H-1→L (9)				
S4	H-1→L+1 (38)	3.11	398.48	0.0522		
	H→L (7)					
	H→L+2 (30)					
S4	H-4→L (10)	3.11	398.48	0.0522		
	H-2→L (56)					
	H-2→L+1 (22)					

H=HOMO, L=LUMO, H-1=HOMO-1, H-2=HOMO-2, H-3=HOMO-3, H-4=HOMO-4, L+1=LUMO+1, L+2=LUMO+2.

porphyrin N3S gave the photocurrent density of 0.83 mA cm⁻², open-circuit voltage of 0.45 V, and fill factor of 58%.

Table 3. Photovoltaic parameters of N4, N3S and N3O dyes

Dye	J_{sc} (mA cm ⁻²)	V_{oc} (V)	ff (%)	η (%)
N4	8.82	0.57	73	3.66
N3S	0.83	0.45	58	0.22
N3O	0.06	0.24	50	0.01

The oxaporphyrin N3O obtained the photocurrent density of 0.06 mA cm⁻², the open-circuit voltage of 0.24, and fill factor of 50%. These parameters gained the overall conversion efficiencies of 0.22% for N3S and 0.01% for N3O. The enhanced non-radiative internal conversion or intersystem crossing for the heteroporphyrins compared to regular porphyrins might decrease the lifetimes of the excited state and decrease the efficiency of electron injection from the dye molecules to the conduction bands of TiO₂. The heavy atom effect of sulfur atom causes faster intersystem crossing rate can be the main reason for the low efficiency of N3S.¹⁶ The incident photon-to-current conversion efficiency (IPCE) spectra (Figure 7) for all the porphyrins are in good agreement with the corresponding absorption spectra on TiO₂ which display the characteristic intense absorption in the *Soret* region. The IPCE maximum for regular N4 porphyrin is found to be 50% in between 400-500 nm re-

gion and those for N3S and N3O are found to be 12% and less than 1%, respectively. The ICPE values for N3S porphyrin are surprisingly small and for N3O it is almost negligible in the *Q* band region. The I-V curves under standard AM 1.5 G illumination are in qualitative agreement with the photo-action spectra.

TCSPC Measurements

As shown in Figure 8, the time-correlated single photon counting (TCSPC) data of N4, N3O and N3S adsorbed on Al₂O₃ or TiO₂ films allow the studies of excited state lifetimes when these dyes were excited at Q(0,0) bands. Because of the complicated relaxation processes at the excited state, the lifetimes have been deconvoluted into two or three components using an iterative non-linear deconvolution fitting method and the mean lifetimes (τ_{av}), as shown in Table 4, are obtained from the weighted average of τ_1 and τ_2 , two main decaying components presence in the data of all dyes. The mean relaxation lifetime of N4 on non-injecting Al₂O₃ film is similar to that of N3S, and is longer than that of N3O. The short excited lifetime for N3O on AlO₃ implies an extremely fast internal conversion and/or intermolecular energy transfer processes caused by dye-aggregations. As expected the fast electron injections into the TiO₂ conduction band after the photo-excitations

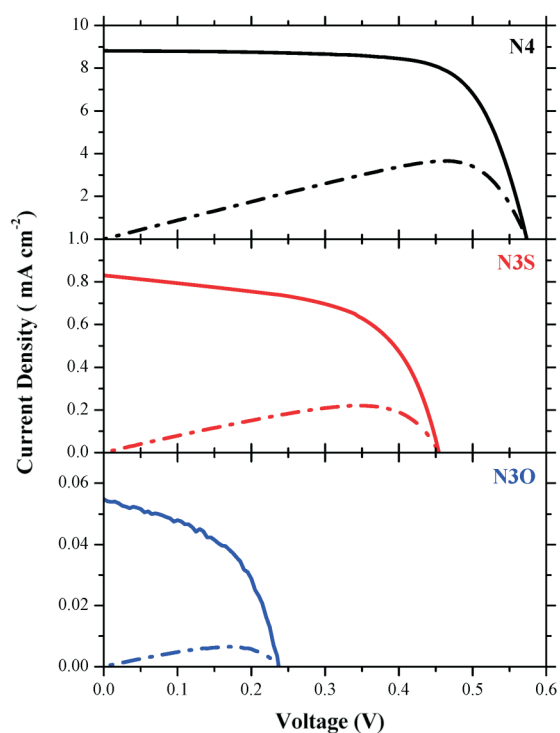


Fig. 6. I-V curves of the DSSCs fabricated with N4, N3S and N3O porphyrins under one sun.

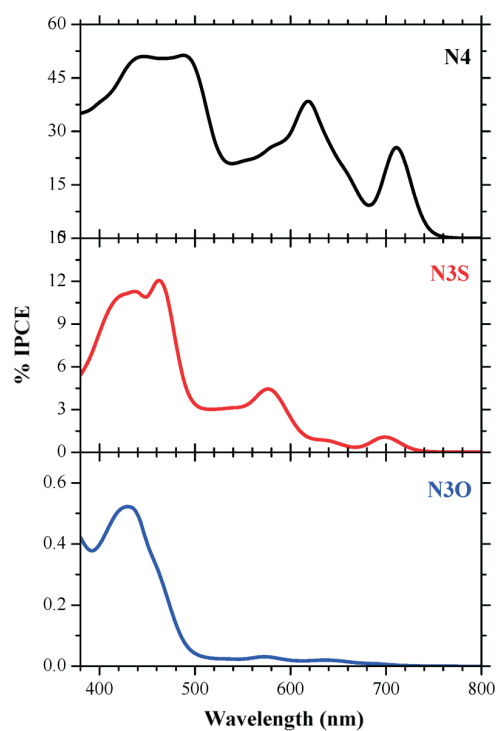


Fig. 7. IPCE spectra of the DSSCs fabricated with N4, N3S and N3O porphyrins.

Table 4. Fluorescence lifetimes and their fractional weights (A_i , normalized to 100%) of emission decays of porphyrin dyes adsorbed on either Al_2O_3 or TiO_2

Dye	τ_1/ns ($A_1\%$)	τ_2/ns ($A_2\%$)	τ_3/ns ($A_3\%$)	Average ($\tau_{\text{av}}/\text{ns}$) ^[a]
N4/ TiO_2	0.194(91)	0.522(9)	-	0.223
N4/ Al_2O_3	0.275(71)	0.87(25)	2.258(4%)	0.413
N3S/ TiO_2	0.234(85)	0.606(15)	-	0.290
N3S/ Al_2O_3	0.354(87)	0.894(13)	-	0.424
N3O/ TiO_2	0.08(96)	0.465(3)	1.534(1%)	0.091
N3O/ Al_2O_3	0.12(95)	0.697(4)	3.216(1%)	0.142

^[a] Average = ($\tau_1 \times A_1\%$) + ($\tau_2 \times A_2\%$)

significantly decrease the fluorescence lifetimes for the dyes adsorbed on TiO_2 films and the relative lifetimes reflect the efficiencies of electron injection. It is interesting to note that the difference of fluorescence transients between TiO_2 and Al_2O_3 are more obvious for N4 than for N3O and N3S. The intrinsic rapid fluorescence quenching of N3O as observed on Al_2O_3 film leads to near static lifetimes between N3O adsorbed on TiO_2 and Al_2O_3 . Overall, the TCSPC data agree with the trend of efficiencies of electron injection as $\text{N4} > \text{N3S} \gg \text{N3O}$.

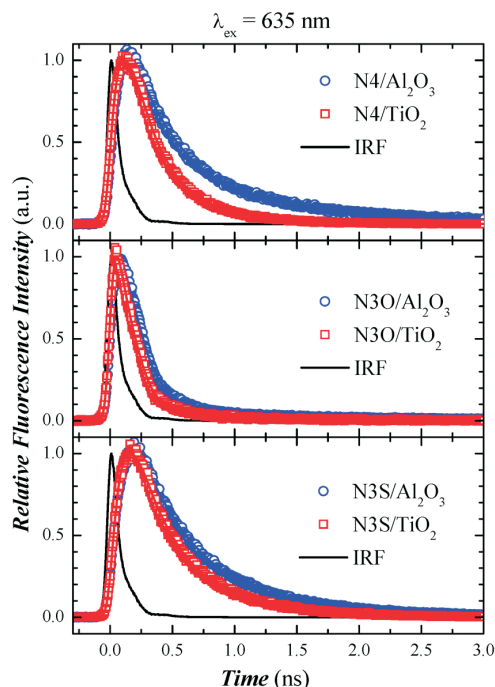


Fig. 8. Picosecond fluorescence transients of the porphyrin sensitizers adsorbed on either TiO_2 or Al_2O_3 ; the fitted lifetimes are summarized in Table 4. (The black curve is instrument response function from picosecond laser source.)

CONCLUSIONS

In summary, three novel free-base porphyrin sensitizers, N4, N3S, and N3O, were synthesized by simple and short routes. It is observed that the alteration of the core atom by group 16 heteroatoms has significant effects on the photophysical as well as photovoltaic properties of the studied porphyrins. The UV-visible spectra of the heteroporphyrins suggest that core-atom modification results in bathochromic enhancement of the absorption bands with the absorption onset reaching the NIR region. The steady-state fluorescence spectra display that the heteroatom substitutions on one of the pyrrolic nitrogens result in faster internal conversion or intersystem crossing which accelerate the non-radiative decay rates. The I-V curves suggest that the photocurrent density and the open-circuit voltage decrease substantially in DSSCs using core-modified porphyrins as the sensitizer. The overall conversion efficiencies of the devices display the order $\text{N4} (3.66\%) \gg \text{N3S} (0.22\%) > \text{N3O} (0.01\%)$. Noticeably, although lower dye loading can decrease the photo-current on N3O based DSSC, the fluorescence lifetimes suggest that poor electron injection caused by rapid excited-state relaxation is the main reason for the poor performance of N3O dye.

EXPERIMENTAL

Materials: All chemicals were obtained from commercial sources and used as received without further purification. All the reactions were carried out under nitrogen atmosphere. Solvents used in the reactions were dried by PureSolv MD 5 system (Innovative Technology, Inc). Flash chromatography was carried out by using basic alumina (63–200 μm , Merck) and silica gel (40–63 μm , Merck). Analytical TLC was performed on Merck silica gel plates. NMR spectra were recorded on a Bruker Avance 400 FT spectrometer. The ESI ion trap mass spectra were measured by a Finnigan MAT LCQ mass spectrometer.

Synthesis: 2-(Hydroxymethyl)-5-[hydroxy(*p*-tolyl)methyl]thiophene,¹⁷ 2-(hydroxymethyl)-5-[hydroxyl(*p*-tolyl)methyl]furan,¹⁷ 10,15,20-tris(*p*-tolyl)porphyrin (**1**),¹⁸ and 4-ethynylbenzoic acid¹⁹ were synthesized by following literature procedures.

10,15,20-Tris(*p*-tolyl)-21-thiaporphyrin (2**):** In a 250 mL one-necked round-bottomed flask fitted with a N_2 gas bubbler, the thiophene diol (335 mg, 1.43 mmol), pyrrole (320 μL , 4.70 mmol), and *p*-tolualdehyde (350 μL , 2.91 mmol) were dissolved in CH_2Cl_2 (150 mL). After purging the solution with N_2 for 15 min, the condensation reaction of the diol, aldehyde and pyrrole was initiated at room temperature by addition of a catalytic

amount of BF_3/OEt_2 (100 μL). After stirring for 1 h, DDQ (240 mg, 1.07 mmol) was added and the reaction mixture was stirred at room temperature in air for an additional hour. The solvent was removed on a rotary evaporator. The crude product was purified by silica gel column chromatography using hexane/ CH_2Cl_2 (1:1) as the eluent to afford a purple solid (62 mg, 7%) after solvent removal. ^1H NMR (400 MHz, CDCl_3) δ , ppm: -2.82 (s, 1H, NH), 2.72 (s, 9H, CH_3), 7.54-7.67 (m, 6H, *m*-tolyl), 8.07-8.19 (m, 6H, *o*-tolyl), 8.64 (d, 1H, $J = 4.44$ Hz, β -pyrrole), 8.74 (m, 2H, β -pyrrole), 8.99 (s, 2H, β -pyrrole), 9.05 (d, 1H, $J = 4.32$ Hz, β -pyrrole), 9.89 (d, 1H, $J = 5.12$ Hz, β -thiophene), 10.02 (d, 1H, $J = 5.04$ Hz, β -thiophene), 10.67 (s, 1H, *meso*); HRMS-ESI: m/z calcd for $\text{C}_{41}\text{H}_{32}\text{N}_3\text{S}$: 598.2317, found 598.2318 $[\text{M}+\text{H}]^+$.

10,15,20-Tris(*p*-tolyl)-21-oxaporphyrin (3): In a 250 mL one-necked round-bottomed flask fitted with a N_2 gas bubbler, the furan diol (500 mg, 2.29 mmol), pyrrole (500 μL , 7.31 mmol), and *p*-tolualdehyde (590 μL , 5.06 mmol) were dissolved in CH_2Cl_2 (200 mL). After purging with N_2 for 15 min, the condensation reaction of the diol, aldehyde, and pyrrole was initiated at room temperature by the addition of a catalytic amount of BF_3/OEt_2 (60 μL , 0.23 mmol). After stirring for 1 h, DDQ (520 mg, 2.32 mmol) was added and the reaction mixture was stirred at room temperature in air for an additional hour. The solvent was removed on a rotary evaporator. The crude product was purified by basic alumina column chromatography using hexane/ CH_2Cl_2 (1:1) and then CH_2Cl_2 as the eluent to afford a purple solid (67 mg, 5%) after solvent removal. ^1H NMR (400 MHz, CDCl_3) δ , ppm: 2.74 (s, 9H, CH_3), 7.60 (m, 6H, *m*-tolyl), 8.12 (m, 6H, *o*-tolyl), 8.68 (d, 2H, β -pyrrole), 8.89 (s, 1H, β -pyrrole), 8.95 (d, 2H, β -pyrrole), 9.15 (s, 1H, β -pyrrole), 9.39 (s, 1H, β -furan), 9.71 (s, 1H, β -furan), 10.17 (s, 1H, *meso*); HRMS-ESI: m/z calcd for $\text{C}_{41}\text{H}_{32}\text{N}_3\text{O}$: 582.2545, found 582.2542 $[\text{M}+\text{H}]^+$.

5-Bromo-10,15,20-tris(*p*-tolyl)porphyrin (4): To a stirred solution of 10,15,20-tris(*p*-tolyl)porphyrin (1) (200 mg, 0.34 mmol) in chloroform (50 mL) at room temperature, *N*-bromosuccinimide (NBS) (73 mg, 0.41 mmol) was added. The progress of the reaction was monitored by TLC and absorption spectroscopy. After complete consumption of the starting porphyrin as confirmed by TLC, the reaction was quenched with acetone (10 mL) and the solvent was removed on a rotary evaporator under vacuum. The crude reaction mixture was purified by silica gel column chromatography with hexane/ CH_2Cl_2 (70:30) as the eluent and the pure brominated porphyrin were obtained as a purple solid in 70% yield (157 mg, 0.24 mmol). ^1H NMR (400 MHz, CDCl_3) δ , ppm: -2.74 (s, 2H, NH), 2.69 (s, 3H, CH_3), 2.71 (s, 6H, CH_3), 7.53-7.58 (m, 6H, *m*-tolyl), 8.05-8.08 (m, 6H, *o*-tolyl), 8.81 (s, 4H, β -pyrrole), 8.91 (d, 2H, $J = 4.7$ Hz, β -pyrrole), 9.65 (d, 2H, $J = 4.8$ Hz,

β -pyrrole); HRMS-ESI: m/z calcd for $\text{C}_{41}\text{H}_{32}\text{N}_4\text{Br}$: 659.1810, found 659.1806 $[\text{M}+\text{H}]^+$.

5-Bromo-10,15,20-tris(*p*-tolyl)-21-thiaporphyrin (5): To a solution of 10,15,20-tris(*p*-tolyl)-21-thiaporphyrin (2) (137 mg, 0.23 mmol) in dry dichloromethane (25 mL) in a 50 mL round-bottomed flask was added NBS (49 mg, 0.28 mmol) at 0 $^\circ\text{C}$ and the reaction mixture was stirred at room temperature for 30 min. After complete consumption of the starting thiaporphyrin as confirmed by TLC, the reaction was quenched with acetone and the solvent was removed with a rotary evaporator under vacuum. The crude compound was subjected to silica gel column chromatography using hexane/ CH_2Cl_2 (2:1) as the eluent and the pure bromoporphyrin was isolated as a purple solid (118 mg, 77%) after drying. ^1H NMR (400 MHz, CDCl_3) δ , ppm: -2.59 (s, 1H, NH), 2.70 (s, 9H, CH_3), 7.52-7.65 (m, 6H, *m*-tolyl), 8.03-8.13 (m, 6H, *o*-tolyl), 8.58 (d, 1H, $J = 4.52$ Hz, β -pyrrole), 8.64 (m, 2H, β -pyrrole), 8.91 (d, 2H, $J = 1.80$ Hz, β -pyrrole), 9.30 (d, 1H, $J = 4.56$ Hz, β -pyrrole), 9.83 (d, 1H, $J = 5.24$ Hz, β -thiophene), 10.19 (d, 1H, $J = 5.28$ Hz, β -thiophene); HRMS-ESI: m/z calcd for $\text{C}_{41}\text{H}_{31}\text{BrN}_3\text{S}$: 676.1422, found 676.1417 $[\text{M}+\text{H}]^+$.

5-Bromo-10,15,20-tris(*p*-tolyl)-21-oxaporphyrin (6): To a solution of 10,15,20-tris(*p*-tolyl)-21-oxaporphyrin (3) (58 mg, 0.1 mmol) in dry CH_2Cl_2 (10 mL) in a 50 mL round-bottomed flask was added NBS (22 mg, 0.12 mmol) at 0 $^\circ\text{C}$ and then the reaction mixture was stirred at room temperature for 30 min. The progress of the reaction was monitored by TLC. After complete consumption of the starting oxaporphyrin as confirmed by TLC, the reaction was quenched with acetone and the solvent was removed with a rotary evaporator under vacuum. The crude compound was subjected to silica gel column chromatography with acetone/ CH_2Cl_2 (1:9) as the eluent and the pure bromoporphyrin was collected as a purple solid (52 mg, 78%) after drying. ^1H NMR (400 MHz, CDCl_3) δ , ppm: 2.71 (m, 9H, CH_3), 7.54-7.58 (m, 6H, *m*-tolyl), 8.03-8.07 (m, 6H, *o*-tolyl), 8.52 (d, 1H, $J = 4.64$ Hz, β -pyrrole), 8.59 (d, 1H, $J = 4.64$ Hz, β -pyrrole), 8.70 (d, 1H, $J = 4.68$ Hz, β -pyrrole), 8.86 (s, 2H, β -pyrrole), 9.31 (d, 1H, $J = 4.88$ Hz, β -pyrrole), 9.51 (d, 1H, $J = 4.68$ Hz, β -furan), 10.06 (d, 1H, $J = 4.92$ Hz, β -furan); HRMS-ESI: m/z calcd for $\text{C}_{41}\text{H}_{31}\text{BrN}_3\text{O}$: 660.1650, found 660.1652 $[\text{M}+\text{H}]^+$.

5-(4-Ethynylbenzoic acid)-10,15,20-tris(*p*-tolyl)porphyrin (7) [N4]: A mixture of 4-ethynylbenzoic acid (55 mg, 0.38 mmol) and 5-bromo-10,15,20-tris(*p*-tolyl)porphyrin (50 mg, 0.076 mmol) in dry THF (5 mL) and Et_3N (5 mL) was degassed with N_2 for 10 min, and then $\text{Pd}_2(\text{dba})_3$ (27 mg, 0.03 mmol) and AsPh_3 (58 mg, 0.19 mmol) were added to the mixture. The solution was stirred at room temperature for 12 h under N_2 . The solvent was removed in vacuo, and the residue was purified by silica gel column chromatography with $\text{CH}_2\text{Cl}_2/\text{methanol} = 9/1$ as the eluent to give purple

solid (31 mg, 56% yield) after drying. Mp > 300 °C; ^1H NMR (400 MHz, THF-*d*8) δ , ppm: -2.22 (s, 2H, NH), 2.68 (s, 3H, CH₃), 2.71 (s, 6H, CH₃), 7.57-7.63 (m, 6H, *m*-tolyl), 8.04-8.11 (m, 6H, *o*-tolyl), 8.16 (d, 2H, J = 8.3 Hz, Ph), 8.24 (d, 2H, J = 8.4 Hz, Ph), 8.76 (s, 4H, β -pyrrole), 8.94 (d, 2H, J = 4.7 Hz, β -pyrrole), 9.78 (d, 2H, J = 4.7 Hz, β -pyrrole) ppm; ^{13}C NMR (125 MHz, THF-*d*8) δ : 20.55, 94.41, 95.91, 98.02, 121.29, 122.33, 124.43, 124.92, 127.30, 127.42, 128.12, 129.03, 129.84, 130.71, 131.21, 131.43, 131.68, 134.14, 134.30, 137.52, 138.83, 139.11, 166.19 ppm; IR (Neat, cm⁻¹): 3312, 1684, 1603, 1424, 1312, 1292, 1174, 965, 794; UV-vis (THF) $\lambda_{\text{max}}/\text{nm}$ ($\epsilon/10^3 \text{ M}^{-1}\text{cm}^{-1}$) = 433 (245), 534 (11), 575 (31), 610 (4), 668 (11); HRMS-ESI: m/z calcd for C₅₀H₃₇N₄O₂: 725.2917, found 725.2919 [M+H]⁺. **5-(4-Ethynylbenzoic acid)-10,15,20-tris(*p*-tolyl)-21-thiaporphyrin (8) [N3S]:** 5-Bromo-10,15,20-tris(*p*-tolyl)-21-thiaporphyrin (5) (100 mg, 0.15 mmol), Pd₂(dba)₃ (55 mg, 0.06 mmol), AsPh₃ (113 mg, 0.37 mmol) and 4-ethynyl benzoic acid (26 mg, 0.18 mmol) were added to a 100 ml round bottom flask and the flask is attached to high vacuum for 30 min. A flow of N₂ gas was then flushed for 15 min before dry THF (40 mL) and triethylamine (10 mL) were added. The reaction mixture was stirred under N₂ at room temperature until completion of the reaction as monitored by TLC. The solvent was removed under vacuum and the crude product was purified by silica gel column chromatography using 5% methanol/CH₂Cl₂ as the eluent to isolate the pure product as a purple solid (99 mg, 90%) after drying. Mp > 300 °C; ^1H NMR (400 MHz, DMSO-*d*6) δ , ppm: -2.31 (s, 1H, NH), 2.67 (s, 9H, CH₃), 7.61-7.74 (m, 6H, *m*-tolyl), 8.04-8.16 (m, 6H, *o*-tolyl), 8.19 (d, 2H, Ph), 8.27 (d, 2H, Ph), 8.46 (d, 1H, β -pyrrole), 8.58 (m, 2H, β -pyrrole), 8.90 (s, 2H, β -pyrrole), 9.44 (d, 1H, β -pyrrole), 9.84 (d, 1H, β -thiophene), 10.48 (d, 1H, β -thiophene) ppm; ^{13}C NMR (100 MHz, DMSO-*d*6) δ : 21.01, 92.07, 98.29, 108.29, 124.80, 125.66, 126.76, 127.49, 127.60, 128.64, 129.15, 129.45, 129.76, 130.86, 131.96, 132.70, 133.12, 133.58, 133.91, 135.51, 136.03, 136.66, 137.63, 137.79, 138.04, 138.23, 138.38, 138.89, 145.28, 149.18, 153.70, 157.15, 157.95, 166.72 ppm; IR (Neat, cm⁻¹): 3326, 1684, 1603, 1429, 1313, 1293, 1176, 967, 795; UV-vis (THF) $\lambda_{\text{max}}/\text{nm}$ ($\epsilon/10^3 \text{ M}^{-1}\text{cm}^{-1}$) = 442 (257), 529 (17), 571 (37), 633 (5), 696 (9); HRMS-ESI: m/z calcd for C₅₀H₃₆N₃O₂S: 742.2528, found 742.2535 [M+H]⁺. **5-(4-Ethynylbenzoic acid)-10,15,20-tris(*p*-tolyl)-21-oxaporphyrin (9) [N3O]:** 5-Bromo-10,15,20-tris(*p*-tolyl)-21-oxaporphyrin (6) (52 mg, 0.08 mmol), Pd₂(dba)₃ (28 mg, 0.03 mmol), AsPh₃ (60 mg, 0.19 mmol) and 4-ethynyl benzoic acid (17 mg, 0.12 mmol) were added to a 100 ml round bottom flask and the flask is attached to high vacuum for 30 min. N₂ gas was then flushed for 15 min before dry THF (20 mL) and triethylamine (5 mL) were added. The reaction mixture was

stirred under N₂ at room temperature until completion of the reaction as monitored by TLC. The solvent was removed under pressure and the crude product was purified by silica gel column chromatography using 5% methanol/CH₂Cl₂ as eluent to afford the pure product as a purple solid (29 mg, 51%). Mp > 300 °C; ^1H NMR (400 MHz, THF-*d*8) δ : 2.69 (m, 9H, CH₃), 7.56-7.62 (m, 6H, *m*-tolyl), 8.01-8.17 (m, 6H, *o*-tolyl), 8.15 (d, 2H, J = 8.20 Hz, Ph), 8.24 (d, 2H, J = 8.24 Hz, Ph), 8.38 (d, 1H, J = 4.60 Hz, β -pyrrole), 8.44 (d, 1H, J = 4.56 Hz, β -pyrrole), 8.64 (d, 1H, J = 4.60 Hz, β -pyrrole), 8.78 (s, 2H, β -pyrrole), 9.32 (d, 1H, J = 4.80 Hz, β -pyrrole), 9.56 (d, 1H, J = 4.56 Hz, β -furan), 10.15 (d, 1H, J = 4.76 Hz, β -furan) ppm; ^{13}C NMR (125 MHz, THF-*d*8) δ : 21.55, 94.17, 97.23, 98.88, 120.43, 125.12, 126.03, 127.27, 127.73, 128.34, 128.39, 128.60, 128.76, 130.00, 130.31, 130.43, 130.75, 131.75, 135.11, 135.27, 135.76, 136.02, 138.50, 138.77, 139.60, 139.83, 140.08, 140.62, 155.67, 157.17, 157.66, 157.84, 157.87, 168.98 ppm; IR (Neat, cm⁻¹): 3233, 1707, 1603, 1462, 1376, 1258, 1181, 967, 798; UV-vis (THF) $\lambda_{\text{max}}/\text{nm}$ ($\epsilon/10^3 \text{ M}^{-1}\text{cm}^{-1}$) = 436 (247), 525 (9), 565 (19), 629 (3), 691 (5); HRMS-ESI: m/z calcd for C₅₀H₃₆N₃O₃: 726.2757, found 726.2759 [M+H]⁺.

Optical Spectroscopy: Transmittance and reflection UV-visible absorption spectra of the porphyrins in tetrahydrofuran (THF) and adsorbed on TiO₂ electrodes, respectively, were recorded on a JASCO V-670 UV-vis/NIR spectrophotometer. Steady-state fluorescence spectra were acquired by using a Varian Cary Eclipse fluorescence spectrophotometer.

Cyclic Voltammetry: The cyclic voltammetry measurements of the porphyrins were carried out on CHI 621B electrochemical analyzer (CH Instruments, Austin, TX, USA) in degassed THF containing 0.1 M tetrabutylammonium hexafluorophosphate (Bu₄NPF₆) as the supporting electrolyte. The cell assembly consists of a glossy carbon as the working electrode, a silver wire as the pseudo-reference electrode, and a platinum wire as the auxiliary electrode. The scan rate for all measurements was fixed at 50 mV/sec. A ferrocene^{+1/0} redox couple was used as the internal standard and the potential values obtained in reference to the silver electrode were converted to the vacuum scale.

Theoretical Calculations: The DFT and TD-DFT calculations were performed with Gaussian 09 package to study the distribution of electron density of the frontier molecular orbitals and the photo-excitation transitions.²⁰ All ground state geometries of studied porphyrins were optimized in the gas phase by the hybrid B3LYP functional and the 6-31G basis set, and the TD-DFT calculations were based on the same functional and basis set. The molecular orbitals were visualized by the Chemoffice software.

Photovoltaic Measurements: To characterize the photovoltaic performance of the DSSC devices, fluorine-doped tin ox-

ide glass (FTO; 6–8 Ω /sq, Pilkington Tec-7, USA, thickness 2.2 mm) plates were washed with a soap solution in an ultrasonic bath for 10 min, and then rinsed with deionized (DI) water and methanol. The FTO glass plates were immersed in 40 mM aqueous TiCl_4 at 70 °C for 30 min and washed with DI water and methanol. A transparent nanocrystalline layer was prepared on the FTO glass plate by repeated screen printing with TiO_2 paste (Solaronix, 15–20 nm Ti-Nanoxide T/SP), then drying for 2 h at room temperature. The TiO_2 electrodes were gradually heated at 110 °C for 1 h and 450 °C for 1 h. The resulting layer was composed of a ~ 11 μm thickness, measured by DekTak 150 stylus profiler. Finally a scattering layer containing >100 nm anatase particles (Solaronix, Ti-Nanoxide R/SP) was deposited by screen printing and then dried at room temperature for 2 h. The FTO glass plates were again immersed in 40 mM aqueous TiCl_4 at 70 °C for 30 min and washed with DI water and methanol. The TiO_2 electrodes were gradually heated at 110 °C for 1 h and 450 °C for 1 h. The porphyrin/ TiO_2 layer was served as a working electrode (anode). We immersed the TiO_2 coated FTO (TiO_2 active size 0.4×0.4 cm^2) films in a THF solution containing porphyrins (1×10^{-4} M) at 40 °C for 2 h. The FTO glass plate used as cathode was coated with Pt particles by using the thermal platinum nano-cluster catalyst method. The Pt catalyst was deposited from a precursor solution composed of 5 mM solution of hexachloroplatinic acid in anhydrous isopropanol. The precursor solution was spin-coated on FTO glass (10 L/cm^2) and dried in air for 3 min. Coated Pt electrode was placed in an oven and temperature was gradually increased to 360 °C and kept under 360 °C for 15 min. To fabricate the DSSC device, the two electrodes were assembled into a sandwich-type cell. The thin layer of electrolyte was introduced into the space between the two electrodes. A typical redox electrolyte containing lithium iodide (LiI, 0.1 M), diiodine (I_2 , 0.05 M), 1,2-dimethyl-3-propylimidazolium iodide (DMII, 0.5 M), and 0.5 M 4-*tert*-butylpyridine in dry acetonitrile. The photoelectrochemical characterizations of the solar cells were carried out by using an Oriol Class-A solar simulator (Oriol 91195A, Newport Corp.). Photocurrent and voltage curves were recorded with a potentiostat/galvanostat (CHI 650B, CH Instruments, Inc., USA) at a light intensity of one-sun irradiation calibrated by an Oriol reference solar cell (Oriol 91150, Newport Corp.). The incident photon-to-current conversion efficiency (IPCE) measurements were carried out with a monochromator (Oriol 74100) at short circuit conditions.

TCSPC Measurements: Fluorescence transients were recorded with a time-correlated single-photon counting (TCSPC) system (FluoTime 200, PicoQuant) with the picosecond laser source (PicoQuant) for excitation at $\lambda_{\text{ex}} = 635$ nm. The excitation

pulse was focused onto a rotating sample holder with a lens. A lens collected emission emitted from the sample at a right angle. An iris attenuated the intensity of the detected signal; the polarization of the detected emission relative to the excitation laser pulse was set at 54.7° with a polarizer. A double monochromator of a subtractive type compensated the group-velocity dispersion of emission and selected the detection wavelength; the resolution was 8 nm with a slit of width 1 mm. A micro-channel plate photomultiplier was connected to a computer with a TCSPC-module card (SPC-630, Becker & Hickl GmbH) for data acquisition. The FWHM of the instrument response function (IRF) was typically 80 ps, measured with scattered light at the laser excitation wavelength.

ACKNOWLEDGEMENTS

This work is supported by the National Science Council of Taiwan. Mass spectrometry analyses and NMR spectrometry measurements were performed by Mass Spectrometry facility and NMR Center of the Institute of Chemistry, Academia Sinica, Taiwan. The authors would like to thank Dr. Jiann-T'suen Lin for his assistance on the efficiency measurements of studied DSSCs.

REFERENCES

- (a) O'Regan, B.; Grätzel, M. *Nature* **1991**, *353*, 737; (b) Burschka, J.; Pellet, N.; Moon, S. J.; Humphry-Baker, R.; Gao, P.; Nazeeruddin, M. K.; Grätzel, M. *Nature* **2003**, *422*, 51; (c) Goncalves, L. M.; de Zea Bermudez, V.; Ribeiro, H. A.; Mendes, A. M. *Energy Environ. Sci.* **2008**, *1*, 655; (d) Grätzel, M. *Acc. Chem. Res.* **2009**, *42*, 1788; (e) Hagfeldt, A.; Boschloo, G.; Sun, L.; Kloo, L.; Pettersson, H. *Chem. Rev.* **2010**, *110*, 6595.
- (a) Imahori, H.; Umeyama, T.; Ito, S. *Acc. Chem. Res.* **2009**, *42*, 1809; (b) Mishra, A.; Fischer, M. K. R.; Bäuerle, P. *Angew. Chem. Int. Ed.* **2009**, *48*, 2474; (c) Martinez-Diaz, M. V.; de la Torre, G.; Torres, T. *Chem. Commun.* **2010**, *46*, 7090.
- (a) Muthiah, C.; Taniguchi, M.; Kim, H.-J.; Schmidt, I.; Kee, H. L.; Holten, D.; Bocian, D. F.; Lindsey, J. S. *Photochem. Photobiol.* **2007**, *83*, 1513; (b) Lee, C. Y.; She, C.; Jeong, N. C.; Hupp, J. T. *Chem. Commun.* **2010**, *46*, 6090; (c) He, H.; Gurung, A.; Si, L. *Chem. Commun.* **2012**, *48*, 5910.
- (a) Rochford, J.; Chu, D.; Hagfeldt, A.; Galoppini, E. *J. Am. Chem. Soc.* **2007**, *129*, 4655; (b) Lin, C.-Y.; Lo, C.-F.; Luo, L.; Lu, H.-P.; Hung, C.-S.; Diao, E. W.-G. *J. Phys. Chem. C* **2008**, *113*, 755.
- (a) Nazeeruddin, M. K.; Humphry-Baker, R.; Officer, D. L.; Campbell, W. M.; Burrell, A. K.; Grätzel, M. *Langmuir* **2004**, *20*, 6514; (b) Gervald, M.; Fungo, F.; Durantini, E. N.; Silber, J. J.; Sereno, L.; Otero, L. *J. Phys. Chem. B* **2005**,

- 109, 20953; (c) Alibabaei, L.; Wang, M.; Giovannetti, R.; Teuscher, J.; Di Censo, D.; Moser, J.-E.; Comte, P.; Pucciarelli, F.; Zakeeruddin, S. M.; Grätzel, M. *Energy Environ. Sci.* **2010**, *3*, 956; (d) Xiang, N.; Zhou, W.; Jiang, S.; Deng, L.; Liu, Y.; Tan, Z.; Zhao, B.; Shen, P.; Tan, S. *Sol. Energy Mater. Sol. Cells* **2011**, *95*, 1174.
6. Li, L.-L.; Diau, E. W.-G. *Chem. Soc. Rev.* **2013**, *42*, 291.
7. Han, L.; Islam, A.; Chen, H.; Malapaka, C.; Chiranjeevi, B.; Zhang, S.; Yang, X.; Yanagida, M. *Energy Environ. Sci.* **2012**, *5*, 6057.
8. Yella, A.; Lee, H.-W.; Tsao, H. N.; Yi, C.; Chandiran, A. K.; Nazeeruddin, M. K.; Diau, E. W.-G.; Yeh, C.-Y.; Zakeeruddin, S. M.; Grätzel, M. *Science* **2011**, *334*, 629.
9. (a) Campbell, W. M.; Jolley, K. W.; Wagner, P.; Wagner, K.; Walsh, P. J.; Gordon, K. C.; Schmidt-Mende, L.; Nazeeruddin, M. K.; Wang, Q.; Grätzel, M.; Officer, D. L. *J. Phys. Chem. C* **2007**, *111*, 11760; (b) Mozer, A. J.; Griffith, M. J.; Tsekouras, G.; Wagner, P.; Wallace, G. G.; Mori, S.; Sunahara, K.; Miyashita, M.; Earles, J. C.; Gordon, K. C.; Du, L.; Katoh, R.; Furube, A.; Officer, D. L. *J. Am. Chem. Soc.* **2009**, *131*, 15621; (c) Bessho, T.; Zakeeruddin, S. M.; Yeh, C.-Y.; Diau, E. W.-G.; Grätzel, M. *Angew. Chem. Int. Ed.* **2010**, *49*, 6646; (d) Kira, A.; Matsubara, Y.; Iijima, H.; Umeyama, T.; Matano, Y.; Ito, S.; Niemi, M.; Tkachenko, N. V.; Lemmetyinen, H.; Imahori, H. *J. Phys. Chem. C* **2010**, *114*, 11293; (e) Mai, C.-L.; Huang, W.-K.; Lu, H.-P.; Lee, C.-W.; Chiu, C.-L.; Liang, Y.-R.; Diau, E. W.-G.; Yeh, C.-Y. *Chem. Commun.* **2010**, *46*, 809; (f) Chang, Y.-C.; Wang, C.-L.; Pan, T.-Y.; Hong, S.-H.; Lan, C.-M.; Kuo, H.-H.; Lo, C.-F.; Hsu, H.-Y.; Lin, C.-Y.; Diau, E. W.-G. *Chem. Commun.* **2011**, *47*, 8910; (g) Ball, J. M.; Davis, N. K. S.; Wilkinson, J. D.; Kirkpatrick, J.; Teuscher, J.; Gunning, R.; Anderson, H. L.; Snaith, H. J. *RSC Advances* **2012**, *2*, 6846.
10. Latos-Grazynski, L. *The Porphyrin Handbook Vol. 2*; Academic Press: New York, 2010.
11. (a) Hung, C.-H.; Lin, C.-Y.; Lin, P.-Y.; Chen, Y.-J. *Tetrahedron Lett.* **2004**, *45*, 129; (b) Chuang, C.-H.; Ou, C.-K.; Liu, S.-T.; Kumar, A.; Ching, W.-M.; Chiang, P.-C.; dela Rosa, M. A. C.; Hung, C.-H. *Inorg. Chem.* **2011**, *50*, 11947; (c) Ambre, R.; Yu, C.-Y.; Mane, S. B.; Yao, C.-F.; Hung, C.-H. *Tetrahedron* **2011**, *67*, 4680.
12. Mane, S. B.; Hu, J.-Y.; Chang, Y.-C.; Luo, L.; Diau, E. W.-G.; Hung, C.-H. *Chem. Commun.* **2013**, *49*, 6882-6884.
13. (a) Chmielewski, P. J.; Latos-Grażyński, L. *Coord. Chem. Rev.* **2005**, *249*, 2510; (b) Gupta, I.; Ravikanth, M. *Coord. Chem. Rev.* **2006**, *250*, 468; (c) Arnold, L.; Müllen, K. *J. Porphyrins Phthalocyanines* **2011**, *15*, 757.
14. Xie, Y.; Joshi, P.; Ropp, M.; Galipeau, D.; Zhang, L.; Fong, H.; You, Y.; Qiao, Q. *J. Porphyrins Phthalocyanines* **2009**, *13*, 903.
15. Ha, J.-H.; Ko, S.; Lee, C.-H.; Lee, W.-y.; Kim, Y.-R. *Chem. Phys. Lett.* **2001**, *349*, 271.
16. Ambre, R.; Chen, K.-B.; Yao, C.-F.; Luo, L.; Diau, E. W.-G.; Hung, C.-H. *J. Phys. Chem. C* **2012**, *116*, 11907.
17. Punidha, S.; Agarwal, N.; Burai, R.; Ravikanth, M. *Eur. J. Org. Chem.* **2004**, *2004*, 2223.
18. Horn, S.; Senge, M. O. *Eur. J. Org. Chem.* **2008**, *2008*, 4881.
19. Wright, A. T.; Song, J. D.; Cravatt, B. F. *J. Am. Chem. Soc.* **2009**, *131*, 10692.
20. Frisch, M. J. Gaussian 09, Revision A.1 Gaussian, Inc.: Wallingford CT 2009.

Novel expanded porphyrin sensitized solar cells using boryl oxasmaragdyrin as the sensitizer†

Cite this: *Chem. Commun.*, 2013, **49**, 6882

Received 15th April 2013,
Accepted 6th June 2013

DOI: 10.1039/c3cc42769b

www.rsc.org/chemcomm

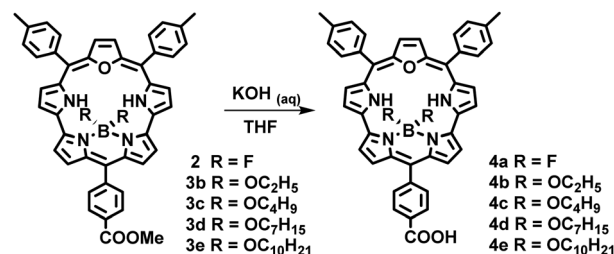
Oxasmaragdyrin boron complexes were prepared and applied in DSSCs. The HOMO–LUMO energy gap analyses and theoretical calculations revealed that these expanded porphyrins are ideal sensitizers for DSSCs. A device containing oxasmaragdyrin–BF₂ as the sensitizer achieves an energy conversion efficiency of 5.7%.

Dye-sensitized solar cells¹ (DSSCs) have emerged as promising candidates amongst the green energy sources due to their advantages such as low cost, high performance, and easy processing.² Although a lot of factors determine the efficiency of DSSCs, the light-harvesting properties of a photosensitizer remain utmost importance. Recently, Yella *et al.* reported a Zn(II) porphyrin with the D–π–A push–pull structure showing a remarkable power conversion efficiency of 12.3% when incorporated with an organic dye into the [Co(bipy)₃]^{2+/3+}-based electrolyte under AM 1.5G simulated sunlight.³ It is projected that the accessibility of high efficiency near-infrared (NIR) and panchromatic dyes might further improve the efficiency of DSSCs. From the spectroscopic point of view, the expanded porphyrins offer a broad range of compounds with absorption energies down to infrared regions.⁴ Expanded porphyrins with more than four pyrrole subunits in the porphyrinic macrocycle have been widely used in a variety of applications including anion and metal sensors,⁵ NIR sensing dyes,⁶ two-photon absorption (TPA) materials,⁷ and photodynamic therapy⁸ due to their increased cavity sizes and unique properties in association with extended π-conjugation. Although enormous literature is available on porphyrin-sensitized solar cells⁹ and red-shifted absorption bands of expanded porphyrins match well with the demands for a low energy sensitizer, surprisingly an expanded porphyrin has never been used as the sensitizer for DSSCs. To uncover the potential of applying expanded porphyrins to

DSSC studies, herein we report the syntheses and photophysical and photovoltaic properties of boron chelated oxasmaragdyrins, a class of aromatic core-modified expanded porphyrin with a 22 π-electron conjugation. The oxasmaragdyrin boron complexes **4a–4e** with structures depicted in Scheme 1 demonstrate panchromatic incident photon-to-current efficiencies (IPCEs), high short-circuit photocurrent densities (*J*_{sc}), and moderate-to-good overall efficiencies revealing an opportunity to develop expanded porphyrin-based highly efficient sensitizers for DSSCs.

The desired oxasmaragdyrin complexes **4a–4e** were prepared in four steps in decent yields under mild reaction conditions. Oxasmaragdyrin **1** was prepared from 3+2 condensation of *meso*-(4-methoxyphenyl)dipyrromethane and 16-oxatripyrrane in the presence of TFA as the acid catalyst.¹⁰ The BF₂ chelated complex **2** was prepared by treating **1** with triethylamine and BF₃·OEt₂ in CH₂Cl₂ at room temperature. The treatment of oxasmaragdyrin–BF₂ complex **2** with an excess amount of the corresponding alcohol in the presence of AlCl₃ at refluxing temperature for 10 min yielded dialkoxyboranyl chelated **3b–3e**.¹¹ The final oxasmaragdyrins **4a–4e** were isolated in moderate yields by hydrolysis of the precursors **2** and **3b–3e** with aqueous KOH in THF under reflux conditions (Scheme 1). In our design, alkoxy groups with long chains from C₂ to C₁₀ were introduced to shield oxasmaragdyrins from aggregation and to increase their solubility.

The absorption spectra of oxasmaragdyrins **4a–4e** display split *Soret* bands in the 400–500 nm region and Q-bands in the 550–750 nm region as shown in Fig. 1. Markedly, the split *Soret* band covers a broader range of absorption wavelengths than regular porphyrins. Additionally, the Q-bands, which are more intense than



Scheme 1 Synthesis of boryl oxasmaragdyrins **4a–4e**.

^a Institute of Chemistry, Academia Sinica, Taipei 115, Taiwan. E-mail: chung@gate.sinica.edu.tw; Tel: +886-2-27898570

^b Department of Chemistry, National Taiwan Normal University, Taipei, 11677, Taiwan

^c Department of Applied Chemistry and Institute of Molecular Science, National Chiao Tung University, Hsinchu 300, Taiwan. E-mail: diau@mail.nctu.edu.tw; Tel: +886-3-5131524

^d Department of Chemistry, Chung Yuan Christian University, Chung Li, 32023, Taiwan

† Electronic supplementary information (ESI) available. See DOI: 10.1039/c3cc42769b

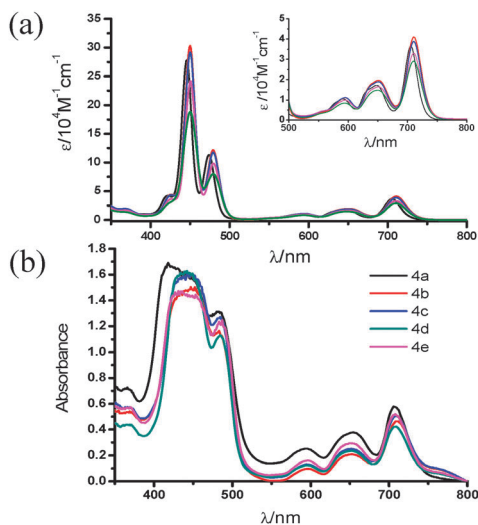


Fig. 1 Absorption spectra of oxasmaragdyrins **4a–4e**: (a) in THF (inset: expansion of Q-bands) and (b) adsorbed on TiO₂.

those for typical zinc or free base porphyrins and are mainly contributed from the HOMO to LUMO transition (Table S-1, ESI[†]), give the highest extinction coefficient (ϵ) at 710 nm, a shift of almost 100 nm in the NIR region compared to Zn(TPP).

The quantum-chemical calculations of structural optimization were performed for compounds **4a–4e** using the density functional theory (DFT) with the B3LYP functional and the 6-31G basis set. The results show planar structures for all studied dyes (see Fig. S-16, ESI[†]). Two alkoxide long chains lie on opposite sides of the oxasmaragdyrin plane and extend over to shield the furan ring. The calculations indicate that in the HOMO and HOMO – 1 orbitals, the majority of the electron density localizes on the macrocyclic π -system of the oxasmaragdyrin ring whereas in the LUMO and LUMO + 2 orbitals, electron densities delocalized further to the *meso*-carboxyphenyl anchoring group. The effective electron density redistribution should facilitate efficient electron injection from the excited state of oxasmaragdyrin to the conduction band of TiO₂. Significantly, theoretical calculations also revealed a higher molecular dipole moment (8.60 D) for the BF₂ chelated **4a** than an average of 7.86 D for B(OR)₂ chelated oxasmaragdyrins. The higher polarizability is beneficial to facilitate intramolecular photoinduced electron transfer. The cyclic voltammetry (CV) measurements of all oxasmaragdyrins **4a–4e** showed two reversible oxidation and one reversible reduction couples (Fig. S-15, ESI[†]). The static potentials and currents under multiple scans suggest high stability and reversibility of these compounds. The data in Table 1 show that the oxidation potentials of oxasmaragdyrins **4b–4e** shifted towards less positive by 140 to 170 mV resulting in elevated HOMO levels compared to oxasmaragdyrin-BF₂ **4a**. The reduction potentials of **4b–4e** shifted toward more negative by approximately 120 mV than that of the oxasmaragdyrin-BF₂ complex. Based on $E_{(0,0)}$ obtained from absorption and emission spectra and the first oxidation potential obtained from CV, the ground state oxidation potentials (E_{ox}) and excited state oxidation potentials (E_{ox}^*) were calculated as listed in Table 1. For all of the oxasmaragdyrin boryl complexes, E_{ox}^* are more negative than the conduction band edge of the TiO₂ electrode while the E_{ox} are more positive than the redox potential of Γ^-/I_3^- . Although the red-shift in the absorption band of

Table 1 Photophysical and electrochemical data for oxasmaragdyrin dyes

Dye	λ_{abs}^a [nm] (ϵ [$10^3 \text{ M}^{-1} \text{ cm}^{-1}$])	E_{ox}^b [V]	$E_{(0,0)}^c$ [eV]	$E_{\text{ox}}^*^d$ [V]
4a	446 (278), 474 (113), 706 (36)	0.86	1.75	–0.89
4b	450 (303), 479 (121), 711 (41)	0.69	1.73	–1.04
4c	450 (291), 479 (117), 711 (38)	0.71	1.73	–1.02
4d	450 (242), 480 (98), 710 (32)	0.72	1.73	–1.01
4e	450 (188), 480 (79), 710 (29)	0.71	1.73	–1.02

^a In THF. ^b First oxidation potentials vs. NHE in THF calibrated by the Fc/Fc⁺ couple. ^c Estimated from the intersection of the absorption and emission spectra. ^d Approximated from E_{ox} and $E_{(0,0)}$.

oxasmaragdyrins indicated a smaller band gap between HOMO and LUMO levels, the electrochemical data confirm the high driving force for both electron injection and dye regeneration.

The BF₂ and B(OR)₂ chelated oxasmaragdyrins **4a–4e** were fabricated into the solar cell devices in the presence of CDCA as a co-adsorbent as detailed in the ESI[†]. Fig. 2a shows the current–voltage plots of the devices measured under standard AM 1.5G simulated solar conditions; the photovoltaic parameters are summarized in Table 2. The DSSCs sensitized with oxasmaragdyrin-BF₂ complex **4a** exhibited the best performance with a short-circuit photocurrent density (J_{sc} /mA cm^{–2}) of 13.71, an open-circuit voltage (V_{oc} /V) of 0.591, and a fill factor (FF) of 0.703, corresponding to an overall power conversion efficiency (η) of 5.70%. The oxasmaragdyrin derivatives **4b–4e** all had efficiencies lower than that of the BF₂ complex **4a**, with a typical trend of an improved device performance upon increasing the length of alkoxy chains. The trend of J_{sc} in this series can be understood from the variation of IPCE action spectra shown in Fig. 2b. The lower efficiencies of devices **4b** and **4c** can be partly attributed to the lower dye-loading (DL) as shown in Table 2. We noted that the IPCE values corresponding to the absorption region of the *Soret* band of device **4a** reached 60%, and those of the Q band were around 50%. Also the dip between 500 and 600 nm was much higher (around 40%) for device **4a** compared to the devices **4b–4e**. To understand the key factors accounting for the IPCE values observed herein, we carried out transient photoelectric and charge-extraction (CE) measurements for the five devices under investigation.

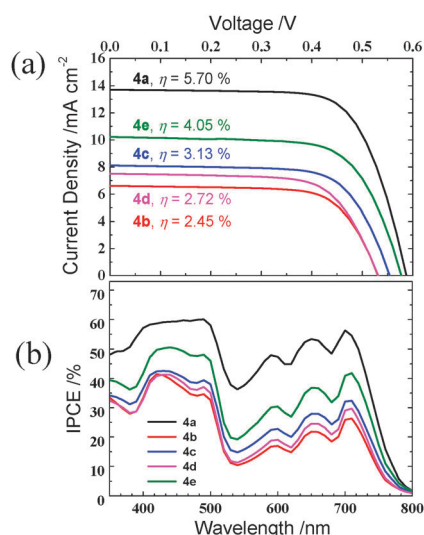


Fig. 2 (a) I – V characteristics and (b) IPCE spectra of DSSCs fabricated with oxasmaragdyrins **4a–4e** under 100% sun (AM 1.5G).

Table 2 Photovoltaic properties of devices with **4a–4e** dyes^a

Dye	DL [nmol cm ⁻²]	J_{sc} [mA cm ⁻²]	V_{oc} [V]	FF [%]	η [%]
4a	184	13.71	0.591	703	5.70
4b	110	6.60	0.535	695	2.45
4c	119	8.12	0.558	690	3.13
4d	146	7.51	0.534	679	2.72
4e	194	10.22	0.581	682	4.05

^a Immersion in EtOH at room temperature for 6–8 h.

The charge densities (N_e) of the devices under a certain bias light irradiation and open-circuit conditions were determined *via* CE measurements when the circuit of the system was switched to the short-circuit conditions.¹³ The CE results show that the extracted charge densities were much smaller than those of highly efficient devices reported elsewhere,¹³ indicating that either less electrons were injected into the conduction band of TiO₂, or the system involved a serious problem in expediting the charge recombination at the dye/TiO₂ interface. As a result, transient photovoltage decay (ΔV_{oc} vs. time) was performed using the small-amplitude approach based on seven white-light intensities (power densities in the range 7–102 mW cm⁻²) as bias irradiation under open-circuit conditions.¹³ Decay curves of ΔV_{oc} vs. time for the five devices were fitted according to a single exponential function to determine time coefficients for charge recombination (τ_R). Fig. 3a and b show the plots of τ_R vs. N_e and V_{oc} vs. N_e , respectively. The plots of V_{oc} vs. N_e show that the potentials were down-shifted upon increasing the length of the alkoxy chains, and this trend is against the variation of V_{oc} showing the opposite trend (Table 2). On the other hand, we found that the values of τ_R in this series are much smaller than those reported for highly efficient dyes,¹³ confirming that the relatively poor device performances of these porphyrins are due to the effect of rapid charge recombination. This effect causes significant reduction of the charge densities in the conduction band of TiO₂, and thus leads to a decrease in the performance for both J_{sc} and V_{oc} . The plots of τ_R vs. N_e shown in Fig. 3a display a systematic trend of τ_R for B(OR)₂ complexes with **4e** > **4d** > **4b** > **4c**, consistent with the variation of V_{oc} in this series. These results indicate that the

two alkoxy chains attached to the boron center could help in retarding the charge recombination. Typically, a longer alkoxy chain would have a better retardation effect to repel the approach of triiodide anion species toward the surface of TiO₂ for a larger τ_R and a higher V_{oc} , but an exception for the **4d** complex with heptoxyl chains was observed. Interestingly, we observed that the τ_R values of **4e** were significantly greater than those of **4a**, which cannot explain the fact that V_{oc} of **4a** was slightly larger than that of **4e**. We expect that the electron injection efficiency of the **4a** device should be greater than that of the **4e** device so as to generate more injected electrons in the CB of TiO₂ to give a larger Fermi level for the observed higher V_{oc} for the former than for the latter. The effect of electron injection can also be applied to rationalize the observed trend of J_{sc} , which is higher for **4a** than for **4e**.¹⁴

In conclusion, we were able to demonstrate for the first time that boron complexes of oxasmaragdyrin, a class of core-modified expanded porphyrin, can be applied as efficient photosensitizers for DSSC. In contrast to the relatively low efficiencies of the devices using BODIPY derivatives as the sensitizers,¹⁵ boron chelated oxasmaragdyrins provide desired redox potentials, high absorption coefficients, high stability, and higher power conversion efficiencies suitable for an effective sensitizer in DSSCs. More importantly, broad absorption spreading over the entire visible region and its lower energy Q band covering part of the NIR region make this class of compound an optimistic candidate for being one of the future selections of porphyrin-sensitized solar cells.

Notes and references

- B. O'Regan and M. Gratzel, *Nature*, 1991, **353**, 737.
- (a) L. M. Goncalves, V. de Zea Bermudez, H. A. Ribeiro and A. M. Mendes, *Energy Environ. Sci.*, 2008, **1**, 655; (b) Y. Luo, D. Li and Q. Meng, *Adv. Mater.*, 2009, **21**, 4647; (c) M. Grätzel, *Acc. Chem. Res.*, 2009, **42**, 1788; (d) A. Hagfeldt, G. Boschloo, L. Sun, L. Klöö and H. Pettersson, *Chem. Rev.*, 2010, **110**, 6595.
- A. Yella, H.-W. Lee, H. N. Tsao, C.-Y. Yi, A. K. Chandiran, M. K. Nazeeruddin, E. W.-G. Diao, C.-Y. Yeh, S. M. Zakeeruddin and M. Grätzel, *Science*, 2011, **334**, 629.
- J. M. Lim, Z. S. Yoon, J.-Y. Shin, K. S. Kim, M.-C. Yoon and D. Kim, *Chem. Commun.*, 2009, 261.
- (a) B. Sridevi, S. J. Narayanan, R. Rao, T. K. Chandrashekar, U. Englich and K. Ruhlandt-Senge, *Inorg. Chem.*, 2000, **39**, 3669; (b) J. L. Sessler, S. Camiolo and P. A. Gale, *Coord. Chem. Rev.*, 2003, **240**, 17; (c) Y. Ikawa, M. Takeda, M. Suzuki, A. Osuka and H. Furuta, *Chem. Commun.*, 2010, **46**, 5689.
- K. Naoda, H. Mori, N. Aratani, B. S. Lee, D. Kim and A. Osuka, *Angew. Chem., Int. Ed.*, 2012, **51**, 9856.
- R. Misra, R. Kumar, T. K. Chandrashekar, C. H. Suresh, A. Nag and D. Goswami, *J. Am. Chem. Soc.*, 2006, **128**, 16083.
- (a) S. K. Pushpan, V. G. Anand, S. Venkatraman, J. Sankar, D. Parmeswaran, S. Ganesan and T. K. Chandrashekar, *Curr. Med. Chem.: Anti-Cancer Agents*, 2002, **2**, 187; (b) J. Seenisamy, S. Bashyam, V. Gokhale, H. Vankayalapati, D. Sun, A. Siddiqui-Jain, N. Streiner, K. Shin-ya, E. White, W. D. Wilson and L. H. Hurley, *J. Am. Chem. Soc.*, 2005, **127**, 2944.
- L.-L. Li and E. W.-G. Diao, *Chem. Soc. Rev.*, 2013, **42**, 291.
- S. J. Narayanan, B. Sridevi, T. K. Chandrashekar, U. Englich and K. Ruhlandt-Senge, *Org. Lett.*, 1999, **1**, 587.
- M. Rajeswara Rao and M. Ravikanth, *J. Org. Chem.*, 2011, **76**, 3582.
- Y. Li, P. Lu, X. Yan, L. Jin and Z. Peng, *RCS Adv.*, 2013, **3**, 545.
- L.-L. Li, Y.-C. Chang, H.-P. Wu and E. W.-G. Diao, *Int. Rev. Phys. Chem.*, 2012, **31**, 420.
- C. Y. Lee, C. She, N. C. Jeong and J. T. Hupp, *Chem. Commun.*, 2010, **46**, 6090.
- S. Kolem, O. A. Bozdemir, Y. Cakmak, G. Barin, S. Erten-Ela, M. Marszalek, J.-H. Yum, S. M. Zakeeruddin, M. K. Nazeeruddin, M. Gratzel and E. U. Akkaya, *Chem. Sci.*, 2011, **2**, 949.

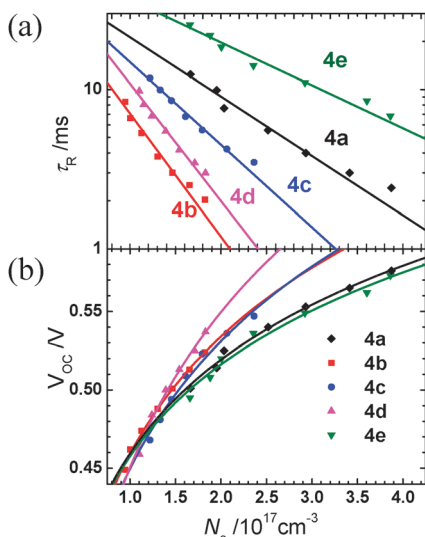


Fig. 3 Plots of (a) charge recombination time coefficient (τ_R) vs. electron density (N_e) and (b) V_{oc} vs. N_e for DSSCs fabricated with **4a–4e**.